

VIBRONIC COUPLING, SYMMETRY AND DYNAMICS  
IN UNSATURATED HYDROCARBONS

by

CHRISTOPHER ROBERTSON

A thesis submitted to  
the University of Birmingham  
for the degree of  
DOCTOR OF PHILOSOPHY

School of Chemistry  
University of Birmingham  
2014

UNIVERSITY OF  
BIRMINGHAM

**University of Birmingham Research Archive**

**e-theses repository**

This unpublished thesis/dissertation is copyright of the author and/or third parties. The intellectual property rights of the author or third parties in respect of this work are as defined by The Copyright Designs and Patents Act 1988 or as modified by any successor legislation.

Any use made of information contained in this thesis/dissertation must be in accordance with that legislation and must be properly acknowledged. Further distribution or reproduction in any format is prohibited without the permission of the copyright holder.

# Abstract

This theoretical work looks at excited state photochemistry - the study of the molecular processes triggered by the absorption/emission of light to/from electronically excited states. Although the Born-Oppenheimer has been often called the most successful approximation in theoretical Chemistry, when studying the excited state surfaces of most molecular systems, one quickly reaches an impasse. Excited states exhibit high-dimensional crossings through conical intersections where the adiabatic approximation gives rise to discontinuities and where population transfer between states occurs. We therefore need to resort to more careful considerations of the system that take into account the interactions of the electronic and nuclear wavefunctions. The approach taken here is that of using approximate vibronic coupling models, as well as extending the methods and algorithms to construct them. These models are then used in quantum dynamic calculations to obtain time-dependent properties, compute spectra and calculate dissociation cross-sections.

A Genetic Algorithm which aids to the fitting of diabatic model parameters is described in detail and tested in two systems. A speciation routine performs multiple local optimizations of all possible subsets of inter-state coupling parameters to prepare the initial guess population. A covariance matrix constructed from the population is then used to generate moderate adaptive mutations on members. The neutral and cationic surfaces of cyclobutadiene is one of the systems for which this fitting algorithm was used. A 10-dimensional model was fitted along important geometries using normal coordinates and the photo-electron spectrum was then calculated to compare with the experimentally recorded one. The diabatic coupling is typically in-

ferred from topological features exhibited between states. A more powerful way of constraining the coupling relationship between nuclei and electrons is the use of symmetry. We show how one can generate polynomial functions which are invariant with respect to the non-Abelian point groups  $D_{\infty h}$  and  $O$ . These polynomials are then calculated and listed to fourth and third order respectively. These  $D_{\infty h}$  invariant polynomials are then used for the construction of an acetylene model, where they reduce the number of fitted polynomials entering the construction of the model by an order of magnitude. Acetylene is a linear system which exhibits Renner-Teller (RT) and pseudo Jahn-Teller (pJT) interactions between states. The spectra of normal coordinate model systems which either explicitly contain these RT-interactions or are ‘folded’ into the diabatic model are compared to help understand these non-adiabatic effects. A more rigorous 10-state full-dimensional model of acetylene is then constructed using curvilinear coordinates which allow us to use  $D_{\infty h}$  constraints and which result in a remarkably simple kinetic energy operator. A pulse polarized laser field is modeled as a Gaussian enveloped sinusoidal function and used to model the experimental technique of vibrationally mediated dissociation (VMD) of acetylene. Dissociation cross sections are calculated for all possible angles. A bigger system Tolan (di-Phenyl acetylene), the monomial of a family of a photo-active dendritic antenna, is under study. Standard Geometry optimization methods locate the  $S_1$  minima far from the Franck-Condon (FC) region towards a *trans*-stilbene geometry. Comparison between the experimental and calculated absorption spectra validates the model and is subsequently used to model the first few picoseconds of population transfer, to qualitatively match the experimentally observed fluorescence decay lifetimes of the FC optically active bright state.



# Glossary

BOA =	Born–Oppenheimer approximation	MO =	Molecular orbital
CAP =	Complex absorbing potential	MPI =	Multi-photon ionization
CAS =	Complete active space	MRCI =	Multi-reference configuration interaction
CBD =	cyclo butadiene	NA =	Non-adiabatic
CC =	Coupled-cluster (SD = singles doubles)	NADPH =	Nicotinamide adenine di nucleotide phosphate
CI =	Conical intersection/ Configuration interaction	ND =	Normal distribution mutations (S = with speciation)
CMA =	Covariance matrix adaptation (S = with speciation)	PCA =	Principal component analysis
CMF =	Constant mean-field	PES =	Potential energy surface
DFT =	Density functional theory	pJT =	pseudo Jahn-Teller
DOF =	Degree of freedom	PT2 =	Perturbation theory, second order
DPA =	Di-phenyl acetylene	RMSD =	Root mean squared deviation
DVR =	Discreet variable representation		Rayleigh Schrodinger
EOM =	Equations of motion	RS2 =	perturbation theory, second order
FC =	Franck-Condon	RT =	Renner-Teller
FWHM =	Full width half maximum	SCF =	Self-consistent field
GA =	Genetic algorithm	SE =	Schroedinger equation
GS =	Ground state	SPF =	Single particle function
HF =	Hartree-Fock	TDDFT =	Time dependent density functional theory
HO =	Harmonic oscillator		Time-dependent
HOMO =	Highest occupied molecular orbital	TDSE =	Schroedinger equation
IR =	Infra-red		Time-independent
IrRep =	Irreducible representation	TISE =	Schroedinger equation
JT =	Jahn-Teller	TOF =	Time of flight
KE =	Kinetic energy	UV =	Ultra-violet
LED =	Light emitting diode	VCHAM =	Vibronic coupling hamiltonian
LIF =	Laser-induced fluorescence		Vibrationally mediated
LUMO =	Lowest unoccupied molecular orbital	VMD =	dissociation
MCTDH =	Multi-configurational time-dependent Hartree	ZPE =	Zero point energy
MP2 =	Moller-Plesset perturbation theory, second order	ZPVE =	Zero point vibrational energy

# Acknowledgements

As an undergraduate I remember reading a history of science book about the life of those classically ‘great scientists’ like Einstein, Maxwell and the like. Although well written, it is not the best format for any book, really. One of the chapters was dedicated to Neils Bohr and was entitled "science through conversations" or to the effect. At the time I was not impressed with Bohr’s portrayed personality; here was a great man, I thought, that needed to bounce off other peoples ideas to come up with something worthwhile. He was nothing like the those other ‘greats’, standing alone in the darkness of uncertainty, searching for that eureka moment to bring back fire from mount Olympus. Ironically, looking back at my first few steps in research, I’ve concluded that I am that sort of bouncy person! (alas, I would not draw any other similarities between myself and the great man). This is because I could honestly say that without some of the conversations I have had with colleagues, I would have stagnated for longer in those endless ditches that are the everyday condition of the computer chemist. Over these years, I felt happy to arrive in the office and start pestering my poor friends into discussions. It was an environment where I felt at liberty to display my endless ignorance in the light of scrutiny of friends.

I would therefore first like to thank Graham Worth for allowing me to join his group. I would also like to thank him for his endless (albeit endless) optimism; for the space and patience with which he allowed me to explore some ideas and without which I would have had to give up some of the projects, for his good advice and his friendship. I thank the The School of Chemistry with all its characters and drama that makes life interesting and my flat-mates for their friendship and tolerance of my sharp edges. It

would feel wrong to start listing all the lovely people in the Worth group (and outside it) that I feel indebted to for my work, without making this a long and somewhat tawdry section. I hope the words above suffice to express my gratitude towards them. Having said this, I would like thank three people whom had so palpable effect on my work that deserve special mention. I thank Gareth Richings for turning around with patience and sympathy almost everyday, every time I uttered his name with a tone of helplessness. His clarity of thought and ability with the pencil consistently served as a universal acid for many of my more nebulous ideas. For similar reasons I would thank Simon Neville. He warned me of many of the caveats involved in constructing vibronic coupling models (the endless mine-fields and ideosyncrasies of the VCHAM code!) and provided several germinal ideas. I valued the heated discussions we had together and for which I must confess, because of his un-faulting rigour, I typically suffered the bigger wounds ( :P ). Finally I would also like to thank Pietro S. Oliveto that, through casual drinks in the dreaded Bratby bar, directed me towards the work of Hansen and from where I cheaply extracted some valuable ideas.

Finally I would like to specially thank my parents, brother, my family in the UK and my girlfriend Elaine Yip for the un-waving love and support I required for the completion of this work.

This thesis and the work described in it are entirely my own, except where I have acknowledged *either* help from a named person *or* a reference is given to a published source or a thesis.

# List of Publications

C. Robertson, G. A. Worth. “*Generating symmetry adapted bases for non-abelian point groups to be used in vibronic coupling models.*” JT special issue of J. Chem. Phys., submitted

C. Robertson, G. A. Worth. “*A genetic algorithm for the optimization of multi-state multi-mode vibronic coupling model parameters.*” in preparation

C. Robertson, G. A. Worth. “*The vibrationally mediated dissociation of Acetylene: a vibronic coupling model.*” in preparation

C. Robertson, G. A. Worth. “*Modelling the singlet excited state internal conversion of Tolane: a vibronic coupling model.*” in preparation

C. Robertson, G. A. Worth. “*Whiplash mechanism in the energy transfer in extended phenyl-acetylene dendrimers.*” In preparation

# Contents

<b>List of Figures</b>	<b>xvii</b>
<b>List of Tables</b>	<b>xxi</b>
<b>1 Introduction</b>	<b>1</b>
<b>2 Methodology and Theory</b>	<b>12</b>
2.1 Schroedinger equation . . . . .	12
2.2 The Born-Oppenheimer Approximation . . . . .	16
2.2.1 Adiabatic and diabatic representations . . . . .	16
2.2.2 Vibronic coupling Hamiltonian models . . . . .	19
2.2.3 Conical intersections. . . . .	23
2.3 Electronic Structure Methods . . . . .	25
2.3.1 SCF techniques and configuration interaction . . . . .	25
2.3.2 Correlated wavefunction methods . . . . .	28
2.3.3 Rayleigh Schroedinger perturbation theory (RSPT) . .	30
2.3.4 Density functional theory and methods . . . . .	31
2.3.5 Local geometry optimisation and normal mode analysis	33
2.4 Solving the Vibronic TDSE . . . . .	36
2.4.1 Variational approach and equations of motion . . . . .	36
2.4.2 Integral evaluation: spectral and DVR basis . . . . .	38
2.4.3 Wavefunction relaxation . . . . .	41

## Contents

---

2.4.4	Complex absorbing potential (CAP) and flux operator	41
2.4.5	Autocorrelation function and spectra. . . . .	43
<b>3</b>	<b>Genetic Algorithm for VCHAM Parameter Optimisations</b>	<b>45</b>
3.1	Introduction . . . . .	45
3.2	Implementation . . . . .	47
3.2.1	Speciation: generating an initial population . . . . .	48
3.2.2	Statistical analysis and covariance matrix . . . . .	51
3.2.3	Mutations . . . . .	52
3.2.4	Uniform Crossover . . . . .	57
3.2.5	Tournaments and Selection . . . . .	57
3.3	GA tests . . . . .	58
3.3.1	Introduction . . . . .	58
3.3.2	Trends across models . . . . .	60
3.3.3	Acetylene . . . . .	67
3.3.4	Cyclo-butadiene . . . . .	70
3.3.5	Conclusions . . . . .	72
3.A	CBD; trends between test-runs with different user-setting parameters. . . . .	74
3.B	Acetylene; trends between test-runs with different user-setting parameters. . . . .	78
<b>4</b>	<b>CBD Photo-Electron Spectra</b>	<b>82</b>
4.1	Introduction . . . . .	82
4.2	CBD photoelectron spectra. . . . .	88
4.3	Discussion and conclusions . . . . .	91
<b>5</b>	<b>Non-Abelian Symmetry in Vibronic Coupling Models</b>	<b>95</b>
5.1	Introduction . . . . .	95

---

## Contents

---

5.2	Generating symmetry-adapted basis . . . . .	96
5.2.1	Basis generating operator . . . . .	96
5.2.2	$D_{\infty h}$ Renner-Teller symmetry-adapted basis . . . . .	97
5.2.3	$O$ (3D) Jahn-Teller symmetry-adapted basis . . . . .	101
5.3	Conclusions . . . . .	103
5.A	Tables of matrix representation of symmetry operations for $D_{\infty h}$ and $\mathbf{O}$ in a symmetrised spherical harmonic basis. . . . .	105
<b>6</b>	<b>Acetylene</b>	<b>107</b>
6.1	Introduction . . . . .	107
6.2	Excited State Landscape . . . . .	114
6.3	Normal coordinates and spectra . . . . .	115
6.4	Curvilinear model and dynamics . . . . .	124
6.4.1	Introduction . . . . .	124
6.4.2	Potential surface and Fitting . . . . .	128
6.4.3	Modelling the vibrationally mediated dissociation of acetylene . . . . .	141
6.5	Conclusions . . . . .	149
6.A	Theoretical flux across dissociation coordinates in the vibra- tionally mediated dissociation of acetylene . . . . .	151
<b>7</b>	<b>Tolane</b>	<b>161</b>
7.1	Introduction . . . . .	161
7.2	Electronic structure and geometry optimisations . . . . .	170
7.3	Potential energy landscape and fitting. . . . .	172
7.4	Calculating absorption spectra . . . . .	176
7.5	Internal conversion . . . . .	179
7.6	Discussion and conclusions . . . . .	182



<b>8</b>	<b>Conclusions</b>	<b>190</b>
----------	--------------------	------------

## Appendix A

<b>A</b>	<b><math>D_{\infty h}</math> group</b>	<b>i</b>
A.1	First Order, $D_{\infty h}$ group . . . . .	ii
A.2	Second Order, $D_{\infty h}$ group . . . . .	iv
A.3	Third Order, $D_{\infty h}$ group . . . . .	vii
A.4	Fourth Order, $D_{\infty h}$ group . . . . .	x
A.5	Fifth Order, $D_{\infty h}$ group . . . . .	xv
A.6	Sixth Order, $D_{\infty h}$ group . . . . .	xix

## Appendix B

<b>B</b>	<b><math>O</math> group</b>	<b>xxiv</b>
B.1	First Order, $O$ group . . . . .	xxv
B.2	Second Order, $O$ group . . . . .	xxvii
B.3	Third Order, $O$ group . . . . .	xxxii

## Supplementary Information A, B and C

# List of Figures

1.1	Electrostatic PES of different ‘excited state’ solutions to TISE determined their fate in BOA (modified from ref. [3]). . . . .	3
1.2	Schematic representation of the landscape features in excited state photo-chemistry; local minima in excited (B,D,G) and ground states (A,L,H) transition states in excited (I,C,F) and ground states (E,K); dipole transitions (A-B),(G-H); non-adiabatic transitions, avoided crossing (D-E) and conical intersection (J). Reprinted from ref. [10] . . . . .	5
1.3	An example in the family of extended phenyl-acetylene dendrimers, taken from ref. [13] . . . . .	6
1.4	$E \otimes \epsilon$ Jahn-Teller ‘Mexican hat’ CI in the adiabatic ( <i>top</i> ) and diabatic ( <i>bottom</i> ) representations (only diabatic diagonal terms shown). . . . .	7
2.1	Two surfaces under the diabatic and adiabatic representations	17
3.1	Best RMSD (y-axis) in population over 2000 generation (x-axis). Representative subfigure obtained from Fig 3.6 in sub-Appendix 3.A showing test-runs with NID+CDM, $N_{pop}=600$ and three cell containing test-runs with $n_{mut}=0.15$ ( <i>left</i> ), 0.25 ( <i>center</i> ) and 0.35 ( <i>right</i> ). Each cell has a number of test-runs with parameters $r_{mut}$ and $\beta$ as shown in legend provided. . . .	61

---

## List of Figures

---

- 3.2 RMSD Standard deviation (y-axis) of the population over 2000 generation (x-axis). Representative subfigure obtained from Fig 3.11 in sub-Appendix 3.B showing test-runs with NID+NDM,  $N_{pop}=400$  and three cell containing test-runs with  $n_{mut}=0.15$  (*left*), 0.25 (*center*) and 0.35 (*right*). Each cell has a number of test-runs with parameters  $r_{mut}$  and  $\beta$  as shown in legend provided. . . . . 62
- 3.3 Average standard deviation relative to all test-runs (y-axis, see Eq. 3.8) of the population over 2000 generation (x-axis). Representative subfigure obtained from Fig 3.8 in sub-Appendix 3.A showing test-runs with NID+NDM,  $N_{pop}=400$  and three cell containing test-runs with  $n_{mut}=0.15$  (*left*), 0.25 (*center*) and 0.35 (*right*). Each cell has a number of test-runs with parameters  $r_{mut}$  and  $\beta$  as shown in legend provided. . . . . 63
- 3.4 Average parameter-mutation ratio (y-axis, see Eq. 3.9) of the population over 2000 generation (x-axis). Representative subfigure obtained from Fig 3.13 in sub-Appendix 3.B showing test-runs with SID+CDM,  $N_{pop}=400$  and three cell containing test-runs with  $n_{mut}=0.15$  (*left*), 0.25 (*centre*) and 0.35 (*right*). Each cell has a number of test-runs with parameters  $r_{mut}$  and  $\beta$  as shown in legend provided. . . . . 66
- 3.5 Some representative initial distributions for some parameters generated using the speciation routine, to be contrasted with a purely normal distribution. 1-4: Morse Oscillator parameters; 5-8: inter-state coupling parameters; 8-9: second order intra-state parameters; 10-12: higher order parameters. . . . . 68

---

## List of Figures

---

3.6	Cyclo-butadiene tests; Comparing the best fit of each test-run over 2000 generations of all the test-run combinations mentioned in the text (section 3.3). The tests are divided into sub-figures identified by a given method pair ([NID,SID] + [NDM,CDM]), $N_{pop}$ (300 and 600) and $n_{mut}$ (0.1,0.25,3.5). Within these sub-figures there are tests showing different settings for $r_{mut}$ (0.1,0.25,0.40) and $\beta$ (0.05,0.15,0.50). . . . .	74
3.7	CBD tests; Comparing the RMSD standard deviation of each test-run over 2000 generations of all the test-run combinations mentioned in the text (section 3.3). The tests are divided into sub-figures identified by a given method pair ([NID,SID] + [NDM,CDM]), $N_{pop}$ (300 and 600) and $n_{mut}$ (0.1,0.25,3.5). Within these sub-figures there are tests showing different settings for $r_{mut}$ (0.1,0.25,0.40) and $\beta$ (0.05,0.15,0.50). . . . .	75
3.8	CBD tests; Comparing the test-run average standard deviation relative to all test-runs (see Eq. 3.8) over 2000 generations of all the test-run combinations mentioned in the text (section 3.3). The tests are divided into sub-figures identified by a given method pair ([NID,SID] + [NDM,CDM]), $N_{pop}$ (300 and 600) and $n_{mut}$ (0.1,0.25,3.5). Within these sub-figures there are tests showing different settings for $r_{mut}$ (0.1,0.25,0.40) and $\beta$ (0.05,0.15,0.50). . . . .	76

3.9	CBD tests; Comparing the test-run average parameter-mutation ratio (see Eq. 3.9) over 2000 generations of all the test-run combinations mentioned in the text (section 3.3). The tests are divided into sub-figures identified by a given method pair ([NID,SID] + [NDM,CDM]), $N_{pop}$ (300 and 600) and $n_{mut}$ (0.1,0.25,3.5). Within these sub-figures there are tests showing different settings for $r_{mut}$ (0.1,0.25,0.40) and $\beta$ (0.05,0.15,0.50).	77
3.10	Acetylene tests; Comparing the best fit of each test-run over 2000 generations of all the test-run combinations mentioned in the text (section 3.3). The tests are divided into sub-figures identified by a given method pair ([NID,SID] + [NDM,CDM]), $N_{pop}$ (400 and 800) and $n_{mut}$ (0.1,0.25,3.5). Within these sub-figures there are tests showing different settings for $r_{mut}$ (0.1,0.25,0.40) and $\beta$ (0.05,0.15,0.50).	78
3.11	Acetylene tests; Comparing the RMSD standard deviation of each test-run over 2000 generations of all the test-run combinations mentioned in the text (section 3.3). The tests are divided into sub-figures identified by a given method pair ([NID,SID] + [NDM,CDM]), $N_{pop}$ (400 and 800) and $n_{mut}$ (0.1,0.25,3.5). Within these sub-figures there are tests showing different settings for $r_{mut}$ (0.1,0.25,0.40) and $\beta$ (0.05,0.15,0.50).	79

## List of Figures

---

3.12	Acetylene tests; Comparing the test-run average standard deviation relative to all test-runs (see Eq. 3.8) over 2000 generations of all the test-run combinations mentioned in the text (section 3.3). The tests are divided into sub-figures identified by a given method pair ([NID,SID] + [NDM,CDM]), $N_{pop}$ (400 and 800) and $n_{mut}$ (0.1,0.25,3.5). Within these sub-figures there are tests showing different settings for $r_{mut}$ (0.1,0.25,0.40) and $\beta$ (0.05,0.15,0.50). . . . .	80
3.13	Acetylene tests; Comparing the test-run average parameter-mutation ratio (see Eq. 3.9) over 2000 generations of all the test-run combinations mentioned in the text (section 3.3). The tests are divided into sub-figures identified by a given method pair ([NID,SID] + [NDM,CDM]), $N_{pop}$ (400 and 800) and $n_{mut}$ (0.1,0.25,3.5). Within these sub-figures there are tests showing different settings for $r_{mut}$ (0.1,0.25,0.40) and $\beta$ (0.05,0.15,0.50). . . . .	81
4.1	Diagram of active space $e_g$ degenerate orbitals occupying different singlet configurations that determine the character and symmetry of the first three excited states. Reprinted from Saddique [53] . . . . .	84
4.2	Calculated photo-electron spectra with different reduced dimensionality models. . . . .	89
4.3	Comparison between experimental spectra [58] and model spectra. . . . .	91

## List of Figures

---

4.4	Fitting of CBD 3 state model to normal (dimensionless) coordinates. $\{\tilde{v}_1\}$ means $\tilde{v}_1$ is kept constant at its minimum geometry (value $\sim 3$ ), while the other coordinate is displaced. From left to right: <i>first row</i> : $\tilde{v}_1, \tilde{v}_2, \tilde{v}_9, \tilde{v}_{10}$ ; <i>second row</i> : $\tilde{v}_{12}, \tilde{v}_{18}, \{\tilde{v}_1\}+\tilde{v}_2, \{\tilde{v}_1\}+\tilde{v}_7$ <i>third row</i> : $\tilde{v}_1+\tilde{v}_9, \tilde{v}_1+\tilde{v}_{10}, \{\tilde{v}_1\}+\tilde{v}_{12}, \{\tilde{v}_1\}+\tilde{v}_{18}$ . . . . .	92
4.5	Fitting of CBD <sup>+</sup> 2 state model to normal (dimensionless) coordinates. $\{\tilde{v}_1\}$ means $\tilde{v}_1$ is kept constant at its minimum geometry (value $\sim 2$ ), while the other coordinate is displaced. From left to right: <i>first row</i> : $\tilde{v}_1, \tilde{v}_2, \tilde{v}_9, \tilde{v}_{10}$ ; <i>second row</i> : $\tilde{v}_{12}, \tilde{v}_{18}, \{\tilde{v}_1\}+\tilde{v}_2, \{\tilde{v}_1\}+\tilde{v}_7$ ; <i>third row</i> : $\tilde{v}_1+\tilde{v}_9, \tilde{v}_1+\tilde{v}_{10}, \{\tilde{v}_1\}+\tilde{v}_{12}, \{\tilde{v}_1\}+\tilde{v}_{18}$ . . . . .	93
4.6	Contour plots. <i>from left to right</i> : <i>first row</i> : CBD S <sub>0</sub> along branching space $\tilde{v}_1$ (x), $\tilde{v}_9$ (y), CBD S <sub>1</sub> along branching space $\tilde{v}_1$ (x), $\tilde{v}_9$ (y) ; <i>second row</i> : CBD S <sub>0</sub> along b <sub>1</sub> $\tilde{v}_1$ (x), $\tilde{v}_9$ (y), CBD <sup>+</sup> S <sub>1</sub> along b <sub>1</sub> $\tilde{v}_1$ (x), $\tilde{v}_{10}$ (y) . . . . .	93
5.1	Depicting which elements of the diabatic potential matrix in the complex representation given in Eq. 5.5 share relationships; along the diagonal they are equal and real; off diagonal are complex conjugates. Identical relationships are shared between the other u/g,+/- IrReps. . . . .	101
5.2	Depicting which elements of the diabatic potential matrix in the complex representation given in Eq. 5.13 share relationships; along the diagonal they are equal and real; off diagonal elements are complex conjugates. . . . .	104
6.1	Laruelle dissociation [81] . . . . .	110

## List of Figures

---

6.2	Comparison of PE cuts along CCH angle using <i>left</i> : EOM-CCSD/aug-cc-pV(q+d)Z, <i>right</i> : EOM-CCSD/aug-pVTZ . . .	116
6.3	Fitting of 4-state model to <i>ab-initio</i> energies along to normal (dimensionless) coordinates. <i>From left to right</i> : $Q_{cc}$ , $Q_{as}$ , $Q_{ss}$	118
6.4	Comparing the fitting of the 4-dimensional space of <i>cis</i> and <i>trans</i> normal (dimensionless) coordinates between N4 ( <i>above</i> ) and N8 ( <i>below</i> ) models. <i>From left to right</i> : $Q_{tx}$ , $Q_{tx} + Q_{ty}$ , $Q_{cx}$ , $Q_{cx} + Q_{cy}$ . . . . .	118
6.5	Herzberg-Teller coupling; $\Pi_g$ nuclear coordinate dependence of <i>x</i> -polarised light ( $\Pi_u$ ) adiabatic transition dipole between ground state and the following; ( $\Pi_u$ ) Blue and red are $\Sigma_u^-$ and $\Delta_u$ states along $Q_{ty}$ mode, green is $\Delta_u$ along $Q_{tx}$ mode . . . .	120
6.6	Comparing reduced dimensionality spectra for models N4 and N8. Spectra have been shifted by their excited state zero-point energy (relative intensities arbitrary). . . . .	121
6.7	Diagrammatic representation of the curvilinear coordinates used in this subsection . . . . .	126
6.8	Adiabatic potential surfaces from a 10-state model that uses curvilinear coordinates compared to EOM-CCSD/aug-cc-pVTZ calculations (points). Energy in eV, coordinates in radians. $S_0$ is not shown in plots. Each slide shows a physically distinct vector generated by exploring diagonal and anti-diagonal vectors of $D_{\infty h}$ and $C_{2v}$ coordinates. <i>From left to right</i> : <i>first row</i> : $(\theta_a)$ , $(\theta_a + \theta_b)$ , $(\theta_a + \theta_b + \phi_a - \phi_b)$ , $(\theta_a - \theta_b)$ <i>second row</i> : $(2\theta_a - \theta_b - \phi_a)$ , $(\theta_a + \phi_a)$ , $(\theta_a + \phi_a + \phi_b)$ , $(\theta_a + \phi_b)$ <i>third row</i> : $(-\theta_a + \theta_b - \phi_a + \phi_b)$ , $(\theta_b + \phi_b)$ , dihedral path between minima in 4D, $\{\theta, \phi\}$ sub-space: $S_1$ , $S_2$ . . . . .	129



## List of Figures

---

- 6.9 Vector cuts showing diagonal elements of diabatic model along both Renner-Teller curvilinear coordinates (eV); *left*:  $\theta_a + \theta_b$  (*cis*); *right*:  $\theta_a - \theta_b$  (*trans*). Strict diabatic states should not exhibit any stablization away from the linear geometry. . . . . 130
- 6.10 Cuts of fitted excited states model correlating  $Q_{ccs}$  and  $R_{a|b}$  coordinates. First two top left frames also show  $S_0$ . Curly brackets mean the coordinate is kept constant but not at reference geometry. Energy in eV, coordinates in Å[amu]<sup>1/2</sup>. Coordinate underlined indicates which coordinate is shown in the x-axis (for mixed angular/radial/normal vectors). From left to right: *first row*:  $(R_a)$ ,  $(Q_{ccs})$ ,  $(\underline{R_a} + Q_{ccs})$ ,  $(\underline{R_a} - Q_{ccs})$ ; *second row*:  $(\underline{R_a} + \underline{R_b})$ ,  $(\underline{\theta_a} + Q_{ccs})$ ,  $(\underline{\theta_a} + \underline{\theta_b} + \{Q_{ccs}\})$ ,  $(\underline{\theta_a} - \underline{\theta_b} + \{Q_{ccs}\})$  132
- 6.11  $G(x)$  function,  $\beta = 1$  . . . . . 133
- 6.12 Comparing qualitatively the diabatic (diagonal elements) and adiabatic representations along a dissociating coordinate from a *trans* geometry. . . . . 134
- 6.13 Diagram of Jacobi coordinates, re-printed from ref [80] . . . . . 135
- 6.14 Comparing model energy surfaces from ref [82] and this model.  $S_1$  (*top*) and  $S_2$  (*bottom*). *left*: Model from [82] along Jacobi  $\Phi_1$  and  $\Phi_2$ , *centre*: this model along Jacobi  $\Phi_1$  and  $\Phi_2$ , *right*: this model along  $\theta_1$  and  $\theta_2$  (analogous angular displacements to Jacobi  $\Phi_1$  and  $\Phi_2$  described in this chapter). . . . . 136
- 6.15 Cut along H-dissociation using CAS+RS2 (*green*) and MRCI+Davidson (*red*). . . . . 137

---

## List of Figures

---

- 6.16 Cuts of fitted model correlating  $\theta, \phi$  and  $R_{a|b}$  coordinates.  
 Curly brackets mean the coordinate is kept constant but not at reference geometry. Energy in eV, coordinates in  $\text{\AA}[\text{amu}]^{\frac{1}{2}}$ .  
 Coordinate underlined indicates which coordinate is shown in the x-axis (for mixed angular/radial/normal vectors). From left to right: *first row* : *cis* dissociation ( $\{\theta_a - \theta_b\} + \underline{R_a}$ ), *trans* dissociation ( $\{\theta_a + \theta_b\} + \underline{R_a}$ ), bent dissociation ( $\{\theta_a\} + \underline{R_a}$ ), 2D bent-dissociation ( $\{\phi_a + \theta_a\} + \underline{R_a}$ ); *second row*: out-of-plane dissociation ( $\{\theta_a + \phi_b\} + \underline{R_a}$ ), skewed, out-of-plane dissociation ( $\{\theta_a + \theta_b + \phi_a - \phi_b\} + \underline{R_b}$ ), angle while CH stretched ( $\underline{\phi_b} + \{R_b\}$ ), simultaneous ( $\phi_a + \underline{R_a}$ ) . . . . . 138
- 6.17 Energy ordered simplex optimisations with initial geometries making a full DOF grid over most of the potential landscape.  
*first row*: *left* cell shows critical points of  $S_1$  with one radial coordinate stretched to  $\sim 1.9 \text{ \AA}$ , *right*  $S_1$  full optimisation *second row*: *left*  $S_2$  as above *right*  $S_2$  as above . . . . . 139
- 6.18 *top left*: Calculated spectra for 4D Renner-Teller subspace, ten state model. *top right*: Calculated 5D spectra including CC stretch ( $Q_{ccs}$ ) in first excited state. *bottom left*: Calculated 7D spectra including radial coordinates ( $R_{a|b}$ ). *bottom right*: Experimental Spectra [79]; Image edited from Malsch *et al* [80], providing assignments for *cis/trans* progressions in  $S_1$ - $S_3$ . 140
- 6.19 Transition dipole along  $\theta_a$ ; *black*: x-plane for  $1\Sigma_u^-$ , *blue*: x-plane for  $1\Delta_u^x$ , *green*: y-plane for  $1\Delta_u^y$  with the ground state.  
 The sign of the surface is reversed for coordinate  $\theta_b$ . . . . . 142

---

## List of Figures

---

6.20	Cumulative flux (y-axis) across dissociation channel along $R_a$ for 36 experiments over 265 fm (x-axis). Time=0 fs determines when the UV-pulse has finished. Key labels refer to Table 6.7 and to flux maps in sub-Appendix 6.A. . . . .	145
6.21	Four sub-figures representing a 3D angular-coordinate subspace (in ten 2D frames) displaying the total flux across a $R_a$ dissociation channel 200 fs after pulse. On the top LHS of each frame, the contribution (Normalised to 10.0) of the given frame to the total density across this subspace for each propagation is printed. In brackets (Total E (eV), Morse Overtone). <i>top left</i> :25p-uv4-ir0 (7.52,0) - near linear, <i>top right</i> :9p-uv1-ir2 (6.68,2) - <i>trans</i> (with slight out of plane), <i>bot left</i> :5p-uv0-ir4 (6.4 ,5) - mixture of <i>cis</i> and <i>trans</i> (with slight out of plane), <i>bot right</i> :29p-uv4-ir4 (7.52,5) - bent and <i>cis</i> (with strong out of plane) . . . . .	146
6.22	<i>top left</i> : 1p-uv0-ir0 (6.4,0), <i>top right</i> : 2p-uv0-ir1 (6.4,1), <i>bot left</i> : 3p-uv0-ir2 (6.4,2), <i>bot right</i> : 4p-uv0-ir3 (6.4,3) . . . . .	152
6.23	<i>top left</i> : 5p-uv0-ir4 (6.4,5), <i>top right</i> : 6p-uv0-ir5 (6.4,7), <i>bot left</i> : 7p-uv1-ir0 (6.68,0), <i>bot right</i> : 8p-uv1-ir1 (6.68,1) . . . . .	153
6.24	<i>top left</i> : 9p-uv1-ir2 (6.68,2), <i>top right</i> : 10p-uv1-ir3 (6.68,3), <i>bot left</i> : 11p-uv1-ir4 (6.68,5), <i>bot right</i> : 12p-uv1-ir5 (6.68,7) . . . . .	154
6.25	<i>top left</i> : 13p-uv2-ir0 (6.96,0), <i>top right</i> : 14p-uv2-ir1 (6.96,1), <i>bot left</i> : 15p-uv2-ir2 (6.96,2), <i>bot right</i> : 16p-uv2-ir3 (6.96,3) . . . . .	155
6.26	<i>top left</i> : 17p-uv2-ir4 (6.96,5), <i>top right</i> : 18p-uv2-ir5 (6.96,7), <i>bot left</i> : 19p-uv3-ir0 (7.24,0), <i>bot right</i> : 20p-uv3-ir1 (7.24,1) . . . . .	156
6.27	<i>top left</i> : 21p-uv3-ir2 (7.24,2), <i>top right</i> : 22p-uv3-ir3 (7.24,3), <i>bot left</i> : 23p-uv3-ir4 (7.24,5), <i>bot right</i> : 24p-uv3-ir5 (7.24,7) . . . . .	157

## List of Figures

---

6.28	<i>top left</i> : 25p-uv4-ir0 (7.52,0), <i>top right</i> : 26p-uv4-ir1 (7.52,1), <i>bot left</i> : 27p-uv4-ir2 (7.52,2), <i>bot right</i> : 28p-uv4-ir3 (7.52,3) . .	158
6.29	<i>top left</i> : 29p-uv4-ir4 (7.52,5), <i>top right</i> : 30p-uv4-ir5 (7.52,7), <i>bot left</i> : 31p-uv5-ir0 (7.8,0), <i>bot right</i> : 32p-uv5-ir1 (7.8,1) . . .	159
6.30	<i>top left</i> : 33p-uv5-ir2 (7.8,2), <i>top right</i> : 34p-uv5-ir3 (7.8,3), <i>bot left</i> : 35p-uv5-ir4 (7.8,5), <i>bot right</i> : 36p-uv5-ir5 (7.8,7) . . . . .	160
7.1	An example in the family of <i>extended</i> phenyl-acetylene dendrimers, taken from ref. [13] . . . . .	161
7.2	TDDFT/6-31G* surface cuts with bonds optimised at $S_0$ ( <i>top</i> ) and $1A_u$ ( <i>bottom</i> geometries. Reprinted from Zgierski <i>et al</i> [112]) . . . . .	163
7.3	Schematic representation of the photochemistry of DPA (by Amatatsu <i>et al</i> [115]) . . . . .	166
7.4	12 HF orbitals with significant contributions in the CAS wavefunctions. . . . .	170
7.5	Fit to $ts-1A_u$ ( <i>below</i> ) and 5D vector ( <i>above</i> ) along important modes of $A_g$ and $B_{3g}$ symmetry. . . . .	173
7.6	Comparison of the PES along $1B_{1u}$ to $ts-1A_u$ vector (normal coordinates) using CASSCF (active space (h) in table 7.2) ( <i>left</i> ) and MRCI ( <i>right</i> ) . . . . .	178
7.7	Comparing full spectra with different sets of reduced dimensionality spectra. . . . .	178
7.8	Calculated absorption spectra (in eV) with states $1B_{2g}$ and $1B_{3g}$ above ( <i>row 1</i> ) and below ( <i>row 2</i> ) state $1B_{1u}$ , with population: <i>From left to right</i> :100,30,15,0 %. Initial wavefunction is the relaxed ground state lowest eigenstate wavefunction. . .	180

## List of Figures

---

7.9	Calculated absorption spectra (in eV) with state $1B_{2g}$ and $1B_{3g}$ above ( <i>row 1</i> ) and below ( <i>row 2</i> ) state $1B_{1u}$ , with population: <i>From left to right</i> :100,30,15,0 %. Initial wavefunction is built from a relaxed $S_0$ state wavefunction with low frequency modes excited to higher vibrational overtones. . . . .	180
7.10	Fitting of surfaces along modes of $A_g$ and $B_{3g}$ symmetry. From left to right: <i>first row</i> : $(\tilde{\nu}_6 + \tilde{\nu}_5)$ , $(\tilde{\nu}_{38} + \tilde{\nu}_5)$ , $(\tilde{\nu}_{56} + \tilde{\nu}_5)$ <i>second row</i> : $(\tilde{\nu}_6 + \tilde{\nu}_{14})$ , $(\tilde{\nu}_{38} + \tilde{\nu}_{14})$ , $(\tilde{\nu}_{56} + \tilde{\nu}_{14})$ . . . . .	182
7.11	Calculated spectra ( <i>below</i> ) with different populations in states $B_{3g}$ and $B_{2u}$ (30% ( <i>left</i> ) and 0% ( <i>right</i> )) compared to experimental spectra ( <i>above</i> ) at high ( <i>left</i> ) and low ( <i>right</i> ) temperatures. . . . .	183
7.12	Fitting of surfaces along modes of $A_g$ symmetry. $S_0$ shown for cuts alone single modes. From left to right: <i>first row</i> : $(\tilde{\nu}_6)$ , $(\tilde{\nu}_{20})$ , $(\tilde{\nu}_{33})$ <i>second row</i> : $(\tilde{\nu}_{38})$ , $(\tilde{\nu}_{54})$ , $(\tilde{\nu}_{56})$ . . . . .	184
7.13	Fitting of surfaces along modes of $B_{1g}$ and $B_{3g}$ symmetry. $S_0$ shown for cuts alone single modes. From left to right: <i>first row</i> : $(\tilde{\nu}_{10})$ , $(\tilde{\nu}_{24})$ , $(\tilde{\nu}_{29})$ , <i>second row</i> : $(\tilde{\nu}_5 + \tilde{\nu}_{14} + \tilde{\nu}_{10})$ , $(\tilde{\nu}_5 + \tilde{\nu}_{14} + \tilde{\nu}_{24})$ , $(\tilde{\nu}_5 + \tilde{\nu}_{14} + \tilde{\nu}_{29})$	185
7.14	Fitting of surfaces along modes of $B_{2g}$ and $B_{3g}$ symmetry. $S_0$ shown for cuts alone single modes. From left to right: <i>first row</i> : $(\tilde{\nu}_4)$ , $(\tilde{\nu}_7)$ , $(\tilde{\nu}_4 + \tilde{\nu}_{14})$ <i>second row</i> : $(\tilde{\nu}_4 + \tilde{\nu}_5)$ , $(\tilde{\nu}_7 + \tilde{\nu}_{14})$ , $(\tilde{\nu}_7 + \tilde{\nu}_5)$ .	186
7.15	Fitting of surfaces along modes of $B_{3g}$ symmetry. $S_0$ shown for cuts along single modes. From left to right: <i>first row</i> : $(\tilde{\nu}_5)$ , $(\tilde{\nu}_{14})$ , $(\tilde{\nu}_5 + \tilde{\nu}_{14})$ , $(\tilde{\nu}_5 - \tilde{\nu}_{14})$ . . . . .	186

## List of Figures

---

7.16 Population transfer from $1B_{1u}$ to states involved in the internal conversion to $ts-1A_u$ using a hot ( <i>above</i> , 3 ps) and cold ( <i>below</i> , 2 ps) wavefunctions. $1B_{1u}$ (red), $1A_u$ (green), $2A_u$ (brown), $B_{3g}$ (blue) . . . . .	188
--	-----

# List of Tables

3.1	How the best of each subfigure in 3.6 and 3.10 in sub-Appendix 3.A and 3.B rank against each other. Each subfigure displays the set for a given method pair ([NID,SID] + [NDM,CDM]), $N_{pop}$ (400,800 for acetylene; 300,600 for CBD) and $n_{mut}$ (0.1,0.25,3.5)	60
4.1	CBD equilibrium $C_1C_2$ and $C_2C_3$ bond lengths for $S_0$ , $^1A_g$ ( $D_{2h}$ ) rectangular geometries . . . . .	86
4.2	CBD equilibrium CC bond length and angle for $S_1$ rhomboidal/square geometries . . . . .	86
4.3	$CBD^+$ equilibrium CC bond length and angle for $S_0$ rhomboidal geometries . . . . .	87
4.4	$CBD^+$ equilibrium c-c bond length and angle for $S_0$ rectangular geometries . . . . .	87
4.5	Vertical excitation energies (eV) at CBD $S_0$ square $D_{4h}$ (TS) geometry . . . . .	87
4.6	Vertical excitation energies (eV) at CBD $S_0$ rectangular $D_{2h}$ (equilibrium) geometry . . . . .	87
4.7	TS barrier for CBD $S_0$ automerization between rectangular $D_{2h}$ (equilibrium) geometries (excluding ZPVE) . . . . .	88

## List of Tables

---

4.8	D <sub>4h</sub> Harmonic frequencies of neutral cyclo-butadiene obtained at the CASSCF(4,4)+MP2 frequencies with a 6-31G* basis set level of theory. . . . .	94
5.1	Table of matrix representations of D <sub>∞h</sub> group under the representation given in Eq. 5.5. Contents taken from [ [73]] . . .	105
5.2	Table of matrix representations of <b>O</b> group under the representation given in Eq 5.13. $\eta = \exp(2i\pi/3)$ Modified from [73]	106
6.1	Experiments involving Singlet photodissociation of acetylene. $\Delta E$ refers to the total energy of excitation (IR + UV). . . .	114
6.2	Vertical excitation energy (eV) comparison between CAS(6,9)+PT2 and EOM-CCSD with different basis-sets. S <sub>0</sub> in Hartree A) CAS(6,9)+PT2//aug-cc-pVTZ B) CAS(6,9)+PT2//pVTZ C) EOM-CCSD//aug-cc-pVTZ D) EOM-CCSD//aug-cc-pV(q+d)Z E) EOM-CCSD//pVTZ . . . . .	122
6.3	Acetylene excited state critical structures and energies S <sub>1</sub> -S <sub>3</sub> . Energies in brackets refer to adiabatic vertical excitation energies from the ground state geometry. If two values are given by & it means the CH bonds/angles where different for both protons. Cisoid refers to differing-angles for CCH <sub>a</sub> and CCH <sub>b</sub> . Prefix d- refers to a proton being stretched to near dissociation before minimising model energy. <sub>a</sub> EOM-CCSD/cc-pVTZ (CASPT2 for energy). <sub>b</sub> CASSCF/ANO (PT2 for energies). <sub>c</sub> MR-AQCC/cc-pVQZ, <sub>d</sub> EOM-CCSD/aug-cc-pVTZ . . . . .	123
6.4	Harmonic Frequencies. Obtained from an MP2 calculation with an cc-pVTZ basis. . . . .	124



## List of Tables

---

6.5	Singlet state and symmetry correlation tables. Character of Rydberg states is based on Ref [81]. Last column refers to the doublet state which correlates adiabatically via dissociation. .	124
6.6	Approx. geometries of dissociating H atom based on VMD flux maps like those in Fig. 6.21. <i>Legend: letters</i> ; T=trans, C=cis, B=bent, L=linear, P=out-of-plane coordinate contribution to T or C. <i>numbers</i> : $0=0^\circ$ , $1=\frac{\pi}{8}^\circ$ , $2=\frac{2\pi}{8}^\circ$ , $3=\frac{3\pi}{8}^\circ$ . Note: B geometries P cannot refer to out-of plane geometries (dihedral angle not defined), but instead corresponds the location of the density in the 2D flux maps. . . . .	149
6.7	$a$ = Total energy (MO excitation + central pulse) includes Zero Point Energy. ; $b$ = Morse potential Overtone. ; $c$ = Ground state energy after using Morse ladder Operator (includes ZPE). ; $d$ = Central Frequency of pulse. ; $e$ = Population remaining in ground state after pulse. ; $f$ = Density (x1000) absorbed by dissociation CAP's after Pulse (65fs). ; $g$ = Final density (x1000) absorbed by dissociation CAP's after Pulse (265 fs). . . . .	151
7.1	Previous work on excited states. . . . .	169
7.2	Vertical excitation energies (eV) and symmetry of excited states from ground state geometry of Tolane. . . . .	169
7.3	CASSCF ts-1A <sub>u</sub> geometry in normal coordinates . . . . .	171
7.4	Important bonds lengths and angles in critical geometries. $a$ = acetylene frag. bond length, $b$ = acetylene-benzene bond length, $c$ = acetylene/benzene <i>trans</i> angle . . . . .	172
7.5	ts-1A <sub>u</sub> geom. in model . . . . .	175

## List of Tables

---

7.6	Mode combination and number of SPF used for each state. $^a$ =Symmetry; $^b$ =Mode combination; $^c$ =(states $1B_{1u}, 1B_{3g}, 1B_{2u},$ $1A_u, 2A_u, 1B_{3u}$ ). . . . .	176
7.7	Labels and coordinates of the different reduced dimensional models used to calculate absorption spectra. . . . .	179
7.8	Vibrational overtones used for initial wavefunctions (see text for details). . . . .	181
7.9	$D_{2h}$ Harmonic frequencies of Tolane (MP2/cc-pVDZ basis) . .	189

# Chapter 1

## Introduction

The rich and escalating complexity of the biosphere begins its journey with the production of complex molecular structures catalyzed by incoming light from the sun; without the capacity of chlorophyll to interconvert photons into chemical potential stored in the bonds of NADPH (nicotinamide adenine dinucleotide phosphate), life may have been reduced to small isolated pockets near the warmth of thermal vents and not covered the earth surface. These same photons must have also threatened early life, as ultra-violet light has the power to destabilise the bonds of essential genetic information carrying molecules. This must have prompted the evolution of the photo-stable DNA helix, whose bases are now known to have the capacity to dissipate the energy of light via non-radiative relaxation channels [1]. Closer to home, light is the medium through which our strongest sensory organ opens the world into our minds; Rhodopsin, the signalling protein which, through the seemingly simple conformational change on the chromophore it encapsules, the retinal molecule, sparks the cascade which culminates in the complex response by the organism. It has been suggested this signalling mechanism to work it must occur in the ultrafast regime [2], in order to avoid the inevitable loss of energy from its dissipative environment.

So how do we know about the intimate details of these essential mechanisms

in life? Yet again, how we came to understand owes much to experiments which probed the interactions of light and matter. Spectroscopy and diffraction experiments, like the microscope before them, showed us the smallest structures that make up the bedrock of the physical universe and gave inception to the new theory of Quantum Mechanics. The picture that emerged tells us the vast majority of complexity can be ultimately explained in terms of the interactions of four particles; protons, neutrons, electrons and photons. How the electrons and protons, which determine the structure (and therefore function) of molecules, behave can be to a great approximation described by the time-dependent Schroedinger equation (TDSE).

$$i\hbar\frac{\partial}{\partial t}|\Psi(t)\rangle = \hat{H}(t)|\Psi(t)\rangle \quad (1.1)$$

And its time independent equivalent (TISE)

$$E|\Psi\rangle = \hat{H}|\Psi\rangle, \quad (1.2)$$

Where  $\hat{H}$ , the Hamiltonian operator, contains the mathematical representation of the motion and interactions of the particles involved, and whose solution  $\Psi(t)$ , the wavefunction, describes how the aforementioned particles evolve in time. Historically, this description of the world represented a fundamental shift on the understanding of the cosmos. TDSE tells us that the position and motion of particles are probabilities that can be described as the propagation of waves that disperse over time. From the description of the hydrogen atom giving us the orbital description of electrons, to the hybridisation of these orbitals uncovering the nature of bonding in organic molecules, much of the fundamental understanding and intuitions of chemical bonding and structure has sprung from this equation.

Since the motion of electrons and nuclei depend on their masses, their ratio typically being on the order of  $10^3 - 10^4$ , the timescales at which elec-

tron evolve (attoseconds,  $10^{-18}$ ) compared to nuclei (femtoseconds,  $10^{-15}$ ) makes their interaction adiabatic; the electrons minimise the interactions with the seemingly ‘static’ nuclei, while the nuclei experience the electron re-arrangement as ‘instantaneous’. This picture, which is more rigorously cited as the Born-Oppenheimer approximation (BOA) of the Schroedinger equation, is perhaps the most celebrated approximation in Physical Chemistry. The Coulomb field of the electronic charges which the nuclei experience as they move adiabatically leads us to the picture of a potential energy surface (PES) which maps the possible nuclear geometries onto some high-dimensional landscape on which the energy is represented as the altitude surface.

Another consequence of the Schroedinger equation which contrasts with our classical expectations is the discrete nature of solutions the wavefunction can possibly take for a given set of conditions given by  $H$ , each solution requiring higher energy to exist (or be ‘populated’). It is this feature which explains the famous photo-electric effect and which led Albert Einstein to first posit the quantised nature of the interactions of matter and light and the concept of ‘excited’ states.

Combining BOA and the discrete arrangements (energies) electrons can take for a given nuclear geometry results in a collection of PES with increasing energy. The fate of systems is determined

by whichever excited state they initially find themselves in (see Fig 1.1). The BOA brought the Harmonic Oscillator

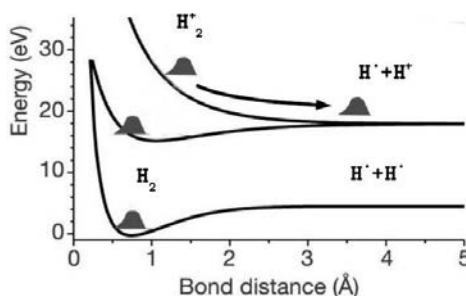


Fig. 1.1: Electrostatic PES of different ‘excited state’ solutions to TISE determined their fate in BOA (modified from ref. [3]).

and Rigid Rotor models from the classical into the quantum world, allowing

us to characterise infra-red spectra as the interaction of photons with the vibrations of chemical bonds and the rotations of molecules. These in turn gave us information on bond-lengths and angles, allowing today's chemists to speak of molecular structure with great confidence and physicists to explore the chemical composition of the interstellar medium [4]. Despite this, when we reach the visible and ultra-violet light regime, where photons are able to interact with the (dipole) electronic charge distribution and populate electronic excited states, the BOA has had more confused results. It predicts that the only form of coupling between electronic states in a molecular system occurs through the absorption/emission of photons. We would therefore expect all molecules to exhibit fluorescence following the population of excited electronic states.

However, half a century ago, experimentalists were already finding gaps in fluorescence spectra, like in the classic example of azulene [5] or in benzene [6], suggesting transfer between states was occurring in a non-adiabatic manner. Decades prior, Neumann and Wigner [7] had shown that there would exist regions of the geometry space where PESs would become degenerate. The story of these (singular) points is reminiscent of the prediction of 'black holes' in astronomy; due to the success of the BOA and the perhaps comforting 'non-crossing rule' for diatoms, these intersecting regions were thought rare oddities in an otherwise well separated landscape. Ironically, with the advent of better methods of calculating excited state energies [8] as well as time resolved, ultra-fast laser-spectroscopy [9], these regions of degeneracy are now understood to be ubiquitous in excited state photo-chemistry. The region of intersection generally has a 2-dimensional double cone shape for which it owes the name 'conical intersection' (CI). It plays the central role for the mechanism that explains photochemical decay [10] along which non-

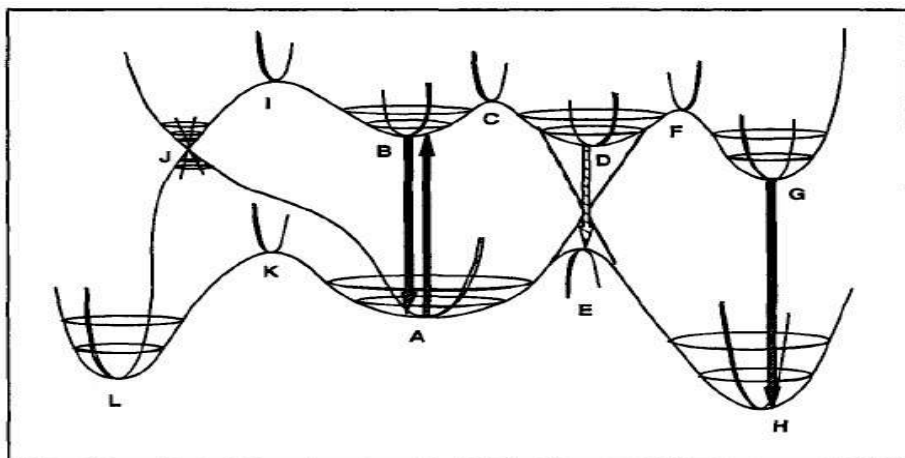


Fig. 1.2: Schematic representation of the landscape features in excited state photochemistry; local minima in excited (B,D,G) and ground states (A,L,H) transition states in excited (I,C,F) and ground states (E,K); dipole transitions (A-B),(G-H); non-adiabatic transitions, avoided crossing (D-E) and conical intersection (J). Reprinted from ref. [10]

adiabatic coupling occurs between adiabatic states. It is along this bottleneck that excited state populations get funnelled at sub-picosecond time-scales, and explains the gaps in fluorescence spectra of azulene and the remarkable DNA base ability to fight photo-degradation [1].

A more adequate picture of the modern view of the excited states landscape is given in Fig 1.2. Often the path towards the photo product drives the reaction to geometries unlike those of the ground state, as with the example of the ring opening of cyclohexadiene [11]. So to understand the electronic excited state landscape, the inclusion of interactions between electronic states by nuclear motion becomes fundamental. Under the BOA however, we reach an impasse. Due to the cusp character of CI, the coupling between states becomes singular leading to the break-down of the BOA. Therefore, understanding the fate of these wavefunctions becomes a less certain task that cannot be easily determined by looking at the static PES and the old paradigm of structure  $\rightarrow$  function loses some of its explanatory power. When reaching a conical intersection, how much population transfer one gets will depend

on non-adiabatic coupling, the shape of the CI, as well as the momentum of the wavefunction. From a coherent initial wavefunction projected to the excited landscape the wavefunction spreads through all possible pathways along the, often far from equilibrium, excited state topology. A dynamical approach to understand this complex web of outcomes becomes the most efficient way to understand photo-processes. As with the examples of retinal and DNA, where timing becomes crucial, instances where the need for a dynamic perspective of photochemistry abound in nature; an example is the green fluorescent protein, GFP, whose bright green fluorescence (under blue light) revolutionised fluorescence microscopy and cell-biology practice [12]. This photo process involves a proton transfer undergoing tunnelling, a dynamic effect describing the transfer of population across classically forbidden potential barriers. The photo-funnelling properties of phenyl-acetylene dendritic antennae are another example; dendrimers are a class of macromolecules with branching units parting from a central node in a regular geometry (Fig 1.3).

Upon excitation from the peripheral diphenyl-acetylene monomer segments, the energy is transferred through the branches via vibrational motion along localised electronic states. At the perylene locus, light is re-emitted 600 times brighter at a lower frequency. Many pa-

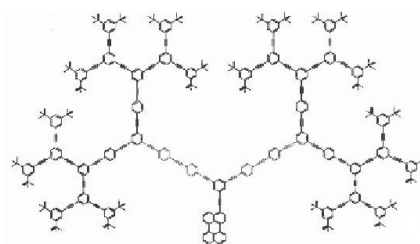


Fig. 1.3: An example in the family of extended phenyl-acetylene dendrimers, taken from ref. [13]

pers have been written highlighting their promise and practice in applications like photoactive arrays in polymeric systems [14] and single-molecular LED [15].

Going beyond the BOA means leaving the adiabatic picture.

The diabatic representation was devised more than 30 years ago [16] to deal



with atom-diatom collisions, but has since become the ideal way of representing non-adiabatic dynamics. Under this representation, states cross smoothly, no conical-shaped topologies are formed and coupling between states is also a smoothly varying function with respect to nuclear motion. Since diabatic states vary smoothly they follow the character of the electronic wavefunction over long displacements. This ‘smoothness’ has yet another valuable and beautiful property; the symmetry that states represent at a point of high symmetry can be used to characterise the interactions between states at displacements away from this point. It can be taken further if we analyse the nuclear displacements along some symmetry representation of the same symmetry group. We can then use a perturbative series to understand the different features of the potential from a Group Theory perspective.

The canonical example of the power of group theory in Chemistry is the Jahn-Teller effect; The underlying theorem shows that all non-linear degenerate irreducible representations of all symmetry groups allow non-totally symmetric linear perturbative terms to break symmetry [17]. This means the degenerate electronic states of polyatomic systems forming a representation of a non-Abelian point group will experience a force away from the high-symmetry geometry along some coordinate of specified symmetry. Any atom arrangement forming a representation of a non-

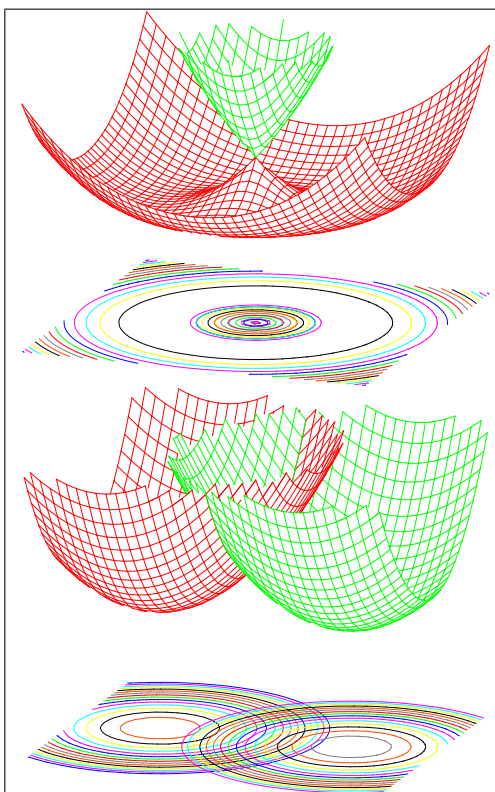


Fig. 1.4:  $E \otimes e$  Jahn-Teller ‘Mexican hat’ CI in the adiabatic (*top*) and diabatic (*bottom*) representations (only diabatic diagonal terms shown).

Abelian symmetry group will have a CI splitting the degenerate states. The ‘Mexican hat’ intersection has become a textbook image depicting the central role that CI and non-adiabatic effects have on the excited states of some of the most common molecules in the planet or the cosmos (like Ozone [18] or  $H_3^+$  [19]). Figure 1 displays this CI and its branching space surfaces in the diabatic and adiabatic representations.

Today’s forefront algorithms for the propagation of fully-quantum mechanical wavefunctions across diabatic surfaces ‘on-the-fly’ have been developed to satisfy the demands highlighted [20]. However, the evaluation of accurate excited state energies, as well as the evaluation of non-adiabatic coupling elements continue to be expensive, and have become a bottleneck for these methods. This work uses one of the most successful approaches in bridging the gap between the edge of the BOA and future, ‘on-the-fly’ propagations. The construction of vibronic coupling Hamiltonian (VCHAM) models is used for the most efficient grid-based method of wave-packet propagation, the multi-configurational time-dependent Hartree method (MCTDH) [21]. MCTDH has been used to obtain spectra for model systems of up to 24 degrees of freedom (DOF) [21]. Vibronic coupling models are simple analytic (typically polynomial) representations of the diabatic surface and coupling and were originally devised to describe the non-adiabatic coupling on two-state systems along a single DOF, or of Jahn-teller systems. Cederbaum *et al* [22] took the same approach and used it for a larger number of states and coordinates. The approximate nature of VCHAM models limits their use to system with some degree of symmetry, which allows us to analyse the order of inter/intra coupling functions. This way we can considerably trim down the number of terms that enter into our guess diabatic model.

Any N-dimensional cut that contains some of the CI 2D branching space

conical surface, but does not directly cut through the intersection, will result in an avoided-crossing topology. This gives the impression of two adiabatic states "pushing" each other away, with a gradient and coupling that is related to the strength of non-adiabatic effects. This feature allows the VCHAM models to piggyback on *ab-initio* energies to obtain estimates of non-adiabatic effects. The parameters constructing the guess diabatic models are optimised by transforming to the adiabatic representation and fitting to match *ab-initio* energies. The limits of VCHAM models come from both electronic and nuclear fronts;

- The increase in nuclear DOF makes fitting models a non-trivial and time consuming task. If the potential has strong correlation amongst coordinates, low-order polynomials become unsuitable. Higher order polynomials lead to unbounded potentials models owing to their monotonic behaviour at sufficiently far distances from the point of expansion.
- The increase in electronic states makes drawing incisions to carve out an adequate Hilbert subspaces on which to build a model more difficult. The correct estimation of non-adiabatic coupling also becomes less certain.

This work is an effort to stretch the limits of VCHAM models.

**Chapter 3** tries to tackle the inevitable increase in analytic terms to construct the VCHAM guess diabatic models fitted to adiabatic energies. A genetic algorithm (GA) was implemented to handle this general optimisation problem. A speciation routine performs multiple local optimisations of all possible subsets of inter-state coupling parameters to prepare the initial guess population. A covariance matrix constructed from the population is then used to generate moderate adaptive mutations on members. Two model systems analysed in subsequent chapters with different optimisation demands

are used to test the GA, the advantages and disadvantages of using a covariance matrix or speciation are discussed.

The neutral and Jahn-Teller cationic surfaces of cyclo-butadiene is one of the systems for which this fitting algorithm was used; the results presented in **Chapter 4**. A 3-state, 10-dimensional model was fitted ‘at once’ along important geometries using normal coordinates. A set of different reduced dimensionality photo-electron spectra was calculated so as to disentangle the experimentally recorded ones.

For non-Abelian Point Groups the eigenvectors of the matrix representation of degenerate symmetry species are complex. In the context of vibronic coupling models, some of the real representations of our diabatic states will be related to each other. This gives rise to constraints between diabatic parameters so as to make our Hamiltonian model polynomial functions totally symmetric.

In **Chapter 5** we therefore present two strategies for obtaining some of these invariant polynomials for the linear  $D_{\infty h}$  and octahedral/tetrahedral  $O$  groups (with 3D irreducible representations). These  $D_{\infty h}$  invariant polynomials are then used in the construction of a linear acetylene model in **Chapter 6**; in order to use these polynomials to describe the first 3 excited states, pseudo Jahn-Teller (pJT) coupling to higher lying Rydberg states was necessary. We compare the spectra between this model and one where these pJT couplings are approximately ‘folded’ into functions that then represent the diagonal elements of a smaller 3-state model. This allowed us to analyse any non-adiabatic effects on the spectra of the models and to compare the approaches when representing the diabatic potential. A more rigorous 10-state full-dimensional model of acetylene is then constructed using curvilinear coordinates which allow us to use  $D_{\infty h}$  constraints and which

result in a remarkably simple Kinetic energy operator. A pulse polarised laser field is modelled as a Gaussian enveloped sinusoidal function to model the experimental technique of vibrationally mediated dissociation (VMD) on acetylene, some of the earliest examples of control in photochemistry [23]. A vibrational eigenstate localised in a CH bond stretch is IR excited, followed by UV-excitation to some dissociating channel. Dissociation cross sections are calculated for all possible angles, providing new insights into this photo-process.

A bigger system tolane (di-phenyl acetylene), the monomial of the dendritic antenna mentioned earlier, is under study in **Chapter 7**. Standard Geometry optimisation methods locate the S1 minima far from the Franck-Condon (FC) region towards a *trans*-stilbene geometry. We interpret the stabilisation towards this geometry as the strong diabatic coupling occurring between  $10A_u$  state and a higher lying state. Symmetry considerations allow us to locate the crucial distortions that couple states leading towards the S1 minima and include them on the model. Comparison between the experimental and calculated absorption spectra validates the model, which is subsequently used to describe the first few picoseconds of transfer of population. This qualitatively matches the experimentally observed fluorescence decay lifetimes of the FC optically active bright state, and suggests a timescale in the order of picoseconds.

*It is one of the most extraordinary things in science that something as simple and abstract as the theory of groups should be so useful in the practical and everyday problems of the chemist.* [David M. Bishop] [24]

# Chapter 2

## Methodology and Theory

### 2.1 Schroedinger equation

In quantum mechanics the dynamic evolution of a system is represented by a matrix that performs a unitary transformation on the states of a system in Hilbert space. This transformation is analogous to the symplectic differential operator in classical mechanics, determining how the system evolves with time. Unitarity ensures that ortho-normality relationships (and therefore identity) of states are conserved:

$$U(t)|\Psi(\mathbf{t}_0)\rangle \rightarrow |\Psi(\mathbf{t}_0 + \mathbf{t})\rangle \quad (2.1)$$

For an infinitesimal time interval  $\varepsilon$ , the time evolution operator  $U(\varepsilon)$ , is conventionally written as:

$$U(\varepsilon) = (\mathbb{1} - \frac{i\varepsilon}{\hbar}\hat{H}) \quad (2.2)$$

Defining the Hamiltonian  $\hat{H}$ , this way enforces hermiticity (by ignoring higher orders of  $\varepsilon$ ), and it represents the observable energy of the system. To obtain a differential expression of the time evolution of the system, we write an infinitesimal step descriptor:

$$|\Psi(\mathbf{t}_0 + \varepsilon)\rangle = (\mathbb{1} - \frac{i\varepsilon}{\hbar}\hat{H})|\Psi(\mathbf{t})\rangle \quad (2.3)$$

Rearranging the above equation, dividing by  $\varepsilon$  and taking the limit  $\varepsilon \rightarrow 0$  results in the non-relativistic time-dependent Schroedinger equation in its most general form:

$$i\hbar \frac{\partial}{\partial t} |\Psi(t)\rangle = \hat{H} |\Psi(t)\rangle \quad (2.4)$$

with a formal solution given by:

$$|\Psi(t)\rangle = e^{\frac{-i\hat{H}}{\hbar}(t-t_0)} |\Psi(t_0)\rangle, \quad (2.5)$$

the state of the system unfolds in time according to this equation (given some initial conditions). Unfortunately the Hamiltonian in most cases is described by a very complicated expression and not easily evaluated in this form. In the cases where  $H$  is explicitly time dependent, there is no certainty whether it will commute with itself at later times, exacerbating things further. The Hilbert space of states of any quantum mechanical systems span the  $L_2(-\infty, \infty)$  space, containing functions which are square integrable (so-called rapidly decreasing functions) and Fourier invertible. A given state (of the system) can therefore be represented by a linear combination of complex basis functions spanning this *linear vector space* (LVS). According to the choice of representation (e.g. using the eigenfunctions of position or momentum operators to describe  $\Psi$ ) we obtain a wavefunction from which all physical information can be extracted as a probability distribution  $|\Psi|^2$ . One tractable approach for solving the Schroedinger equation is obtained by assuming the wavefunction to be separable into a product of time-dependent and time-independent functions  $\Psi = \xi(t)\psi$ . Substituting this back into 2.4 and separating variables we arrive at:

$$i\hbar\dot{\xi}(t) = E\xi(t) \quad (a) \quad (2.6)$$

$$H\psi_E(x) = E\psi_E(x) \quad (b)$$

for which the first can be readily solved as

$$\xi(t) = \xi_0 e^{-\frac{i}{\hbar}Et} \quad (2.7)$$

This gives rise to the time-dependent and time-independent Schroedinger equations (TDSE and TISE respectively). Equation 2.6b is an eigenvalue problem, whose solutions are the eigenvalues and eigenvectors of the Hamiltonian operator and decouple the equation. These in turn become the phase-factors and basis of the first equation. The wavefunction for non trivial systems will consist of linear combinations of the eigenfunction of H (and is generally termed a *wave-packet*). The interference resulting from the phase-factors (the ‘speed’ of the eigenfunction) then determine the way in which the wave-packet diffuses.

Many methods for wave-packet propagation have been devised. The dynamics simulations performed in this work will use the Multi-configurational time-dependent hartree (MCTDH) method and will be the subject later in this chapter. The full expression for the Hamiltonian of a molecule is [25]:

$$\hat{H} = \hat{H}_{trans} + \hat{H}_{rve} + \hat{H}_{es} + \hat{H}_{hfs} \quad (2.8)$$

The last three terms; the rovibronic, electron magnetic spin and nuclear spin-orbit interactions (‘hyperfine’ structure) correspond to the internal components of the Hamiltonian (and are separable from  $\hat{H}_{trans}$ ). For an electronic part of  $\hat{H}$ , only the rovibronic electronic Hamiltonian needs to be considered. For a molecule with  $N_n$  nuclei and  $N_e$  electrons,  $\hat{H}_{rve}$  is expanded as follows:



$$\begin{aligned}
\hat{H}_{rve} &= \hat{T}_e + \hat{T}_N + \hat{V}_{ee} + \hat{V}_{NN} + \hat{V}_{eN} \quad (a) \\
\hat{T}_e &= - \sum_{i=1}^{N_e} \frac{1}{2} \nabla_i^2 \quad (b) & \hat{T}_N &= - \sum_{A=1}^{N_n} \frac{1}{2M_A} \nabla_A^2 \quad (c) \\
\hat{V}_{eN} &= - \sum_{i=1}^{N_e} \sum_{A=1}^{N_n} \frac{Z_A}{r_{iA}} \quad (d) & \hat{V}_{ee} &= \sum_{i=1}^{N_e} \sum_{j>1}^{N_e} \frac{1}{r_{ij}} \quad (e) \\
\hat{V}_{NN} &= \sum_{A=1}^{N_n} \sum_{B>1}^{N_n} \frac{Z_A Z_B}{R_{AB}} \quad (f)
\end{aligned} \tag{2.9}$$

where indexes  $i$  and  $j$  label the electrons and  $A$  and  $B$  the nuclei. How tractable the evaluation of this operator is depends largely on the form of the wavefunction used. It is assumed that we can further separate the wavefunction into its electronic and nuclear parts (Born Representation);  $\psi_{rve}(\mathbf{r}, \mathbf{R}) = \phi_{elec,n}(\mathbf{r}; \mathbf{R}) \chi_{rv,nj}(\mathbf{R})$ . we obtain [18]:

$$\begin{aligned}
\hat{H} \phi_{elec,n}(\mathbf{r}; \mathbf{R}) \chi_{rv,nj}(\mathbf{R}) &= (\hat{V}_{elec,n} + \hat{V}_{NN}) [\phi_{elec,n}(\mathbf{r}; \mathbf{R}) \chi_{rv,nj}(\mathbf{R})] + \\
&\sum_{A=1}^M -\frac{1}{2M_A} [\phi_{elec,n}(\mathbf{r}; \mathbf{R}) \nabla^2 \chi_{rv,nj}(\mathbf{R}) + 2 \nabla \phi_{elec,n}(\mathbf{r}; \mathbf{R}) \cdot \nabla \chi_{rv,nj}(\mathbf{R}) \\
&\quad + \nabla^2 \phi_{elec,n}(\mathbf{r}; \mathbf{R}) \chi_{rv,nj}(\mathbf{R})] \tag{2.10} \\
&= E_{rve,nj} \phi_{elec,n}(\mathbf{r}; \mathbf{R}) \chi_{rv,nj}(\mathbf{R})
\end{aligned}$$

The summation (obtained from  $T_N$ ) runs over the nuclear coordinates, and its last two terms are *usually* orders of magnitude smaller than the other terms (due to the mass ratio of electrons with respect to the nuclei).  $2 \nabla \phi_{elec,n}(\mathbf{r}; \mathbf{R})$  is referred to as the non-adiabatic coupling operator and  $\nabla^2 \phi_{elec,n}(\mathbf{r}; \mathbf{R})$  as the scalar coupling operator. This equation is discussed in more detail in the following section. If we ignore these last two terms we arrive at the Born-Oppenheimer approximation (BOA):

$$\begin{aligned}
[\hat{T}_e + \hat{V}_{ee} + \hat{V}_{Ne}] \phi_{elec,n} &= \hat{H}_{elec} \phi_{elec,n} = E_{elec,n} \phi_{elec,n} \quad (a) \\
[\hat{T}_N + \hat{V}_{NN} + \hat{V}_{elec,n}] \chi_{rv,nj} &= E_{rve,nj}^0 \chi_{rv,nj} \quad (b) \\
\text{and } (E_{rve,nj}^0 &= E_{rv,nj} + E_{elec,n})
\end{aligned} \tag{2.11}$$

These are termed the coupled nuclear and electronic Schroedinger equations, we quantise the motion of electrons for a parameterised nuclear configuration. This leads to the concept of a potential energy surface (PES) for the nuclear wavefunction by a given electronic configuration.  $E_{rve,nj}^0$  is the Born-Oppenheimer rovibrational and electronic energy. The eigenstates obtained for  $\hat{H}_{elec}$  are orthogonal, and when used as a basis for the description of the rovibronic Hamiltonian, we get PES which preserve their energy level ordering. This picture is called the Adiabatic Representation (see Fig 2.1 ). Along totally symmetric displacements, states of same symmetry never intersect. In diatomic, this exceptional circumstance was enshrined as the so-called non-crossing rule. The exact electronic Hamiltonian would be ideally represented by a Hermitian matrix with the full eigenfunction space. Unfortunately, since these are infinite, the evaluation (diagonalisation) is un-feasible. However, in practice only the leading excited states are needed to obtain good agreement with experiments, and many approximate methods to calculate  $V_{elec,n}$  (and hence  $E_{rve,nj}$ ) have been devised. A summary of those methods used in this work are given in section 2.3.

## 2.2 The Born-Oppenheimer Approximation

### 2.2.1 Adiabatic and diabatic representations

As mentioned in the introduction, the BO approximation is obtained by ignoring the last two terms of the full expression of the Born-Oppenheimer representation (equation 2.10). This approximation assumes a quasi-static picture, where the character of the electron wavefunction is allowed to adapt gradually to the changes in the nuclear configuration, thereby remaining in the same eigenstate of the electronic Hamiltonian. However, there are many instances where the BO approximation breaks down. When the electronic

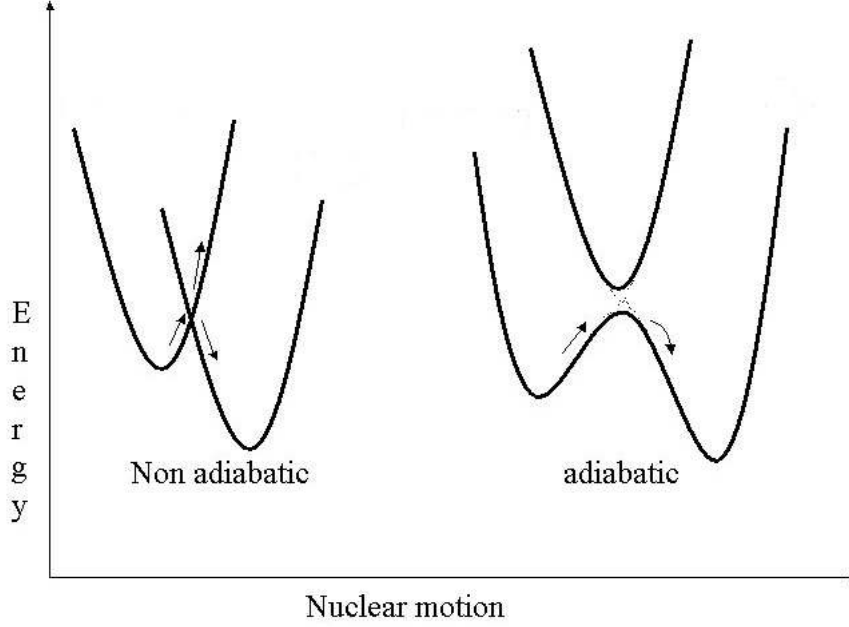


Fig. 2.1: Two surfaces under the diabatic and adiabatic representations

wavefunction changes rapidly as a function of the nuclear coordinates, or when two electronic states approach degeneracy, the aforementioned picture is rendered inapt. The last two terms can no longer be ignored and they must be included in any dynamical model if it is aimed at describing the system accurately. Following the adiabatic picture and no longer ignoring the coupling terms, we can project from the left with the electronic eigenfunction basis  $\phi_{elec,m}^*(\mathbf{r}; \mathbf{R})$  and obtain (ignoring the nuclear, rovibronic quantum number  $j$ ):

$$\sum_n [(\hat{T}_N + \hat{V}_{elec,n})\delta_{nm} + \hat{\Lambda}_{nm}]\chi_{rv,n} = E_n\chi_m,$$

where  $\hat{\Lambda}_{nm}$  arises from nuclear kinetic energy operator

$$\hat{\Lambda}_{nm} = -\frac{1}{2M}(2F_{nm} \cdot \nabla + G_{nm}) = -\frac{1}{2M}[2 \cdot \langle \phi_{elec,m} | \nabla \phi_{elec,n} \rangle \nabla + \langle \phi_m | \nabla^2 \phi_n \rangle]$$

$$F_{nm} = \frac{\langle \phi_{elec,m} | \nabla \hat{H}_{elec} | \phi_{elec,n} \rangle}{\hat{V}_{elec,m} - \hat{V}_{elec,n}} \quad (2.12)$$

$\Lambda_{nm}$  is the non-adiabatic coupling operator which contains  $F_{nm}$ , the deriva-

tive coupling vector (expressed above via the Hellman-Feynman theorem) and  $G_{nm}$  the scalar coupling. The last equation in 2.12 shows that when two electronic states start approaching each other the derivative coupling vector becomes singular. Therefore, at the points of intersection, the adiabatic wavefunction exhibits discontinuities. The adiabatic picture will be inappropriate for any system that involves such crossings (which turn out to be the majority of vibronic systems, as noted in chapter 1).

To proceed further, the full Schroedinger equation can be written in a more compact form, where the kinetic and non-adiabatic coupling operators form part of a bilinear expansion (so called ‘dressed kinetic energy operator’):

$$\left[-\frac{1}{2M}(\nabla + F_{nm})^2 + \hat{V}_{elec,n}\right]\chi_j = E\chi_j \quad (2.13)$$

having used the relationship:

$$\hat{G} = (\nabla \cdot \hat{F}) + \hat{F} \cdot \hat{F} \quad (2.14)$$

$F$  and  $G$  shown in matrix form. It is possible to restrict the problem at hand to those states that are relevant and to those whose coupling coefficients in the non-adiabatic operator are significant. Such a truncation is often referred to as the group adiabatic approximation. It is often too complicated to solve the above equation, since  $F$  is a non-local operator that exhibits poles. Instead, we can perform a similarity transformation on the electronic eigenfunction basis that can simplify the expression by minimising the non-adiabatic coupling operator contribution (the nuclear wavefunction undergoes the adjoint transformation).

The unitary matrix  $\mathbf{S}$ , that performs a similarity transformation, has to satisfy the condition:

$$(\nabla + \hat{F})\hat{S}^\dagger = 0 \quad (2.15)$$

Such a matrix is defined so as to turn a problem containing a derivative operator into the one with the off diagonal coordinate couplings in the potential operator. In general  $F_{nm}$  will only be analytic, and satisfy the above relation if the extended curl equation is satisfied [26]:

$$\text{Curl}(\hat{F})\mathbb{1} - \hat{F} \otimes \hat{F} = \mathbf{0} \quad (2.16)$$

This representation makes the electronic wavefunction dependence on the nuclear coordinates as minimal as possible. However, in general, the wavefunctions are dependent on nuclear coordinates and strictly diabatic basis has only been shown to exist for diatomics [27] or two-state problems.

After rotating we obtain:

$$\begin{aligned} [-\frac{1}{2M}\nabla^2\mathbb{1} + \hat{W}]\chi &= E\chi, \\ \hat{W} &= \hat{S}^\dagger \hat{V} \hat{S} \end{aligned} \quad (2.17)$$

This is the quasi-diabatic Schroedinger equation. Its appeal is that we have a more intuitive understanding of coupling between states that is now represented via potential operators rather than momenta. The new diabatic basis is usually arbitrarily fixed so that it is equal to the adiabatic basis at some suitable set of nuclear coordinates. Some nuclear configuration where  $S = \mathbb{1}$  is typically chosen to be at a point where non-adiabatic effects are minimal, making the comparison between diabatic and adiabatic representations useful for understanding where non-adiabatic effects might be important. Couplings between the diabatic surfaces are caused by the off-diagonal elements of  $W$ .

### 2.2.2 Vibronic coupling Hamiltonian models

One of the simplest approaches to approximately representing the potential is by Taylor expanding the potential about some critical geometry, since low order polynomials do a good job around slowly varying energies. However,

Polynomials struggle to approximate adiabatic surfaces which exhibits significant *non-adiabatic* (NA) coupling. It typically increases when two adiabatic states cross or their characters become similar. In such cases the adiabatic electronic wavefunction will vary rapidly with respect to the nuclear coordinates and, typically, so will the energy. Expansion of a Taylor series about such points would result in a slow convergence of the series, and high order terms would be required (with the extreme case being when two states cross and differentiability breaks down). The diabatic potential is the starting point for vibronic coupling models with which one can analytically model the Hamiltonian of polyatomic molecules. Quasi-diabatic states are defined to minimise their dependence on the nuclear coordinates. As the molecule distorts away from the Franck Condon (FC) geometry from which the Taylor series is expanded, quasi-diabatic states should approximately retain the character of the irreducible representation (IrRep) they belong to at the Franck Condon (FC) geometry. This leads to smooth changes in the energy and making the convergence of the Taylor series quicker, with only low-order polynomials required to describe such surfaces. Furthermore, in the diabatic representation electronic coupling is also represented in potential form and can also be easily approximated by low order polynomials. In the simplest of models, the potential is Taylor expanded to second order about the Frank-Condon point. Adopting mass-frequency scaled dimensionless coordinates,  $\mathbf{Q}$ , we get:

$$\begin{aligned}
\mathbf{H} &= \mathbf{H}^{(0)} + \mathbf{W}^{(0)} + \mathbf{W}^{(1)} + \mathbf{W}^{(2)} + \dots \\
\mathbf{H}^{(0)} &= \sum_{\alpha} \frac{\omega_{\alpha}}{2} \left( -\frac{\partial^2}{\partial Q_{\alpha}^2} + Q_{\alpha}^2 \right) \\
\mathbf{W}_{nm}^{(0)} &= \langle \phi_n | H_{el} | \phi_m \rangle \\
\mathbf{W}_{nm}^{(1)} &= \sum_{\alpha} (\kappa_{\alpha}^n + \lambda_{\alpha}^{nm}) Q_{\alpha} = \\
&\sum_{\alpha} \left( \frac{\partial}{\partial Q_{\alpha}} \langle \phi_n | H_{el} | \phi_n \rangle |_{\mathbf{Q}=0} + \frac{\partial}{\partial Q_{\alpha}} \langle \phi_n | H_{el} | \phi_m \rangle |_{\mathbf{Q}=0} \right) Q_{\alpha} \\
\mathbf{W}_{nm}^{(2)} &= \frac{1}{2} \sum_{\alpha, \beta} (\gamma_{\alpha\beta}^n + \mu_{\alpha\beta}^{nm}) Q_{\alpha} Q_{\beta} = \\
&\frac{1}{2} \sum_{\alpha \geq \beta} \left( \frac{\partial^2}{\partial Q_{\alpha} \partial Q_{\beta}} \langle \phi_n | H_{el} | \phi_n \rangle |_{\mathbf{Q}=0} + \frac{\partial^2}{\partial Q_{\alpha} \partial Q_{\beta}} \langle \phi_n | H_{el} | \phi_m \rangle |_{\mathbf{Q}=0} \right) Q_{\alpha} Q_{\beta}
\end{aligned} \tag{2.18}$$

The diagonal matrix  $\mathbf{W}^{(0)}$  contains the vertical excitation energies from the ground state equilibrium geometry. The parameters of the  $\mathbf{W}^{(1)}$  and  $\mathbf{W}^{(2)}$  off-diagonal matrix elements contain the non-adiabatic couplings between states. Parameters such as  $\lambda$  can be obtained from electronic structure calculations, as they are related to derivative coupling terms. The diabatic model parameters are fitted by diagonalizing the model at multiple geometries so that the resulting adiabatic model energies map to those obtained from *ab initio* calculations. The diagonalisation is done via a similarity transformation:

$$\mathbf{V} = \mathbf{SWS}^{\dagger} \tag{2.19}$$

When expanding a model from a point of high symmetry, one can take advantage of the fact that diabatic states will only weakly change their electronic character away from the point of expansion (as they only weakly depend on nuclear coordinates). This makes such states conserve the symmetry character of the irreducible representation they belong to.

Taking symmetry into consideration simplifies the construction of vibronic coupling models significantly, since many of these element evaluations

of our Hamiltonian model vanish due to symmetry arguments. We first note that scalar products of two spatial function defined by integral evaluations over the whole space domain have the following symmetry property:

$$\int \mathbf{O}_R(A(x') \cdot B(x')) d\tau = \int \mathbf{O}_R A(x') \cdot \mathbf{O}_R B(x') d\tau = \chi \int A(x) \cdot B(x) d\tau \quad (2.20)$$

Where  $\mathbf{O}_R$  represents some linear operator belonging to some point group which either acts on the coordinates.  $A$  and  $B$  functions spanning different reducible representations of that group and the integral is over the coordinates  $x'$  and  $x$ .  $\chi$  is the product of the characters belonging to  $A$  and  $B$ . Using the great orthogonality theorem (see chapter 5), we can construct a projection operator  $\mathbf{P}_1$  [24]:

$$\begin{aligned} \mathbf{P}_1 \int A(x) \cdot B(x) d\tau &= \int g^{-1} \sum_R \mathbf{O}_R(A(x) \cdot B(x)) d\tau = \chi \int A(x) \cdot B(x) d\tau \\ \chi &\neq 0, \quad \Gamma_A \otimes \Gamma_B \supset \Gamma_1 \end{aligned} \quad (2.21)$$

the integral is zero if the product of the IrReps that  $A$  and  $B$  belong to does not contain the totally symmetric IrRep (labelled  $\Gamma_A, \Gamma_B$  and  $\Gamma_1$ ).  $g^{-1} \sum_R \mathbf{O}_R$  is a projector onto the totally symmetric irreducible representation ( $g$  the order of the group). Therefore, an integral is non-zero only if the direct products between the different symmetry species in the integrand span a totally symmetric irreducible representation. For a polynomial function representing some irreducible representation, and representing some diabatic element of the potential operator of some symmetric molecule, the following sufficient conditions need to be satisfied:

$$\begin{aligned} \kappa_\alpha^n &\neq 0, \Gamma_\alpha \supset \Gamma_A \quad (a) \\ \lambda_\alpha^{nm} &\neq 0, \Gamma_n \otimes \Gamma_\alpha \otimes \Gamma_m \supset \Gamma_A \quad (b) \\ \gamma_{\alpha\beta}^n &\neq 0, \Gamma_\alpha \otimes \Gamma_\beta \supset \Gamma_A \quad (c) \\ \mu_{\alpha\beta}^{nm} &\neq 0, \Gamma_n \otimes \Gamma_\alpha \otimes \Gamma_\beta \otimes \Gamma_m \supset \Gamma_A \quad (d) \end{aligned} \quad (2.22)$$



$\Gamma$  referring to some irreducible representation of the point group. Assuming our coordinates and diabatic states form a representation in some group (see normal coordinates below), these conditions determine the order of different interactions between the states along some coordinate (i.e. interstate ( $\lambda$  and  $\mu$ ) and intrastate ( $\kappa$  and  $\gamma$ ) couplings. It is also instructive to note that, from the symmetry of the geometry, only the gradient  $\kappa$ , along totally symmetric modes of excited states will give non-vanishing integrals. This gives us a prescription for where to begin the analysis of photo-relaxation pathways.

### 2.2.3 Conical intersections.

Surface crossings are one of the most important non-adiabatic effects which drive many photochemical processes and will therefore be fundamental for this work. To simplify the picture, we will consider a two state model and approximate the potential to first order. It is possible to write the diabatic potential as follows:

$$W = \begin{pmatrix} W_{11} & W_{12} \\ W_{12} & W_{22} \end{pmatrix} \equiv \mathbb{1}\Sigma \pm \begin{pmatrix} -\Delta & W_{12} \\ W_{12} & \Delta \end{pmatrix} \quad (2.23)$$

$$\Sigma = \frac{1}{2}(W_{11} + W_{22}); \quad \Delta = \frac{1}{2}(W_{22} - W_{11})$$

and approximating these elements linearly we get:

$$\frac{1}{2}(W_{22} - W_{11}) \sim \delta \cdot \mathbf{Q}; \quad (2.24)$$

$$W_{12} \sim \lambda \cdot \mathbf{Q}$$

where

$$W_{11} = \kappa_1 \cdot Q; \quad W_{22} = \kappa_2 \cdot Q \quad (2.25)$$

Where we have introduced  $\delta$ , the gradient difference vector and  $\lambda$ , the derivative coupling vector. A Taylor expansion from the point where the diabatic and adiabatic representation are equal would equate the linear coupling vector (in the diabatic representation) and the derivative coupling vector. Following Eq. 2.19, it is possible to obtain the adiabatic energies by solving the

secular equation:

$$\begin{vmatrix} W_{11} - V & W_{12} \\ W_{12} & W_{22} - V \end{vmatrix} = 0$$

Which gives

(2.26)

$$V_{\pm} = \Sigma \pm \sqrt{\Delta^2 + W_{12}^2}$$

As noted from 2.18, the linear coupling and gradient difference vectors contain a sum of modes that couple states linearly. The linear coupling vector is equated with the derivative coupling when we are using strictly diabatic states (and related to the non-adiabatic coupling like in equation 2.12 ). These two vectors are linearly independent, defining a plane in hyperspace. In addition, we can see from Eq. 2.26 that the selection rules for having a hyper point of degeneracy (the root term disappears) is given by [28];

$$\Delta^2 = 0; \quad W_{12}^2 = 0$$
(2.27)

The lifting of degeneracy can often be understood as a pair of degenerate vibrations, played by modes that break the symmetry of the molecule. Along this 2D branching subspace one finds the derivative coupling and gradient difference vectors breaking the energy degeneracy to first order, forming a conically shaped intersection. Any cut along this 2D space which does not cross the intersection, but instead ‘pushes’ adiabatic states away from each other is referred to as an avoided crossing. The derivative coupling vector is large in this region, where non-adiabatic effects are typically encountered. It is possible to describe the degeneracy topology by identifying conical intersections with nearest seam paths between them in an analogous way to stable conformations with transition pathways between them. Since moving along other coordinates does not break the degeneracy (to first order), this space forms what is termed the seam space of the intersection.

From the above symmetry considerations, it is clear that there exist a constellation of integrals which allow for points of degeneracy between different

surfaces. For molecules with non-Abelian symmetry groups with degenerate electronic states, the Jahn-Teller theorem [17] states that all non-linear degenerate irreducible representations of all symmetry groups allow non-totally symmetric linear perturbative terms to break symmetry. This means the degenerate electronic states of polyatomic systems forming a representation of a non-Abelian point group will experience a force away from the high-symmetry geometry along some coordinates. This coordinate must span some irrep contained in the direct product of a generate irreps with itself. In the diabatic representation of the JT problem, this implies that the derivative coupling and gradient difference vectors must span a totally symmetric irrep and a non-totally symmetric irrep respectively, forming a conical intersection (CI). For linear molecules, Renner-Teller theorem states that degeneracy breaking occurs to second order (forming a slanted intersection), or via a pseudo Jahn-Teller coupling (pJT) to first order [29] (see chapter 5 for the generation of polynomials elements obeying  $D_{\infty h}$  invariance and suitable for Renner-Teller systems.)

## 2.3 Electronic Structure Methods

### 2.3.1 SCF techniques and configuration interaction

The different methods for electronic excited state energy calculation will be summarised in this section. The aim is to approximate the eigenvalues/vectors of the electronic Hamiltonian (the electronic potential energy). The variational theorem states that, given a trial wavefunction with which to represent the expectation value of the electronic Hamiltonian, the approximation to the exact energy will always be an upper bound [30]. This allows for correction techniques on the trial wavefunction and therefore for systematic improvements on the computed energy:

$$\langle \tilde{\phi} | \hat{H}_{elec} | \tilde{\phi} \rangle \geq V_{elec,0}, \quad (2.28)$$

where  $\tilde{\phi}$  is the trial electronic wavefunction and  $V_{elec,0}$  the ground state electronic energy. The Slater-determinant *ansatz* wavefunction,  $\phi$ , is built up by an anti-symmetrised spin-orbital basis in a determinantal expansion:

$$\phi = |\chi_1 \chi_2 \dots \chi_K\rangle = \frac{1}{\sqrt{N!}} \begin{vmatrix} \psi_1(\mathbf{x}_1) & \psi_2(\mathbf{x}_1) & \dots & \psi_K(\mathbf{x}_1) \\ \psi_1(\mathbf{x}_2) & \psi_2(\mathbf{x}_2) & \dots & \psi_K(\mathbf{x}_2) \\ \vdots & \vdots & \ddots & \vdots \\ \psi_1(\mathbf{x}_N) & \psi_2(\mathbf{x}_N) & \dots & \psi_K(\mathbf{x}_N) \end{vmatrix} \quad (2.29)$$

To obtain energies we wish to minimise  $\phi * H\phi$  under normalisation constraints. We therefore need to add the constraints as a Lagrange multiplier into the expression  $L = \phi * H\phi - E(\phi * \phi - 1)$ , and find  $\frac{\partial L}{\partial c} = 0$  where  $c$  represents variational parameter in our functional space. For the Slater-determinant wavefunction in particular, we have a linear variational problem which results in an eigenvalue problem. We obtain a coupled set of differential operators called the Fock Operators:

$$[\hat{T}_e + \hat{V}_{ee} + \hat{V}_{Ne}] \phi_{hf} = [h + v] \phi_{hf} = \hat{V}_{hf} \phi_{hf} \quad (2.30)$$

where

$$h = \hat{T}_e + \hat{V}_{Ne} = \sum_{i=1}^{N/2} \frac{1}{2} \nabla_i^2 - \sum_{i=1}^{N/2} \sum_{A=1}^M \frac{Z_A}{r_{iA}} \quad (2.31)$$

and

$$v = \hat{V}_{ee} = \sum_{i=1}^{N/2} \sum_{j>1}^{N/2} \frac{1}{r_{ij}} \quad (2.32)$$

The spin orbitals are built by the product of a spatial  $\chi$ , and spin component functions, and represent solutions to the Fock operator. Integrating over the spin-orbital basis we get for  $h$ :

$$\langle i | h | i \rangle = 2 \sum_{i=1}^{N/2} \int d\mathbf{x}_1 \chi_i^*(\mathbf{x}_1) h(\mathbf{r}_i) \chi_i(\mathbf{x}_1) \quad (2.33)$$

and for  $v$ :

$$\begin{aligned}
\langle ij|v|ij\rangle &= 2\hat{J}_{ij} - \hat{K}_{ij} = \\
2\langle ii|jj\rangle - \langle ij|ji\rangle &= \\
\sum_{i=1}^{N/2} \sum_{j>1}^{N/2} [2 \int d\mathbf{x}_1 d\mathbf{x}_2 \chi_i^*(\mathbf{x}_1) \chi_i^*(\mathbf{x}_2) \frac{1}{r_{12}} \chi_j(\mathbf{x}_1) \chi_j(\mathbf{x}_2)] - & \quad (2.34) \\
\int d\mathbf{x}_1 d\mathbf{x}_2 \chi_i^*(\mathbf{x}_1) \chi_j^*(\mathbf{x}_2) \frac{1}{r_{12}} \chi_j(\mathbf{x}_1) \chi_i(\mathbf{x}_2)] &
\end{aligned}$$

where  $\hat{J}_{ij}$  and  $\hat{K}_{ij}$  are the Coulomb and exchange operators.  $\chi$  are solutions to an approximate *one electron* spatial wavefunction feeling the average field of other electrons via those terms in the Fock operator representing the interactions between electrons (exchange and Coulomb operators). To solve these equations, we need some set of orbitals to evaluate the elements of the exchange and Coulomb operator, the resulting energy being dependent on them. The *self-consistent field* (SCF) procedure therefore involves a recursive construction of this eigenvalue problem, but with a better guess for the exchange and Coulomb operators obtained from the previous diagonalisation (solution of the eigenvalue problem). Since the variational theorem ensures that we cannot obtain energies below the exact, we will progressively converge on the correct energy (provided the initial guess wavefunction is reasonable). The Hartree-Fock ground state energy is obtained by filling the  $N/2$  optimised (molecular) HF spin-orbitals with  $N$  electrons. The SCF algorithm based on a HF wavefunction has become a benchmark as well as a starting point for more modern methods (some detailed below). One of the downside of such a restricted basis is that long range correlation between electrons is not properly described, giving rise to substantial overestimates (especially at dissociation). The difference between the Hartree-Fock limit energy and the exact energy is termed the *correlation energy*, since no correlation is taken into account between electrons of opposite spins (under HF). Although the HF energy accounts for  $\sim 99\%$  of the systems energy, the remaining correla-

tion energy determines most of the interesting chemical properties one finds in molecular systems.

### 2.3.2 Correlated wavefunction methods

HF orbitals are often subsequently used to improve on the correlation energy or to calculate excited state energies by using linear combinations of determinants with other virtual (non-occupied) HF molecular orbitals to describe the electronic wavefunction. The greater the use of determinants and of basis functions as variational parameters, the higher accuracy of the final wavefunction (and better energies). A multi-configurational wavefunction *ansatz* is defined by [30]:

$$|\Phi_{MCSFC}\rangle = \sum c_i |\chi_1 \chi_2 \dots \chi_K\rangle \quad (2.35)$$

the coefficients  $c_i$ , as well as the spin orbitals entering every determinant become variational parameters. In principle, we would obtain an exact solution by letting the orbital basis set (Hartree-Fock limit) and the linear combination of all possible determinants become complete (Full CI). Many different approximations are defined by the way in which the CI wavefunction is truncated. An arbitrarily truncated CI expansion suffers from size-consistency - for a given approximation, it is not possible to estimate the energy of a molecule from separate calculations of the smaller segments that compose it. The Coupled Cluster and CAS methods were devised to maintain this property.

#### *Complete active space (CAS) SCF.*

Since a full CI expansion is prohibitively large for a given basis, it is usually rendered un-feasible (even for small molecules). CAS methods have been devised to perform full CI expansion only on an *active space*, a subset of HF spin orbitals determinants that are known to contribute significantly to

the energy. An analysis of the orbitals to go into the active space has to be performed, aided typically by ‘chemical’ intuition. To date this method provides one of the most reliable SCF results of excited state calculations of relatively small molecules.

### *Coupled cluster (CC) methods.*

To cope with size extensivity without having to use a full CI expansion, the CI expansion is recast in an exponential second quantisation operator form

$$|\Phi_{CI}\rangle = \exp(-\hat{T})\hat{H}\exp(\hat{T})|\Phi_{HF}\rangle \quad (2.36)$$

where

$$\hat{T} = \hat{T}_1 + \hat{T}_2 + \dots, \quad \hat{T}_1 = \sum_{A,I} t_I^A a_A^\dagger a_I, \quad \hat{T}_2 = \sum_{A>I, B>J} t_{IJ}^{AB} a_A^\dagger a_I a_B^\dagger a_J \quad (2.37)$$

$T_n$  are excitation operators given in second quantisation, where  $a^\dagger$  and  $a$  are creation and annihilation operators. By expanding a Taylor series of  $\exp(-\hat{T})\hat{H}\exp(\hat{T})$  in Hausdorff form, and together with the anti-commutation relations this gives exactly [31]:

$$\begin{aligned} \exp(-\hat{T})\hat{H}\exp(\hat{T}) = & \hat{H} + [\hat{H}, \hat{T}] + \frac{1}{2}[[\hat{H}, \hat{T}], \hat{T}] + \\ & \frac{1}{3!}[[[\hat{H}, \hat{T}], \hat{T}], \hat{T}] + \frac{1}{4!}[[[[\hat{H}, \hat{T}], \hat{T}], \hat{T}], \hat{T}] \end{aligned} \quad (2.38)$$

It is possible to truncate the cluster expansion operator,  $\hat{T}$ , to any order, and continue to have a size extensive wavefunction, while obtaining contributions from all possible determinants built out HF orbitals (unlike CASSCF). The most common truncation involves single and double excitation operators, CCSD. As a single determinant reference method, it may perform poorly for systems that are strongly multi configurational in their character (e.g. dissociation problems). The energy is obtained by projecting the cluster operator onto the HF wavefunction and as such, is not variational in character.

### 2.3.3 Rayleigh Schroedinger perturbation theory (RSPT)

Perturbation theory is yet another method by which we can obtain a correlation energy correction not included in the Hartree-Fock approximation. One of the strengths of perturbation theory is its size consistency which enables us to improve on the HF correlation energy at a scalable rate with the number of atoms. This is not a variational method. RSPT is done by dividing the Hamiltonian into two parts: a zeroth-order Hamiltonian  $\hat{H}_0$  for which we can calculate its eigenvalues exactly, and a small perturbation expression  $V$  which might be too complicated to compute directly or easily. The exact eigenfunctions/values are expanded as a Taylor series, using the zeroth-order Hamiltonian eigenfunctions  $\psi_n^{(0)}$  as basis, which in this case are the anti-symmetrised spin-orbitals of from HF (or other excited state calculations):

$$\begin{aligned}
 H|\phi_n\rangle &= (H_0 + V)|\phi_n\rangle = E_n|\phi_n\rangle \quad (a) \\
 H_0|\psi_n^{(0)}\rangle &= E_n^{(0)}|\psi_n^{(0)}\rangle \quad (b) \\
 E_n &= E_n^{(0)} + \lambda E_n^{(1)} + \lambda^2 E_n^{(2)} + \dots \quad (c) \\
 |\phi_n\rangle &= |\psi_n^{(0)}\rangle + \lambda|\psi_n^{(1)}\rangle + \lambda^2|\psi_n^{(2)}\rangle + \dots \quad (d)
 \end{aligned}
 \tag{2.39}$$

Using an intermediate normalisation by which  $\langle\psi_0^{(0)}|\phi_n\rangle = 1$ , we can express the higher order terms for the exact energy in terms for the eigenvalues/functions and the perturbation:

$$\begin{aligned}
 E_n^{(1)} &= \langle\psi_n^{(0)}|V|\psi_n^{(0)}\rangle \\
 E_n^{(2)} &= \sum_{a=1} \frac{|\langle\psi_0^{(0)}|V|\psi_n^{(a)}\rangle|^2}{E_0^{(0)} - E_n^{(0)}}
 \end{aligned}
 \tag{2.40}$$

Caution has to be taken when choosing the function representing the perturbation. Not all functions expanded in a Taylor series converge, or do so quickly enough to give a reasonable approximation. The most common per-



turbation expression used in electronic calculations is the difference between the Hartree Fock correlation energy and the exact correlation energy. It is sometimes called the Moller-Plesset (MP) perturbation theory:

$$\begin{aligned} H_0 &= \sum_i [h(i) + v^{HF}(i)] \\ V &= [V_{ee} - \sum_i v^{HF}(i)] = \sum_{i=1}^K \sum_{j>1}^K \frac{1}{r_{ij}} - \sum_i v^{HF}(i) \end{aligned} \quad (2.41)$$

the first and second orders of the energies then become:

$$\begin{aligned} E_0^{(1)} &= -\frac{1}{2} [\langle ij|ij \rangle - \langle ij|ji \rangle] \\ E_0^{(2)} &= \sum_{i>j} \sum_{k>l} \frac{\langle ij|kl \rangle - \langle ij|lk \rangle}{E_i^{(0)} + E_j^{(0)} - E_k^{(0)} - E_l^{(0)}} \end{aligned} \quad (2.42)$$

where  $i, j, k, l$  refer to orbital indices as defined in equation 2.34. Even though the denominator of the second-order correction should include all possible excited states, triply excited states and above don't mix with  $|\phi_0\rangle$ , in this type of two electron integral (spin-orbital) of perturbation. Furthermore, given Brillouin's theorem, which states that singly-excited determinants don't interact with  $|\phi_0\rangle$ , we only need to sum over all possible double excitations.

### 2.3.4 Density functional theory and methods

By making the assumption that two potentials can give rise to the same electron density, Hohenberg and Kohn proved by contradiction that there only is a one-to-one correspondence between the electron density and the electronic potential and therefore with the electronic Hamiltonian [32]. It can be shown that all but the exact density functional expression representing the energy of a system will give an upper bound to the exact energy (which is a functional of it). In other words, given a trial electron density function  $\rho'$  which integrates over space to give  $N$ , the total number of electrons in our system:

$$\begin{aligned} \int \rho'(\mathbf{r}) d\mathbf{r} &= N \\ E_0[\rho'] &\geq E_0[\rho] \end{aligned} \quad (2.43)$$

This makes DFT variational and therefore similar techniques can be applied as those for wave mechanics. One of the strengths of DFT is that, unlike dealing with wavefunctions, where the need to integrate over all electron coordinates makes the problem insoluble for large systems, the expression for the electron density of molecules has the same number of variables (3) irrespective of the number of electrons. Unfortunately, the exact functional connecting the density and the energy is not known, making the principal task of DFT methods that of designing functionals to approximate the energy.

There is an analogous (but not equivalent) way to express kinetic, (nuclear and Coulomb) potential and exchange-correlation contributions to the energy arising from the electron density as done in the HF formalism. DFT also uses an orbital basis to obtain the electron density arising from non-interacting electrons. The functional describing the exchange and kinetic energy term of electrons has to be designed in a semi-empirical way, contrasting with HF (the exact expression). The choice of a functional for the exchange and correlation terms defines a given DFT method. This work uses a BLYP approximation, which includes an exchange functional introduced by Becke [33] and a correlation term by Lee, Yang and Parr [34]. Like HF, DFT also uses orbitals introduced into ‘Roothan like’ equations which produce *Kohn-Sham* orbitals. These orbitals don’t carry the same significance as the HF orbitals, since the functionals for the exchange-correlation are not the same. They can, however, also provide some qualitative information about the electronic structure of molecules.

DFT does a reasonable job at recovering some electron dynamic correlation, but poor at static correlation. For the description of excited states with multi- configurational character, DFT-MRCI (multi-reference CI) [35] can

be used to approximately recover some of the static correlation; it is a hybrid approach, where some of the multi-reference wavefunction Hamiltonian elements that correct the HF wavefunction are replaced by DFT approximations to them.

### 2.3.5 Local geometry optimisation and normal mode analysis

Under the BO approximation, a non-linear molecule consisting of  $N$  nuclei under the potential created by electrons ( $V(\mathbf{X}) = V_{elec,n}$ ), (in a given electronic state) has  $3N-6$  thermally accessible internal degrees of freedom  $\mathbf{X} = (x_1, x_2, \dots, x_{3N-6})$  which span the potential energy hypersurface. The topography of such surface contains many minima and maxima and does have poles (given energy conservation) that define possible stable conformations of the molecule. Many very good approaches (e.g. Monte-Carlo, genetic algorithms, molecular dynamics) have been devised for the sampling of this hypersurface, searching for the global optimum. At any "basin of attraction", a local optimisation must be performed in order to converge to its energy minima. By defining a displacement  $\mathbf{q} = (\mathbf{X}_1 - \mathbf{X})$  (where  $\mathbf{X}_1$  is a column vector representing a displacement), expanding the energy about  $\mathbf{X}$  in a Taylor series up to second order we obtain:

$$V(\mathbf{X}_1) = V(\mathbf{X}) + \mathbf{q}^T \mathbf{f}(\mathbf{X}) + \frac{1}{2} \mathbf{q}^T \mathbf{H}(\mathbf{X}) \mathbf{q}$$

where (2.44)

$$f_i = \frac{\partial V(\mathbf{X})}{\partial x_i} \quad \text{and} \quad H_{ij} = \frac{\partial^2 V(\mathbf{X})}{\partial x_i \partial x_j}$$

where  $\mathbf{f}$  and  $\mathbf{H}$  stand for the gradient vector and Hessian matrix. At a stationary point  $\mathbf{f}(\mathbf{X}_e) = 0$ . From this, we can derive an expression that serves as a general starting point for local optimisation procedures:

$$\begin{aligned}
\mathbf{f}(\mathbf{X}_1) &= \mathbf{f}(\mathbf{X}) + \mathbf{H}(\mathbf{X})\mathbf{q} \\
\text{at } \mathbf{X}_1 &= \mathbf{X}_e, \\
\mathbf{f}(\mathbf{X}) &= -\mathbf{H}(\mathbf{X})\mathbf{q} \quad \text{rearranges to:} \\
\mathbf{q} &= -\mathbf{H}^{-1}(\mathbf{X})\mathbf{f}(\mathbf{X})
\end{aligned} \tag{2.45}$$

which gives us a prescription for finding a stationary point  $\mathbf{X}_e$  from a point  $\mathbf{X}$  nearby, so that the energy function is quadratic to a good approximation.

It is clear that the potential function can be expanded on any arbitrary coordinate system. In practice, however, we would like to choose one which will simplify  $\mathbf{H}$  and  $\mathbf{f}$ . At a given critical point where the first order (gradients) of  $V$  vanish, we are left with the expression:

$$V(\mathbf{X}_1) = V(\mathbf{X}) + \frac{1}{2}\mathbf{q}^\dagger \mathbf{H}(\mathbf{X})\mathbf{q} \tag{2.46}$$

The above equation also holds if we include the subspace of molecular rotations and translations, with a total of  $3N$  coordinates. Finding ourselves at some critical point where  $\mathbf{f}(\mathbf{X}_e) = 0$ , we now represent the Lagrangian of the system as

$$L = T - V = \frac{1}{2} \sum_i^{3N} \left\{ \delta_{ij} \dot{q}_i^2 - B_{ij} q_i q_j \right\} \tag{2.47}$$

Where  $B_{ij}$  are the harmonic force constants and  $q$  are mass-weighted coordinates. The Euler-Lagrange equation of motion thus gives [36]:

$$\sum_j^{3N} \left\{ \frac{d^2 q_i}{dt^2} \delta_{ij} + B_{ij} q_j \right\} = 0 \quad i = 1, 2, \dots, 3N \tag{2.48}$$

This can be reformulated as the more general vector equation

$$\frac{d^2 \mathbf{Q}}{dt^2} + \lambda \mathbf{Q} = 0 \quad \text{where} \quad \mathbf{Q} = \sum_j^{3N} c_j q_j \tag{2.49}$$

Which gives an eigenvalue problem from which we obtain  $3N$  eigenvalues and vectors. These vectors satisfy the above equation, as well as leaving the Hamiltonian in a decoupled form:

$$H = T + V = \frac{1}{2} \sum_i^{3N} \left\{ \dot{Q}_i^2 + \lambda_i Q_i^2 \right\} \tag{2.50}$$

for which the nuclear wavefunction becomes separable into one-dimensional differential equations, giving Hermite polynomial eigenfunctions and eigenvalues as solutions. Any vector displacements departing from a geometry where the molecule belongs to a symmetry group, will form a representation of that point group. If we use normal coordinates (the eigenvectors of the Hessian as a basis), the representation of any operation of the group becomes block diagonal, where the blocks are related to those modes that share eigenvalues. Normal coordinates form an irreducible representation of the point group of the molecule and can be used for the efficient construction of vibronic coupling models. This enables to categorise them in a non-arbitrary way, allowing for more structured insight on how different symmetric regions of the potential surfaces interact. It also gives symmetry rules for integral of evaluation of transition dipole moment elements and therefore aids in many aspects of rovibronic spectra (such as band assignments).

## 2.4 Solving the Vibronic TDSE

### 2.4.1 Variational approach and equations of motion

To solve the vibronic TDSE variationally for functions in complex space, we can use the Dirac-Frenkel principle:

$$\langle \delta\Phi | \hat{H} - i \frac{\partial}{\partial t} | \Phi \rangle = 0 \quad (2.51)$$

It can be shown that under linear variations of this kind the resulting equations of motion conserve the norm and the energy [37]. If we expand our wavefunction as a product of 1D time-independent orthonormal functions:

$$\Phi(q_1, q_2, \dots, q_f, t) = \sum_{j_1}^{N_1} \cdots \sum_{j_f}^{N_f} C_{j_1, \dots, j_f}(t) \prod_{\kappa=1}^f \chi_{j_\kappa}^{(\kappa)}(q_\kappa) \quad (2.52)$$

Or using the notation  $J \equiv (j_1, \dots, j_f)$ , and  $\chi_J \equiv \prod_{\kappa=1}^f \chi_{j_\kappa}^{(\kappa)}(q_\kappa)$

$$\Phi(\mathbf{q}, t) = \sum_J C_J(t) \chi_J \quad (2.53)$$

Note that only the coefficients carry the time-dependency. Introducing this *ansatz* into the variational equation we get

$$i\dot{C}_L = \sum_J \langle \chi_L | \hat{H} | \chi_J \rangle C_J \quad (2.54)$$

We get a system of coupled differential equations which scales exponentially with the number of degrees of freedom. Beyond six dimensions we reach a bottleneck where the evaluation of these matrices becomes prohibitive. We therefore have to resort to more sophisticated methods, the most successful of which is the multi-configurational time-dependent Hartree (MCTDH) [21]. It uses time-dependent multi-dimensional basis functions termed single-particle functions (SPF), built out of time independent functions

$$\varphi_j^{(\kappa)}(Q_\kappa, t) = \sum_{i_1}^{N_1} \cdots \sum_{i_d}^{N_d} C_{i_1, \dots, i_d}^{(\kappa, 1)}(t) \prod_{v=1}^d \chi^{(\kappa, v)}(q_{k, d}) \quad (2.55)$$

where  $Q_k$  refers to a mode combination

$$Q_k \equiv (q_{k,1}, q_{k,2}, \dots, q_{k,d}) \quad d < f \quad (2.56)$$

and are the nuclear coordinate basis over which the so-called Hartree products  $\Phi_J \equiv \prod_{\kappa=1}^p \varphi_{jk}^{(\kappa)}(Q_\kappa, t)$  are constructed. These are linearly combined as a full product expansion to give the final MCTDH *ansatz*:

$$\Psi(\mathbf{Q}, t) = \sum_J A_J \Phi_J = \sum_{j_1}^{n_1} \cdots \sum_{j_p}^{n_p} A_{j_1, \dots, j_p}(t) \prod_{\kappa=1}^p \varphi_{j_k}^{(\kappa)}(Q_\kappa, t) \quad (2.57)$$

Since every SPF basis function is now time-dependent, the  $A$  coefficients add a redundancy into the MCTDH wavefunction. For the parameter space to be linearly variational and non-singular, a further constraint must be imposed on the wavefunction. Choosing the constraint

$$i\langle \varphi_i^{(\kappa)} | \dot{\varphi}_j^{(\kappa)} \rangle = \langle \varphi_i^{(\kappa)} | \hat{g}^{(\kappa)} | \varphi_j^{(\kappa)} \rangle \quad (2.58)$$

where  $\hat{g}^{(\kappa)}$  is some arbitrary constraint operator, ensures that the SPF basis remains orthonormal over time

$$\partial_t \langle \varphi_l | \varphi_k \rangle = \langle \dot{\varphi}_l | \varphi_k \rangle + \langle \varphi_l | \dot{\varphi}_k \rangle = -i(\mathbf{g} - \mathbf{g}^\dagger)_{lk} \quad (2.59)$$

so long as  $\mathbf{g}$  remains Hermitian. Different forms of  $\mathbf{g}$  are used for purely numerical reasons. They all result in slightly different forms of the equations of motion, but the basis functions propagated by them are all related by a similarity transformation. The choice of constraint does not affect the accuracy of the representation of the wavefunction. By choosing  $\mathbf{g} = 0$ , we obtain the following equations of motion from the variational principle:

$$\begin{aligned} i\dot{A}_J &= \sum_I \mathcal{K}_{JI} A_I \\ i\dot{\varphi}^{(\kappa)} &= \left[ (1 - P^{(\kappa)}) (\rho^{(\kappa)})^{-1} \mathcal{H}^{(\kappa)} \right] \varphi^{(\kappa)} \end{aligned} \quad (2.60)$$

These are a pair of coupled set of differential equations, where  $\mathcal{K}_{JL}$  is the Hartree product representation of the Hamiltonian operator  $\langle \Phi_J | H | \Phi_L \rangle$ .  $(1 - P^{(\kappa)})$  projects onto the space outside of the current SPF space.  $\mathcal{H}^{(\kappa)}$  is a Hamiltonian mean-field operator of SPF  $j$  integrated over the rest of the SPF functions,  $\mathcal{H}^{(\kappa)} = \langle \Phi_j^{(\kappa)} | H | \Phi_l^{(\kappa)} \rangle$  where  $\Psi_j^{(\kappa)} = \langle \varphi_j^{(\kappa)} | \Psi \rangle$  and  $\rho^{(\kappa)}$  is the density matrix, integrated over all modes but  $\kappa$ ,  $\rho_{ij}^{(\kappa)} = \langle \Psi_j^{(\kappa)} | \Psi_i^{(\kappa)} \rangle$ . These non-linear differential equations propagate the SPF functions using standard integration algorithms (e.g. Runge-Kutta). It has been observed that the mean-field  $\mathcal{H}^{(\kappa)}$  only varies slowly for problems that are not functions of time operators (e.g. fields). For such problems, the constant mean field (CMF) scheme is used, where  $\mathcal{H}^{(\kappa)}$  is updated at much longer time-steps than the propagation of SPFs. This has the advantage of decoupling the individual SPF differential equations in Eq 2.60, making the evaluation of the  $A$  vector, in turn, cheaper. Given the MCTDH wavefunctions are a product of mono-modal functions, assuming the combined modes can be factorised into one-dimensional functions, construction of the equation of motion operators decomposes into separable, one dimensional integral evaluations:

$$\mathcal{K}_{IJ} = \langle \varphi_{i_1}^{(1)} \cdots \varphi_{i_p}^{(p)} | \hat{H} | \varphi_{j_1}^{(1)} \cdots \varphi_{j_p}^{(p)} \rangle = \sum_{r=1}^{n_s} c_r \prod_{\kappa=1}^p \langle \varphi_{i_\kappa}^{(\kappa)} | \hat{h}_r^{(\kappa)} | \varphi_{j_\kappa}^{(\kappa)} \rangle \quad (2.61)$$

The memory requirements scale as  $n^f + f \cdot n \cdot N$ , continuing to scale exponentially with the number of degrees of freedom, but with  $n$ , the number of SPF per degree of freedom having replaced  $N$ , the total number of grid points. This allows the propagation of wavefunction from model Hamiltonian of up to 24 degrees of freedom [38].

### 2.4.2 Integral evaluation: spectral and DVR basis

The above derivations say little of our choice of basis. Since we are using a direct product expansion *ansatz*, the most common point of departure is to



consider using one-dimensional square-integrable basis functions. Typically these are the complete orthonormal sets of functions, mostly obtained from the Sturm-Liouville system of partial differential equations [36]: Hermite, Lagrange, Laguerre and Chebychev polynomials, as well as the Fourier series. These sets of functions are often referred to as spectral bases. We can project the exact wavefunction to an  $N$ -dimensional subspace of these polynomials, with the condition that the coefficients  $b_n$  on our spectral basis  $\{\phi(x)_n\}$  satisfy the following collocation relation:

$$\Psi(x_i) = \sum_{n=1}^N b_n \phi_n(x_i) \quad i = 1, \dots, N \quad (2.62)$$

and satisfying the orthogonality relation  $\sum_{j=1}^N \phi_m^*(x_j) \phi_n(x_j) \Delta_j = \delta_{mn}$  (termed orthogonal collocation), where  $\Delta_j$  normalises the functions. This projection ensures that our basis has the exact values of the wavefunction at  $\{x_j\}$ . In this representation we can easily analytically evaluate derivative operators such as the kinetic energy operators in the equations of the previous section. However, the potential integral evaluations are not trivially solved in this basis. Instead, from this new basis, a unitary transformation that localises each function about some point  $x_i$  with a value of weight of  $\Delta_i^{\frac{1}{2}}$  and close to zero everywhere else, gives us a pseudo-spectral basis;

$$\theta_j(x) \equiv \sum_{n=1}^N \phi_n(x) \Phi_n^*(x_j), \quad \Phi_n(x_j) = \sqrt{\Delta_j} \phi_n(x_j) \quad (2.63)$$

satisfying the modified Kronecker delta  $\delta$  property  $\theta_j(x_i) = \Delta_j^{\frac{1}{2}} \delta_{ij}$ . When the basis becomes complete our functions become Dirac  $\delta$ -functions (a useful approximation used later). Since the above collocation relation continues to hold:

$$\begin{aligned} \Psi(x) &= \sum_{n=1}^N b_n \phi_n(x) = \sum_{i=1}^N \left\{ \sum_{n=1}^N b_n \Phi_n(x_i) \right\} \theta_i(x) \\ &= \sum_{i=1}^N \Psi(x_i) \theta_i(x) \Delta_i^{\frac{1}{2}} \end{aligned} \quad (2.64)$$

we get

$$\begin{aligned} \int \Psi(x)^* \Psi(x) dx &= \sum_{i,j}^N \int \Psi(x_j)^* \theta_j^*(x) \theta_i(x) \Psi(x_i) \Delta_i^{\frac{1}{2}} \Delta_j^{\frac{1}{2}} dx \\ &= \sum_{i=1}^N \Psi(x_i)^* \Psi(x_i) \Delta_i \end{aligned} \quad (2.65)$$

We can therefore evaluate integrals in a projected  $2N-1$  dimensional Hilbert space with  $N$  quadrature points exactly. It can be shown that there is a complete correspondence between Gaussian quadrature and our pseudo-spectral functions, evaluated at the Gaussian quadrature points [18]. To find the Gaussian quadrature set  $\{x_i\}$  for a given set of polynomials, the position operator is evaluated under some representation:

$$\int \phi_m(x) \hat{x} \phi_n(x) dx = \int \sum_{i,j=0}^{N-1} \Phi_n(x_i) x \Phi_m(x_j) dx = \sum_{i,j=0}^{N-1} \Phi_{ni} x_{ij} \Phi_{mj} \quad (2.66)$$

since Sturm-Liouville polynomials have exactly one member per order of polynomial, the matrix above would be tri-diagonal. By diagonalizing the above operator, the eigenvalues obtained  $\{x_i\}$ , are the Gaussian quadrature points, and whose eigenvectors are  $\theta_i(x) = \sum_{n=1}^N \Phi_{ni}^\dagger \phi_n(x)$ , the pseudo-spectral basis functions.

This means that if we evaluate the position operator in the pseudo-spectral basis we obtain a diagonal representation

$$\langle \theta_i | \hat{x}_N | \theta_j \rangle = x_i \delta_{ij}, \quad (2.67)$$

where  $\hat{x}_N$  is the operator projected onto the subspace of our truncated basis. Since  $\sum_{i=0}^{N-1} \Phi_{ni} \cdot \Phi_{mi} = \delta_{nm}$  is unitary and the first member of our basis is a constant

$$\Phi_0(x_i) = \left( \int w(x) dx \right)^{-1/2} \quad (2.68)$$

from equation 2.63 we therefore get:  $\Delta_i = \Phi_{0i}^2 \int w(x) dx$ , where  $w(x)$  is the weighting function belonging to the given set of orthogonal polynomials (e.g.

$\exp(-x^2)$  for Hermite). Folded into the weights one also finds the volume elements obtained from the Jacobian determinant of whatever choice of coordinates one takes (e.g.  $r^2 dr, \sin \theta d\theta$ ). The discrete variable representation (DVR) of the potential operator is then the following approximation:

$$V_{ij} = \langle \theta_i | V(\hat{x}) | \theta_j \rangle \rightarrow V(x_i) \delta_{ij} \quad (2.69)$$

This approximation works because of the localisation of the pseudo spectral functions. This makes the DVR evaluation of potential operators remarkably simple.

### 2.4.3 Wavefunction relaxation

The vibrational ground state wavefunction can be obtained by setting  $t \rightarrow -i \cdot t$ , so the Schrodinger equation becomes

$$\dot{\Psi} = -H\Psi, \quad (2.70)$$

with the formal solution given by

$$\Psi(t) = \sum_n a_n e^{-E_n t} \Psi_n \quad (2.71)$$

As we propagate in the negative "imaginary" time, the negative exponential weighting will minimise the contributions arising from eigenfunctions  $\Psi_n$  at rates depending on their eigenvalue  $E_n$ . After a sufficiently long time, the wave packet converges onto the lowest eigenstate, typically the ground eigenstate.

### 2.4.4 Complex absorbing potential (CAP) and flux operator

Since the propagation of wave packets often involves the description of scattering problems, where unbounded regions of the potential function would in principle require a grid as long as the length traversed by the packet.

To overcome this, it is possible to construct operators which annihilate the wavefunction beyond certain regions, so as to keep the grid size practical. Complex absorbing potentials (CAP) have just these properties, usually of the form:

$$-i\eta W(r) = -i\eta(r - r_c)^n \Theta(r - r_c) \quad \text{so that} \quad \hat{H} = \hat{H}_0 - i\eta W(r) \quad (2.72)$$

where  $W(r)$  is a real low order monomial and  $\Theta(r - r_c)$  is a step function. Modifying the Hamiltonian in this manner makes it non-Hermitian (not norm conserving), with the desired effect of decreasing the norm when the wavefunction enters the CAP region. The norm depends on the Hamiltonian as follows

$$\begin{aligned} \frac{d}{dt} ||\Psi||^2 &= \frac{d}{dt} \langle \Psi | \Psi \rangle = \langle \dot{\Psi} | \Psi \rangle + \langle \Psi | \dot{\Psi} \rangle \\ &= \langle -iH\Psi | \Psi \rangle + \langle \Psi | -iH\Psi \rangle \\ &= i\langle \Psi | H^\dagger - H | \Psi \rangle \end{aligned} \quad (2.73)$$

When  $\hat{H}$  is Hermitian the norm is conserved, when  $\hat{H} = \hat{H}_0 - i\eta W(r)$

$$\begin{aligned} \frac{d}{dt} ||\Psi||^2 &= 2||\Psi|| \cdot \frac{d}{dt} ||\Psi|| = -2\eta \langle \Psi | W | \Psi \rangle \\ \frac{d}{dt} ||\Psi|| &= -\eta \frac{\langle \Psi | W | \Psi \rangle}{||\Psi||} \end{aligned} \quad (2.74)$$

with a formal solution:

$$||\Psi(t)|| \propto e^{-\eta W} ||\Psi(0)|| \quad (2.75)$$

Thus the norm falls exponentially over time for regions of the wavefunction within the CAP. The flux operator evaluates how the rate of change of probability density across some arbitrary subspace. If we denote  $\Theta$ , a heavy-side step function projecting onto the sub-space of interest, then;

$$\begin{aligned} \text{Flux} &= \frac{\partial}{\partial t} \langle \Psi | \Theta | \Psi \rangle = \langle \Psi | \dot{\Theta} | \Psi \rangle + \langle \Psi | \Theta | \dot{\Psi} \rangle \\ &= -i\langle \Psi | \Theta H | \Psi \rangle + i\langle \Psi | H \Theta | \Psi \rangle = i\langle \Psi | [H, \Theta] | \Psi \rangle \end{aligned} \quad (2.76)$$

Noting that  $[V, \Theta] = 0$  generally, we get

$$\begin{aligned} [H, \Theta] &= [T, \Theta] = \frac{-1}{2m} \left[ \frac{d^2}{dq^2} \Theta - \Theta \frac{d^2}{dq^2} \right] \quad \text{but} \\ \frac{d^2}{dq^2} \Theta &= \frac{d}{dq} \delta + \delta \frac{d}{dq} + \Theta \frac{d^2}{dq^2}, \quad \text{so} \\ \hat{F} &= [T, \Theta] = \frac{-1}{2m} \left[ \frac{d}{dq} \delta + \delta \frac{d}{dq} \right] \end{aligned} \quad (2.77)$$

defines the flux operator. Finally, if we obtain the flux through a channel for a Hamiltonian with a CAP defining the channel:

$$\hat{F} = i[H, \Theta] = i[H - iW, \Theta] = i(H\Theta - \Theta H) + 2W \quad (2.78)$$

so that the total flux over the channel

$$\int_0^\infty dt \langle \Psi | \hat{F} | \Psi \rangle = \int_0^\infty dt i \langle \Psi | [H, \Theta] | \Psi \rangle + 2 \int_0^\infty dt \langle \Psi | W | \Psi \rangle \quad (2.79)$$

where the first term in RHS is the Heisenberg picture of the step operator.

Note that

$$\int_0^\infty dt \frac{\partial}{\partial t} \langle \Psi | \Theta | \Psi \rangle = \langle \Psi(\infty) | \Theta | \Psi(\infty) \rangle - \langle \Psi(0) | \Theta | \Psi(0) \rangle = 0 \quad (2.80)$$

so that to get the total flux, we only need to evaluate  $2 \int_0^\infty dt \langle \Psi | W | \Psi \rangle$ , a much simpler operator than the formal flux expression.

### 2.4.5 Autocorrelation function and spectra.

The power spectrum is given by the Fourier transform of the autocorrelation function  $a(t) = \langle \Psi(0) | \Psi(t) \rangle$ :

$$\begin{aligned} \sigma(E) &= \langle \Psi | \delta(E - H) | \Psi \rangle = \frac{1}{2\pi} \int_{-\infty}^{\infty} dt \langle \Psi | e^{i(E-H)t} | \Psi \rangle \\ &= \frac{1}{2\pi} \int_{-\infty}^{\infty} dt e^{iEt} a(t) = \frac{1}{\pi} \text{Re} \int_0^\infty dt e^{iEt} a(t) \end{aligned} \quad (2.81)$$

where we have used the Fourier-transform definition of the Dirac  $\delta$ -function and the fact that, if  $H$  is Hermitian,  $a(t) = a(-t)^*$ . Another advantage comes from

$$a(t) = \langle \Psi | e^{iHt} | \Psi \rangle = \langle (e^{-iHt/2} \Psi)^* | e^{-iHt/2} \Psi \rangle = \langle (\Psi(t/2))^* | \Psi(t/2) \rangle, \quad (2.82)$$

so if the wavefunction is real and symmetric, we obtain an autocorrelation function for twice the time propagated. To reduce the Gibbs phenomenon which results from truncation of our integral to time  $T$ , the following damping function is used to smoothly bring the autocorrelation function to zero

$$g_k(t) = \cos^k\left(\frac{\pi t}{2T}\right)\Theta\left(1 - \frac{|t|}{T}\right) \quad (2.83)$$

where  $\Theta$  is a step function and  $k$  determines the order of our damping function. Using this family of functions has the effect of convoluting our original spectrum with the Fourier transform of our damping function (which is another trigonometric function). The convolution of a trigonometric function with a delta function (ie. our power spectra) has a broadening effect on our calculated spectra, thereby mimicking the effect that a limited measurement window has on an experimental spectra. By adopting the Franck-Condon approximation, the  $t = 0$  wavefunction of the absorption spectra is the ground state wavefunction operated with the transition dipole operator of the excited state of interest. Its subsequent propagation gives us the autocorrelation function and thereby its spectra.

# Chapter 3

## Genetic Algorithm for VCHAM Parameter Optimisations

### 3.1 Introduction

The vibronic coupling Hamiltonian (VCHAM) introduced in chapter 2, is parameterised in order to reproduce the adiabatic PES of a coupled set of electronic states. The number of parameters depends on the number of states and the number of degrees of freedom (DOF) of the system. The VCHAM parameters that represent the model set of coupled diabatic states are optimised in order to minimise the root mean square deviation (RMSD):

$$\sigma_{RMSD}^2 = \frac{\sum_i w_i (V_i^{calc} - V_i^{mod})^2}{N} \quad (3.1)$$

between the diagonal representation of the model,  $V_i^{mod}$  (the adiabatic representation), and the *ab-initio* points obtained from electronic structure calculations  $V_i^{calc}$  ( $w_i$  is a weighting function,  $N$  is the total number of *ab initio* points for a given state).

Since the number of internal nuclear DOF goes as  $3N-6$  with the number of atoms, fitting procedure can quickly become a non-trivial stage in the construction of these kinds of models. It is therefore desirable to have a global optimisation tool which simultaneously fits vibronic coupling parameters along those DOF for which one provides *ab-initio* energies.

---

Genetic algorithms (GA) are a family of heuristic procedures inspired by biological evolution that serve as general global optimisation tools. Therefore, GA start to become useful for problems involving the optimisation of typically more than 20 parameters [39]. The minimum requisite elements for an evolving GA system are: inheritance, mutation, fitness-selection and DNA-crossover. The generality of such steps gives flexibility in their implementation and explains the diversity of approaches found in the literature [39, 40].

A typical GA works by having a population of candidate solutions (‘individuals’ or ‘members’ of the population) whose DNA or genotype forms a vector in the basis of some parameter space that are to be optimised. Members inherit their genotype from their parents (through genetic crossover) who have been members of the population over generations. The survival of individuals over generations depends on how they compare to other members when passed through a fitness function that interprets their phenotypic effect (trait) from their genes. Finally, some mutations are injected into the gene pool at every generation in order to introduce variability and allow for the exploration of the parameter space. These steps thereby determine the evolution of the population towards greater fitness (i.e, fitness function) and culminating in the adaptation of the population towards the optimal solution in the DNA/parameter space. Because the adaptation occurs to the entire gene-pool in a gradual manner this optimisation approach is generally less susceptible to local optimisation, provided the population size and gene-pool are sufficiently diverse.

This chapter presents a GA implementation and applied to specific task of optimising parameters for vibronic coupling models. The algorithms is part of the VCHAM family of programs found in the MCTDH package (version 101).



Details of the implementation are given in the following section (3.2). The following two aspects of the implementation are worth highlighting briefly here:

- A speciation routine performs multiple local optimisations of all possible subsets of inter-state coupling parameters to prepare the initial guess population.
- A covariance matrix constructed from the population is then used to generate moderate adaptive mutations on members.

The advantages and disadvantages of using these two routines, as well as other implementation parameters, are tested and discussed for two systems with different demands testing the GA flexibility:

- An acetylene model with nine electronic states strongly coupled along four correlated DOF.
- A cyclo-butadiene (CBD) model with three electronic states weakly coupled along ten largely uncorrelated DOF.

The resulting acetylene model is the subject of chapter 6 and discussed in detail there. In chapter 4 the fitted CBD model is used to obtain a theoretical estimate for the photo-electron spectra for CBD; a new interpretation to the origins of some spectral bands is suggested.

## 3.2 Implementation

Each parameter determining the diabatic model is represented by the locus in the DNA strand of an individual (an element in an array holding VCHAM parameters). The fitness of an individual (member in the population) is given by the RMSD between the model generated by the individuals DNA and the

adiabatic points in a database. This current implementation uses similar (but not the same) hybrid GA techniques as those found in the literature [41] to generate an initial population, and extracts statistical information about the population in order to determine the strength and direction of mutations in the population (loosely based on Hansen’s covariance matrix adaptation, CMA-ES [42]). Besides this, the main steps in the algorithm are those of a typical GA outlined above. A fixed number of generations is assigned from the beginning and this is used to assign values for some of the parameters used during the optimisation. The detailed steps on every generation are given below.

### 3.2.1 Speciation: generating an initial population

Population size is one of the crucial parameters affecting the efficiency of any GA. The larger the population, greater memory and time are required for every generation. However, a bigger population size can explore a wider parameter space and is thus more likely to locate the global minima. It is therefore important to have a conservative size for the population number which samples the pertinent regions of parameter space; an initial population that reflects the relevant diversity of minima found in the landscape.

For this implementation, the speciation routine was built with this goal in mind. Like the GA itself, this routine also draws inspiration from biological evolution; when a small genetic subpopulation of a species becomes trapped by environmental/geographical barriers, it often exhibits quick speciation, whereby the small gene-pool (from the subpopulation) and the new differing ecological/geographical conditions accelerate their evolution. If the ecological/geographical environment is more constraining, such as in islands or lakes, selection pressures often lead to very diverse adaptations with high specificity to the more constraining ecological niches. In other words, such a

mechanism to evolution could provide a way to obtain the desired diversity we seek in our implementation.

In the context of this GA implementation, the reduced gene-pool worked on by the GA simply translates to the optimisation of smaller set of parameters; in this instance, sets of parameters that affect the RMSD along, at most, two degrees of freedom. This allows us to approximate the evolution of this reduced gene-pool as local optimisations (more below). In turn, to mimic the demands that different ecological niche have, and which drive the optimisation of differing adaptive traits, we form all possible subpopulations of genes by generating the combinations of subsets of states that are connected by diabatic interstate coupling parameters (the meaning of this will be clarified further with an example below). Interstate coupling parameters are the coefficients of (typical) polynomial functions entering the off-diagonal elements of the diabatic potential energy matrix. Interstate coupling parameters play a big role in correlating the topology of multiple states surfaces, as their linear combination plays an important role in their description. For example, in a 2x2 matrix, interstate coupling terms enter inside the square root part of the diagonalised diabatic model (the adiabatic model which we compare to *ab initio* data) which gives rise to most complicated topological features (e.g. crossings, double wells). So we wish to produce a population that exhibits as many diverse ways states can correlate with each other in order to produce reasonable fits. Having at least one interstate coupling parameters between some, but not each, pair of states would mean that for for N states, we could form N! combinations, which can quickly turn unwieldy. A solution is to only use those combinations of states that are coupled directly through a coupling parameter and that can form a *connected network* (with links given by interstate coupling terms). Its worth mentioning that these networks are

also built across terms involving at most two DOF.

As a concrete example: Suppose three states are connected in series: A-B-C, where state B connects A and C in the network. The possible subpopulations obtained in this problem would be the following combinations: ABC, AB and BC. Note that AC would not be a subpopulation.

Since such subpopulation combinations involve typically less than 20 parameters, their ‘evolution’ can be approximated by simple local minimisations. Parameters that are not involved in either the two modes or connected states (subpopulation of a niche) are then assigned normally distributed (ND) values with a standard deviation which is estimated from values obtained from previous locally optimised parameters (during the generation of the initial population). The parameter that determines the spread of the ND values, is henceforth referred to as  $\hat{L}_j$  and is also used later on to determine some of the mutation algorithms used. Since the optimisation of parameters occurs to the entire gene-pool, if there is a large discrepancy between the fitness of members in the population, those with high RMSD (poor fitness) are removed rather quickly from the population. This is normally a sought property, but not in this first instance; we wish to generate a balanced population that will allow (locally) optimised parameters to survive for enough time in the population to successfully generate good solutions. In other words, those combinations of subpopulations with a large number of locally optimised parameters are more likely to give better overall RMSD values initially. However, the purpose of the speciation routine is to bring relevant genetic diversity into the pool; those un-fit member may actually contain alleles (specific values for a gene) which may prove valuable if combined appropriately with other genes (at a later stage). So in order to avoid this loss of diversity and premature convergence to a local minima, the alleles of subpopulations are thoroughly

shuffled to make up the initial population. Other methods that exploit local minimisations for the generation of initial populations can be found in the literature [41].

### 3.2.2 Statistical analysis and covariance matrix

At every generation the mean, standard deviation and kurtosis of every parameter class  $j$  is calculated for the population of survivors and of the survivors and their offspring together as well.

$$\text{excess kurtosis} = \kappa_j = \sum_{i=1}^N \frac{(x_i - \bar{x})^4}{(N-1)\sigma_j^4} - 3 \quad (3.2)$$

Index  $j$  is omitted from  $\bar{x}$  and  $x_i$  on the RHS for clarity.  $\sigma_j$  is the parameter standard deviation. The same properties are calculated for the RMSD of the population of size  $N$ . These properties are used to determine the amount and kinds of mutations occurring in several ways as described in the following section (3.2.3). A covariance matrix is also constructed in order to accelerate ‘adaptation’, and is loosely based on one of the most effective evolutionary algorithms in the literature associated with Nikolaus Hansen and Ostermeier [43]. They construct the following sample covariance matrix:

$$C^{(g+1)} = \sum_{i=1}^N w_i (\mathbf{x}_i^{(g+1)} - \mathbf{m}^{(g)})(\mathbf{x}_i^{(g+1)} - \mathbf{m}^{(g)})^T \quad (3.3)$$

The mean  $\mathbf{m}^{(g)}$  used here is that of the population without the offspring, whereas the construction of the  $\mathbf{x}_i^{(g+1)}$  vector includes an (perhaps overall less fit) offspring. This makes the covariance matrix an approximately better unbiased estimator (see [44]). A weight function,  $w_i$ , is used against every sample that enters into the covariance matrix; the samples are ranked by their RMSD and a decaying exponential function determines their weight

according to their ranking position.

$$w_j = \frac{N}{\gamma} \exp(-Or(\sigma_{RMSD}^j) \cdot \lambda),$$

$$\text{where: } \lambda = -\ln(\beta)/N, \quad \text{and} \quad \gamma = \sum_j^N \exp(-Or(\sigma_{RMSD}^j) \cdot \lambda) \quad (3.4)$$

The weight is normalised to the total population number,  $N$ .  $Or()$  function gives an integer ranking  $0 < Or(\sigma_{RMSD}^j) \leq N$  based on the RMSD of the sample (1 for best RMSD). In the spirit of principal component analysis (PCA), by performing an orthogonal transformation to diagonalise our positive definite matrix, we should obtain an eigenvector basis which is linearly uncorrelated. These describe an orthogonal set of vectors determining the main ellipsoid axis of a normal multivariate distribution. The eigenvalues of such matrix are interpreted as the variance of the population along our new basis. In other words, with regards to our old basis the first principal component with the highest eigenvalue accounts for the largest variability in our data. This technique is strongly reminiscent of the normal mode decomposition of molecular systems as the covariance matrix approximates the inverse Hessian matrix up to a constant factor [44].

### 3.2.3 Mutations

In order to inject variability into the gene-pool and to explore our parameter space,  $n_{mut}$ , a small proportion of mutations are introduced at every generation. Each individual chosen for mutation has  $r_{mut}$  of its parameters mutated.  $n_{mut}$  and  $r_{mut}$  are user parameters and are their effect studied in the test cases detailed in the section 3.3. There are three kinds of mutations that are used in the current implementation.

- A mutation obtained from a random sample following a normal distribution, centred at the mean,  $\bar{x}_j/3$ , of parameter  $j$  being mutated.

The standard deviation is given by  $\sigma_j = (\hat{L}_j - |x_j| - \bar{x}_j)/3$ , where  $\hat{L}_j$  describes the bounds of the parameter range (relative to  $\bar{x}_j$ ) considered in the statistical analysis (thus any parameters beyond these bounds are dismissed as outliers) and  $x_j$  the current value for that parameter to be mutated.  $\hat{L}_j$  can be estimated from the speciation routine or else provided with some foresight. The variance of this normal distribution also slowly decreases as the generations progress, since we expect the population to eventually find itself near the global basin.

- Parameters that belong to the same kind of order and element (such as linear intra-state coupling terms) are shuffled amongst each other. This has the advantage that the mutations will probably have some reasonable effect on the surfaces; if the algorithm has already found a good fit along a cut/state it is likely that other cuts/states will have similar properties and would benefit from having alleles of those values.
- Covariance matrix: One can generate a set of vectors in the eigenvector basis of the covariance matrix (as described above), with magnitudes following a normal distribution with variance given by the eigenvalues of these covariance eigenvectors. These vectors are then used as a source of mutations. One could loosely interpret the evolution of our population as ‘Lamarckian’, considering the foresighted mutations thus generated. Normal distributions are useful for these problems as they generate isotropic search points and are the only stable distributions with finite variance (see [43]). As will be shown in section 3.3, the covariance matrix can speed up significantly the convergence to the global solution. If we only use the covariance matrix to generate mutations, the population eventually collapses into a delta distribution. However, if the population has not sampled the parameter space sufficiently or

the weight function in the covariance matrix is not carefully balanced, it can lead to a premature convergence to a local minima. It is therefore important to give enough generations for selection and recombination to drive the evolution of the population into the right basin. To this end the following strategies were taken:

### Strategy 1

If the distribution of a particular parameter in the population becomes too narrow, noise is added to the data (for that specific parameter) used to construct the covariance matrix. This ensures the population of that parameter does not collapse by making the covariance matrix generate mutations in its direction. This noise is introduced when adding the parameter value for every member (sample) into the elements of the covariance matrix. The following heuristic solutions are used with regards to the noise distribution:

- The kurtosis for a given parameter is used as a measure of non-normality and peakedness of its distribution for this parameter (calculated ignoring outliers determined by  $\hat{L}_j$  away from the mean).
- The standard deviation,  $\sigma_j^m$ , of noise distribution is switched on gradually as the given parameter's kurtosis increases. With the constraint that  $0 \leq \sigma_j^m \leq \hat{L}_j$ , where  $\hat{L}_j$  is the bounds of the range of mutations for this parameter.
- The noise is allowed (if needed) to be significant for most of the optimisation (specially as the population begins to decrease in size) but should decrease over the generations.

If the speciation routine is used,  $\hat{L}_j$  are obtained from local minimisa-



tions and also used to estimate the maximum value a parameter can take. This attempts to reduce the amount of a-priori information regarding the choice of domain boundaries in which to explore the RMSD landscape. The following function determines the standard deviation for the noise amplitude following a normal distribution, centred at the current value of the parameter of the sample, that was used to satisfy these conditions:

$$\sigma_j^m = \left\{ \frac{1}{2} (\tanh(\alpha(\kappa_j - \kappa_{max})) + 1) \right\} \{G \cdot \beta \cdot \sigma_j(\hat{L}_j)\}, \quad (3.5)$$

where  $\alpha$  is defined such to make the tanh function unity when parameter  $\kappa_j$  becomes equal to  $\kappa_{max} \cdot 2$ . When this happens  $\sigma_j^m$  becomes equal to  $G \cdot \beta \cdot \sigma_j$ , where  $\sigma_j$  is the standard deviation for parameter  $j$  (calculated ignoring outliers determined by  $\hat{L}_j$  away from the mean).  $\beta$  is a factor that determines the largest value that this distribution can take (typically 4.0, but has not been optimised in the current implementation);  $G$  is a Gaussian weight function that reduces the noise as the generations progress (essentially no noise by the last 20% of the generations in the calculation, regardless of high kurtosis). If the kurtosis, which is calculated from samples within  $\hat{L}_j$  reaches  $\kappa_{max}$  (typically  $\sim 20$ ), the information fed into the covariance matrix becomes a Gaussian distribution with a slightly bigger standard deviation than the current distribution. This generates suggested mutations that favour the production of a more normal distribution, avoiding a population with too high kurtosis.

### Strategy 2

If the kurtosis of some parameter  $\kappa_j$ , becomes close to  $\kappa_{max}$   $P_j^{max}$ , the probability of mutating that parameter increases. This increase in

probability is given by:

$$\Delta P(j) = \Delta^\kappa \left( \frac{1}{2} (\tanh(\beta(\kappa_j - \kappa_{max})) + 1) \right) \quad (3.6)$$

where  $\Delta^\kappa$  is the increase in mutation. Typically  $r_{mut} + \Delta^\kappa$  above 0.6 ( $r_{mut}$ , the baseline probability of genes mutated in an individual) leads to too many mutations and is likely to make mutants so unfit they never survive in the gene-pool.

### Strategy 3

If the population is becoming too narrow,  $n_{mut}$ , the number of mutations per generation increases and individuals with DNA close to the average are mutated more often. The average kurtosis of all parameters is used as a measure of the gene-pool diversity of the population; reaching values near  $\kappa_{max}$  (narrow gene-pool), the probability of mutation of individuals with a high overlap with the first principal component increases. However, the best 5% are never mutated. This probability is also Gaussian weighted to generate a strongly biased mutation towards the best solutions near the end of the generations. The following function was used to satisfy these conditions:

$$P(j) = \frac{-\chi}{N} (Or(x_j \cdot x_{1st \text{ comp}}) - N/2) + 1/2 \quad (0 < j \leq N) \quad (3.7)$$

$$\chi = \frac{1}{2} (\tanh(\alpha(\bar{\kappa} - \kappa_{max})) + 1)$$

$\alpha$  is defined similarly than in strategy 1.  $\chi$  modulates the gradient of this linear equation determining  $P(j)$ , the probability of individual  $j$  being mutated. Function  $Or()$  ranks member  $j$  by their overlap with the first principal component  $0 < Or() \leq N$  (highest overlap ranks 1);  $N$  is the total population number and  $\bar{\kappa}$  is the average kurtosis of the population. Simultaneously,  $n_{mut}$ , the number of members to be mutated per generation increases as a tanh function (asymptotically

adding 0.25%, percentage. this feature was not optimised in current implementation).

If adiabatic energies correlating different DOF are not included, the sign of the interstate coupling parameters is often arbitrary (with regards to fitness). If this is the case, we will obtain a bimodal distribution centred at zero (with a mean of zero). If the mean is zero, the resulting covariance matrix will tend to generate mutation vectors which drive mutations towards an (erroneous) zero valued parameter. To avoid this, the interstate coupling parameters are split into a positive and negative domains parameters when used to build the covariance matrix. This way the mean correctly describes the centre position of this bimodal distribution. The parameters used in this algorithm (e.g.  $\kappa_{max}$ ,  $P_j^{max}$  and  $\beta$ ) were optimised for small test systems, but could be subject to further rigorous investigation.

### 3.2.4 Uniform Crossover

The population is randomly arranged into a set of pairs to recombine their genes into a pair of offspring. A random number algorithm assigns a 0.5 probability to allocate the gene from one parent or the other to a first offspring. Independent of the outcome, a second offspring receives the complementary set of genes.

### 3.2.5 Tournaments and Selection

The population of parents and offsprings are randomly arranged into a set of pairs and their RMSD compared. Those with a lower RMSD value gets selected for the next generation and the other one discarded. This has been

termed an ‘elite’ selection as both parents and offspring are allowed to compete.

### 3.3 GA tests

#### 3.3.1 Introduction

We test the GA for two model systems with a large number of optimisation parameters (78 and 58), where simple local optimisers consistently fail to give accurate solutions or else require very good initial guesses. Specifically, four different user-setting parameters are studied for both systems:

- Population size; this number refers to the number of survivors every generation. Labelled  $N_{pop}$
- Average fraction of mutated parameters per mutated individual. Labelled  $r_{mut}$ .
- Number of individuals mutated every generation. Labelled  $n_{mut}$ .
- Parameter  $\beta$  related to the weight function entering in the construction of the covariance matrix (see section 3.2.2). This parameter only makes sense if we are using the covariance matrix to generate mutations. Labelled  $\beta$ .

As well as the use of the following types of mutations and types of initial distributions (as described in the previous section):

- Normally distributed parameter values for initial population (referred to as NID). Normally distributed mutations centred at the mean value  $\bar{x}_j$  of the mutated parameter  $j$  and with standard deviation  $\sigma_j = (\hat{L}_j - |x_j| - \bar{x}_j)/3$  (detailed in section , refereed to as NDM). Together Labelled NID+NDM

- Speciation routine used to generate initial population (section 3.2.1, referred to as SID). Normally distributed mutations. Labelled SID+NDM
- Normally distributed parameter values for initial population. Covariance matrix used to generate mutations (see section 3.2.2, referred to as CDM). Labelled NID+CDM
- Speciation routine used to generate initial population. Covariance matrix used to generate mutations. Labelled SID+CDM

First we present the trends observed for both model systems. Then we present results for the fitting of a nine singlet state, four DOF model of acetylene. These states have a large number of coupling parameters and functions correlating DOF. We follow with results for the first three singlet electronic states of cyclo-butadiene (CBD) along ten DOF. The parameters fitting these states and DOF are only weakly coupled, with very few interstate coupling parameters. Together with the fitted surfaces of the first two ion states we calculate a theoretical photoelectron spectra for this molecule (chapter 4). As mentioned before, these two systems are likely to have qualitatively different RMSD surfaces, given the differing number of interstate coupling parameters and functions correlating DOF. These contrasting systems should suitably test the flexibility or applicability of some of the routines described in the previous section. For each model we present test-runs using all possible combinations resulting from the just mentioned user parameters, covariance matrix and speciation routine. This will allow us to ascertain for which kinds of problems the aforementioned options are necessary, preferred or to be avoided.

Genetic algorithms are stochastic by nature and depend on chance events (brought by seeds in the random number algorithm) to the explore parameter

landscape; two identical tests settings but with different seeds could therefore lead to results with significant differences. As such, a thorough investigation would require statistical samples to accurately explore the effects of different controllable parameters on the GA. For each of the mentioned test settings, four different test-runs were performed using different seeds used for the random number algorithm. Most of the results presented below correspond to the average of those four-runs (unless otherwise specified). This number of tests is clearly not statistically meaningful; conclusions we can draw from these are only tentative, borne out of a small set of test-runs and only likely to show the most salient trends. The number of function evaluations is the computer-time bottleneck and these scale linearly with population size; at every generation, all new offspring RMSD have to be evaluated as well as  $n_{mut} \cdot N_{pop}$ , those members which are mutated per generation. This step could be easily parallelized to tackle even larger problems, but currently not implemented.

### 3.3.2 Trends across models

The effects all the just-mentioned possible combinations of user-setting parameter/options for the different test-runs are presented in figures like 3.6 or	Rank	cyclo-butadiene	acetylene
		[Methods], $N_{pop}$ , $n_{mut}$	[Methods], $N_{pop}$ , $n_{mut}$
	1	[CDM+NID], 600, 0.25	[CDM+SID], 800, 0.25
	2	[CDM+SID], 600, 0.25	[CDM+SID], 400, 0.25
	3	[NDM+SID], 600, 0.25	[CDM+NID], 800, 0.10
	4	[NDM+NID], 600, 0.25	[CDM+NID], 400, 0.25
	5	[NDM+NID], 300, 0.25	[NDM+NID], 800, 0.10
	6	[CDM+SID], 300, 0.25	[NDM+SID], 800, 0.10
	7	[NDM+SID], 300, 0.25	[NDM+NID], 400, 0.10
	8	[CDM+NID], 300, 0.25	[NDM+SID], 400, 0.10

3.10 in sub-Appendix 3.A and 3.B respectively.

The statistical and quantitative data displayed in these figures

Table 3.1: How the best of each subfigure in 3.6 and 3.10 in sub-Appendix 3.A and 3.B rank against each other. Each subfigure displays the set for a given method pair ([NID,SID] + [NDM,CDM]),  $N_{pop}$  (400,800 for acetylene; 300,600 for CBD) and  $n_{mut}$  (0.1,0.25,3.5)

(provided in the sub-Appendix) and described below highlight the most general trends across the test-runs as a function of generations. The test-runs

are displayed to highlight the most significant determining user-setting parameters of the optimisation; they are divided into subfigures identified by a given method pair ([NID,SID] + [NDM,CDM]),  $N_{pop}$  (300, 600 for CBD and 400, 800 for acetylene) and  $n_{mut}$  (0.1,0.25,3.5). Within these subfigures there are tests showing different settings for  $r_{mut}$  (0.1,0.25,0.40) and  $\beta$  (0.05,0.15,0.50). Representative subfigures are re-printed in the following subsections, provided for quick reference in the discussion (Figures 3.1, 3.2, 3.3 and 3.4).

### Best RMSD:

Figures 3.6 (CBD) and 3.10 (acetylene) in sub-Appendix 3.A and 3.B respectively show the average RMSD of the best fitted individual over 2000 generations (a representative subfigure is shown in Fig. 3.1). As mentioned previously, the displayed results are an average from four test-runs with different seeds for the random number algorithm. Table 3.1 ranks the best result from each of the different combinations of mutation method, initial distribution, population ( $N_{pop}$ ) and mutants per generation

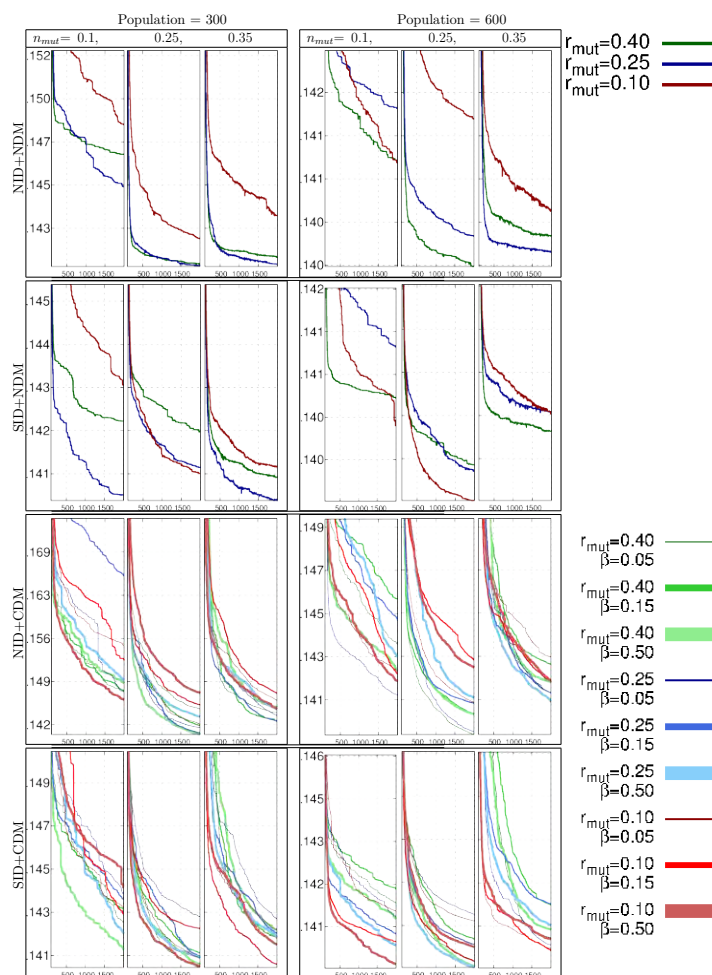


Fig. 3.1: Best RMSD (y-axis) in population over 2000 generation (x-axis). Representative subfigure obtained from Fig 3.6 in sub-Appendix 3.A showing test-runs with NID+CDM,  $N_{pop}=600$  and three cell containing test-runs with  $n_{mut}=0.15$  (left), 0.25 (center) and 0.35 (right). Each cell has a number of test-runs with parameters  $r_{mut}$  and  $\beta$  as shown in legend provided.

( $n_{mut}$ ) as shown in these figures. The average of the standard deviation of best RMSD fit for each four seeded test-runs gave 0.001667 for Acetylene and 0.0005127 for CBD. This gives us confidence that the best fit graphs give reasonably meaningful trends that do not depend significantly on the stochastic elements of the implementation. A determining factor for a reasonable fit is population size; all else being equal, a bigger population gives consistently better results. Similarly important is wheather one uses CDM or SID . The effective use of these options however, significantly depends on the model system in question (covered closely below). Finally the number of mutants per generations,  $n_{mut}$ , also markedly affects the optimization; under this implementation, values around 0.15-0.25 (15-25% of the population gets mutated every generation) work consistently well for most situations. Parameters  $r_{mut}$  and  $\beta$  have more blurred and less determining effects with respect to the final RMSD outome. The uncertainty on the effect of these two parameters is possibly a result of the stochastic nature of the algorithm.

### RMSD distribution:

Another useful statistical measure is the RMSD standard deviation for the populations, as these can provide some indirect insight into the fitness of the population as a whole and its

stability. In sub-Appendix 3.A and 3.B we provide graphs of these trends over generations, and a representative subfigure shown in Fig. 3.2. As before,

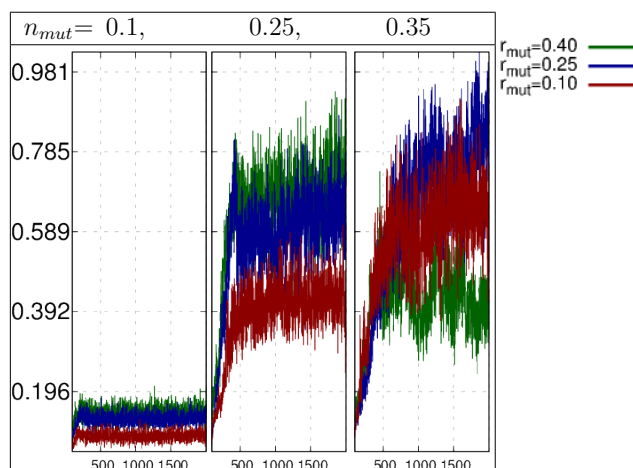


Fig. 3.2: RMSD Standard deviation (y-axis) of the population over 2000 generation (x-axis). Representative subfigure obtained from Fig 3.11 in sub-Appendix 3.B showing test-runs with NID+NDM,  $N_{pop}=400$  and three cell containing test-runs with  $n_{mut}=0.15$  (*left*), 0.25 (*center*) and 0.35 (*right*). Each cell has a number of test-runs with parameters  $r_{mut}$  and  $\beta$  as shown in legend provided.



we can see what the different effects the parameters/options here tested might have on the populations RMSD spread. Most test-runs show a simple monotonic dependence between parameters  $n_{mut}$  and  $r_{mut}$ ; as the amount of new genes in the pool is increases, the RMSD standard deviation of the population increases concomitantly (last frame in acetylene discused further below). Like the best RMSD figures, the effect of using of CDM or SID depend on the model system used. On the other hand, population size seems to have little effect on this statistical measure. It is worth mentioning that the kurtosis of the rmsd distribution increases significantly for all calculations; after a thousand generations aproximately a third of all members lie near the best RMSD for the given test-run, the rest being thinly spread over large RMSD values.

### Parameter distribution:

The RMSD can only indirectly suggest what is occuring to the gene-pool; one cannot directly asses how the gene diversity or spread might relate to the RMSD distribution. To ob-

tain further insight on the effect different user-setting parameters/options have on parameters, we can compare the normality of the distribution of parameters between the different test-runs. Specifically, as a

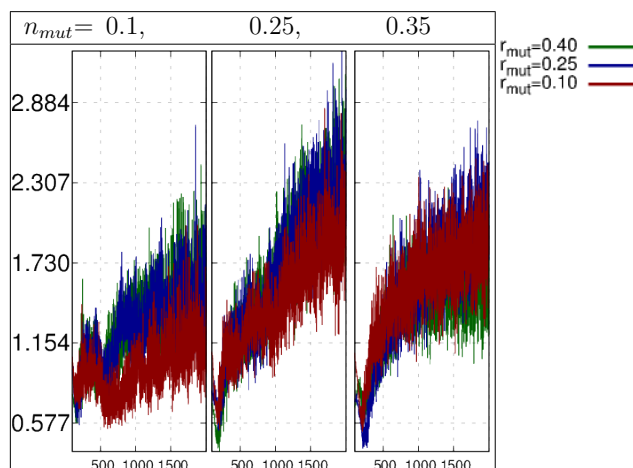


Fig. 3.3: Average standard deviation relative to all test-runs (y-axis, see Eq. 3.8) of the population over 2000 generation (x-axis). Representative subfigure obtained from Fig 3.8 in sub-Appendix 3.A showing test-runs with NID+NDM,  $N_{pop}=400$  and three cell containing test-runs with  $n_{mut}=0.15$  (left), 0.25 (center) and 0.35 (right). Each cell has a number of test-runs with parameters  $r_{mut}$  and  $\beta$  as shown in legend provided.

way of measuring this feature, we calculated the average of the standard deviation of parameters, each normalised to the average of standard deviation of all test-runs for a given population size and generation:

$$\Sigma_t^{G, N_{pop}} = \frac{1}{N_p} \sum_p^{N_p} \frac{\sigma_{tp}}{\frac{1}{N_t} \sum_{t'}^{N_t} \sigma_{t'p}}, \quad G = 1, \dots, 2000 \quad (N_{gen}) \quad (3.8)$$

The  $G$  and  $N_{pop}$  indexes have been omitted in the RHS for the sake of clarity.  $\sigma_{tp}$  refers to the standard deviation of parameter class  $p$  (eg. coefficients of linear/quadratic interstate/intrastate coupling elements of the diabatic hamiltonian) for test-run  $t$ , in the test-set here presented.  $N_p$  and  $N_t$  are the total number of parameter classes and test-runs here discussed (for a given population set  $N_{pop}$  and generation  $G$  in  $N_{gen}$ ). Its worth reminding that each  $\sigma_{tp}$  is an average of four test-runs with identical settings but different seeds for the random number algorithm (as well as all previously discussed statistical measures). The choice of normalisation allows us to both put the same parameters across different test-runs, as well as different classes of parameters (eg inter/intra-state coupling terms) in a common footing. Similar graphs were also obtained for the relative kurtosis of the parameter distribution. With these measures we can approximately represent the relative spread of the gene-pool as the population evolves over generations for the different test-runs settings presented. Figures displaying the resulting trends for all test-runs are provided in sub-Appendix 3.A and 3.B and a representative shown in Fig. 3.3. Although  $n_{mut}$  has a strong relative effect on the parameters standard deviation, it exhibits a slightly different pattern on both models (discussed further below). In either of the test-runs of both models one can claim, to a greater or lesser extent, that increasing  $n_{mut}$  increases the standard deviation of parameters. The use of CDM results in a slightly smaller spread of parameters compared to NDM. It further decreases as generations progress, likely due to the tendency for CDM to form delta function

distributions. The speciation routine (SID) has a variable effect on this measure. The relative kurtosis on the other hand, is consistently reduced by the increase in  $n_{mut}$ . This suggests that increasing the number of mutants has an effect of broadening the distribution. The effect that  $r_{mut}$ , the number of genes mutated per mutant has on the standard deviation or kurtosis of the parameter distribution seems to depend on  $n_{mut}$ , the number of mutants per generation. For most test-runs with  $n_{mut} \geq 0.1$  we observe that small values of  $r_{mut}$  result in higher kurtosis, and the trend reversed for  $n_{mut} = 0.05$ .

### Mutation distribution:

To gain further insight into how the covariance matrix mutations (CDM) perform for different user-setting parameters, we constructed the following quantity per test-run as a measure of comparison between test-runs:

$$\Omega_t^{G, N_{pop}} = \frac{1}{N_p} \sum_p \frac{\sigma_{tp}}{\sigma_{tp}^m}, \quad G = 1, \dots, 2000 \quad (N_{gen}) \quad (3.9)$$

We compare the ratio between the standard deviation of a parameter class  $\sigma_{tp}$  and the mutations generated for that class  $\sigma_{tp}^m$ , and obtain an average for all parameters in a given test-run. Like before,  $\sigma$  are an average of four test-runs with identical settings but different seeds for the random number algorithm. The figures are also provided in sub-Appendix 3.A and 3.B and a representative given in Fig. 3.4. They show for most of the generations the standard deviation of mutations of a parameter is greater than in the population. As mentioned in section 3.2.3, the mutations are weighted by a Gaussian function which decreases the mutation magnitude as the calculation progresses, presuming that by the end of the calculation the GA should find itself in the correct basin and would only require small changes. This gets reflected in the figures as the increase in the ratio as the calculation comes to completion.  $n_{mut}$  increases this ratio further and  $r_{mut}$

only seems to affect the optimisation when coupled with large  $n_{mut}$  values.

Most notably, the ratio is significantly different for both models presented; the increase in this ratio occurs earlier and is more pronounced for CBD. Since this occurs to large populations and small values of

$n_{mut}$ , leading to more homogeneous populations, it is unlikely that the parameters magnitude are increasing faster than mutations over the generations. Instead, it is more likely that mutations decrease quicker, sug-

gesting that the covariance matrix is driving the population to form a delta function. As mentioned before, this may occur when the population lies strongly in a single region of parameter space; in this instance it may well mean that the populations finds itself at the correct global basin earlier in the optimisation, given the lower number of parameters and the weaker coupling between them.

One can approximately assert that moderate values for parameters  $n_{mut}$ ,  $r_{mut}$  and  $\beta$  (as explored in these test-runs) tend to consistently give a more satisfactory optimisation. Although population size is an important factor in all optimisations, it alone cannot guarantee a successful optimisation. Provided the population is not too small, the speciation routine tends to provide a better initial distribution of parameters for the subsequent optimisation,

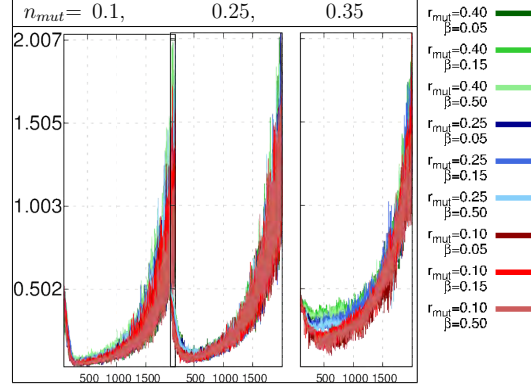


Fig. 3.4: Average parameter-mutation ratio (y-axis, see Eq. 3.9) of the population over 2000 generation (x-axis). Representative sub-figure obtained from Fig 3.13 in sub-Appendix 3.B showing test-runs with SID+CDM,  $N_{pop}=400$  and three cell containing test-runs with  $n_{mut}=0.15$  (*left*),  $0.25$  (*centre*) and  $0.35$  (*right*). Each cell has a number of test-runs with parameters  $r_{mut}$  and  $\beta$  as shown in legend provided.

regardless of whether one uses CDM or NDM. The number of mutants that survive every generation is found to depend largely on  $n_{mut}$ ; the more mutants we have in the population, the higher the number of mutants surviving the generation. This is most likely due to the existence of less fit members that can be easily displaced, for the very reason that more mutations most often lead to less fit members. This is in agreement with the general increase in RMSD as  $n_{mut}$  increases. The often observed increase in standard deviation and strong decrease in kurtosis of parameters as one increases  $n_{mut}$  suggests an overall broadening of the population, and loosely following the RMSD standard deviation. So we can approximately associate an increase in RMSD in the population as a broadening of the parameter distribution. Alas, all of these concomitant changes don't translate in any simple way to the final best RMSD fits. One can at best suggest that by choosing moderate values of  $n_{mut}$ ,  $r_{mut}$  and  $\beta$  (as presented in the test-runs), else being equal, result in moderate values of RMSD standard deviation and correlate with moderate values of standard deviation and kurtosis of parameters, one is likely to do better than otherwise. This is in part because, as mentioned above, the choice of initial distribution or mutation source (i.e. CDM, SID) also have significant effects on the RMSD standard deviation and to the final best fit, and depend on the model system in question. We will therefore analyse in closer detail both models tested.

### 3.3.3 Acetylene

For this model, 78 parameters were fitted in a single calculation. A  $D_{\infty}h$ ,  $\Sigma_g^+$  symmetry adapted basis of polynomial functions representing the nuclear coordinates over the elements of a diabatic electronic wavefunctions was used. The algorithm for the generation of such basis is presented in chapter 5. Energy points for ten states were obtained at approximately 300 geometries

using a EOM-CCSD/aug-cc-pVTZ level of theory (Molpro [45]). The most noticeable result from Fig. 3.10 in sub-Appendix 3.B and Tab. 3.1 is the consistent failure of calculations using normally distributed mutations (NDM) to perform successfully. The relative average distribution of the parameters (as provided Fig.3.12 in sub-Appendix 3.B) does not differ significantly from using CDM. The relative standard deviation RMSD is slightly lower than using CDM, suggesting that the individuals are on average reasonable fits. There is a more pronounced shoulder and plateauing exhibited, suggesting possibly some type of stagnation of the population, unable to continue improving its fitness.

This may indicate that NDM are ineffective generators of mutants that explore new regions of parameter space while simultaneously being good enough to survive enough in the population to spread these new genes. The population starts prematurely converging onto a basin other than the global minima. This is consistent with the lower RMSD standard deviation observed. Another trend in these NDM test-runs is that all  $n_{mut}=0.10-0.25$  performed best as well as  $r_{mut}=0.1$

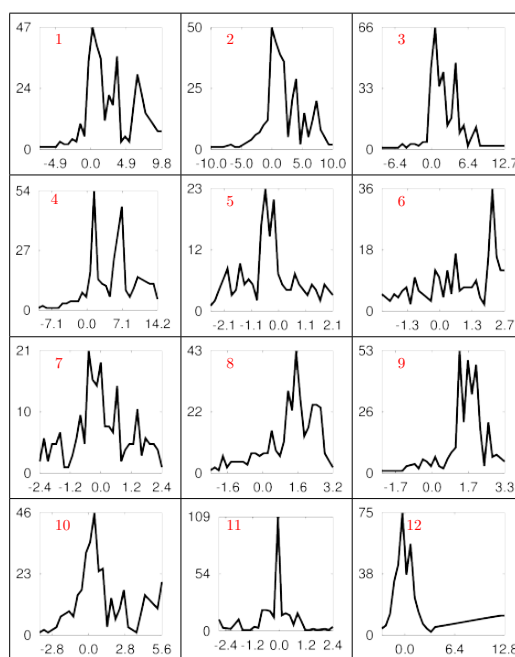


Fig. 3.5: Some representative initial distributions for some parameters generated using the speciation routine, to be contrasted with a purely normal distribution. 1-4: Morse Oscillator parameters; 5-8: inter-state coupling parameters; 8-9: second order intra-state parameters; 10-12: higher order parameters.

performing well; this implies that for the given number of optimisation pa-

rameters, the population is unable to absorb a large numbers of mutations without affecting the best fitted members. Since we do not observe these failure in all instances, like in the CBD test model, we are led to the conclusion that the complexity of fitting a set of strongly coupled parameters poses a specific impasse to the kinds of mutations provided by the NDM test-runs.

The system has 16 independent interstate coupling parameters, which give rise to 75 species. These break down into the following number of interstate connected networks (see section 3.2.1): 39 for 2-state, 23 for 3-state, 11 for 4-state and only 2 for 5-state networks. Figure 3.5 shows the intended slight skewing of the initial population towards more successful parameter values when using SID, instead of a normal distribution (NID) centred at zero (Morse potential function parameters also included from CBD). Using SID gave both the best and the worst calculations. A significant improvement in conjunction with CDM suggests that it provides better initial samples of parameter space with which to generate suggested mutations. Even after 2000 generations the algorithm continues optimising the RMSD significantly. This includes the smaller population of 400, which gave the second best set of results of any of the other type set of calculations. It most notably improves the outcome of  $n_{mut}=0.35$ , where all other types of calculations performed poorly (more on this below). Contrasting these results are those without CDM that used the speciation routine (NDM+SID), giving the poorest results. The symptoms discussed above for the NDM become acute; the slightly lower RMSD than without the speciation routine suggest that stagnation, as suggested above, becomes more pronounced.

This ‘stagnation’ can be more clearly appreciated in test-runs with  $n_{mut}=0.35$  (CDM+SID notwithstanding). Clearly, the failure results from the excessive number of mutations the population suffers, unable to absorb these appro-

priately. Expectedly, the worse fits within this subset come from  $r_{mut}=0.40$ . The distribution of parameters narrows suggesting a smaller gene-pool. We obtain a simultaneous reduction of the RMSD standard deviation, suggesting that this contracted gene population is nevertheless reasonably fit (albeit incorrect). Figure 3.13 in sub-Appendix 3.B shows the parameter/mutation ratio of standard deviations, showing that, being greater than one, the mutations generated are small. These smaller mutations are less able to explore parameter space sufficiently, resulting in the premature convergence onto the incorrect basin.

### 3.3.4 Cyclo-butadiene

This neutral cyclo-butadiene model has 18 normal coordinates and 3 states, only significantly coupled along a few of these DOF. For this test case, only 10 coordinates are fitted, others being well described by the zeroth order model and for which no fitted parameters required. Energy points for the first three excited singlet states were obtained at approximately 250 geometries using a CAS-SCF(4,4)+RS2C/cc-pVDZ level of theory (Molpro [45]). 58 polynomials were used to fit these states and coordinates, a few obeying constraints for Jahn-Teller systems (discussed further in chapter 4) This system is by-and-large well described by a model with uncorrelated normal coordinates and fitting could be performed almost on all degrees of freedom separately, instead of as a single optimisation test-run. Only one DOF is correlated to four others (further details on the model parameters are given in section 4). However, this type of system provides distinct demands on the GA; for example, we can test the performance of the covariance matrix, which locates correlation between parameters. It is reassuring the GA can tackle such problems and one can optimise all DOF in a single calculation, an otherwise tedious procedure. It is also worth mentioning that parameters for



Morse potential function were also optimised at the same time as other polynomials; these parameters have significantly differing domains which again tested the robustness of the algorithm.

Since we have fewer optimisation parameters, smaller populations were used to test the GA (300 and 600) compared to the previous model. Such small populations had a clear effect on the optimisations, all test-runs with  $N_{pop} = 300$  under performing compared to their  $N_{pop} = 600$  counterpart (see figures 3.6 in sub-Appendix 3.A). Any test-run resulting in an RMSD lower than  $\sim 0.140$  was in the correct global basin, resulting in a generally satisfactory fit; the use of local optimisation algorithms starting from such fitted models would result in little improvement and the same fitted model. Although the NDM perform comparatively well, their best RMSD fits often continue to exhibit a plateauing, with pronounced shoulders suggesting stagnation of the population is generally more likely using NDM. Another noticeable trend is that  $n_{mut}=0.10$  gave consistently poor results, suggesting that systems with large number of decoupled parameters benefit more from a larger number of mutations per generation.

Once again, the best and most consistent results were obtained when we used CDM+SID. However, in this instance the use of CDM has less certain results. Although CDM+NDM gave the best test-run in the set, it also results in a significant spread of final best RMSD, many of which compare badly with many NDM. All CDM calculations exhibit large parameter/mutations standard deviation ratio (Fig. 3.9 in sub-Appendix 3.A), which may indicate that mutations are no longer exploring parameter space appropriately and potentially leading to premature convergence. This interpretation is in agreement with the decrease in parameter and RMSD standard deviation over generations; the worst test-runs, typically those with  $n_{mut} = 0.1, 0.35$ ,

show the smallest relative parameter spread. Only 3 DOF couple states via interstate coupling parameters. This low number gives rise to only 6 species (as defined in the previous section). Therefore, we should not expect any drastic improvements/aggravations due to the use of the speciation routine. Although it seems to improve the results when coupled to CDM, it may worsen small populations that are NDM; the RMSD standard deviation is higher and the parameter relative standard deviation is smaller. Since NDM and NID represent the cheapest strategies with regard to computational time (compared with SID and CDM), one can improve these results by increasing the population size of NDM+NID runs as opposed to use SID or CDM. This is specially true in this model system, where CDM+NID does not produce consistent results, despite having resulted in the best RMSD fit of the whole set. We tentatively suggest that for systems with weakly correlated DOF and parameters, NDM provides a successful approach, in contrast to the acetylene model.

### 3.3.5 Conclusions

A genetic algorithm was constructed which successfully optimised up to 78 parameters test-model with continuous domains. We have analysed many of the effects that different parameters have on the optimisation. However, more rigorous work needs to be done to clearly map out the relationships between all different user-settings parameters in this implementation. Moderate values for parameters  $n_{mut}$ ,  $r_{mut}$  and  $\beta$  (as given in sec 3.3) result in the most satisfactory optimisations. Although population size is an crucial factor, specially regarding computation time, it alone does not ensure a sucessfull optimisation. The methods for mutation and generation of initial population also have decisive effects on the GA performance. CDM give a more gradual evolution with less risk of stagnation when contrasted

with NDM, specially clear in the acetylene model case. We tentatively suggest that NDM distributed mutations alone are not suited for demands that the penalty functions with continuous domains and with highly correlated parameters. The ‘stagnation’ effect in NDM is exacerbated by the use of the speciation routine, SID. Conversely, for systems with weakly uncoupled parameters, NDM mutations perform well and giving the lowest function evaluation cost, provided the population size / number of parameters ratio is adequate. The speciation routine improves the outcome of results, provided the population size is sufficiently large. If little information is available on the domain of the optimised parameters, the speciation routine should be used. Without recourse to this algorithm, it would not have been possible to successfully fit the 78, strongly correlated parameters model.

### 3.A CBD; trends between test-runs with different user-setting parameters.

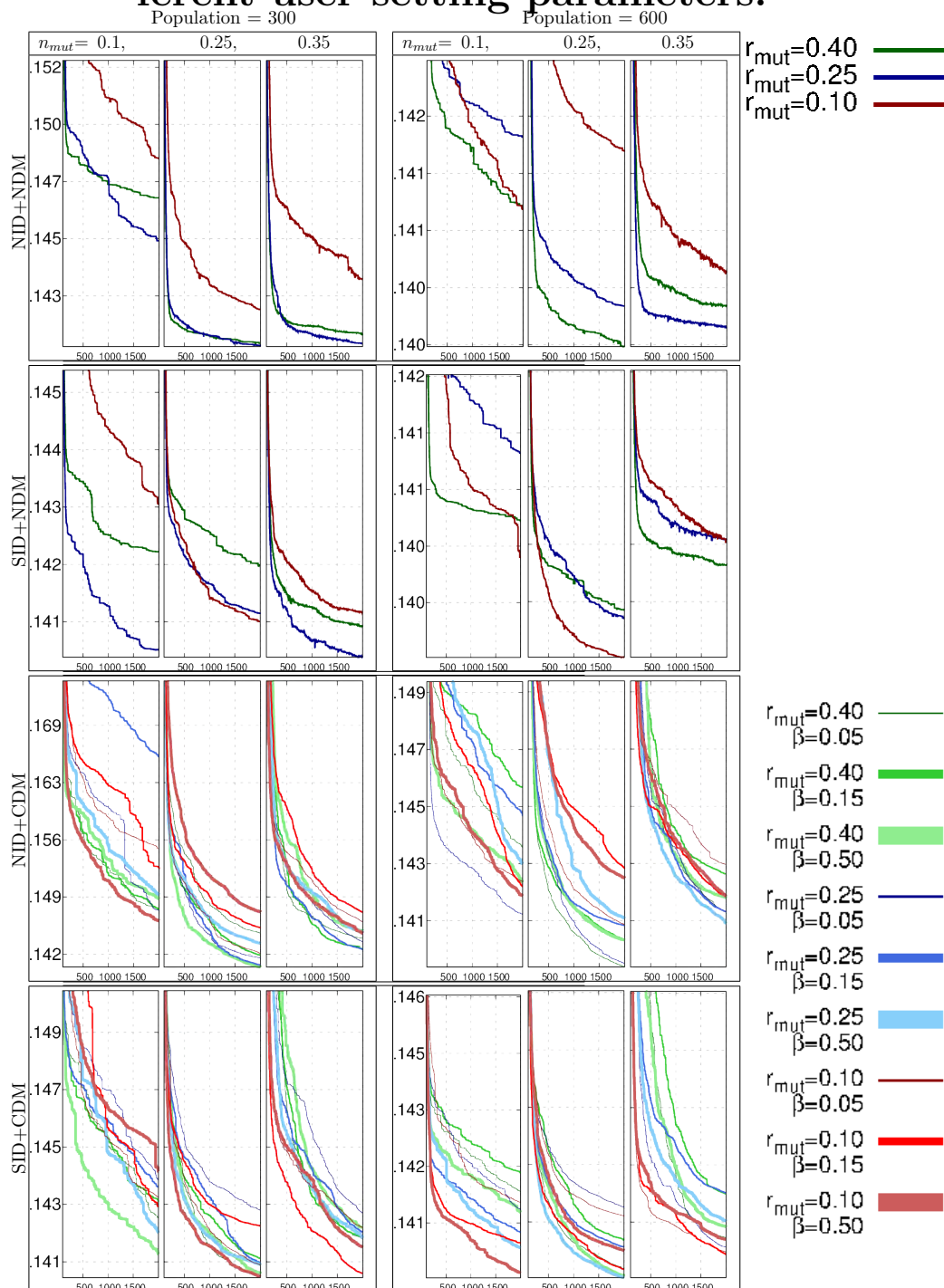


Fig. 3.6: Cyclo-butadiene tests; Comparing the best fit of each test-run over 2000 generations of all the test-run combinations mentioned in the text (section 3.3). The tests are divided into sub-figures identified by a given method pair ([NID,SID] + [NDM,CDM]),  $N_{pop}$  (300 and 600) and  $n_{mut}$  (0.1,0.25,3.5). Within these sub-figures there are tests showing different settings for  $r_{mut}$  (0.1,0.25,0.40) and  $\beta$  (0.05,0.15,0.50).

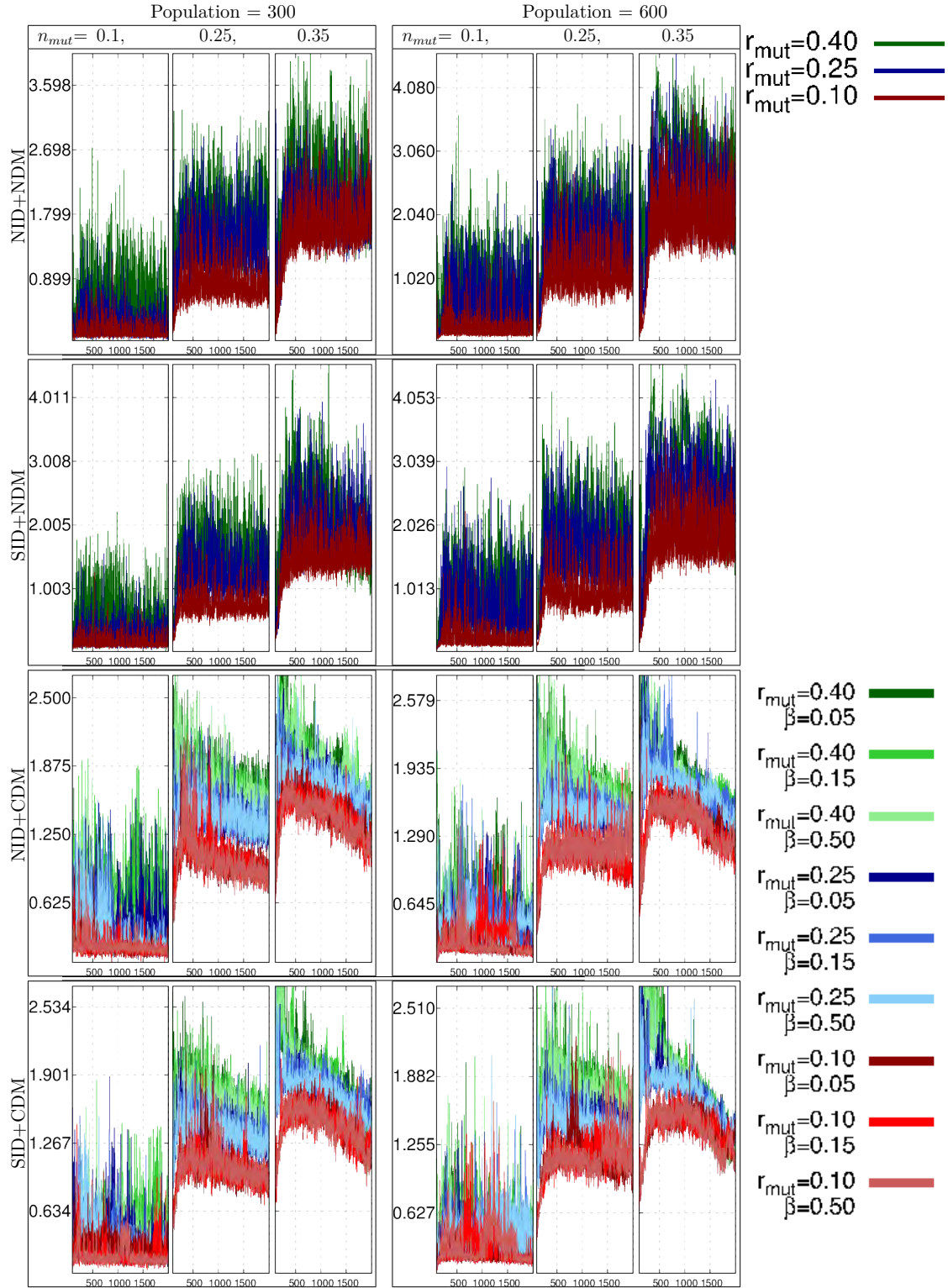


Fig. 3.7: CBD tests; Comparing the RMSD standard deviation of each test-run over 2000 generations of all the test-run combinations mentioned in the text (section 3.3). The tests are divided into sub-figures identified by a given method pair ([NID,SID] + [NDM,CDM]),  $N_{pop}$  (300 and 600) and  $n_{mut}$  (0.1,0.25,3.5). Within these sub-figures there are tests showing different settings for  $r_{mut}$  (0.1,0.25,0.40) and  $\beta$  (0.05,0.15,0.50).

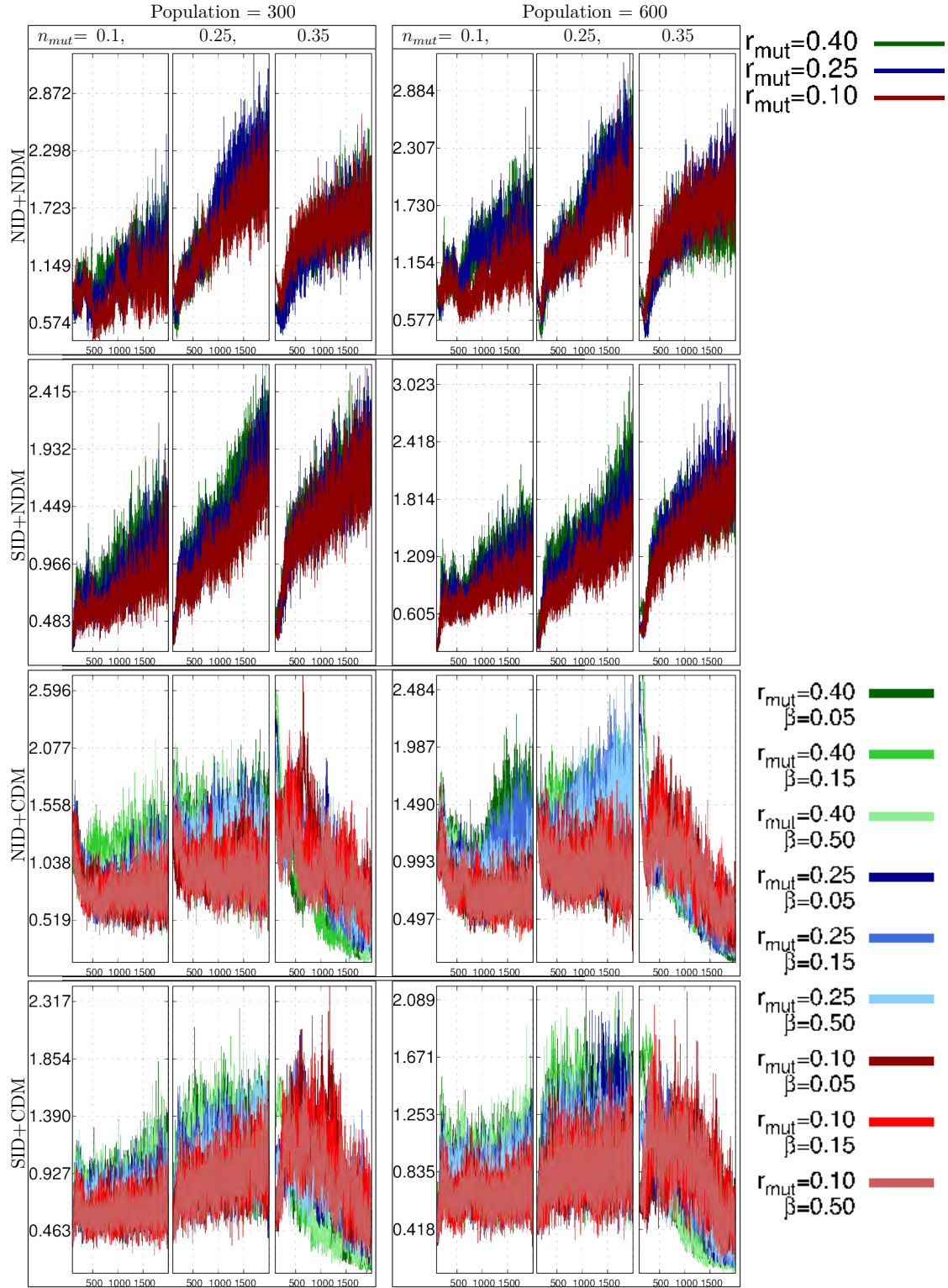


Fig. 3.8: CBD tests; Comparing the test-run average standard deviation relative to all test-runs (see Eq. 3.8) over 2000 generations of all the test-run combinations mentioned in the text (section 3.3). The tests are divided into sub-figures identified by a given method pair ([NID,SID] + [NDM,CDM]),  $N_{pop}$  (300 and 600) and  $n_{mut}$  (0.1,0.25,0.35). Within these sub-figures there are tests showing different settings for  $r_{mut}$  (0.1,0.25,0.40) and  $\beta$  (0.05,0.15,0.50).

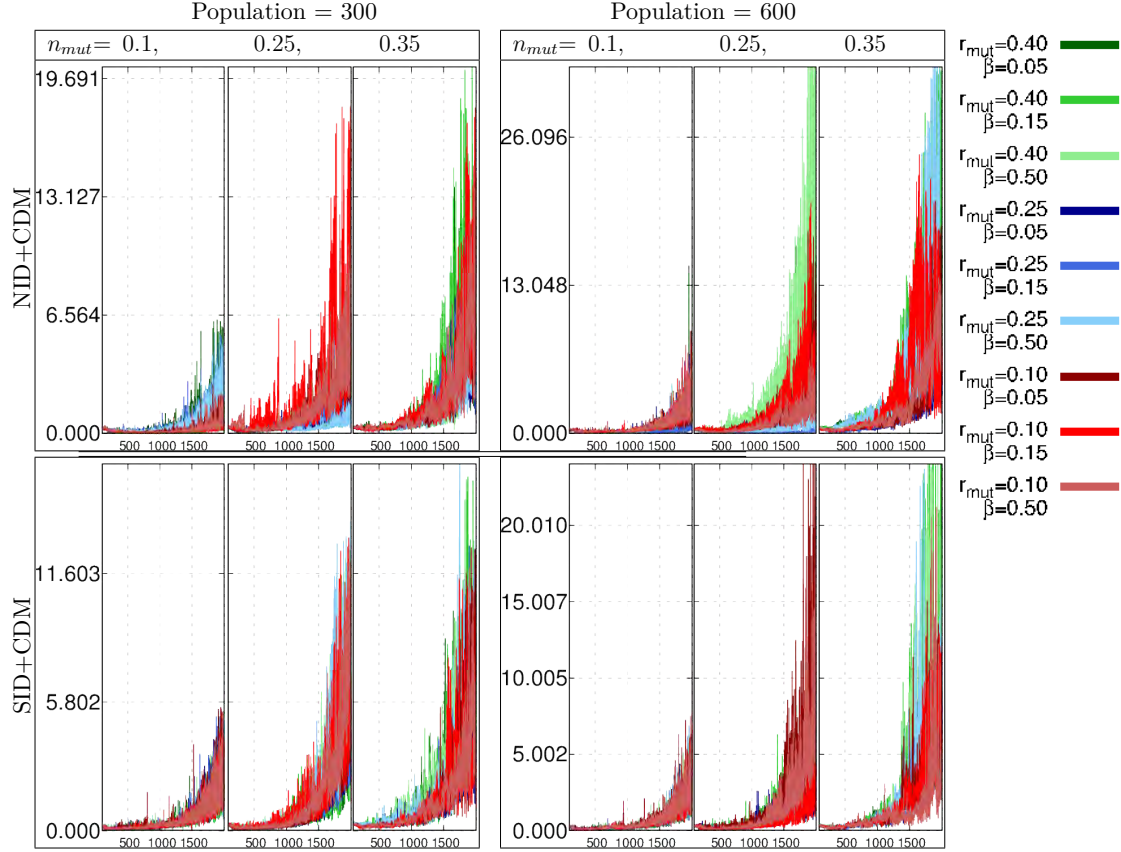


Fig. 3.9: CBD tests; Comparing the test-run average parameter-mutation ratio (see Eq. 3.9) over 2000 generations of all the test-run combinations mentioned in the text (section 3.3). The tests are divided into sub-figures identified by a given method pair ([NID,SID] + [NDM,CDM]),  $N_{pop}$  (300 and 600) and  $n_{mut}$  (0.1,0.25,3.5). Within these sub-figures there are tests showing different settings for  $r_{mut}$  (0.1,0.25,0.40) and  $\beta$  (0.05,0.15,0.50).



### 3.B Acetylene; trends between test-runs with different user-setting parameters.

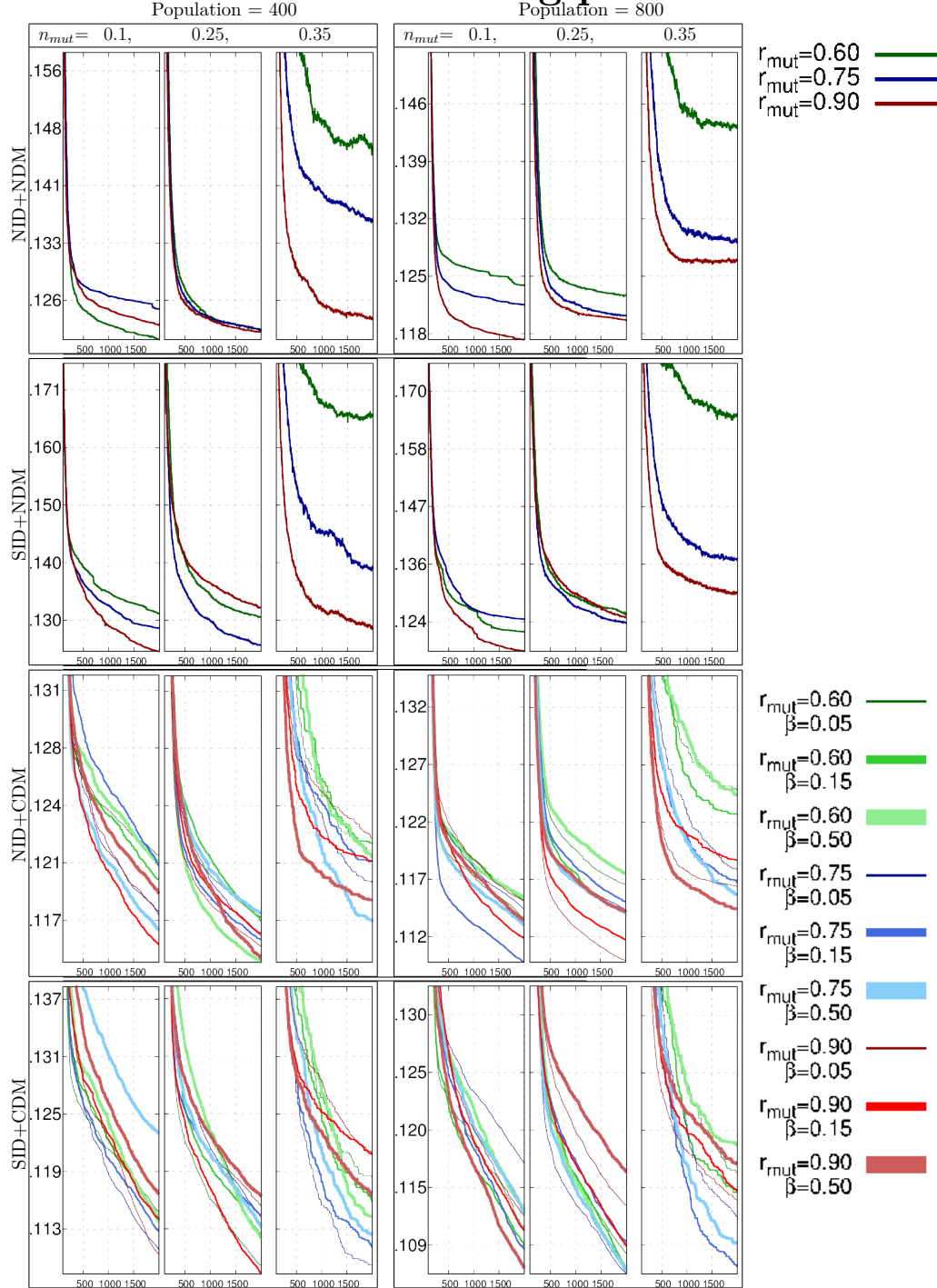


Fig. 3.10: Acetylene tests; Comparing the best fit of each test-run over 2000 generations of all the test-run combinations mentioned in the text (section 3.3). The tests are divided into sub-figures identified by a given method pair ([NID,SID] + [NDM,CDM]),  $N_{pop}$  (400 and 800) and  $n_{mut}$  (0.1,0.25,3.5). Within these sub-figures there are tests showing different settings for  $r_{mut}$  (0.1,0.25,0.40) and  $\beta$  (0.05,0.15,0.50).



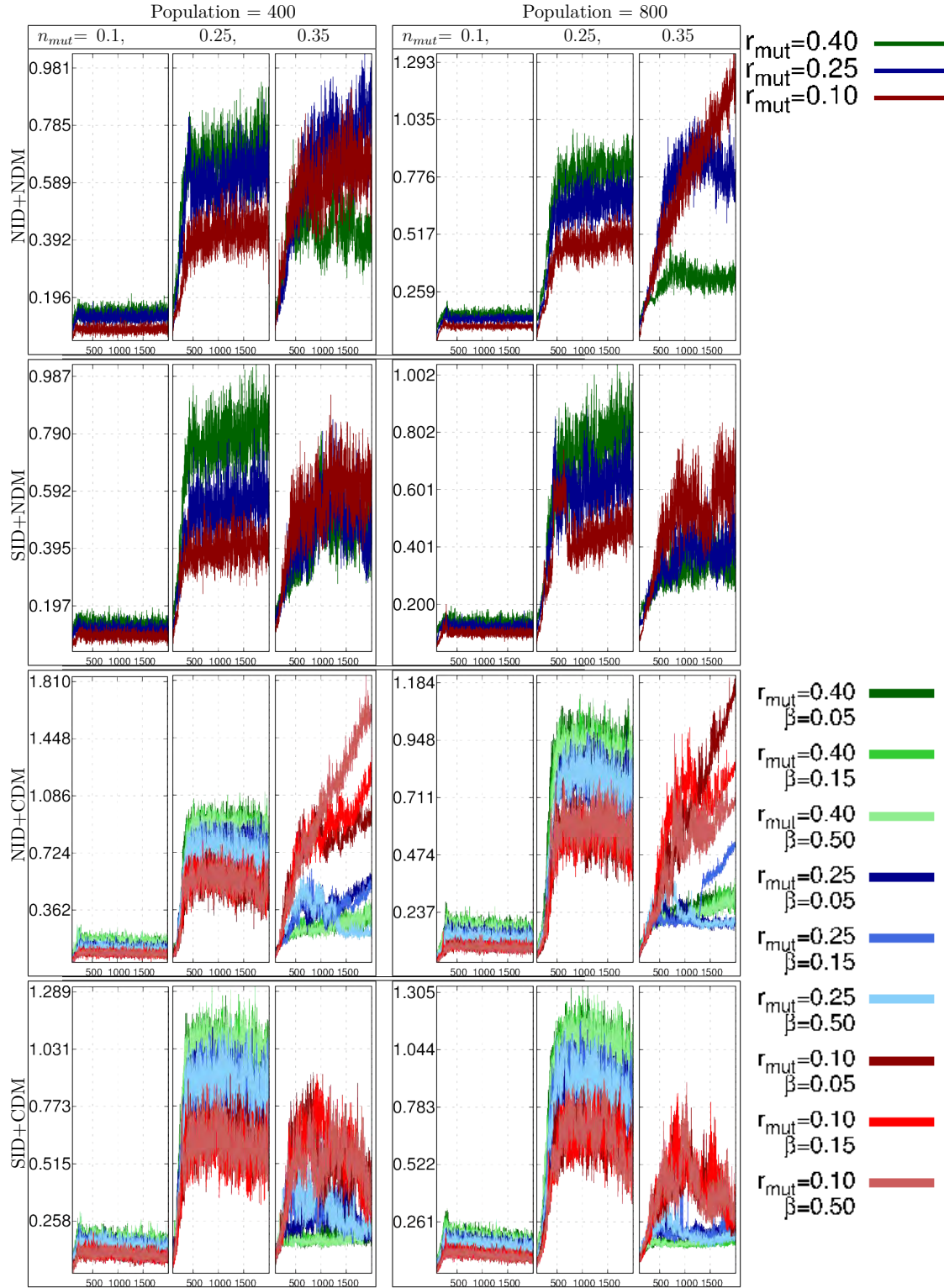


Fig. 3.11: Acetylene tests; Comparing the RMSD standard deviation of each test-run over 2000 generations of all the test-run combinations mentioned in the text (section 3.3). The tests are divided into sub-figures identified by a given method pair ([NID,SID] + [NDM,CDM]),  $N_{pop}$  (400 and 800) and  $n_{mut}$  (0.1,0.25,3.5). Within these sub-figures there are tests showing different settings for  $r_{mut}$  (0.1,0.25,0.40) and  $\beta$  (0.05,0.15,0.50).

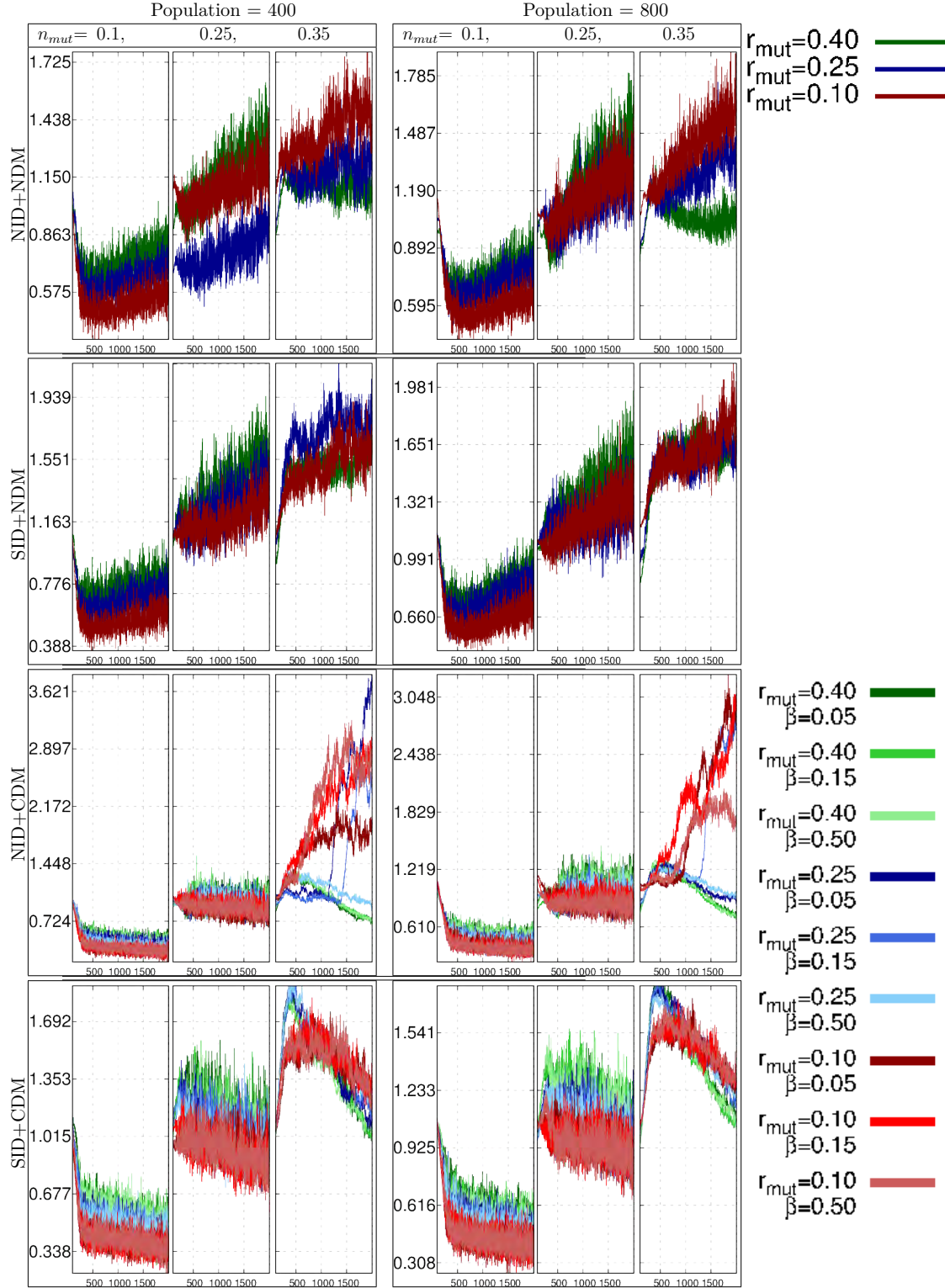


Fig. 3.12: Acetylene tests; Comparing the test-run average standard deviation relative to all test-runs (see Eq. 3.8) over 2000 generations of all the test-run combinations mentioned in the text (section 3.3). The tests are divided into sub-figures identified by a given method pair ([NID,SID] + [NDM,CDM]),  $N_{pop}$  (400 and 800) and  $n_{mut}$  (0.1,0.25,0.35). Within these sub-figures there are tests showing different settings for  $r_{mut}$  (0.1,0.25,0.40) and  $\beta$  (0.05,0.15,0.50).

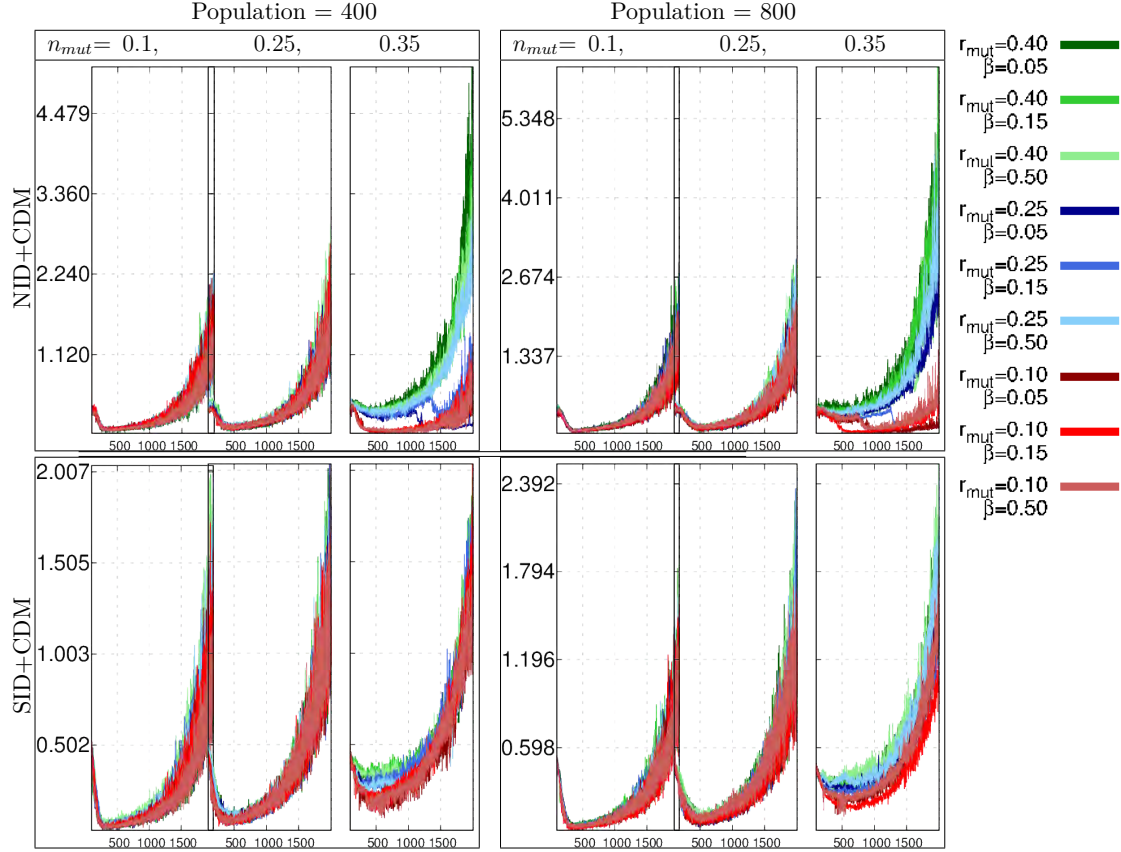


Fig. 3.13: Acetylene tests; Comparing the test-run average parameter-mutation ratio (see Eq. 3.9) over 2000 generations of all the test-run combinations mentioned in the text (section 3.3). The tests are divided into sub-figures identified by a given method pair ([NID,SID] + [NDM,CDM]),  $N_{pop}$  (400 and 800) and  $n_{mut}$  (0.1,0.25,3.5). Within these sub-figures there are tests showing different settings for  $r_{mut}$  (0.1,0.25,0.40) and  $\beta$  (0.05,0.15,0.50).

# Chapter 4

## CBD Photo-Electron Spectra

### 4.1 Introduction

Cyclo-butadiene (CBD) has been the subject of much theoretical and experimental work over the last 5 decades. Although no experimental work has conclusively determined the ground state geometry, a large body of theoretical work indicates it is rectangular with two equivalent minima; an exhaustive review [46] of work done up to 1980 suggests that C. A. Coluson was the first to propose that pseudo Jahn-Teller effects explain the rectangular ground state geometry of CBD. For similar group theoretical arguments, the transition state describing the bond-flipping automerization between these rectangular geometries is likely to be near square planar (in contrast to other options only open to true JT-systems). This symmetry argument is physically attributed to a mixture of internuclear and  $\sigma$  inter electronic repulsion, lowering the energy towards the ‘bond-alternated’ rectangular structure, with a contraction of the  $\pi$ -bonds due to polarisation of bond-charges and nuclear- $\pi$  electron attraction [47]. Although regarded as a paradigm for anti-aromatic molecule’s [46, 48] the aforementioned review still cautioned classifying CBD as an anti-aromatic  $4[n]$   $\pi$  electron annulene (Hückel rules) since the ring strain could be enough to keep the molecules cyclic conjugation (and its planar geometry).

More recently [49] theoretical work was done by Karadakov who calculated several magnetic properties and characterised different geometries and states as anti/aromatic annulene; rectangular  $S_1$ ,  $S_0$  and square  $S_2$  are classified as anti-aromatic, square  $S_1$  as aromatic and rectangular  $S_2$  as non-aromatic. A more recent study also cautioned any quick conclusion for the rectangular geometry as one should also need to consider stabilisation energy obtained from these rectangular resonance structures [50] that could lead to square geometries and to aromaticity.

Table 4.1 shows some of the ground state CC bond distances obtained from geometry optimisation found in the literature. Unlike the equilibrium geometry, the square geometry is an open shell system, where the HOMO is a pair of degenerate  $e_g$  orbitals housing two electrons (bi-radical configuration according to Hückel diagrams), this transition state is described by strongly quasi-degenerate electronic orbital configurations which demand an accurate multi-reference/configuration wavefunction. Together with the fact the barrier [51] to automerization has a large experimental uncertainty ( 0.07-0.434 eV range ) has made this automerization in recent years a benchmark problem to compare different new electronic structure energy algorithms (it is a well know fact that CCSD(T), a typically reliable method gives poor results in this system).

Table 4.7 lists some of the recent methods used to estimate the automerization barrier which, like the vertical excitation energies, can also serve as a way of discerning the accuracy of our electronic structure technique of choice. Some of the excited state topology has also been investigated; at the  $D_{4h}$  (square) geometry, two electrons are occupied by degenerate  $e_g^2$  orbitals ( $^1B_{3g}$  and  $^1B_{2g}$  in  $D_2$ ) from which we can construct the three singlet states aforementioned (some vertical excitation energies given in Tables 4.5 and

4.6).

Nakamura [52] performed MCSCF calculations and the major spin-orbit configurations determining these states. This description agrees with Saddique and this work and the configurations are shown in the Hückel-like diagram in Fig. 4.1.

They attribute the stabilisation energy of the  $S_0$  equilibrium geometry as well as the  $S_1$  rhomboidal equilibrium geometry to a second-order JT effect. Their use of second-order JT effect corresponds to Sad-

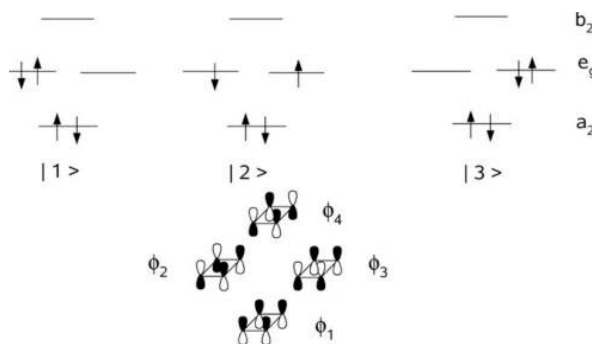


Fig. 4.1: Diagram of active space  $e_g$  degenerate orbitals occupying different singlet configurations that determine the character and symmetry of the first three excited states. Reprinted from Saddique [53]

dique's [53] use of the linear vibronic coupling between non-degenerate states (which are allowed to couple to first order using  $D_{4h}$  symmetry product arguments). Both agree that it is sufficient to account for the stabilisation of  $S_0$ . Wang *et al.* [54] performed EOM-CCSD calculation and arrived to a similar conclusion about the main configurations playing a role in the first three excited states; at the  $D_{4h}$  (square) geometry, with an identical picture to Nakamura [52] (and later Saddique). They note that at this geometry, the triplet state is higher in energy than the singlet, thus in violation of Hund's rules. At the  $D_{2h}$  (rectangular) geometry, these configurations change to make the  $S_2$  ( $2^1A_{1g}$ ) correspond to a  $1^1B_{3g}$  to  $1^1B_{2g}$  double orbital excitations, while the  $S_1$  ( $1^1B_{1g}$ ) corresponds to a single excitation configuration.

Saito *et al.* [55] performed MCSCF and EOM-CCSD calculations and found two  $S_0/S_1$  conical intersections involving the excited state automerization;

the ‘ionic’ (rhomboidal) structure where both electrons find themselves at opposite carbons from each other (leading to the automerization via the heterolytic mechanism); the "tetra-radical" structure involves one electron in each carbon atom (drives the homolytic mechanism to automerization) and conclude that the ionic structure is the minimum energy pathway (which consolidates Nakamura’s earlier work).

Tables 4.5 and 4.6 show some of the vertical excitation energies found in the literature. Experimental work has been referred to sparse and contradictory [54, 56]; the UV spectrum only shows only one peak before 300 nm, no peaks after 250 nm and a very weak absorbing tail near( $\sim 3$  eV). Photo decomposition happens above  $\sim 5$  eV and the high-angular strain and anti-aromaticity make this molecule highly reactive [57].

The cleanest photoelectron-spectrum (which is reproduced in this work) was obtained using a jet-cooled supersonic expansion [58]. They used vibrational structure to fit to a 2-state 2D harmonic Jahn-Teller model (FC factors depend sensitively on the differences between the geometries and surfaces of the neutral and cationic CBD), from which they deduce that the cation surfaces also have rectangular equilibrium geometries, but with a smaller deviation from the square geometry. This conclusion agrees with theoretical work done on the radical cation; efforts to understand the surfaces started as far back as 3 decades ago [59], when it was calculated to have an electronically degenerate ground state with true  $E_g \otimes \beta$  Jahn-Teller coupling; a pair of  $E_g$  electronic states ( $D_{4h}$ ) are lifted from their degeneracy by a branching space built from  $b_{2g}$  and  $b_{1g}$  ( $D_{4h}$ ) modes. Similar conclusions can be drawn from degenerate Hückel MO’s picture; a rhomboidal or rectangular stable structures can be formed for which they concluded the rectangular geometry would dominate due to  $\pi$  interactions being stronger between neighbouring atoms. The pres-

ence of a single non-bonding electron in the CBD cation then explains the existence of a stable rhombic (or square) structure. They contrast it with the restriction to rectangular geometry of the neutral CBD; it would have to pass through the square transition state and place the non-bonding electrons at diagonal orbitals from a rectangular geometry and therefore increase Columbic repulsion. An earlier spectrum [60] obtained at higher temperatures and by subtracting spectra from other compounds is shown in Fig 4.2, exhibiting another band at higher energies. Further work [61] has corroborated the picture of a Jahn-Teller sombrero surface with branching space minima connected by a pseudo-rotation about the square geometry conical intersection (undergoing  $b_{1g}$  puckered rhomboidal and  $b_{2g}$  rectangular distortions with a barrier of  $\leq 0.1$  eV ). Bond lengths and angles for rhomboidal and rectangular geometries from literature are included in Tables 4.3 and 4.4 respectively optimised at MCSCF [52] and RMP2/CCSD(T) [62] levels.

source	Method	$C_1C_2$ length (Å)	$C_2C_3$ length (Å)
Nakamura [52]	CAS(4,4)/6-31g*	1.3657	1.5532
Koseki [47]	MCSCF/6-31(d)	1.3530	1.5461
Levchenko [54]	CCSD(T)/cc-pVTZ	1.3943	1.5660
Eckert-maksi [57]	MR-AQCC/cc-pVTZ	1.3490	1.5620
Sumita [55]	CAS(8,8)MRMP2/cc-pVDZ	1.3510	1.5930
Lyakh [63]	TCCSD(T)/cc-pVTZ	1.3700	1.5750
This model	CAS(4,4)PT2/6-31g*	1.3444	1.5437

Table 4.1: CBD equilibrium  $C_1C_2$  and  $C_2C_3$  bond lengths for  $S_0$ ,  $^1A_g$  ( $D_{2h}$ ) rectangular geometries

source	Method	$CC$ length (Å)	angle (deg)
Nakamura [52]	CAS(4,4)/6-31g*	1.4503	85.5
Koseki [47]	MCSCF/6-31(d)	1.4364	84.8
Eckert-maksi [57]	MR-AQCC/cc-pVTZ	1.447	-
This Model	CAS(4,4)PT2/6-31g*	1.440	86.1

Table 4.2: CBD equilibrium  $CC$  bond length and angle for  $S_1$  rhomboidal/square geometries



source	Method	$C_1C_2$ length (Å)	angle (deg)
Nakamura [52]	CAS(4,4)/6-31g*	1.443	87.70
Bally [62]	RMP2/6-31g(2d,p)	1.428	83.01
This model	CAS(4,4)PT2/6-31g*	1.473 (1.403)	86.67

Table 4.3: CBD<sup>+</sup> equilibrium CC bond length and angle for S<sub>0</sub> rhomboidal geometries

source	Method	$C_1C_2$ length (Å)	$C_2C_3$ length(Å)
1 Nakamura [52]	CAS(4,4)/6-31g*	0.3897	1.4977
2 Bally [62]	RMP2/6-31g(2d,p)	1.380	1.5
This model	CAS(4,4)PT2/6-31g*	1.396	1.501

Table 4.4: CBD<sup>+</sup> equilibrium c-c bond length and angle for S<sub>0</sub> rectangular geometries

source	Method	S <sub>1</sub> <sup>1</sup> A <sub>1g</sub>	S <sub>2</sub> <sup>1</sup> B <sub>2g</sub>
Levchenko [54]	ROHF-EOM-SF-CCSD	1.8140	2.1370
Levchenko [54]	EOM-CCSD/cc-PVTZ	1.5340	-
Eckert-maksi [57]	MR-AQCC/aug-cc-pVTZ	1.3313	1.8039
Karadakov [49]	CAS(4,4)/6-311++G(2d,2p)	2.2400	3.4800
Saddique [53]	CAS(4,4)/6-31g*	2.2300	3.8400
This Model	CAS(4,4)PT2/6-31g*	1.5121	1.8543

Table 4.5: Vertical excitation energies (eV) at CBD S<sub>0</sub> square D<sub>4h</sub> (TS) geometry

source	Method	S <sub>1</sub> <sup>1</sup> B <sub>1g</sub>	S <sub>2</sub> <sup>1</sup> A <sub>g</sub>
Levchenko [54]	ROHF-EOM-SF-CCSD	3.4170	4.3630
Levchenko [54]	CCSD(T)/cc-PVTZ	3.3190	-
Karadakov [49]	CAS(4,4)/6-311++G(2d,2p)	4.3800	4.6600
Sumita [55]	MRMP2//CAS(8,8)/cc-pVDZ	3.2762	4.3339
This Model	CAS(4,4)PT2/6-31g*	3.0280	3.7200

Table 4.6: Vertical excitation energies (eV) at CBD S<sub>0</sub> rectangular D<sub>2h</sub> (equilibrium) geometry

source	Method	$\Delta E$ (eV)
Eckert-Maksi [57]	MR-AQCC/aug-cc-pVTZ	$\sim 0.350$
Li [64]	MkCCSD/cc-pVTZ	0.4163
Bhaskaran-Nair [65]	MkCCSD(T)/cc-pVTZ	0.3859
Saito [48]	ULO-MRCCSD	0.3079
Saito [48]	UNO-MRCCSD	0.3729
Shen [66]	CASPT2/cc-pVTZ	0.3770
Shen [66]	CASBCCC4/cc-pVTZ	0.1626
Mahapatra [67]	SS-MRMPPT/CASSCF(4,4)	0.4644
Lyakh [63]	TCCSD(T)/cc-pVTZ	0.4076
Saddique [53]	CAS(4,4)/6-31g*	$\sim 0.181$
This Model	CAS(4,4)PT2/6-31g*	0.3330

Table 4.7: TS barrier for CBD  $S_0$  automerization between rectangular  $D_{2h}$  (equilibrium) geometries (excluding ZPVE)

## 4.2 CBD photoelectron spectra.

Saddique and Worth [53] constructed a vibronic model to reproduce the photoelectron spectra. They used CASSCF(4,4) to calculate the first three neutral state and the first degenerate cation state surfaces. Their vibronic model includes second order terms of up to six DOF. Due to limited inclusion of dynamic correlation by CASSCF methods, the authors overestimated the automerization barrier and  $S_0/S_1$  vertical excitation energy which they acknowledge might have made their spectra calculations inaccurate.

This model improves the electronic structure determination by adding perturbation theory corrections to CASSCF(4,4) wavefunction, and including more degrees of freedom and correlation between them. Like theirs, our typical vibronic model was built by fitting low order polynomial functions representing the diabatic potential to adiabatic energies along the normal DOF of a square CBD geometry (frequency calculations were performed with Gaussian 03 [68], energies with Molpro [45]). Details of this approach have been described in the introduction. For ground  $E_g$  cation states we have a  $E_g \otimes b_{1g} \otimes b_{2g}$  Jahn-Teller problem [28] electrons occupying orbitals of sym-

metry  $E_g$  generate IrReps  $E_g \otimes E_g = A_{1g} \oplus \{A_{2g}\} \oplus B_{1g} \oplus B_{2g}$ , the branching space must be formed from those modes that break the symmetry of the system,  $b_{1g}$  and  $b_{2g}$  (modes  $\tilde{v}_1$  and  $\tilde{v}_9$ ). The vibronic coupling model potential describing this branching space is written succinctly:

$$V_{CI} = \frac{1}{2} \left( \sum_j^2 \omega^2 q_j^2 \right) + \begin{pmatrix} -\alpha q_1 & \beta q_2 \\ \beta q_2 & \alpha q_1 \end{pmatrix} \quad (4.1)$$

borne out of arguments akin to those seen in chapter 5 ( $q_1$  and  $q_2$  refer to modes  $\tilde{v}_1$  and  $\tilde{v}_9$  respectively) Stabilisation of the neutral molecule occurs via pseudo-Jahn Teller coupling along mode  $\tilde{v}_1$  (see Figs 4.6 and 4.4). Since this geometry is not the ground state global minima, it is worth considering the space correlating normal coordinates which stabilise the molecule to a rectangular geometry. Bi-linear corrections to the cation, degenerate states are allowed along JT modes correlating modes of  $a_{1g}$  or  $b_{1g}$  symmetry. For the neutral states only modes of  $b_{1g}$  symmetry correlate these JT modes with symmetry allowed bi-linear terms.

Figures 4.4 and 4.5 show cuts of the fitted model along ten DOF for which either anharmonicity or surfaces which

break the cation state degeneracy. Fitting was done using the Genetic Algorithm described in chapter 3. These are either  $e_g$  modes, branching space

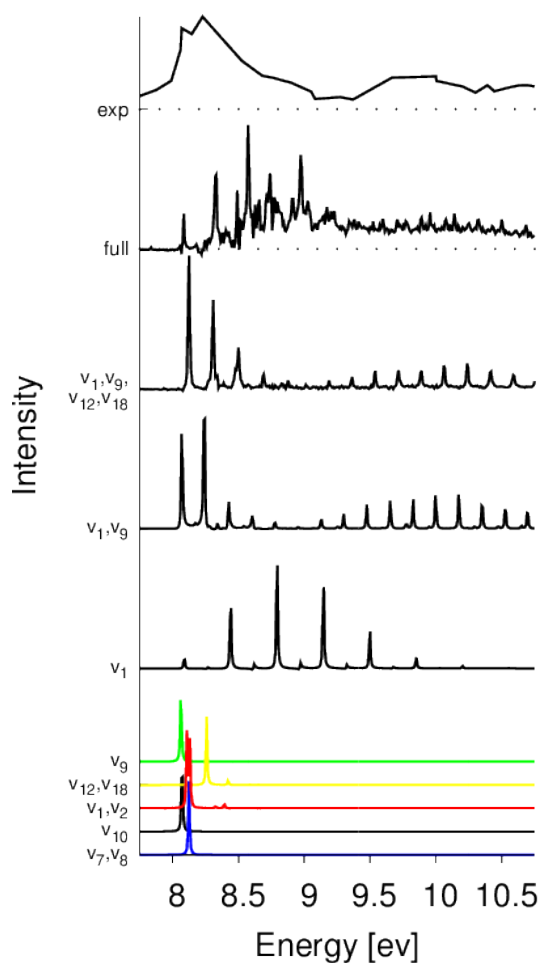


Fig. 4.2: Calculated photo-electron spectra with different reduced dimensionality models.

modes or totally symmetric modes. Cuts showing some correlated DOF are also shown. Contour plots of the branching space coordinates as well as the contour plots for the space of  $b_{1g}$ , modes  $\tilde{v}_1$  and  $\tilde{v}_{10}$  are shown in Fig 4.6. Only these two modes showed interesting behaviour beyond a zeroth order model. By minimising our model potential, some geometries obtained for different critical structures are given in tables 4.1-4.3. Geometries obtained in this model, as well as vertical excitation energies from these, are comparable to those in the literature and given in tables 4.5 and 4.6. From the cut along  $\tilde{v}_9$  neutral CBD, we can see a double well minima, agreeing with previous work regarding the rhomboidal geometry of  $S_1$  (see introduction and table 4.2) and not apparent at the CASSCF(4,4) level. The MCTDH operator file for model presented here is provided in supplementary information c. To obtain the spectra, we propagated a wave-packet in imaginary time ( $\sim 200$  fs) using the MCTDH relaxation method to obtain the ground state energy relaxed wavefunction. In the diabatic representation, the relaxed wavefunction is spread through the first three excited states. For the 10-mode model, the populations are 0.7392 ( $S_0$ ), 0.2606 ( $S_1$ ), 0.0002 ( $S_2$ ). This is caused principally by linear coupling between  $S_0$  and  $S_1$  along  $\tilde{v}_1$ , and  $S_1$  and  $S_2$  along  $\tilde{v}_9$  (branching space). The ground state wavefunction relaxes with an maximum amplitude around the double well in  $\tilde{v}_1$ , which undoubtedly determines much of the dynamical behaviour and spectra of CBD. This relaxed, 3-state wavefunction is projected evenly to both cation states and propagated for 500 fs. To help us unweave the final spectra, a collection reduced dimensionality models where also constructed and their theoretical spectrum calculated. The results of these propagations are shown in Fig 4.2.

### 4.3 Discussion and conclusions

The final spectra have a very poor resemblance to the experimentally recorded ones; the onset of peaks starts very progressively and it has a very broad tail, with line spacings poorly matching experimental ones. Better results are obtained by only including the branching space and totally symmetric coordinates. The

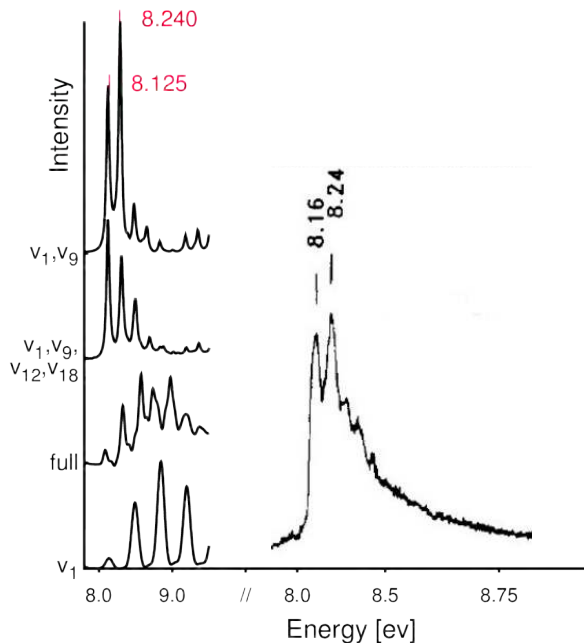


Fig. 4.3: Comparison between experimental spectra [58] and model spectra.

best result, like Saddique and Worth [53] before us, was obtained when we only propagated along the branching space. It would seem the most salient features of the spectra arise from this space, giving rise to bands around 8-8.5 and 9.5-10.5 eV. Figure 4.3 compares the TOF photoelectron spectra [58] with the obtained model spectra in the range available. Note that the spectra have a non-linear scaling of the energy axis, thereby showing only the 8-9 eV region. Figure 4.2 shows a spectrum at a higher temperature obtained through subtraction of the benzene spectra but covering a larger energy range. We can see a second shoulder arising, previously assigned by the authors (using MNDO methods) to a higher lying ion state. No theoretical work has previously made comments on the bands appearing at energies around 9.5-10.5 eV. We propose the origin of the second band to also be caused by population onto these  $E_g$  states. Although spectra and surfaces of  $e_g$  degenerate modes  $\tilde{v}_{7,8}$  and  $\tilde{v}_{2,3}$  are harmonic and simple, they had a significant effect on the final

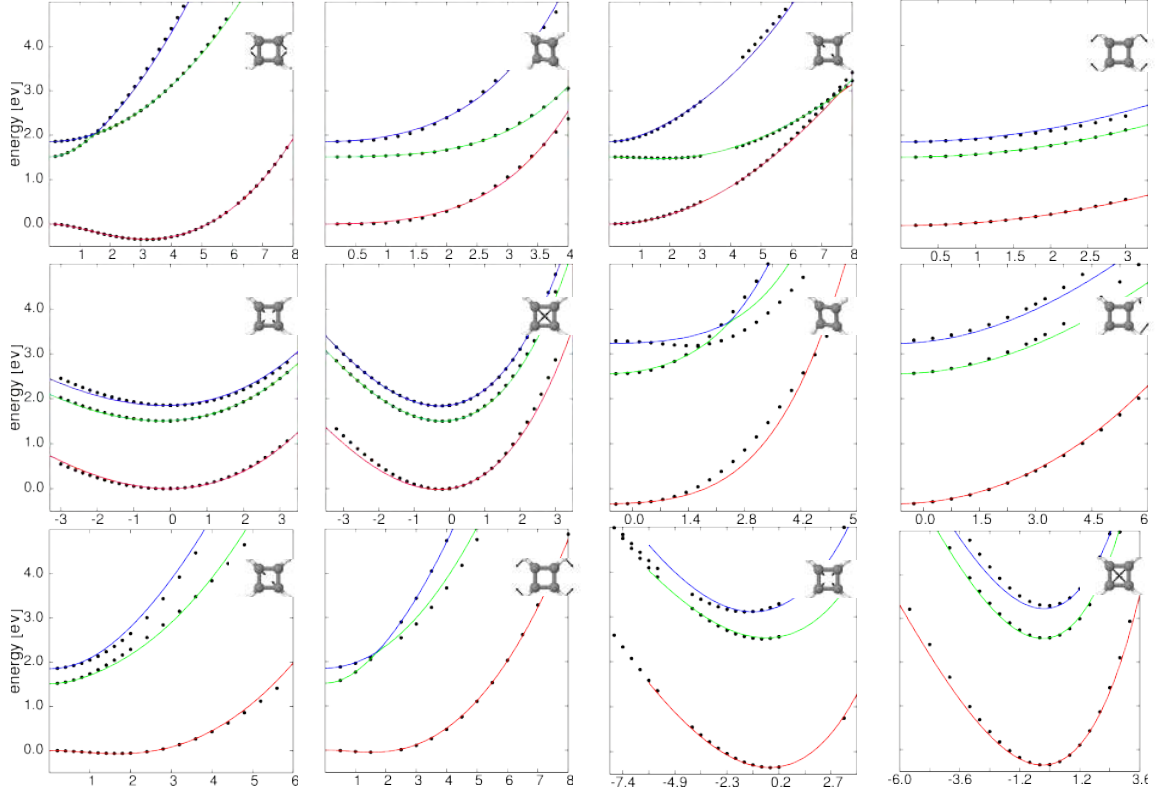


Fig. 4.4: Fitting of CBD 3 state model to normal (dimensionless) coordinates.  $\{\tilde{v}_1\}$  means  $\tilde{v}_1$  is kept constant at its minimum geometry (value  $\sim 3$ ), while the other coordinate is displaced. From left to right:  
*first row:*  $\tilde{v}_1, \tilde{v}_2, \tilde{v}_9, \tilde{v}_{10}$  ; *second row:*  $\tilde{v}_{12}, \tilde{v}_{18}, \{\tilde{v}_1\}+\tilde{v}_2, \{\tilde{v}_1\}+\tilde{v}_7$   
*third row:*  $\tilde{v}_1+\tilde{v}_9, \tilde{v}_1+\tilde{v}_{10}, \{\tilde{v}_1\}+\tilde{v}_{12}, \{\tilde{v}_1\}+\tilde{v}_{18}$

aspect of the 10-dimensional spectra. In hindsight, the JT-theorem dictates these states should form a peaked intersection, forming part of the branching space. However, a gradient and coupling terms like those of equation 4.1 were not included in the model, instead the simple condition the parameters determining these modes should swap the state identity. Although these terms may seem to constitute a small correction (based on the cuts shown), they may have contributed to the poor overall 10-dimensional model spectra. We echo the conclusions of reference [53] regarding the electronic structure methods giving poor energy surfaces, but we suggest PT2 corrections are not yet sufficient to match the experimental line spacing. Instead, more accurate methods like some given in the tables here provided should be necessary.

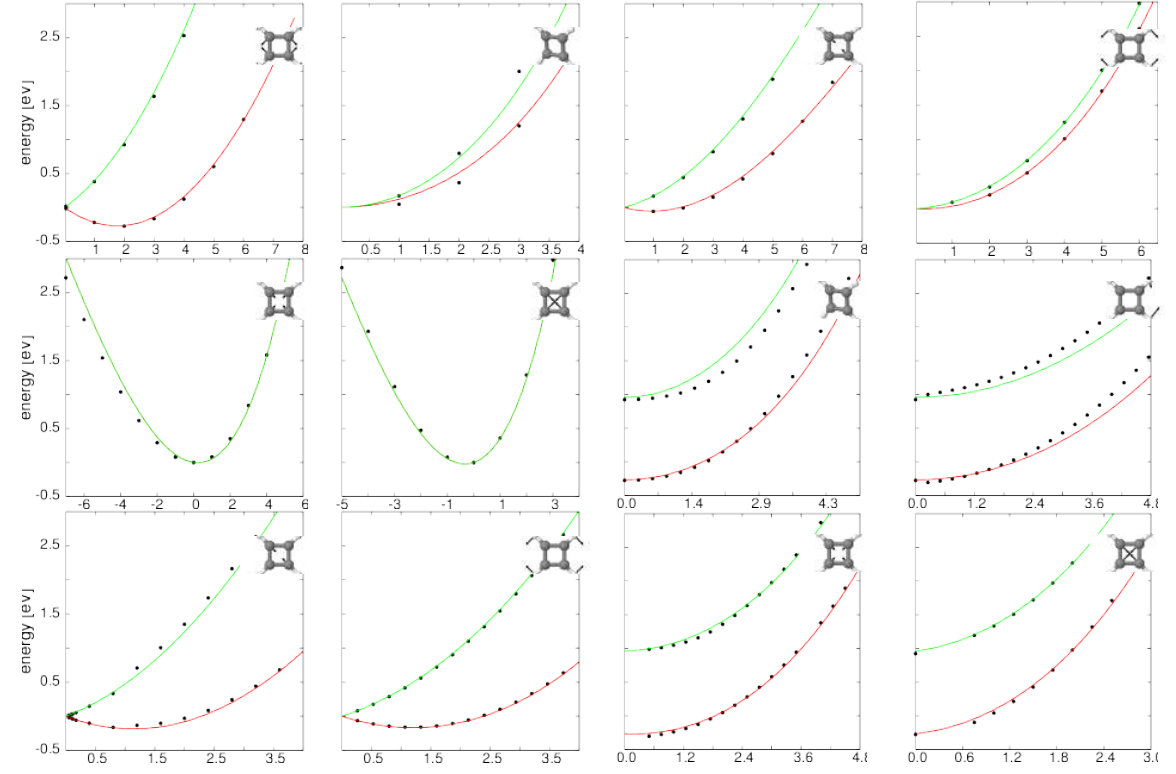


Fig. 4.5: Fitting of CBD<sup>+</sup> 2 state model to normal (dimensionless) coordinates.  $\{\tilde{v}_1\}$  means  $\tilde{v}_1$  is kept constant at its minimum geometry (value  $\sim 2$ ), while the other coordinate is displaced. From left to right: *first row*:  $\tilde{v}_1, \tilde{v}_2, \tilde{v}_9, \tilde{v}_{10}$  ; *second row*:  $\tilde{v}_{12}, \tilde{v}_{18}, \{\tilde{v}_1\}+\tilde{v}_2, \{\tilde{v}_1\}+\tilde{v}_7$  ; *third row*:  $\tilde{v}_1+\tilde{v}_9, \tilde{v}_1+\tilde{v}_{10}, \{\tilde{v}_1\}+\tilde{v}_{12}, \{\tilde{v}_1\}+\tilde{v}_{18}$

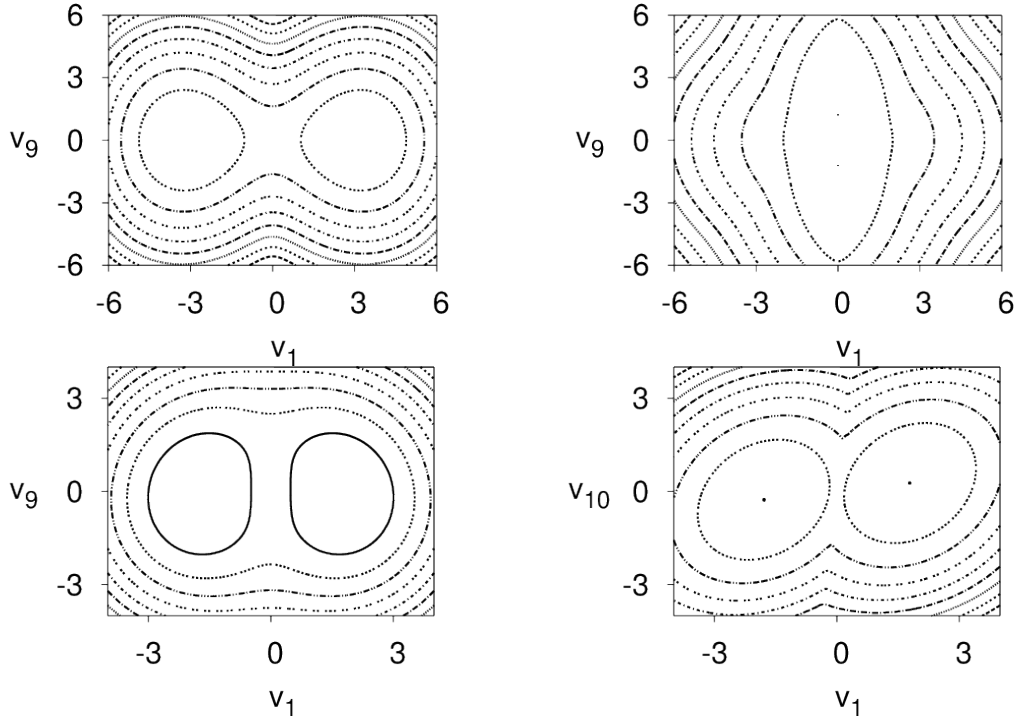


Fig. 4.6: Contour plots. *from left to right*: *first row*: CBD S<sub>0</sub> along branching space  $\tilde{v}_1(x), \tilde{v}_9(y)$ , CBD S<sub>1</sub> along branching space  $\tilde{v}_1(x), \tilde{v}_9(y)$  ; *second row*: CBD S<sub>0</sub> along  $b_1 \tilde{v}_1(x), \tilde{v}_9(y)$ , CBD<sup>+</sup> S<sub>1</sub> along  $b_1 \tilde{v}_1(x), \tilde{v}_{10}(y)$











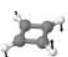







#	D <sub>4h</sub>	D <sub>2h</sub>	e-vector	$\omega(cm^{-1})$	#	D <sub>4h</sub>	D <sub>2h</sub>	e-vector	$\omega(cm^{-1})$
$\tilde{\nu}_1$	b <sub>1g</sub>	a <sub>g</sub>		-1421.05	$\tilde{\nu}_{10}$	b <sub>1g</sub>	a <sub>g</sub>		1162.04
$\tilde{\nu}_2$	e <sub>g</sub>	b <sub>2g</sub>		391.25	$\tilde{\nu}_{11}$	a <sub>2g</sub>	b <sub>1g</sub>		1319.62
$\tilde{\nu}_3$	e <sub>g</sub>	b <sub>3g</sub>		391.25	$\tilde{\nu}_{12}$	a <sub>1g</sub>	a <sub>g</sub>		1326.89
$\tilde{\nu}_4$	a <sub>2u</sub>	b <sub>1u</sub>		497.00	$\tilde{\nu}_{13}$	e <sub>u</sub>	b <sub>3u</sub>		1457.30
$\tilde{\nu}_5$	b <sub>1u</sub>	a <sub>u</sub>		498.19	$\tilde{\nu}_{14}$	e <sub>u</sub>	b <sub>2u</sub>		1457.30
$\tilde{\nu}_6$	b <sub>1u</sub>	a <sub>u</sub>		600.22	$\tilde{\nu}_{15}$	b <sub>2g</sub>	b <sub>1g</sub>		3421.83
$\tilde{\nu}_7$	e <sub>u</sub>	b <sub>2u</sub>		996.53	$\tilde{\nu}_{16}$	e <sub>u</sub>	b <sub>3u</sub>		3437.85
$\tilde{\nu}_8$	e <sub>u</sub>	b <sub>3u</sub>		996.53	$\tilde{\nu}_{17}$	e <sub>u</sub>	b <sub>2u</sub>		3437.85
$\tilde{\nu}_9$	b <sub>2g</sub>	b <sub>1g</sub>		1018.45	$\tilde{\nu}_{18}$	a <sub>1g</sub>	a <sub>g</sub>		3460.98

Table 4.8: D<sub>4h</sub> Harmonic frequencies of neutral cyclo-butadiene obtained at the CASSCF(4,4)+MP2 frequencies with a 6-31G\* basis set level of theory.



# Chapter 5

## Non-Abelian Symmetry in Vibronic Coupling Models

### 5.1 Introduction

For a model Hamiltonian to correctly approximate the eigenvectors of the true Hamiltonian they have to span the totally symmetric irreducible representation (IrRep) of the point groups the molecule belongs to, at the appropriate symmetric geometries [24]. We present an approach for generating polynomial bases over diabatic elements spanning the totally symmetric irreducible representation (IrRep) of any point group. Such symmetry-adapted bases are of special interest in the case of non-Abelian groups and here we present as examples the  $\mathbf{O}$  and  $D_{\infty h}$  groups.

Molecules that belong to either of these groups will exhibit Jahn-Teller and Renner-Teller effects respectively. The Jahn-Teller (JT) effect occurs when a molecule in a high-symmetry configuration has degenerate electronic states. Vibronic coupling leads to a conical intersection being formed at the high symmetry point which removes the degeneracy away from this point. The result is a lowering of symmetry of the system. In the most common case, doubly degenerate states interact with doubly degenerate vibrations to form the well-known “mexican hat” potential. The Renner-Teller (RT) effect is a special case that happens in linear molecules. Due to symmetry

considerations a glancing intersection rather than a conical intersection is formed [28].

To generate the  $D_{\infty h}$  basis we followed a similar approach to Viel and Eisfeld [69], who generated a basis up to sixth order for  $E \otimes e$  Jahn-Teller Hamiltonians. This basis was fitted to the  ${}^2E'$  anharmonic surfaces along twofold  $e'$  stretches of  $\text{NO}_3$  obtained from *ab initio* MR-SDCI calculations. They demonstrate that wavefunctions propagated on models built by the inclusion of extra *ad-hoc*, symmetry non-allowed polynomial functions do not match the expectation value, population transfer and autocorrelation of wavefunctions obtained from the  $E \otimes e$  Jahn-Teller basis alone. This work was followed by the generation of a basis properly describing pseudo Jahn-Teller (pJT) coupling between  $E$  degenerate states to nondegenerate  $A$  states [70]. They tested this basis on the pJT coupling between the ground state  ${}^2A_2''$  and excited  ${}^2E'$  state along the twofold  $e$  bending mode surfaces of cation  $\text{NH}_3^+$  obtained from *ab initio* MRCI calculations. A large decrease in fitting error was obtained as higher order terms were included.

For the  $\mathbf{O}$  group, we used a basis generating operator, devised by Wigner, Lowdin and Shapiro, amongst others [71]. This is a well known method for generating symmetry-adapted functions and only briefly presented here.

## 5.2 Generating symmetry-adapted basis

### 5.2.1 Basis generating operator

A given function from a set of  $n_v$  orthonormal basis functions  $f_1^v, f_2^v, f_3^v, \dots, f_{n_v}^v$  spanning the space of IrRep  $v$  in a group with  $k$  classes, under a given operation  $\mathbf{R}$  of the group, must satisfy:

$$\mathbf{O}_R f_q^v = \sum_{p=1}^{n_v} D_{pq}^v(R) f_p^v \quad q = 1, 2, \dots, n_v, \quad v = 1, 2, \dots, k \quad (5.1)$$

where  $D_{pq}^v(R)$  is the matrix representation of operation  $\mathbf{R}$  on IrRep  $v$ . Operating further on the above expression by the sum of all operations  $\mathbf{R}$  of some arbitrary IrRep of the group  $\sum_R D_{ij}^\mu(R)$  we get:

$$\begin{aligned} \sum_R D_{ij}^\mu(R) \cdot \mathbf{O}_R f_q^v &= \sum_{p=1}^{n_v} \sum_R D_{ij}^\mu(R) \cdot D_{pq}^v(R) f_p^v \\ &= (g/n_\mu) \delta_{v\mu} \delta_{jq} f_i^v \end{aligned} \quad (5.2)$$

owing to the great orthogonality theorem:

$$\sum_R D_{ij}^\mu(R) D_{pq}^v(R) = (g/n_\mu) \delta_{v\mu} \delta_{jq} \quad (5.3)$$

In other words, operating with  $\sum_R D_{ij}^\mu(R) \cdot \mathbf{O}_R$  on a basis function  $f_q^v$  will generate another basis function  $f_i^v$  of the same IrRep or else annihilate the function (if  $v \neq \mu$ ).

A second operator can be constructed by choosing  $i = j$  and summing over  $j$ :

$$\sum_i \sum_R D_{ii}^\mu(R) \cdot \mathbf{O}_R = \sum_R \chi^\mu(R) \cdot \mathbf{O}_R = \mathbf{P}^\mu \quad (5.4)$$

This operator  $\mathbf{P}^\mu$  has the property of annihilating any function that does not belong to the  $\mu$ th IrRep space, or else project out any function which does. With both these operators it is therefore possible, starting with an arbitrary function within the  $\mu$ th space, to generate the complete set of orthonormal functions belonging to this IrRep. To generate the totally symmetric IrReps of the group, it is therefore only necessary to utilise the latter operator.

To generate all polynomials described here we used the open-source mathematics software SAGE [72].

### 5.2.2 $D_{\infty h}$ Renner-Teller symmetry-adapted basis

There are an infinite number of possible gerade/ungerade  $E_n$  IrReps indexed by  $n$  where  $\alpha = \frac{\pi}{n}$ ,  $\alpha$  being the angle of the  $C_\alpha$  rotation required to interchange any two real basis functions forming a twofold degenerate representation of this group.

The dominant contribution of the first few singlet excited states of organic molecules tend to be from functions with low orbital angular momentum. For linear organic molecules we therefore expect that the low singlet states, being formed from  $\pi$  and  $\sigma$  functions built of  $l = d$ -type functions would result in electronic states forming a representation for low  $n$  representations. Similarly, it is rare to find a full orthonormal set of coordinates with high  $n$  index number for small molecules (for example, it can be shown that normal coordinates do not exceed  $\Pi$  symmetry [24]).

Given these considerations, we will restrict our construction of a symmetry-adapted basis by solely using functions that form a basis for  $\Sigma^{+/-}$ ,  $\Pi_{u/g}$  and  $\Delta_{u/g}$  IrReps ( $A_n$  and  $E_n$  for  $n = 1, 2$ ) to represent diabatic states and only  $\Pi_{u/g}$  functions to represent nuclear coordinates.

The resulting polynomials have been used in the construction of an 10-state 7-dimensional diabatic model describing the vibrationally mediated dissociation of acetylene. Details of the model and dynamical calculations are the subject of chapter 6.

Herzig and Altmann have published the most comprehensive book of point group tables to date [73]. One can use spherical harmonic functions to form a representation of any point group. They provide the matrix representations of the  $\Pi_{g/u}$  and  $\Delta_{u/g}$  IrReps for all the operations of the group, in the complex symmetrised spherical harmonic basis:

$$\begin{aligned}\Pi_u &:= (\Pi_u^+, \Pi_u^-) = \langle Y_1^1, Y_1^{-1} | \\ \Pi_g &:= (\Pi_g^+, \Pi_g^-) = \langle Y_2^1, -Y_2^{-1} | \\ \Delta_g &:= (\Delta_g^+, \Delta_g^-) = \langle Y_2^2, Y_2^{-2} | \\ \Delta_u &:= (\Delta_u^+, \Delta_u^-) = \langle Y_2^3, -Y_3^{-2} |\end{aligned}\tag{5.5}$$

where  $Y_l^m$  are the ortho-normalised spherical harmonics using the Condon-Shortley phase convention [73]. The corresponding real Cartesian basis func-

tions forming the same representation are related by (ignoring normalisation factors):

$$\begin{aligned}
 Y_1^1 &= -(x + i \cdot y) & Y_1^{-1} &= (x - i \cdot y) \\
 Y_2^1 &= -(zx + i \cdot yz) & Y_2^{-1} &= (zx - i \cdot yz) \\
 Y_2^2 &= (x^2 - y^2 + i \cdot 2xy) & Y_2^{-2} &= (x^2 - y^2 - i \cdot 2xy) \\
 Y_3^2 &= (z(x^2 - y^2) + i \cdot 2xyz) & Y_3^{-2} &= (z(x^2 - y^2) - i \cdot 2xyz)
 \end{aligned} \tag{5.6}$$

One advantage of working in the complex representation is immediately apparent from the tables: every operation reduces itself to a permutation operation multiplied by a factor. Another is that our basis functions for each IrRep are complex conjugates of one another, from which we can deduce that the on-diagonal Hamiltonian elements are equal and real and that some elements in the upper-triangular elements are complex conjugates of one another. For example:

$$\frac{\partial \langle \Sigma_g^+ | \hat{H} | \Pi_u^+ \rangle}{\partial Q_{\Delta_u^+}} = \left( \frac{\partial \langle \Sigma_g^+ | \hat{H} | \Pi_u^- \rangle}{\partial Q_{\Delta_u^-}} \right)^* \tag{5.7}$$

The above relation implies that the Taylor coefficients of such Hamiltonian elements are related. Fig 5.2 shows the relationship between elements of states of symmetries pertinent to this work.

Given that operations like  $\sigma_v(\phi)$  have the effect of permuting the complex conjugate basis pair in the 2D IrReps (see tables in reference [73] or in table 5.2 in sub-Appendix 5.A), any invariant expression (totally symmetric) must be constructed from some linear combination of some polynomial element with its permuted (complex conjugate) counterpart. Concretely, for a term such as

$$|\Pi_{u^+}\rangle (Q_{\Sigma_g^+})^n \cdot (Q_{\Delta_g^+})^m \langle \Sigma_u^- | \tag{5.8}$$

to be invariant it must be part of the totally symmetric combination

$$\begin{aligned}
 P^{\pi_u^+, \sigma_u^+}(Q_\pi, Q_\sigma) &= |\Pi_{u^+}\rangle (Q_{\Sigma_g^+})^n \cdot (Q_{\Delta_g^+})^m \langle \Sigma_u^- | + \\
 &|\Pi_{u^-}\rangle (Q_{\Sigma_g^+})^n \cdot (Q_{\Delta_g^-})^m \langle \Sigma_u^- |
 \end{aligned} \tag{5.9}$$

where operating with any arbitrary operator of the point group  $O_R$ ;

$$\begin{aligned} \hat{O}_R P^{\pi_u^+, \sigma_u^+}(Q_\pi, Q_\sigma) = \\ \Lambda_f^R(\Pi_u^+, (\Sigma_g^+)^n, (\Delta_g^+)^m, (\Sigma_u^-)^*) |\Pi_u^+\rangle (Q_{\Sigma_g^+})^n \cdot (Q_{\Delta_g^+})^m \langle \Sigma_u^-| + \\ \Lambda_g^R(\Pi_u^-, (\Sigma_g^+)^n, (\Delta_g^-)^m, (\Sigma_u^-)^*) |\Pi_u^-\rangle (Q_{\Sigma_g^+})^n \cdot (Q_{\Delta_g^-})^m \langle \Sigma_u^-| \end{aligned} \quad (5.10)$$

where  $\Lambda_f^R$  and  $\Lambda_g^R$  are the products of factors from each IrRep making up the element, obtained from operating with the matrices given in the  $D_{\infty h}$  tables found in Herzog and Altmann (or table 5.1 in sub-Appendix 5.A). Since each term has to give a factor +1 for the expression above to be totally symmetric, and both terms are complex conjugates of each other, it follows that it is only necessary to test either  $\Lambda^R$  in order to test for invariance. A similar approach was devised by Eisfeld and Viel [69, 70] for Jahn-Teller systems.

Using the projection operator formalism is one possible approach. It is, however, unnecessary as starting with one of the terms in the expression, it is straightforward to see how the operator would construct the totally symmetric bases by operating with  $\sigma_v(\phi)$  and adding both terms (times the appropriate eigenvalue factor). Finally, to obtain real polynomials and states for our model diabatic potential one is required to rotate to a real basis:

$$\begin{pmatrix} \Pi_g^+ \\ \Pi_g^- \end{pmatrix} = \frac{1}{\sqrt{2}} \begin{pmatrix} -1 & -i \\ -1 & +1 \end{pmatrix} \begin{pmatrix} \Pi_g^x \\ \Pi_g^y \end{pmatrix} \quad \begin{pmatrix} \Pi_u^+ \\ \Pi_u^- \end{pmatrix} = \frac{1}{\sqrt{2}} \begin{pmatrix} -1 & -i \\ -1 & +1 \end{pmatrix} \begin{pmatrix} \Pi_u^x \\ \Pi_u^y \end{pmatrix} \quad (5.11)$$

$$\begin{pmatrix} \Delta_g^+ \\ \Delta_g^- \end{pmatrix} = \frac{1}{\sqrt{2}} \begin{pmatrix} +1 & +i \\ +1 & -1 \end{pmatrix} \begin{pmatrix} \Delta_g^x \\ \Delta_g^y \end{pmatrix} \quad \begin{pmatrix} \Delta_u^+ \\ \Delta_u^- \end{pmatrix} = \frac{1}{\sqrt{2}} \begin{pmatrix} +1 & +i \\ -1 & +1 \end{pmatrix} \begin{pmatrix} \Delta_u^x \\ \Delta_u^y \end{pmatrix} \quad (5.12)$$

where  $\Pi_{u/g}^{x/y}$  and  $\Delta_{g/u}^{x/y}$  are a shorthand notation for the real, Cartesian basis functions. Appendix A lists the polynomial elements generated in this way up to sixth order. One can easily generate polynomials of higher order. This basis is used in chapter 6 to construct a 4-dimensional sub-space of coordinates exhibiting strong Renner-Teller and pseudo Jahn-Teller coupling.

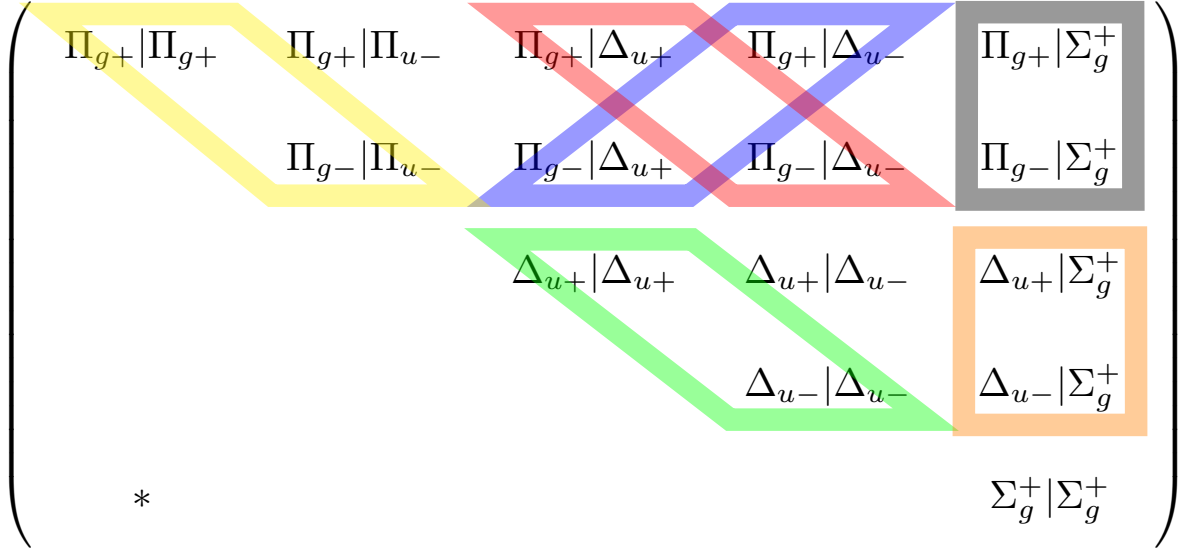


Fig. 5.1: Depicting which elements of the diabatic potential matrix in the complex representation given in Eq. 5.5 share relationships; along the diagonal they are equal and real; off diagonal are complex conjugates. Identical relationships are shared between the other u/g,+/- IrReps.

### 5.2.3 $O$ (3D) Jahn-Teller symmetry-adapted basis

The strategy described above breaks down for the case of 3-dimensional non-Abelian groups, where the operations of the group become harder to disentangle; in the available representation [73], operations permute one basis in the subspace onto either one or two others, multiplied by some complex factor. Therefore, the possible number of terms that make up the invariant expression increase (unlike  $D_{\infty h}$  with a predictable number of 2 terms). Here we take recourse to the projection operator. Although it should be mentioned that other, more general techniques have been devised to generate  $T_2$  related polynomials [74].

The complex matrix representations for the  $O$  group were obtained from Herzog and Altmann. They use the following representation in the symmetrised spherical harmonic basis (matrices given in ref. [73] or sub-Appendix

B):

$$\begin{aligned}
T_1 &:= (T_{1+}, T_{1z}, T_{1-}) = \langle \frac{1}{\sqrt{2}}(Y_1^1 + Y_1^{-1}), Y_1^0, \frac{1}{\sqrt{2}}(Y_1^1 - Y_1^{-1}) | \\
E &:= (E_+, E_-) = \langle \frac{1}{\sqrt{2}}Y_2^0 - \frac{i}{\sqrt{2}}(Y_2^2 + Y_2^{-2}), \frac{1}{\sqrt{2}}Y_2^0 + \frac{i}{\sqrt{2}}(Y_2^2 + Y_2^{-2}) |
\end{aligned} \tag{5.13}$$

which relate to the cartesian tensor basis (ignoring common factors) as:

$$\begin{aligned}
x &= -(Y_1^1 - Y_1^{-1}) & 2z^2 - x^2 - y^2 &= Y_2^0 \\
y &= (Y_1^1 + Y_1^{-1})i & x^2 - y^2 &= \frac{1}{\sqrt{6}}(Y_1^1 + Y_1^{-1}) \\
z &= \sqrt{2}Y_1^0
\end{aligned} \tag{5.14}$$

so that the unitary matrices to the real representation are given by:

$$\begin{aligned}
\begin{pmatrix} T_+ \\ T_z \\ T_- \end{pmatrix} &= \frac{1}{\sqrt{2}} \begin{pmatrix} -i & 0 & 0 \\ 0 & 1 & 0 \\ 0 & 0 & -1 \end{pmatrix} \begin{pmatrix} T_y \\ T_z \\ T_x \end{pmatrix} \\
\begin{pmatrix} E_+ \\ E_- \end{pmatrix} &= \frac{1}{\sqrt{2}} \begin{pmatrix} 1 & -\sqrt{3}i \\ 1 & +\sqrt{3}i \end{pmatrix} \begin{pmatrix} E_y \\ E_x \end{pmatrix}
\end{aligned} \tag{5.15}$$

where  $E_{x/y}$  and  $T_{y/x}$  are shorthands for the appropriate Cartesian tensors given in Eq. 5.14. The projection operator is expensive to construct given that we need to add all polynomials generated by operating with all 24 operators on a single generating function. For IrReps  $T_1$ ,  $E$  and  $A_1$  (6 functions) testing all possible terms such as  $|a\rangle Q_b^i \cdot Q_c^j \cdot Q_d^k |e\rangle$  would mean that we could construct up to, say fourth order  $\sim 15000$  combinations.

It is therefore desirable to find a more efficient way of discriminating terms without immediate recourse to the projection operator. We decrease this number drastically if we can work in the representation which reduces the operation to a multiplicative factor. For the  $E$  IrRep, we already have such a representation available (one for which all operations are in their eigenvector representation). For  $T_1$ , we could achieve a similar result by switching to the representation of the eigenfunctions of some operator of the group whose eigenvalues are preferably distinct.



To clarify, consider  $T_1$  under the representation of the eigenvectors of  $C_{31}^+$ , which belongs to the class of operators with eigenvalues  $(e^{\frac{+i\pi}{3}}, e^{\frac{-i\pi}{3}}, 1)$ . The effect of operating with  $C_{31}^+$  on any term such as  $|a\rangle Q_b^i \cdot Q_c^j \cdot Q_d^k \langle e|$  will simply be to multiply out the product of eigenvalues of the different terms forming the element. For a given sum  $A + B$ , where  $A$  and  $B$  are terms like the aforementioned, to be totally symmetric both  $A$  and  $B$  separately have to give  $+1$  factors. If such a product gives  $+1$  we can consider it to potentially form part of a totally symmetric polynomial. This way, all possible combinations of terms are easily trimmed into a constellation of terms that satisfy these more stringent conditions. Under such a representation, we also obtain an analogous set of relationships between elements to those seen in  $D_{\infty h}$  (i.e. Fig 5.2). Under this eigenvector representation we therefore further cut the number of elements we need to test. For those terms that survive, we can rotate back using the eigenvector matrix:

$$\begin{pmatrix} T_{\lambda+} \\ T_{\lambda-} \\ T_0 \end{pmatrix} = \frac{1}{\sqrt{3}} \begin{pmatrix} 1 & e^{\frac{+i\pi}{3}} & e^{\frac{-i\pi}{3}} \\ 1 & e^{\frac{-i\pi}{3}} & e^{\frac{+i\pi}{3}} \\ -1 & 1 & 1 \end{pmatrix} \begin{pmatrix} T_+ \\ T_- \\ T_z \end{pmatrix} \quad (5.16)$$

Once back in this representation we can use the projection operator method to reconstruct any totally symmetric polynomial elements that might be possible from this subset.

Appendix B lists the polynomial elements generated in this way up to third order between  $\{A_g, E, T_1\}$  states and modes. For practical reasons, only three dimensional complex polynomials were tested to generate it; this guarantees all three dimensional terms possible.

## 5.3 Conclusions

We have presented two strategies to generate symmetry-adapted bases of real polynomials representing nuclear coordinates over electronic diabatic

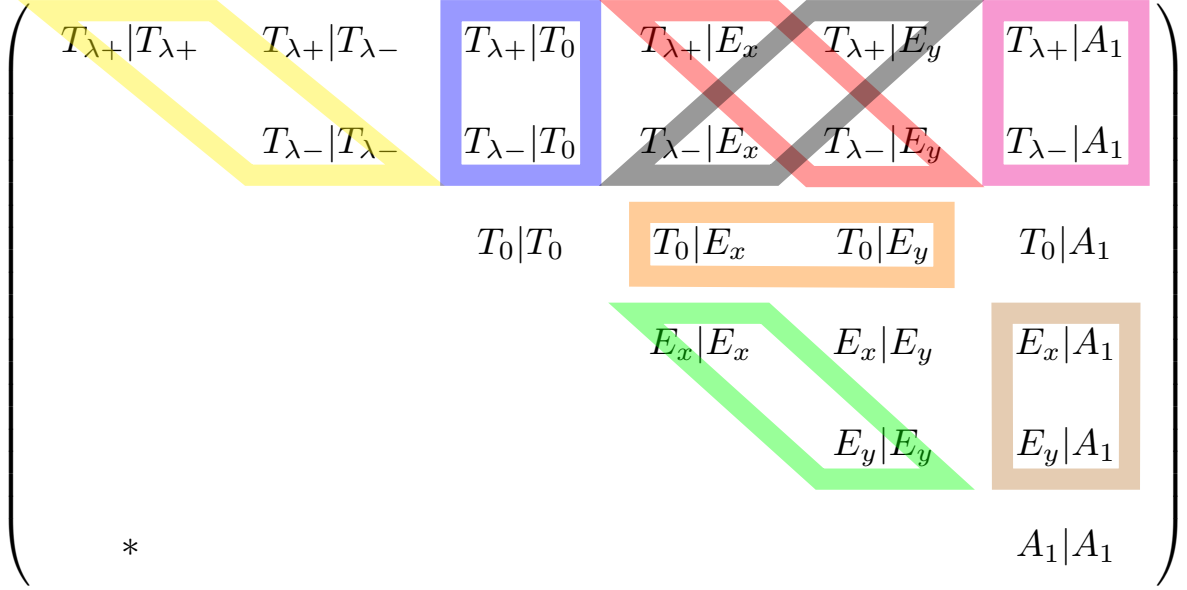


Fig. 5.2: Depicting which elements of the diabatic potential matrix in the complex representation given in Eq. 5.13 share relationships; along the diagonal they are equal and real; off diagonal elements are complex conjugates.

Elements that are invariant with respect to non-Abelian point group operations. The two cases for which we generated these bases are the  $D_{\infty h}$  and  $\mathbf{O}$ , but this approach should work for any group. Working in the simplest representation, i.e. the complex representation of the eigenvectors of the operators of the group, and the use of the projection operator where two indispensable tools used to make the generation of these polynomials tractable.

## 5.A Tables of matrix representation of symmetry operations for $D_{\infty h}$ and $O$ in a symmetrised spherical harmonic basis.

$D_{\infty h}$	$\Pi_u$	$\Pi_g$	$\Delta_g$	$\Delta_u$
E	$\begin{bmatrix} 1 & 0 \\ 0 & 1 \end{bmatrix}$	$\begin{bmatrix} 1 & 0 \\ 0 & 1 \end{bmatrix}$	$\begin{bmatrix} 1 & 0 \\ 0 & 1 \end{bmatrix}$	$\begin{bmatrix} 1 & 0 \\ 0 & 1 \end{bmatrix}$
$C_{\infty}^+(\psi)$	$\begin{bmatrix} e^{-i\psi} & 0 \\ 0 & e^{i\psi} \end{bmatrix}$	$\begin{bmatrix} e^{-i\psi} & 0 \\ 0 & e^{i\psi} \end{bmatrix}$	$\begin{bmatrix} e^{-2i\psi} & 0 \\ 0 & e^{2i\psi} \end{bmatrix}$	$\begin{bmatrix} e^{-2i\psi} & 0 \\ 0 & e^{2i\psi} \end{bmatrix}$
$C_{\infty}^-(\psi)$	$\begin{bmatrix} e^{i\psi} & 0 \\ 0 & e^{-i\psi} \end{bmatrix}$	$\begin{bmatrix} e^{i\psi} & 0 \\ 0 & e^{-i\psi} \end{bmatrix}$	$\begin{bmatrix} e^{2i\psi} & 0 \\ 0 & e^{-2i\psi} \end{bmatrix}$	$\begin{bmatrix} e^{2i\psi} & 0 \\ 0 & e^{-2i\psi} \end{bmatrix}$
$C_2$	$\begin{bmatrix} -1 & 0 \\ 0 & -1 \end{bmatrix}$	$\begin{bmatrix} -1 & 0 \\ 0 & -1 \end{bmatrix}$	$\begin{bmatrix} 1 & 0 \\ 0 & 1 \end{bmatrix}$	$\begin{bmatrix} 1 & 0 \\ 0 & 1 \end{bmatrix}$
$\sigma_v(\phi)$	$\begin{bmatrix} 0 & e^{-2i\phi} \\ e^{2i\phi} & 0 \end{bmatrix}$	$\begin{bmatrix} 0 & -e^{-2i\phi} \\ -e^{2i\phi} & 0 \end{bmatrix}$	$\begin{bmatrix} 0 & e^{-4i\phi} \\ e^{4i\phi} & 0 \end{bmatrix}$	$\begin{bmatrix} 0 & -e^{-4i\phi} \\ -e^{4i\phi} & 0 \end{bmatrix}$
$\sigma_h$	$\begin{bmatrix} 1 & 0 \\ 0 & 1 \end{bmatrix}$	$\begin{bmatrix} -1 & 0 \\ 0 & -1 \end{bmatrix}$	$\begin{bmatrix} 1 & 0 \\ 0 & 1 \end{bmatrix}$	$\begin{bmatrix} -1 & 0 \\ 0 & -1 \end{bmatrix}$
$S_{\infty}^+(\psi)$	$\begin{bmatrix} e^{-i\psi} & 0 \\ 0 & e^{i\psi} \end{bmatrix}$	$\begin{bmatrix} -e^{-i\psi} & 0 \\ 0 & -e^{i\psi} \end{bmatrix}$	$\begin{bmatrix} e^{-2i\psi} & 0 \\ 0 & e^{2i\psi} \end{bmatrix}$	$\begin{bmatrix} -e^{-2i\psi} & 0 \\ 0 & -e^{2i\psi} \end{bmatrix}$
$S_{\infty}^-(\psi)$	$\begin{bmatrix} e^{i\psi} & 0 \\ 0 & e^{-i\psi} \end{bmatrix}$	$\begin{bmatrix} -e^{i\psi} & 0 \\ 0 & -e^{-i\psi} \end{bmatrix}$	$\begin{bmatrix} e^{2i\psi} & 0 \\ 0 & e^{-2i\psi} \end{bmatrix}$	$\begin{bmatrix} -e^{2i\psi} & 0 \\ 0 & -e^{-2i\psi} \end{bmatrix}$
i	$\begin{bmatrix} -1 & 0 \\ 0 & -1 \end{bmatrix}$	$\begin{bmatrix} 1 & 0 \\ 0 & 1 \end{bmatrix}$	$\begin{bmatrix} 1 & 0 \\ 0 & 1 \end{bmatrix}$	$\begin{bmatrix} -1 & 0 \\ 0 & -1 \end{bmatrix}$
$C_2'(\phi + \frac{\pi}{2})$	$\begin{bmatrix} 0 & e^{-2i\phi} \\ e^{2i\phi} & 0 \end{bmatrix}$	$\begin{bmatrix} 0 & -e^{-2i\phi} \\ -e^{2i\phi} & 0 \end{bmatrix}$	$\begin{bmatrix} 0 & e^{-4i\phi} \\ e^{4i\phi} & 0 \end{bmatrix}$	$\begin{bmatrix} 0 & -e^{-4i\phi} \\ -e^{4i\phi} & 0 \end{bmatrix}$

Table 5.1: Table of matrix representations of  $D_{\infty h}$  group under the representation given in Eq. 5.5. Contents taken from [ [73]]

Tables of matrix representation of symmetry operations for  $D_{\infty h}$  and  $O$  in a symmetrised spherical harmonic basis. 5.1

O	E	$T_1$	O	E	$T_1$
E	$\begin{bmatrix} 1 & 0 \\ 0 & 1 \end{bmatrix}$	$\begin{bmatrix} 1 & 0 & 0 \\ 0 & 1 & 0 \\ 0 & 0 & 1 \end{bmatrix}$	$S_{4x}^-$	$\begin{bmatrix} 0 & \eta^* \\ \eta & 0 \end{bmatrix}$	$\begin{bmatrix} 0 & \bar{1} & 0 \\ 1 & 0 & 0 \\ 0 & 0 & 1 \end{bmatrix}$
$C_{2x}$	$\begin{bmatrix} 1 & 0 \\ 0 & 1 \end{bmatrix}$	$\begin{bmatrix} 1 & 0 & 0 \\ 0 & \bar{1} & 0 \\ 0 & 0 & \bar{1} \end{bmatrix}$	$S_{4z}^-$	$\begin{bmatrix} 0 & 1 \\ 1 & 0 \end{bmatrix}$	$\begin{bmatrix} 1 & 0 & 0 \\ 0 & 0 & 1 \\ 0 & \bar{1} & 0 \end{bmatrix}$
$C_{2y}$	$\begin{bmatrix} 1 & 0 \\ 0 & 1 \end{bmatrix}$	$\begin{bmatrix} \bar{1} & 0 & 0 \\ 0 & 1 & 0 \\ 0 & 0 & \bar{1} \end{bmatrix}$	$S_{4y}^-$	$\begin{bmatrix} 0 & \eta \\ \eta^* & 0 \end{bmatrix}$	$\begin{bmatrix} 0 & 0 & 1 \\ 0 & 1 & 0 \\ \bar{1} & 0 & 0 \end{bmatrix}$
$C_{2z}$	$\begin{bmatrix} 1 & 0 \\ 0 & 1 \end{bmatrix}$	$\begin{bmatrix} \bar{1} & 0 & 0 \\ 0 & \bar{1} & 0 \\ 0 & 0 & 1 \end{bmatrix}$	$S_{4x}^+$	$\begin{bmatrix} 0 & \eta^* \\ \eta & 0 \end{bmatrix}$	$\begin{bmatrix} 0 & 1 & 0 \\ \bar{1} & 0 & 0 \\ 0 & 0 & 1 \end{bmatrix}$
$C_{31}^-$	$\begin{bmatrix} \eta & 0 \\ 0 & \eta^* \end{bmatrix}$	$\begin{bmatrix} 0 & \bar{1} & 0 \\ 0 & 0 & 1 \\ \bar{1} & 0 & 0 \end{bmatrix}$	$S_{4y}^+$	$\begin{bmatrix} 0 & 1 \\ 1 & 0 \end{bmatrix}$	$\begin{bmatrix} 1 & 0 & 0 \\ 0 & 0 & \bar{1} \\ 0 & 1 & 0 \end{bmatrix}$
$C_{32}^-$	$\begin{bmatrix} \eta & 0 \\ 0 & \eta^* \end{bmatrix}$	$\begin{bmatrix} 0 & 1 & 0 \\ 0 & 0 & \bar{1} \\ \bar{1} & 0 & 0 \end{bmatrix}$	$S_{4z}^+$	$\begin{bmatrix} 0 & \eta \\ \eta^* & 0 \end{bmatrix}$	$\begin{bmatrix} 0 & 0 & \bar{1} \\ 0 & 1 & 0 \\ 1 & 0 & 0 \end{bmatrix}$
$C_{33}^-$	$\begin{bmatrix} \eta & 0 \\ 0 & \eta^* \end{bmatrix}$	$\begin{bmatrix} 0 & \bar{1} & 0 \\ 0 & 0 & \bar{1} \\ 1 & 0 & 0 \end{bmatrix}$	$\sigma_{d1}$	$\begin{bmatrix} 0 & 1 \\ 1 & 0 \end{bmatrix}$	$\begin{bmatrix} 0 & 0 & \bar{1} \\ 0 & \bar{1} & 0 \\ \bar{1} & 0 & 0 \end{bmatrix}$
$C_{34}^-$	$\begin{bmatrix} \eta & 0 \\ 0 & \eta^* \end{bmatrix}$	$\begin{bmatrix} 0 & 1 & 0 \\ 0 & 0 & 1 \\ 1 & 0 & 0 \end{bmatrix}$	$\sigma_{d2}$	$\begin{bmatrix} 0 & 1 \\ 1 & 0 \end{bmatrix}$	$\begin{bmatrix} 0 & 0 & 1 \\ 0 & \bar{1} & 0 \\ 1 & 0 & 0 \end{bmatrix}$
$C_{31}^+$	$\begin{bmatrix} \eta^* & 0 \\ 0 & \eta \end{bmatrix}$	$\begin{bmatrix} 0 & 0 & \bar{1} \\ \bar{1} & 0 & 0 \\ 0 & 1 & 0 \end{bmatrix}$	$\sigma_{d3}$	$\begin{bmatrix} 0 & \eta \\ \eta^* & 0 \end{bmatrix}$	$\begin{bmatrix} \bar{1} & 0 & 0 \\ 0 & 0 & 1 \\ 0 & 1 & 0 \end{bmatrix}$
$C_{32}^+$	$\begin{bmatrix} \eta^* & 0 \\ 0 & \eta \end{bmatrix}$	$\begin{bmatrix} 0 & 0 & \bar{1} \\ 1 & 0 & 0 \\ 0 & \bar{1} & 0 \end{bmatrix}$	$\sigma_{d4}$	$\begin{bmatrix} 0 & \eta^* \\ \eta & 0 \end{bmatrix}$	$\begin{bmatrix} 0 & \bar{1} & 0 \\ \bar{1} & 0 & 0 \\ 0 & 0 & \bar{1} \end{bmatrix}$
$C_{33}^+$	$\begin{bmatrix} \eta^* & 0 \\ 0 & \eta \end{bmatrix}$	$\begin{bmatrix} 0 & 0 & 1 \\ \bar{1} & 0 & 0 \\ 0 & \bar{1} & 0 \end{bmatrix}$	$\sigma_{d5}$	$\begin{bmatrix} 0 & \eta \\ \eta^* & 0 \end{bmatrix}$	$\begin{bmatrix} \bar{1} & 0 & 0 \\ 0 & 0 & \bar{1} \\ 0 & \bar{1} & 0 \end{bmatrix}$
$C_{34}^+$	$\begin{bmatrix} \eta^* & 0 \\ 0 & \eta \end{bmatrix}$	$\begin{bmatrix} 0 & 0 & 1 \\ 1 & 0 & 0 \\ 0 & 1 & 0 \end{bmatrix}$	$\sigma_{d6}$	$\begin{bmatrix} 0 & \eta^* \\ \eta & 0 \end{bmatrix}$	$\begin{bmatrix} 0 & 1 & 0 \\ 1 & 0 & 0 \\ 0 & 0 & \bar{1} \end{bmatrix}$

Table 5.2: Table of matrix representations of  $O$  group under the representation given in Eq 5.13.  $\eta = \exp(2i\pi/3)$  Modified from [73]

# Chapter 6

## Acetylene

### 6.1 Introduction

The excited state landscape of acetylene has been one of the most carefully studied systems to date. It is the simplest molecule that contains all the features of vibrational dynamics of polyatomic systems [75] and has a labile H atoms that undergo large amplitude motions. It was the first molecule to be shown to have differing equilibrium structures in the excited and ground states [76,77]. Its photo fragment, the C<sub>2</sub>H radical was observed in the interstellar medium [4] and is a reactive intermediate in combustion processes [78]. The absorption spectrum has been recorded in the range 5.4-7.8 eV. Figure 6.18 (final section of this chapter) shows the experimental spectrum from reference [79], image edited by Malsch *et al* [80] together with peak assignments. The maximum intensity of the S<sub>0</sub>-S<sub>1</sub> transition lies near the vertical transition (~6.9 eV), a somewhat unexpected result given that all valence states in this region are optically forbidden at a linear geometry. In this region we find singlet valence and Rydberg states as well as triplet states in the 4.5-6.0 eV range. Acetylene is a conjugated system and the valence states arising in the absorption spectra region are generated by  $\pi \rightarrow \pi^*$  orbital excitations.

From these degenerate HOMO-LUMO orbitals of symmetry  $\Pi \otimes \Pi$  we can obtain  $\Sigma$  and  $\Delta$  triplet and singlet states. Double excitations can in turn produce similar *gerade* states. The contribution of a  $\pi^*$  orbital to valence states has the effect of stabilising the molecule towards a bent geometry. In contrast, Rydberg states found in this range arise from orbital excitations  $\pi \rightarrow n/\Lambda$  ( $\Lambda$  = hydrogenic wavefunction) which give stabilisation energies favouring a linear geometry [81].

The  $S_1$  minimum has been found experimentally and theoretically to be at *trans* bent geometry with an isomerisation barrier to its *cis* conformer via a torsional motion. Consequently, the absorption spectrum is dominated by a long progression arising from  $S_1$  *trans*-bending mode and a CC stretch mode. The transition states for the *cis-trans* isomerisation have been calculated to be at one CCH angle near-linear and the other at  $120^\circ$  [80]. The  $S_0 \rightarrow S_1$  maximum intensity is not discernible as it lies higher than the  $S_0 \rightarrow S_2$  onset (6.71 eV). The  $S_0 \rightarrow S_1$  onset is believed to lie 1.5 eV above the band origin. A linear isomerisation barrier of 0.8 eV was calculated [80]. Questions regarding the validity of using CASPT2 to calculate this barrier have been raised [82], where a barrier of 1.24 eV was obtained using MRCISD (1.06 eV from the *cis* minimum).

For  $S_2$ , a non-planar differing-angle *cis* geometry has been calculated using ab initio methods [80,83]. Table 6.3 provides those critical points found in the literature as well as their adiabatic transition energies. Over the last decade Koppel and co-workers [82,84] have built vibronic models to help unweave the absorption spectra. They use Liu *et al* [85] Jacobi coordinate formulation with two angles that approximately describe CCH angles, a CC bond and a torsional angle. The most complete of their models includes non-adiabatic interactions between  $S_1$  and  $S_2$  along the torsional motion which allows for

interstate diabatic coupling elements between them and approximating this coupling in a regularised diabatic representation. They observe an S<sub>1</sub>-S<sub>2</sub> internal conversion in less than 50 fs. Acetylene in its ground state belongs to the D<sub>∞h</sub> point group and therefore should exhibit Renner-Teller (RT) and pseudo Jahn-Teller (pJT) stabilisation effects. At the linear geometry, S<sub>2</sub> forms part of a degenerate  $\Delta_u$  state which should exhibit Renner-Teller effects. Such consideration has been acknowledged [84], but not taken into account in order to reproduce the spectra around the 6.9 eV range.

Cederbaum *et al* were the first to analyse the topological effects of linear molecular systems [22] and their effect in spectra. More recently Bersuker and Liu [86] highlighted the small contribution RT might have to the stabilisation energy of degenerate states. This study was followed by work proving that for all RT systems, all instabilities arise from pseudo Jahn-Teller coupling, having implications for spectroscopic selection rules, transition dipole moments and line intensities [29].

A large body of spectroscopic work exists to further the understanding of hydrogen dissociation when irradiated around the threshold energy range. Dissociation by excitation to valence states has been observed to correlate adiabatically with two doublet states; the  $\tilde{X}^2\Sigma^+$  ground state (~5.71 eV) and a degenerate  $\tilde{A}^2\Pi$  state (~6.15 eV) from the ground state minima (5.81 and 6.15 eV using *ab-initio* methods [83]). The most careful theoretical study of critical points was done by Cui and Morokuma [83,87], proposing a dissociation mechanism near the experimentally observed threshold. Starting from S<sub>1</sub>, they distinguished possible pathways as a function of energy, leading to either the doublet ground state  $\tilde{X}^2\Sigma^+$  or excited  $\tilde{A}^2\Pi$  states of the C<sub>2</sub>H moiety. From S<sub>1</sub> they found a transition state barrier of 6.48 eV (including ZPE) to adiabatic dissociation leading to the 6.15 eV  $\tilde{A}^2\Pi$  state. An alternative

route to the same doublet state but with a lower barrier of 6.28 eV (including ZPE) to dissociation occurs via a conical intersection with the  $S_2$  state at an out-of-plane geometry and then possibly via a  $S_2/S_0$  avoided crossing at 6.10 eV. They suggest this pathway should be a slow process compared to tunnelling directly from  $S_1$  at those energies. More recent work [81] has shown that another avoided crossing is found by dissociation from the linear geometry where the degenerate  $\Pi_u$  state is strongly pre-dissociated by the  $\Pi_g$  states which then exhibit (ref [81] and shown in Fig. 6.1) an avoided crossing with  $S_0$  at a CH bond distance of 2.5 Angstroms (more on this crossing will be discussed in section 6.4.2).

The lowest energy pathway has received abundant attention from the spectroscopy community [75, 88–90] and is most often associated with R. W. Field [91, 92]; the common view is that the  $S_1$  state undergoes intersystem crossing to a manifold of triplet states where pre-dissociation takes place (a drastic decrease in fluorescence yield has been reported above 5.7 eV [93]). This picture agrees with many

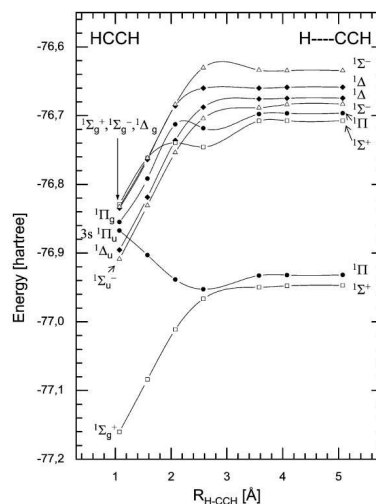


Fig. 6.1: Laruelle dissociation [81]

*ab-initio* calculations [83, 94, 95], which suggest that after intersystem crossing there would have to be a sequential energy transfer along several modes involving large molecular contortions that would make such a mechanism slow and inefficient [83]. This agrees with the observed  $\mu$ s metastable state lifetimes of the excited acetylene upon irradiation [88, 92] and a lower limit for a pre-dissociation lifetime has been put at tens of picoseconds [96] at least.

Excitations around 193 nm (6.42 eV) have been studied by Wodke [97]



and Fletcher *et al* [78]. The former obtain centre of mass translational energy distributions with an estimated 0.694 eV maximum translational energy for the nascent proton. The latter obtained rotational state distributions (for the  $\tilde{A}^2\Pi$  state) of the dissociating moiety. They estimate that the CC double bond increases by 0.2 Å in the  $S_1$  ( $\Sigma_u^-$ ) state. Both experiments suggest that the *trans* mode is active at the time of excitation and it is likely that such a bent configuration occurs at the time of dissociation. Emission lifetimes of 10-50  $\mu$ s are estimated. At energies below the dark pre-dissociative (triplet) state, long lived (260  $\mu$ s) acetylene has been reported [88].

Several groups performed vibrationally mediated photo-dissociation experiments (VMD); with rovibrational excitations ( $\sim$ 1.5-2.0 eV) prior to photodissociation with UV at 230-260 nm (4.7-5.4 eV). The rovibrationally excited wavefunction correlates differently with the excited electronic states and provides new insights into the excited state topology as well as facilitating the assignment of vibrational progressions. Valence  $\pi\pi^*$  orbital excitations typically don't significantly affect the CH bond length, vibronic CH stretch bands are usually missing from electronic transitions. VMD allows experimentalists to probe the excited state surface along these modes as well as to drive photochemical reactions (especially true due the high IR absorption coefficients for these modes) [93]. Changes in Frank-Condon factors effectively influence the electronic excitation. Haijima *et al* [89] irradiated above 46400  $\text{cm}^{-1}$  (5.74 eV) where they observed a substantial drop in fluorescence quantum yield which was interpreted as a pre-dissociation channel leading to the  $\tilde{A}^2\Pi$  states. Their justification is based on the low  $J(J+1)$  dependence of the band lying just above the threshold (vibrational pre-dissociation) and high dependence below it. In later work [93] they performed vibrationally-excited anti-symmetric and symmetric CH stretch mode combinations prior to UV

double resonance exciting in the region of 43000-47000  $\text{cm}^{-1}$  (5.1-5.7 eV). Below their posited dissociation threshold they assign bands in their LIF spectra originating from *trans* and CC combinations with anti-symmetric CH stretches. Above the threshold they use IR-UV double resonance multi photon ionisation (MPI) spectroscopy to study the range 49500-52000  $\text{cm}^{-1}$  (6.1-6.4 eV). They IR excite anti-symmetric and symmetric CH stretch mode combinations around 6556  $\text{cm}^{-1}$  (0.78678 eV) and observe many progressions involving quanta along *trans* vibrations in three different excited states. At 51,740  $\text{cm}^{-1}$  (6.24 eV) they suggest that a non-radiative relaxation channel becomes available. Zhang *et al* [98] pre-excited 4 quanta of CH stretch and then UV excited to 248.3 nm (5.0 eV) with a total energy of 6.56 eV leading to dissociation along the  $\tilde{A}^2\Pi$  state states. They posit a dissociation threshold just above 193.3 nm (6.41 eV) leading to an efficient adiabatic  $^2\Pi$  production when exceeded (with little asymmetric CH stretch excitation). In similar work, Schmidt and co-workers [75] excite  $\sim 1.9$  eV (5 quanta) into CH stretch modes and then excite by  $\sim 5.1$  eV; they deduce that two photo-dissociating channels must be taking place that lead to  $\tilde{X}^2\Sigma^+$  and  $\tilde{A}^2\Pi$  states with nascent proton maximum kinetic energies of 1.34 and 0.67 eV, respectively. The non-adiabatic channel to  $\tilde{X}^2\Sigma^+$  is thought to occur with bent geometries. Their work is interpreted in line with the Cui and Morokuma theoretical study; when the total energy is higher than the  $A_u$  barrier the  $C_{2h}$  internal energy is used for bond breaking and the adiabatic  $\tilde{A}^2\Pi$  channel is preferred but when the bending mode is excited it may enhance the propensity for the singlet non-adiabatic channel ( $\tilde{X}^2\Sigma^+$ ). In later work with Ganot [99], by pre-exciting bending modes (both *cis* or *trans*) and UV exciting to a total energy of  $\sim 7.0$  eV (similar as before) they find a significant increase in the photolytic yield (above the adiabatic dissociation barrier). In later comple-

mentary work [94,100] they excite just below the barrier estimated by Cui *et al* at 6.3 eV but pre-excite the second CH stretch overtone and UV excite to bent and CH stretch combinations to find an increased cleavage efficiency at those energies. They interpret their findings as an increase in non-adiabatic pre-dissociation to dark states. It is worth mentioning that the energy range marginally allows for some possible dissociation occurring via the  $S_1/S_2$  conical intersection also proposed by Cui *et al* and for the possibility of tunnelling via the  $S_1$ . Table 6.1 collates some of the information regarding the aforementioned vibrationally mediated photodissociation experiments. Exciting at *trans* bent geometries is experimentally seen to have better transition probabilities and theoretically supported by the strong vibronic dependence on the transition dipole moment surfaces [82]. Zhang irradiated acetylene around the 8.17-8.36 eV range exciting to an *un-gerade* state (most likely bound  $\Pi_u$  pre-dissociative state). They observe two dissociation lifetimes of 47 fs (8.16 eV) and 22-39 fs (8.37 eV) which they correlate with states  $\tilde{X}^2\Sigma^+$  (8.16 eV) and  $\tilde{A}^2\Pi$  (8.37 eV), the latter being the major component. Experimental [101] and theoretical [81] work suggests that this pre-dissociation state is described by a  $\pi \rightarrow 3s\sigma^*$  transition, which undergoes rydberdisation along the dissociation coordinate. Pre-dissociation is thought to happen at a near linear geometry but undergoing *trans*-bending and CC bending stretching. Finally exciting in the  $\sim 10$  eV range, below the  $C_2 + H + H$  channel,  $\Pi_g$  was observed to predominantly dissociate in the doublet  $^2\Pi$  states. [98]. Above this range one finds the first ionisation potential ( $\sim 11.0$  eV) [102].

In this work we construct a vibronic model which describe the dynamics of acetylene in the first three excited states, including non-adiabatic effects between them as Renner-Teller (RT) and pseudo Jahn-Teller (pJT) diabatic coupling. We will use the  $D_{\infty h}$  polynomials generated in chapter 5 to con-

Authors, Year	IR (cm <sup>-1</sup> )	UV (nm)	$\Delta E$ (eV)	Relevant Observations
Wodke & Lee, 85 [97]		193	6.424	0.694 eV estimated for the maximum mass translational energy distributions of the nascent proton
Fletcher <i>et al.</i> , 89 [78]		193	6.424	The <i>trans</i> mode is active at the time of excitation and it is likely that such an bent configuration occurs at the time of dissociation
Haijima <i>et al.</i> , 90 [89]		209-240	5.2-5.9	Posit a pre-dissociation channel opening at 5.74 eV
Fuji <i>et al.</i> , 94 [93]	6556 cm <sup>-1</sup> anti-symmetric and symmetric CH stretch mode combinations	192-231	5.3-7.1	At 51,740 cm <sup>-1</sup> (6.24 eV) a non-radiative relaxation channel becomes available. Observe many progressions involving quanta along <i>trans</i> -bends in three different excited states
Zhang <i>et al.</i> , 95 [98]	12582 cm <sup>-1</sup> : 4 quanta of CH-stretch local mode $\hat{v}_1'' + \hat{v}_3''$ ; $\hat{v}_1''$ = CH symmetric stretch, $\hat{v}_3''$ = CH anti-symmetric stretch	248.3	6.56	Posit a dissociation threshold just above 193.3 nm (6.41 eV) leading to an efficient adiabatic $\tilde{A}^2\Pi$ production when exceeded (with little asymmetric CH stretch excitation)
Schmid <i>et al.</i> , 97 [75]	15600 cm <sup>-1</sup> : CH stretch fourth overtone (2030 <sup>0</sup> 0 <sup>0</sup> )	243.13	7.02	Posit two photo-dissociating channels leading to $\tilde{X}^2\Sigma^+$ and $\tilde{A}^2\Pi$ states, where the non-adiabatic channel to $\tilde{X}^2\Sigma^+$ is thought to occur under bent geometries
Schmid <i>et al.</i> , 99 [99]	15600 cm <sup>-1</sup> : CH stretch fourth overtone (2030 <sup>0</sup> 0 <sup>0</sup> ); CC, CH stretch, <i>cis</i> -bend (1410 <sup>0</sup> 2 <sup>0</sup> ); CH stretch, <i>trans</i> -bend (2031 <sup>1</sup> 0 <sup>1</sup> )	243.13	7.02	Dissociation via bent and CH stretch modes with similar character to the initial rovibrational states. CH rupture increased by pre-excitation. Dark states might play a factor
Ganot <i>et al.</i> , 02, 03 [94, 100]	9998.33 cm <sup>-1</sup> : second CH stretch overtone	243.10	6.30	Dissociation below the adiabatic channel. Proton cleavage enhanced by exciting second CH overtone

Table 6.1: Experiments involving Singlet photodissociation of acetylene.  $\Delta E$  refers to the total energy of excitation (IR + UV).

construct a vibronic models in normal coordinates that includes pJT coupling. Comparison with another model which does not represent pJT explicitly tells us if there are any differences in the representation or any Renner-Teller effects present. Through the construct of a model using curvilinear coordinates to describe the full space of internal DOF. We obtain theoretical absorption spectra for different dimensionality models to validate the model. We then use it to model VMD experiments like those described above. The model predicts different preferred geometries at the time of dissociation that depend on the pre-excitation and UV excitation used.

## 6.2 Excited State Landscape

Table 6.2 shows vertical excitation energies obtained using two methods, CASSCF/PT2 and EOM-CCSD with increasing basis completeness. The active space for the former was obtained by performing single point calcu-

lations with different low-energy orbitals, including up to 17 orbitals at any time. By weighting the contribution that every orbital has on N states proportionally to the energy of the states which they describe, it is possible to reduce the active space to those orbitals that best describe the lowest N states. These orbitals were in agreement with those of EOM-CCSD calculations with the same basis. For an MP2 optimised geometry (cc-pVDZ), the following symmetry and energy ordering in a HF calculation labels the active space orbitals:  $4A_g$ ,  $1B_{3u}$ ,  $2B_{3u}$ ,  $1B_{2u}$ ,  $2B_{2u}$ ,  $3B_{1u}$ ,  $4B_{1u}$ ,  $1B_{2g}$ ,  $2B_{2g}$ , (using a aug-cc-pvtz basis). Geometry optimisations were done with Gaussian 03 [68] and excited state calculations with Molpro 09 [45]. For a given basis, neither a second or third order-perturbation changes state ordering and the results agree with those of EOM-CCSD calculations. However, the inclusion of augmented diffuse functions has the effect of swapping degenerate  $\Pi_u$  with  $\Pi_g$  states. Finally, inclusion of polarisable pV(q+d)Z functions has the effect of further lowering the energy. Performing a cut on the PES, Fig. 6.2 shows that the main effect of polarisable functions is to lower the absolute energies of the states without perturbing their topology and relative energies. Since the difference between the relative energies of excited states is slight, for practical purposes, models were fitted to an EOM-CCSD/aug-cc-pVTZ energies.

## 6.3 Normal coordinates and spectra

To reproduce the spectrum of acetylene we constructed a simple vibronic model. We used normal coordinates, ensuring we obtain the main harmonic bands in our calculated absorption spectrum. More crucially, these coordinates allow us to include RT and pJT coupling in a rigorous manner, allowing us to analyse the effect on its spectra (see below). From symmetry argu-

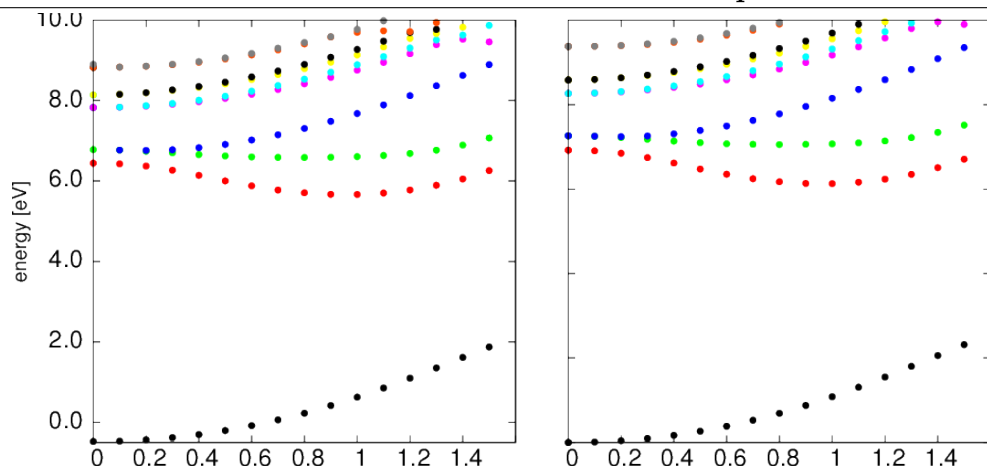


Fig. 6.2: Comparison of PE cuts along CCH angle using *left*: EOM-CCSD/aug-cc-pV(q+d)Z, *right*: EOM-CCSD/aug-pVTZ

ments [24] and the ortho-normality of normal coordinates, it can be shown that for an even number of  $N$  atoms, there will be  $(N-1)/2$  modes belonging to  $\Sigma+$ ,  $(N-1)/2$  to  $\Sigma-$  (symmetric and anti symmetric linear stretches), and  $(N-1)/2$  to  $\Pi_u$  and  $(N-3)/2$   $\Pi_g$  each. A frequency calculation was done for the ground state using a MP2 expansion over a HF wavefunction using a cc-pVDZ basis set. The geometry was first obtained by an optimisation at the same level. Table 6.4 shows the frequencies obtained and their corresponding displacements. Acetylene gives rise to a pair of degenerate  $\Pi_u$  and  $\Pi_g$  modes corresponding to *trans* and *cis* like flapping of the H atoms about the plane orthogonal to the axis of the molecule (further on referred to as  $[Q_{cx}, Q_{cy}]$  and  $[Q_{tx}, Q_{ty}]$ ). In addition we get the symmetric and anti-symmetric stretches of the H-atoms ( $Q_{ss}, Q_{as}$  modes) and the symmetric CC stretch ( $Q_{ccs}$ ).

The experimental absorption spectrum [79] (Fig. 6.18) ranges from 6.0 to 8.5 eV, we were concerned with the dynamics occurring in the first three excited states. Since we have  $\Pi$  normal coordinates and  $\Pi$  and  $\Delta$  states in this region, we should expect RT and pseudo Jahn-Teller coupling between these. We can therefore use the techniques of chapter 5 to generate totally symmetric polynomial elements with which to construct our model Hamiltonian (henceforth referred to as RT-polynomials). The PES along the seven

normal coordinates are shown in Figs 6.3-6.4.

The most salient feature of the landscape is the noticeably marked double well from the FC geometry to an either bent *cis* or *trans* geometry on  $S_1$ . Valence  $\pi$  orbitals are in the main orbital configurations determining these states. From a symmetry perspective, this stabilisation towards the bent geometry is caused by a pJT diabatic coupling to higher lying states, like all other RT systems [86]. Furthermore, from our RT-polynomials, the degeneracy of  $\Delta_u$  states is only lifted to fourth order due to inter-state coupling between such degenerate states. So if we only wanted to take the first 4-states into account, we would be assuming that the topology of the first three excited states should be well described by pJT coupling between  $1\Sigma_u^-$  and  $1\Delta_u$  and fourth order RT coupling alone. Questions about the potential need to account for RT coupling between  $S_2$ - $S_3$  to correctly describe the spectrum arising from them were raised by Koppel *et al* [82, 84]. But as noted, this subtle, fourth order, stabilisation energy will probably have a weak effect compared to linear pJT coupling. It turns out to be impossible to fit low order RT-polynomial functions that fit the topology along the  $\Pi$  degenerate coordinates on our 3 excited state manifold. So even if we wish to correctly build a simple model that only correlates degenerate degree of freedom, we will have to take into account pJT diabatic interactions to higher lying states.

Therefore, in this section we evaluate the effect and importance of including higher lying states in calculations by contrasting two models; one in which we include the excited states and coupling (model N8) explicitly in our model and a second where the diabatic 4 highest excited state coupling terms are ‘folded’ into the diagonal part (model N4). By comparing the calculated spectrum obtained we can judge the effect that not including such states and their pJT coupling could have in dynamic calculations. By ‘folding’ cou-

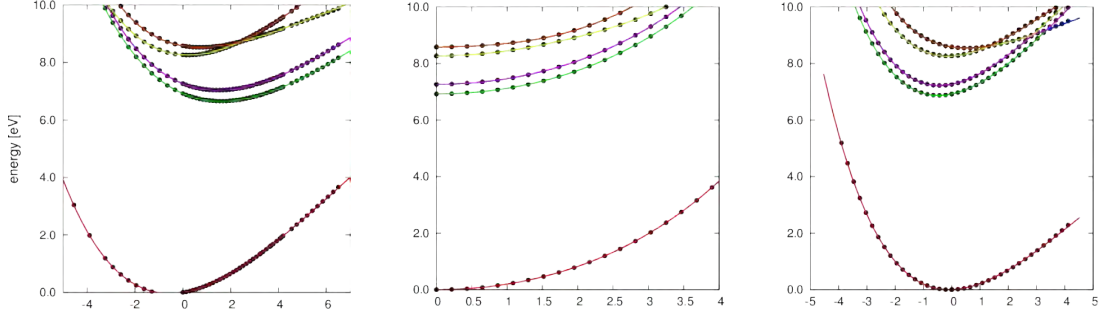


Fig. 6.3: Fitting of 4-state model to *ab-initio* energies along to normal (dimensionless) coordinates. *From left to right:  $Q_{cc}$ ,  $Q_{as}$ ,  $Q_{ss}$*

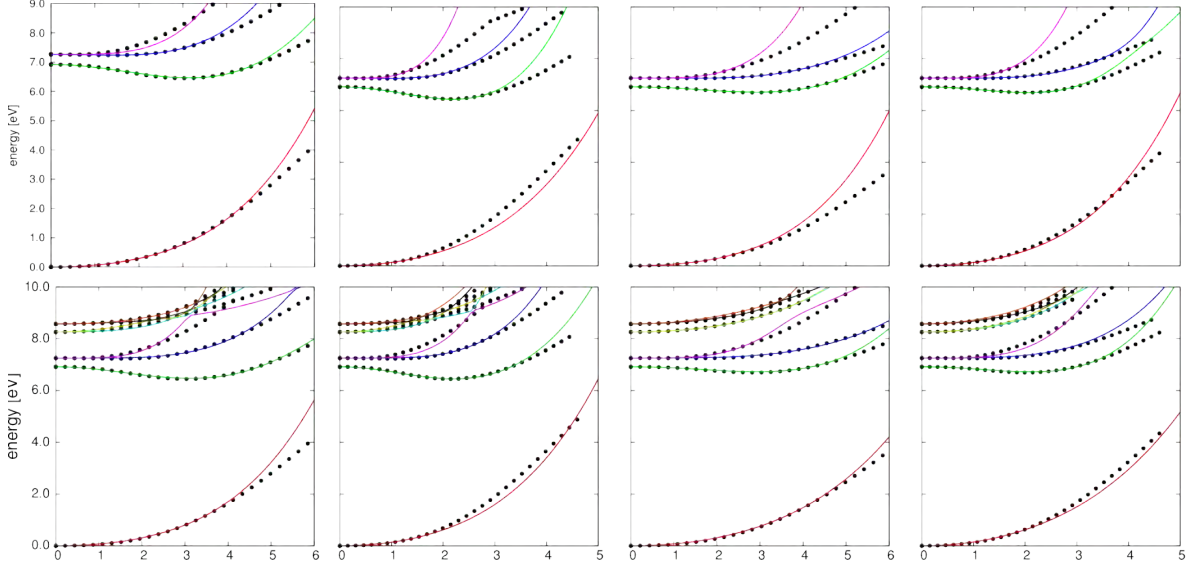


Fig. 6.4: Comparing the fitting of the 4-dimensional space of *cis* and *trans* normal (dimensionless) coordinates between N4 (*above*) and N8 (*below*) models. *From left to right:  $Q_{tx}$ ,  $Q_{tx} + Q_{ty}$ ,  $Q_{cx}$ ,  $Q_{cx} + Q_{cy}$*

pling terms, it is meant using the following form of a diabatic model for the diagonal element of the diabatic potential:

$$W_{11} = \frac{V_{eff}(\Delta E, \gamma, \epsilon) + D_{11}}{2} - \frac{\sqrt{(V_{eff}(\Delta E, \gamma, \epsilon) - D_{11})^2 - 4\lambda_{eff} \cdot Q^2}}{2} \quad (6.1)$$

This has the form of a 2x2 diagonalised diabatic vibronic model going into the diabatic on-diagonal element. All parameters but  $\Delta E$  are functions of our coordinate.  $V_{eff}$  and  $\lambda_{eff}$  represent the diabatic on-diagonal term and coupling to some single effective state. Underlying this model there is an assumption that the states interacting with the state of interest are approx-



imately described by a single linear coupling parameter,  $\lambda_{eff}$ .  $V_{eff}$  represents the effective higher lying state described; in this instance, by a vertical excitation energy ( $\Delta E$ ), quadratic ( $\gamma$ ) and quartic ( $\epsilon$ ) polynomial terms.  $D_{11}$  will similarly contain the usual on-diagonal terms of a simple vibronic Hamiltonian. Given the direct-product expansion of the Hamiltonian operator requested by the MCTDH algorithm, it is not possible to 'fold' coupling functions that correlate multiple DOF explicitly using this form.

For the totally symmetric modes given in Fig. 6.3 we use the Morse oscillator diabatic model:

$$\begin{aligned} W_{ii}(R) &= D_{0,i} (1 - \exp(-\alpha_i(R - R_{0,i})))^2 + E_{0,i}; \quad i \neq 6, \\ E_{0,i} &= -D_{0,i} (1 - \exp(\alpha_i R_{0,i}))^2, \end{aligned} \quad (6.2)$$

From symmetry arguments, for  $\Delta_u$  states to exhibit pJT coupling along  $\Pi_u$  and  $\Pi_g$  modes, we needed to include at least the next 4-states which are  $\Pi_u$  and  $\Pi_g$  states (coupling along  $\Pi_g$  and  $\Pi_u$  modes), since  $\Sigma^+ \subset \Pi_{u/g} \otimes \Pi_{u/g}$ . The fit to the adiabatic energies along normal coordinates of N4 and N8 models is shown in Fig. 6.4. As expected from the above discussions, model N4 gives a poorer fit for the first three excited states when correlating *cis* and *trans* coordinates. It is worth briefly noting that all zeroth order quadratic terms for all states are positive, which provides some confidence that the correct coupling between states has been included in our N8 model (from symmetry considerations [29]). To obtain the spectrum, the MCTDH package was used; since these are bound systems undergoing approximate harmonic motion, Harmonic Oscillator, HO-DVR functions were used as a primitive grid on which 9 SPF functions per state propagated a series of wavefunctions on the coupled manifold for 500 femtoseconds. The Fourier transform of the autocorrelation function on the resulting wavefunction gives us a spectrum (detailed in 2). To obtain a reasonable approximation to the initial wavefunction

determining the absorption spectrum, the relaxed, ground-state wavefunction is projected onto the excited state surfaces weighted by their optical activity.

The first 3 excited states are nominally forbidden, but exhibit Herzberg-Teller coupling along the *trans* bending coordinates. Figure 6.5 shows the coordinate dependence of the transition dipole of the first three excited states. The adiabatic and diabatic representations are chosen to be equal at the high-symmetry point of expansion, and the transition dipole surfaces track the overlap between the character of electronic

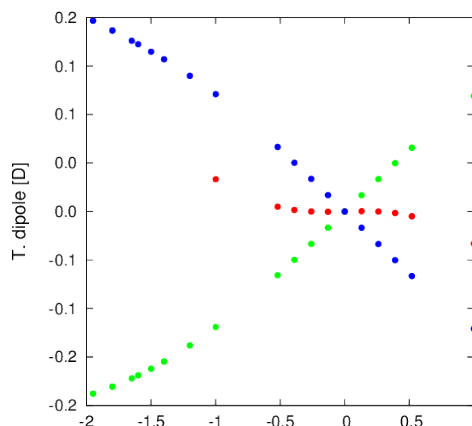


Fig. 6.5: Herzberg-Teller coupling;  $\Pi_g$  nuclear coordinate dependence of  $x$ -polarised light ( $\Pi_u$ ) adiabatic transition dipole between ground state and the following; ( $\Pi_u$ ) Blue and red are  $\Sigma_u^-$  and  $\Delta_u$  states along  $Q_{ty}$  mode, green is  $\Delta_u$  along  $Q_{tx}$  mode.

states. This means the transition dipole surfaces depend weakly on the nuclear coordinates, making it a reasonable approximation to use the linear terms of the *diabatic* transition dipole surfaces to be equal to those in the *adiabatic* representation. By symmetry,  $x$  and  $y$  components of the transition dipole operator span the  $\Pi_u$  IrRep and generate symmetrically equivalent excited state wavefunctions. It is worth noting that the  $\langle 0|\mu|i\rangle$  transition dipole surface about the  $x$  and  $y$  axis (where  $i$  is any excited state) can be interpreted as another RT pair of degrees of freedom, that exhibit pJT and RT coupling to electronic states. This linear approximation to the diabatic transition dipole surfaces is then used to operate on the relaxed ground state wavefunction prior to its projection to the appropriate state. This sets up the initial wavefunction. The well-depth obtained for  $S_1$  in normal coordinates in Fig. 6.4 is very shallow compared to the true well-depth (see following section or introduction). This will miss

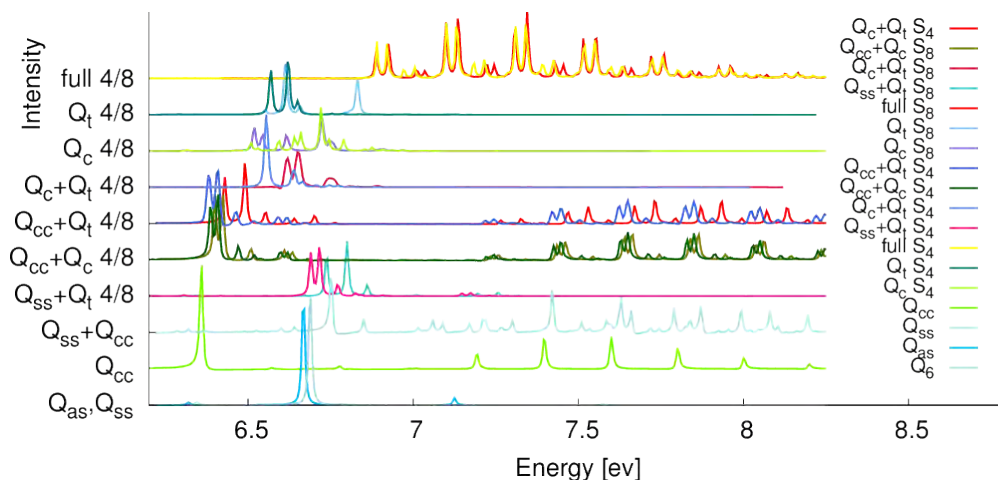


Fig. 6.6: Comparing reduced dimensionality spectra for models N4 and N8. Spectra have been shifted by their excited state zero-point energy (relative intensities arbitrary).

the  $S_1$  onset and much of the front tail seen in Fig. 6.18. Figure 6.6 shows the spectra obtained from models N4 and N8 under different dimensionalities, so as to help disentangle some of the spectral features arising in the full spectrum. Those spectra which have been overlaid compare the N8 and N4 models fitting the same DOF. All spectra were shifted by the ground state ZPE ( $\sim 0.75$  eV). Overall N4 and N8 exhibit very similar spectra, and their differences most likely come from fitting performed with different functions, and not as a result of different effects arising from pJT coupling. Especially clear is the close similarity between the full-dimensional spectra. The intensity of peaks from pure  $Q_{as}$  and  $Q_{ss}$ , like those from  $Q_{tx,ty}$ ,  $Q_{cx,cy}$  are notably weak in the full spectra (hardly visible, suggesting the  $Q_{as}$  and  $Q_{ss}$  bands don't contribute significantly). The spectra obtained for models with one pair of RT modes ( $Q_{tx,ty}$ ,  $Q_{cx,cy}$ ) together with  $Q_{ccs}$  produce two qualitatively different spectral bands clearly originating from the individual modes, but with some splitting effects for the  $Q_{ccs}$  band. Note that the  $Q_{tx,ty}+Q_{ccs}$  have slightly shifted set of peaks when comparing N4 and N8 and the same effect can be seen in the full spectra for the smaller intensity peaks. Therefore,

State	A	B	C	D	E
S <sub>0</sub>	-77.164 ( $\Sigma_g^+$ )	-77.091 ( $\Sigma_g^+$ )	-77.175 ( $\Sigma_g^+$ )	-77.193 ( $\Sigma_g^+$ )	-77.171 ( $\Sigma_g^+$ )
S <sub>1</sub>	7.025 ( $\Sigma_u^+$ )	7.596 ( $\Sigma_u^+$ )	7.213 ( $\Sigma_u^+$ )	7.213 ( $\Sigma_u^+$ )	7.367 ( $\Sigma_u^+$ )
S <sub>2</sub>	7.342 ( $\Delta_u$ )	7.990 ( $\Delta_u$ )	7.538 ( $\Delta_u$ )	7.534 ( $\Delta_u$ )	7.730 ( $\Delta_u$ )
S <sub>3</sub>	7.343 ( $\Delta_u$ )	8.035 ( $\Delta_u$ )	7.538 ( $\Delta_u$ )	7.534 ( $\Delta_u$ )	7.730 ( $\Delta_u$ )
S <sub>4</sub>	8.117 ( $\Pi_u$ )	9.788 ( $\Pi_g$ )	8.375 ( $\Pi_u$ )	8.415 ( $\Pi_u$ )	9.536 ( $\Pi_g$ )
S <sub>5</sub>	8.117 ( $\Pi_u$ )	9.788 ( $\Pi_g$ )	8.375 ( $\Pi_u$ )	8.415 ( $\Pi_u$ )	9.536 ( $\Pi_g$ )
S <sub>6</sub>	8.520 ( $\Pi_g$ )	10.638 ( $\Pi_u$ )	8.736 ( $\Pi_g$ )	8.776 ( $\Pi_g$ )	10.118 ( $\Pi_u$ )
S <sub>7</sub>	8.520 ( $\Pi_g$ )	10.638 ( $\Pi_u$ )	8.736 ( $\Pi_g$ )	8.776 ( $\Pi_g$ )	10.118 ( $\Pi_u$ )
S <sub>8</sub>	n/a	11.768 ( $\Sigma_g^-$ )	9.476 ( $\Delta_g$ )	9.404 ( $\Delta_g$ )	11.578 ( $\Sigma_g^-$ )
S <sub>9</sub>	n/a	13.106 ( $\Delta_g$ )	9.476 ( $\Delta_g$ )	9.404 ( $\Delta_g$ )	12.249 ( $\Delta_g$ )

Table 6.2: Vertical excitation energy (eV) comparison between CAS(6,9)+PT2 and EOM-CCSD with different basis-sets. S<sub>0</sub> in Hartree A) CAS(6,9)+PT2//aug-cc-pVTZ B) CAS(6,9)+PT2//pVTZ C) EOM-CCSD//aug-cc-pVTZ D) EOM-CCSD//aug-cc-pV(q+d)Z E) EOM-CCSD//pVTZ

we suggest the full spectrum is formed from coupling between both bands  $Q_{tx,ty}+Q_{ccs}$  and  $Q_{cx,cy}+Q_{ccs}$ ; the high intensity progression originating from the  $Q_{cx,cy}+Q_{ccs}$  and the low intensity from  $Q_{tx,ty}+Q_{ccs}$ . The small difference in spectral effects between N8 and N4 can be rationalised by noting the energies of the wavefunction during the propagation since we project up to S<sub>3</sub> and energies thereby, the higher lying states are populated via diabatic coupling that shouldn't reflect any non-adiabatic coupling effects, but merely be another unitary way of representing states. Although the energy difference between S<sub>1</sub> and S<sub>2/3</sub> is considerably smaller than to S<sub>4</sub> upwards and might justifiably lead to non-adiabatic coupling, this simple model does not describe the known regions where these states actually cross [87]. RT coupling was present in both models, but the removal of these fourth order terms had essentially no effect on the propagations. These results give us some confidence that MCTDH gives consistent results under either representations, for which we will continue to take a similar approach in the following subsection.

State	Geom	CH/CC/Ang/Dih	Adiabatic ex. Energy (eV)	Reference and method
S <sub>1</sub>	trans	1.105/1.377/122.4	5.26	Cui 97 <sup>9</sup> <sub>a</sub>
S <sub>1</sub>	cis	1.107/1.341/NA	5.77	Cui 97 <sup>9</sup> <sub>a</sub>
S <sub>1</sub>	trans	1.094/1.382/122.0	5.14	Malsch 01 <sup>8</sup> <sub>b</sub>
S <sub>1</sub>	cis	1.097/1.353/132.0	5.55	Malsch 01 <sup>8</sup> <sub>b</sub>
S <sub>1</sub>	linear	1.067/1.341/180.0	5.99 (6.96)	Malsch 01 <sup>8</sup> <sub>b</sub>
S <sub>1</sub>	cis	1.094/1.342/132.7	5.58	Ventura 03 <sup>18</sup> <sub>c</sub>
S <sub>1</sub>	trans	1.092/1.372/122.2	5.23	Ventura 03 <sup>18</sup> <sub>c</sub>
S <sub>1</sub>	cis	(1.078&1.315)/1.316/ (129.1&129.0)/2.6	5.60	this work <sub>d</sub>
S <sub>1</sub>	trans	(1.133&1.078)/1.422/ (123.4&127.3)/2.6	5.39	this work <sub>d</sub>
S <sub>1</sub>	linear	(1.053&1.048)/1.239	6.78	this work <sub>d</sub>
S <sub>1</sub>	d-trans	(0.979&1.859)/1.362/ (123.2&124.7)/1.2	6.50	this work <sub>d</sub>
S <sub>1</sub>	d-cis	(1.095&1.889)/1.333/ (134.2&123.0)/4.0	7.00	this work <sub>d</sub>
S <sub>2</sub>	trans	1.092/1.350/146.0	6.68	Malsch 01 <sup>8</sup> <sub>b</sub>
S <sub>2</sub>	cis	1.127/1.346/146.0	6.60	Malsch 01 <sup>8</sup> <sub>b</sub>
S <sub>2</sub>	linear	1.061/1.322/180.0	6.87 (7.30)	Malsch 01 <sup>8</sup> <sub>b</sub>
S <sub>2</sub>	cis	1.098/1.328/140.0	6.55	Ventura 03 <sup>18</sup> <sub>c</sub>
S <sub>2</sub>	trans	1.071/1.327/149.9	6.80	Ventura 03 <sup>18</sup> <sub>c</sub>
S <sub>2</sub>	cisoid	(1.216&1.154)/1.3718/ (137.6&115.5)/60	6.5	this work <sub>d</sub>
S <sub>2</sub>	cisoid	(1.116&1.092)/1.418/ (116.1&129.0)/82.3	6.7	this work <sub>d</sub>
S <sub>2</sub>	linear	(1.060&1.054)/1.239/	7.23	this work <sub>d</sub>
S <sub>2</sub>	d-out plane	(1.077&1.830)/1.311/ (115.1&125.0)/105.3	7.6	this work <sub>d</sub>
S <sub>2</sub>	d-cisoid	(1.052&1.856)/1.278/ (155.1&121.0)/55.3	7.6	this work <sub>d</sub>
S <sub>3</sub>	cis	1.080/1.328/169.0	6.82	Malsch 01 <sup>8</sup> <sub>b</sub>
S <sub>3</sub>	trans	1.078/1.325/168.1	6.83	Malsch 01 <sup>8</sup> <sub>b</sub>
S <sub>3</sub>	out-plane	(1.097&1.103)/1.377/ (121.8&121.8)/96.33	6.9	this work <sub>d</sub>
S <sub>3</sub>	cisoid	(1.083&1.096)/1.310/ (132.01&133.4)/76.8	6.9	this work <sub>d</sub>
S <sub>3</sub>	linear	(1.096&1.054)/1.239/	7.2	this work <sub>d</sub>

Table 6.3: Acetylene excited state critical structures and energies S<sub>1</sub>-S<sub>3</sub>. Energies in brackets refer to adiabatic vertical excitation energies from the ground state geometry. If two values are given by & it means the CH bonds/angles where different for both protons. Cisoid refers to differing-angles for CCH<sub>a</sub> and CCH<sub>b</sub>. Prefix d- refers to a proton being stretched to near dissociation before minimising model energy. <sub>a</sub> EOM-CCSD/cc-pVTZ (CASPT2 for energy). <sub>b</sub> CASSCF/ANO (PT2 for energies). <sub>c</sub> MR-AQCC/cc-pVQZ, <sub>d</sub> EOM-CCSD/aug-cc-pVTZ






Mode	Motion	Symmetry	$\omega$ (cm <sup>-1</sup> )
$Q_{tx,ty}$ ( $\tilde{\nu}_{1,2}$ )		$\Pi_g$	557.8506
$Q_{cx,cy}$ ( $\tilde{\nu}_{3,4}$ )		$\Pi_u$	749.5317
$Q_{ccs}$ ( $\tilde{\nu}_5$ )		$\Sigma_g^+$	1965.0605
$Q_{as}$ ( $\tilde{\nu}_6$ )		$\Sigma_u^+$	3455.1418
$Q_{ss}$ ( $\tilde{\nu}_7$ )		$\Sigma_g^+$	3540.0541

Table 6.4: Harmonic Frequencies. Obtained from an MP2 calculation with an cc-pVTZ basis.

State	Char	$D_{\infty h}$	$C_{2h}$	$C_{2v}$	$C_s$	$C_{\infty v}$
$S_0$		$\Sigma_g^+$	$A_g$	$A_1$	$A'$	$^2\Sigma^+$
$S_1$	$1\pi_g$	$\Sigma_u^-$	$A_u$	$A_2$	$A''$	$^2\Pi$
$S_2/S_3$	$1\pi_g$	$\Delta_u$	$A_u \otimes A_u$	$A_2 \otimes B_1$	$A'' \otimes A'$	$^2\Pi$
$S_4/S_5$	$3s\sigma_g$	$\Pi_u$	$B_u \otimes B_u$	$B_2 \otimes B_1$	$A'' \otimes A'$	
$S_6/S_7$	$3p\sigma_u$	$\Pi_g$	$B_g \otimes B_g$	$B_1 \otimes B_2$	$A' \otimes A''$	
$S_8/S_9$	$3s\pi_u$	$\Delta_g$	$A_g \otimes A_g$	$A_1 \otimes A_2$	$A' \otimes A''$	

Table 6.5: Singlet state and symmetry correlation tables. Character of Rydberg states is based on Ref [81]. Last column refers to the doublet state which correlates adiabatically via dissociation.

## 6.4 Curvilinear model and dynamics

### 6.4.1 Introduction

Some of the optimised geometries or critical points on excited state surfaces in the literature are given in tables 6.3 and were mentioned in the introduction. Some cells in Fig. 6.16 show cuts starting from near the excited state minima towards a dissociation channel; for dissociation to occur from  $S_1$ , almost 1.5 eV have to be overcome; it is unlikely to get dissociation by exciting near the fundamental of  $S_1$ . However, given that the relaxed ground state wavefunction prefers a linear geometry it is likely, when exciting to these valence states, the wavefunction will gain momentum owing to the high vi-

brational eigenfunctions that will be projected in the excited state. From such an initial wavefunction we are more likely to observe some dissociation occurring; as the angular coordinates would start undergoing a double well oscillation, it would require the inclusion of coupling to dissociating coordinates to observe some energy going into the proton dissociation.

As mentioned in the introduction, experimentalists have gone further and prepared initial wavefunctions with high momentum along linear dissociation by IR exciting mode combinations to produce these excited local modes [98] which are then UV excited to a narrow energy band to enhance dissociation of the molecule. This section aims to model such a vibrationally mediated photodissociation process (VMD).

We have already seen that the surfaces exhibit very strong diabatic coupling of which some, and potentially much, could be attributable to NA-coupling. This would also suggest that the true vibronic surfaces might be different so as to affect the barrier height of the system. Properly modelling such landscape requires an accurate description of the *cis-trans* isomerisation and out-of-plane torsion as a function of the dissociating coordinates. It is clear that normal modes are inadequate for the natural description of such excited state critical points; their un-physically rectilinear character makes them restrictive on the kind of molecular distortions one can naturally describe (typically small and bound displacements) often giving rise to rapidly changing potential state energies that make a low order polynomial model prohibitive. Jacobi [85] and valence [103] curvilinear coordinates are offered in the literature but have disadvantages when we try to use them for the construction of vibronic models built out of products of 1D operators. They require the molecule to be non-linear for the dihedral angle to be defined, resulting in strong correlation of the energy along this degree of freedom

(DOF) with regards the others (when using 1D-product functions). Additionally, this same feature reduces the symmetry of the coordinates from  $D_{\infty h}$  to  $C_{2h}$  which allows for potentially a much larger number of parameters into the model, complicating the optimisation procedure.

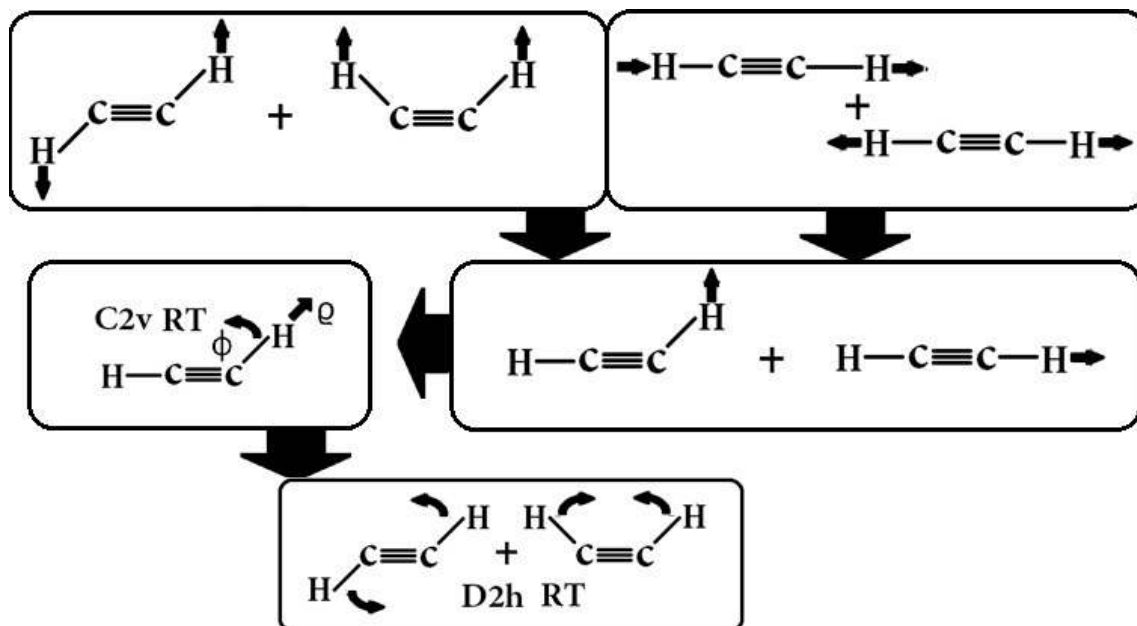


Fig. 6.7: Diagrammatic representation of the curvilinear coordinates used in this subsection

Unable to use  $D_{\infty h}$  totally symmetric adapted basis, this increase becomes prohibitive if we hope to describe many DOF and states. The above implications suggest we would like curvilinear coordinates that ideally span as many  $D_{\infty h}$  irreps as possible so as to reduce the terms that enter into our model. The most obvious solution is therefore to use the same kinds of displacements that the  $D_{\infty h}$  normal coordinates have, but involving CCH angles and radial (valence like) coordinates. To obtain such coordinates, we start by performing rotations of normal coordinates to obtain a set of quasi-Cartesian coordinates describing the position of the hydrogen atoms:

$$\begin{pmatrix} Q_{ay} \\ Q_{by} \end{pmatrix} = \frac{1}{\sqrt{2}} \begin{pmatrix} 1 & -1 \\ 1 & 1 \end{pmatrix} \begin{pmatrix} Q_{cy} \\ Q_{ty} \end{pmatrix} \quad (6.3)$$



where  $Q_{ay}$  refers to the quasi y-coordinate of hydrogen atom ‘a’ (similar definition for  $Q_{by}$ ) and  $Q_{cy}$  and  $Q_{ty}$  refer to the *cis* and *trans* coordinates along the yz-plane. A similar operation is done for the xz-plane coordinates, and for the symmetric and anti-symmetric stretches to give single H-atom stretches along the z-axis. The only difference between the Cartesian coordinates and these are that the other bond distances change slightly so as to fix the centre of mass and to maintain the linear space of rotations and translations outside our coordinate space. Since we are using mass-scaled normal coordinates, the KE operator is invariant with respect to rotations. From there we performed a spherical polar transformation of each H atom quasi-Cartesian coordinates to obtain two sets of quasi-spherical polar coordinates:

$$\begin{aligned} Q_{ax} &= R_a \cdot \cos(\theta_a) \\ Q_{ay} &= R_a \cdot \sin(\theta_a) \cdot \sin(\phi_a) \\ Q_{az} &= R_a \cdot \sin(\theta_a) \cdot \cos(\phi_a) - Q_0^z \end{aligned} \tag{6.4}$$

defined in such a way that the linear minima in the ground state lies at  $\theta_a = \frac{\pi}{2}, \phi_a = \pi, R_a = Q_0^z$ . A similar set of coordinates is obtained for atom ‘b’. For these coordinates, the resulting KE operator is potentially the simplest form this system could have: it consists of a pair of angular momentum operators, radial KE terms and a normal KE term for  $Q_{ccs}$ :

$$2 \cdot \hat{T} = \hat{p}_i^2 + \frac{\hat{L}_i^2}{R_i^2} + \nabla_{ccs}, \quad i = a, b \tag{6.5}$$

where

$$\begin{aligned} \hat{L} &= \frac{1}{\sin(\theta)} \frac{\partial}{\partial \theta} \sin(\theta) \frac{\partial}{\partial \theta} + \frac{1}{\sin^2 \theta} \frac{\partial^2}{\partial \phi^2} \\ \frac{\hat{p}_i^2}{2} &= \frac{1}{R_i^2} \frac{\partial}{\partial R_i} R_i^2 \frac{\partial}{\partial R_i} \end{aligned} \tag{6.6}$$

In comparison, the KE operator for valence coordinates obtained in reference [103] contains just under 100 terms. We can simplify this operator further if we factor the radial part of the wavefunction by  $R_i$ ,  $\Phi_R(R_i) \equiv R_i \cdot \Phi(R_i)$ . This

way the radial kinetic energy term takes an “equivalent one-dimensional” form [104]:

$$2 \cdot \hat{T} = \left( \frac{1}{i} \frac{\partial}{\partial R_i} \right)^2 + \frac{\hat{L}_i^2}{R_i^2} + \nabla_{ccs}, \quad i = a, b \quad (6.7)$$

One could have conceivably used valence coordinates to obtain an analogous set of coordinates, but the resulting transformed kinetic energy operator would have been more complicated. These coordinates possess  $C_{2v}$  symmetry. By operating with the analogous but inverse rotation matrix of equation 6.3 on the angular coordinates, we recover a coordinate representation spanning the  $D_{\infty h}$  point group. Crucially, these coordinates give a much more accurate description of excited state critical points than do normal coordinates.

### 6.4.2 Potential surface and Fitting

Due to symmetry considerations, combined displacements along several of these high symmetry coordinates can result in identical potential energy to some other. For example, since  $\phi_a + \theta_b$  and  $\phi_b + \theta_a$  are related by a reflection, they are physically (energetically) indistinguishable. By cutting along all possible 2-dimensional diagonal and anti-diagonal cuts of all modes, rotating to the lower  $C_{2v}$  symmetry coordinates (before applying inverse of Equation 6.3 as explained above) and similarly obtaining all possible 2 dimensional cuts, we obtained 10 *distinct* vector cuts (Fig. 6.8). A more sparse four dimensional grid with 6 points per coordinate was also calculated (these ignore the potential energy symmetry considerations just mentioned). We fitted 78 totally symmetric functions generated in the 4-dimensional space of the Renner-Teller coordinates (*cis* and *trans* angles), 10-state landscape with strong coupling terms.

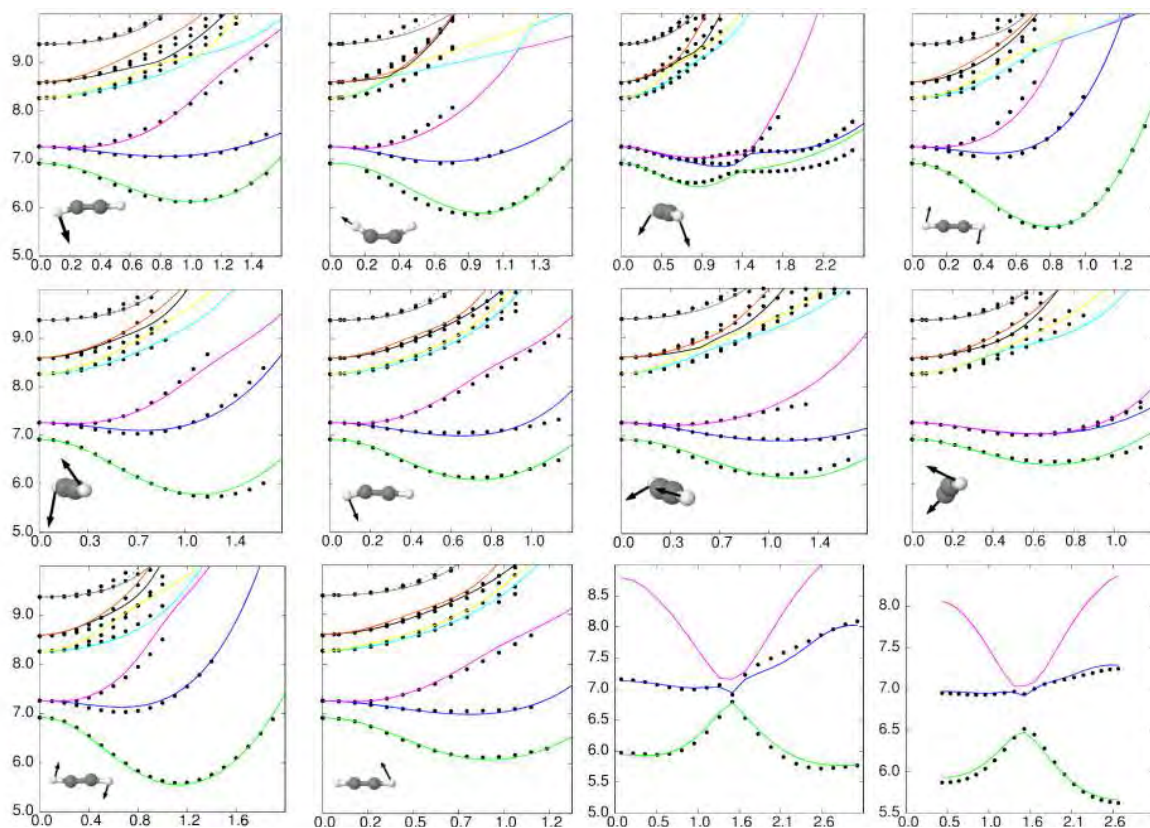


Fig. 6.8: Adiabatic potential surfaces from a 10-state model that uses curvilinear coordinates compared to EOM-CCSD/aug-cc-pVTZ calculations (points). Energy in eV, coordinates in radians.  $S_0$  is not shown in plots. Each slide shows a physically distinct vector generated by exploring diagonal and anti-diagonal vectors of  $D_{\infty h}$  and  $C_{2v}$  coordinates. *From left to right: first row:  $(\theta_a)$ ,  $(\theta_a + \theta_b)$ ,  $(\theta_a + \theta_b + \phi_a - \phi_b)$ ,  $(\theta_a - \theta_b)$  second row:  $(2\theta_a - \theta_b - \phi_a)$ ,  $(\theta_a + \phi_a)$ ,  $(\theta_a + \phi_a + \phi_b)$ ,  $(\theta_a + \phi_b)$  third row:  $(-\theta_a + \theta_b - \phi_a + \phi_b)$ ,  $(\theta_b + \phi_b)$ , dihedral path between minima in 4D,  $\{\theta, \phi\}$  sub-space:  $S_1$ ,  $S_2$*

These energies were used to fit  $D_{\infty h}$  the totally symmetric adapted polynomial basis generated in chapter 5 using the genetic algorithm described in chapter 3. The fitting included up to four dimensional, fourth order polynomials to fit the surfaces shown in Fig. 6.8. Where appropriate, fourth order terms were constrained to have positive values in order to ensure a bounded potential. All states and modes are coupled by inclusion of all first and second order terms. Only a few third and fourth order terms were included, as the increasing number of parameters pushed the limits of the

optimisation algorithm. Fewer terms were used to fit  $S_0$  - no coupling was assumed to occur between  $S_0$  and any excited state (fit not shown in Fig. 6.8). Against the suggestion that the model might be over-parametrised, a 8 state model with terms up to the same order was attempted but yielded no satisfactory fitting. It is worth mentioning a relaxed wavefunction in the  $S_1$  state for this Renner-Teller subspace of coordinates retains a  $D_{\infty h}$  symmetry; the position expectation value results in a linear molecule. This demonstrates that the symmetry adapted functions indeed obey  $D_{\infty h}$  operations, with no region in the potential being asymmetrically favoured.

The  $S_1$ - $S_2$  crossing mentioned in the literature [83] can be seen in Fig. 6.8 at an out-of-plane geometry ( $\theta_a + \theta_b + \phi_a - \phi_b$ ). The last two sub-figures show the  $S_1$  and  $S_2$  potential energy around the dihedral angle that takes us between the *cis* and *trans* minima (in this 4D subspace) of the  $S_1$  and  $S_2$  surfaces respectively.

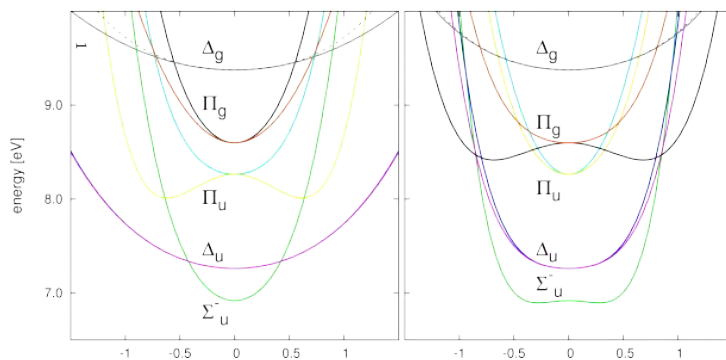


Fig. 6.9: Vector cuts showing diagonal elements of diabatic model along both Renner-Teller curvilinear coordinates (eV); *left*:  $\theta_a + \theta_b$  (*cis*); *right*:  $\theta_a - \theta_b$  (*trans*). Strict diabatic states should not exhibit any stabilisation away from the linear geometry.

The model therefore allows for a proper free dihedral rotation to occur. Figure 6.9 shows the model diabatic surfaces (the interstate elements) along the  $\Pi_g$  and  $\Pi_u$  modes. According to literature [29], there should be no stabilisation away from the linear geometry in the inter-state elements, but should all arise solely via pJT coupling. Since the diagonal elements of this diabatic model potential exhibit stabilisation away from the linear geometry, it therefore does not account for all diabatic coupling and cannot be said to be a separable Hilbert subspace. But given the strong pJT effect present in this

system, it is an approximation that yields good qualitative agreements. The first three states show stabilisation away from the linear geometry that must arise from pJT coupling to higher lying states [29]. As mentioned before, ten states were required to fit satisfactorily the RT coordinates, with a modest 78 symmetry adapted basis function. After rotating the model back to the  $C_{2v}$  coordinates (to keep the simple KE form), these four dimensions alone contribute 337 monomials into the potential energy matrix. Where no symmetry to be used at all, the number of terms possible entering such a model would become prohibitive.

The dissociation coordinates,  $R_{a,b}$ , shown in Fig. 6.10 (top left) were not rotated to the higher  $\Sigma^{+/-}$  symmetries; being CH radial coordinates, these are the most relevant coordinates for dissociation and where fitted with the Morse potential functions. Along these dissociating coordinates, states  $\Pi_g$  are likely shaped by strong diabatic coupling to some other high lying repulsive state (of  $\Pi_g$  or  $\Delta_g$  symmetry) resulting in a barrier-less dissociating surface. Since we can only expect the density of states to increase at higher energies and compound the complexity of interactions, the dissociative  $\Pi_g$  state was approximated by a function which ‘folds’ the diabatic coupling with the higher lying state into the diagonal element:

$$W_{11} = \frac{1}{2} \left\{ v_M + v_d - \sqrt{(v_M - v_d)^2 + 4[\alpha \tanh(\beta Q)]^2} \right\} \quad (6.8)$$

where  $v_M$  is the Morse potential function,  $v_d$  a decaying exponential and  $\alpha \tanh(\beta Q)$  describes the coupling between these states; as the coordinate dissociates the coupling reaches some asymptotic value. The cost of using this approximate function is that it fails to properly describe the correct topology when moving across several DOF (along which the missing higher lying states that couple diabatically would have appropriately correlated the surfaces).

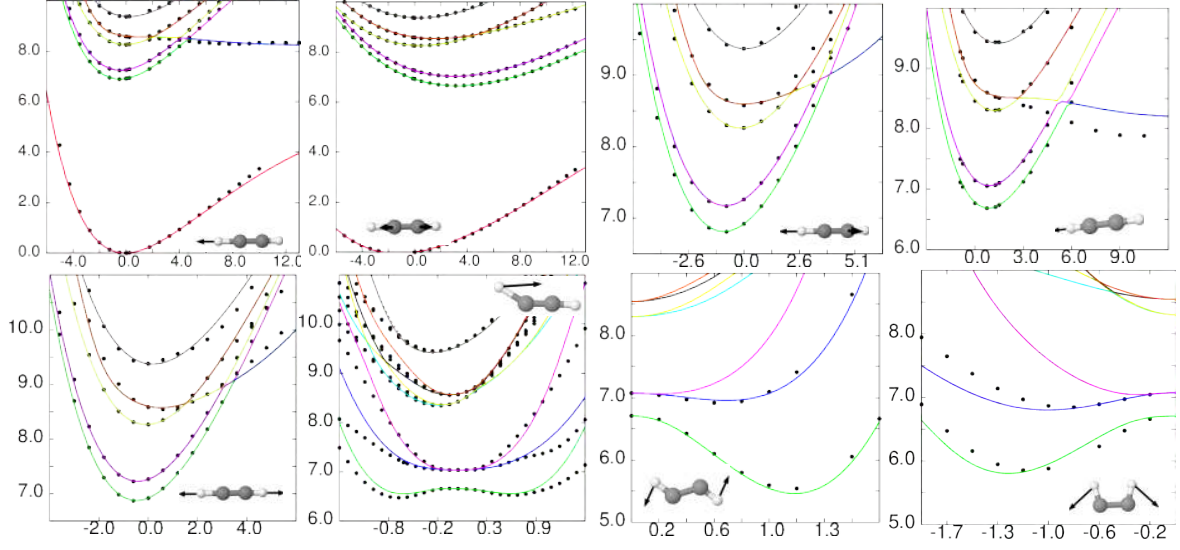


Fig. 6.10: Cuts of fitted excited states model correlating  $Q_{ccs}$  and  $R_{a|b}$  coordinates. First two top left frames also show  $S_0$ . Curly brackets mean the coordinate is kept constant but not at reference geometry. Energy in eV, coordinates in  $\text{\AA}[\text{amu}]^{\frac{1}{2}}$ . Coordinate underlined indicates which coordinate is shown in the x-axis (for mixed angular/radial/normal vectors). From left to right: *first row*: ( $R_a$ ), ( $Q_{ccs}$ ), ( $R_a + Q_{ccs}$ ), ( $R_a - Q_{ccs}$ ); *second row*: ( $R_a + R_b$ ), ( $\theta_a + Q_{ccs}$ ), ( $\theta_a + \theta_b + \{Q_{ccs}\}$ ), ( $\theta_a - \theta_b + \{Q_{ccs}\}$ )

Specifically, when correlating both dissociative,  $R_a$  and  $R_b$ , coordinates the model surface (Fig. 6.10) does not rise as quickly as it should and when correlating  $Q_{ccs}$  with  $R_a$  the dissociating channel does not fall as quickly as it should (Fig. 6.10). Therefore additional *ad-hoc* functions were also used to fits these spaces. For  $j=1,2$ , indexing degenerate state  $\Pi_g$ . Between  $R_a$  and  $R_b$ ;

$$W_{j\Pi_g,j\Pi_g} = \gamma_{R_a,R_b} \cdot \Theta^+(R_a - 0)\Theta^+(R_b - 0) \cdot R_a R_b$$

$$W_{j\Pi_g,j\Pi_g} = \epsilon_{R_a,R_b} \cdot \left\{ \Theta^-(R_a - 0)\Theta^+(R_b - 0) \cdot R_a R_b + \right.$$

$$\left. \Theta^+(R_a - 0)\Theta^-(R_b - 0) \cdot R_a R_b \right\}$$

and between  $Q_{ccs}$  and  $R_a$ ;

$$W_{j\Pi_g,j\Pi_g} = \beta_{R_a,ccs} \cdot \Theta^-(R_b - 0) \cdot \tanh(\lambda_{R_b} R_b) \cdot$$

$$\tanh(\lambda_{R_a} R_a) \cdot \frac{1}{2}(\tanh(\lambda_{ccs}(Q_{ccs} - Q_{ccs}^0)))$$

Bilinear parameters ( $\gamma_{R_a,R_b}$  and  $\epsilon_{R_a,R_b}$ ) correlate  $R_a$  and  $R_b$  with different values along different quadrants.  $\Theta^{+/-}$  are forward/backward step functions.

Although non-differentiable at  $R_{a/b} = 0$  (albeit continuous), these functions do not break symmetry. The bottom right cells in figure 6.10 show the *cis*, *trans* displacement correlating mode  $Q_{ccs}$ ; these cuts approximately show the two important  $S_1$  minima.

Finally, functions that correlate the four dimensional RT modes to the radial  $R_{a/b}$  coordinates were fitted to single point energies along the same selection of distinct vectors in the RT  $\{\phi, \theta\}$  subspace described earlier but including  $R_{a/b}$  contribution. A sample of interesting cuts, describing out-of-plane, bent,

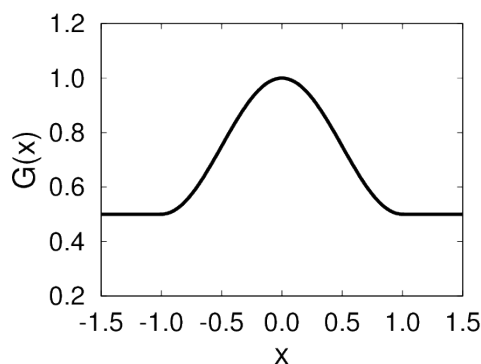


Fig. 6.11:  $G(x)$  function,  $\beta = 1$

*cis* and *trans* geometries leading to dissociation, are shown in Fig. 6.16. The fitting procedure was non-trivial and the genetic algorithm was used (chapter 3), involving 40 optimisation parameters. Since polynomials are not asymptotic functions they are inappropriate for coordinates describing dissociation. The following functions adequately fit these asymptotic surfaces. For pJT coupling elements:

$$W_{ij}(R_a, \theta_a, \phi_a) = \gamma \cdot \tanh(\lambda \cdot R_a) \cdot \sin(\alpha \cdot \theta_a) \cdot G(\beta, \phi_a) \quad (6.9)$$

where

$$G(\beta, \phi_a) = \frac{1}{4} \cdot (\cos(\beta \cdot \phi_a) + 3) \cdot \Theta^+(\phi_a - \frac{\pi}{\beta}) \cdot \Theta^-(\phi_a + \frac{\pi}{\beta}) + \frac{1}{2} \cdot (\Theta^-(\phi_a - \frac{\pi}{\beta}) + \Theta^+(\phi_a + \frac{\pi}{\beta})) \quad (6.10)$$

where  $\gamma$ ,  $\lambda$ ,  $\alpha$  and  $\beta$  are parameters to be optimised. Linear terms corresponding to radial displacements have been replaced by tanh functions, and even/odd polynomial functions were replaced by even/odd trigonometric functions. It is worth mentioning that this function obeys  $D_{2h}$  symmetry op-

erations. One can make it obey  $D_{\infty h}$  constraints, if for, say  $\Pi \otimes \Delta$  coupling, with:

$$\begin{aligned}
 +W_{\Pi_x, \Delta_y}(R_a, \theta_a, \phi_a) &= -W_{\Pi_x, \Delta_y}(R_b, \theta_b, \phi_b) \\
 = +W_{\Pi_x, \Delta_x}(R_a, \phi_a, \theta_a) &= -W_{\Pi_x, \Delta_x}(R_b, \phi_b, \theta_b) \\
 = -W_{\Pi_y, \Delta_x}(R_b, \theta_b, \phi_b) &= +W_{\Pi_y, \Delta_x}(R_a, \theta_a, \phi_a) \\
 = +W_{\Pi_y, \Delta_y}(R_b, \phi_b, \theta_b) &= -W_{\Pi_y, \Delta_y}(R_a, \phi_a, \theta_a)
 \end{aligned}$$

$W_{ij}$  as defined above. For diagonal inter-state diabatic coupling:

$$W_{ii}(R_a, \theta_a, \phi_a) = \gamma \cdot \tanh(\lambda \cdot R_a) \cdot 2(1 - \cos(\alpha \cdot \theta_a)) \cdot G(\beta, \phi_a) \quad (6.11)$$

with similar symmetry conditions and parameters as the aforementioned coupling elements.  $G$  ensures that the functions do not couple too strongly when, say, both  $\theta_a$  and  $\phi_a$  are displaced;  $W_{ii}(R_a, \theta_a, \phi_a) + W_{ii}(R_a, \phi_a, \theta_a)$  asymptotically reach the same value as moving on either  $\theta_a$  or  $\phi_a$  alone).

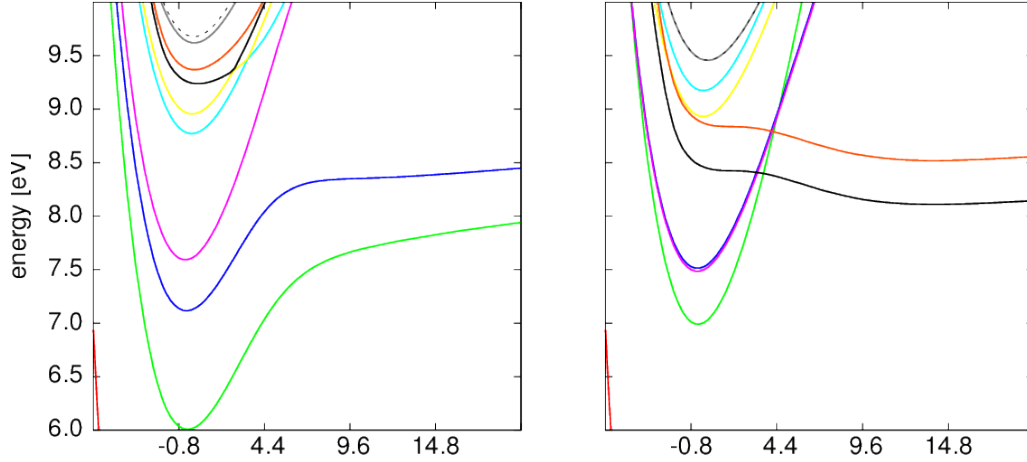


Fig. 6.12: Comparing qualitatively the diabatic (diagonal elements) and adiabatic representations along a dissociating coordinate from a *trans* geometry.

Fig. 6.12 compares a cut along some *trans* dissociation channel in the diabatic and adiabatic representations; the diabatic dissociative  $6\Pi_g$  states get mixed strongly (via pJT coupling) with  $1\Sigma_u^-$  and  $2\Delta_u$  states so that they instead become the dissociative channel.

We can compare the final fitted model to others in the literature; in three papers, Koppel, Lischka *et al* [80,82] reproduced the  $S_1$  and  $S_2$  spectra. They



propagated a wavefunction in a 3 dimensional subspace enabling the in-plane *cis-trans* isomerisation. Later work [84] included non-adiabatic interactions along out-of plane motion. They used the Jacobi coordinates depicted in Fig. 6.13. The CC and CH bond lengths were kept constant,  $R$  denotes the distance between the centres of mass of the two CH subunits,  $\Phi_1$  and  $\Phi_2$  are the angles between  $R$  and the CH bonds.

Their resulting potential energy is reproduced in the left cells of Fig. 6.14 next to the energy obtained in this model along those same coordinates.

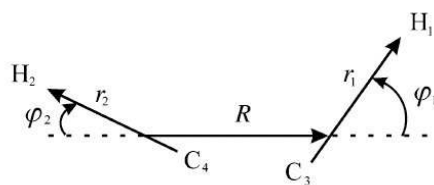


Fig. 6.13: Diagram of Jacobi coordinates, re-printed from ref [80]

This model does not reproduce either plot qualitatively suggesting the way the curval coordinates carve geometry space

differs significantly from Jacobi, struggling to reproduce the detailed features around these regions.  $S_1$  seems to be  $\sim 0.22$  eV lower than the CASPT2/ANO reported ones [82]. However, the  $S_1$  *trans*-linear relative barrier heights are in agreement ( $\sim 1.1$  eV).

The right-most cell in Fig. 6.14 shows the *cis-trans* isomerisation along  $\theta_a \pm \theta_b$  curval modes; although qualitatively closer they still fail to exhibit the *trans* double minima with differing-angles for  $\theta_a$  and  $\theta_b$  in  $S_2$  obtained by Malsch *et al* [80]. It is worth mentioning that this double minima is found when moving slightly out of plane for both for non-planar differing-angle *cis* (referring to the CCH angle) and differing-angle *trans* geometries (see Table 6.3). A significant approximation to this model is that no effort was made to include any coupling to the ground state, so that non-radiative relaxation to the ground state will not be reproduced (as observed by Schmidt *et al* [75], see Table 6.1). Theoretically, such possible pathway was found by Cui and

Morokuma [87] along a geometry with strong dihedral and angle values ( $\sim 90^\circ$  for both angles) with a CH bond length of 2.111 Å, very close to dissociation.

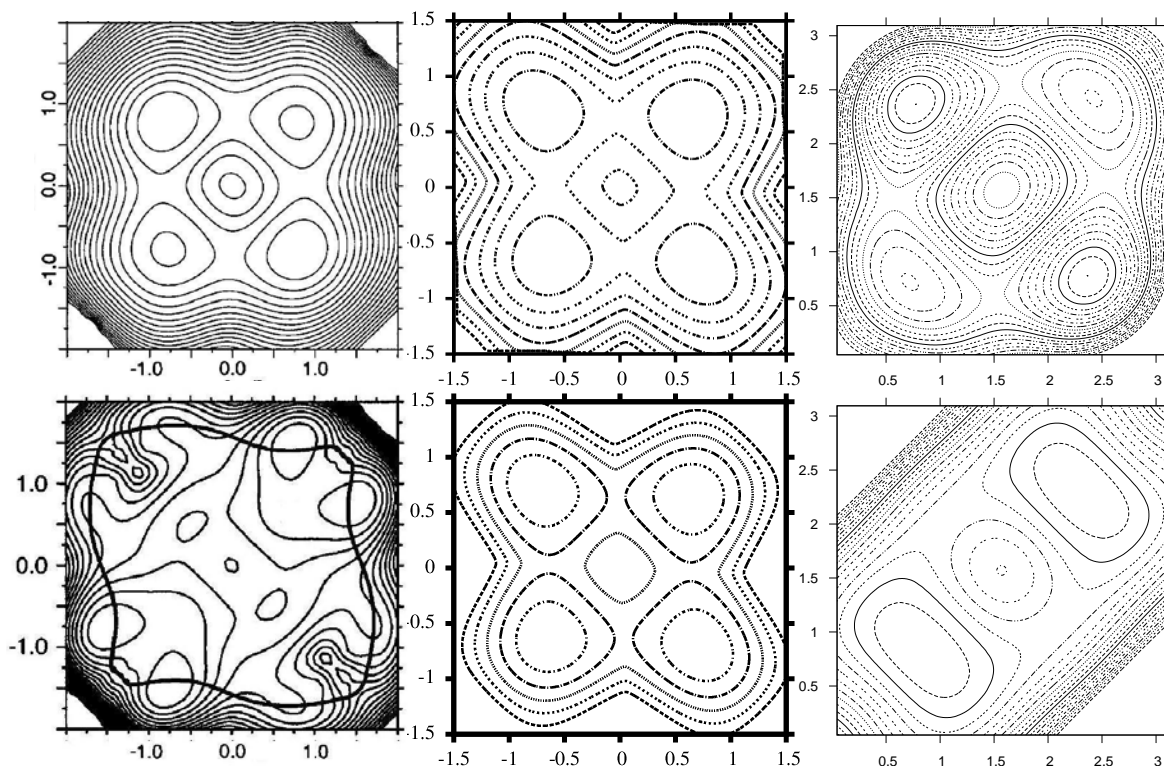


Fig. 6.14: Comparing model energy surfaces from ref [82] and this model.  $S_1$  (top) and  $S_2$  (bottom). left: Model from [82] along Jacobi  $\Phi_1$  and  $\Phi_2$ , centre: this model along Jacobi  $\Phi_1$  and  $\Phi_2$ , right: this model along  $\theta_1$  and  $\theta_2$  (analogous angular displacements to Jacobi  $\Phi_1$  and  $\Phi_2$  described in this chapter).

Such long displacements are poorly described by the present curved modes; as the H atom dissociates the conservation of centre of mass makes the triple carbon bond contract, thus raising the potential energy. Such crossing cannot be realistically fitted with these coordinates. Another potential crossing was suggested by Laruelle *et al* [81] in a figure showing an avoided crossing along the CH dissociation coordinate. Based on the electronic structure calculations shown in Table 6.2 we suggest their symmetry label assignment to  $\Pi_g$  and  $\Pi_u$  states were incorrectly swapped; at the  $D_{\infty h}$  geometry, it is  $\Pi_g$  which is the dissociative coordinate.

To certify whether such crossing occurs or not, a high accuracy calculation was performed; a aug-cc-pVTZ basis with 3 extra even-tempered functions (ratio=2.5) [45] on the dissociating carbon and hydrogen atoms were added. Using  $C_{2v}$  symmetry and starting at a 1.713 Å bond length, a CAS(8,8) energy was obtained after several calculations with different active orbitals to test for their contribution to the first three ex-

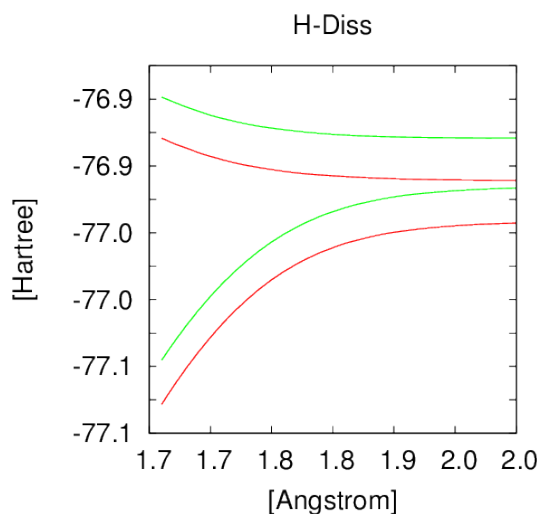


Fig. 6.15: Cut along H-dissociation using CAS+RS2 (*green*) and MRCI+Davidson (*red*).

cited states. From this active space, RS2C and MR CI (cluster corrected Pople/Davidson) calculations were performed, plotting the hydrogen dissociation coordinate (Fig. 6.15). No crossing is found between  $S_0$ - $S_1$  at the linear geometry with these methods. No crossing was found along any other geometry with the level of theory used for the model construction. This model therefore assumes that all density past the  $S_{1/2}$  asymptotic regions ( $> 1.5$  Å C–H bond length) of all states above  $S_0$  does not cross with any other state. To explore the adiabatic potential energy landscape of this model, we performed thousands of simplex optimisations with initial geometries set at different points in an equidistant grid. Fig. 6.17 shows the energies that each simplex optimisation gave, arranged in increasing energy. They give some qualitative insight into the basin landscape of the model. For the left cells of the figure, one of the dissociative coordinates was stretched to 1.9 Å and frozen during the optimisation to give some perspective on the landscape near dissociation; the model suggests a *trans* geometry to be the lowest energy towards dissociation in  $S_1$ , but with *cis* conformations only  $\sim 0.4$  eV

above.

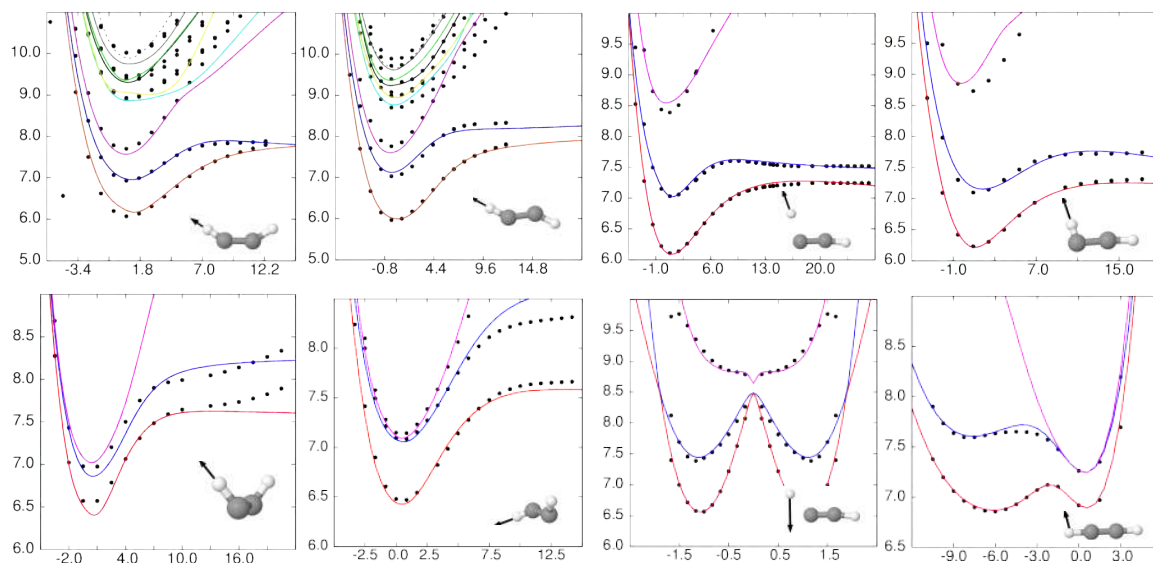


Fig. 6.16: Cuts of fitted model correlating  $\theta$ ,  $\phi$  and  $R_{a|b}$  coordinates. Curly brackets mean the coordinate is kept constant but not at reference geometry. Energy in eV, coordinates in  $\text{\AA}[\text{amu}]^{\frac{1}{2}}$ . Coordinate underlined indicates which coordinate is shown in the x-axis (for mixed angular/radial/normal vectors). From left to right: *first row* : *cis* dissociation ( $\{\theta_a - \theta_b\} + \underline{R_a}$ ), *trans* dissociation ( $\{\theta_a + \theta_b\} + \underline{R_a}$ ), bent dissociation ( $\{\theta_a\} + \underline{R_a}$ ), 2D bent-dissociation ( $\{\phi_a + \theta_a\} + \underline{R_a}$ ); *second row*: out-of-plane dissociation ( $\{\theta_a + \phi_b\} + \underline{R_a}$ ), skewed, out-of-plane dissociation ( $\{\theta_a + \theta_b + \phi_a - \phi_b\} + \underline{R_b}$ ), angle while CH stretched ( $\underline{\phi_b} + \{R_b\}$ ), simultaneous ( $\phi_a + \underline{R_a}$ )

For  $S_2$  the dissociation geometries favoured are out-of-plane or unequal-angle *cis*. Some sampled energies and geometries are given in Table 6.3; these are simply representative of the frequency with which these were found based on a few samples chosen and shouldn't be taken to be too precise (a more accurate picture will be provided in section 6.4.3). For  $S_3$  only basins of out-of-plane unequal-angle *cis* geometries with closely similar energies were found. A wavefunction relaxation in the  $S_1$  state gives energies of 5.4 eV + ZPE = 6.024 eV, using ZPE in line with literature [87].

## Absorption spectra

The  $S_1$  minimum has been found experimentally [76] and theoretically [83] to be at a *trans* bent geometry with an isomerisation barrier to its *cis* conformer via a torsional motion. Consequently, the absorption spectra is dominated by a long progression arising from  $S_1$  *trans*-bending mode as well as contributions arising from CC and possibly CH (totally symmetric) stretch modes. The  $S_0 \rightarrow S_1$  maximum intensity is not discernible as it lies higher than the onset of the  $S_0 \rightarrow S_2$  transition (6.71 eV). The  $S_0 \rightarrow S_1$

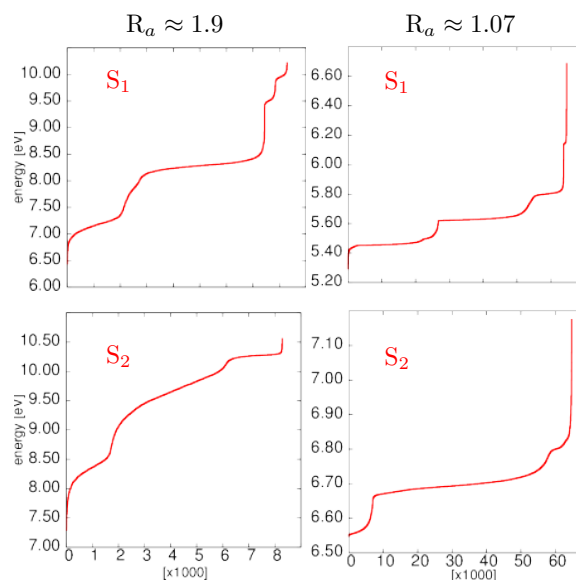


Fig. 6.17: Energy ordered simplex optimisations with initial geometries making a full DOF grid over most of the potential landscape. *first row: left cell shows critical points of  $S_1$  with one radial coordinate stretched to  $\sim 1.9$  Å, right  $S_1$  full optimisation second row: left  $S_2$  as above right  $S_2$  as above*

maximum is believed to lie 1.5 eV above the band origin [80]. From the discussion in section 6.3, it is likely that the spectrum arises from a combination of symmetric CC stretches together with *cis/trans* vibrations. To confirm this, we calculated three different theoretical spectra from reduced dimensionality models; a 4-dimensional model of Renner-Teller, *cis/trans* coordinates ( $\{\theta, \phi\}$ ), a 5-dimensional model including the CC symmetric stretch ( $Q_{ccs}$ ) and a full, 6-dimensional model further including the radial CH coordinates ( $R_{a|b}$ ). To reproduce such spectra, a nuclear wave-packet was propagated for 120 fs on these surfaces using the MCTDH algorithm [21]. Mode combination for coordinates  $\{\theta_a, \phi_a\}$  (and similarly for b) were used, since these are coupled via the kinetic energy operator (equation 6.7). The radial co-

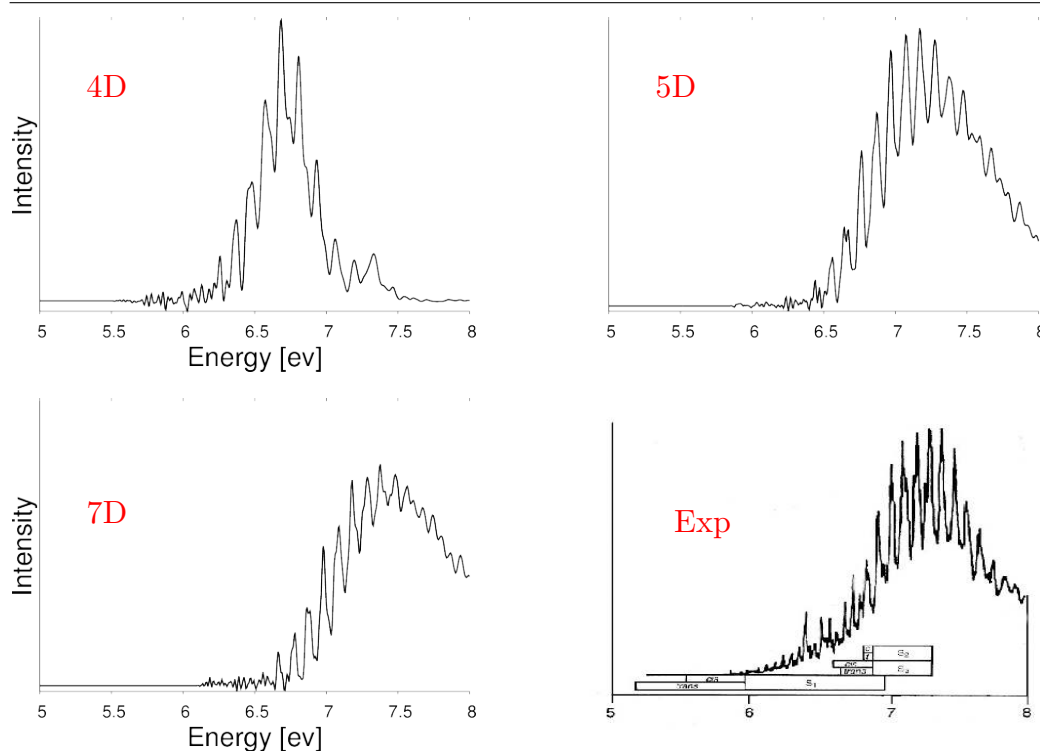


Fig. 6.18: *top left*: Calculated spectra for 4D Renner-Teller subspace, ten state model. *top right*: Calculated 5D spectra including CC stretch ( $Q_{ccs}$ ) in first excited state. *bottom left*: Calculated 7D spectra including radial coordinates ( $R_{a|b}$ ). *bottom right*: Experimental Spectra [79]; Image edited from Malsch *et al* [80], providing assignments for *cis/trans* progressions in  $S_1$ - $S_3$ .

ordinates were also mode-combined, since they have terms correlating them (Fig. 6.10). At least twelve single particle, two-dimensional functions (SPF) were used to represent the time dependent basis for each state. The relaxed ground state wavefunction is initially operated on by the transition dipole from the  $\langle S_0 | \mu | S_1 \rangle$  elements of this coordinate subspace using a linear approximation. By multiplying the autocorrelation of the resulting propagated wavefunction by a trigonometric damping function and fourier transforming this product, we obtain a theoretical estimate for the experimental absorption spectra (Fig. 6.18). It should be mentioned that this propagation time (120) may have not been sufficient to resolve the 7D peaks properly (this correction will be done in in future work). The resulting 4D spectra (top left in Figure 6.18) is in qualitative agreement with experiment around the energy range corresponding to  $S_1$  and  $S_{2/3}$  *cis* and *trans* progressions, but is

clearly missing progressions at energies 6.75-7.5. Both the 5D and 7D spectra gave results that qualitatively match the experimental spectrum (also provided in 6.18) and resemble each other significantly, suggesting that the radial vibrations may not be significantly excited during the excitation. This is in agreement with the models built using normal coordinates (section 6.3). It is also in accord with the fact that valence  $\pi\pi^*$  orbital excitations typically don't significantly affect the CH bond length. Therefore, we can have some confidence the model reproduces the qualitative behaviour of acetylene.

### 6.4.3 Modelling the vibrationally mediated dissociation of acetylene

As discussed in the previous section, the coordinates used are essentially a pair of spherical polar coordinates and a normal mode, the most natural choice of primitive basis function with which to construct our nuclear wavefunctions are the Legendre polynomials (being eigenfunctions of  $L^2$ ), radial Harmonic Oscillator (HO) functions and harmonic oscillator eigen functions for the bound  $Q_{ccs}$ . The radial HO representation is defined on  $[0, \infty)$  and has only the odd harmonic oscillator functions as a basis [21],  $\phi_{2j-1}^{HO}(R)$ , related to the Hermite polynomials. When diagonalizing the position operator, the weights of every DVR grid point are given by:

$$w_{\alpha}^{\frac{1}{2}} \propto R^{-1} \cdot U_{1\alpha} \quad (6.12)$$

where  $U$  is the matrix that transforms from the FBR to DVR representation. The factor  $R^{-1}$  ensures the differential volume element from the Jacobian determinant ( $r^2$  factor) for the radial part of the spherical harmonic transformation is properly treated. This allows us to simplify the KE into the form given in equation 6.7.

Table 6.1 describes how experimentalist have performed energy resolved VMD experiments probing the range 5.5-7.0 eV. They have done so by preparing the initial ground state wavefunction to have quanta along local dissociation modes [98] with IR field followed by UV-excitations to the appropriate energy band. Though there exist methods [21] in the MCTDH package to ex-

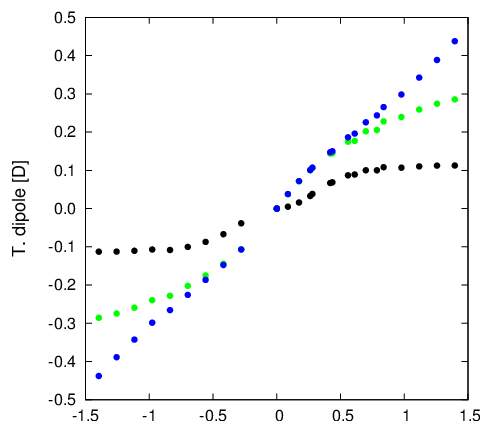


Fig. 6.19: Transition dipole along  $\theta_a$ ; *black*:x-plane for  $1\Sigma_u^-$ , *blue*: x-plane for  $1\Delta_u^x$ , *green*:y-plane for  $1\Delta_u^y$  with the ground state. The sign of the surface is reversed for coordinate  $\theta_b$ .

plore the eigenfunctions of a vibronic Hamiltonian, locating the appropriate mode combination eigenstates require the computation of a large number of eigenfunctions making such a method prohibitively expensive. Instead, for the Morse Hamiltonian describing the ground state  $R_{a|b}$  coordinate:

$$H = \frac{p^2}{2m} + D(e^{-2\alpha(R_{a|b}-r_0)} - 2e^{-\alpha(R_{a|b}-r_0)}) \quad (6.13)$$

the following approximate raising operator was used on a previously relaxed ground state wavefunction:

$$L = \frac{1}{\sqrt{2m\omega}} \left[ \left( \Lambda - \frac{1}{2} \right) \alpha - \Lambda \alpha e^{-\alpha(R_{a|b}-r_0)} + i \cdot p \right] \quad (6.14)$$

$$\omega = \alpha \sqrt{2D/m} \quad \text{and} \quad \Lambda = \frac{\sqrt{2D/m}}{\alpha}$$

The next step is to simulate the UV-excitation in a narrow energy range. To do this, we modelled a laser field as a Gaussian envelope with the appropriate central frequency interacting with the transition dipole surface of the molecule. The transition dipole surfaces has been linearly approximated; Fig. 6.19 shows some of the surface cuts along the coordinates with some contribution. These surfaces peak at *trans* geometries and cancel along *cis* for  $S_1$  and  $S_2$ . The transition dipole along the z-component also has some



significant value. To keep things manageable, in this work we are only exciting along the x-component. This should give identical results than along the y-component since the x and y vectors form a  $\Pi_u$  representation. Like diabatic coupling, transition dipole coupling also exhibits pJT like relations amongst the states. For example, from symmetry considerations, it is possible to show that  $\langle \Sigma_g^+ | \mu | \Delta_u \rangle$  transition dipole surfaces expanded to first order in nuclear coordinates have the following relations:

$$\begin{aligned}
 \langle \Sigma_g^+ | \mu_x(\theta_a) | \Delta_u \rangle &= -\langle \Sigma_g^+ | \mu_y(\theta_b) | \Delta_u \rangle = -\langle \Sigma_g^+ | \mu_x(\theta_b) | \Delta_u \rangle = \\
 \langle \Sigma_g^+ | \mu_y(\theta_a) | \Delta_u \rangle &= +\langle \Sigma_g^+ | \mu_y(\phi_a) | \Delta_u \rangle = -\langle \Sigma_g^+ | \mu_y(\phi_b) | \Delta_u \rangle = \\
 \langle \Sigma_g^+ | \mu_x(\phi_b) | \Delta_u \rangle &= -\langle \Sigma_g^+ | \mu_x(\phi_a) | \Delta_u \rangle
 \end{aligned} \tag{6.15}$$

Similar terms can be obtained for  $\langle \Sigma_g^+ | \mu | \Sigma_u^- \rangle$ . The field was enveloped under a Gaussian function to avoid the cost of propagating a wavefunction under a permanent time-dependent external field; under such conditions, the constant mean-field integration scheme [21], where the mean-field matrices are kept constant for longer time-steps than the single-particle functions and MCTDH coefficients, cannot be used. Due to computational limitations, it was only possible to model pulses in the range of tens of femtoseconds. Modelling a femtosecond laser pulse restricts the energy resolution we can achieve as its Fourier decomposition will result in a spread of frequencies given by the uncertainty principle; a bandwidth with a full width at half maximum (FWHM) of 0.14 eV was obtained with a pulse of  $\Delta t = h/\Delta E = [\text{eV} \cdot \text{fs}]/[\text{eV}] = 4.135/0.14 \sim 30$  fs FWHM long. The pulse is modelled using a Gaussian envelope

$$\varepsilon(t) = \frac{s}{\sigma} \sqrt{\frac{4\ln 2}{\pi}} \exp\left(-\frac{4\ln 2}{\sigma^2}(t-t_0)^2\right) \cos(\omega(t-t_0)) \tag{6.16}$$

where  $\sigma$  is the FWHM,  $s$  the strength parameter of the pulse and  $\omega$  the central frequency. Since the excited states have different resonances to different

central frequencies, the population transferred is variable. However, to ensure that at least 1% of the population is transferred for all tests (in some instances it is full population transfer), the strength parameter was set to 70. Step functions were placed at the tails of the Gaussian envelope to help with numerics. At least eight SPF per state were required to ensure that, for every mode combination, the last SPF contributes at most  $\sim 1.0 \cdot 10^{-4}$  to the wavefunction. Together with a sufficiently large grid in momentum space we guarantee the convergence of the wavefunction. This required 51 grid points for  $\theta$ , 39 for  $\phi$ , 91 for  $R$  and 75 for  $Q_{ccs}$ . After the pulse had ensued ( $\sim 65$  fs), the propagation was halted and the CMF algorithm was used to continue the propagation for another 200 femtoseconds.

Six equidistant central frequencies with energies of  $6.4\text{-}7.8 \text{ eV} + (\text{ZPE}_{S_0}) - \Delta^{IR}$  were used, where  $\Delta^{IR}$  is the energy gained from the Morse raising operator. With this operator we ‘IR’ pre-excite wavefunctions with the fundamental and overtones 2, 3, 5 and 7 to test with the mentioned pulses. Complex absorbing potential (CAP) were used to annihilate any components to the wavefunction that attempt to leave the grid along the  $R_{a|b}$  coordinates. Details for 36 propagations where we vary the initial overtone and central UV frequency are tabulated in 6.7. From this table, the following trends are apparent: with increasing total excitation energy, we obtain more population transferred from the ground state to excited states and greater dissociation. Exciting with a total energy centred around 6.4 eV might reduce the number of states available to populate (resonant), probably being near the first vibrational  $S_1$  state. Although pre-exciting to higher overtones reduces the overall transfer of population when applying the UV-pulse, the flux across dissociation channels increases significantly compared to no pre-excitation.

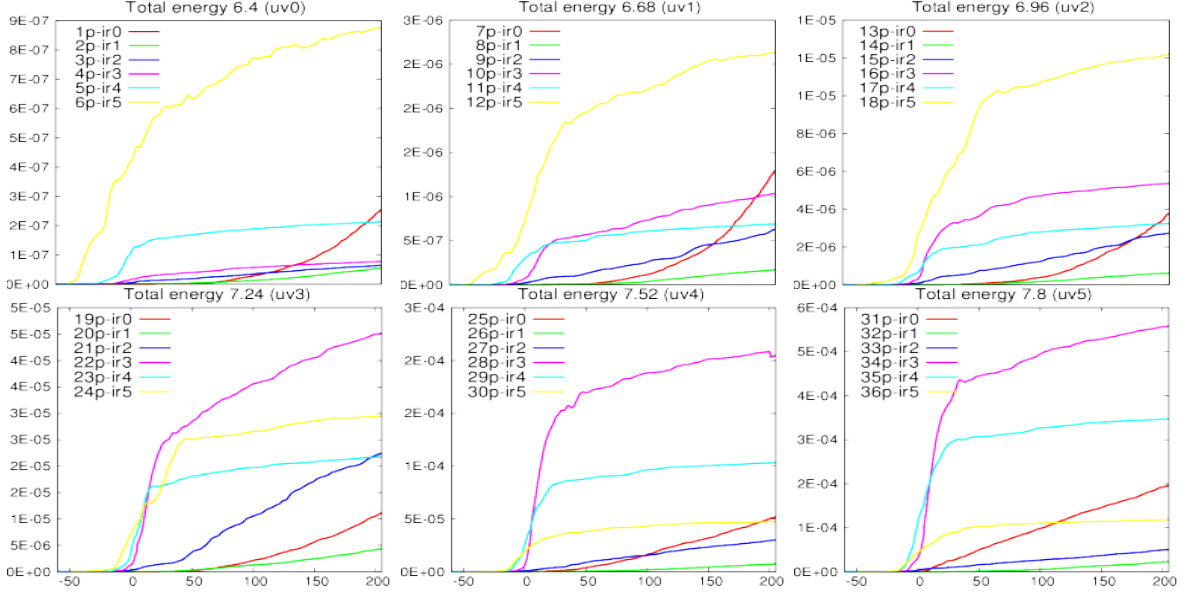


Fig. 6.20: Cumulative flux (y-axis) across dissociation channel along  $R_a$  for 36 experiments over 265 fm (x-axis). Time=0 fs determines when the UV-pulse has finished. Key labels refer to Table 6.7 and to flux maps in sub-Appendix 6.A.

This can be best illustrated, using the labelling in table 6.7, by noting that run 25p-uv4-ir0 (no pre-excitation, but almost full transfer from the ground state) dissociates as much as 30p-uv4-ir5 (large pre-excitation, but less 0.5% transfer from the ground state). It seems that preparing the initial wavefunction in a higher local CH mode reduces the ground state wavefunction overlap with excited state eigenfunctions but increases the energy imparted towards dissociation. From Fig. 6.20 we can see that for pre-excited pulses most of the transfer occurs shortly after the pulse, whereas for the ground state wavefunction the transfer often continues to accelerate even after 200 fs. We were able to determine the favoured geometries at the time of dissociation for the first 265 fs of dynamics. Figures 14-22 provided in sub-Appendix 6.A (some examples reprinted in Fig. 6.21) show sets of frames of flux across the dissociating channels of  $R_a$  for coordinates  $\theta_a$  (y-axis:  $(\frac{\pi}{2}, 0)$ ) and  $\phi_a$  (x-axis:  $(\frac{\pi}{2}, \frac{3\pi}{2})$ ) while keeping some  $\theta_b$  fixed in each frame.

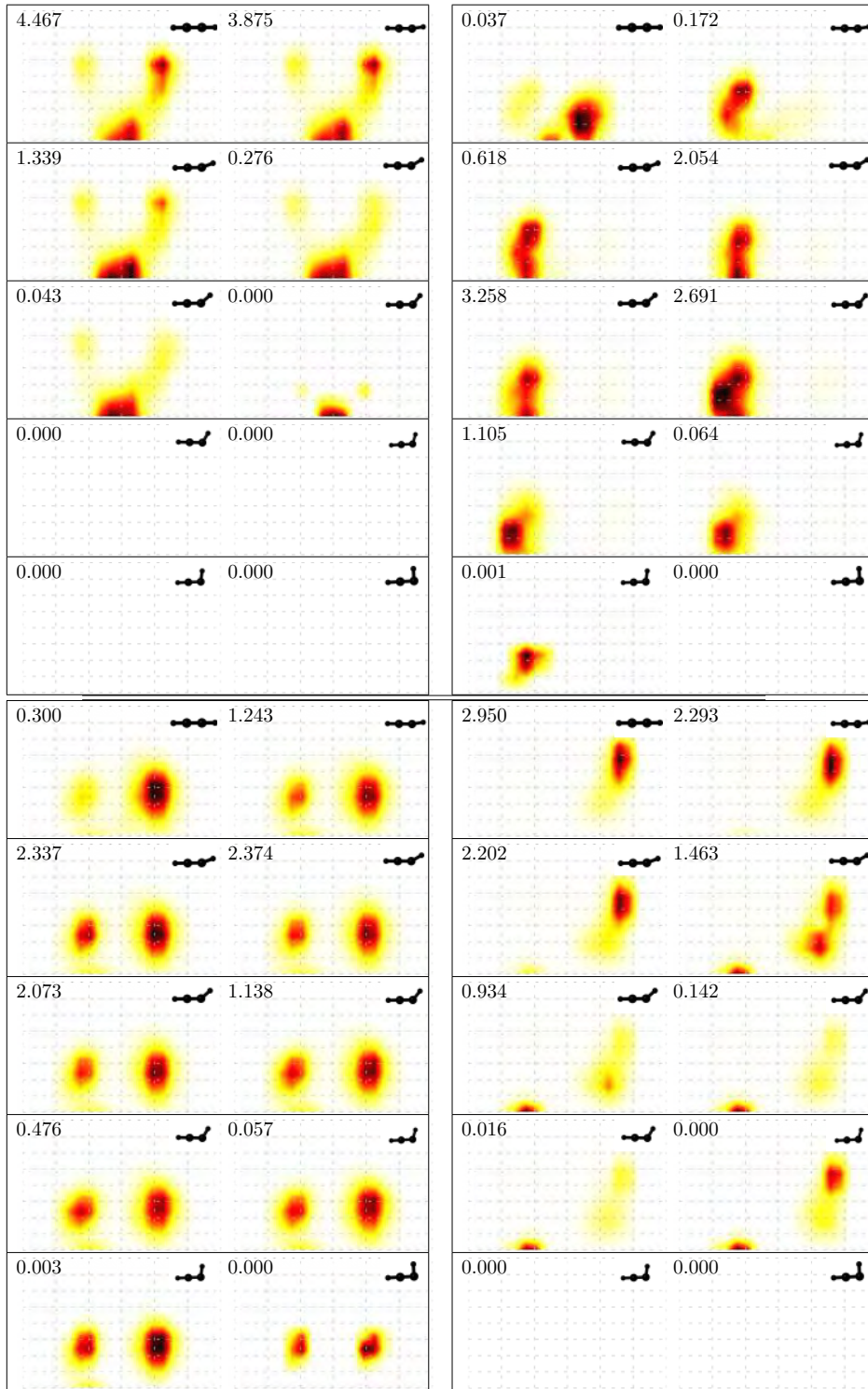


Fig. 6.21: Four sub-figures representing a 3D angular-coordinate subspace (in ten 2D frames) displaying the total flux across a  $R_a$  dissociation channel 200 fs after pulse. On the top LHS of each frame, the contribution (Normalised to 10.0) of the given frame to the total density across this subspace for each propagation is printed. In brackets (Total E (eV), Morse Overtone). *top left*: 25p-uv4-ir0 (7.52,0) - near linear, *top right*: 9p-uv1-ir2 (6.68,2) - *trans* (with slight out of plane), *bot left*: 5p-uv0-ir4 (6.4,5) - mixture of *cis* and *trans* (with slight out of plane), *bot right*: 29p-uv4-ir4 (7.52,5) - bent and *cis* (with strong out of plane)

Each frame shows a value of  $i$  for  $\theta_b = (\pi/2 - \frac{\pi/2 \times i}{10})$ ,  $i = 0, 1, \dots, 9$ . Recall that  $\theta_b = \pi/2$  (in equilibrium).  $\phi_a$  roughly describes out-of-plane geometries (for given  $\theta_a$  and  $\theta_b \neq$  equilibrium). Throughout all maps  $\phi_b = \pi$ , fixed in the equilibrium geometry. In other words, each set of frames shows a 3D subspace representing distinguishable geometries (i.e. *trans*, *cis*, linear, bent and out-of-plane geometries), with a colour map determining the flux across that dissociation channel. It should be mentioned that in the present experiment, where we modelled a plane polarised pulse along the  $xz$ -plane, the flux across *trans*, *cis* motion in the  $yz$ -plane should not result in the same as the  $xz$ -plane (not shown in figures). Each frame was obtained by generating a collection of geometry grid points representing the final flux across  $R_a$  dissociation of the wavefunction around this region. The flux in this subspace is obtained by first acting on the wavefunction with a product of box functions so as to only leave density around the specific grid geometry  $\theta_a = \theta_{a0}$ ,  $\phi_a = \phi_{a0}$ ,  $\theta_b = \theta_{b0}$ ,  $\phi_b = \pi$ :

$$\begin{aligned} \hat{\Theta}|\Psi\rangle = & \left[ \begin{aligned} & [\Theta^+(\theta_a - \theta_{a0}^+) \cdot \Theta^-(\theta_a - \theta_{a0}^-)] \cdot \\ & [\Theta^+(\phi_a - \phi_{a0}^+) \cdot \Theta^-(\phi_a - \phi_{a0}^-)] \cdot \\ & [\Theta^+(\theta_b - \theta_{b0}^+) \cdot \Theta^-(\theta_b - \theta_{b0}^-)] \cdot \\ & [\Theta^+(\phi_b - \frac{21\pi}{20}) \cdot \Theta^-(\phi_b - \frac{19\pi}{20})] \end{aligned} \right] |\Psi\rangle \end{aligned} \quad (6.17)$$

where  $\Theta^\pm$  are the forward and backward step functions.  $\theta_{a0}^\pm = \theta_{a0} \pm \frac{\pi}{20}$ . By setting  $\theta_{a0}^\pm$  so as to make a 4D box function of width  $\frac{\pi}{10}$  and centred at  $\{\theta_a = \theta_{a0}, \phi_a = \phi_{a0}, \theta_b = \theta_{b0}\}$ . The flux is evaluated by taking the expectation value of the commutator of a step function along  $R_a$  with the kinetic energy operator:

$$\langle \Psi | \left[ \Theta^+(R_a - R_{diss}), \hat{p}_i^2 + \frac{\hat{L}_i^2}{R_a^2} \right] | \Psi \rangle \quad (6.18)$$

Table 6.6 clarifies the results by giving the most likely geometries at the moment of dissociation for a given IR pre-excitation (Morse overtone using the ladder operator) and UV pulse. The observations and predictions this model makes can be summarised as follows:

- Exciting in the region of 6-7 eV (including ZPE) should lead to dissociation in a slightly out-of-plane *trans* geometry, unless we pre-excite with more than 2.2 eV along the CH vibration, where the molecule is likely to dissociate at near-linear and bent geometries. These channels are likely to belong to  $S_1$ .
- Exciting above 7 eV (including ZPE) from the ground state we obtain a mixture of out-of-plane *cis* and *trans* geometries. These channels are likely to belong to  $S_1$ .
- We obtain strong out-of-plane, *cis* geometries by exciting from high overtones to energies in the 7.5-7.8 eV range. These channels are likely to belong to  $S_2$ .
- No pure *cis* dissociating geometries were seen, having at least some out-of-plane contribution. No *cis* was found below  $\sim 7$  eV

Since we are working in a diabatic representation which was built from strongly mixed adiabatic of states and a pulse which results in an energy band of 0.14 eV width, it is not possible to determine with confidence to which adiabatic states these different dissociating channels belong to. However, based on the simplex minimisation Fig. 6.17 and geometries given in Table 6.3, we suggested the most likely adiabatic state responsible for the results obtained. The MCTDH operator file for this curvilinear model is provided as supplementary information B.

## 6.5 Conclusions

The  $D_{\infty h}$  totally symmetric symmetry adapted polynomials basis generated in chapter 5 were used to fit full internal DOF models using normal and curvilinear coordinates. A pair of normal coordinate models was built to test any effects pseudo Jahn-Teller or Renner-Teller coupling might have on spectra and dynamics. They also tested the equivalence between the explicit inclusion of higher lying diabatic states with strong coupling to the lower states of interest against a representation where the diabatic coupling to these higher lying states is folded into the diagonal part of the potential matrix of our lower diabatic states. The conclusions, albeit far from definitive, are that Renner-Teller coupling has little effect in the spectra of the first three excited states, and dynamics is equally well described by either representations mentioned. Since the mode did not include correlation along out-of plane motion, where coupling between  $S_1$  and  $S_2$  is known to occur, this model could not probe the effect pseudo Jahn-Teller coupling has on the non-adiabatic interactions between these states. A second set of coordinates were used to construct a model that include Renner-Teller and pseudo Jahn-Teller coupling along dissociation coordinates. To use the symmetry adapted

Over tone	Total Energy (eV): IR + UV					
	6.4 (uv0)	6.68 (uv1)	6.96 (uv2)	7.24 (uv3)	7.52 (uv4)	7.8 (uv5)
0 (ir0)	[T2-P1][T2-P1][T2-P1][T2-P1][C2-P2][B2-P2] [T2-P2][T2-P2][C2-P2]					
1 (ir1)	[T2-P1][T2-P1][T2-P1][T2-P2][T2-P2][T2-P2]					
2 (ir2)	[T2-P0][T2-P0][T2-P0][T2-P1][T2-P0][T1-P0]					
3 (ir3)	[L -P0][T2-P0][T2-P0][T2-P1][T2-P0][T1-P0] [B2-P2]					
5 (ir4)	[L -P0] [B2-P1]	[L -P0] [B2-P2]	[L -P0] [B2-P2]	[B2-P2] [T2-P0]	[B2-P3] [C2-P2]	[B2-P3] [C2-P3]
7 (ir5)	[L -P0]	[L -P0]	[L -P0]	[B2-P2] [T2-P2] [C2-P2]	[B2-P3] [C2-P2]	[B2-P3] [C2-P3]

Table 6.6: Approx. geometries of dissociating H atom based on VMD flux maps like those in Fig. 6.21. *Legend:* letters; T=trans, C=cis, B=bent, L=linear, P=out-of-plane coordinate contribution to T or C. *numbers:* 0=0°, 1= $\frac{\pi}{8}$ °, 2= $\frac{2\pi}{8}$ °, 3= $\frac{3\pi}{8}$ °.

Note: B geometries P cannot refer to out-of plane geometries (dihedral angle not defined), but instead corresponds the location of the density in the 2D flux maps.

matrix of our lower diabatic states. The conclusions, albeit far from definitive, are that Renner-Teller coupling has little effect in the spectra of the first three excited states, and dynamics is equally well described by either representations mentioned. Since the mode did not include correlation along out-of plane motion, where coupling between  $S_1$  and  $S_2$  is known to occur, this model could not probe the effect pseudo Jahn-Teller coupling has on the non-adiabatic interactions between these states. A second set of coordinates were used to construct a model that include Renner-Teller and pseudo Jahn-Teller coupling along dissociation coordinates. To use the symmetry adapted

basis, coordinates spanning  $D_{\infty h}$  irreducible representations were devised by a spherical polar transformation from rotated Normal coordinates. Ten states were required to more accurately fit the first three excited states using these 1D product-form functions. The model agrees well with the critical points reported in the literature, correctly describing the  $S_1$  and  $S_{2/3}$  minima as well as out-of-plane geometries. Theoretical absorption spectra were calculated and compared well with the experimental spectra, serving as validation of the model. The model was used to emulate VMD experiments akin to those found in the literature. This was done by operating the initial ground state wavefunction with Morse ladder operators, mimicking IR pre-excitation, followed by a Gaussian enveloped sinusoidal function representing an experimental pulse polarised laser field. The model suggests that for energies in the range 6.4-7.0 eV,  $S_1$  can give *trans* or linear/bent geometries depending on the IR pre-excitation of CH stretch local modes. Similar control can be obtained in the range 7-8 eV for state  $S_2$ , where we can also obtain dissociation at *cis* geometries. These results complement and agree with many of the observations reported in the literature; indeed the *trans* mode plays an important part in the dissociation mechanism, but this work adds further light into the dynamic behaviour of this archetypal system.



**Theoretical flux across dissociation coordinates in the vibrationally mediated dissociation of acetylene**

**6.A**

Tot E (eV) <sup>a</sup>	Label	M O b	GS En (eV) <sup>c</sup>	C Freq E (eV) <sup>d</sup>	% S <sub>0</sub> Pop <sup>e</sup>	Tot Diss <sup>f</sup>	Tot Diss <sup>g</sup>
6.40	1p-uv0-ir0	0	0.755812	5.644188	0.93272611	0.00001	0.01035
	2p-uv0-ir1	1	1.243326	5.156674	0.99513311	0.00001	0.00219
	3p-uv0-ir2	2	1.452592	4.947408	0.99889976	0.00003	0.00216
	4p-uv0-ir3	3	1.693773	4.706227	0.99984823	0.00006	0.00208
	5p-uv0-ir4	5	2.208312	4.191688	0.99994895	0.00166	0.00826
	6p-uv0-ir5	7	2.728493	3.671507	0.99983620	0.03261	0.08193
6.68	7p-uv1-ir0	0	0.755812	5.924188	0.80290768	0.00002	0.03805
	8p-uv1-ir1	1	1.243326	5.436674	0.97325940	0.00004	0.00853
	9p-uv1-ir2	2	1.452592	5.227408	0.99135512	0.00016	0.02151
	10p-uv1-ir3	3	1.693773	4.986227	0.99791293	0.00045	0.02577
	11p-uv1-ir4	5	2.208312	4.471688	0.99977558	0.00170	0.01856
	12p-uv1-ir5	7	2.728493	3.951507	0.99937751	0.00184	0.05784
6.96	13p-uv2-ir0	0	0.755812	6.204188	0.63214908	0.00011	0.14830
	14p-uv2-ir1	1	1.243326	5.716674	0.90362589	0.00050	0.03097
	15p-uv2-ir2	2	1.452592	5.507408	0.96092724	0.00203	0.09330
	16p-uv2-ir3	3	1.693773	5.266227	0.98791055	0.00902	0.16378
	17p-uv2-ir4	5	2.208312	4.751688	0.99849079	0.02113	0.11037
	18p-uv2-ir5	7	2.728493	4.231507	0.99840603	0.10555	0.46281
7.24	19p-uv3-ir0	0	0.755812	6.484188	0.44770916	0.00034	0.46996
	20p-uv3-ir1	1	1.243326	5.996674	0.75210196	0.00156	0.16474
	21p-uv3-ir2	2	1.452592	5.787408	0.86979412	0.00807	0.81784
	22p-uv3-ir3	3	1.693773	5.546227	0.94852116	0.04258	1.07881
	23p-uv3-ir4	5	2.208312	5.031688	0.99267406	0.34027	1.13715
	24p-uv3-ir5	7	2.728493	4.511507	0.99669197	0.96607	2.54839
7.52	25p-uv4-ir0	0	0.755812	6.764188	0.10565797	0.00224	2.17146
	26p-uv4-ir1	1	1.243326	6.276674	0.59616333	0.00616	0.30913
	27p-uv4-ir2	2	1.452592	6.067408	0.73817475	0.01522	1.01600
	28p-uv4-ir3	3	1.693773	5.826227	0.84498736	0.12002	4.61980
	29p-uv4-ir4	5	2.208312	5.311688	0.97359007	0.67901	3.47766
	30p-uv4-ir5	7	2.728493	4.791507	0.99154697	2.67559	6.33137
7.80	31p-uv5-ir0	0	0.755812	7.044188	0.04684333	0.00636	8.57936
	32p-uv5-ir1	1	1.243326	6.556674	0.37867083	0.01286	0.98093
	33p-uv5-ir2	2	1.452592	6.347408	0.57932659	0.04972	1.72780
	34p-uv5-ir3	3	1.693773	6.106227	0.69098010	0.15060	11.9383
	35p-uv5-ir4	5	2.208312	5.591688	0.92338604	0.41226	8.03986
	36p-uv5-ir5	7	2.728493	5.071507	0.97904797	0.95607	4.33664

Table 6.7: *a* = Total energy (MO excitation + central pulse) includes Zero Point Energy. ; *b* = Morse potential Overtone. ; *c* = Ground state energy after using Morse ladder Operator (includes ZPE). ; *d* = Central Frequency of pulse. ; *e* = Population remaining in ground state after pulse. ; *f* = Density (x1000) absorbed by dissociation CAP's after Pulse (65fs). ; *g* = Final density (x1000) absorbed by dissociation CAP's after Pulse (265 fs).

## 6.A Theoretical flux across dissociation coordinates in the vibrationally mediated dissociation of acetylene

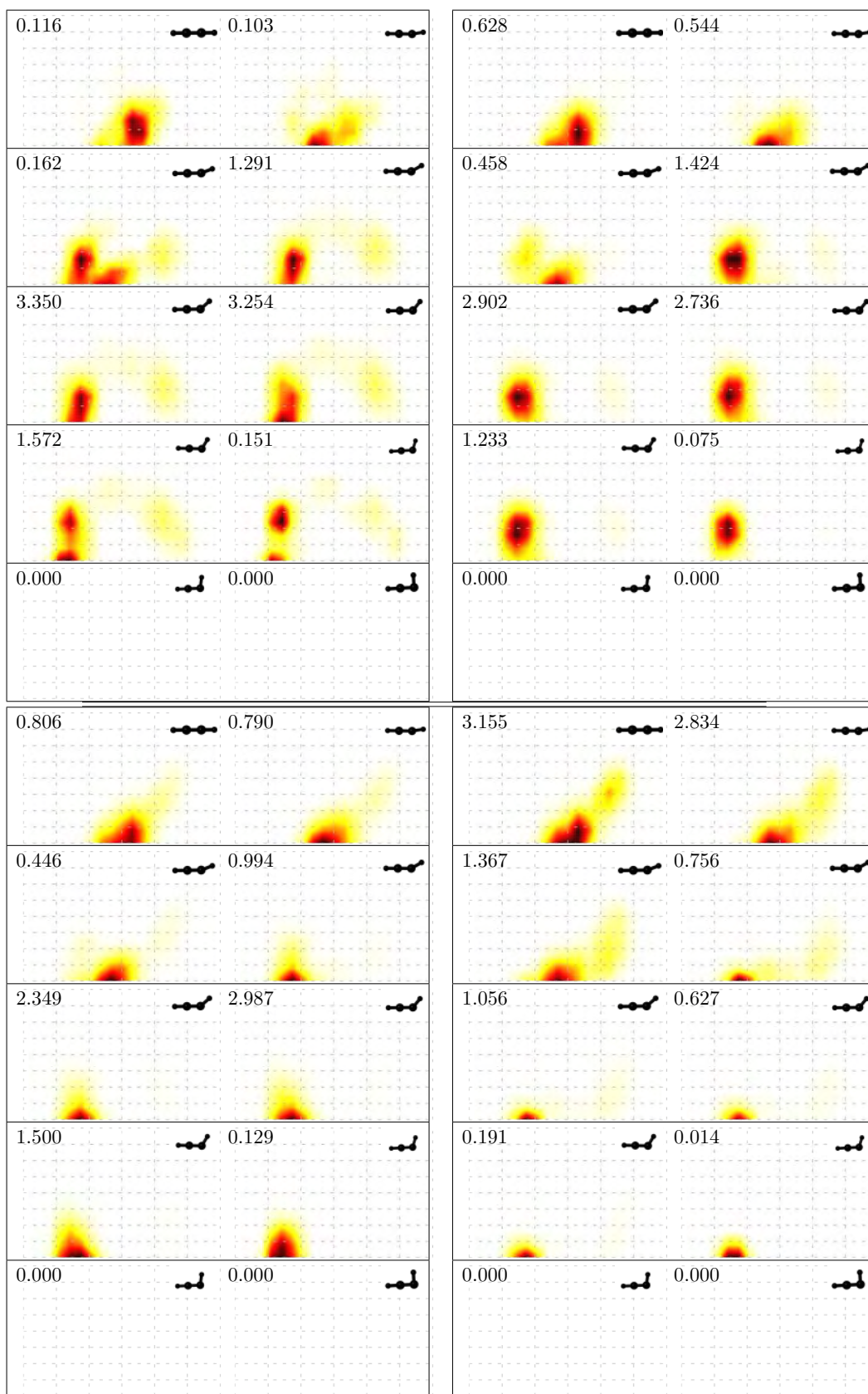


Fig. 6.22: *top left*: 1p-uv0-ir0 (6.4,0), *top right*: 2p-uv0-ir1 (6.4,1), *bot left*: 3p-uv0-ir2 (6.4,2), *bot right*: 4p-uv0-ir3 (6.4,3)

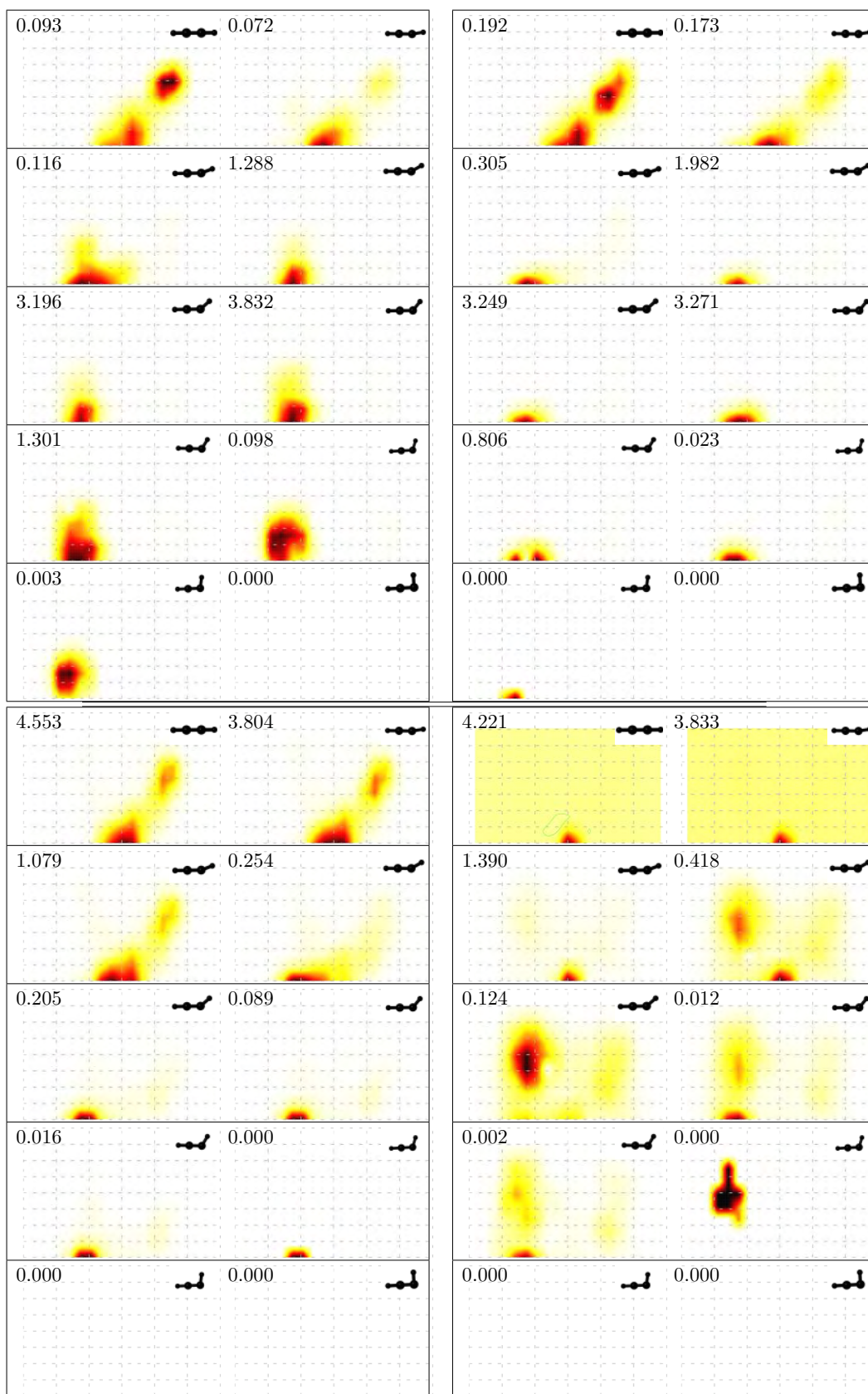


Fig. 6.24: *top left*: 9p-uv1-ir2 (6.68,2), *top right*: 10p-uv1-ir3 (6.68,3), *bot left*: 11p-uv1-ir4 (6.68,5), *bot right*: 12p-uv1-ir5 (6.68,7)

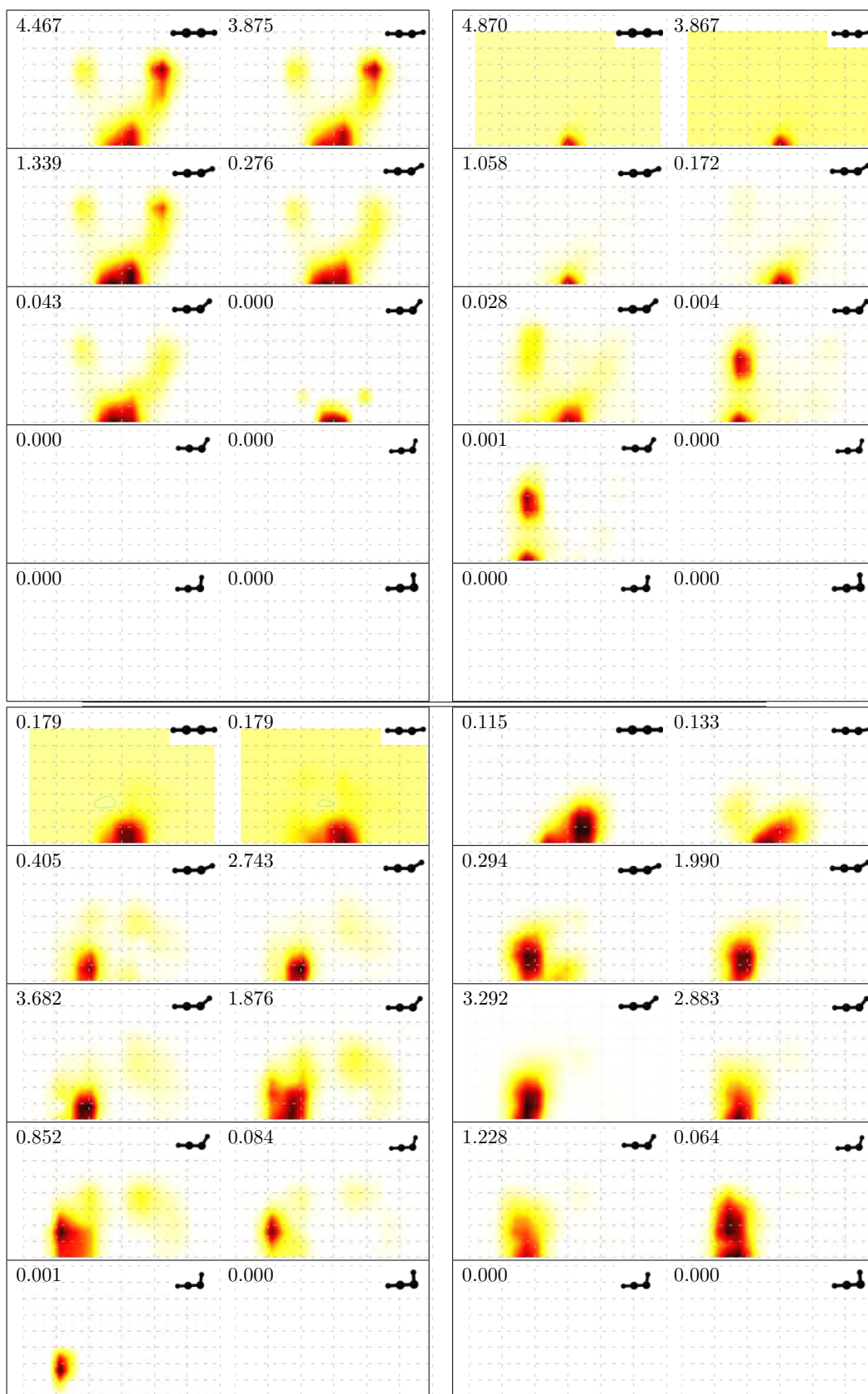


Fig. 6.23: *top left*: 5p-uv0-ir4 (6.4,5), *top right*: 6p-uv0-ir5 (6.4,7), *bot left*: 7p-uv1-ir0 (6.68,0), *bot right*: 8p-uv1-ir1 (6.68,1)



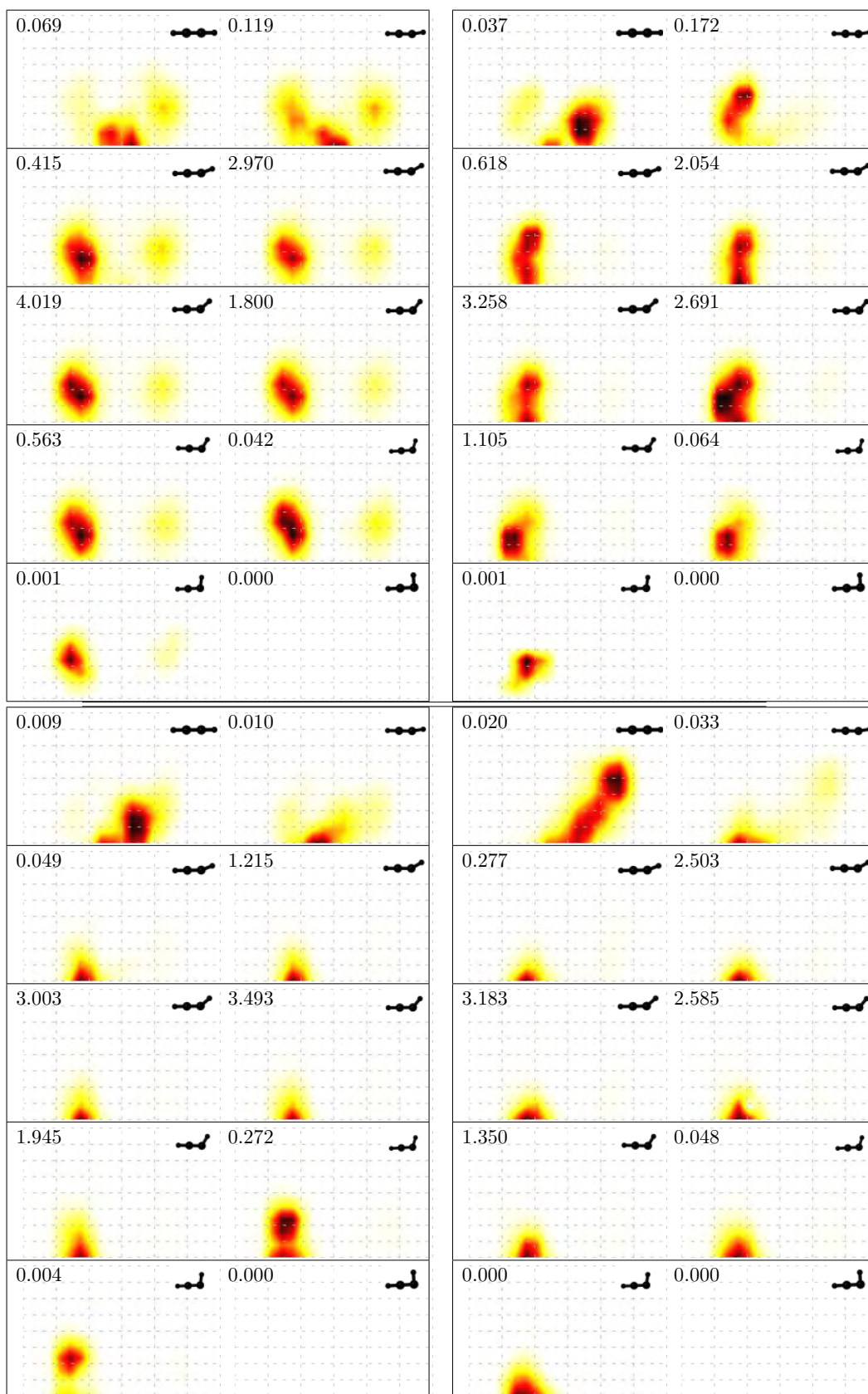


Fig. 6.25: *top left*: 13p-uv2-ir0 (6.96,0), *top right*: 14p-uv2-ir1 (6.96,1), *bot left*: 15p-uv2-ir2 (6.96,2), *bot right*: 16p-uv2-ir3 (6.96,3)

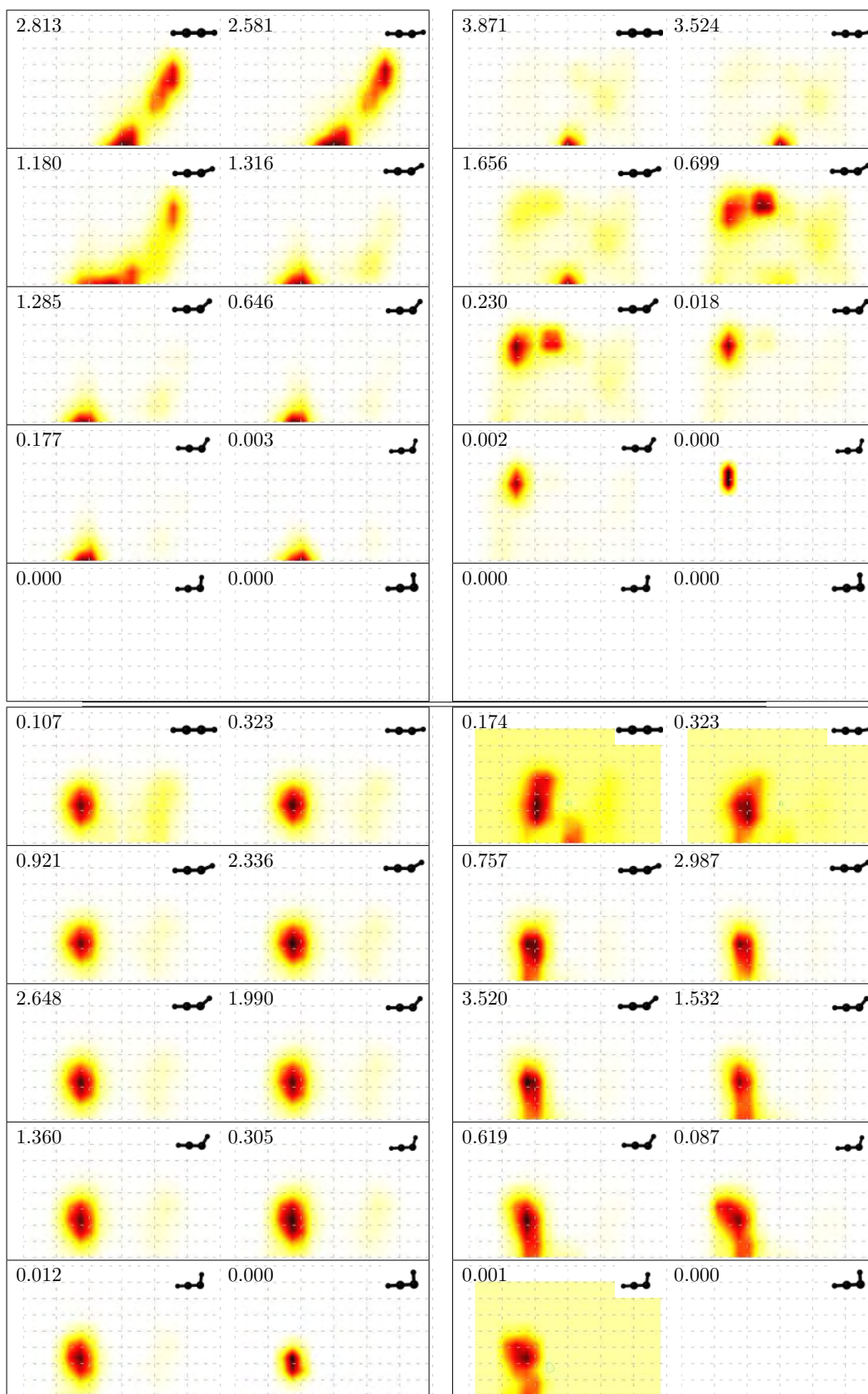


Fig. 6.26: *top left*: 17p-uv2-ir4 (6.96,5), *top right*: 18p-uv2-ir5 (6.96,7), *bot left*: 19p-uv3-ir0 (7.24,0), *bot right*: 20p-uv3-ir1 (7.24,1)



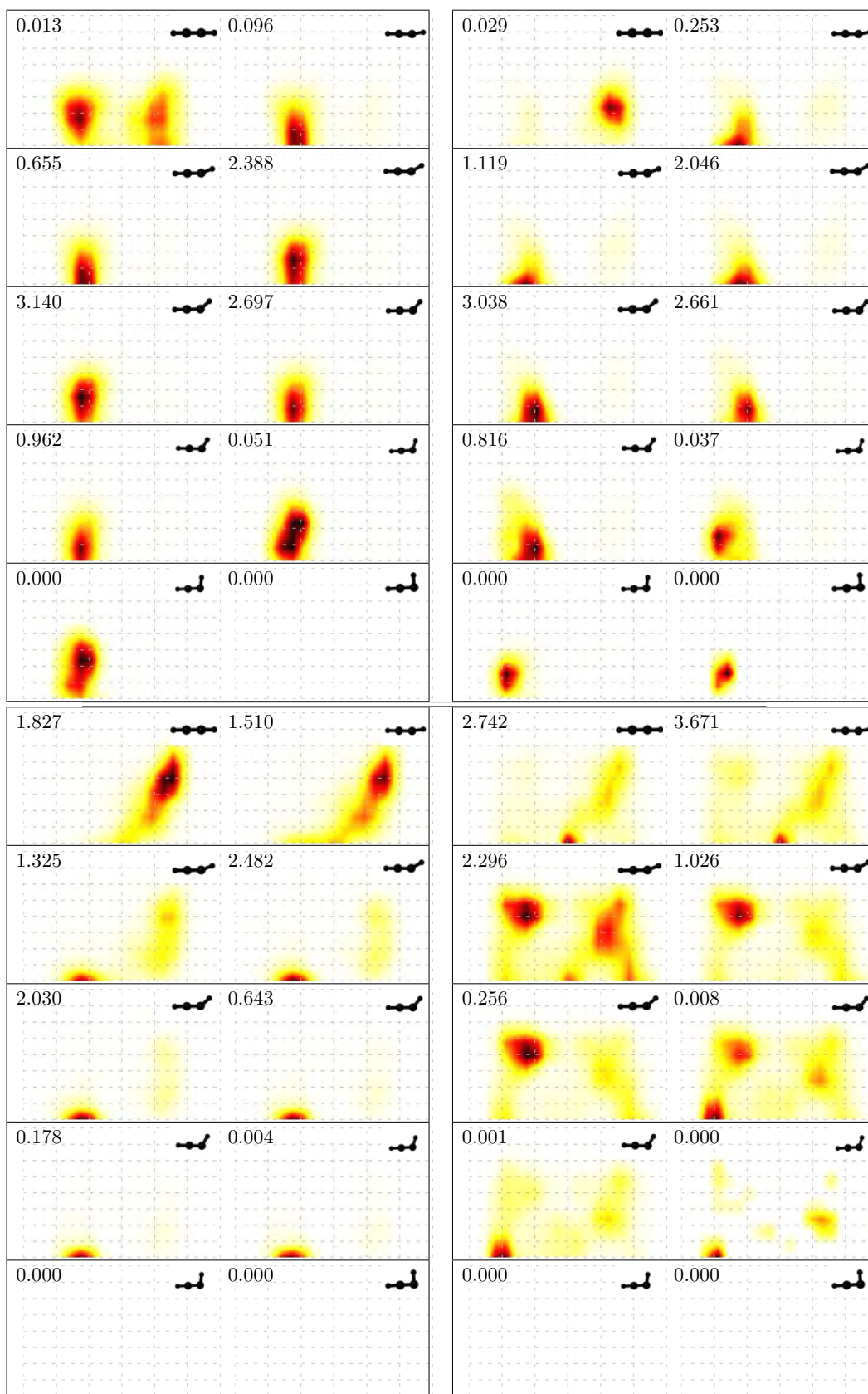


Fig. 6.27: *top left*: 21p-uv3-ir2 (7.24,2), *top right*: 22p-uv3-ir3 (7.24,3), *bot left*: 23p-uv3-ir4 (7.24,5), *bot right*: 24p-uv3-ir5 (7.24,7)

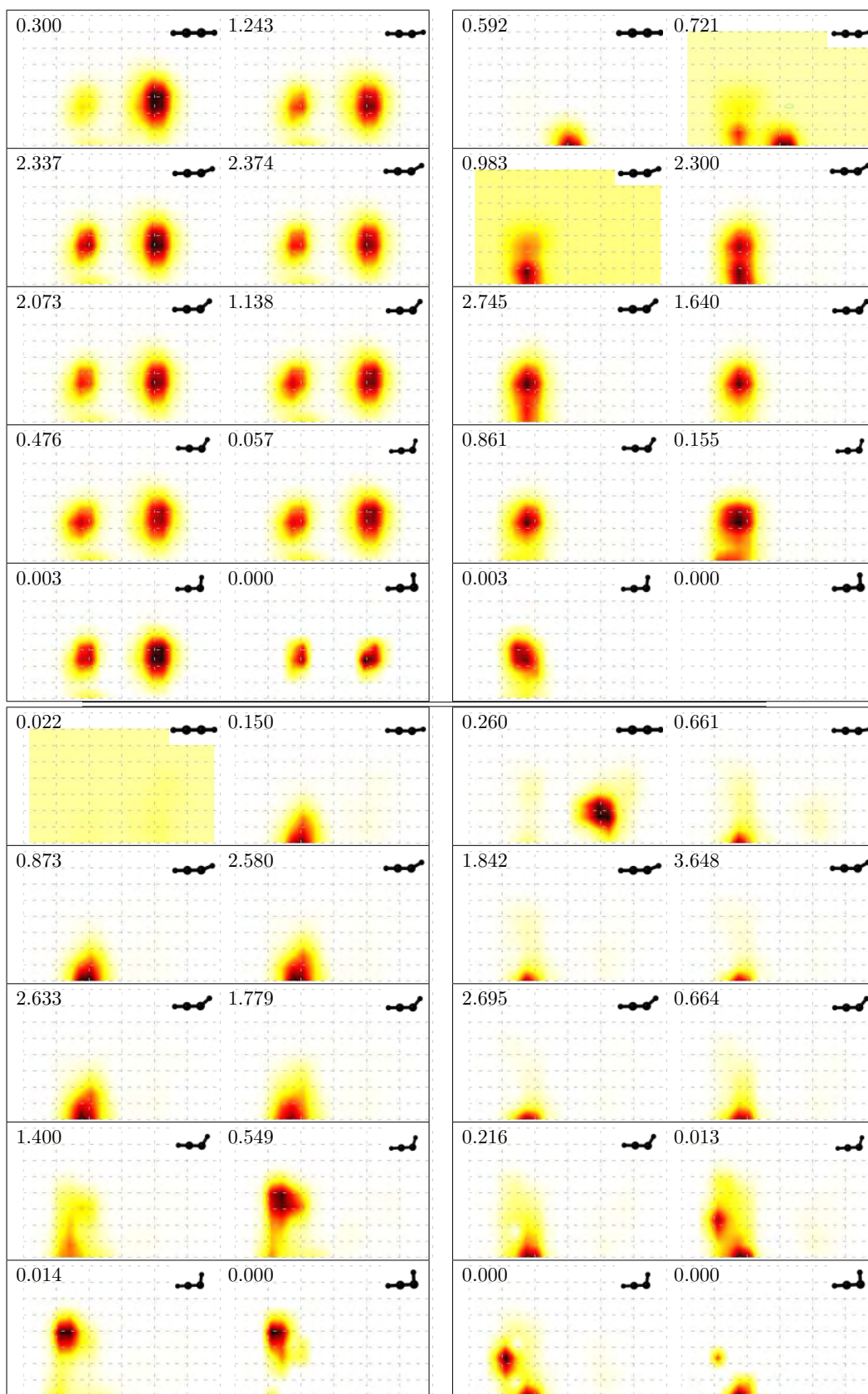


Fig. 6.28: *top left*: 25p-uv4-ir0 (7.52,0), *top right*: 26p-uv4-ir1 (7.52,1), *bot left*: 27p-uv4-ir2 (7.52,2), *bot right*: 28p-uv4-ir3 (7.52,3)



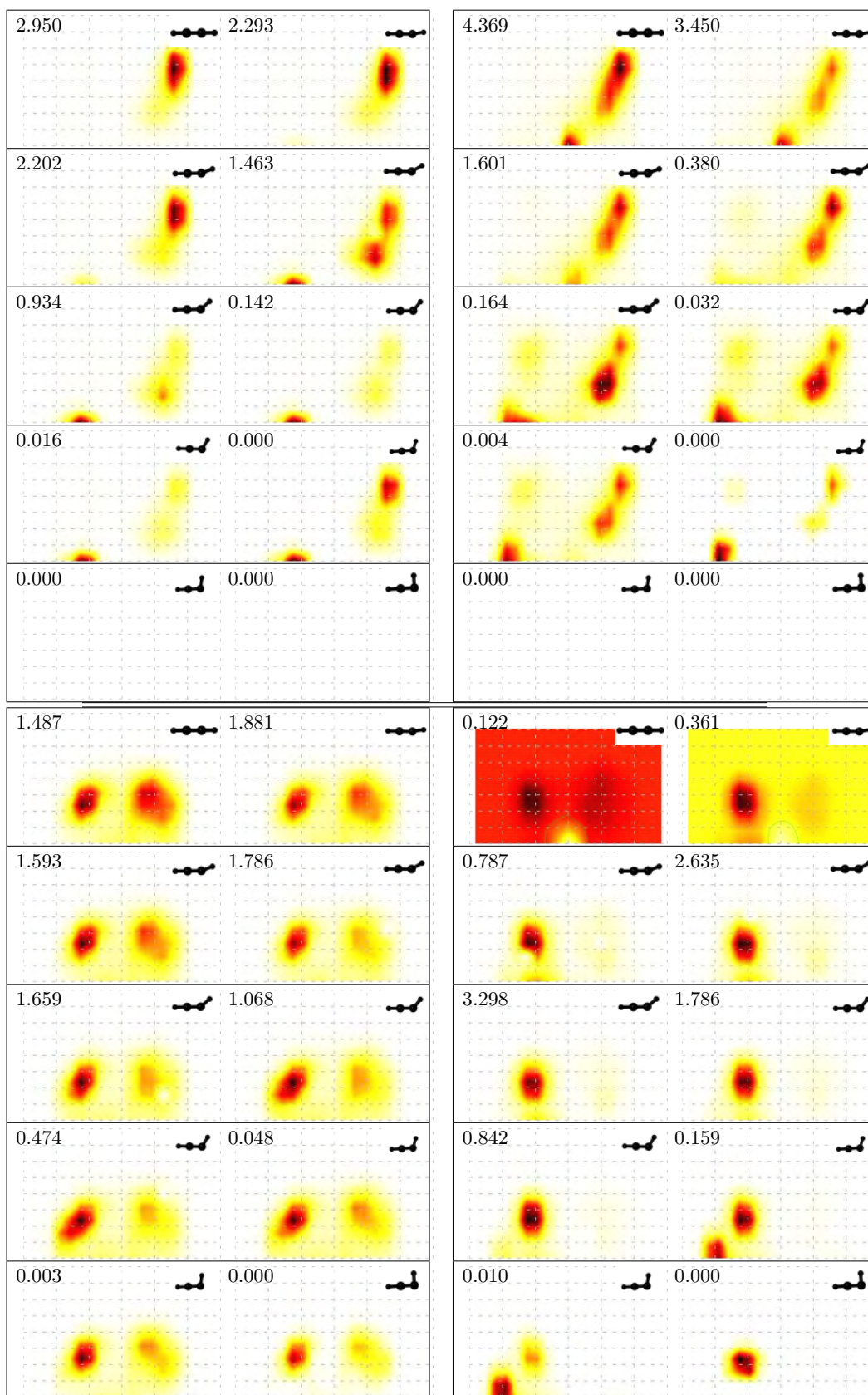


Fig. 6.29: *top left*: 29p-uv4-ir4 (7.52,5), *top right*: 30p-uv4-ir5 (7.52,7), *bot left*: 31p-uv5-ir0 (7.8,0), *bot right*: 32p-uv5-ir1 (7.8,1)

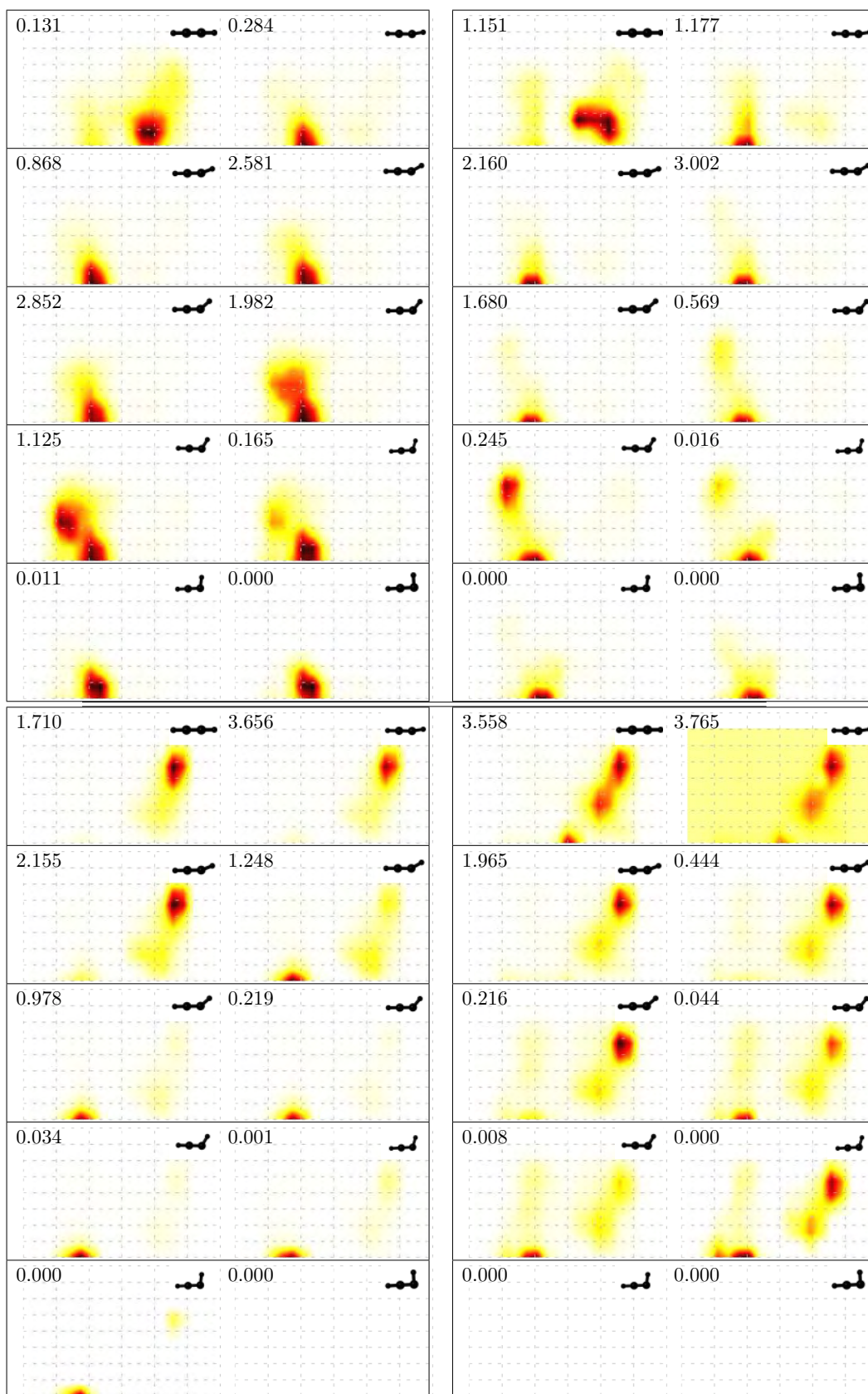


Fig. 6.30: *top left*: 33p-uv5-ir2 (7.8,2), *top right*: 34p-uv5-ir3 (7.8,3), *bot left*: 35p-uv5-ir4 (7.8,5), *bot right*: 36p-uv5-ir5 (7.8,7)

# Chapter 7

## Tolane

### 7.1 Introduction

In the last 20 years, efforts to understand the spectra of diphenyl-acetylene (Tolane or DPA) have mounted, being the monomial of a family of extended dendrimer segments exhibiting remarkable photo-funnelling properties [13]. Dendrimers are a class of macromolecules with branching units parting from a central node in a regular geometry (Fig 7.1).

Upon excitation from the peripheral diphenyl-acetylene (Tolane) monomer segments, the energy is transferred through the branches via vibrational motion along localised electronic states.

At the perylene locus (see Fig 7.1), light is re-emitted 600 times brighter at a

lower frequency. Much work has been done highlighting their promise and practice in applications like photoactive arrays in polymeric systems [14] and single-molecular LED [15].

No other dendrimer segment has been studied nearly as well as Tolane (DPA), and an overall mechanism of its photo-relaxation is emerging.

Tolane has been observed experimentally to possess a planar structure of

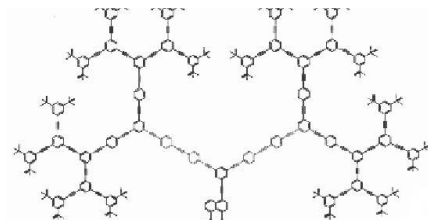


Fig. 7.1: An example in the family of *extended* phenyl-acetylene dendrimers, taken from ref. [13]

$D_{2h}$  symmetry at the ground-state equilibrium geometry [105]. Although theoretical excited state calculations had been performed earlier [106], we start this introduction with the work done by Hirata *et al* [107]. They performed picosecond time-resolved absorption spectrum measurements (in various solvents), following the work by Okuyama *et al* [108] who found dual fluorescence present in the gas phase (using supersonic free jet spectroscopy) but absent in solution. Hirata *et al* proposed a state transfer mechanism based on their observations:  $S_0 \rightarrow X \rightarrow Y \rightarrow T_1$ . They found a short-lived (8 ps) optically active state X (absorption at 290 nm (4.27 eV) from the ground state, fluoresces at 500 nm), being a precursor to a long-lived (200 ps) ‘dark’ (optically forbidden, fluoresces at 700 nm) state Y (the decay of X coincides with the rise time of Y), which undergoes intersystem crossing to a fluorescing triplet state  $T_1$  (fluoresces for  $\sim 1 \mu s$ ). They found a temperature dependence for the lifetime of X with a small activation barrier of 10.77 kJ/mol ( $\sim 0.11$  eV). They also rule out the possibility for X and Y to correspond to conformational changes in one state, since they did not observe any viscosity effects for the lifetimes of X and Y. At very low temperatures (180 K) they observed nearly no fluorescence from Y. They propose identities for the states but as Gutmann *et al* [109] noted (see below), they misinterpreted earlier work (the notation of polarisation axis) in which their labelling scheme was based on.

More recent experimental work has clarified the picture further. The one-photon allowed optically active state X has been identified by Saltiel *et al* [110] and Borst *et al* [111] to have the  $B_{1u}$  symmetry (and energy 4.37 eV), also suggesting this state to be  $S_2$  at the FC geometry. Saltiel *et al* suggests  $S_1$  to be an orbitally forbidden state with  $B_{2u}$  identity [110] (4.33 eV) based on the onset of phosphorescence excitation spectra. This state is marginally

lower than the suggested  $S_2$  of  $B_{1u}$  symmetry. Both [110,111] conclude that formation of the vibrationally relaxed  $B_{1u}$  state giving rise to fluorescence occurs in competition with internal conversion to the ‘Dark’ Y state with  $1A_u$  symmetry.

They record excitation spectra of fluorescence originating from  $1A_u$ , and they argue that its close resemblance to the absorption spectra shows that competition between vibrational cooling and internal conversion to the  $1A_u$  (with *trans*-stilbene geometry, see below) is significant at room temperature. Saltiel *et al* [110] conclude that below 77K the internal conversion to  $1A_u$  shuts down, although between the 0-70 °C range, increasing temperature improves the vibrational cooling (collisions with medium) which competes with internal conversion to  $1A_u$ . Contrary to previous studies, they conclude that solvent effects also play an important role in the competition between vibrational cooling and internal conversion. They

argue that conversion between  $B_{2u}$  and  $B_{1u}$  at low or room temperatures does not compete with internal conversion to  $A_u$ , being consistent with the  $B_{1u}$ - $B_{2u}$  interconversion being orbitally forbidden (they don’t freely equilibrate in condensed media). They also conclude, contrary to earlier interpretations,

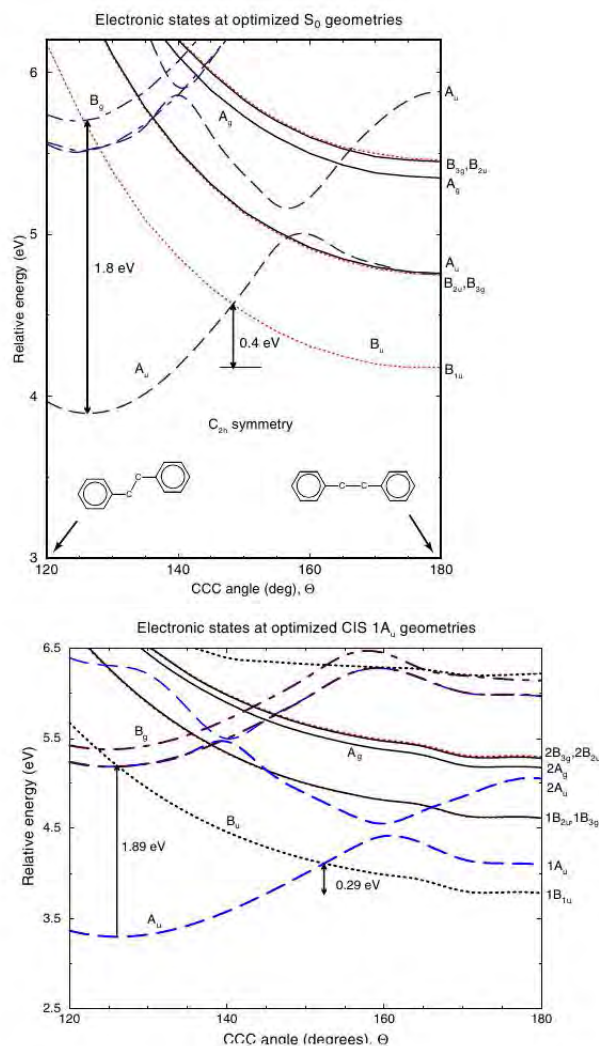


Fig. 7.2: TDDFT/6-31G\* surface cuts with bonds optimised at  $S_0$  (top) and  $1A_u$  (bottom) geometries. Reprinted from Zgierski *et al* [112])



that solvent effects play a role in determining the activation barrier height of isomerisation.

Kleiman *et al* [113] (transient absorption) experimentally found the two exponential decay components with lifetimes of 3 and 14 ps, as well as a reproducibly complex oscillatory component for the nano-star dendrimer. Most notably, they found no band responsible for the  $T_1$  state, showing that intersystem crossing does not take place. Their estimation of the lifetime for the DPA molecule was 6.3 ps (slightly faster than earlier work). Gutmann *et al* [109] performed both experimental (site selective matrix isolation spectroscopy) and theoretical calculations (using semi-empirical CNDO/S-CI method). They notice that the earlier computational work (and which Hirata *et al* analysis was based on) could not calculate  $A_u$  symmetry states, which they find as  $S_2$  in their work. They could not see any other bands to the red of  $B_{1u}$ , and they suggest a possible  $B_{3g}$  state, but acknowledge that their equipment might have not detected them (relevant to the plausibility of the CASSCF results by Amatatsu *et al*, see below). They therefore conclude that  $S_1$  must be of  $B_{1u}$  symmetry. They note the discrepancy between their experimental results in condensed phase compared to the gas phase (supersonic jet), and suggest that the  $A_u$  state might be lower in energy in the gas phase. Their experimental results give a barrier for the  $X \rightarrow Y$  transition of 15 kJ/mol (0.155 eV). They observe that because the transitions are either one or two photon allowed (mutual exclusion principle is observed), the molecule must conserve its centre of symmetry in the excited states (leaving either  $C_{2h}$  or  $C_i$  symmetry groups as a possible distorted excited state geometry).

Following this line of reasoning, Ferrante *et al* [114] agrees with the  $B_{1u}$  labelling of  $S_1$ , but only at the ground state geometry. They perform

INDO/S calculations (AM1 for geometry optimisations) that suggest that the  $2A_u$  state crosses  $1B_{1u}$  to become the first excited state stable geometry. They reason that the lack of viscosity noted by Hirata *et al* is due to the stable  $1A_u$  geometry corresponding primarily to a simple elongation of the central acetylene bond (with a new bond length of 1.28 Å, closer to a double bond), contrary to suggestions of conformational change. Their calculations give a barrier of 14 kJ/mol (0.145 eV) between the  $1B_{1u}$  (X) and  $1A_u$  (Y). These results agree with Gutmann, and suggest the discrepancy with Hirata *et al* work might be due to the limiting temperature dependency of the fluorescence quantum yields, since Hirata *et al* worked at low temperatures. They [114] also note that the  $\sigma\pi^*$  character of the  $A_u$  state could explain the strong spin-orbit coupling with triplet states giving rise to intersystem crossing. They suggest that the weak lines observed to the red of the  $B_{1u}$  absorption band in the supersonic jet calculations might be due to the direct, non-vertical excitation to the  $A_u$  state. This said, it is worth commenting that these bands could be better explained by the  $B_{2u}$  optically allowed (but with a small transition probability) state, predicted by Amatatsu *et al* (see below) to be below the  $B_{1u}$  state. Triplet state calculations gave two well separated states  $1^3B_{1u}$  and  $2^3A_g$ , with the lowest being the one involved in intersystem crossing.

The two most recent theoretical papers [112, 115] have sedimented the experimental observations and the conformational studies by Ferrante *et al*, bringing a clearer picture of the dynamic pathway mechanisms originally observed by Hirata *et al*. However, there continue to be differences in their energy level ordering (read below). Zgierki *et al* [112] observes that the crossing between  $\sigma\pi^*$   $A_u$  state and the  $\pi\pi^*$   $B_{1u}$  state that Ferrante *et al* suggested to be purely along the central CC stretching coordinate might not be accu-

rate, having used a semi-empirical method AM1 (Fig [112]). They performed TDDFT and CIS (CASSCF(8,8) for geometry confirmation) calculations to cut energy surfaces along the Ph-CC-Ph, the linkage angles in the plane of the molecule.

Following the findings by Ferrante *et al*, a lower basin of the  $1A_u$  state is found at a geometry that resembles a *trans*-stilbene molecule (with a  $C_{2h}$  point group, in agreement with the previous optical selection rules noted by Gutmann *et al*) with CCBz angle of  $125^\circ$ . They [112] also performed a geometry optimisation using a CASSCF(8,8) wavefunction, confirming that the states are well described by a singly excited configura-

tions. They performed cuts interpolating the  $S_0$  and  $1A_u$  CIS optimised geometries, energies calculated at a TDDFT/6-31G\* level. They measured the barrier height for the  $S_0$  and  $1A_u$  isomerisation by interpolating along the bending angle (see reprint in Fig 7.2) using the valence coordinates optimised at either the  $S_0$  or  $1A_u$  minimum (see Fig 7.2). Activation barriers of 38.59 kJ/mol (0.4 eV) and 27.98 kJ/mol (0.29 eV) were obtained respectively, both being significantly above the experimentally observed value. The ordering of the states for both geometries is given in table 7.1. Many of their results agree with coherent anti-Stokes Raman spectroscopy (CARS) results for the vibrational frequencies [116]. Physical insight of the character and stability of the *trans* stilbene structure is suggested to come from the stabilisation that the  $\sigma^*$  orbital (which play a role in the  $A_u$  state) gains compared to the  $\pi^*$  orbital (in the  $B_{1u}$  state) in the acetylene bond. An optically allowed  $A_u$

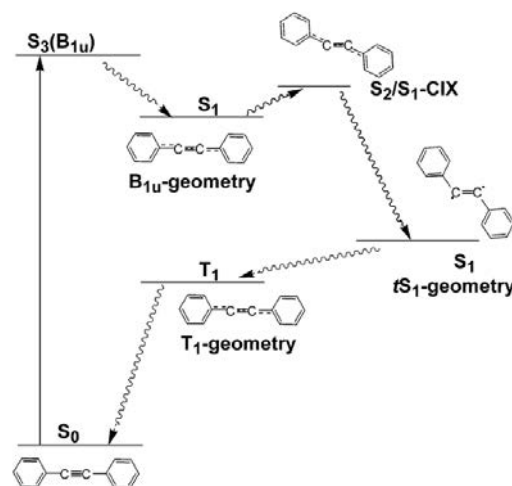


Fig. 7.3: Schematic representation of the photochemistry of DPA (by Amatatsu *et al* [115])



→ B<sub>g</sub> transition is found at the A<sub>u</sub> (S<sub>1</sub>) stable geometry, with 1.8 eV vertical excitation (688.7 nm), suggesting it as a falsification test. Their results are also able to explain why at low temperatures the 700 nm transient absorption (the A<sub>u</sub> state) was not observed by Hirata *et al.*

The work with the most computationally demanding results was done by Amatatsu *et al* [115]. They performed CASSCF calculations (Huziange-Dunning double- $\xi$  basis set) with MRMP2 corrections. They use a (10,10) active space including 5 HOMO and 5 LUMO  $\pi$  orbitals which they observed to be relatively invariant under conformational change. They also demonstrate that the qualitative picture (ordering of levels and relative energies) does not change by improving the energy by MP2 calculations on the CASSCF wavefunction. They note B<sub>1u</sub> is the only strong optically active state around that band. Their work agrees with Zgierki *et al* on the globally stable S<sub>1</sub> geometry being like a *trans*-stilbene molecule. It is also in agreement with Raman and IR work suggesting that by the mutual exclusion selection rules, the excited state stable geometry should belong to the either C<sub>2h</sub> or C<sub>i</sub> point groups [116]. In salient contrast to most of the earlier studies, Zgierki *et al* found the B<sub>3g</sub> and B<sub>2u</sub> states lower than the B<sub>1u</sub> and A<sub>u</sub> states. However, as mentioned before, this was considered a possibility by Gutmann and Ferrante *et al.* The B<sub>2u</sub> and B<sub>3g</sub> states are constructed primarily from  $\pi$  orbitals from the benzene rings, in contrast to the B<sub>1u</sub> and A<sub>u</sub> states, built from the HOMO-LUMO,  $\pi\pi^*$  out- and in- plane orbitals, respectively. The B<sub>2u</sub> and B<sub>3g</sub> geometries are characterised by an enlargement of the benzene rings, due to local  $\pi\pi^*$  excitations in the rings. The B<sub>1u</sub> geometry is characterised as a quinoid structure (similar to that suggested by Ferrante *et al*, who also gave a similar orbital explanation), where the aromaticity of the benzene ring is lost; the ethylene bond is stretched and the linkage bonds are

contracted (consistent with the orbital interpretation above). By looking at the LUMO orbitals that compose the  $S_1$  stilbene-like stable structure, they conclude that it has a di-radical character, and the orbital involved seem to be the in-plane  $\pi^*$  orbital (also noted by Gutman and Zgierki *et al*). They compare their results with the vibrational frequency calculations and obtain good agreements [116].

Amatatsu *et al* also propose that the main mechanism for relaxation is a vertical excitation to the  $S_3$  ( $1B_{1u}$ ) state (corresponding to the short-lived 8 ps state) which relaxes into its conformationally stable structure (they looked at the forces on the molecule at the FC geometry). From FC the system crosses barrier into a conical intersection with the long lived ' $S_4$ ' or  $tS_1$  ( $A_u$ ) state (at the *trans* stilbene geometry, lower in energy than  $S_3$ ) that undergoes intersystem crossing to the  $T_1$  state (Fig 7.3). Although the bending CC-C linkage angle is found to change proportionally along the reaction coordinate, it alone was not found to lead directly to the conical intersection (and the transition pathway). Instead, the molecule needs to drastically extend both the central and linkage bonds (bonds in the aromatic ring don't change significantly). By looking at different conformation pathways that brake the  $C_{2h}$  symmetry, they concluded that the molecule conserves its planar structure throughout the relaxation.

The aim of the work covered in this chapter is to aid the assignment of the bands observed in the absorption spectrum as well as to model the internal conversion to the  $S_1$  minima, shedding light on the mechanism and timescales involved in the process. This was done by constructing a vibronic model using normal (dimensionless) coordinates. The high symmetry of this system will, yet again, prove useful and provide insights into the coupling between states.

Table 7.1: Previous work on excited states.

state	(a)	(b)	(c)	(d)	(e)	(f)	(g)	(h)
S <sub>1</sub>	A <sub>u</sub> (266.7)	B <sub>1u</sub> (286.8)	(290) B <sub>1u</sub>	B <sub>1u</sub> (299.8)	B <sub>1u</sub> (296.6)	B <sub>1u</sub> (327.1)	B <sub>2u</sub> (305.9)	B <sub>2u</sub> (286.0)
S <sub>2</sub>	B <sub>1u</sub> (264.7)	A <sub>u</sub> (285.1)	(295) B <sub>2u</sub>	B <sub>2u</sub> (288.9)	B <sub>2u</sub> ( 261)	A <sub>u</sub> (319.55)(378*)	B <sub>3g</sub> (305.9)	B <sub>1u</sub> (283.0)
S <sub>3</sub>	B <sub>2u</sub> (240.6)	B <sub>2u</sub> (256.7)		B <sub>3g</sub> (288.7)	A <sub>u</sub> ( 261)(326.31*)	B <sub>2u</sub> ( 275)	B <sub>1u</sub> (275.1)	
S <sub>4</sub>	B <sub>3g</sub> (240.5)	B <sub>3g</sub> (256.6)		A <sub>u</sub> (287.5)	B <sub>3g</sub> ( 261)	B <sub>3g</sub> ( 270.7)	A <sub>u</sub> (255.8)	
S <sub>5</sub>	A <sub>u</sub> (228.9)	(237) A <sub>u</sub>		A <sub>g</sub> (248.1)	A <sub>g</sub> ( 261)	A <sub>u</sub>		

(a): X-ray data, (b): Gutmann [109] (AM1, Mopac) (c): Hirata [107] (exp) (d): Ferrante [114] (INDO/S Mopac)  
(e): Zgierski [112] (TDDFT at g.s. geom) (f): Zgierski [112] (TDDFT at A<sub>u</sub> geom) (g) Amatatsu [115] (CAS/RS2)  
(h) Saltiel [110]. \* = at the A<sub>u</sub> basin (adiabatic excitation energy).

Table 7.2: Vertical excitation energies (eV) and symmetry of excited states from ground state geometry of Toluene.

State	(a)	(b)	(c)	(d)	(e)	(f)	(g)	(h)
S <sub>1</sub>	4.11 (B <sub>1u</sub> )	4.90 (B <sub>2u</sub> )	5.32 (B <sub>2u</sub> )	5.03 (B <sub>3g</sub> )	4.49 (B <sub>1u</sub> )	4.68 (B <sub>3g</sub> )	4.71 (B <sub>2u</sub> )	4.69 (B <sub>3g</sub> )
S <sub>2</sub>	4.15 (B <sub>2u</sub> )	4.90 (B <sub>3g</sub> )	5.58 (B <sub>3g</sub> )	5.03 (B <sub>2u</sub> )	5.18 (B <sub>2u</sub> )	4.68 (B <sub>2u</sub> )	4.72 (B <sub>3g</sub> )	4.75 (B <sub>2u</sub> )
S <sub>3</sub>	4.16 (B <sub>3g</sub> )	6.68 (A <sub>g</sub> )	5.72 (B <sub>1u</sub> )	5.53 (B <sub>1u</sub> )	5.18 (B <sub>3g</sub> )	4.88 (B <sub>1u</sub> )	5.04 (B <sub>1u</sub> )	4.90 (B <sub>1u</sub> )
S <sub>4</sub>	4.81 (A <sub>u</sub> )	6.87 (B <sub>1u</sub> )	6.60 (A <sub>g</sub> )	6.43 (A <sub>g</sub> )	5.72 (A <sub>g</sub> )	5.74 (A <sub>u</sub> )	6.05 (A <sub>u</sub> )	5.76 (A <sub>u</sub> )
S <sub>5</sub>	5.04 (A <sub>g</sub> )	7.24 (A <sub>u</sub> )	6.73 (A <sub>u</sub> )	6.61 (A <sub>u</sub> )	5.76 (A <sub>u</sub> )	6.10 (A <sub>g</sub> )	6.21 (A <sub>g</sub> )	6.13 (A <sub>g</sub> )
S <sub>6</sub>	5.51 (A <sub>g</sub> )	7.76 (B <sub>1u</sub> )	7.24 (B <sub>2u</sub> )	6.98 (B <sub>3g</sub> )	6.66 (A <sub>u</sub> )	6.27 (B <sub>3g</sub> )	6.27 (B <sub>3g</sub> )	6.30 (B <sub>3g</sub> )
S <sub>7</sub>	5.54 (B <sub>3g</sub> )	8.06 (B <sub>3g</sub> )	7.88 (B <sub>1u</sub> )	7.02 (B <sub>2u</sub> )	6.92 (B <sub>2u</sub> )	6.29 (B <sub>2u</sub> )	6.32 (B <sub>2u</sub> )	6.44 (B <sub>2u</sub> )
A <sub>u</sub>	S <sub>10</sub> 5.57	S <sub>9</sub> 8.27	S <sub>13</sub> 11.2	S <sub>9</sub> 7.22	S <sub>6</sub> 6.66	S <sub>9</sub> 6.55	S <sub>9</sub> 7.12	S <sub>9</sub> 6.56

(a): DFT-MRCI/TZVP (b): (SA)-CAS(16,16)/6-31g(p,d) (c): (SA)-CAS(8,8)+RS2C/6-31g(p,d)  
(d): (SA)-CAS(10,10)+RS2C/6-31g(p,d) (e): (SA)-CAS(8,10)+RS2C/aug-cc-pvdz (f): (SA)-CAS(10,10)+RS2C/cc-pvdz  
(g): (SA)-CAS(12,12)+RS2C/cc-pvdz (h): (SA)-CAS(13,10)+RS2C/cc-pvdz  
Last row indicates which adiabatic state the A<sub>u</sub> diatomic state is at the ground state minima (energy provided).

## 7.2 Electronic structure and geometry optimisations

To construct a vibronic model for the excited states in Tolane, we will need a stable and efficient electronic structure method. Table 7.2 compares the first eight excited states obtained with CASSCF calculations using different active spaces involving HF  $\pi$  and  $\pi^*$  MO's built from conjugating p-orbitals (shown in Fig 7.4). Calculations were done with Molpro 09 [45]. Calculation (f), (g) and (h) in table 7.2, the more expensive (active-space and theory) methods, situate states in the same order as Amatatsu *et al*, and agrees with experimental data [110] with regard to the  $B_{1u}$  and  $B_{2u}$  ordering.

State  $B_{3g}$  seems to consistently give similar results as  $B_{2u}$  and  $B_{1u}$  lying not far either. It was not possible to achieve the predicted RS2 energy ordering when only using CASSCF, even when including all 16 p-orbitals (table 7.2 (b)). Since it is experimentally suggested [111] that the first one-photon allowed absorption state is the bright  $B_{1u}$  state, we performed a geometry optimisation in this state to obtain the  $S_1$  minima. We ran a CAS(10,10) to obtain the minima using  $C_s$  symmetry. From this minima, a conical intersection optimisation for  $1B_{1u}$ - $2A_u$ -CI at  $C_s$  symmetry gave a geometry with elongated ‘acetylene bridge’ bonds. This result disagrees with the the CI of Amatatsu *et al* who suggest a slight *trans* geometry. Efforts to find the transition state starting from the CI yielded no results. The same active space was used to locate the

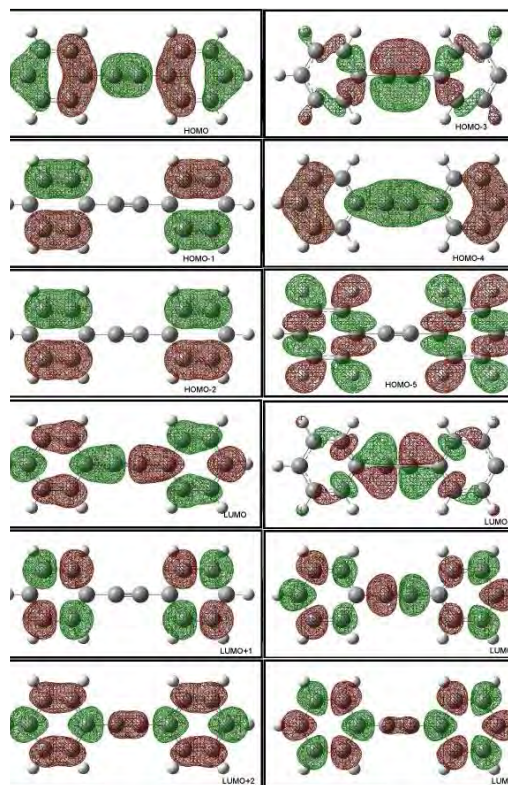


Fig. 7.4: 12 HF orbitals with significant contributions in the CAS wavefunctions.

$S_1$ , *trans*-stilbene minima (a “ts” prefix label will be used henceforth to refer to this geometry).

Bond lengths of the acetylene bridge, acetylene and the benzene segments and angles are given in table 7.4. A cut from the  $1B_{1u}$  minima to the  $ts-1A_u$  minima (the same diabatic state labelled as  $2A_u$  at the FC geometry) using the same level of theory is shown in Fig 7.6. These calculations fail to locate state  $B_{3g}$ , despite being the same active space used in the  $D_{2h}$  calculations. The  $2A_u$  state exhibits dramatic drop from several eV above to become the global  $S_1$  minima.

To construct the vibronic model, a large number of points are required along distortions that involve breaking  $C_s$  symmetry, thereby increasing the computational cost of every energy calculation. Running CASPT2 calculations would require a very large active space that will ensure the CASSCF wavefunction converges smoothly along any foreseeable geometry, including distortions that break  $C_s$  symmetry. Since this requires us to calculate a large number of states with a very large active space, making it too expensive.

Since CASSCF energies give poor results compared to PT2 calculations and match poorly to experimental frequencies, a more efficient, albeit more approximate method was used for obtaining energies; DFT-MRCI is a DFT based method for computing excited singlet/triplet states which includes both dynamic and static correlation (further details in chapter 2). Energies and states obtained from this method are given in table 7.2. Despite placing  $1B_{1u}$  as the  $S_1$  minima at the FC geometry, energies obtained are in good agreement with experimental

Mode	disp.
$\tilde{v}_5(B_{3g})$	5.107
$\tilde{v}_6(A_g)$	4.273
$\tilde{v}_{14}(B_{3g})$	-2.972
$\tilde{v}_{17}(B_{3g})$	-0.615
$\tilde{v}_{20}(A_g)$	1.763
$\tilde{v}_{33}(A_g)$	1.055
$\tilde{v}_{38}(A_g)$	0.884
$\tilde{v}_{54}(A_g)$	0.165
$\tilde{v}_{56}(A_g)$	-3.163

Table 7.3:  
CASSCF  $ts-1A_u$   
geometry in nor-  
mal coordinates

spectra (Fig 7.11). The second frame in Fig 7.6 shows the same cut towards

the  $ts-1A_u$  minima obtained with DFT-MRCI; topologically, there is qualitative agreement between both methods, which differ significantly on quantitative estimates of the barrier and minima involved (the DFT-MRCI cut shown is vector towards the CASSCF optimised minima). A significant risk is taken by using a method that misplaces the first three excited states (albeit by a slight value); the mechanism for overcoming the isomerisation barrier might involve population transfer to state  $B_{3g}$  or  $B_{2u}$ . However, experimental data [110] suggest the population between these do not freely equilibrate in condensed media and show little signs of being part of the mechanism leading to internal conversion at either low or room temperatures (being an orbitally forbidden interconversion).

### 7.3 Potential energy landscape and fitting.

A frequency calculation using an MP2 wavefunction (cc-pVDZ basis) was performed using Gaussian 03 [68], at an optimised geometry in the ground state at the same level of theory. There are 66 normal coordinates, the most relevant to this

Geometry	CC <sup>a</sup> (Å)	CC <sup>b</sup> (Å)	Ang <sup>c</sup> (deg)
$B_{1u}$ min.	1.2391	1.3699	180.0
$B_{1u}-A_u$ CI	1.2979	1.3814	180.0
$tS-1A_u$ min.	1.3678	1.4310	127.2

Table 7.4: Important bonds lengths and angles in critical geometries.

a = acetylene frag. bond length,  
b = acetylene-benzene bond length,  
c = acetylene/benzene *trans* angle

work tabulated in 7.9. By projecting the vector describing the  $1B_{1u} \rightarrow ts-1A_u$  internal conversion in the basis of the normal coordinate basis, we can analyse what kinds of symmetry distortions determine this process. The  $ts-1A_u$  minima is principally described by displacement along coordinates of  $B_{3g}$  and  $A_g$  symmetries; the basis vectors with largest displacements are shown in table 7.3. By exploring cuts along normal coordinates spanning these irreps, we were able to find the space which determines both the spectra and evolution

of the system. From symmetry consideration,  $A_g$  modes are the only that can exhibit gradients away from the FC geometry in excited states. These impart momentum on the wave-packet as well as typically being responsible for spectral progressions. Most crucially, two  $B_{3g}$  modes,  $\tilde{\nu}_5$  and  $\tilde{\nu}_{14}$ , provide most of the stabilisation arising in the  $2A_u$  state (shown in Fig 7.15). Fig 7.15 shows cuts along  $\tilde{\nu}_5$  and  $\tilde{\nu}_{14}$ , as well as their diagonal and anti-diagonal cuts (referring to quadrants in this 2D space). Eight states were calculated using DFT-MRCI; although state  $2A_u$  is  $S_{10}$  at the FC geometry, its energy is very close to those in  $S_8$  and since we are only interested in the dynamics of low lying states, we only need to describe properly the  $2A_u$  stabilisation onto  $ts-1A_u$  (other states not exhibiting any interesting topological features).

Since it is along these two modes alone that stabilisation of  $2A_u$  occurs, we approximate the states along other coordinates as harmonic, with a character similar to all the states in the figures shown henceforth. Insight into the kind of electronic configurations that play a role in this stabilisation might be suggested by the topology of this 2D space. Notice the contrast between the diagonal and anti-diagonal cuts; there is a sharp gradient along the anti-diagonal direction. Our attempt to fit quadratic, quartic and bilinear polynomials to this 2D surface was in vain; it is our conclusion therefore that low order polynomi-

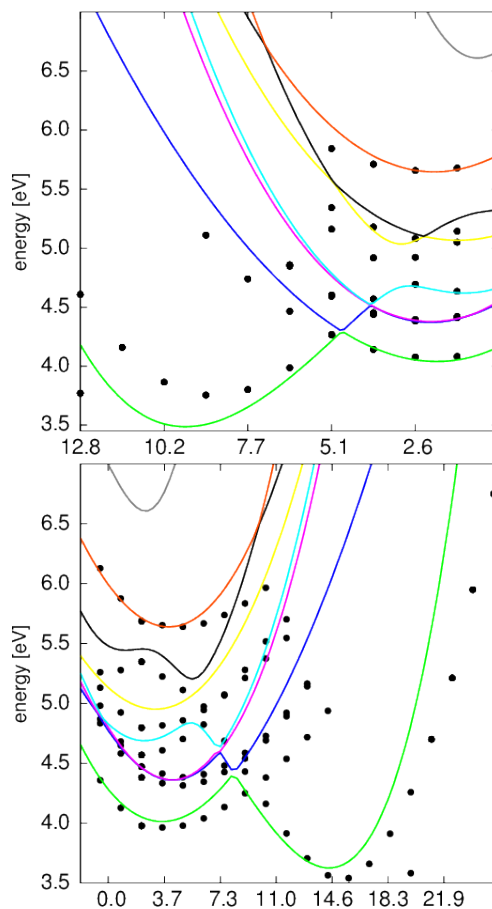


Fig. 7.5: Fit to  $ts-1A_u$  (*below*) and 5D vector (*above*) along important modes of  $A_g$  and  $B_{3g}$  symmetry.

als do a very poor job to fitting these surfaces accurately in an intra-state diabatic manner. Instead, a much more natural fit was achieved by assuming that stabilisation was caused by linear coupling to a higher lying state so that the functional form of the adiabatic energies between these coupled states could be written as:

$$W_{11} = \frac{D_{11} + D_{22}}{2} - \frac{\sqrt{((D_{22} - D_{11})^2 - 4(\lambda_5 \cdot Q_5 + \lambda_{14} \cdot Q_{14})^2)}}{2} \quad (7.1)$$

$D_{11}$  and  $D_{22}$  refer to the intra-state elements of  $2A_u$  and the higher lying state, respectively and  $\lambda_5$  and  $\lambda_{14}$  to the inter-state coupling parameters along  $\tilde{v}_5$  and  $\tilde{v}_{14}$ . The discriminant gives a sharper, more adequately shaped surfaces near the FC region due to the linear terms entering the expansion. The state to which  $2A_u$  couples needs to be of  $B_{3u}$  symmetry and DFT-MRCI situates the next state of that symmetry at 6.45 eV. This state was included in the model, but without any considerations into its shape along other DOF, where the ground state harmonic potential was used to approximate them (similar treatment to  $2A_u$ ). This suggests the adiabatic state is formed by the mixing of diabatic states with  $A_u$  and  $B_{3u}$  character. Fig 7.12 shows those  $A_g$  modes with significant gradient (at the FC geometry) or that play a role in the vector towards  $ts-1A_u$ . Terms correlating these coordinates are also fitted in the model, but not shown here for clarity. The most significant of these modes is  $\tilde{v}_{56}$ , which shows interesting crossings between many high lying states and might play an important role in dynamics at higher energies. The  $ts-1A_u$  minima is a highly correlated point in the normal coordinate basis, with the small contributions from tens of the modes. As a result, some of the modes correlating  $A_g$  modes to  $B_{3g}$  modes gave higher RMSD fits compared to other spaces. 2D functions were fitted to points in the  $A_g \times B_{3g}$  space. Cuts between these modes and their fits are shown (along the diagonals) in Fig 7.10. By fitting functions that correlate only up to two coordinates, we were



able to obtain a reasonable fit to the vector towards ts-1A<sub>u</sub> CASSCF(10,10) minima mentioned above, shown in Fig 7.5 together with another 5D vector displacing equally along each coordinate involved.

By performing local optimisation starting from a *trans* bent geometry, we were able to obtain an approximate energy for the minimum of 3.04 eV, underestimating the experimental energies. We obtain 1.425 Å for the acetylene benzene fragment bond length and 1.401 Å for the acetylene bridge bond length, overestimating the latter compared to the optimisation data in table 7.4. The minimum in terms of normal modes in this  $A_g \oplus B_{3g}$  subspace are given in table 7.5; we should not expect the vectors from table 7.3 and 7.5 to match exactly since we are fitting to DFT-MRCI energies and the 1B<sub>1u</sub> to ts-1A<sub>u</sub> minima vector was generated using a CASSCF geometry optimisation. We obtain two identical minima corresponding to either of the symmetrically equivalent *trans* geometries. Having obtained surfaces which exhibit the correct critical features for states 1B<sub>1u</sub> and 2A<sub>u</sub>, we are left with the task of understanding the coupling mechanisms that lead to the transfer of population.

Modes B<sub>3g</sub> and A<sub>g</sub> do not allow for any coupling between 1B<sub>1u</sub> and 2A<sub>u</sub>, not even indirectly via any of the intermediate states. Given the high symmetry of this molecule, we have to explore a restricted number of coordinates which would allow by symmetry considerations any direct B<sub>3g</sub> and A<sub>g</sub> coupling. Modes that allow linear coupling have B<sub>1g</sub> symmetry and are shown in Fig 7.13; there is little evidence of any direct coupling between our states

Mode	disp.
$\tilde{v}_5(B_{3g})$	4.829
$\tilde{v}_6(A_g)$	6.261
$\tilde{v}_{14}(B_{3g})$	-5.735
$\tilde{v}_{20}(A_g)$	2.066
$\tilde{v}_{33}(A_g)$	0.251
$\tilde{v}_{38}(A_g)$	0.812
$\tilde{v}_{54}(A_g)$	0.138
$\tilde{v}_{56}(A_g)$	-2.78

Table 7.5: ts-1A<sub>u</sub> geom. in model

of interest along any single B<sub>1g</sub> cut. This is clearly a result of the large energy separation between these states at the FC region. Therefore, we get a better estimate of coupling by exploring cuts that include the B<sub>3g</sub> subspace,

as these enable states to get close and exhibit any coupling effects near the crossing region. Fig 7.13 also depict 3D cuts along the  $\tilde{v}_5 + \tilde{v}_{14}(\text{B}_{3g})$  diagonal with the three  $\text{B}_{1g}$  modes. Third order terms were fitted along these. Third order coupling is generally weak, but can be inferred from the gap between  $\text{A}_u\text{B}_{1u}$  states in Fig. 7.13. To obtain second-order coupling between  $1\text{B}_{1u}$  and  $2\text{A}_u$  but simultaneously reduce the energy separation between these states (i.e. coordinates  $\tilde{v}_5$  or  $\tilde{v}_{14}$ ) we have to explore coordinates of symmetry  $\text{B}_{1g} \otimes \text{B}_{3g} = \text{B}_{2g}$ . Fig 7.14 shows 2D cuts along two coordinates,  $\tilde{v}_4$  and  $\tilde{v}_7$ , of  $\text{B}_{2g}$  symmetry which exhibit clear signs of coupling between states  $\text{A}_u$  and  $\text{B}_{1u}$  when simultaneously displacing along  $\tilde{v}_5$  or  $\tilde{v}_{14}$  ( $\text{B}_{3g}$ ).

## 7.4 Calculating absorption spectra

We now use the minimal model described above to run wave-packet simulations to help us characterise the absorption spectra, and to serve as a validation when we subsequently obtain an estimate for the timescales involved in population transfer. Figure 7.11 shows the experimental spectra at 10 K and 298 K (taken from ref. [117] and [107] respectively). Table 7.6 shows the mode combinations and number of SPF used for the different DOF in MCTDH calculations. The wave-packets were propagated for 500 fs, and spectra obtained by calculating the Fourier transform of the autocorrelation function (as described in chapter 2). The

$a$	$b$	grid-points, (range)	SPF <sup>c</sup>
$\text{B}_{3g}$	$\tilde{v}_5$	39 (-10,10)	5, 4, 4
	$\tilde{v}_{14}$	39 (-13,13)	4, 5, 5
$\text{A}_g$	$\tilde{v}_6$	39 (-11,13)	5, 4, 4
	$\tilde{v}_{38}$	35 (-7,7)	4, 5, 5
	$\tilde{v}_{56}$	45 (-9,13)	
$\text{B}_{1g}$	$\tilde{v}_{10}$	31 (-8,8)	5, 3, 3
	$\tilde{v}_{24}$	31 (-6,6)	3, 4, 4
	$\tilde{v}_{29}$	41 (-6,6)	
$\text{B}_{2g}$	$\tilde{v}_4$	31 (-10,10)	5, 4, 4
	$\tilde{v}_7$	31 (-8,8)	4, 5, 5
$\text{A}_g$	$\tilde{v}_{20}$	27 (-8,8)	5, 3, 3, 3, 4, 4
$\text{A}_g$	$\tilde{v}_{33}$	27 (-5,5)	5, 3, 3, 3, 4, 4
$\text{A}_g$	$\tilde{v}_{38}$	35 (-7,7)	5, 3, 3, 3, 4, 4

Table 7.6: Mode combination and number of SPF used for each state. <sup>a</sup>=Symmetry; <sup>b</sup>=Mode combination; <sup>c</sup>=(states  $1\text{B}_{1u}, 1\text{B}_{3g}, 1\text{B}_{2u}, 1\text{A}_u, 2\text{A}_u, 1\text{B}_{3u}$ ).

$1B_{1u}$  state is the only significant bright state in the energy range shown in the absorption spectra. Population transfer can only be expected to occur between states with comparable energies, namely  $1B_{2u}$ ,  $1B_{3g}$  and  $ts-1A_u$ . As mentioned above, there is some uncertainty in the order of these first three excited states (at the FC geometry) shown in table 7.2, reflecting some of the disagreements in theoretical and experimental literature. Furthermore, none of the coordinates explored in the above model shows any signs of coupling (most being symmetry forbidden). It is possible to answer these questions (energy order and population transfer) by calculating the absorption spectrum for systems that probe these possibilities and matching to experiments. We performed a series of calculations where we varied the following conditions:

- The initial wavefunction; either a fully relaxed wavefunction (0 K temperature) or a wavefunction with some of the low frequency components (modes  $\tilde{\nu}_5$ ,  $\tilde{\nu}_6$ ,  $\tilde{\nu}_7$  and  $\tilde{\nu}_{10}$ ) having the second vibrational states populated (obtained by diagonalizing the 1D operators of these modes), thus approximately representing a wavefunction at 298 K according to the Boltzmann distribution .
- Vertical excitation energies of  $1B_{2u}$  and  $1B_{3g}$ ; either the DFT-MRCI determined energies or those states shifted to energies lower than  $B_{1u}$ , to the relative position obtained by the (SA)-CAS(13,10)+RS2C calculation (shown in table 7.2 (h) and giving 3.84 and 3.83 respectively)
- The amount of density projected into states  $B_{2u}$  and  $B_{3g}$ : 0, 15, 30, 100 % which should be representative of the amount of internal conversion over fluorescence timescales.

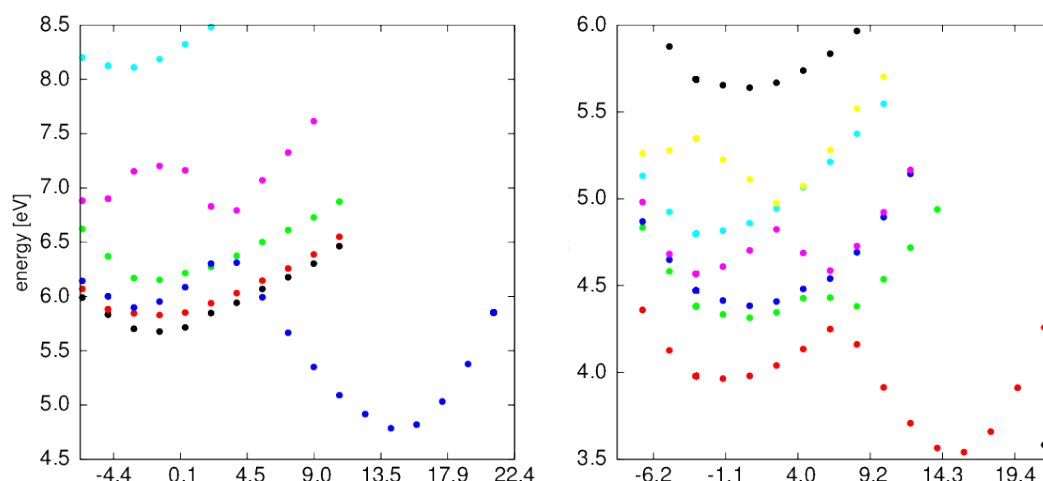


Fig. 7.6: Comparison of the PES along  $1B_{1u}$  to  $ts-1A_u$  vector (normal coordinates) using CASSCF (active space (h) in table 7.2) (*left*) and MRCI (*right*)

Figures 7.8 and 7.9 show the spectra labelled ‘full’ in table 7.7 (with all modes mentioned above being fitted) for the different populations for states  $B_{2u}$  and  $B_{3g}$  (0, 15, 30, 100 %) and for different vertical excitation energies. The calculated spectrum that resembles

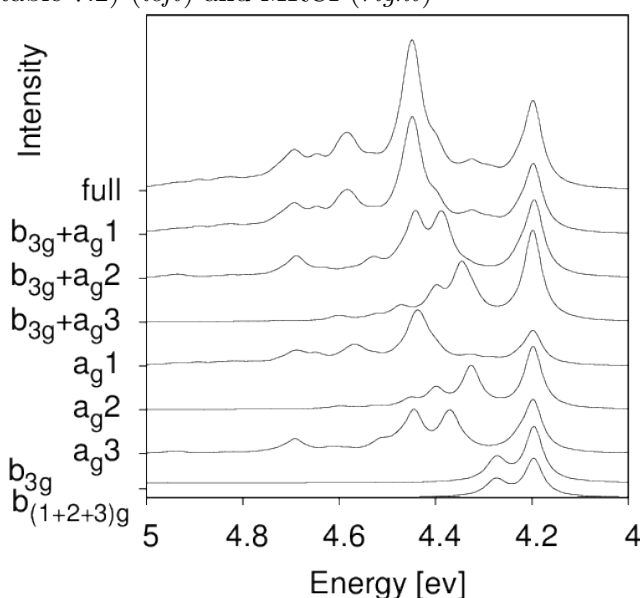


Fig. 7.7: Comparing full spectra with different sets of reduced dimensionality spectra.

the room temperature experimental spectrum is the fully relaxed initial wavefunction and with  $1B_{2u}$  and  $1B_{3g}$  states placed according to the DFT-MRCI method and with 30% of the population initially transferred to these states. In turn, the spectrum resembling the low-temperature experimental spectrum is also one with the DFT-MRCI determined energies, with the fully relaxed wavefunction but with no population entering states  $1B_{2u}$  and  $1B_{3g}$ . An enlarged images of the calculated spectra are also shown in Fig 7.11. That transfer to states  $1B_{2u}$  and  $1B_{3g}$  occurs at low temperature might be expected, as modes that

might couple such states would not be significantly excited. In the case of the former (room temperature) matching model, absorption spectra for different sets of reduced dimensional models (tabulated in 7.2) were also calculated in order to help us unweave the spectra (Fig 7.7). From this figure we can see that the final spectra are principally built from vibrational progressions arising from totally symmetric modes labelled  $a_{g1}$  with some contribution from modes labelled  $b_{3g}$  (table 7.7).

## 7.5 Internal conversion

As mentioned in the introduction, experimental data strongly suggests that the dual fluorescence exhibited by Toluene corresponds to the internal conversion from  $1B_{1u}$  to the *trans*-stilbene like geometry due to the strong stabilisation of the  $2A_u$  state.

It is also known that this process is susceptible to temperature dependence - shutting down at low temperatures and competing with vibrational cooling at room temperature. This implies that population transfer between these states must be on similar timescales as those of vibrational energy relaxation, which is known to occur from hundreds of femtosecond [118] to a few picosecond [119] timescales. Since no transfer occurs at low temperatures, this transfer must be due to energy components arising from higher vibrational states being populated in the ground electronic state prior to absorption.

Label	Coordinates
full	$\tilde{v}_5\tilde{v}_{14}(B_{3g}), \tilde{v}_4\tilde{v}_7(B_{2g}),$ $\tilde{v}_{10}\tilde{v}_{24}\tilde{v}_{29}(B_{1g}),$ $\tilde{v}_6\tilde{v}_{20}\tilde{v}_{33}\tilde{v}_{38}\tilde{v}_{54}\tilde{v}_{56}(A_g)$
$b_{3g}+a_{g1}$	$\tilde{v}_5\tilde{v}_{14}(B_{3g}),$ $\tilde{v}_6\tilde{v}_{20}\tilde{v}_{33}\tilde{v}_{38}\tilde{v}_{54}\tilde{v}_{56}(A_g)$
$b_{3g}+a_{g2}$	$\tilde{v}_5\tilde{v}_{14}(B_{3g}),$ $\tilde{v}_6\tilde{v}_{38}\tilde{v}_{56}(A_g)$
$b_{3g}+a_{g3}$	$\tilde{v}_5\tilde{v}_{14}(B_{3g}),$ $\tilde{v}_{20}\tilde{v}_{33}\tilde{v}_{54}(A_g)$
$a_{g1}$	$\tilde{v}_6\tilde{v}_{20}\tilde{v}_{33}\tilde{v}_{38}\tilde{v}_{54}\tilde{v}_{56}(A_g)$
$a_{g2}$	$\tilde{v}_6\tilde{v}_{38}\tilde{v}_{56}(A_g)$
$a_{g3}$	$\tilde{v}_{20}\tilde{v}_{33}\tilde{v}_{54}(A_g)$
$b_{(1+2+3)g}$	$\tilde{v}_5\tilde{v}_{14}(B_{3g}), \tilde{v}_4\tilde{v}_7(B_{2g}),$ $\tilde{v}_{10}\tilde{v}_{24}\tilde{v}_{29}(B_{1g})$
$b_{3g}$	$\tilde{v}_5\tilde{v}_{14}(B_{3g})$

Table 7.7: Labels and coordinates of the different reduced dimensional models used to calculate absorption spectra.

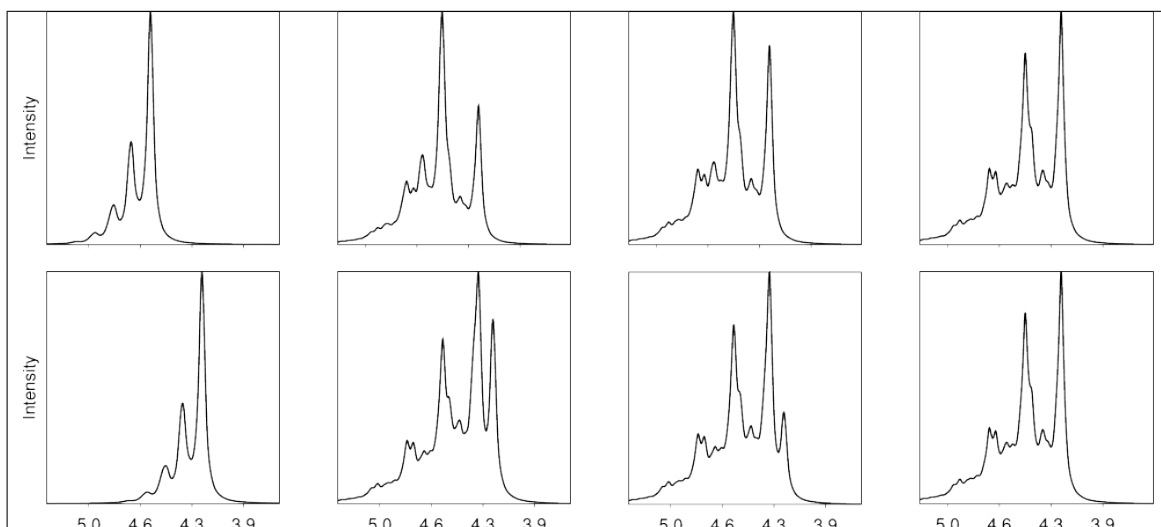


Fig. 7.8: Calculated absorption spectra (in eV) with states  $1B_{2g}$  and  $1B_{3g}$  above (row 1) and below (row 2) state  $1B_{1u}$ , with population: *From left to right*: 100, 30, 15, 0 %. Initial wavefunction is the relaxed ground state lowest eigenstate wavefunction.

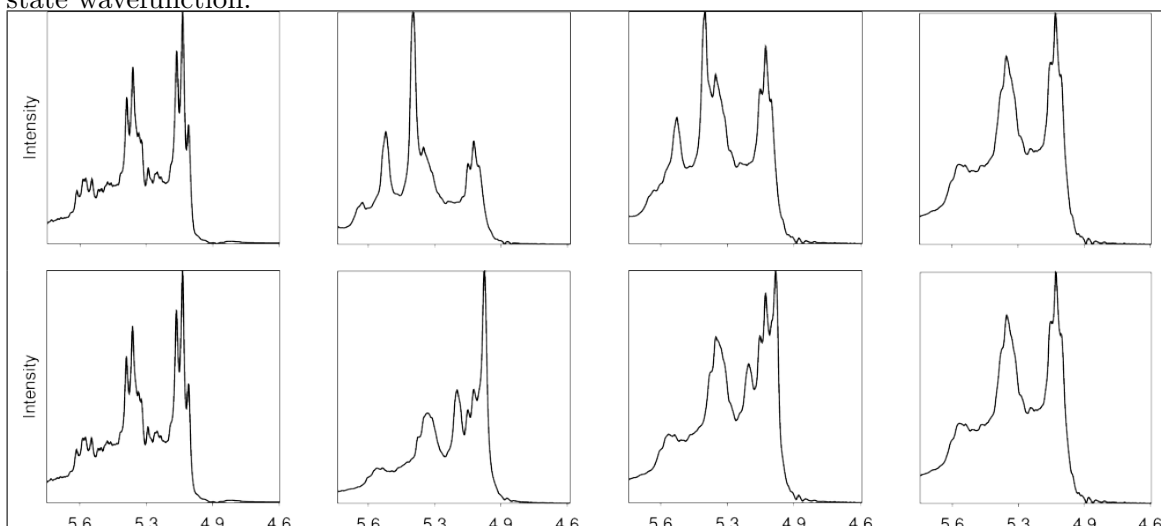


Fig. 7.9: Calculated absorption spectra (in eV) with state  $1B_{2g}$  and  $1B_{3g}$  above (row 1) and below (row 2) state  $1B_{1u}$ , with population: *From left to right*: 100, 30, 15, 0 %. Initial wavefunction is built from a relaxed  $S_0$  state wavefunction with low frequency modes excited to higher vibrational overtones.

The minimal model described above should therefore remain in line with the two experimental observations just mentioned. In other words, if we project the fully relaxed ground state wavefunction corresponding to a 0 K state (to compare with 10 K in the experiment [117] in Fig 7.11) we should not observe any transfer occurring. On the other hand, preparing a wavefunction with

eigenvector components populated at room temperature according to the Boltzmann distribution should lead to transfer of energy on the femtosecond to picosecond timescales. Since we do not include any dissipative effects to the media in our model, we should not expect purely unidirectional energy transfer but an initial transfer followed by an eventual equilibration between the populations. The model does not include coupling to states  $1B_{2u}$ ,  $1B_{3g}$  or  $2A_g$ , since along the coordinates explored and shown above, coupling was either symmetry forbidden or there was little evidence of coupling. Only four states are involved in the modelling of this process, and we assume the transfer to occur between  $1B_{1u}$  and  $2A_u$  via the second-order coupling terms (mentioned above) to be the main source of population transfer.

Figure 7.16 contains two plots showing the state populations resulting of two propagations with the two different initial wavefunctions (but otherwise identical) shown. States  $2A_u$   $1B_{3g}$  (shown in plot) diabatically represent the adiabatic state  $S_1$  which becomes  $ts-1A_u$ . Only  $\sim 2\%$  of the wavefunction has transferred after 2 ps, when we start from the fully relaxed wavefunction (top frame in Fig 7.16). Intriguingly, a very weak but clear transfer of population can be discerned over 5 ps timescales. For the

second calculation (top frame in Fig 7.16), the ‘hot’ initial wavefunction was built by obtaining the eigenfunctions of the ground state 1D model operators. Since they are largely harmonic, we essentially obtain the harmonic oscillator approximation to vibrational energies and functions. The excited eigenstates chosen for this propagation are given in table 7.8, all others being in their mono modal ground state. State  $1A_u$  ( $S_5$ ) is also populated and acts as another channel that couples  $2A_u$  and  $1B_{1u}$ , using totally symmetric modes to

Mode	Overt.
$\tilde{v}_4(B_{2g})$	3
$\tilde{v}_5(B_{3g})$	3
$\tilde{v}_6(A_g)$	3
$\tilde{v}_7(B_{2g})$	2
$\tilde{v}_{10}(B_{1g})$	2
$\tilde{v}_{14}(B_{3g})$	2

Table 7.8: Vibrational overtones used for initial wavefunctions (see text for details).

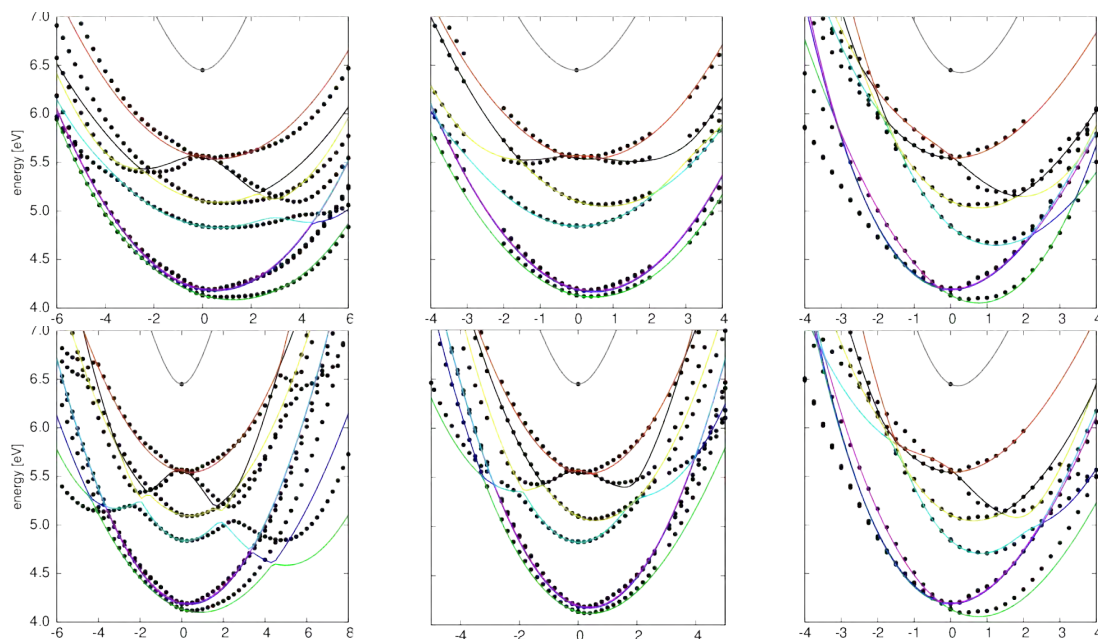


Fig. 7.10: Fitting of surfaces along modes of  $A_g$  and  $B_{3g}$  symmetry. From left to right: *first row*:  $(\tilde{v}_6 + \tilde{v}_5)$ ,  $(\tilde{v}_{38} + \tilde{v}_5)$ ,  $(\tilde{v}_{56} + \tilde{v}_5)$  *second row*:  $(\tilde{v}_6 + \tilde{v}_{14})$ ,  $(\tilde{v}_{38} + \tilde{v}_{14})$ ,  $(\tilde{v}_{56} + \tilde{v}_{14})$

couple the  $A_u$  states. Signs that these states are strongly interacting can be observed in Fig 7.5, where the energy gap at the nearest region between these two states is likely to be caused by non-adiabatic effects. These two calculations agree well with experimental observations of transfer at different temperatures, with an estimated population transfer occurring in picosecond timescales for temperatures above 77K [110,113]. The MCTDH operator file for model presented here is provided in supplementary information C.

## 7.6 Discussion and conclusions

We performed several different CASSCF+PT2 calculations to investigate the energy ordering of the first 10 excited electronic states. These suggest the energy ordering of the first five excited states to be  $B_{3g}$ ,  $B_{2u}$ ,  $B_{1u}$ ,  $A_u$  and  $A_g$ . Due to computational costs, a more approximate DFT-MRCI method was used to generate the set of points required for constructing a vibronic model.



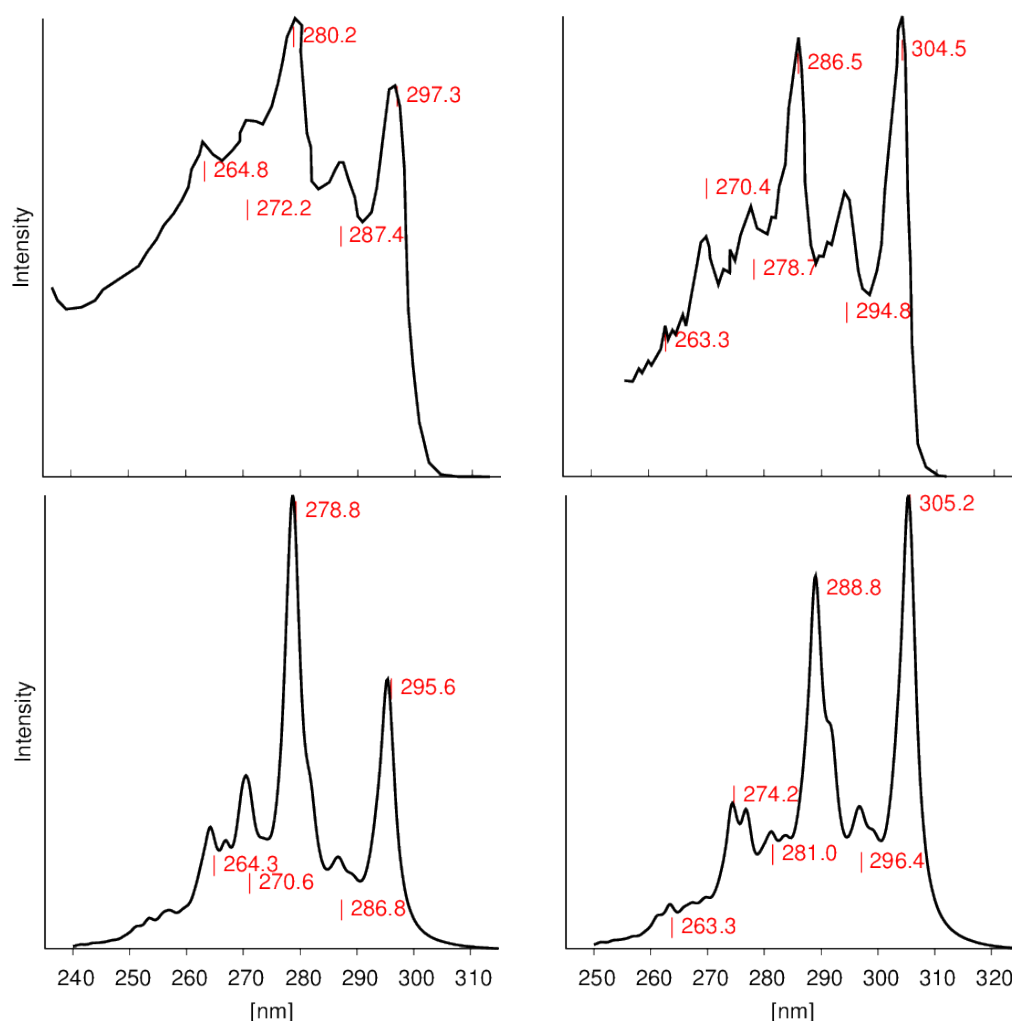


Fig. 7.11: Calculated spectra (*below*) with different populations in states  $B_{3g}$  and  $B_{2u}$  (30% (*left*) and 0% (*right*)) compared to experimental spectra (*above*) at high (*left*) and low (*right*) temperatures.

It predicts  $B_{1u}$  to be lower in energy than  $B_{3g}, B_{2u}$ . Starting from the optically bright  $B_{1u}$  state, we performed geometry optimisations to obtain the  $B_{1u}$  and (trans-stilbene like)  $ts-1A_u$  minimum and  $B_{1u}/A_u$  intersection (predicted to have  $D_{2h}$  symmetry).  $ts-1A_u$  is the  $S_1$  global minimum and at the FC geometry it is estimated to be  $S_{10}$ . Projecting the  $B_{1u}$ - $ts-1A_u$  vector into the basis of normal coordinates tells us that such distortion largely involves  $A_g$  and  $B_{3g}$  modes. By analysing the topological features of the  $B_{3g}$  subspace, we conclude that the stabilisation of  $2A_u$  is likely to be explained by diabatic coupling to a higher lying state with  $B_{3u}$  character. No signs of first order coupling between states  $1B_{1u}$  and  $2A_u$  were found, but instead

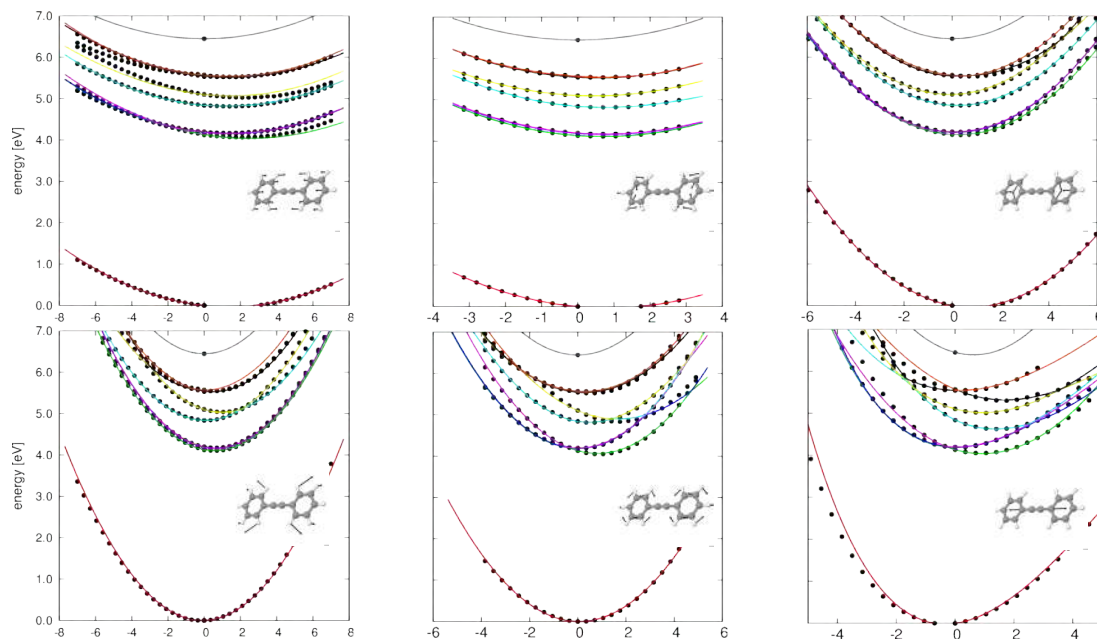


Fig. 7.12: Fitting of surfaces along modes of  $A_g$  symmetry.  $S_0$  shown for cuts along single modes. From left to right: *first row*:  $(\tilde{v}_6)$ ,  $(\tilde{v}_{20})$ ,  $(\tilde{v}_{33})$  *second row*:  $(\tilde{v}_{38})$ ,  $(\tilde{v}_{54})$ ,  $(\tilde{v}_{56})$

second order coupling along  $B_{3g}$  and  $B_{2g}$  modes was found to clearly exhibit non-adiabatic effects. This suggests that the transfer between states should occur via an out-of-plane distortion. On hindsight, we probably failed to find the transition state leading to the  $ts-1A_u$  minimum because we constrained our calculations to have  $C_s$  symmetry given that the branching space (where the transition state is likely to occur) is likely to contain distortion along  $B_{2g}$  modes, breaking the planar,  $C_s$  symmetry. By calculating a set of different spectra under different conditions, the best match for room temperature spectra was obtained where 30% of the excited state population is initially found in states  $B_{3g}$  and  $B_{2u}$ , lying higher than  $B_{1u}$  and with a fully relaxed ground state initial wavefunction. In the case of low temperature (10K) experimental spectra, no population onto states  $B_{3g}$  and  $B_{2u}$  gives the best match. Since states  $B_{3g}$  and  $B_{2u}$  are higher than  $B_{1u}$ , this could be interpreted as the effect of higher temperatures giving sufficient energy to populate them. Where  $B_{3g}$  and  $B_{2u}$  lower in energy, we might then expect  $B_{1u}$  to transfer

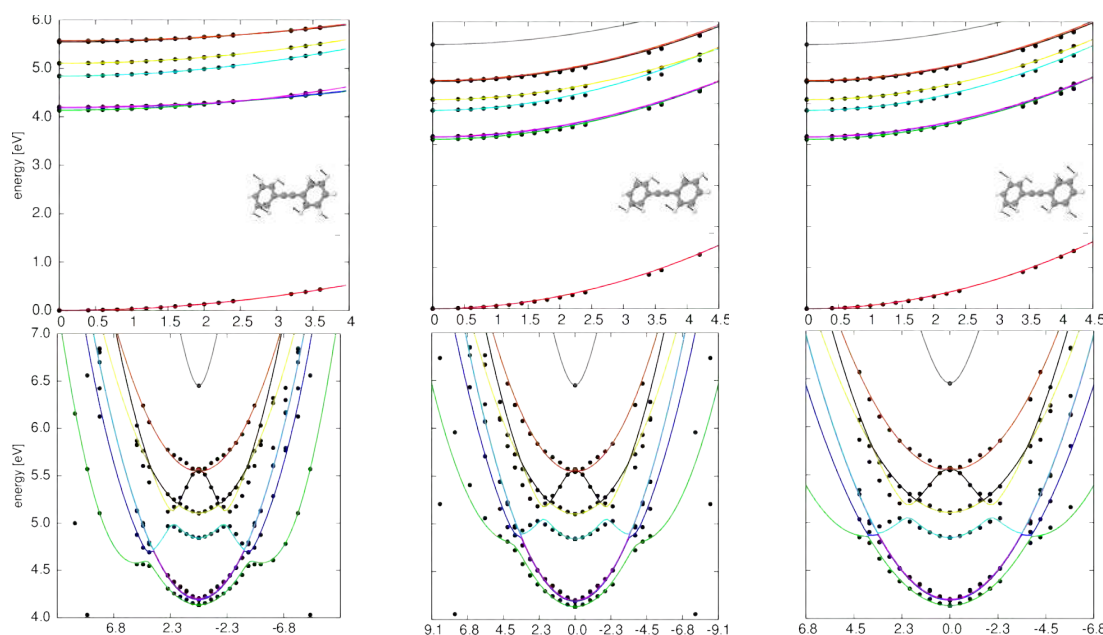


Fig. 7.13: Fitting of surfaces along modes of  $B_{1g}$  and  $B_{3g}$  symmetry.  $S_0$  shown for cuts along single modes. From left to right: *first row*:  $(\tilde{\nu}_{10}), (\tilde{\nu}_{24}), (\tilde{\nu}_{29})$ , *second row*:  $(\tilde{\nu}_5 + \tilde{\nu}_{14} + \tilde{\nu}_{10}), (\tilde{\nu}_5 + \tilde{\nu}_{14} + \tilde{\nu}_{24}), (\tilde{\nu}_5 + \tilde{\nu}_{14} + \tilde{\nu}_{29})$

some energy as it relaxes. There is a very good agreement between the position of the calculated peaks and those of the experimental spectra. This provides some support to energies calculated using DFT-MRCI, its assignment of the energy ordering of  $B_{1g}$  and confidence for the further use of this model to calculate the timescales for internal conversion to  $ts-1A_u$ . It also suggests that there is some transfer to states  $B_{3g}$  and  $B_{2u}$  despite being orbitally forbidden. Finally, the model was used to get a rough estimate of ps timescales for the internal conversion to  $ts-1A_u$ . Further confidence on the model is provided by the lack of transfer when using a fully relaxed wavefunction corresponding to 0 K, where no transfer was shown experimentally to occur. However, much work remains to be done on this model to properly understand the dynamics of this process. To obtain a proper estimate of the rate constant for the population transfer of this process at room temperature, we need to include in the model some way of representing energy loss to the environment (e.g. using complex absorbing potentials or some weakly

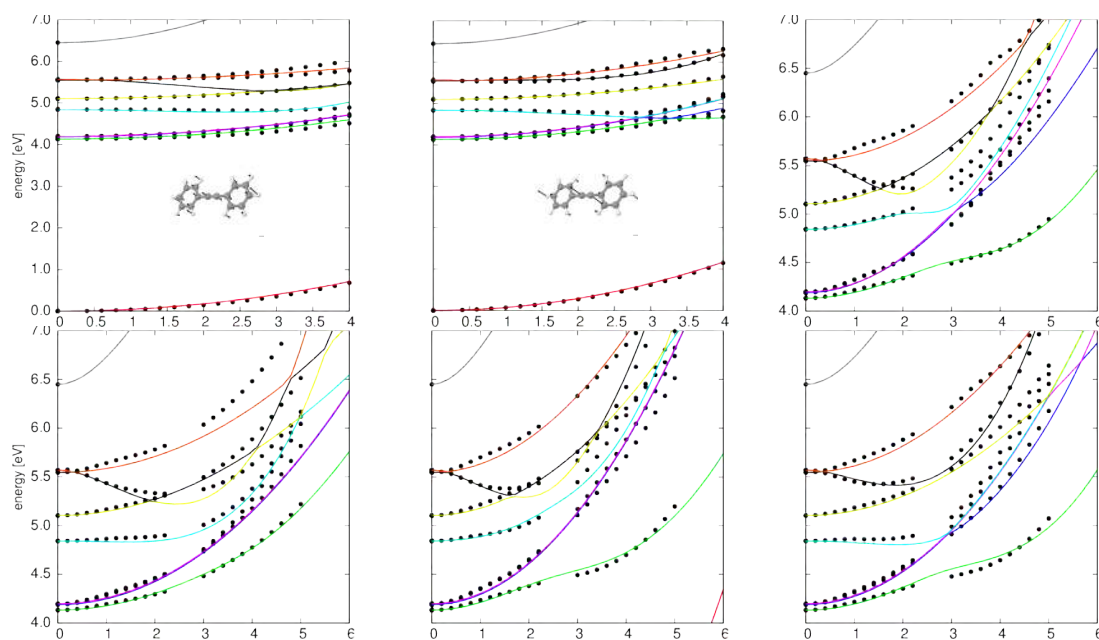


Fig. 7.14: Fitting of surfaces along modes of  $B_{2g}$  and  $B_{3g}$  symmetry.  $S_0$  shown for cuts along single modes. From left to right: *first row*:  $(\tilde{v}_4), (\tilde{v}_7), (\tilde{v}_4 + \tilde{v}_{14})$  *second row*:  $(\tilde{v}_4 + \tilde{v}_5), (\tilde{v}_7 + \tilde{v}_{14}), (\tilde{v}_7 + \tilde{v}_5)$

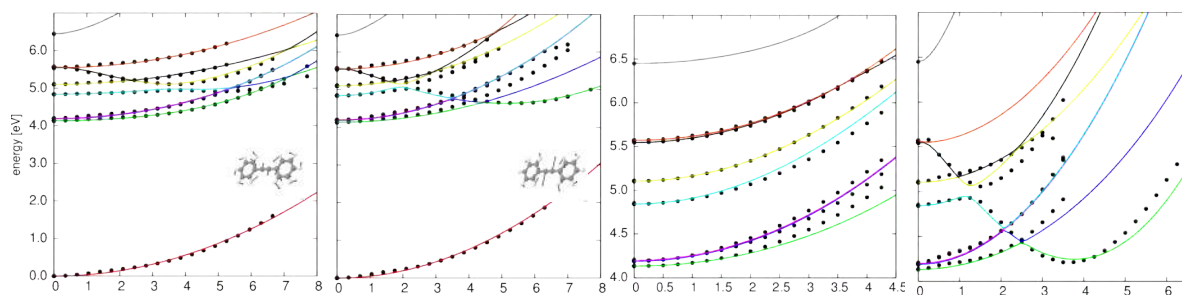


Fig. 7.15: Fitting of surfaces along modes of  $B_{3g}$  symmetry.  $S_0$  shown for cuts along single modes. From left to right: *first row*:  $(\tilde{v}_5), (\tilde{v}_{14}), (\tilde{v}_5 + \tilde{v}_{14}), (\tilde{v}_5 - \tilde{v}_{14})$

coupled "bath" of harmonic oscillators) as well as using a density matrix representation [21] of our system with the statistical distribution of initial states given by the Boltzmann distribution at the appropriate energies. The slow picosecond transfer occurring for the propagation with fully relaxed ground state wavefunction (0 K) might suggest other longer timescale mechanisms occurring such as tunnelling effects, allowing the system to overcome the isomerisation barrier. The important modes involved in this mechanism as well as the extent of out-of-plane distortions required for efficient coupling could be further explored and more carefully analysed.

Study of this system has been principally driven because Tolane is the monomer of the family of dendrimers described in the introduction. Kleiman *et al* [113] observed that the longer lived fluorescence (150-200 ps) arising from the  $ts-1A_u$  state is missing in one of the dendrimers referred to as nano-star (shown in the introduction), but the short fluorescence band is still present. It has been shown these dendritic antenna have states that are localised along the *meta*-deconjugated phenyl-acetylene branches. One suggested mechanism could be that, upon absorption at the peripheral Tolane branches, population is transferred via a *trans*-stilbene geometry, where it must immediately couple to states localised in the next segment. Given the work just presented, acetylene stretches, out-of-plane and *trans*-distortions might be playing a role in the energy funnelling mechanisms of this remarkable family of molecules.

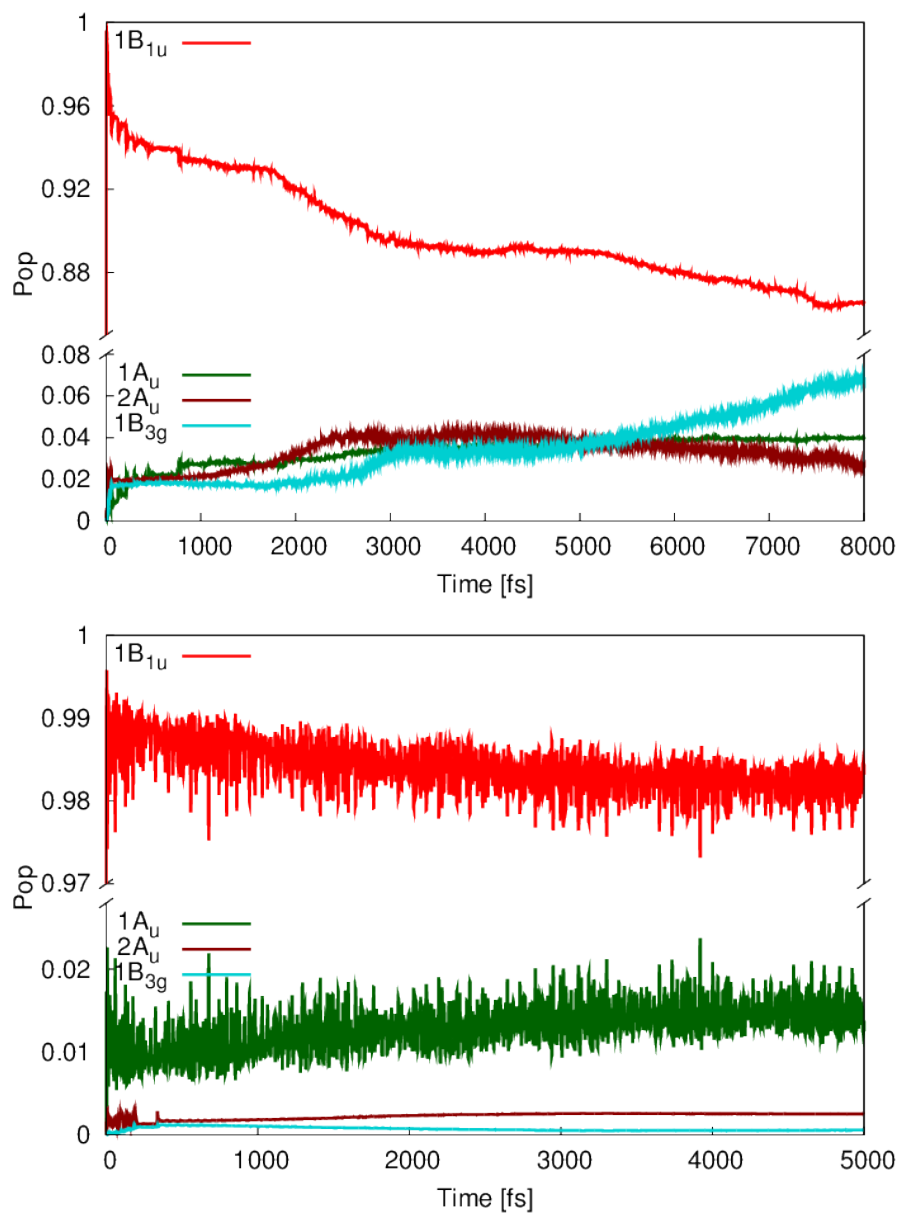


Fig. 7.16: Population transfer from  $1B_{1u}$  to states involved in the internal conversion to  $ts-1A_u$  using a hot (*above*, 3 ps) and cold (*below*, 2 ps) wavefunctions.  $1B_{1u}$  (red),  $1A_u$  (green),  $2A_u$  (brown),  $B_{3g}$  (blue)


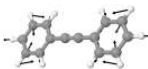


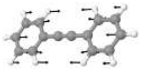



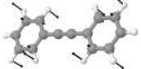
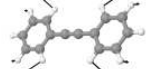






#	$D_{2h}$	e-vector	$\omega(cm^{-1})$	#	$D_{2h}$	e-vector	$\omega(cm^{-1})$
$\tilde{\nu}_2$	$B_{2u}$		0.00540	$\tilde{\nu}_{20}$	$A_g$		0.08718
$\tilde{\nu}_4$	$B_{2g}$		0.01519	$\tilde{\nu}_{24}$	$B_{1g}$		0.10490
$\tilde{\nu}_5$	$B_{3g}$		0.01679	$\tilde{\nu}_{29}$	$B_{1g}$		0.11780
$\tilde{\nu}_6$	$A_g$		0.03189	$\tilde{\nu}_{33}$	$A_g$		0.12502
$\tilde{\nu}_7$	$B_{2g}$		0.03209	$\tilde{\nu}_{38}$	$A_g$		0.14381
$\tilde{\nu}_{10}$	$B_{1g}$		0.04933	$\tilde{\nu}_{54}$	$A_g$		0.20414
$\tilde{\nu}_{14}$	$B_{3g}$		0.06379	$\tilde{\nu}_{56}$	$A_g$		0.27476
$\tilde{\nu}_{17}$	$B_{3g}$		0.07729	$\tilde{\nu}_{66}$	$A_g$		0.40244

Table 7.9:  $D_{2h}$  Harmonic frequencies of Tolane (MP2/cc-pVDZ basis)

# Chapter 8

## Conclusions

For decades, vibronic coupling models [22, 28, 120] have served as bridges connecting nuclear dynamics studies with the static studies of electronic structure calculations. Although diabatisation by anzats circumvents many problems of the description of non-adiabatic systems, it relies heavily in the topological features of the system to express non-adiabatic effects. It must be therefore conceded that as molecules become large, loose symmetry and exhibit large geometric distortions, one can no longer rely on such features to properly capture such non-adiabatic interactions. However, we have attempted to show that one can continue using these techniques fruitfully and rigorously for many systems with significant demands and for which direct-dynamic methods, with also an approximate descriptions of non-adiabatic coupling (like Tully’s fewest-switches algorithm [121]), might sometimes conceal mechanistic insight. The aim of this work was to find ways to extend the use of vibronic coupling models to describe systems of increasing complexity. As the number of states and nuclear coordinates of interest increases the following obstacles are typically apparent:

- The manifold of coupling states increases.
- Larger number of nuclear coordinates to include.



- Stronger correlation between our nuclear coordinates.
- Number of model parameters increases.

The most general of problems in the list is the increasing number of optimisation parameters. For this, many general optimisation algorithms could have performed well. However, we developed a genetic algorithm (built into the VCHAM package in MCTDH) that focuses on the specific problems that vibronic coupling models suffer. Such examples as the development of the speciation routine, which we demonstrate that it improves significantly the optimisation; the development of a number of mutation strategies that target types of coupling parameters. This includes the construction of a covariance matrix to generate adaptive mutations which is modulated by information regarding the type and domain of such vibronic model parameters.

Anyone who wishes to construct vibronic models with a large number of uncoupled DOF will soon appreciate the tediousness of the construction procedure. With the genetic algorithm we demonstrated how we can fit a cyclo-butadiene model ‘at once’, and save human time. With this CBD model we suggested a new interpretation to the high-energy photo-electron spectrum band seen in experimental one.

Another way of increasing the number of parameters is through the number of electronic states involved; the number of coupling states can quickly become unwieldy if one cannot restrict how states interact. This is why symmetry is another crucial factor for these models; to reduce the number and order of coupling between states, to allow one to correctly describe the potential energy topology with polynomial functions and to provide meaningful insights into physical mechanism by classifying in a non-arbitrary manner the way molecular distortions couple electronic states. Modelling the vibrationally mediated dissociation of acetylene was only possible thanks to the

genetic algorithm and the generation of totally symmetric invariant polynomials. This model added some flesh to the VMD experiments in the literature and allowed us to tentatively suggest some ways to control the geometry of acetylene at the time of dissociation. The invariant basis and curvilinear coordinates generated for this model could also prove valuable for the study of many other important linear molecules like  $\text{CO}_2$  and  $\text{H}_2\text{O}$ . The triply degenerate, Jahn-Teller totally symmetric invariant polynomials in turn, could be used for tetrahedral molecules, as used previously with  $T_2$  states by Mondal and Varandas [122] and for many octahedral water complexes with transition metal centres like  $\text{Fe}^+$  or  $\text{Co}^{2+}$  [123].

Finally, symmetry allowed us to analyse a system with both a large number of electronic and nuclear DOF (Chapter 7, the photo-relaxation of Tolane). It occurs via internal conversion towards a *trans*-stilbene like geometry. Both the absorption spectra and population transfer timescales agree with experiments at different temperatures. The model suggests that transfer happens primarily via out-of-plane vibrations, a new observation allowed by the careful use of symmetry considerations. Since this is the monomer for a family of energy funnelling dendritic antenna [13], this model provides clues of how these systems more generally transfer energy through the different segments of the dendritic branches. This demonstrates that vibronic coupling models can be used to understand the operations of even larger molecular systems, allowing us to include essential features in more approximate models.

# Appendix A

## $D_{\infty h}$ group

Presented below are the symmetry adapted basis function for the construction of diabatic model potential matrices representing molecules belonging to the  $D_{\infty h}$  point group. Elements of these matrices representing states spanning IrReps A and B are labelled as  $|A\rangle\hat{H}\langle B|$ . The nuclear coordinate, polynomial terms approximating these elements are similarly labelled by their IrReps such as  $Q_C^2 \cdot Q_D$ , for given C and D IrReps (a quadratic, linear term). The following functions are listed by the order of the polynomials approximating the matrix elements. Up to sixth order, two dimensional terms are provided for IrReps  $\Sigma^{+/-}$ ,  $\Pi_{u/g}$  and  $\Delta_{u/g}$  ( $A_n$  and  $E_n$  for  $n = 1, 2$ ).

## A.1 First Order, D<sub>∞h</sub> group

$$\begin{aligned}
 & \left| \Pi_g^x \right\rangle \hat{H} \left\langle \Sigma_g^+ \right| : Q_{\Pi_g^x} \\
 & \left| \Pi_g^y \right\rangle \hat{H} \left\langle \Sigma_g^+ \right| : Q_{\Pi_g^y}
 \end{aligned} \tag{1.1}$$

$$\begin{aligned}
 & \left| \Pi_g^x \right\rangle \hat{H} \left\langle \Sigma_u^- \right| : Q_{\Pi_u^y} \\
 & \left| \Pi_g^y \right\rangle \hat{H} \left\langle \Sigma_u^- \right| : -Q_{\Pi_u^x}
 \end{aligned} \tag{1.2}$$

$$\begin{aligned}
 & \left| \Pi_g^x \right\rangle \hat{H} \left\langle \Delta_g^x \right| : Q_{\Pi_g^x} \\
 & \left| \Pi_g^x \right\rangle \hat{H} \left\langle \Delta_g^y \right| : Q_{\Pi_g^y} \\
 & \left| \Pi_g^y \right\rangle \hat{H} \left\langle \Delta_g^x \right| : -Q_{\Pi_g^y} \\
 & \left| \Pi_g^y \right\rangle \hat{H} \left\langle \Delta_g^y \right| : Q_{\Pi_g^x}
 \end{aligned} \tag{1.3}$$

$$\begin{aligned}
 & \left| \Pi_g^x \right\rangle \hat{H} \left\langle \Delta_u^x \right| : Q_{\Pi_u^x} \\
 & \left| \Pi_g^x \right\rangle \hat{H} \left\langle \Delta_u^y \right| : Q_{\Pi_u^y} \\
 & \left| \Pi_g^y \right\rangle \hat{H} \left\langle \Delta_u^x \right| : -Q_{\Pi_u^y} \\
 & \left| \Pi_g^y \right\rangle \hat{H} \left\langle \Delta_u^y \right| : Q_{\Pi_u^x}
 \end{aligned} \tag{1.4}$$

$$\begin{aligned}
 & \left| \Pi_u^x \right\rangle \hat{H} \left\langle \Sigma_g^+ \right| : -Q_{\Pi_u^x} \\
 & \left| \Pi_u^y \right\rangle \hat{H} \left\langle \Sigma_g^+ \right| : -Q_{\Pi_u^y}
 \end{aligned} \tag{1.5}$$

$$\left| \Pi_u^x \right\rangle \hat{H} \left\langle \Sigma_u^- \right| : -Q_{\Pi_g^y}$$

$$\left| \Pi_u^y \right\rangle \hat{H} \left\langle \Sigma_u^- \right| : Q_{\Pi_g^x} \quad (1.6)$$

$$\begin{aligned} & \left| \Pi_u^x \right\rangle \hat{H} \left\langle \Delta_u^x \right| : Q_{\Pi_g^x} \\ & \left| \Pi_u^x \right\rangle \hat{H} \left\langle \Delta_u^y \right| : Q_{\Pi_g^y} \\ & \left| \Pi_u^y \right\rangle \hat{H} \left\langle \Delta_u^x \right| : -Q_{\Pi_g^y} \\ & \left| \Pi_u^y \right\rangle \hat{H} \left\langle \Delta_u^y \right| : Q_{\Pi_g^x} \end{aligned} \quad (1.7)$$

$$\begin{aligned} & \left| \Pi_u^x \right\rangle \hat{H} \left\langle \Delta_g^x \right| : Q_{\Pi_u^x} \\ & \left| \Pi_u^x \right\rangle \hat{H} \left\langle \Delta_g^y \right| : Q_{\Pi_u^y} \\ & \left| \Pi_u^y \right\rangle \hat{H} \left\langle \Delta_g^x \right| : -Q_{\Pi_u^y} \\ & \left| \Pi_u^y \right\rangle \hat{H} \left\langle \Delta_g^y \right| : Q_{\Pi_u^x} \end{aligned} \quad (1.8)$$

## A.2 Second Order, D<sub>∞h</sub> group

$$\left| \Sigma_g^+ \right\rangle \hat{H} \left\langle \Sigma_g^+ \right| : Q_{\Pi_g^x}^2 + Q_{\Pi_g^y}^2 \quad (2.1)$$

$$\left| \Sigma_g^+ \right\rangle \hat{H} \left\langle \Sigma_u^- \right| : -Q_{\Pi_u^x} \cdot Q_{\Pi_g^y} + Q_{\Pi_g^x} \cdot Q_{\Pi_u^y} \quad (2.2)$$

$$\left| \Sigma_u^- \right\rangle \hat{H} \left\langle \Sigma_u^- \right| : Q_{\Pi_g^x}^2 + Q_{\Pi_g^y}^2 \quad (2.3)$$

$$\begin{aligned} \left| \Delta_g^x \right\rangle \hat{H} \left\langle \Sigma_g^+ \right| &: Q_{\Pi_g^x}^2 - Q_{\Pi_g^y}^2 \\ \left| \Delta_g^y \right\rangle \hat{H} \left\langle \Sigma_g^+ \right| &: +2 \cdot Q_{\Pi_g^x} \cdot Q_{\Pi_g^y} \end{aligned} \quad (2.4)$$

$$\begin{aligned} \left| \Delta_g^x \right\rangle \hat{H} \left\langle \Sigma_g^+ \right| &: Q_{\Pi_u^x}^2 - Q_{\Pi_u^y}^2 \\ \left| \Delta_g^y \right\rangle \hat{H} \left\langle \Sigma_g^+ \right| &: +2 \cdot Q_{\Pi_u^x} \cdot Q_{\Pi_u^y} \end{aligned} \quad (2.5)$$

$$\begin{aligned} \left| \Delta_g^x \right\rangle \hat{H} \left\langle \Delta_g^x \right| &: Q_{\Pi_g^x}^2 + Q_{\Pi_g^y}^2 \\ \left| \Delta_g^y \right\rangle \hat{H} \left\langle \Delta_g^y \right| &: Q_{\Pi_g^x}^2 + Q_{\Pi_g^y}^2 \end{aligned} \quad (2.6)$$

$$\begin{aligned} \left| \Delta_g^x \right\rangle \hat{H} \left\langle \Delta_u^x \right| &: Q_{\Pi_g^x} \cdot Q_{\Pi_u^x} + Q_{\Pi_g^y} \cdot Q_{\Pi_u^y} \\ \left| \Delta_g^x \right\rangle \hat{H} \left\langle \Delta_u^y \right| &: -Q_{\Pi_u^x} \cdot Q_{\Pi_g^y} + Q_{\Pi_g^x} \cdot Q_{\Pi_u^y} \\ \left| \Delta_g^y \right\rangle \hat{H} \left\langle \Delta_u^x \right| &: Q_{\Pi_u^x} \cdot Q_{\Pi_g^y} - Q_{\Pi_g^x} \cdot Q_{\Pi_u^y} \\ \left| \Delta_g^y \right\rangle \hat{H} \left\langle \Delta_u^y \right| &: Q_{\Pi_g^x} \cdot Q_{\Pi_u^x} + Q_{\Pi_g^y} \cdot Q_{\Pi_u^y} \end{aligned} \quad (2.7)$$

$$\begin{aligned}
\left| \Delta_u^x \right\rangle \hat{H} \left\langle \Sigma_u^- \right| &: -Q_{\Pi_g^x} \cdot Q_{\Pi_g^y} \\
\left| \Delta_u^y \right\rangle \hat{H} \left\langle \Sigma_u^- \right| &: Q_{\Pi_g^x}^2 - Q_{\Pi_g^y}^2
\end{aligned} \tag{2.8}$$

$$\begin{aligned}
\left| \Delta_u^x \right\rangle \hat{H} \left\langle \Sigma_u^- \right| &: -Q_{\Pi_u^x} \cdot Q_{\Pi_u^y} \\
\left| \Delta_u^y \right\rangle \hat{H} \left\langle \Sigma_u^- \right| &: Q_{\Pi_u^x}^2 - Q_{\Pi_u^y}^2
\end{aligned} \tag{2.9}$$

$$\begin{aligned}
\left| \Delta_u^x \right\rangle \hat{H} \left\langle \Delta_u^x \right| &: Q_{\Pi_g^x}^2 + Q_{\Pi_g^y}^2 \\
\left| \Delta_u^y \right\rangle \hat{H} \left\langle \Delta_u^y \right| &: Q_{\Pi_g^x}^2 + Q_{\Pi_g^y}^2
\end{aligned} \tag{2.10}$$

$$\begin{aligned}
\left| \Pi_g^x \right\rangle \hat{H} \left\langle \Pi_g^x \right| &: Q_{\Pi_g^x}^2 - Q_{\Pi_g^y}^2 \\
\left| \Pi_g^x \right\rangle \hat{H} \left\langle \Pi_g^y \right| &: Q_{\Pi_g^x} \cdot Q_{\Pi_g^y} \\
\left| \Pi_g^y \right\rangle \hat{H} \left\langle \Pi_g^y \right| &: -Q_{\Pi_g^x}^2 + Q_{\Pi_g^y}^2
\end{aligned} \tag{2.11}$$

$$\begin{aligned}
\left| \Pi_g^x \right\rangle \hat{H} \left\langle \Pi_u^x \right| &: Q_{\Pi_g^x} \cdot Q_{\Pi_u^x} + Q_{\Pi_g^y} \cdot Q_{\Pi_u^y} \\
\left| \Pi_g^x \right\rangle \hat{H} \left\langle \Pi_u^y \right| &: -Q_{\Pi_u^x} \cdot Q_{\Pi_g^y} + Q_{\Pi_g^x} \cdot Q_{\Pi_u^y} \\
\left| \Pi_g^y \right\rangle \hat{H} \left\langle \Pi_u^x \right| &: Q_{\Pi_u^x} \cdot Q_{\Pi_g^y} - Q_{\Pi_g^x} \cdot Q_{\Pi_u^y} \\
\left| \Pi_g^y \right\rangle \hat{H} \left\langle \Pi_u^y \right| &: Q_{\Pi_g^x} \cdot Q_{\Pi_u^x} + Q_{\Pi_g^y} \cdot Q_{\Pi_u^y}
\end{aligned} \tag{2.12}$$

$$\left| \Pi_g^x \right\rangle \hat{H} \left\langle \Pi_g^x \right| : Q_{\Pi_u^x}^2 - Q_{\Pi_u^y}^2$$

$$\begin{aligned}
\left| \Pi_g^x \right\rangle \hat{H} \left\langle \Pi_g^y \right| &: Q_{\Pi_u^x} \cdot Q_{\Pi_u^y} \\
\left| \Pi_g^y \right\rangle \hat{H} \left\langle \Pi_g^y \right| &: -Q_{\Pi_u^x}^2 + Q_{\Pi_u^y}^2
\end{aligned} \tag{2.13}$$

$$\begin{aligned}
\left| \Pi_u^x \right\rangle \hat{H} \left\langle \Pi_u^x \right| &: -Q_{\Pi_g^x}^2 + Q_{\Pi_g^y}^2 \\
\left| \Pi_u^x \right\rangle \hat{H} \left\langle \Pi_u^y \right| &: -Q_{\Pi_g^x} \cdot Q_{\Pi_g^y} \\
\left| \Pi_u^y \right\rangle \hat{H} \left\langle \Pi_u^y \right| &: Q_{\Pi_g^x}^2 - Q_{\Pi_g^y}^2
\end{aligned} \tag{2.14}$$

$$\begin{aligned}
\left| \Pi_u^x \right\rangle \hat{H} \left\langle \Pi_u^x \right| &: -Q_{\Pi_u^x}^2 + Q_{\Pi_u^y}^2 \\
\left| \Pi_u^x \right\rangle \hat{H} \left\langle \Pi_u^y \right| &: -Q_{\Pi_u^x} \cdot Q_{\Pi_u^y} \\
\left| \Pi_u^y \right\rangle \hat{H} \left\langle \Pi_u^y \right| &: Q_{\Pi_u^x}^2 - Q_{\Pi_u^y}^2
\end{aligned} \tag{2.15}$$



### A.3 Third Order, D<sub>∞h</sub> group

$$\begin{aligned}
|\Pi_g^x\rangle\hat{H}\langle\Sigma_g^+| &: Q_{\Pi_g^x}^3 + Q_{\Pi_g^x} \cdot Q_{\Pi_g^y}^2 \\
|\Pi_g^y\rangle\hat{H}\langle\Sigma_g^+| &: Q_{\Pi_g^x}^2 \cdot Q_{\Pi_g^y} + Q_{\Pi_g^y}^3
\end{aligned} \tag{3.1}$$

$$\begin{aligned}
|\Pi_g^x\rangle\hat{H}\langle\Sigma_g^+| &: Q_{\Pi_g^x} \cdot Q_{\Pi_u^x}^2 + Q_{\Pi_u^x} \cdot Q_{\Pi_g^y} \cdot Q_{\Pi_u^y} - Q_{\Pi_g^x} \cdot Q_{\Pi_u^y}^2 \\
|\Pi_g^y\rangle\hat{H}\langle\Sigma_g^+| &: -Q_{\Pi_u^x}^2 \cdot Q_{\Pi_g^y} + Q_{\Pi_g^x} \cdot Q_{\Pi_u^x} \cdot Q_{\Pi_u^y} + Q_{\Pi_g^y} \cdot Q_{\Pi_u^y}^2
\end{aligned} \tag{3.2}$$

$$\begin{aligned}
|\Pi_g^x\rangle\hat{H}\langle\Sigma_u^-| &: -Q_{\Pi_g^x} \cdot Q_{\Pi_u^x} \cdot Q_{\Pi_g^y} + Q_{\Pi_g^x}^2 \cdot Q_{\Pi_u^y} - Q_{\Pi_g^y}^2 \cdot Q_{\Pi_u^y} \\
|\Pi_g^y\rangle\hat{H}\langle\Sigma_u^-| &: Q_{\Pi_g^x}^2 \cdot Q_{\Pi_u^x} - Q_{\Pi_u^x} \cdot Q_{\Pi_g^y}^2 + Q_{\Pi_g^x} \cdot Q_{\Pi_g^y} \cdot Q_{\Pi_u^y}
\end{aligned} \tag{3.3}$$

$$\begin{aligned}
|\Pi_g^x\rangle\hat{H}\langle\Delta_g^x| &: Q_{\Pi_g^x}^3 - 3 \cdot Q_{\Pi_g^x} \cdot Q_{\Pi_g^y}^2 \\
|\Pi_g^x\rangle\hat{H}\langle\Delta_g^y| &: +3 \cdot Q_{\Pi_g^x}^2 \cdot Q_{\Pi_g^y} - Q_{\Pi_g^y}^3 \\
|\Pi_g^y\rangle\hat{H}\langle\Delta_g^x| &: +3 \cdot Q_{\Pi_g^x}^2 \cdot Q_{\Pi_g^y} - Q_{\Pi_g^y}^3 \\
|\Pi_g^y\rangle\hat{H}\langle\Delta_g^y| &: -Q_{\Pi_g^x}^3 + 3 \cdot Q_{\Pi_g^x} \cdot Q_{\Pi_g^y}^2
\end{aligned} \tag{3.4}$$

$$\begin{aligned}
|\Pi_g^x\rangle\hat{H}\langle\Delta_g^x| &: Q_{\Pi_g^x} \cdot Q_{\Pi_u^x}^2 + Q_{\Pi_u^x} \cdot Q_{\Pi_g^y} \cdot Q_{\Pi_u^y} - Q_{\Pi_g^x} \cdot Q_{\Pi_u^y}^2 \\
|\Pi_g^x\rangle\hat{H}\langle\Delta_g^y| &: -Q_{\Pi_u^x}^2 \cdot Q_{\Pi_g^y} + Q_{\Pi_g^x} \cdot Q_{\Pi_u^x} \cdot Q_{\Pi_u^y} + Q_{\Pi_g^y} \cdot Q_{\Pi_u^y}^2 \\
|\Pi_g^y\rangle\hat{H}\langle\Delta_g^x| &: Q_{\Pi_u^x}^2 \cdot Q_{\Pi_g^y} - Q_{\Pi_g^x} \cdot Q_{\Pi_u^x} \cdot Q_{\Pi_u^y} - Q_{\Pi_g^y} \cdot Q_{\Pi_u^y}^2 \\
|\Pi_g^y\rangle\hat{H}\langle\Delta_g^y| &: Q_{\Pi_g^x} \cdot Q_{\Pi_u^x}^2 + Q_{\Pi_u^x} \cdot Q_{\Pi_g^y} \cdot Q_{\Pi_u^y} - Q_{\Pi_g^x} \cdot Q_{\Pi_u^y}^2
\end{aligned} \tag{3.5}$$

$$|\Pi_g^x\rangle\hat{H}\langle\Delta_u^x| : Q_{\Pi_u^x}^3 - 3 \cdot Q_{\Pi_u^x} \cdot Q_{\Pi_u^y}^2$$

$$\begin{aligned}
\left| \Pi_g^x \right\rangle \hat{H} \left\langle \Delta_u^y \right| &: +3 \cdot Q_{\Pi_u^x}^2 \cdot Q_{\Pi_u^y} - Q_{\Pi_u^y}^3 \\
\left| \Pi_g^y \right\rangle \hat{H} \left\langle \Delta_u^x \right| &: +3 \cdot Q_{\Pi_u^x}^2 \cdot Q_{\Pi_u^y} - Q_{\Pi_u^y}^3 \\
\left| \Pi_g^y \right\rangle \hat{H} \left\langle \Delta_u^y \right| &: -Q_{\Pi_u^x}^3 + 3 \cdot Q_{\Pi_u^x} \cdot Q_{\Pi_u^y}^2
\end{aligned} \tag{3.6}$$

$$\begin{aligned}
\left| \Pi_g^x \right\rangle \hat{H} \left\langle \Delta_u^x \right| &: -Q_{\Pi_g^x}^2 \cdot Q_{\Pi_u^x} + Q_{\Pi_u^x} \cdot Q_{\Pi_g^y}^2 - Q_{\Pi_g^x} \cdot Q_{\Pi_g^y} \cdot Q_{\Pi_u^y} \\
\left| \Pi_g^x \right\rangle \hat{H} \left\langle \Delta_u^y \right| &: -Q_{\Pi_g^x} \cdot Q_{\Pi_u^x} \cdot Q_{\Pi_g^y} + Q_{\Pi_g^x}^2 \cdot Q_{\Pi_u^y} - Q_{\Pi_g^y}^2 \cdot Q_{\Pi_u^y} \\
\left| \Pi_g^y \right\rangle \hat{H} \left\langle \Delta_u^x \right| &: Q_{\Pi_g^x} \cdot Q_{\Pi_u^x} \cdot Q_{\Pi_g^y} - Q_{\Pi_g^x}^2 \cdot Q_{\Pi_u^y} + Q_{\Pi_g^y}^2 \cdot Q_{\Pi_u^y} \\
\left| \Pi_g^y \right\rangle \hat{H} \left\langle \Delta_u^y \right| &: -Q_{\Pi_g^x}^2 \cdot Q_{\Pi_u^x} + Q_{\Pi_u^x} \cdot Q_{\Pi_g^y}^2 - Q_{\Pi_g^x} \cdot Q_{\Pi_g^y} \cdot Q_{\Pi_u^y}
\end{aligned} \tag{3.7}$$

$$\begin{aligned}
\left| \Pi_u^x \right\rangle \hat{H} \left\langle \Sigma_g^+ \right| &: Q_{\Pi_g^x}^2 \cdot Q_{\Pi_u^x} - Q_{\Pi_u^x} \cdot Q_{\Pi_g^y}^2 + Q_{\Pi_g^x} \cdot Q_{\Pi_g^y} \cdot Q_{\Pi_u^y} \\
\left| \Pi_u^y \right\rangle \hat{H} \left\langle \Sigma_g^+ \right| &: Q_{\Pi_g^x} \cdot Q_{\Pi_u^x} \cdot Q_{\Pi_g^y} - Q_{\Pi_g^x}^2 \cdot Q_{\Pi_u^y} + Q_{\Pi_g^y}^2 \cdot Q_{\Pi_u^y}
\end{aligned} \tag{3.8}$$

$$\begin{aligned}
\left| \Pi_u^x \right\rangle \hat{H} \left\langle \Sigma_u^- \right| &: -Q_{\Pi_g^x}^2 \cdot Q_{\Pi_g^y} - Q_{\Pi_g^y}^3 \\
\left| \Pi_u^y \right\rangle \hat{H} \left\langle \Sigma_u^- \right| &: Q_{\Pi_g^x}^3 + Q_{\Pi_g^x} \cdot Q_{\Pi_g^y}^2
\end{aligned} \tag{3.9}$$

$$\begin{aligned}
\left| \Pi_u^x \right\rangle \hat{H} \left\langle \Sigma_u^- \right| &: Q_{\Pi_u^x}^2 \cdot Q_{\Pi_g^y} - Q_{\Pi_g^x} \cdot Q_{\Pi_u^x} \cdot Q_{\Pi_u^y} - Q_{\Pi_g^y} \cdot Q_{\Pi_u^y}^2 \\
\left| \Pi_u^y \right\rangle \hat{H} \left\langle \Sigma_u^- \right| &: Q_{\Pi_g^x} \cdot Q_{\Pi_u^x}^2 + Q_{\Pi_u^x} \cdot Q_{\Pi_g^y} \cdot Q_{\Pi_u^y} - Q_{\Pi_g^x} \cdot Q_{\Pi_u^y}^2
\end{aligned} \tag{3.10}$$

$$\left| \Pi_u^x \right\rangle \hat{H} \left\langle \Delta_u^x \right| : -Q_{\Pi_g^x}^3 + 3 \cdot Q_{\Pi_g^x} \cdot Q_{\Pi_g^y}^2$$

$$\begin{aligned}
|\Pi_u^x\rangle\hat{H}\langle\Delta_u^y| &: -3 \cdot Q_{\Pi_g^x}^2 \cdot Q_{\Pi_g^y} + Q_{\Pi_g^y}^3 \\
|\Pi_u^y\rangle\hat{H}\langle\Delta_u^x| &: -3 \cdot Q_{\Pi_g^x}^2 \cdot Q_{\Pi_g^y} + Q_{\Pi_g^y}^3 \\
|\Pi_u^y\rangle\hat{H}\langle\Delta_u^y| &: Q_{\Pi_g^x}^3 - 3 \cdot Q_{\Pi_g^x} \cdot Q_{\Pi_g^y}^2
\end{aligned} \tag{3.11}$$

$$\begin{aligned}
|\Pi_u^x\rangle\hat{H}\langle\Delta_u^x| &: Q_{\Pi_g^x} \cdot Q_{\Pi_u^x}^2 + Q_{\Pi_u^x} \cdot Q_{\Pi_g^y} \cdot Q_{\Pi_u^y} - Q_{\Pi_g^x} \cdot Q_{\Pi_u^y}^2 \\
|\Pi_u^x\rangle\hat{H}\langle\Delta_u^y| &: -Q_{\Pi_u^x}^2 \cdot Q_{\Pi_g^y} + Q_{\Pi_g^x} \cdot Q_{\Pi_u^x} \cdot Q_{\Pi_u^y} + Q_{\Pi_g^y} \cdot Q_{\Pi_u^y}^2 \\
|\Pi_u^y\rangle\hat{H}\langle\Delta_u^x| &: Q_{\Pi_u^x}^2 \cdot Q_{\Pi_g^y} - Q_{\Pi_g^x} \cdot Q_{\Pi_u^x} \cdot Q_{\Pi_u^y} - Q_{\Pi_g^y} \cdot Q_{\Pi_u^y}^2 \\
|\Pi_u^y\rangle\hat{H}\langle\Delta_u^y| &: Q_{\Pi_g^x} \cdot Q_{\Pi_u^x}^2 + Q_{\Pi_u^x} \cdot Q_{\Pi_g^y} \cdot Q_{\Pi_u^y} - Q_{\Pi_g^x} \cdot Q_{\Pi_u^y}^2
\end{aligned} \tag{3.12}$$

$$\begin{aligned}
|\Pi_u^x\rangle\hat{H}\langle\Delta_g^x| &: -Q_{\Pi_u^x}^3 + 3 \cdot Q_{\Pi_u^x} \cdot Q_{\Pi_u^y}^2 \\
|\Pi_u^x\rangle\hat{H}\langle\Delta_g^y| &: -3 \cdot Q_{\Pi_u^x}^2 \cdot Q_{\Pi_u^y} + Q_{\Pi_u^y}^3 \\
|\Pi_u^y\rangle\hat{H}\langle\Delta_g^x| &: -3 \cdot Q_{\Pi_u^x}^2 \cdot Q_{\Pi_u^y} + Q_{\Pi_u^y}^3 \\
|\Pi_u^y\rangle\hat{H}\langle\Delta_g^y| &: Q_{\Pi_u^x}^3 - 3 \cdot Q_{\Pi_u^x} \cdot Q_{\Pi_u^y}^2
\end{aligned} \tag{3.13}$$

$$\begin{aligned}
|\Pi_u^x\rangle\hat{H}\langle\Delta_g^x| &: -Q_{\Pi_g^x}^2 \cdot Q_{\Pi_u^x} + Q_{\Pi_u^x} \cdot Q_{\Pi_g^y}^2 - Q_{\Pi_g^x} \cdot Q_{\Pi_g^y} \cdot Q_{\Pi_u^y} \\
|\Pi_u^x\rangle\hat{H}\langle\Delta_g^y| &: -Q_{\Pi_g^x} \cdot Q_{\Pi_u^x} \cdot Q_{\Pi_g^y} + Q_{\Pi_g^x}^2 \cdot Q_{\Pi_u^y} - Q_{\Pi_g^y}^2 \cdot Q_{\Pi_u^y} \\
|\Pi_u^y\rangle\hat{H}\langle\Delta_g^x| &: Q_{\Pi_g^x} \cdot Q_{\Pi_u^x} \cdot Q_{\Pi_g^y} - Q_{\Pi_g^x}^2 \cdot Q_{\Pi_u^y} + Q_{\Pi_g^y}^2 \cdot Q_{\Pi_u^y} \\
|\Pi_u^y\rangle\hat{H}\langle\Delta_g^y| &: -Q_{\Pi_g^x}^2 \cdot Q_{\Pi_u^x} + Q_{\Pi_u^x} \cdot Q_{\Pi_g^y}^2 - Q_{\Pi_g^x} \cdot Q_{\Pi_g^y} \cdot Q_{\Pi_u^y}
\end{aligned} \tag{3.14}$$

## A.4 Fourth Order, D<sub>∞h</sub> group

$$\left| \Sigma_g^+ \right\rangle \hat{H} \left\langle \Sigma_g^+ \right| : Q_{\Pi_g^x}^4 + Q_{\Pi_g^x}^2 \cdot Q_{\Pi_g^y}^2 + Q_{\Pi_g^y}^4 \quad (4.1)$$

$$\begin{aligned} \left| \Sigma_g^+ \right\rangle \hat{H} \left\langle \Sigma_g^+ \right| : & Q_{\Pi_g^x}^2 \cdot Q_{\Pi_u^x}^2 - Q_{\Pi_u^x}^2 \cdot Q_{\Pi_g^y}^2 + 4 \cdot Q_{\Pi_g^x} \cdot Q_{\Pi_u^x} \\ & \cdot Q_{\Pi_g^y} \cdot Q_{\Pi_u^y} - Q_{\Pi_g^y}^2 \cdot Q_{\Pi_u^x}^2 + Q_{\Pi_g^y}^2 \cdot Q_{\Pi_u^y}^2 \end{aligned} \quad (4.2)$$

$$\left| \Sigma_u^- \right\rangle \hat{H} \left\langle \Sigma_u^- \right| : Q_{\Pi_g^x}^4 + Q_{\Pi_g^x}^2 \cdot Q_{\Pi_g^y}^2 + Q_{\Pi_g^y}^4 \quad (4.3)$$

$$\begin{aligned} \left| \Sigma_u^- \right\rangle \hat{H} \left\langle \Sigma_u^- \right| : & Q_{\Pi_g^x}^2 \cdot Q_{\Pi_u^x}^2 - Q_{\Pi_u^x}^2 \cdot Q_{\Pi_g^y}^2 + 4 \cdot Q_{\Pi_g^x} \cdot Q_{\Pi_u^x} \\ & \cdot Q_{\Pi_g^y} \cdot Q_{\Pi_u^y} - Q_{\Pi_g^y}^2 \cdot Q_{\Pi_u^x}^2 + Q_{\Pi_g^y}^2 \cdot Q_{\Pi_u^y}^2 \end{aligned} \quad (4.4)$$

$$\begin{aligned} \left| \Delta_g^x \right\rangle \hat{H} \left\langle \Sigma_g^+ \right| : & Q_{\Pi_g^x}^4 - Q_{\Pi_g^y}^4 \\ \left| \Delta_g^y \right\rangle \hat{H} \left\langle \Sigma_g^+ \right| : & +2 \cdot Q_{\Pi_g^x}^3 \cdot Q_{\Pi_g^y} + 2 \cdot Q_{\Pi_g^x} \cdot Q_{\Pi_g^y}^3 \end{aligned} \quad (4.5)$$

$$\begin{aligned} \left| \Delta_g^x \right\rangle \hat{H} \left\langle \Sigma_u^- \right| : & -3 \cdot Q_{\Pi_g^x}^2 \cdot Q_{\Pi_u^x} \cdot Q_{\Pi_g^y} + Q_{\Pi_u^x} \cdot Q_{\Pi_g^y}^3 + Q_{\Pi_g^x}^3 \cdot Q_{\Pi_u^y} - 3 \cdot Q_{\Pi_g^x} \cdot Q_{\Pi_g^y}^2 \cdot Q_{\Pi_u^y} \\ \left| \Delta_g^y \right\rangle \hat{H} \left\langle \Sigma_u^- \right| : & Q_{\Pi_g^x}^3 \cdot Q_{\Pi_u^x} - 3 \cdot Q_{\Pi_g^x} \cdot Q_{\Pi_u^x} \cdot Q_{\Pi_g^y}^2 + 3 \cdot Q_{\Pi_g^x}^2 \cdot Q_{\Pi_g^y} \cdot Q_{\Pi_u^y} - Q_{\Pi_g^y}^3 \cdot Q_{\Pi_u^y} \end{aligned} \quad (4.6)$$

$$\begin{aligned} \left| \Delta_g^x \right\rangle \hat{H} \left\langle \Sigma_u^- \right| : & -Q_{\Pi_u^x}^3 \cdot Q_{\Pi_g^y} + 3 \cdot Q_{\Pi_g^x} \cdot Q_{\Pi_u^x}^2 \cdot Q_{\Pi_u^y} + 3 \cdot Q_{\Pi_u^x} \cdot Q_{\Pi_g^y} \cdot Q_{\Pi_u^y}^2 - Q_{\Pi_g^x} \cdot Q_{\Pi_u^y}^3 \\ \left| \Delta_g^y \right\rangle \hat{H} \left\langle \Sigma_u^- \right| : & -Q_{\Pi_g^x} \cdot Q_{\Pi_u^x}^3 - 3 \cdot Q_{\Pi_u^x}^2 \cdot Q_{\Pi_g^y} \cdot Q_{\Pi_u^y} + 3 \cdot Q_{\Pi_g^x} \cdot Q_{\Pi_u^x} \cdot Q_{\Pi_u^y}^2 + Q_{\Pi_g^y} \cdot Q_{\Pi_u^y}^3 \end{aligned} \quad (4.7)$$

$$\begin{aligned} \left| \Delta_g^x \right\rangle \hat{H} \left\langle \Delta_g^x \right| : & Q_{\Pi_g^x}^4 - 6 \cdot Q_{\Pi_g^x}^2 \cdot Q_{\Pi_g^y}^2 + Q_{\Pi_g^y}^4 \\ \left| \Delta_g^x \right\rangle \hat{H} \left\langle \Delta_g^y \right| : & +4 \cdot Q_{\Pi_g^x}^3 \cdot Q_{\Pi_g^y} - 4 \cdot Q_{\Pi_g^x} \cdot Q_{\Pi_g^y}^3 \end{aligned}$$

$$\left| \Delta_g^y \right\rangle \hat{H} \left\langle \Delta_g^y \right| : -Q_{\Pi_g^x}^4 + 6 \cdot Q_{\Pi_g^x}^2 \cdot Q_{\Pi_g^y}^2 - Q_{\Pi_g^y}^4 \quad (4.8)$$

$$\begin{aligned} \left| \Delta_g^x \right\rangle \hat{H} \left\langle \Delta_g^x \right| : & Q_{\Pi_g^x}^2 \cdot Q_{\Pi_u^x}^2 - Q_{\Pi_u^x}^2 \cdot Q_{\Pi_g^y}^2 + Q_{\Pi_g^x} \cdot Q_{\Pi_u^x} \\ & \cdot Q_{\Pi_g^y} \cdot Q_{\Pi_u^y} - Q_{\Pi_g^x}^2 \cdot Q_{\Pi_u^y}^2 + Q_{\Pi_g^y}^2 \cdot Q_{\Pi_u^y}^2 \\ \left| \Delta_g^y \right\rangle \hat{H} \left\langle \Delta_g^y \right| : & Q_{\Pi_g^x}^2 \cdot Q_{\Pi_u^x}^2 - Q_{\Pi_u^x}^2 \cdot Q_{\Pi_g^y}^2 + Q_{\Pi_g^x} \cdot Q_{\Pi_u^x} \\ & \cdot Q_{\Pi_g^y} \cdot Q_{\Pi_u^y} - Q_{\Pi_g^x}^2 \cdot Q_{\Pi_u^y}^2 + Q_{\Pi_g^y}^2 \cdot Q_{\Pi_u^y}^2 \end{aligned} \quad (4.9)$$

$$\begin{aligned} \left| \Delta_g^x \right\rangle \hat{H} \left\langle \Delta_g^x \right| : & Q_{\Pi_u^x}^4 - 6 \cdot Q_{\Pi_u^x}^2 \cdot Q_{\Pi_u^y}^2 + Q_{\Pi_u^y}^4 \\ \left| \Delta_g^x \right\rangle \hat{H} \left\langle \Delta_g^y \right| : & +4 \cdot Q_{\Pi_u^x}^3 \cdot Q_{\Pi_u^y} - 4 \cdot Q_{\Pi_u^x} \cdot Q_{\Pi_u^y}^3 \\ \left| \Delta_g^y \right\rangle \hat{H} \left\langle \Delta_g^y \right| : & -Q_{\Pi_u^x}^4 + 6 \cdot Q_{\Pi_u^x}^2 \cdot Q_{\Pi_u^y}^2 - Q_{\Pi_u^y}^4 \end{aligned} \quad (4.10)$$

$$\begin{aligned} \left| \Delta_u^x \right\rangle \hat{H} \left\langle \Sigma_g^+ \right| : & Q_{\Pi_g^x}^3 \cdot Q_{\Pi_u^x} - 3 \cdot Q_{\Pi_g^x} \cdot Q_{\Pi_u^x} \cdot Q_{\Pi_g^y}^2 + 3 \cdot Q_{\Pi_g^x}^2 \cdot Q_{\Pi_g^y} \cdot Q_{\Pi_u^y} - Q_{\Pi_g^y}^3 \cdot Q_{\Pi_u^y} \\ \left| \Delta_u^y \right\rangle \hat{H} \left\langle \Sigma_g^+ \right| : & +3 \cdot Q_{\Pi_g^x}^2 \cdot Q_{\Pi_u^x} \cdot Q_{\Pi_g^y} - Q_{\Pi_u^x} \cdot Q_{\Pi_g^y}^3 - Q_{\Pi_g^x}^3 \cdot Q_{\Pi_u^y} + 3 \cdot Q_{\Pi_g^x} \cdot Q_{\Pi_g^y}^2 \cdot Q_{\Pi_u^y} \end{aligned} \quad (4.11)$$

$$\begin{aligned} \left| \Delta_u^x \right\rangle \hat{H} \left\langle \Sigma_g^+ \right| : & -Q_{\Pi_g^x} \cdot Q_{\Pi_u^x}^3 - 3 \cdot Q_{\Pi_u^x}^2 \cdot Q_{\Pi_g^y} \cdot Q_{\Pi_u^y} + 3 \cdot Q_{\Pi_g^x} \cdot Q_{\Pi_u^x} \cdot Q_{\Pi_u^y}^2 + Q_{\Pi_g^y} \cdot Q_{\Pi_u^y}^3 \\ \left| \Delta_u^y \right\rangle \hat{H} \left\langle \Sigma_g^+ \right| : & Q_{\Pi_u^x}^3 \cdot Q_{\Pi_g^y} - 3 \cdot Q_{\Pi_g^x} \cdot Q_{\Pi_u^x}^2 \cdot Q_{\Pi_u^y} - 3 \cdot Q_{\Pi_u^x} \cdot Q_{\Pi_g^y} \cdot Q_{\Pi_u^y}^2 + Q_{\Pi_g^x} \cdot Q_{\Pi_u^y}^3 \end{aligned} \quad (4.12)$$

$$\begin{aligned} \left| \Delta_u^x \right\rangle \hat{H} \left\langle \Sigma_u^- \right| : & -Q_{\Pi_g^x}^3 \cdot Q_{\Pi_g^y} - Q_{\Pi_g^x} \cdot Q_{\Pi_g^y}^3 \\ \left| \Delta_u^y \right\rangle \hat{H} \left\langle \Sigma_u^- \right| : & Q_{\Pi_g^x}^4 - Q_{\Pi_g^y}^4 \end{aligned} \quad (4.13)$$

$$\left| \Delta_u^x \right\rangle \hat{H} \left\langle \Delta_u^x \right| : -Q_{\Pi_g^x}^4 + 6 \cdot Q_{\Pi_g^x}^2 \cdot Q_{\Pi_g^y}^2 - Q_{\Pi_g^y}^4$$

$$\begin{aligned}
\left| \Delta_u^x \right\rangle \hat{H} \left\langle \Delta_u^y \right| &: -4 \cdot Q_{\Pi_g^x}^3 \cdot Q_{\Pi_g^y} + 4 \cdot Q_{\Pi_g^x} \cdot Q_{\Pi_g^y}^3 \\
\left| \Delta_u^y \right\rangle \hat{H} \left\langle \Delta_u^y \right| &: Q_{\Pi_g^x}^4 - 6 \cdot Q_{\Pi_g^x}^2 \cdot Q_{\Pi_g^y}^2 + Q_{\Pi_g^y}^4
\end{aligned} \tag{4.14}$$

$$\begin{aligned}
\left| \Delta_u^x \right\rangle \hat{H} \left\langle \Delta_u^x \right| &: Q_{\Pi_g^x}^2 \cdot Q_{\Pi_u^x}^2 - Q_{\Pi_u^x}^2 \cdot Q_{\Pi_g^y}^2 + Q_{\Pi_g^x} \cdot Q_{\Pi_u^x} \\
&\quad \cdot Q_{\Pi_g^y} \cdot Q_{\Pi_u^y} - Q_{\Pi_g^x}^2 \cdot Q_{\Pi_u^y}^2 + Q_{\Pi_g^y}^2 \cdot Q_{\Pi_u^y}^2 \\
\left| \Delta_u^y \right\rangle \hat{H} \left\langle \Delta_u^y \right| &: Q_{\Pi_g^x}^2 \cdot Q_{\Pi_u^x}^2 - Q_{\Pi_u^x}^2 \cdot Q_{\Pi_g^y}^2 + Q_{\Pi_g^x} \cdot Q_{\Pi_u^x} \\
&\quad \cdot Q_{\Pi_g^y} \cdot Q_{\Pi_u^y} - Q_{\Pi_g^x}^2 \cdot Q_{\Pi_u^y}^2 + Q_{\Pi_g^y}^2 \cdot Q_{\Pi_u^y}^2
\end{aligned} \tag{4.15}$$

$$\begin{aligned}
\left| \Delta_u^x \right\rangle \hat{H} \left\langle \Delta_u^x \right| &: -Q_{\Pi_u^x}^4 + 6 \cdot Q_{\Pi_u^x}^2 \cdot Q_{\Pi_u^y}^2 - Q_{\Pi_u^y}^4 \\
\left| \Delta_u^x \right\rangle \hat{H} \left\langle \Delta_u^y \right| &: -4 \cdot Q_{\Pi_u^x}^3 \cdot Q_{\Pi_u^y} + 4 \cdot Q_{\Pi_u^x} \cdot Q_{\Pi_u^y}^3 \\
\left| \Delta_u^y \right\rangle \hat{H} \left\langle \Delta_u^y \right| &: Q_{\Pi_u^x}^4 - 6 \cdot Q_{\Pi_u^x}^2 \cdot Q_{\Pi_u^y}^2 + Q_{\Pi_u^y}^4
\end{aligned} \tag{4.16}$$

$$\begin{aligned}
\left| \Pi_g^x \right\rangle \hat{H} \left\langle \Pi_g^x \right| &: Q_{\Pi_g^x}^4 - Q_{\Pi_g^y}^4 \\
\left| \Pi_g^x \right\rangle \hat{H} \left\langle \Pi_g^y \right| &: Q_{\Pi_g^x}^3 \cdot Q_{\Pi_g^y} + Q_{\Pi_g^x} \cdot Q_{\Pi_g^y}^3 \\
\left| \Pi_g^y \right\rangle \hat{H} \left\langle \Pi_g^y \right| &: -Q_{\Pi_g^x}^4 + Q_{\Pi_g^y}^4
\end{aligned} \tag{4.17}$$

$$\begin{aligned}
\left| \Pi_g^x \right\rangle \hat{H} \left\langle \Pi_g^x \right| &: Q_{\Pi_g^x}^4 + 2 \cdot Q_{\Pi_g^x}^2 \cdot Q_{\Pi_g^y}^2 + Q_{\Pi_g^y}^4 \\
\left| \Pi_g^y \right\rangle \hat{H} \left\langle \Pi_g^y \right| &: Q_{\Pi_g^x}^4 + 2 \cdot Q_{\Pi_g^x}^2 \cdot Q_{\Pi_g^y}^2 + Q_{\Pi_g^y}^4
\end{aligned} \tag{4.18}$$

$$\begin{aligned}
\left| \Pi_g^x \right\rangle \hat{H} \left\langle \Pi_g^x \right| &: Q_{\Pi_g^x}^2 \cdot Q_{\Pi_u^x}^2 - Q_{\Pi_u^x}^2 \cdot Q_{\Pi_g^y}^2 + Q_{\Pi_g^x} \cdot Q_{\Pi_u^x} \\
&\quad \cdot Q_{\Pi_g^y} \cdot Q_{\Pi_u^y} - Q_{\Pi_g^x}^2 \cdot Q_{\Pi_u^y}^2 + Q_{\Pi_g^y}^2 \cdot Q_{\Pi_u^y}^2
\end{aligned}$$

$$\begin{aligned} \left| \Pi_g^y \right\rangle \hat{H} \left\langle \Pi_g^y \right| : & Q_{\Pi_g^x}^2 \cdot Q_{\Pi_u^x}^2 - Q_{\Pi_u^x}^2 \cdot Q_{\Pi_g^y}^2 + Q_{\Pi_g^x} \cdot Q_{\Pi_u^x} \\ & \cdot Q_{\Pi_g^y} \cdot Q_{\Pi_u^y} - Q_{\Pi_g^x}^2 \cdot Q_{\Pi_u^y}^2 + Q_{\Pi_g^y}^2 \cdot Q_{\Pi_u^y}^2 \end{aligned} \quad (4.19)$$

$$\begin{aligned} \left| \Pi_g^x \right\rangle \hat{H} \left\langle \Pi_u^x \right| : & -Q_{\Pi_g^x}^3 \cdot Q_{\Pi_u^x} + 3 \cdot Q_{\Pi_g^x} \cdot Q_{\Pi_u^x} \cdot Q_{\Pi_g^y}^2 - 3 \cdot Q_{\Pi_g^x}^2 \cdot Q_{\Pi_g^y} \cdot Q_{\Pi_u^y} + Q_{\Pi_g^y}^3 \cdot Q_{\Pi_u^y} \\ \left| \Pi_g^x \right\rangle \hat{H} \left\langle \Pi_u^y \right| : & -3 \cdot Q_{\Pi_g^x}^2 \cdot Q_{\Pi_u^x} \cdot Q_{\Pi_g^y} + Q_{\Pi_u^x} \cdot Q_{\Pi_g^y}^3 + Q_{\Pi_g^x}^3 \cdot Q_{\Pi_u^y} - 3 \cdot Q_{\Pi_g^x} \cdot Q_{\Pi_g^y}^2 \cdot Q_{\Pi_u^y} \\ \left| \Pi_g^y \right\rangle \hat{H} \left\langle \Pi_u^x \right| : & -3 \cdot Q_{\Pi_g^x}^2 \cdot Q_{\Pi_u^x} \cdot Q_{\Pi_g^y} + Q_{\Pi_u^x} \cdot Q_{\Pi_g^y}^3 + Q_{\Pi_g^x}^3 \cdot Q_{\Pi_u^y} - 3 \cdot Q_{\Pi_g^x} \cdot Q_{\Pi_g^y}^2 \cdot Q_{\Pi_u^y} \\ \left| \Pi_g^y \right\rangle \hat{H} \left\langle \Pi_u^y \right| : & Q_{\Pi_g^x}^3 \cdot Q_{\Pi_u^x} - 3 \cdot Q_{\Pi_g^x} \cdot Q_{\Pi_u^x} \cdot Q_{\Pi_g^y}^2 + 3 \cdot Q_{\Pi_g^x}^2 \cdot Q_{\Pi_g^y} \cdot Q_{\Pi_u^y} - Q_{\Pi_g^y}^3 \cdot Q_{\Pi_u^y} \end{aligned} \quad (4.20)$$

$$\begin{aligned} \left| \Pi_g^x \right\rangle \hat{H} \left\langle \Pi_u^x \right| : & Q_{\Pi_g^x} \cdot Q_{\Pi_u^x}^3 + 3 \cdot Q_{\Pi_u^x}^2 \cdot Q_{\Pi_g^y} \cdot Q_{\Pi_u^y} - 3 \cdot Q_{\Pi_g^x} \cdot Q_{\Pi_u^x} \cdot Q_{\Pi_u^y}^2 - Q_{\Pi_g^y} \cdot Q_{\Pi_u^y}^3 \\ \left| \Pi_g^x \right\rangle \hat{H} \left\langle \Pi_u^y \right| : & -Q_{\Pi_u^x}^3 \cdot Q_{\Pi_g^y} + 3 \cdot Q_{\Pi_g^x} \cdot Q_{\Pi_u^x}^2 \cdot Q_{\Pi_u^y} + 3 \cdot Q_{\Pi_u^x} \cdot Q_{\Pi_g^y} \cdot Q_{\Pi_u^y}^2 - Q_{\Pi_g^x} \cdot Q_{\Pi_u^y}^3 \\ \left| \Pi_g^y \right\rangle \hat{H} \left\langle \Pi_u^x \right| : & -Q_{\Pi_u^x}^3 \cdot Q_{\Pi_g^y} + 3 \cdot Q_{\Pi_g^x} \cdot Q_{\Pi_u^x}^2 \cdot Q_{\Pi_u^y} + 3 \cdot Q_{\Pi_u^x} \cdot Q_{\Pi_g^y} \cdot Q_{\Pi_u^y}^2 - Q_{\Pi_g^x} \cdot Q_{\Pi_u^y}^3 \\ \left| \Pi_g^y \right\rangle \hat{H} \left\langle \Pi_u^y \right| : & -Q_{\Pi_g^x} \cdot Q_{\Pi_u^x}^3 - 3 \cdot Q_{\Pi_u^x}^2 \cdot Q_{\Pi_g^y} \cdot Q_{\Pi_u^y} + 3 \cdot Q_{\Pi_g^x} \cdot Q_{\Pi_u^x} \cdot Q_{\Pi_u^y}^2 + Q_{\Pi_g^y} \cdot Q_{\Pi_u^y}^3 \end{aligned} \quad (4.21)$$

$$\begin{aligned} \left| \Pi_u^x \right\rangle \hat{H} \left\langle \Pi_u^x \right| : & -Q_{\Pi_g^x}^4 + Q_{\Pi_g^y}^4 \\ \left| \Pi_u^x \right\rangle \hat{H} \left\langle \Pi_u^y \right| : & -Q_{\Pi_g^x}^3 \cdot Q_{\Pi_g^y} - Q_{\Pi_g^x} \cdot Q_{\Pi_g^y}^3 \\ \left| \Pi_u^y \right\rangle \hat{H} \left\langle \Pi_u^y \right| : & Q_{\Pi_g^x}^4 - Q_{\Pi_g^y}^4 \end{aligned} \quad (4.22)$$

$$\begin{aligned} \left| \Pi_u^x \right\rangle \hat{H} \left\langle \Pi_u^x \right| : & Q_{\Pi_g^x}^4 + 2 \cdot Q_{\Pi_g^x}^2 \cdot Q_{\Pi_g^y}^2 + Q_{\Pi_g^y}^4 \\ \left| \Pi_u^y \right\rangle \hat{H} \left\langle \Pi_u^y \right| : & Q_{\Pi_g^x}^4 + 2 \cdot Q_{\Pi_g^x}^2 \cdot Q_{\Pi_g^y}^2 + Q_{\Pi_g^y}^4 \end{aligned} \quad (4.23)$$

$$\begin{aligned}
\left| \Pi_u^x \right\rangle \hat{H} \left\langle \Pi_u^x \right| : & Q_{\Pi_g^x}^2 \cdot Q_{\Pi_u^x}^2 - Q_{\Pi_u^x}^2 \cdot Q_{\Pi_g^y}^2 + Q_{\Pi_g^x} \cdot Q_{\Pi_u^x} \\
& \cdot Q_{\Pi_g^y} \cdot Q_{\Pi_u^y} - Q_{\Pi_g^x}^2 \cdot Q_{\Pi_u^y}^2 + Q_{\Pi_g^y}^2 \cdot Q_{\Pi_u^y}^2 \\
\left| \Pi_u^y \right\rangle \hat{H} \left\langle \Pi_u^y \right| : & Q_{\Pi_g^x}^2 \cdot Q_{\Pi_u^x}^2 - Q_{\Pi_u^x}^2 \cdot Q_{\Pi_g^y}^2 + Q_{\Pi_g^x} \cdot Q_{\Pi_u^x} \\
& \cdot Q_{\Pi_g^y} \cdot Q_{\Pi_u^y} - Q_{\Pi_g^x}^2 \cdot Q_{\Pi_u^y}^2 + Q_{\Pi_g^y}^2 \cdot Q_{\Pi_u^y}^2
\end{aligned} \tag{4.24}$$



## A.5 Fifth Order, D<sub>∞h</sub> group

$$\begin{aligned}
\left| \Pi_g^x \right\rangle \hat{H} \left\langle \Sigma_g^+ \right| &: Q_{\Pi_g^x}^5 + Q_{\Pi_g^x}^3 \cdot Q_{\Pi_g^y}^2 + Q_{\Pi_g^x} \cdot Q_{\Pi_g^y}^4 \\
\left| \Pi_g^y \right\rangle \hat{H} \left\langle \Sigma_g^+ \right| &: Q_{\Pi_g^y}^4 \cdot Q_{\Pi_g^y} + Q_{\Pi_g^x}^2 \cdot Q_{\Pi_g^y}^3 + Q_{\Pi_g^y}^5
\end{aligned} \tag{5.1}$$

$$\begin{aligned}
\left| \Pi_g^x \right\rangle \hat{H} \left\langle \Sigma_g^+ \right| &: Q_{\Pi_g^x}^3 \cdot Q_{\Pi_u^x}^2 - 3 \cdot Q_{\Pi_g^x} \cdot Q_{\Pi_u^x}^2 \cdot Q_{\Pi_g^y}^2 + 3 \cdot Q_{\Pi_g^x}^2 \cdot Q_{\Pi_u^x} \cdot Q_{\Pi_g^y} \cdot Q_{\Pi_u^y} \\
&\quad - Q_{\Pi_u^x} \cdot Q_{\Pi_g^y}^3 \cdot Q_{\Pi_u^y} - Q_{\Pi_g^x}^3 \cdot Q_{\Pi_u^y}^2 + 3 \cdot Q_{\Pi_g^x} \cdot Q_{\Pi_u^y}^2 \cdot Q_{\Pi_u^y}^2 \\
\left| \Pi_g^y \right\rangle \hat{H} \left\langle \Sigma_g^+ \right| &: +3 \cdot Q_{\Pi_g^x}^2 \cdot Q_{\Pi_u^x}^2 \cdot Q_{\Pi_g^y} - Q_{\Pi_u^x}^2 \cdot Q_{\Pi_g^y}^3 - Q_{\Pi_g^x}^3 \cdot Q_{\Pi_u^x} \cdot Q_{\Pi_u^y} + 3 \\
&\quad \cdot Q_{\Pi_g^x} \cdot Q_{\Pi_u^x} \cdot Q_{\Pi_g^y}^2 \cdot Q_{\Pi_u^y} - 3 \cdot Q_{\Pi_g^x}^2 \cdot Q_{\Pi_g^y} \cdot Q_{\Pi_u^y}^2 + Q_{\Pi_g^x}^3 \cdot Q_{\Pi_u^y}^2
\end{aligned} \tag{5.2}$$

$$\begin{aligned}
\left| \Pi_g^x \right\rangle \hat{H} \left\langle \Sigma_u^- \right| &: -Q_{\Pi_g^x} \cdot Q_{\Pi_u^x}^3 \cdot Q_{\Pi_g^y} + 3 \cdot Q_{\Pi_g^x}^2 \cdot Q_{\Pi_u^x}^2 \cdot Q_{\Pi_u^y} - 3 \cdot Q_{\Pi_u^x}^2 \cdot Q_{\Pi_g^y}^2 \\
&\quad \cdot Q_{\Pi_u^y} + 3 \cdot Q_{\Pi_g^x} \cdot Q_{\Pi_u^x} \cdot Q_{\Pi_g^y} \cdot Q_{\Pi_u^y}^2 - Q_{\Pi_g^x}^2 \cdot Q_{\Pi_u^y}^3 + Q_{\Pi_g^x}^2 \cdot Q_{\Pi_u^y}^3 \\
\left| \Pi_g^y \right\rangle \hat{H} \left\langle \Sigma_u^- \right| &: -Q_{\Pi_g^x}^2 \cdot Q_{\Pi_u^x}^3 + Q_{\Pi_u^x}^3 \cdot Q_{\Pi_g^y}^2 - 3 \cdot Q_{\Pi_g^x} \cdot Q_{\Pi_u^x}^2 \cdot Q_{\Pi_g^y} \cdot Q_{\Pi_u^y} + 3 \\
&\quad \cdot Q_{\Pi_g^x}^2 \cdot Q_{\Pi_u^x} \cdot Q_{\Pi_u^y}^2 - 3 \cdot Q_{\Pi_u^x} \cdot Q_{\Pi_g^y}^2 \cdot Q_{\Pi_u^y}^2 + Q_{\Pi_g^x} \cdot Q_{\Pi_g^y} \cdot Q_{\Pi_u^y}^3
\end{aligned} \tag{5.3}$$

$$\begin{aligned}
\left| \Pi_g^x \right\rangle \hat{H} \left\langle \Delta_g^x \right| &: Q_{\Pi_g^x}^5 - Q_{\Pi_g^x}^3 \cdot Q_{\Pi_g^y}^2 - 3 \cdot Q_{\Pi_g^x} \cdot Q_{\Pi_g^y}^4 \\
\left| \Pi_g^x \right\rangle \hat{H} \left\langle \Delta_g^y \right| &: +3 \cdot Q_{\Pi_g^x}^4 \cdot Q_{\Pi_g^y} + Q_{\Pi_g^x}^2 \cdot Q_{\Pi_g^y}^3 - Q_{\Pi_g^y}^5 \\
\left| \Pi_g^y \right\rangle \hat{H} \left\langle \Delta_g^x \right| &: +3 \cdot Q_{\Pi_g^x}^4 \cdot Q_{\Pi_g^y} + Q_{\Pi_g^x}^2 \cdot Q_{\Pi_g^y}^3 - Q_{\Pi_g^y}^5 \\
\left| \Pi_g^y \right\rangle \hat{H} \left\langle \Delta_g^y \right| &: -Q_{\Pi_g^x}^5 + Q_{\Pi_g^x}^3 \cdot Q_{\Pi_g^y}^2 + 3 \cdot Q_{\Pi_g^x} \cdot Q_{\Pi_g^y}^4
\end{aligned} \tag{5.4}$$

$$\begin{aligned}
\left| \Pi_g^x \right\rangle \hat{H} \left\langle \Delta_u^x \right| &: Q_{\Pi_g^x}^2 \cdot Q_{\Pi_u^x}^3 - Q_{\Pi_u^x}^3 \cdot Q_{\Pi_g^y}^2 + 3 \cdot Q_{\Pi_g^x} \cdot Q_{\Pi_u^x}^2 \cdot Q_{\Pi_g^y} \cdot Q_{\Pi_u^y} - 3 \\
&\quad \cdot Q_{\Pi_g^x}^2 \cdot Q_{\Pi_u^x} \cdot Q_{\Pi_u^y}^2 + 3 \cdot Q_{\Pi_u^x} \cdot Q_{\Pi_g^y}^2 \cdot Q_{\Pi_u^y}^2 - Q_{\Pi_g^x} \cdot Q_{\Pi_g^y} \cdot Q_{\Pi_u^y}^3 \\
\left| \Pi_g^x \right\rangle \hat{H} \left\langle \Delta_u^y \right| &: -Q_{\Pi_g^x} \cdot Q_{\Pi_u^x}^3 \cdot Q_{\Pi_g^y} + 3 \cdot Q_{\Pi_g^x}^2 \cdot Q_{\Pi_u^x}^2 \cdot Q_{\Pi_u^y} - 3 \cdot Q_{\Pi_u^x}^2 \cdot Q_{\Pi_g^y}^2 \\
&\quad \cdot Q_{\Pi_u^y} + 3 \cdot Q_{\Pi_g^x} \cdot Q_{\Pi_u^x} \cdot Q_{\Pi_g^y} \cdot Q_{\Pi_u^y}^2 - Q_{\Pi_g^x}^2 \cdot Q_{\Pi_u^y}^3 + Q_{\Pi_g^x}^2 \cdot Q_{\Pi_u^y}^3
\end{aligned}$$

$$\begin{aligned}
\left| \Pi_g^y \right\rangle \hat{H} \left\langle \Delta_u^x \right| : & Q_{\Pi_g^x} \cdot Q_{\Pi_u^x}^3 \cdot Q_{\Pi_g^y} - 3 \cdot Q_{\Pi_g^x}^2 \cdot Q_{\Pi_u^x}^2 \cdot Q_{\Pi_u^y} + 3 \cdot Q_{\Pi_u^x}^2 \cdot Q_{\Pi_g^y}^2 \cdot Q_{\Pi_u^y} \\
& - 3 \cdot Q_{\Pi_g^x} \cdot Q_{\Pi_u^x} \cdot Q_{\Pi_g^y} \cdot Q_{\Pi_u^y}^2 + Q_{\Pi_g^x}^2 \cdot Q_{\Pi_u^y}^3 - Q_{\Pi_g^y}^2 \cdot Q_{\Pi_u^y}^3 \\
\left| \Pi_g^y \right\rangle \hat{H} \left\langle \Delta_u^y \right| : & Q_{\Pi_g^x}^2 \cdot Q_{\Pi_u^x}^3 - Q_{\Pi_u^x}^3 \cdot Q_{\Pi_g^y}^2 + 3 \cdot Q_{\Pi_g^x} \cdot Q_{\Pi_u^x}^2 \cdot Q_{\Pi_g^y} \cdot Q_{\Pi_u^y} - 3 \\
& \cdot Q_{\Pi_g^x}^2 \cdot Q_{\Pi_u^x} \cdot Q_{\Pi_u^y}^2 + 3 \cdot Q_{\Pi_u^x} \cdot Q_{\Pi_g^y}^2 \cdot Q_{\Pi_u^y}^2 - Q_{\Pi_g^x} \cdot Q_{\Pi_g^y} \cdot Q_{\Pi_u^y}^3
\end{aligned} \tag{5.5}$$

$$\begin{aligned}
\left| \Pi_g^x \right\rangle \hat{H} \left\langle \Delta_u^x \right| : & -Q_{\Pi_g^x}^4 \cdot Q_{\Pi_u^x} + 6 \cdot Q_{\Pi_g^x}^2 \cdot Q_{\Pi_u^x} \cdot Q_{\Pi_g^y}^2 - Q_{\Pi_u^x} \cdot Q_{\Pi_g^y}^4 \\
& - 4 \cdot Q_{\Pi_g^x}^3 \cdot Q_{\Pi_g^y} \cdot Q_{\Pi_u^y} + 4 \cdot Q_{\Pi_g^x} \cdot Q_{\Pi_g^y}^3 \cdot Q_{\Pi_u^y} \\
\left| \Pi_g^x \right\rangle \hat{H} \left\langle \Delta_u^y \right| : & -4 \cdot Q_{\Pi_g^x}^3 \cdot Q_{\Pi_u^x} \cdot Q_{\Pi_g^y} + 4 \cdot Q_{\Pi_g^x} \cdot Q_{\Pi_u^x} \cdot Q_{\Pi_g^y}^3 \\
& + Q_{\Pi_g^x}^4 \cdot Q_{\Pi_u^y} - 6 \cdot Q_{\Pi_g^x}^2 \cdot Q_{\Pi_g^y}^2 \cdot Q_{\Pi_u^y} + Q_{\Pi_g^y}^4 \cdot Q_{\Pi_u^y} \\
\left| \Pi_g^y \right\rangle \hat{H} \left\langle \Delta_u^x \right| : & -4 \cdot Q_{\Pi_g^x}^3 \cdot Q_{\Pi_u^x} \cdot Q_{\Pi_g^y} + 4 \cdot Q_{\Pi_g^x} \cdot Q_{\Pi_u^x} \cdot Q_{\Pi_g^y}^3 \\
& + Q_{\Pi_g^x}^4 \cdot Q_{\Pi_u^y} - 6 \cdot Q_{\Pi_g^x}^2 \cdot Q_{\Pi_g^y}^2 \cdot Q_{\Pi_u^y} + Q_{\Pi_g^y}^4 \cdot Q_{\Pi_u^y} \\
\left| \Pi_g^y \right\rangle \hat{H} \left\langle \Delta_u^y \right| : & Q_{\Pi_g^x}^4 \cdot Q_{\Pi_u^x} - 6 \cdot Q_{\Pi_g^x}^2 \cdot Q_{\Pi_u^x} \cdot Q_{\Pi_g^y}^2 + Q_{\Pi_u^x} \cdot Q_{\Pi_g^y}^4 \\
& + 4 \cdot Q_{\Pi_g^x}^3 \cdot Q_{\Pi_g^y} \cdot Q_{\Pi_u^y} - 4 \cdot Q_{\Pi_g^x} \cdot Q_{\Pi_g^y}^3 \cdot Q_{\Pi_u^y}
\end{aligned} \tag{5.6}$$

$$\begin{aligned}
\left| \Pi_g^x \right\rangle \hat{H} \left\langle \Delta_g^x \right| : & Q_{\Pi_g^x} \cdot Q_{\Pi_u^x}^4 + 4 \cdot Q_{\Pi_u^x}^3 \cdot Q_{\Pi_g^y} \cdot Q_{\Pi_u^y} - 6 \cdot Q_{\Pi_g^x} \\
& \cdot Q_{\Pi_u^x}^2 \cdot Q_{\Pi_u^y}^2 - 4 \cdot Q_{\Pi_u^x} \cdot Q_{\Pi_g^y} \cdot Q_{\Pi_u^y}^3 + Q_{\Pi_g^x} \cdot Q_{\Pi_u^y}^4 \\
\left| \Pi_g^x \right\rangle \hat{H} \left\langle \Delta_g^y \right| : & -Q_{\Pi_u^x}^4 \cdot Q_{\Pi_g^y} + 4 \cdot Q_{\Pi_g^x} \cdot Q_{\Pi_u^x}^3 \cdot Q_{\Pi_u^y} + 6 \cdot Q_{\Pi_u^x}^2 \\
& \cdot Q_{\Pi_g^y} \cdot Q_{\Pi_u^y}^2 - 4 \cdot Q_{\Pi_g^x} \cdot Q_{\Pi_u^x} \cdot Q_{\Pi_u^y}^3 - Q_{\Pi_g^y} \cdot Q_{\Pi_u^y}^4 \\
\left| \Pi_g^y \right\rangle \hat{H} \left\langle \Delta_g^x \right| : & -Q_{\Pi_u^x}^4 \cdot Q_{\Pi_g^y} + 4 \cdot Q_{\Pi_g^x} \cdot Q_{\Pi_u^x}^3 \cdot Q_{\Pi_u^y} + 6 \cdot Q_{\Pi_u^x}^2 \\
& \cdot Q_{\Pi_g^y} \cdot Q_{\Pi_u^y}^2 - 4 \cdot Q_{\Pi_g^x} \cdot Q_{\Pi_u^x} \cdot Q_{\Pi_u^y}^3 - Q_{\Pi_g^y} \cdot Q_{\Pi_u^y}^4 \\
\left| \Pi_g^y \right\rangle \hat{H} \left\langle \Delta_g^y \right| : & -Q_{\Pi_g^x} \cdot Q_{\Pi_u^x}^4 - 4 \cdot Q_{\Pi_u^x}^3 \cdot Q_{\Pi_g^y} \cdot Q_{\Pi_u^y} + 6 \cdot Q_{\Pi_g^x} \\
& \cdot Q_{\Pi_u^x}^2 \cdot Q_{\Pi_u^y}^2 + 4 \cdot Q_{\Pi_u^x} \cdot Q_{\Pi_g^y} \cdot Q_{\Pi_u^y}^3 - Q_{\Pi_g^x} \cdot Q_{\Pi_u^y}^4
\end{aligned} \tag{5.7}$$

$$\begin{aligned}
|\Pi_u^x\rangle\hat{H}\langle\Sigma_g^+| &: -Q_{\Pi_g^x}^2 \cdot Q_{\Pi_u^x}^3 + Q_{\Pi_u^x}^3 \cdot Q_{\Pi_g^y}^2 - 3 \cdot Q_{\Pi_g^x} \cdot Q_{\Pi_u^x}^2 \cdot Q_{\Pi_g^y} \cdot Q_{\Pi_u^y} + 3 \\
&\quad \cdot Q_{\Pi_g^x}^2 \cdot Q_{\Pi_u^x} \cdot Q_{\Pi_u^y}^2 - 3 \cdot Q_{\Pi_u^x} \cdot Q_{\Pi_g^y}^2 \cdot Q_{\Pi_u^y}^2 + Q_{\Pi_g^x} \cdot Q_{\Pi_g^y} \cdot Q_{\Pi_u^y}^3 \\
|\Pi_u^y\rangle\hat{H}\langle\Sigma_g^+| &: Q_{\Pi_g^x} \cdot Q_{\Pi_u^x}^3 \cdot Q_{\Pi_g^y} - 3 \cdot Q_{\Pi_g^x}^2 \cdot Q_{\Pi_u^x}^2 \cdot Q_{\Pi_u^y} + 3 \cdot Q_{\Pi_u^x}^2 \cdot Q_{\Pi_g^y}^2 \cdot Q_{\Pi_u^y} \\
&\quad - 3 \cdot Q_{\Pi_g^x} \cdot Q_{\Pi_u^x} \cdot Q_{\Pi_g^y} \cdot Q_{\Pi_u^y}^2 + Q_{\Pi_g^x}^2 \cdot Q_{\Pi_u^y}^3 - Q_{\Pi_g^y}^2 \cdot Q_{\Pi_u^y}^3
\end{aligned} \tag{5.8}$$

$$\begin{aligned}
|\Pi_u^x\rangle\hat{H}\langle\Sigma_u^-| &: -Q_{\Pi_g^x}^4 \cdot Q_{\Pi_g^y} - Q_{\Pi_g^x}^2 \cdot Q_{\Pi_g^y}^3 - Q_{\Pi_g^y}^5 \\
|\Pi_u^y\rangle\hat{H}\langle\Sigma_u^-| &: Q_{\Pi_g^x}^5 + Q_{\Pi_g^x}^3 \cdot Q_{\Pi_g^y}^2 + Q_{\Pi_g^x} \cdot Q_{\Pi_g^y}^4
\end{aligned} \tag{5.9}$$

$$\begin{aligned}
|\Pi_u^x\rangle\hat{H}\langle\Sigma_u^-| &: -3 \cdot Q_{\Pi_g^x}^2 \cdot Q_{\Pi_u^x}^2 \cdot Q_{\Pi_g^y} + Q_{\Pi_u^x}^2 \cdot Q_{\Pi_g^y}^3 + Q_{\Pi_g^x}^3 \cdot Q_{\Pi_u^x} \cdot Q_{\Pi_u^y} - 3 \\
&\quad \cdot Q_{\Pi_g^x} \cdot Q_{\Pi_u^x} \cdot Q_{\Pi_g^y}^2 \cdot Q_{\Pi_u^y} + 3 \cdot Q_{\Pi_g^x}^2 \cdot Q_{\Pi_g^y} \cdot Q_{\Pi_u^y}^2 - Q_{\Pi_g^y}^3 \cdot Q_{\Pi_u^y}^2 \\
|\Pi_u^y\rangle\hat{H}\langle\Sigma_u^-| &: Q_{\Pi_g^x}^3 \cdot Q_{\Pi_u^x}^2 - 3 \cdot Q_{\Pi_g^x} \cdot Q_{\Pi_u^x}^2 \cdot Q_{\Pi_g^y}^2 + 3 \cdot Q_{\Pi_g^x}^2 \cdot Q_{\Pi_u^x} \cdot Q_{\Pi_g^y} \cdot Q_{\Pi_u^y} \\
&\quad - Q_{\Pi_u^x} \cdot Q_{\Pi_g^y}^3 \cdot Q_{\Pi_u^y} - Q_{\Pi_g^x}^3 \cdot Q_{\Pi_u^y}^2 + 3 \cdot Q_{\Pi_g^x} \cdot Q_{\Pi_g^y}^2 \cdot Q_{\Pi_u^y}^2
\end{aligned} \tag{5.10}$$

$$\begin{aligned}
|\Pi_u^x\rangle\hat{H}\langle\Delta_u^x| &: -Q_{\Pi_g^x}^5 + Q_{\Pi_g^x}^3 \cdot Q_{\Pi_g^y}^2 + 3 \cdot Q_{\Pi_g^x} \cdot Q_{\Pi_g^y}^4 \\
|\Pi_u^x\rangle\hat{H}\langle\Delta_u^y| &: -3 \cdot Q_{\Pi_g^x}^4 \cdot Q_{\Pi_g^y} - Q_{\Pi_g^x}^2 \cdot Q_{\Pi_g^y}^3 + Q_{\Pi_g^y}^5 \\
|\Pi_u^y\rangle\hat{H}\langle\Delta_u^x| &: -3 \cdot Q_{\Pi_g^x}^4 \cdot Q_{\Pi_g^y} - Q_{\Pi_g^x}^2 \cdot Q_{\Pi_g^y}^3 + Q_{\Pi_g^y}^5 \\
|\Pi_u^y\rangle\hat{H}\langle\Delta_u^y| &: Q_{\Pi_g^x}^5 - Q_{\Pi_g^x}^3 \cdot Q_{\Pi_g^y}^2 - 3 \cdot Q_{\Pi_g^x} \cdot Q_{\Pi_g^y}^4
\end{aligned} \tag{5.11}$$

$$\begin{aligned}
|\Pi_u^x\rangle\hat{H}\langle\Delta_g^x| &: Q_{\Pi_g^x}^2 \cdot Q_{\Pi_u^x}^3 - Q_{\Pi_u^x}^3 \cdot Q_{\Pi_g^y}^2 + 3 \cdot Q_{\Pi_g^x} \cdot Q_{\Pi_u^x}^2 \cdot Q_{\Pi_g^y} \cdot Q_{\Pi_u^y} - 3 \\
&\quad \cdot Q_{\Pi_g^x}^2 \cdot Q_{\Pi_u^x} \cdot Q_{\Pi_u^y}^2 + 3 \cdot Q_{\Pi_u^x} \cdot Q_{\Pi_g^y}^2 \cdot Q_{\Pi_u^y}^2 - Q_{\Pi_g^x} \cdot Q_{\Pi_g^y} \cdot Q_{\Pi_u^y}^3 \\
|\Pi_u^x\rangle\hat{H}\langle\Delta_g^y| &: -Q_{\Pi_g^x} \cdot Q_{\Pi_u^x}^3 \cdot Q_{\Pi_g^y} + 3 \cdot Q_{\Pi_g^x}^2 \cdot Q_{\Pi_u^x}^2 \cdot Q_{\Pi_u^y} - 3 \cdot Q_{\Pi_u^x}^2 \cdot Q_{\Pi_g^y}^2 \\
&\quad \cdot Q_{\Pi_u^y} + 3 \cdot Q_{\Pi_g^x} \cdot Q_{\Pi_u^x} \cdot Q_{\Pi_g^y} \cdot Q_{\Pi_u^y}^2 - Q_{\Pi_g^x}^2 \cdot Q_{\Pi_u^y}^3 + Q_{\Pi_g^y}^2 \cdot Q_{\Pi_u^y}^3
\end{aligned}$$

$$\begin{aligned}
|\Pi_u^y\rangle\hat{H}\langle\Delta_g^x| &: Q_{\Pi_g^x} \cdot Q_{\Pi_u^x}^3 \cdot Q_{\Pi_g^y} - 3 \cdot Q_{\Pi_g^x}^2 \cdot Q_{\Pi_u^x}^2 \cdot Q_{\Pi_u^y} + 3 \cdot Q_{\Pi_u^x}^2 \cdot Q_{\Pi_g^y}^2 \cdot Q_{\Pi_u^y} \\
&\quad - 3 \cdot Q_{\Pi_g^x} \cdot Q_{\Pi_u^x} \cdot Q_{\Pi_g^y} \cdot Q_{\Pi_u^y}^2 + Q_{\Pi_g^x}^2 \cdot Q_{\Pi_u^y}^3 - Q_{\Pi_g^y}^2 \cdot Q_{\Pi_u^y}^3 \\
|\Pi_u^y\rangle\hat{H}\langle\Delta_g^y| &: Q_{\Pi_g^x}^2 \cdot Q_{\Pi_u^x}^3 - Q_{\Pi_u^x}^3 \cdot Q_{\Pi_g^y}^2 + 3 \cdot Q_{\Pi_g^x} \cdot Q_{\Pi_u^x}^2 \cdot Q_{\Pi_g^y} \cdot Q_{\Pi_u^y} - 3 \\
&\quad \cdot Q_{\Pi_g^x}^2 \cdot Q_{\Pi_u^x} \cdot Q_{\Pi_u^y}^2 + 3 \cdot Q_{\Pi_u^x} \cdot Q_{\Pi_g^y}^2 \cdot Q_{\Pi_u^y}^2 - Q_{\Pi_g^x} \cdot Q_{\Pi_g^y} \cdot Q_{\Pi_u^y}^3 \\
&\hspace{15em} (5.12)
\end{aligned}$$

$$\begin{aligned}
|\Pi_u^x\rangle\hat{H}\langle\Delta_g^x| &: Q_{\Pi_g^x}^4 \cdot Q_{\Pi_u^x} - 6 \cdot Q_{\Pi_g^x}^2 \cdot Q_{\Pi_u^x} \cdot Q_{\Pi_g^y}^2 + Q_{\Pi_u^x} \cdot Q_{\Pi_g^y}^4 \\
&\quad + 4 \cdot Q_{\Pi_g^x}^3 \cdot Q_{\Pi_g^y} \cdot Q_{\Pi_u^y} - 4 \cdot Q_{\Pi_g^x} \cdot Q_{\Pi_g^y}^3 \cdot Q_{\Pi_u^y} \\
|\Pi_u^x\rangle\hat{H}\langle\Delta_g^y| &: +4 \cdot Q_{\Pi_g^x}^3 \cdot Q_{\Pi_u^x} \cdot Q_{\Pi_g^y} - 4 \cdot Q_{\Pi_g^x} \cdot Q_{\Pi_u^x} \cdot Q_{\Pi_g^y}^3 \\
&\quad - Q_{\Pi_g^x}^4 \cdot Q_{\Pi_u^y} + 6 \cdot Q_{\Pi_g^x}^2 \cdot Q_{\Pi_g^y}^2 \cdot Q_{\Pi_u^y} - Q_{\Pi_g^y}^4 \cdot Q_{\Pi_u^y} \\
|\Pi_u^y\rangle\hat{H}\langle\Delta_g^x| &: +4 \cdot Q_{\Pi_g^x}^3 \cdot Q_{\Pi_u^x} \cdot Q_{\Pi_g^y} - 4 \cdot Q_{\Pi_g^x} \cdot Q_{\Pi_u^x} \cdot Q_{\Pi_g^y}^3 \\
&\quad - Q_{\Pi_g^x}^4 \cdot Q_{\Pi_u^y} + 6 \cdot Q_{\Pi_g^x}^2 \cdot Q_{\Pi_g^y}^2 \cdot Q_{\Pi_u^y} - Q_{\Pi_g^y}^4 \cdot Q_{\Pi_u^y} \\
|\Pi_u^y\rangle\hat{H}\langle\Delta_g^y| &: -Q_{\Pi_g^x}^4 \cdot Q_{\Pi_u^x} + 6 \cdot Q_{\Pi_g^x}^2 \cdot Q_{\Pi_u^x} \cdot Q_{\Pi_g^y}^2 - Q_{\Pi_u^x} \cdot Q_{\Pi_g^y}^4 \\
&\quad - 4 \cdot Q_{\Pi_g^x}^3 \cdot Q_{\Pi_g^y} \cdot Q_{\Pi_u^y} + 4 \cdot Q_{\Pi_g^x} \cdot Q_{\Pi_g^y}^3 \cdot Q_{\Pi_u^y} \\
&\hspace{15em} (5.13)
\end{aligned}$$

$$\begin{aligned}
|\Pi_u^x\rangle\hat{H}\langle\Delta_u^x| &: -Q_{\Pi_g^x} \cdot Q_{\Pi_u^x}^4 - 4 \cdot Q_{\Pi_g^x}^3 \cdot Q_{\Pi_g^y} \cdot Q_{\Pi_u^y} + 6 \cdot Q_{\Pi_g^x} \\
&\quad \cdot Q_{\Pi_u^x}^2 \cdot Q_{\Pi_u^y}^2 + 4 \cdot Q_{\Pi_u^x} \cdot Q_{\Pi_g^y} \cdot Q_{\Pi_u^y}^3 - Q_{\Pi_g^x} \cdot Q_{\Pi_u^y}^4 \\
|\Pi_u^x\rangle\hat{H}\langle\Delta_u^y| &: Q_{\Pi_u^x}^4 \cdot Q_{\Pi_g^y} - 4 \cdot Q_{\Pi_g^x} \cdot Q_{\Pi_u^x}^3 \cdot Q_{\Pi_u^y} - 6 \cdot Q_{\Pi_u^x}^2 \\
&\quad \cdot Q_{\Pi_g^y} \cdot Q_{\Pi_u^y}^2 + 4 \cdot Q_{\Pi_g^x} \cdot Q_{\Pi_u^x} \cdot Q_{\Pi_u^y}^3 + Q_{\Pi_g^y} \cdot Q_{\Pi_u^y}^4 \\
|\Pi_u^y\rangle\hat{H}\langle\Delta_u^x| &: Q_{\Pi_u^x}^4 \cdot Q_{\Pi_g^y} - 4 \cdot Q_{\Pi_g^x} \cdot Q_{\Pi_u^x}^3 \cdot Q_{\Pi_u^y} - 6 \cdot Q_{\Pi_u^x}^2 \\
&\quad \cdot Q_{\Pi_g^y} \cdot Q_{\Pi_u^y}^2 + 4 \cdot Q_{\Pi_g^x} \cdot Q_{\Pi_u^x} \cdot Q_{\Pi_u^y}^3 + Q_{\Pi_g^y} \cdot Q_{\Pi_u^y}^4 \\
|\Pi_u^y\rangle\hat{H}\langle\Delta_u^y| &: Q_{\Pi_g^x} \cdot Q_{\Pi_u^x}^4 + 4 \cdot Q_{\Pi_g^x}^3 \cdot Q_{\Pi_g^y} \cdot Q_{\Pi_u^y} - 6 \cdot Q_{\Pi_g^x} \\
&\quad \cdot Q_{\Pi_u^x}^2 \cdot Q_{\Pi_u^y}^2 - 4 \cdot Q_{\Pi_u^x} \cdot Q_{\Pi_g^y} \cdot Q_{\Pi_u^y}^3 + Q_{\Pi_g^x} \cdot Q_{\Pi_u^y}^4 \\
&\hspace{15em} (5.14)
\end{aligned}$$

## A.6 Sixth Order, D<sub>∞h</sub> group

$$\left| \Sigma_g^+ \right\rangle \hat{H} \left\langle \Sigma_g^+ \right| : Q_{\Pi_g^x}^6 + 3 \cdot Q_{\Pi_g^x}^4 \cdot Q_{\Pi_g^y}^2 + 3 \cdot Q_{\Pi_g^x}^2 \cdot Q_{\Pi_g^y}^4 + Q_{\Pi_g^y}^6 \quad (6.1)$$

$$\begin{aligned} \left| \Sigma_g^+ \right\rangle \hat{H} \left\langle \Sigma_u^- \right| : & -3 \cdot Q_{\Pi_g^x}^2 \cdot Q_{\Pi_u^x}^3 \cdot Q_{\Pi_g^y} + Q_{\Pi_u^x}^3 \cdot Q_{\Pi_g^y}^3 + 3 \cdot Q_{\Pi_g^x}^3 \cdot Q_{\Pi_u^x}^2 \cdot Q_{\Pi_g^y} \\ & - 9 \cdot Q_{\Pi_g^x} \cdot Q_{\Pi_u^x}^2 \cdot Q_{\Pi_g^y}^2 \cdot Q_{\Pi_u^y} + 9 \cdot Q_{\Pi_g^x}^2 \cdot Q_{\Pi_u^x} \cdot Q_{\Pi_g^y} \cdot Q_{\Pi_u^y}^2 \\ & - 3 \cdot Q_{\Pi_u^x} \cdot Q_{\Pi_g^y}^3 \cdot Q_{\Pi_u^y}^2 - Q_{\Pi_g^x}^3 \cdot Q_{\Pi_u^y}^3 + 3 \cdot Q_{\Pi_g^x} \cdot Q_{\Pi_g^y}^2 \cdot Q_{\Pi_u^y}^3 \end{aligned} \quad (6.2)$$

$$\left| \Sigma_u^- \right\rangle \hat{H} \left\langle \Sigma_u^- \right| : Q_{\Pi_g^x}^6 + 3 \cdot Q_{\Pi_g^x}^4 \cdot Q_{\Pi_g^y}^2 + 3 \cdot Q_{\Pi_g^x}^2 \cdot Q_{\Pi_g^y}^4 + Q_{\Pi_g^y}^6 \quad (6.3)$$

$$\begin{aligned} \left| \Delta_g^x \right\rangle \hat{H} \left\langle \Sigma_g^+ \right| : & Q_{\Pi_g^x}^6 + Q_{\Pi_g^x}^4 \cdot Q_{\Pi_g^y}^2 - Q_{\Pi_g^x}^2 \cdot Q_{\Pi_g^y}^4 - Q_{\Pi_g^y}^6 \\ \left| \Delta_g^y \right\rangle \hat{H} \left\langle \Sigma_g^+ \right| : & +2 \cdot Q_{\Pi_g^x}^5 \cdot Q_{\Pi_g^y} + 2 \cdot Q_{\Pi_g^x}^3 \cdot Q_{\Pi_g^y}^3 + 2 \cdot Q_{\Pi_g^x} \cdot Q_{\Pi_g^y}^5 \end{aligned} \quad (6.4)$$

$$\begin{aligned} \left| \Delta_g^x \right\rangle \hat{H} \left\langle \Sigma_g^+ \right| : & Q_{\Pi_g^x}^4 \cdot Q_{\Pi_u^x}^2 - 6 \cdot Q_{\Pi_g^x}^2 \cdot Q_{\Pi_u^x}^2 \cdot Q_{\Pi_g^y}^2 + Q_{\Pi_u^x}^2 \cdot Q_{\Pi_g^y}^4 + 2 \\ & \cdot Q_{\Pi_g^x}^3 \cdot Q_{\Pi_u^x} \cdot Q_{\Pi_g^y} \cdot Q_{\Pi_u^y} - 2 \cdot Q_{\Pi_g^x} \cdot Q_{\Pi_u^x} \cdot Q_{\Pi_g^y}^3 \cdot Q_{\Pi_u^y} \\ & - Q_{\Pi_g^x}^4 \cdot Q_{\Pi_u^y}^2 + 6 \cdot Q_{\Pi_g^x}^2 \cdot Q_{\Pi_g^y}^2 \cdot Q_{\Pi_u^y}^2 - Q_{\Pi_g^y}^4 \cdot Q_{\Pi_u^y}^2 \\ \left| \Delta_g^y \right\rangle \hat{H} \left\langle \Sigma_g^+ \right| : & +2 \cdot Q_{\Pi_g^x}^3 \cdot Q_{\Pi_u^x}^2 \cdot Q_{\Pi_g^y} - 2 \cdot Q_{\Pi_g^x} \cdot Q_{\Pi_u^x}^2 \cdot Q_{\Pi_g^y}^3 - 2 \cdot Q_{\Pi_g^x}^4 \\ & \cdot Q_{\Pi_u^x} \cdot Q_{\Pi_u^y} + 12 \cdot Q_{\Pi_g^x}^2 \cdot Q_{\Pi_u^x} \cdot Q_{\Pi_g^y}^2 \cdot Q_{\Pi_u^y} - 2 \cdot Q_{\Pi_g^x} \\ & \cdot Q_{\Pi_g^y}^4 \cdot Q_{\Pi_u^y} - 2 \cdot Q_{\Pi_g^x}^3 \cdot Q_{\Pi_g^y} \cdot Q_{\Pi_u^y}^2 + 2 \cdot Q_{\Pi_g^x} \cdot Q_{\Pi_g^y}^3 \cdot Q_{\Pi_u^y}^2 \end{aligned} \quad (6.5)$$

$$\begin{aligned} \left| \Delta_g^x \right\rangle \hat{H} \left\langle \Delta_g^x \right| : & Q_{\Pi_g^x}^6 - 5 \cdot Q_{\Pi_g^x}^4 \cdot Q_{\Pi_g^y}^2 - 5 \cdot Q_{\Pi_g^x}^2 \cdot Q_{\Pi_g^y}^4 + Q_{\Pi_g^y}^6 \\ \left| \Delta_g^x \right\rangle \hat{H} \left\langle \Delta_g^y \right| : & +4 \cdot Q_{\Pi_g^x}^5 \cdot Q_{\Pi_g^y} - 4 \cdot Q_{\Pi_g^x} \cdot Q_{\Pi_g^y}^5 \\ \left| \Delta_g^y \right\rangle \hat{H} \left\langle \Delta_g^y \right| : & -Q_{\Pi_g^x}^6 + 5 \cdot Q_{\Pi_g^x}^4 \cdot Q_{\Pi_g^y}^2 + 5 \cdot Q_{\Pi_g^x}^2 \cdot Q_{\Pi_g^y}^4 - Q_{\Pi_g^y}^6 \end{aligned} \quad (6.6)$$

$$\begin{aligned}
|\Delta_g^x\rangle\hat{H}\langle\Delta_u^x| &: Q_{\Pi_g^x}^3 \cdot Q_{\Pi_u^x}^3 - 3 \cdot Q_{\Pi_g^x} \cdot Q_{\Pi_u^x}^3 \cdot Q_{\Pi_g^y}^2 + 9 \cdot Q_{\Pi_g^x}^2 \cdot Q_{\Pi_u^x}^2 \cdot Q_{\Pi_g^y} \\
&\quad \cdot Q_{\Pi_u^y} - 3 \cdot Q_{\Pi_u^x}^2 \cdot Q_{\Pi_g^y}^3 \cdot Q_{\Pi_u^y} - 3 \cdot Q_{\Pi_g^x}^3 \cdot Q_{\Pi_u^x} \cdot Q_{\Pi_u^y}^2 + 9 \\
&\quad \cdot Q_{\Pi_g^x} \cdot Q_{\Pi_u^x} \cdot Q_{\Pi_g^y}^2 \cdot Q_{\Pi_u^y}^2 - 3 \cdot Q_{\Pi_g^x}^2 \cdot Q_{\Pi_g^y} \cdot Q_{\Pi_u^y}^3 + Q_{\Pi_g^y}^3 \cdot Q_{\Pi_u^y}^3 \\
|\Delta_g^x\rangle\hat{H}\langle\Delta_u^y| &: -3 \cdot Q_{\Pi_g^x}^2 \cdot Q_{\Pi_u^x}^3 \cdot Q_{\Pi_g^y} + Q_{\Pi_u^x}^3 \cdot Q_{\Pi_g^y}^3 + 3 \cdot Q_{\Pi_g^x}^3 \cdot Q_{\Pi_u^x}^2 \cdot Q_{\Pi_g^y} \\
&\quad - 9 \cdot Q_{\Pi_g^x} \cdot Q_{\Pi_u^x}^2 \cdot Q_{\Pi_g^y}^2 \cdot Q_{\Pi_u^y} + 9 \cdot Q_{\Pi_g^x}^2 \cdot Q_{\Pi_u^x} \cdot Q_{\Pi_g^y} \cdot Q_{\Pi_u^y}^2 \\
&\quad - 3 \cdot Q_{\Pi_u^x} \cdot Q_{\Pi_g^y}^3 \cdot Q_{\Pi_u^y}^2 - Q_{\Pi_g^x}^3 \cdot Q_{\Pi_u^y}^3 + 3 \cdot Q_{\Pi_g^x} \cdot Q_{\Pi_g^y}^2 \cdot Q_{\Pi_u^y}^3 \\
|\Delta_g^y\rangle\hat{H}\langle\Delta_u^x| &: +3 \cdot Q_{\Pi_g^x}^2 \cdot Q_{\Pi_u^x}^3 \cdot Q_{\Pi_g^y} - Q_{\Pi_u^x}^3 \cdot Q_{\Pi_g^y}^3 - 3 \cdot Q_{\Pi_g^x}^3 \cdot Q_{\Pi_u^x}^2 \cdot Q_{\Pi_g^y} \\
&\quad + 9 \cdot Q_{\Pi_g^x} \cdot Q_{\Pi_u^x}^2 \cdot Q_{\Pi_g^y}^2 \cdot Q_{\Pi_u^y} - 9 \cdot Q_{\Pi_g^x}^2 \cdot Q_{\Pi_u^x} \cdot Q_{\Pi_g^y} \cdot Q_{\Pi_u^y}^2 \\
&\quad + 3 \cdot Q_{\Pi_u^x} \cdot Q_{\Pi_g^y}^3 \cdot Q_{\Pi_u^y}^2 + Q_{\Pi_g^x}^3 \cdot Q_{\Pi_u^y}^3 - 3 \cdot Q_{\Pi_g^x} \cdot Q_{\Pi_g^y}^2 \cdot Q_{\Pi_u^y}^3 \\
|\Delta_g^y\rangle\hat{H}\langle\Delta_u^y| &: Q_{\Pi_g^x}^3 \cdot Q_{\Pi_u^x}^3 - 3 \cdot Q_{\Pi_g^x} \cdot Q_{\Pi_u^x}^3 \cdot Q_{\Pi_g^y}^2 + 9 \cdot Q_{\Pi_g^x}^2 \cdot Q_{\Pi_u^x}^2 \cdot Q_{\Pi_g^y} \\
&\quad \cdot Q_{\Pi_u^y} - 3 \cdot Q_{\Pi_u^x}^2 \cdot Q_{\Pi_g^y}^3 \cdot Q_{\Pi_u^y} - 3 \cdot Q_{\Pi_g^x}^3 \cdot Q_{\Pi_u^x} \cdot Q_{\Pi_u^y}^2 + 9 \\
&\quad \cdot Q_{\Pi_g^x} \cdot Q_{\Pi_u^x} \cdot Q_{\Pi_g^y}^2 \cdot Q_{\Pi_u^y}^2 - 3 \cdot Q_{\Pi_g^x}^2 \cdot Q_{\Pi_g^y} \cdot Q_{\Pi_u^y}^3 + Q_{\Pi_g^y}^3 \cdot Q_{\Pi_u^y}^3
\end{aligned} \tag{6.7}$$

$$\begin{aligned}
|\Delta_g^x\rangle\hat{H}\langle\Delta_u^x| &: -Q_{\Pi_g^x}^5 \cdot Q_{\Pi_u^x} + 5 \cdot Q_{\Pi_g^x}^3 \cdot Q_{\Pi_u^x} \cdot Q_{\Pi_g^y}^2 - 5 \cdot Q_{\Pi_g^x} \cdot Q_{\Pi_u^x} \cdot Q_{\Pi_g^y}^4 \\
&\quad - 5 \cdot Q_{\Pi_g^x}^4 \cdot Q_{\Pi_g^y} \cdot Q_{\Pi_u^y} + 5 \cdot Q_{\Pi_g^x}^2 \cdot Q_{\Pi_g^y}^3 \cdot Q_{\Pi_u^y} - Q_{\Pi_g^y}^5 \cdot Q_{\Pi_u^y} \\
|\Delta_g^x\rangle\hat{H}\langle\Delta_u^y| &: -5 \cdot Q_{\Pi_g^x}^4 \cdot Q_{\Pi_u^x} \cdot Q_{\Pi_g^y} + 5 \cdot Q_{\Pi_g^x}^2 \cdot Q_{\Pi_u^x} \cdot Q_{\Pi_g^y}^3 - Q_{\Pi_u^x} \cdot Q_{\Pi_g^y}^5 \\
&\quad + Q_{\Pi_g^x}^5 \cdot Q_{\Pi_u^y} - 5 \cdot Q_{\Pi_g^x}^3 \cdot Q_{\Pi_g^y}^2 \cdot Q_{\Pi_u^y} + 5 \cdot Q_{\Pi_g^x} \cdot Q_{\Pi_g^y}^4 \cdot Q_{\Pi_u^y} \\
|\Delta_g^y\rangle\hat{H}\langle\Delta_u^x| &: -5 \cdot Q_{\Pi_g^x}^4 \cdot Q_{\Pi_u^x} \cdot Q_{\Pi_g^y} + 5 \cdot Q_{\Pi_g^x}^2 \cdot Q_{\Pi_u^x} \cdot Q_{\Pi_g^y}^3 - Q_{\Pi_u^x} \cdot Q_{\Pi_g^y}^5 \\
&\quad + Q_{\Pi_g^x}^5 \cdot Q_{\Pi_u^y} - 5 \cdot Q_{\Pi_g^x}^3 \cdot Q_{\Pi_g^y}^2 \cdot Q_{\Pi_u^y} + 5 \cdot Q_{\Pi_g^x} \cdot Q_{\Pi_g^y}^4 \cdot Q_{\Pi_u^y} \\
|\Delta_g^y\rangle\hat{H}\langle\Delta_u^y| &: Q_{\Pi_g^x}^5 \cdot Q_{\Pi_u^x} - 5 \cdot Q_{\Pi_g^x}^3 \cdot Q_{\Pi_u^x} \cdot Q_{\Pi_g^y}^2 + 5 \cdot Q_{\Pi_g^x} \cdot Q_{\Pi_u^x} \cdot Q_{\Pi_g^y}^4 \\
&\quad + 5 \cdot Q_{\Pi_g^x}^4 \cdot Q_{\Pi_g^y} \cdot Q_{\Pi_u^y} - 5 \cdot Q_{\Pi_g^x}^2 \cdot Q_{\Pi_g^y}^3 \cdot Q_{\Pi_u^y} + Q_{\Pi_g^y}^5 \cdot Q_{\Pi_u^y}
\end{aligned} \tag{6.8}$$

$$|\Delta_u^x\rangle\hat{H}\langle\Sigma_u^-| : -Q_{\Pi_g^x}^5 \cdot Q_{\Pi_g^y} - Q_{\Pi_g^x}^3 \cdot Q_{\Pi_g^y}^3 - Q_{\Pi_g^x} \cdot Q_{\Pi_g^y}^5$$

$$\left| \Delta_u^y \right\rangle \hat{H} \left\langle \Sigma_u^- \right| : Q_{\Pi_g^x}^6 + Q_{\Pi_g^x}^4 \cdot Q_{\Pi_g^y}^2 - Q_{\Pi_g^x}^2 \cdot Q_{\Pi_g^y}^4 - Q_{\Pi_g^y}^6 \quad (6.9)$$

$$\begin{aligned} \left| \Delta_u^x \right\rangle \hat{H} \left\langle \Sigma_u^- \right| : & -Q_{\Pi_g^x}^3 \cdot Q_{\Pi_u^x}^2 \cdot Q_{\Pi_g^y} + Q_{\Pi_g^x} \cdot Q_{\Pi_u^x}^2 \cdot Q_{\Pi_g^y}^3 + Q_{\Pi_g^x}^4 \cdot Q_{\Pi_u^x} \cdot Q_{\Pi_g^y} - 6 \cdot Q_{\Pi_g^x}^2 \cdot Q_{\Pi_u^x} \\ & \cdot Q_{\Pi_g^y}^2 \cdot Q_{\Pi_u^y} + Q_{\Pi_u^x} \cdot Q_{\Pi_g^y}^4 \cdot Q_{\Pi_u^y} + Q_{\Pi_g^x}^3 \cdot Q_{\Pi_g^y} \cdot Q_{\Pi_u^y}^2 - Q_{\Pi_g^x} \cdot Q_{\Pi_g^y}^3 \cdot Q_{\Pi_u^y}^2 \\ \left| \Delta_u^y \right\rangle \hat{H} \left\langle \Sigma_u^- \right| : & Q_{\Pi_g^x}^4 \cdot Q_{\Pi_u^x}^2 - 6 \cdot Q_{\Pi_g^x}^2 \cdot Q_{\Pi_u^x}^2 \cdot Q_{\Pi_g^y}^2 + Q_{\Pi_u^x}^2 \cdot Q_{\Pi_g^y}^4 + 8 \\ & \cdot Q_{\Pi_g^x}^3 \cdot Q_{\Pi_u^x} \cdot Q_{\Pi_g^y} \cdot Q_{\Pi_u^y} - 8 \cdot Q_{\Pi_g^x} \cdot Q_{\Pi_u^x} \cdot Q_{\Pi_g^y}^3 \cdot Q_{\Pi_u^y} \\ & - Q_{\Pi_g^x}^4 \cdot Q_{\Pi_u^y}^2 + 6 \cdot Q_{\Pi_g^x}^2 \cdot Q_{\Pi_g^y}^2 \cdot Q_{\Pi_u^y}^2 - Q_{\Pi_g^y}^4 \cdot Q_{\Pi_u^y}^2 \end{aligned} \quad (6.10)$$

$$\begin{aligned} \left| \Delta_u^x \right\rangle \hat{H} \left\langle \Delta_u^x \right| : & -Q_{\Pi_g^x}^6 + 5 \cdot Q_{\Pi_g^x}^4 \cdot Q_{\Pi_g^y}^2 + 5 \cdot Q_{\Pi_g^x}^2 \cdot Q_{\Pi_g^y}^4 - Q_{\Pi_g^y}^6 \\ \left| \Delta_u^x \right\rangle \hat{H} \left\langle \Delta_u^y \right| : & -4 \cdot Q_{\Pi_g^x}^5 \cdot Q_{\Pi_g^y} + 4 \cdot Q_{\Pi_g^x} \cdot Q_{\Pi_g^y}^5 \\ \left| \Delta_u^y \right\rangle \hat{H} \left\langle \Delta_u^y \right| : & Q_{\Pi_g^x}^6 - 5 \cdot Q_{\Pi_g^x}^4 \cdot Q_{\Pi_g^y}^2 - 5 \cdot Q_{\Pi_g^x}^2 \cdot Q_{\Pi_g^y}^4 + Q_{\Pi_g^y}^6 \end{aligned} \quad (6.11)$$

$$\begin{aligned} \left| \Pi_g^x \right\rangle \hat{H} \left\langle \Pi_g^x \right| : & Q_{\Pi_g^x}^6 + Q_{\Pi_g^x}^4 \cdot Q_{\Pi_g^y}^2 - Q_{\Pi_g^x}^2 \cdot Q_{\Pi_g^y}^4 - Q_{\Pi_g^y}^6 \\ \left| \Pi_g^x \right\rangle \hat{H} \left\langle \Pi_g^y \right| : & Q_{\Pi_g^x}^5 \cdot Q_{\Pi_g^y} + Q_{\Pi_g^x}^3 \cdot Q_{\Pi_g^y}^3 + Q_{\Pi_g^x} \cdot Q_{\Pi_g^y}^5 \\ \left| \Pi_g^y \right\rangle \hat{H} \left\langle \Pi_g^y \right| : & -Q_{\Pi_g^x}^6 - Q_{\Pi_g^x}^4 \cdot Q_{\Pi_g^y}^2 + Q_{\Pi_g^x}^2 \cdot Q_{\Pi_g^y}^4 + Q_{\Pi_g^y}^6 \end{aligned} \quad (6.12)$$

$$\begin{aligned} \left| \Pi_g^x \right\rangle \hat{H} \left\langle \Pi_u^x \right| : & Q_{\Pi_g^x}^3 \cdot Q_{\Pi_u^x}^3 - 3 \cdot Q_{\Pi_g^x} \cdot Q_{\Pi_u^x}^3 \cdot Q_{\Pi_g^y}^2 + 9 \cdot Q_{\Pi_g^x}^2 \cdot Q_{\Pi_u^x}^2 \cdot Q_{\Pi_g^y} \\ & \cdot Q_{\Pi_u^y} - 3 \cdot Q_{\Pi_u^x}^2 \cdot Q_{\Pi_g^y}^3 \cdot Q_{\Pi_u^y} - 3 \cdot Q_{\Pi_g^x}^3 \cdot Q_{\Pi_u^x} \cdot Q_{\Pi_u^y}^2 + 9 \\ & \cdot Q_{\Pi_g^x} \cdot Q_{\Pi_u^x} \cdot Q_{\Pi_g^y}^2 \cdot Q_{\Pi_u^y}^2 - 3 \cdot Q_{\Pi_g^x}^2 \cdot Q_{\Pi_g^y} \cdot Q_{\Pi_u^y}^3 + Q_{\Pi_g^y}^3 \cdot Q_{\Pi_u^y}^3 \\ \left| \Pi_g^x \right\rangle \hat{H} \left\langle \Pi_u^y \right| : & -3 \cdot Q_{\Pi_g^x}^2 \cdot Q_{\Pi_u^x}^3 \cdot Q_{\Pi_g^y} + Q_{\Pi_u^x}^3 \cdot Q_{\Pi_g^y}^3 + 3 \cdot Q_{\Pi_g^x}^3 \cdot Q_{\Pi_u^x}^2 \cdot Q_{\Pi_u^y} \\ & - 9 \cdot Q_{\Pi_g^x} \cdot Q_{\Pi_u^x}^2 \cdot Q_{\Pi_g^y}^2 \cdot Q_{\Pi_u^y} + 9 \cdot Q_{\Pi_g^x}^2 \cdot Q_{\Pi_u^x} \cdot Q_{\Pi_g^y} \cdot Q_{\Pi_u^y}^2 \\ & - 3 \cdot Q_{\Pi_u^x}^3 \cdot Q_{\Pi_g^y}^3 \cdot Q_{\Pi_u^y}^2 - Q_{\Pi_g^x}^3 \cdot Q_{\Pi_u^y}^3 + 3 \cdot Q_{\Pi_g^x} \cdot Q_{\Pi_g^y}^2 \cdot Q_{\Pi_u^y}^3 \end{aligned}$$

$$\begin{aligned}
|\Pi_g^y\rangle\hat{H}\langle\Pi_u^x| : & +3 \cdot Q_{\Pi_g^x}^2 \cdot Q_{\Pi_u^x}^3 \cdot Q_{\Pi_g^y} - Q_{\Pi_u^x}^3 \cdot Q_{\Pi_g^y}^3 - 3 \cdot Q_{\Pi_g^x}^3 \cdot Q_{\Pi_u^x}^2 \cdot Q_{\Pi_u^y} \\
& + 9 \cdot Q_{\Pi_g^x} \cdot Q_{\Pi_u^x}^2 \cdot Q_{\Pi_g^y}^2 \cdot Q_{\Pi_u^y} - 9 \cdot Q_{\Pi_g^x}^2 \cdot Q_{\Pi_u^x} \cdot Q_{\Pi_g^y} \cdot Q_{\Pi_u^y}^2 \\
& + 3 \cdot Q_{\Pi_u^x} \cdot Q_{\Pi_g^y}^3 \cdot Q_{\Pi_u^y}^2 + Q_{\Pi_g^x}^3 \cdot Q_{\Pi_u^y}^3 - 3 \cdot Q_{\Pi_g^x} \cdot Q_{\Pi_g^y}^2 \cdot Q_{\Pi_u^y}^3 \\
|\Pi_g^y\rangle\hat{H}\langle\Pi_u^y| : & Q_{\Pi_g^x}^3 \cdot Q_{\Pi_u^x}^3 - 3 \cdot Q_{\Pi_g^x} \cdot Q_{\Pi_u^x}^3 \cdot Q_{\Pi_g^y}^2 + 9 \cdot Q_{\Pi_g^x}^2 \cdot Q_{\Pi_u^x}^2 \cdot Q_{\Pi_g^y} \\
& \cdot Q_{\Pi_u^y} - 3 \cdot Q_{\Pi_u^x}^2 \cdot Q_{\Pi_g^y}^3 \cdot Q_{\Pi_u^y} - 3 \cdot Q_{\Pi_g^x}^3 \cdot Q_{\Pi_u^x} \cdot Q_{\Pi_u^y}^2 + 9 \\
& \cdot Q_{\Pi_g^x} \cdot Q_{\Pi_u^x} \cdot Q_{\Pi_g^y}^2 \cdot Q_{\Pi_u^y}^2 - 3 \cdot Q_{\Pi_g^x}^2 \cdot Q_{\Pi_g^y} \cdot Q_{\Pi_u^y}^3 + Q_{\Pi_g^y}^3 \cdot Q_{\Pi_u^y}^3
\end{aligned} \tag{6.13}$$

$$\begin{aligned}
|\Pi_g^x\rangle\hat{H}\langle\Pi_g^x| : & Q_{\Pi_g^x}^4 \cdot Q_{\Pi_u^x}^2 - 6 \cdot Q_{\Pi_g^x}^2 \cdot Q_{\Pi_u^x}^2 \cdot Q_{\Pi_g^y}^2 + Q_{\Pi_u^x}^2 \cdot Q_{\Pi_g^y}^4 \\
& + Q_{\Pi_g^x}^3 \cdot Q_{\Pi_u^x} \cdot Q_{\Pi_g^y} \cdot Q_{\Pi_u^y} - Q_{\Pi_g^x} \cdot Q_{\Pi_u^x} \cdot Q_{\Pi_g^y}^3 \cdot Q_{\Pi_u^y} \\
& - Q_{\Pi_g^x}^4 \cdot Q_{\Pi_u^y}^2 + 6 \cdot Q_{\Pi_g^x}^2 \cdot Q_{\Pi_g^y}^2 \cdot Q_{\Pi_u^y}^2 - Q_{\Pi_g^y}^4 \cdot Q_{\Pi_u^y}^2 \\
|\Pi_g^x\rangle\hat{H}\langle\Pi_g^y| : & Q_{\Pi_g^x}^3 \cdot Q_{\Pi_u^x}^2 \cdot Q_{\Pi_g^y} - Q_{\Pi_g^x} \cdot Q_{\Pi_u^x}^2 \cdot Q_{\Pi_g^y}^3 - Q_{\Pi_g^x}^4 \cdot Q_{\Pi_u^x} \cdot Q_{\Pi_u^y} + 6 \cdot Q_{\Pi_g^x}^2 \cdot Q_{\Pi_u^x} \\
& \cdot Q_{\Pi_g^y}^2 \cdot Q_{\Pi_u^y} - Q_{\Pi_u^x} \cdot Q_{\Pi_g^y}^4 \cdot Q_{\Pi_u^y} - Q_{\Pi_g^x}^3 \cdot Q_{\Pi_g^y} \cdot Q_{\Pi_u^y}^2 + Q_{\Pi_g^x} \cdot Q_{\Pi_g^y}^3 \cdot Q_{\Pi_u^y}^2 \\
|\Pi_g^y\rangle\hat{H}\langle\Pi_g^y| : & -Q_{\Pi_g^x}^4 \cdot Q_{\Pi_u^x}^2 + 6 \cdot Q_{\Pi_g^x}^2 \cdot Q_{\Pi_u^x}^2 \cdot Q_{\Pi_g^y}^2 - Q_{\Pi_u^x}^2 \cdot Q_{\Pi_g^y}^4 \\
& - Q_{\Pi_g^x}^3 \cdot Q_{\Pi_u^x} \cdot Q_{\Pi_g^y} \cdot Q_{\Pi_u^y} + Q_{\Pi_g^x} \cdot Q_{\Pi_u^x} \cdot Q_{\Pi_g^y}^3 \cdot Q_{\Pi_u^y} \\
& + Q_{\Pi_g^x}^4 \cdot Q_{\Pi_u^y}^2 - 6 \cdot Q_{\Pi_g^x}^2 \cdot Q_{\Pi_g^y}^2 \cdot Q_{\Pi_u^y}^2 + Q_{\Pi_g^y}^4 \cdot Q_{\Pi_u^y}^2
\end{aligned} \tag{6.14}$$

$$\begin{aligned}
|\Pi_u^x\rangle\hat{H}\langle\Pi_u^x| : & -Q_{\Pi_g^x}^6 - Q_{\Pi_g^x}^4 \cdot Q_{\Pi_g^y}^2 + Q_{\Pi_g^x}^2 \cdot Q_{\Pi_g^y}^4 + Q_{\Pi_g^y}^6 \\
|\Pi_u^x\rangle\hat{H}\langle\Pi_u^y| : & -Q_{\Pi_g^x}^5 \cdot Q_{\Pi_g^y} - Q_{\Pi_g^x}^3 \cdot Q_{\Pi_g^y}^3 - Q_{\Pi_g^x} \cdot Q_{\Pi_g^y}^5 \\
|\Pi_u^y\rangle\hat{H}\langle\Pi_u^y| : & Q_{\Pi_g^x}^6 + Q_{\Pi_g^x}^4 \cdot Q_{\Pi_g^y}^2 - Q_{\Pi_g^x}^2 \cdot Q_{\Pi_g^y}^4 - Q_{\Pi_g^y}^6
\end{aligned} \tag{6.15}$$

$$\begin{aligned}
|\Pi_u^x\rangle\hat{H}\langle\Pi_u^x| : & -Q_{\Pi_g^x}^4 \cdot Q_{\Pi_u^x}^2 + 6 \cdot Q_{\Pi_g^x}^2 \cdot Q_{\Pi_u^x}^2 \cdot Q_{\Pi_g^y}^2 - Q_{\Pi_u^x}^2 \cdot Q_{\Pi_g^y}^4 \\
& - Q_{\Pi_g^x}^3 \cdot Q_{\Pi_u^x} \cdot Q_{\Pi_g^y} \cdot Q_{\Pi_u^y} + Q_{\Pi_g^x} \cdot Q_{\Pi_u^x} \cdot Q_{\Pi_g^y}^3 \cdot Q_{\Pi_u^y} \\
& + Q_{\Pi_g^x}^4 \cdot Q_{\Pi_u^y}^2 - 6 \cdot Q_{\Pi_g^x}^2 \cdot Q_{\Pi_g^y}^2 \cdot Q_{\Pi_u^y}^2 + Q_{\Pi_g^y}^4 \cdot Q_{\Pi_u^y}^2
\end{aligned}$$



$$\begin{aligned}
\left| \Pi_u^x \right\rangle \hat{H} \left\langle \Pi_u^y \right| : & -Q_{\Pi_g^x}^3 \cdot Q_{\Pi_u^x}^2 \cdot Q_{\Pi_g^y} + Q_{\Pi_g^x} \cdot Q_{\Pi_u^x}^2 \cdot Q_{\Pi_g^y}^3 + Q_{\Pi_g^x}^4 \cdot Q_{\Pi_u^x} \cdot Q_{\Pi_u^y} - 6 \cdot Q_{\Pi_g^x}^2 \cdot Q_{\Pi_u^x} \\
& \cdot Q_{\Pi_g^y}^2 \cdot Q_{\Pi_u^y} + Q_{\Pi_u^x} \cdot Q_{\Pi_g^y}^4 \cdot Q_{\Pi_u^y} + Q_{\Pi_g^x}^3 \cdot Q_{\Pi_g^y} \cdot Q_{\Pi_u^y}^2 - Q_{\Pi_g^x} \cdot Q_{\Pi_g^y}^3 \cdot Q_{\Pi_u^y}^2 \\
\left| \Pi_u^y \right\rangle \hat{H} \left\langle \Pi_u^y \right| : & Q_{\Pi_g^x}^4 \cdot Q_{\Pi_u^x}^2 - 6 \cdot Q_{\Pi_g^x}^2 \cdot Q_{\Pi_u^x}^2 \cdot Q_{\Pi_g^y}^2 + Q_{\Pi_u^x}^2 \cdot Q_{\Pi_g^y}^4 \\
& + Q_{\Pi_g^x}^3 \cdot Q_{\Pi_u^x} \cdot Q_{\Pi_g^y} \cdot Q_{\Pi_u^y} - Q_{\Pi_g^x} \cdot Q_{\Pi_u^x} \cdot Q_{\Pi_g^y}^3 \cdot Q_{\Pi_u^y} \\
& - Q_{\Pi_g^x}^4 \cdot Q_{\Pi_u^y}^2 + 6 \cdot Q_{\Pi_g^x}^2 \cdot Q_{\Pi_g^y}^2 \cdot Q_{\Pi_u^y}^2 - Q_{\Pi_g^y}^4 \cdot Q_{\Pi_u^y}^2
\end{aligned} \tag{6.16}$$

# Appendix B

## O group

Presented below are the symmetry adapted basis function for the construction of diabatic model potential matrices representing molecules belonging to the **O** point group. Elements of these matrices representing states spanning IrReps A and B are labelled as  $|A\rangle\hat{H}\langle B|$ . The nuclear coordinate, polynomial terms approximating these elements are similarly labelled by their IrReps such as  $Q_C^2 \cdot Q_D$ , for given C and D IrReps (a quadratic, linear term). The following functions are listed by the order of the polynomials approximating the matrix elements. Up to third order, three dimensional terms are provided for IrReps  $A_{g,E}$  and  $T_1$ .

## B.1 First Order, O group

$$\left| A_1 \right\rangle \hat{H} \left\langle A_1 \right| : Q_{A_1} \quad (1.1)$$

$$\begin{aligned} \left| E_x \right\rangle \hat{H} \left\langle A_1 \right| : Q_{E_x} \\ \left| E_y \right\rangle \hat{H} \left\langle A_1 \right| : Q_{E_y} \end{aligned} \quad (1.2)$$

$$\begin{aligned} \left| E_x \right\rangle \hat{H} \left\langle E_x \right| : Q_{E_x} \\ \left| E_x \right\rangle \hat{H} \left\langle E_y \right| : -Q_{E_y} \\ \left| E_y \right\rangle \hat{H} \left\langle E_y \right| : -Q_{E_x} \end{aligned} \quad (1.3)$$

$$\begin{aligned} \left| E_x \right\rangle \hat{H} \left\langle E_x \right| : Q_{A_1} \\ \left| E_y \right\rangle \hat{H} \left\langle E_y \right| : Q_{A_1} \end{aligned} \quad (1.4)$$

$$\begin{aligned} \left| T_{1x} \right\rangle \hat{H} \left\langle A_1 \right| : Q_{T_{1x}} \\ \left| T_{1y} \right\rangle \hat{H} \left\langle A_1 \right| : Q_{T_{1y}} \\ \left| T_{1z} \right\rangle \hat{H} \left\langle A_1 \right| : Q_{T_{1z}} \end{aligned} \quad (1.5)$$

$$\begin{aligned} \left| T_{1x} \right\rangle \hat{H} \left\langle E_x \right| : -Q_{T_{1x}} \\ \left| T_{1x} \right\rangle \hat{H} \left\langle E_y \right| : -1\sqrt{3} \cdot Q_{T_{1x}} \\ \left| T_{1y} \right\rangle \hat{H} \left\langle E_x \right| : Q_{T_{1y}} \end{aligned}$$

$$\begin{aligned}
|T_{1z}\rangle \hat{H} \langle E_x| &: -Q_{T_{1z}} \\
|T_{1z}\rangle \hat{H} \langle E_y| &: \sqrt{3} \cdot Q_{T_{1z}}
\end{aligned}
\tag{1.6}$$

$$\begin{aligned}
|T_{1x}\rangle \hat{H} \langle T_{1x}| &: -\sqrt{3} \cdot Q_{E_y} - Q_{E_x} \\
|T_{1y}\rangle \hat{H} \langle T_{1y}| &: +2 \cdot Q_{E_x} \\
|T_{1z}\rangle \hat{H} \langle T_{1z}| &: +\sqrt{3} \cdot Q_{E_y} - Q_{E_x}
\end{aligned}
\tag{1.7}$$

$$\begin{aligned}
|T_{1x}\rangle \hat{H} \langle T_{1x}| &: Q_{A_1} \\
|T_{1y}\rangle \hat{H} \langle T_{1y}| &: Q_{A_1} \\
|T_{1z}\rangle \hat{H} \langle T_{1z}| &: Q_{A_1}
\end{aligned}
\tag{1.8}$$

## B.2 Second Order, O group

$$\left| A_1 \right\rangle \hat{H} \left\langle A_1 \right| : Q_{T_{1x}}^2 + Q_{T_{1y}}^2 + Q_{T_{1z}}^2 \quad (2.1)$$

$$\left| A_1 \right\rangle \hat{H} \left\langle A_1 \right| : Q_{A_1}^2 \quad (2.2)$$

$$\left| A_1 \right\rangle \hat{H} \left\langle A_1 \right| : Q_{E_x}^2 + Q_{E_y}^2 \quad (2.3)$$

$$\begin{aligned} \left| E_x \right\rangle \hat{H} \left\langle A_1 \right| : Q_{T_{1x}}^2 - Q_{T_{1y}}^2 + Q_{T_{1z}}^2 \\ \left| E_y \right\rangle \hat{H} \left\langle A_1 \right| : \sqrt{3} \cdot Q_{T_{1x}}^2 - \sqrt{3} \cdot Q_{T_{1z}}^2 \end{aligned} \quad (2.4)$$

$$\begin{aligned} \left| E_x \right\rangle \hat{H} \left\langle A_1 \right| : Q_{E_x}^2 - Q_{E_y}^2 \\ \left| E_y \right\rangle \hat{H} \left\langle A_1 \right| : -2 \cdot Q_{E_x} \cdot Q_{E_y} \end{aligned} \quad (2.5)$$

$$\begin{aligned} \left| E_x \right\rangle \hat{H} \left\langle A_1 \right| : Q_{A_1} \cdot Q_{E_x} \\ \left| E_y \right\rangle \hat{H} \left\langle A_1 \right| : Q_{A_1} \cdot Q_{E_y} \end{aligned} \quad (2.6)$$

$$\begin{aligned} \left| E_x \right\rangle \hat{H} \left\langle E_x \right| : Q_{T_{1x}}^2 + Q_{T_{1y}}^2 + Q_{T_{1z}}^2 \\ \left| E_y \right\rangle \hat{H} \left\langle E_y \right| : Q_{T_{1x}}^2 + Q_{T_{1y}}^2 + Q_{T_{1z}}^2 \end{aligned} \quad (2.7)$$

$$\begin{aligned} \left| E_x \right\rangle \hat{H} \left\langle E_x \right| : Q_{E_x}^2 - Q_{E_y}^2 \\ \left| E_x \right\rangle \hat{H} \left\langle E_y \right| : 2 \cdot Q_{E_x} \cdot Q_{E_y} \end{aligned}$$

$$\left| E_y \right\rangle \hat{H} \left\langle E_y \right| : -Q_{E_x}^2 + Q_{E_y}^2 \quad (2.8)$$

$$\begin{aligned} \left| E_x \right\rangle \hat{H} \left\langle E_x \right| &: Q_{A_1}^2 \\ \left| E_y \right\rangle \hat{H} \left\langle E_y \right| &: Q_{A_1}^2 \end{aligned} \quad (2.9)$$

$$\begin{aligned} \left| E_x \right\rangle \hat{H} \left\langle E_x \right| &: Q_{A_1} \cdot Q_{E_x} \\ \left| E_x \right\rangle \hat{H} \left\langle E_y \right| &: -Q_{A_1} \cdot Q_{E_y} \\ \left| E_y \right\rangle \hat{H} \left\langle E_y \right| &: -Q_{A_1} \cdot Q_{E_x} \end{aligned} \quad (2.10)$$

$$\begin{aligned} \left| T_{1x} \right\rangle \hat{H} \left\langle A_1 \right| &: -\sqrt{3} \cdot Q_{E_y} \cdot Q_{T_{1x}} - Q_{E_x} \cdot Q_{T_{1x}} \\ \left| T_{1y} \right\rangle \hat{H} \left\langle A_1 \right| &: +2 \cdot Q_{E_x} \cdot Q_{T_{1y}} \\ \left| T_{1z} \right\rangle \hat{H} \left\langle A_1 \right| &: +\sqrt{3} \cdot Q_{E_y} \cdot Q_{T_{1z}} - Q_{E_x} \cdot Q_{T_{1z}} \end{aligned} \quad (2.11)$$

$$\begin{aligned} \left| T_{1x} \right\rangle \hat{H} \left\langle A_1 \right| &: Q_{A_1} \cdot Q_{T_{1x}} \\ \left| T_{1y} \right\rangle \hat{H} \left\langle A_1 \right| &: Q_{A_1} \cdot Q_{T_{1y}} \\ \left| T_{1z} \right\rangle \hat{H} \left\langle A_1 \right| &: Q_{A_1} \cdot Q_{T_{1z}} \end{aligned} \quad (2.12)$$

$$\begin{aligned} \left| T_{1x} \right\rangle \hat{H} \left\langle E_x \right| &: \sqrt{3} \cdot Q_{T_{1y}} \cdot Q_{T_{1z}} \\ \left| T_{1x} \right\rangle \hat{H} \left\langle E_y \right| &: -Q_{T_{1y}} \cdot Q_{T_{1z}} \end{aligned}$$

$$\begin{aligned}
|T_{1y}\rangle \hat{H} \langle E_y| &: +2 \cdot Q_{T_{1x}} \cdot Q_{T_{1z}} \\
|T_{1z}\rangle \hat{H} \langle E_x| &: -1\sqrt{3} \cdot Q_{T_{1x}} \cdot Q_{T_{1y}} \\
|T_{1z}\rangle \hat{H} \langle E_y| &: -Q_{T_{1x}} \cdot Q_{T_{1y}}
\end{aligned} \tag{2.13}$$

$$\begin{aligned}
|T_{1x}\rangle \hat{H} \langle E_x| &: Q_{E_x} \cdot Q_{T_{1x}} \\
|T_{1x}\rangle \hat{H} \langle E_y| &: Q_{E_y} \cdot Q_{T_{1x}} \\
|T_{1y}\rangle \hat{H} \langle E_x| &: Q_{E_x} \cdot Q_{T_{1y}} \\
|T_{1y}\rangle \hat{H} \langle E_y| &: Q_{E_y} \cdot Q_{T_{1y}} \\
|T_{1z}\rangle \hat{H} \langle E_x| &: Q_{E_x} \cdot Q_{T_{1z}} \\
|T_{1z}\rangle \hat{H} \langle E_y| &: Q_{E_y} \cdot Q_{T_{1z}}
\end{aligned} \tag{2.14}$$

$$\begin{aligned}
|T_{1x}\rangle \hat{H} \langle E_x| &: -\sqrt{3} \cdot Q_{E_y} \cdot Q_{T_{1x}} + Q_{E_x} \cdot Q_{T_{1x}} \\
|T_{1x}\rangle \hat{H} \langle E_y| &: -\sqrt{3} \cdot Q_{E_x} \cdot Q_{T_{1x}} - Q_{E_y} \cdot Q_{T_{1x}} \\
|T_{1y}\rangle \hat{H} \langle E_x| &: -Q_{E_x} \cdot Q_{T_{1y}} \\
|T_{1y}\rangle \hat{H} \langle E_y| &: Q_{E_y} \cdot Q_{T_{1y}} \\
|T_{1z}\rangle \hat{H} \langle E_x| &: +\sqrt{3} \cdot Q_{E_y} \cdot Q_{T_{1z}} + Q_{E_x} \cdot Q_{T_{1z}} \\
|T_{1z}\rangle \hat{H} \langle E_y| &: +\sqrt{3} \cdot Q_{E_x} \cdot Q_{T_{1z}} - Q_{E_y} \cdot Q_{T_{1z}}
\end{aligned} \tag{2.15}$$

$$|T_{1x}\rangle \hat{H} \langle E_x| : -Q_{A_1} \cdot Q_{T_{1x}}$$

$$\begin{aligned}
|T_{1x}\rangle \hat{H} \langle E_y| &: -1\sqrt{3} \cdot Q_{A_1} \cdot Q_{T_{1x}} \\
|T_{1y}\rangle \hat{H} \langle E_x| &: Q_{A_1} \cdot Q_{T_{1y}} \\
|T_{1z}\rangle \hat{H} \langle E_x| &: -Q_{A_1} \cdot Q_{T_{1z}} \\
|T_{1z}\rangle \hat{H} \langle E_y| &: \sqrt{3} \cdot Q_{A_1} \cdot Q_{T_{1z}}
\end{aligned} \tag{2.16}$$

$$\begin{aligned}
|T_{1x}\rangle \hat{H} \langle T_{1x}| &: 1/3 \cdot Q_{T_{1x}}^2 + 1/3 \cdot Q_{T_{1y}}^2 + 1/3 \cdot Q_{T_{1z}}^2 \\
|T_{1x}\rangle \hat{H} \langle T_{1y}| &: -1/3 \cdot Q_{T_{1x}} \cdot Q_{T_{1y}} \\
|T_{1x}\rangle \hat{H} \langle T_{1z}| &: -1/3 \cdot Q_{T_{1x}} \cdot Q_{T_{1z}} \\
|T_{1y}\rangle \hat{H} \langle T_{1y}| &: 1/3 \cdot Q_{T_{1x}}^2 + 1/3 \cdot Q_{T_{1y}}^2 + 1/3 \cdot Q_{T_{1z}}^2 \\
|T_{1y}\rangle \hat{H} \langle T_{1z}| &: -1/3 \cdot Q_{T_{1y}} \cdot Q_{T_{1z}} \\
|T_{1z}\rangle \hat{H} \langle T_{1z}| &: 1/3 \cdot Q_{T_{1x}}^2 + 1/3 \cdot Q_{T_{1y}}^2 + 1/3 \cdot Q_{T_{1z}}^2
\end{aligned} \tag{2.17}$$

$$\begin{aligned}
|T_{1x}\rangle \hat{H} \langle T_{1x}| &: -\sqrt{3} \cdot Q_{E_x} \cdot Q_{E_y} + Q_{E_x}^2 - Q_{E_y}^2 \\
|T_{1y}\rangle \hat{H} \langle T_{1y}| &: -Q_{E_x}^2 + Q_{E_y}^2 \\
|T_{1z}\rangle \hat{H} \langle T_{1z}| &: +\sqrt{3} \cdot Q_{E_x} \cdot Q_{E_y} + Q_{E_x}^2 - Q_{E_y}^2
\end{aligned} \tag{2.18}$$

$$\begin{aligned}
|T_{1x}\rangle \hat{H} \langle T_{1x}| &: Q_{A_1}^2 \\
|T_{1y}\rangle \hat{H} \langle T_{1y}| &: Q_{A_1}^2 \\
|T_{1z}\rangle \hat{H} \langle T_{1z}| &: Q_{A_1}^2
\end{aligned} \tag{2.19}$$



$$\begin{aligned}
|T_{1x}\rangle \hat{H} \langle T_{1x}| &: Q_{E_x}^2 + Q_{E_y}^2 \\
|T_{1y}\rangle \hat{H} \langle T_{1y}| &: Q_{E_x}^2 + Q_{E_y}^2 \\
|T_{1z}\rangle \hat{H} \langle T_{1z}| &: Q_{E_x}^2 + Q_{E_y}^2
\end{aligned} \tag{2.20}$$

$$\begin{aligned}
|T_{1x}\rangle \hat{H} \langle T_{1x}| &: -\sqrt{3} \cdot Q_{A_1} \cdot Q_{E_y} - Q_{A_1} \cdot Q_{E_x} \\
|T_{1y}\rangle \hat{H} \langle T_{1y}| &: +2 \cdot Q_{A_1} \cdot Q_{E_x} \\
|T_{1z}\rangle \hat{H} \langle T_{1z}| &: +\sqrt{3} \cdot Q_{A_1} \cdot Q_{E_y} - Q_{A_1} \cdot Q_{E_x}
\end{aligned} \tag{2.21}$$

$$\begin{aligned}
|T_{1x}\rangle \hat{H} \langle T_{1y}| &: -\sqrt{3} \cdot Q_{E_x} \cdot Q_{T_{1z}} - Q_{E_y} \cdot Q_{T_{1z}} \\
|T_{1x}\rangle \hat{H} \langle T_{1z}| &: Q_{E_y} \cdot Q_{T_{1y}} \\
|T_{1y}\rangle \hat{H} \langle T_{1z}| &: +\sqrt{3} \cdot Q_{E_x} \cdot Q_{T_{1x}} - Q_{E_y} \cdot Q_{T_{1x}}
\end{aligned} \tag{2.22}$$

### B.3 Third Order, O group

$$\left| A_1 \right\rangle \hat{H} \left\langle A_1 \right| : Q_{E_x}^3 - 3 \cdot Q_{E_x} \cdot Q_{E_y}^2 \quad (3.1)$$

$$\begin{aligned} \left| A_1 \right\rangle \hat{H} \left\langle A_1 \right| : & \sqrt{3} \cdot Q_{E_y} \cdot Q_{T_{1x}}^2 - \sqrt{3} \cdot Q_{E_y} \cdot Q_{T_{1z}}^2 + Q_{E_x} \\ & \cdot Q_{T_{1x}}^2 - Q_{E_x} \cdot Q_{T_{1y}}^2 + Q_{E_x} \cdot Q_{T_{1z}}^2 \end{aligned} \quad (3.2)$$

$$\left| A_1 \right\rangle \hat{H} \left\langle A_1 \right| : Q_{A_1}^3 \quad (3.3)$$

$$\left| A_1 \right\rangle \hat{H} \left\langle A_1 \right| : Q_{A_1} \cdot Q_{T_{1x}}^2 + Q_{A_1} \cdot Q_{T_{1y}}^2 + Q_{A_1} \cdot Q_{T_{1z}}^2 \quad (3.4)$$

$$\left| A_1 \right\rangle \hat{H} \left\langle A_1 \right| : Q_{A_1} \cdot Q_{E_x}^2 + Q_{A_1} \cdot Q_{E_y}^2 \quad (3.5)$$

$$\begin{aligned} \left| E_x \right\rangle \hat{H} \left\langle A_1 \right| : & -\sqrt{3} \cdot Q_{E_y} \cdot Q_{T_{1x}}^2 + \sqrt{3} \cdot Q_{E_y} \cdot Q_{T_{1z}}^2 + Q_{E_x} \\ & \cdot Q_{T_{1x}}^2 - Q_{E_x} \cdot Q_{T_{1y}}^2 + Q_{E_x} \cdot Q_{T_{1z}}^2 \\ \left| E_y \right\rangle \hat{H} \left\langle A_1 \right| : & -\sqrt{3} \cdot Q_{E_x} \cdot Q_{T_{1x}}^2 + \sqrt{3} \cdot Q_{E_x} \cdot Q_{T_{1z}}^2 \\ & - Q_{E_y} \cdot Q_{T_{1x}}^2 + Q_{E_y} \cdot Q_{T_{1y}}^2 - Q_{E_y} \cdot Q_{T_{1z}}^2 \end{aligned} \quad (3.6)$$

$$\begin{aligned} \left| E_x \right\rangle \hat{H} \left\langle A_1 \right| : & Q_{E_x} \cdot Q_{T_{1x}}^2 + Q_{E_x} \cdot Q_{T_{1y}}^2 + Q_{E_x} \cdot Q_{T_{1z}}^2 \\ \left| E_y \right\rangle \hat{H} \left\langle A_1 \right| : & Q_{E_y} \cdot Q_{T_{1x}}^2 + Q_{E_y} \cdot Q_{T_{1y}}^2 + Q_{E_y} \cdot Q_{T_{1z}}^2 \end{aligned} \quad (3.7)$$

$$\begin{aligned} \left| E_x \right\rangle \hat{H} \left\langle A_1 \right| : & Q_{A_1} \cdot Q_{T_{1x}}^2 - Q_{A_1} \cdot Q_{T_{1y}}^2 + Q_{A_1} \cdot Q_{T_{1z}}^2 \\ \left| E_y \right\rangle \hat{H} \left\langle A_1 \right| : & \sqrt{3} \cdot Q_{A_1} \cdot Q_{T_{1x}}^2 - \sqrt{3} \cdot Q_{A_1} \cdot Q_{T_{1z}}^2 \end{aligned} \quad (3.8)$$

$$\begin{aligned}
|E_x\rangle\hat{H}\langle A_1| &: Q_{E_x}^3 + Q_{E_x} \cdot Q_{E_y}^2 \\
|E_y\rangle\hat{H}\langle A_1| &: Q_{E_x}^2 \cdot Q_{E_y} + Q_{E_y}^3
\end{aligned} \tag{3.9}$$

$$\begin{aligned}
|E_x\rangle\hat{H}\langle A_1| &: Q_{A_1} \cdot Q_{E_x}^2 - Q_{A_1} \cdot Q_{E_y}^2 \\
|E_y\rangle\hat{H}\langle A_1| &: -2 \cdot Q_{A_1} \cdot Q_{E_x} \cdot Q_{E_y}
\end{aligned} \tag{3.10}$$

$$\begin{aligned}
|E_x\rangle\hat{H}\langle A_1| &: Q_{A_1}^2 \cdot Q_{E_x} \\
|E_y\rangle\hat{H}\langle A_1| &: Q_{A_1}^2 \cdot Q_{E_y}
\end{aligned} \tag{3.11}$$

$$\begin{aligned}
|E_x\rangle\hat{H}\langle E_x| &: Q_{E_x}^3 - 3 \cdot Q_{E_x} \cdot Q_{E_y}^2 \\
|E_y\rangle\hat{H}\langle E_y| &: Q_{E_x}^3 - 3 \cdot Q_{E_x} \cdot Q_{E_y}^2
\end{aligned} \tag{3.12}$$

$$\begin{aligned}
|E_x\rangle\hat{H}\langle E_x| &: \sqrt{3} \cdot Q_{E_y} \cdot Q_{T_{1x}}^2 - \sqrt{3} \cdot Q_{E_y} \cdot Q_{T_{1z}}^2 + Q_{E_x} \\
&\quad \cdot Q_{T_{1x}}^2 - Q_{E_x} \cdot Q_{T_{1y}}^2 + Q_{E_x} \cdot Q_{T_{1z}}^2 \\
|E_y\rangle\hat{H}\langle E_y| &: \sqrt{3} \cdot Q_{E_y} \cdot Q_{T_{1x}}^2 - \sqrt{3} \cdot Q_{E_y} \cdot Q_{T_{1z}}^2 + Q_{E_x} \\
&\quad \cdot Q_{T_{1x}}^2 - Q_{E_x} \cdot Q_{T_{1y}}^2 + Q_{E_x} \cdot Q_{T_{1z}}^2
\end{aligned} \tag{3.13}$$

$$\begin{aligned}
|E_x\rangle\hat{H}\langle E_x| &: Q_{E_x} \cdot Q_{T_{1x}}^2 + Q_{E_x} \cdot Q_{T_{1y}}^2 + Q_{E_x} \cdot Q_{T_{1z}}^2 \\
|E_x\rangle\hat{H}\langle E_y| &: -Q_{E_y} \cdot Q_{T_{1x}}^2 - Q_{E_y} \cdot Q_{T_{1y}}^2 - Q_{E_y} \cdot Q_{T_{1z}}^2 \\
|E_y\rangle\hat{H}\langle E_y| &: -Q_{E_x} \cdot Q_{T_{1x}}^2 - Q_{E_x} \cdot Q_{T_{1y}}^2 - Q_{E_x} \cdot Q_{T_{1z}}^2
\end{aligned} \tag{3.14}$$

$$\begin{aligned}
|E_x\rangle\hat{H}\langle E_x| &: Q_{A_1}^3 \\
|E_y\rangle\hat{H}\langle E_y| &: Q_{A_1}^3
\end{aligned}
\tag{3.15}$$

$$\begin{aligned}
|E_x\rangle\hat{H}\langle E_x| &: Q_{A_1} \cdot Q_{T_{1x}}^2 + Q_{A_1} \cdot Q_{T_{1y}}^2 + Q_{A_1} \cdot Q_{T_{1z}}^2 \\
|E_y\rangle\hat{H}\langle E_y| &: Q_{A_1} \cdot Q_{T_{1x}}^2 + Q_{A_1} \cdot Q_{T_{1y}}^2 + Q_{A_1} \cdot Q_{T_{1z}}^2
\end{aligned}
\tag{3.16}$$

$$\begin{aligned}
|E_x\rangle\hat{H}\langle E_x| &: Q_{A_1}^2 \cdot Q_{E_x} \\
|E_x\rangle\hat{H}\langle E_y| &: -Q_{A_1}^2 \cdot Q_{E_y} \\
|E_y\rangle\hat{H}\langle E_y| &: -Q_{A_1}^2 \cdot Q_{E_x}
\end{aligned}
\tag{3.17}$$

$$\begin{aligned}
|E_x\rangle\hat{H}\langle E_x| &: Q_{A_1} \cdot Q_{E_x}^2 - Q_{A_1} \cdot Q_{E_y}^2 \\
|E_x\rangle\hat{H}\langle E_y| &: 2 \cdot Q_{A_1} \cdot Q_{E_x} \cdot Q_{E_y} \\
|E_y\rangle\hat{H}\langle E_y| &: -Q_{A_1} \cdot Q_{E_x}^2 + Q_{A_1} \cdot Q_{E_y}^2
\end{aligned}
\tag{3.18}$$

$$\begin{aligned}
|T_{1x}\rangle\hat{H}\langle A_1| &: 1/3 \cdot Q_{T_{1x}}^3 + Q_{T_{1x}} \cdot Q_{T_{1y}}^2 + Q_{T_{1x}} \cdot Q_{T_{1z}}^2 \\
|T_{1y}\rangle\hat{H}\langle A_1| &: Q_{T_{1x}}^2 \cdot Q_{T_{1y}} + 1/3 \cdot Q_{T_{1y}}^3 + Q_{T_{1y}} \cdot Q_{T_{1z}}^2 \\
|T_{1z}\rangle\hat{H}\langle A_1| &: Q_{T_{1x}}^2 \cdot Q_{T_{1z}} + Q_{T_{1y}}^2 \cdot Q_{T_{1z}} + 1/3 \cdot Q_{T_{1z}}^3
\end{aligned}
\tag{3.19}$$

$$|T_{1x}\rangle\hat{H}\langle A_1| : 1/3 \cdot Q_{T_{1x}}^3$$

$$\begin{aligned}
|T_{1y}\rangle \hat{H} \langle A_1| &: 1/3 \cdot Q_{T_{1y}}^3 \\
|T_{1z}\rangle \hat{H} \langle A_1| &: 1/3 \cdot Q_{T_{1z}}^3
\end{aligned} \tag{3.20}$$

$$\begin{aligned}
|T_{1x}\rangle \hat{H} \langle A_1| &: +2\sqrt{3} \cdot Q_{E_x} \cdot Q_{E_y} \cdot Q_{T_{1x}} - Q_{E_x}^2 \cdot Q_{T_{1x}} + Q_{E_y}^2 \cdot Q_{T_{1x}} \\
|T_{1y}\rangle \hat{H} \langle A_1| &: +2 \cdot Q_{E_x}^2 \cdot Q_{T_{1y}} - 2 \cdot Q_{E_y}^2 \cdot Q_{T_{1y}} \\
|T_{1z}\rangle \hat{H} \langle A_1| &: -2\sqrt{3} \cdot Q_{E_x} \cdot Q_{E_y} \cdot Q_{T_{1z}} - Q_{E_x}^2 \cdot Q_{T_{1z}} + Q_{E_y}^2 \cdot Q_{T_{1z}}
\end{aligned} \tag{3.21}$$

$$\begin{aligned}
|T_{1x}\rangle \hat{H} \langle A_1| &: -\sqrt{3} \cdot Q_{E_x} \cdot Q_{T_{1y}} \cdot Q_{T_{1z}} + Q_{E_y} \cdot Q_{T_{1y}} \cdot Q_{T_{1z}} \\
|T_{1y}\rangle \hat{H} \langle A_1| &: -Q_{E_y} \cdot Q_{T_{1x}} \cdot Q_{T_{1z}} \\
|T_{1z}\rangle \hat{H} \langle A_1| &: +\sqrt{3} \cdot Q_{E_x} \cdot Q_{T_{1x}} \cdot Q_{T_{1y}} + Q_{E_y} \cdot Q_{T_{1x}} \cdot Q_{T_{1y}}
\end{aligned} \tag{3.22}$$

$$\begin{aligned}
|T_{1x}\rangle \hat{H} \langle A_1| &: Q_{A_1}^2 \cdot Q_{T_{1x}} \\
|T_{1y}\rangle \hat{H} \langle A_1| &: Q_{A_1}^2 \cdot Q_{T_{1y}} \\
|T_{1z}\rangle \hat{H} \langle A_1| &: Q_{A_1}^2 \cdot Q_{T_{1z}}
\end{aligned} \tag{3.23}$$

$$\begin{aligned}
|T_{1x}\rangle \hat{H} \langle A_1| &: -\sqrt{3} \cdot Q_{A_1} \cdot Q_{E_y} \cdot Q_{T_{1x}} - Q_{A_1} \cdot Q_{E_x} \cdot Q_{T_{1x}} \\
|T_{1y}\rangle \hat{H} \langle A_1| &: +2 \cdot Q_{A_1} \cdot Q_{E_x} \cdot Q_{T_{1y}} \\
|T_{1z}\rangle \hat{H} \langle A_1| &: +\sqrt{3} \cdot Q_{A_1} \cdot Q_{E_y} \cdot Q_{T_{1z}} - Q_{A_1} \cdot Q_{E_x} \cdot Q_{T_{1z}}
\end{aligned} \tag{3.24}$$

$$|T_{1x}\rangle \hat{H} \langle A_1| : Q_{E_x}^2 \cdot Q_{T_{1x}} + Q_{E_y}^2 \cdot Q_{T_{1x}}$$

$$\begin{aligned}
|T_{1y}\rangle \hat{H} \langle A_1| &: Q_{E_x}^2 \cdot Q_{T_{1y}} + Q_{E_y}^2 \cdot Q_{T_{1y}} \\
|T_{1z}\rangle \hat{H} \langle A_1| &: Q_{E_x}^2 \cdot Q_{T_{1z}} + Q_{E_y}^2 \cdot Q_{T_{1z}}
\end{aligned} \tag{3.25}$$

$$\begin{aligned}
|T_{1x}\rangle \hat{H} \langle E_x| &: -1/3 \cdot Q_{T_{1x}}^3 - Q_{T_{1x}} \cdot Q_{T_{1y}}^2 - Q_{T_{1x}} \cdot Q_{T_{1z}}^2 \\
|T_{1x}\rangle \hat{H} \langle E_y| &: -1/3\sqrt{3} \cdot Q_{T_{1x}}^3 - \sqrt{3} \cdot Q_{T_{1x}} \cdot Q_{T_{1y}}^2 - \sqrt{3} \cdot Q_{T_{1x}} \cdot Q_{T_{1z}}^2 \\
|T_{1y}\rangle \hat{H} \langle E_x| &: Q_{T_{1x}}^2 \cdot Q_{T_{1y}} + 1/3 \cdot Q_{T_{1y}}^3 + Q_{T_{1y}} \cdot Q_{T_{1z}}^2 \\
|T_{1z}\rangle \hat{H} \langle E_x| &: -Q_{T_{1x}}^2 \cdot Q_{T_{1z}} - Q_{T_{1y}}^2 \cdot Q_{T_{1z}} - 1/3 \cdot Q_{T_{1z}}^3 \\
|T_{1z}\rangle \hat{H} \langle E_y| &: \sqrt{3} \cdot Q_{T_{1x}}^2 \cdot Q_{T_{1z}} + \sqrt{3} \cdot Q_{T_{1y}}^2 \cdot Q_{T_{1z}} + 1/3\sqrt{3} \cdot Q_{T_{1z}}^3
\end{aligned} \tag{3.26}$$

$$\begin{aligned}
|T_{1x}\rangle \hat{H} \langle E_x| &: -1/3 \cdot Q_{T_{1x}}^3 + Q_{T_{1x}} \cdot Q_{T_{1y}}^2 \\
|T_{1x}\rangle \hat{H} \langle E_y| &: -1/3\sqrt{3} \cdot Q_{T_{1x}}^3 + 1/3\sqrt{3} \cdot Q_{T_{1x}} \cdot Q_{T_{1y}}^2 + 1/3\sqrt{3} \cdot Q_{T_{1x}} \cdot Q_{T_{1z}}^2 \\
|T_{1y}\rangle \hat{H} \langle E_x| &: -Q_{T_{1x}}^2 \cdot Q_{T_{1y}} + 1/3 \cdot Q_{T_{1y}}^3 - Q_{T_{1y}} \cdot Q_{T_{1z}}^2 \\
|T_{1y}\rangle \hat{H} \langle E_y| &: -1/3\sqrt{3} \cdot Q_{T_{1x}}^2 \cdot Q_{T_{1y}} + 1/3\sqrt{3} \cdot Q_{T_{1y}} \cdot Q_{T_{1z}}^2 \\
|T_{1z}\rangle \hat{H} \langle E_x| &: Q_{T_{1y}}^2 \cdot Q_{T_{1z}} - 1/3 \cdot Q_{T_{1z}}^3 \\
|T_{1z}\rangle \hat{H} \langle E_y| &: -1/3\sqrt{3} \cdot Q_{T_{1x}}^2 \cdot Q_{T_{1z}} - 1/3\sqrt{3} \cdot Q_{T_{1y}}^2 \cdot Q_{T_{1z}} + 1/3\sqrt{3} \cdot Q_{T_{1z}}^3
\end{aligned} \tag{3.27}$$

$$\begin{aligned}
|T_{1x}\rangle \hat{H} \langle E_x| &: -1/3 \cdot Q_{T_{1x}}^3 \\
|T_{1x}\rangle \hat{H} \langle E_y| &: -1/3\sqrt{3} \cdot Q_{T_{1x}}^3 \\
|T_{1y}\rangle \hat{H} \langle E_x| &: +1/3 \cdot Q_{T_{1y}}^3
\end{aligned}$$

$$\begin{aligned}
|T_{1z}\rangle\hat{H}\langle E_x| &: -1/3 \cdot Q_{T_{1z}}^3 \\
|T_{1z}\rangle\hat{H}\langle E_y| &: 1/3\sqrt{3} \cdot Q_{T_{1z}}^3
\end{aligned} \tag{3.28}$$

$$\begin{aligned}
|T_{1x}\rangle\hat{H}\langle E_x| &: +1/3 \cdot Q_{T_{1x}}^3 - Q_{T_{1x}} \cdot Q_{T_{1z}}^2 \\
|T_{1x}\rangle\hat{H}\langle E_y| &: 1/3\sqrt{3} \cdot Q_{T_{1x}}^3 - 1/3\sqrt{3} \cdot Q_{T_{1x}} \cdot Q_{T_{1y}}^2 - 1/3\sqrt{3} \cdot Q_{T_{1x}} \cdot Q_{T_{1z}}^2 \\
|T_{1y}\rangle\hat{H}\langle E_x| &: Q_{T_{1x}}^2 \cdot Q_{T_{1y}} - 1/3 \cdot Q_{T_{1y}}^3 + Q_{T_{1y}} \cdot Q_{T_{1z}}^2 \\
|T_{1y}\rangle\hat{H}\langle E_y| &: -1/3\sqrt{3} \cdot Q_{T_{1x}}^2 \cdot Q_{T_{1y}} + 1/3\sqrt{3} \cdot Q_{T_{1y}} \cdot Q_{T_{1z}}^2 \\
|T_{1z}\rangle\hat{H}\langle E_x| &: -Q_{T_{1x}}^2 \cdot Q_{T_{1z}} + 1/3 \cdot Q_{T_{1z}}^3 \\
|T_{1z}\rangle\hat{H}\langle E_y| &: 1/3\sqrt{3} \cdot Q_{T_{1x}}^2 \cdot Q_{T_{1z}} + 1/3\sqrt{3} \cdot Q_{T_{1y}}^2 \cdot Q_{T_{1z}} - 1/3\sqrt{3} \cdot Q_{T_{1z}}^3
\end{aligned} \tag{3.29}$$

$$\begin{aligned}
|T_{1x}\rangle\hat{H}\langle E_x| &: +2\sqrt{3} \cdot Q_{E_x} \cdot Q_{E_y} \cdot Q_{T_{1x}} + Q_{E_x}^2 \cdot Q_{T_{1x}} - Q_{E_y}^2 \cdot Q_{T_{1x}} \\
|T_{1x}\rangle\hat{H}\langle E_y| &: -\sqrt{3} \cdot Q_{E_x}^2 \cdot Q_{T_{1x}} + \sqrt{3} \cdot Q_{E_y}^2 \cdot Q_{T_{1x}} + 2 \cdot Q_{E_x} \cdot Q_{E_y} \cdot Q_{T_{1x}} \\
|T_{1y}\rangle\hat{H}\langle E_x| &: -2 \cdot Q_{E_x}^2 \cdot Q_{T_{1y}} + 2 \cdot Q_{E_y}^2 \cdot Q_{T_{1y}} \\
|T_{1y}\rangle\hat{H}\langle E_y| &: -4 \cdot Q_{E_x} \cdot Q_{E_y} \cdot Q_{T_{1y}} \\
|T_{1z}\rangle\hat{H}\langle E_x| &: -2\sqrt{3} \cdot Q_{E_x} \cdot Q_{E_y} \cdot Q_{T_{1z}} + Q_{E_x}^2 \cdot Q_{T_{1z}} - Q_{E_y}^2 \cdot Q_{T_{1z}} \\
|T_{1z}\rangle\hat{H}\langle E_y| &: +\sqrt{3} \cdot Q_{E_x}^2 \cdot Q_{T_{1z}} - \sqrt{3} \cdot Q_{E_y}^2 \cdot Q_{T_{1z}} + 2 \cdot Q_{E_x} \cdot Q_{E_y} \cdot Q_{T_{1z}}
\end{aligned} \tag{3.30}$$

$$\begin{aligned}
|T_{1x}\rangle\hat{H}\langle E_x| &: Q_{E_x}^2 \cdot Q_{T_{1x}} - Q_{E_y}^2 \cdot Q_{T_{1x}} \\
|T_{1x}\rangle\hat{H}\langle E_y| &: -2 \cdot Q_{E_x} \cdot Q_{E_y} \cdot Q_{T_{1x}}
\end{aligned}$$

$$\begin{aligned}
|T_{1y}\rangle \hat{H} \langle E_x| &: Q_{E_x}^2 \cdot Q_{T_{1y}} - Q_{E_y}^2 \cdot Q_{T_{1y}} \\
|T_{1y}\rangle \hat{H} \langle E_y| &: -2 \cdot Q_{E_x} \cdot Q_{E_y} \cdot Q_{T_{1y}} \\
|T_{1z}\rangle \hat{H} \langle E_x| &: Q_{E_x}^2 \cdot Q_{T_{1z}} - Q_{E_y}^2 \cdot Q_{T_{1z}} \\
|T_{1z}\rangle \hat{H} \langle E_y| &: -2 \cdot Q_{E_x} \cdot Q_{E_y} \cdot Q_{T_{1z}}
\end{aligned} \tag{3.32}$$

$$\begin{aligned}
|T_{1x}\rangle \hat{H} \langle E_x| &: -\sqrt{3} \cdot Q_{E_x} \cdot Q_{T_{1y}} \cdot Q_{T_{1z}} - Q_{E_y} \cdot Q_{T_{1y}} \cdot Q_{T_{1z}} \\
|T_{1x}\rangle \hat{H} \langle E_y| &: +\sqrt{3} \cdot Q_{E_y} \cdot Q_{T_{1y}} \cdot Q_{T_{1z}} - Q_{E_x} \cdot Q_{T_{1y}} \cdot Q_{T_{1z}} \\
|T_{1y}\rangle \hat{H} \langle E_x| &: +2 \cdot Q_{E_y} \cdot Q_{T_{1x}} \cdot Q_{T_{1z}} \\
|T_{1y}\rangle \hat{H} \langle E_y| &: +2 \cdot Q_{E_x} \cdot Q_{T_{1x}} \cdot Q_{T_{1z}} \\
|T_{1z}\rangle \hat{H} \langle E_x| &: +\sqrt{3} \cdot Q_{E_x} \cdot Q_{T_{1x}} \cdot Q_{T_{1y}} - Q_{E_y} \cdot Q_{T_{1x}} \cdot Q_{T_{1y}} \\
|T_{1z}\rangle \hat{H} \langle E_y| &: -\sqrt{3} \cdot Q_{E_y} \cdot Q_{T_{1x}} \cdot Q_{T_{1y}} - Q_{E_x} \cdot Q_{T_{1x}} \cdot Q_{T_{1y}}
\end{aligned} \tag{3.33}$$

$$\begin{aligned}
|T_{1x}\rangle \hat{H} \langle E_x| &: -Q_{A_1}^2 \cdot Q_{T_{1x}} \\
|T_{1x}\rangle \hat{H} \langle E_y| &: -1\sqrt{3} \cdot Q_{A_1}^2 \cdot Q_{T_{1x}} \\
|T_{1y}\rangle \hat{H} \langle E_x| &: Q_{A_1}^2 \cdot Q_{T_{1y}} \\
|T_{1z}\rangle \hat{H} \langle E_x| &: -Q_{A_1}^2 \cdot Q_{T_{1z}} \\
|T_{1z}\rangle \hat{H} \langle E_y| &: \sqrt{3} \cdot Q_{A_1}^2 \cdot Q_{T_{1z}}
\end{aligned} \tag{3.34}$$

$$|T_{1x}\rangle \hat{H} \langle E_x| : \sqrt{3} \cdot Q_{A_1} \cdot Q_{T_{1y}} \cdot Q_{T_{1z}}$$



$$\begin{aligned}
|T_{1x}\rangle\hat{H}\langle E_y| &: -Q_{A_1} \cdot Q_{T_{1y}} \cdot Q_{T_{1z}} \\
|T_{1y}\rangle\hat{H}\langle E_y| &: +2 \cdot Q_{A_1} \cdot Q_{T_{1x}} \cdot Q_{T_{1z}} \\
|T_{1z}\rangle\hat{H}\langle E_x| &: -1\sqrt{3} \cdot Q_{A_1} \cdot Q_{T_{1x}} \cdot Q_{T_{1y}} \\
|T_{1z}\rangle\hat{H}\langle E_y| &: -Q_{A_1} \cdot Q_{T_{1x}} \cdot Q_{T_{1y}}
\end{aligned} \tag{3.35}$$

$$\begin{aligned}
|T_{1x}\rangle\hat{H}\langle E_x| &: Q_{A_1} \cdot Q_{E_x} \cdot Q_{T_{1x}} \\
|T_{1x}\rangle\hat{H}\langle E_y| &: Q_{A_1} \cdot Q_{E_y} \cdot Q_{T_{1x}} \\
|T_{1y}\rangle\hat{H}\langle E_x| &: Q_{A_1} \cdot Q_{E_x} \cdot Q_{T_{1y}} \\
|T_{1y}\rangle\hat{H}\langle E_y| &: Q_{A_1} \cdot Q_{E_y} \cdot Q_{T_{1y}} \\
|T_{1z}\rangle\hat{H}\langle E_x| &: Q_{A_1} \cdot Q_{E_x} \cdot Q_{T_{1z}} \\
|T_{1z}\rangle\hat{H}\langle E_y| &: Q_{A_1} \cdot Q_{E_y} \cdot Q_{T_{1z}}
\end{aligned} \tag{3.36}$$

$$\begin{aligned}
|T_{1x}\rangle\hat{H}\langle E_x| &: +\sqrt{3} \cdot Q_{A_1} \cdot Q_{E_y} \cdot Q_{T_{1x}} - Q_{A_1} \cdot Q_{E_x} \cdot Q_{T_{1x}} \\
|T_{1x}\rangle\hat{H}\langle E_y| &: +\sqrt{3} \cdot Q_{A_1} \cdot Q_{E_x} \cdot Q_{T_{1x}} + Q_{A_1} \cdot Q_{E_y} \cdot Q_{T_{1x}} \\
|T_{1y}\rangle\hat{H}\langle E_x| &: Q_{A_1} \cdot Q_{E_x} \cdot Q_{T_{1y}} \\
|T_{1y}\rangle\hat{H}\langle E_y| &: -Q_{A_1} \cdot Q_{E_y} \cdot Q_{T_{1y}} \\
|T_{1z}\rangle\hat{H}\langle E_x| &: -\sqrt{3} \cdot Q_{A_1} \cdot Q_{E_y} \cdot Q_{T_{1z}} - Q_{A_1} \cdot Q_{E_x} \cdot Q_{T_{1z}} \\
|T_{1z}\rangle\hat{H}\langle E_y| &: -\sqrt{3} \cdot Q_{A_1} \cdot Q_{E_x} \cdot Q_{T_{1z}} + Q_{A_1} \cdot Q_{E_y} \cdot Q_{T_{1z}}
\end{aligned} \tag{3.37}$$

$$\begin{aligned}
|T_{1x}\rangle\hat{H}\langle T_{1x}| &: Q_{E_x}^3 - 3 \cdot Q_{E_x} \cdot Q_{E_y}^2 \\
|T_{1y}\rangle\hat{H}\langle T_{1y}| &: Q_{E_x}^3 - 3 \cdot Q_{E_x} \cdot Q_{E_y}^2 \\
|T_{1z}\rangle\hat{H}\langle T_{1z}| &: Q_{E_x}^3 - 3 \cdot Q_{E_x} \cdot Q_{E_y}^2
\end{aligned} \tag{3.38}$$

$$\begin{aligned}
|T_{1x}\rangle\hat{H}\langle T_{1x}| &: 1/3\sqrt{3} \cdot Q_{E_y} \cdot Q_{T_{1x}}^2 - 1/3\sqrt{3} \cdot Q_{E_y} \cdot Q_{T_{1z}}^2 \\
&\quad + 1/3 \cdot Q_{E_x} \cdot Q_{T_{1x}}^2 - 2/3 \cdot Q_{E_x} \cdot Q_{T_{1y}}^2 + 1/3 \cdot Q_{E_x} \cdot Q_{T_{1z}}^2 \\
|T_{1x}\rangle\hat{H}\langle T_{1y}| &: 1/3\sqrt{3} \cdot Q_{E_y} \cdot Q_{T_{1x}} \cdot Q_{T_{1y}} - 1/3 \cdot Q_{E_x} \cdot Q_{T_{1x}} \cdot Q_{T_{1y}} \\
|T_{1x}\rangle\hat{H}\langle T_{1z}| &: 2/3 \cdot Q_{E_x} \cdot Q_{T_{1x}} \cdot Q_{T_{1z}} \\
|T_{1y}\rangle\hat{H}\langle T_{1y}| &: 1/3\sqrt{3} \cdot Q_{E_y} \cdot Q_{T_{1x}}^2 - 1/3\sqrt{3} \cdot Q_{E_y} \cdot Q_{T_{1z}}^2 \\
&\quad + 1/3 \cdot Q_{E_x} \cdot Q_{T_{1x}}^2 - 2/3 \cdot Q_{E_x} \cdot Q_{T_{1y}}^2 + 1/3 \cdot Q_{E_x} \cdot Q_{T_{1z}}^2 \\
|T_{1y}\rangle\hat{H}\langle T_{1z}| &: -1/3\sqrt{3} \cdot Q_{E_y} \cdot Q_{T_{1y}} \cdot Q_{T_{1z}} - 1/3 \cdot Q_{E_x} \cdot Q_{T_{1y}} \cdot Q_{T_{1z}} \\
|T_{1z}\rangle\hat{H}\langle T_{1z}| &: 1/3\sqrt{3} \cdot Q_{E_y} \cdot Q_{T_{1x}}^2 - 1/3\sqrt{3} \cdot Q_{E_y} \cdot Q_{T_{1z}}^2 \\
&\quad + 1/3 \cdot Q_{E_x} \cdot Q_{T_{1x}}^2 - 2/3 \cdot Q_{E_x} \cdot Q_{T_{1y}}^2 + 1/3 \cdot Q_{E_x} \cdot Q_{T_{1z}}^2
\end{aligned} \tag{3.39}$$

$$\begin{aligned}
|T_{1x}\rangle\hat{H}\langle T_{1x}| &: -1/3\sqrt{3} \cdot Q_{E_y} \cdot Q_{T_{1x}}^2 - 1/3\sqrt{3} \cdot Q_{E_y} \cdot Q_{T_{1y}}^2 \\
&\quad - 1/3\sqrt{3} \cdot Q_{E_y} \cdot Q_{T_{1z}}^2 - 1/3 \cdot Q_{E_x} \cdot Q_{T_{1x}}^2 - 1/3 \cdot Q_{E_x} \cdot Q_{T_{1y}}^2 - 1/3 \cdot Q_{E_x} \cdot Q_{T_{1z}}^2 \\
|T_{1x}\rangle\hat{H}\langle T_{1y}| &: +1/3\sqrt{3} \cdot Q_{E_y} \cdot Q_{T_{1x}} \cdot Q_{T_{1y}} - 1/3 \cdot Q_{E_x} \cdot Q_{T_{1x}} \cdot Q_{T_{1y}} \\
|T_{1x}\rangle\hat{H}\langle T_{1z}| &: +1/3 \cdot Q_{E_x} \cdot Q_{T_{1x}} \cdot Q_{T_{1z}} \\
|T_{1y}\rangle\hat{H}\langle T_{1y}| &: +2/3 \cdot Q_{E_x} \cdot Q_{T_{1x}}^2 + 2/3 \cdot Q_{E_x} \cdot Q_{T_{1y}}^2 + 2/3 \cdot Q_{E_x} \cdot Q_{T_{1z}}^2 \\
|T_{1y}\rangle\hat{H}\langle T_{1z}| &: -1/3\sqrt{3} \cdot Q_{E_y} \cdot Q_{T_{1y}} \cdot Q_{T_{1z}} - 1/3 \cdot Q_{E_x} \cdot Q_{T_{1y}} \cdot Q_{T_{1z}}
\end{aligned}$$

$$\begin{aligned}
& \left| T_{1z} \right\rangle \hat{H} \left\langle T_{1z} \right| \\
& : +1/3\sqrt{3} \cdot Q_{E_y} \cdot Q_{T_{1x}}^2 + 1/3\sqrt{3} \cdot Q_{E_y} \cdot Q_{T_{1y}}^2 \\
& \quad + 1/3\sqrt{3} \cdot Q_{E_y} \cdot Q_{T_{1z}}^2 - 1/3 \cdot Q_{E_x} \cdot Q_{T_{1x}}^2 - 1/3 \cdot Q_{E_x} \cdot Q_{T_{1y}}^2 - 1/3 \cdot Q_{E_x} \cdot Q_{T_{1z}}^2 \\
& \hspace{15em} (3.40)
\end{aligned}$$

$$\begin{aligned}
& \left| T_{1x} \right\rangle \hat{H} \left\langle T_{1x} \right| : +1/3\sqrt{3} \cdot Q_{E_y} \cdot Q_{T_{1x}}^2 - 1/3\sqrt{3} \cdot Q_{E_y} \cdot Q_{T_{1y}}^2 \\
& \quad + 1/3 \cdot Q_{E_x} \cdot Q_{T_{1x}}^2 + 1/3 \cdot Q_{E_x} \cdot Q_{T_{1y}}^2 - 1/3 \cdot Q_{E_x} \cdot Q_{T_{1z}}^2 \\
& \left| T_{1x} \right\rangle \hat{H} \left\langle T_{1y} \right| : -1/3\sqrt{3} \cdot Q_{E_y} \cdot Q_{T_{1x}} \cdot Q_{T_{1y}} + 1/3 \cdot Q_{E_x} \cdot Q_{T_{1x}} \cdot Q_{T_{1y}} \\
& \left| T_{1x} \right\rangle \hat{H} \left\langle T_{1z} \right| : -1/3 \cdot Q_{E_x} \cdot Q_{T_{1x}} \cdot Q_{T_{1z}} \\
& \left| T_{1y} \right\rangle \hat{H} \left\langle T_{1y} \right| : -1/3\sqrt{3} \cdot Q_{E_y} \cdot Q_{T_{1x}}^2 + 1/3\sqrt{3} \cdot Q_{E_y} \cdot Q_{T_{1z}}^2 \\
& \quad + 1/3 \cdot Q_{E_x} \cdot Q_{T_{1x}}^2 - 1/3 \cdot Q_{E_x} \cdot Q_{T_{1y}}^2 + 1/3 \cdot Q_{E_x} \cdot Q_{T_{1z}}^2 \\
& \left| T_{1y} \right\rangle \hat{H} \left\langle T_{1z} \right| : +1/3\sqrt{3} \cdot Q_{E_y} \cdot Q_{T_{1y}} \cdot Q_{T_{1z}} + 1/3 \cdot Q_{E_x} \cdot Q_{T_{1y}} \cdot Q_{T_{1z}} \\
& \left| T_{1z} \right\rangle \hat{H} \left\langle T_{1z} \right| : +1/3\sqrt{3} \cdot Q_{E_y} \cdot Q_{T_{1y}}^2 - 1/3\sqrt{3} \cdot Q_{E_y} \cdot Q_{T_{1z}}^2 \\
& \quad - 1/3 \cdot Q_{E_x} \cdot Q_{T_{1x}}^2 + 1/3 \cdot Q_{E_x} \cdot Q_{T_{1y}}^2 + 1/3 \cdot Q_{E_x} \cdot Q_{T_{1z}}^2 \\
& \hspace{15em} (3.41)
\end{aligned}$$

$$\begin{aligned}
& \left| T_{1x} \right\rangle \hat{H} \left\langle T_{1x} \right| : Q_{A_1}^3 \\
& \left| T_{1y} \right\rangle \hat{H} \left\langle T_{1y} \right| : Q_{A_1}^3 \\
& \left| T_{1z} \right\rangle \hat{H} \left\langle T_{1z} \right| : Q_{A_1}^3 \\
& \hspace{15em} (3.42)
\end{aligned}$$

$$\begin{aligned}
& \left| T_{1x} \right\rangle \hat{H} \left\langle T_{1x} \right| : 2/3 \cdot Q_{A_1} \cdot Q_{T_{1x}}^2 - 1/3 \cdot Q_{A_1} \cdot Q_{T_{1y}}^2 - 1/3 \cdot Q_{A_1} \cdot Q_{T_{1z}}^2 \\
& \left| T_{1x} \right\rangle \hat{H} \left\langle T_{1y} \right| : 4/3 \cdot Q_{A_1} \cdot Q_{T_{1x}} \cdot Q_{T_{1y}} \\
& \left| T_{1x} \right\rangle \hat{H} \left\langle T_{1z} \right| : 4/3 \cdot Q_{A_1} \cdot Q_{T_{1x}} \cdot Q_{T_{1z}}
\end{aligned}$$

$$\begin{aligned}
|T_{1y}\rangle \hat{H} \langle T_{1y}| &: -1/3 \cdot Q_{A_1} \cdot Q_{T_{1x}}^2 + 2/3 \cdot Q_{A_1} \cdot Q_{T_{1y}}^2 - 1/3 \cdot Q_{A_1} \cdot Q_{T_{1z}}^2 \\
|T_{1y}\rangle \hat{H} \langle T_{1z}| &: 4/3 \cdot Q_{A_1} \cdot Q_{T_{1y}} \cdot Q_{T_{1z}} \\
|T_{1z}\rangle \hat{H} \langle T_{1z}| &: -1/3 \cdot Q_{A_1} \cdot Q_{T_{1x}}^2 - 1/3 \cdot Q_{A_1} \cdot Q_{T_{1y}}^2 + 2/3 \cdot Q_{A_1} \cdot Q_{T_{1z}}^2
\end{aligned} \tag{3.43}$$

$$\begin{aligned}
|T_{1x}\rangle \hat{H} \langle T_{1x}| &: +\sqrt{3} \cdot Q_{E_x}^2 \cdot Q_{E_y} + \sqrt{3} \cdot Q_{E_y}^3 + \cdot Q_{E_x}^3 + \cdot Q_{E_x} \cdot Q_{E_y}^2 \\
|T_{1y}\rangle \hat{H} \langle T_{1y}| &: -2 \cdot Q_{E_x}^3 - 2 \cdot Q_{E_x} \cdot Q_{E_y}^2 \\
|T_{1z}\rangle \hat{H} \langle T_{1z}| &: -\sqrt{3} \cdot Q_{E_x}^2 \cdot Q_{E_y} - \sqrt{3} \cdot Q_{E_y}^3 + \cdot Q_{E_x}^3 + \cdot Q_{E_x} \cdot Q_{E_y}^2
\end{aligned} \tag{3.44}$$

$$\begin{aligned}
|T_{1x}\rangle \hat{H} \langle T_{1x}| &: -\sqrt{3} \cdot Q_{A_1}^2 \cdot Q_{E_y} - Q_{A_1}^2 \cdot Q_{E_x} \\
|T_{1y}\rangle \hat{H} \langle T_{1y}| &: +2 \cdot Q_{A_1}^2 \cdot Q_{E_x} \\
|T_{1z}\rangle \hat{H} \langle T_{1z}| &: +\sqrt{3} \cdot Q_{A_1}^2 \cdot Q_{E_y} - Q_{A_1}^2 \cdot Q_{E_x}
\end{aligned} \tag{3.45}$$

$$\begin{aligned}
|T_{1x}\rangle \hat{H} \langle T_{1x}| &: -\sqrt{3} \cdot Q_{A_1} \cdot Q_{E_x} \cdot Q_{E_y} + Q_{A_1} \cdot Q_{E_x}^2 - Q_{A_1} \cdot Q_{E_y}^2 \\
|T_{1y}\rangle \hat{H} \langle T_{1y}| &: -Q_{A_1} \cdot Q_{E_x}^2 + Q_{A_1} \cdot Q_{E_y}^2 \\
|T_{1z}\rangle \hat{H} \langle T_{1z}| &: +\sqrt{3} \cdot Q_{A_1} \cdot Q_{E_x} \cdot Q_{E_y} + Q_{A_1} \cdot Q_{E_x}^2 - Q_{A_1} \cdot Q_{E_y}^2
\end{aligned} \tag{3.46}$$

$$\begin{aligned}
|T_{1x}\rangle \hat{H} \langle T_{1x}| &: Q_{A_1} \cdot Q_{E_x}^2 + Q_{A_1} \cdot Q_{E_y}^2 \\
|T_{1y}\rangle \hat{H} \langle T_{1y}| &: Q_{A_1} \cdot Q_{E_x}^2 + Q_{A_1} \cdot Q_{E_y}^2 \\
|T_{1z}\rangle \hat{H} \langle T_{1z}| &: Q_{A_1} \cdot Q_{E_x}^2 + Q_{A_1} \cdot Q_{E_y}^2
\end{aligned} \tag{3.47}$$

$$\begin{aligned}
\left| T_{1x} \right\rangle \hat{H} \left\langle T_{1y} \right| &: \sqrt{3} \cdot Q_{E_x}^2 \cdot Q_{T_{1z}} - \sqrt{3} \cdot Q_{E_y}^2 \cdot Q_{T_{1z}} - Q_{E_x} \cdot Q_{E_y} \cdot Q_{T_{1z}} \\
\left| T_{1x} \right\rangle \hat{H} \left\langle T_{1z} \right| &: 2 \cdot Q_{E_x} \cdot Q_{E_y} \cdot Q_{T_{1y}} \\
\left| T_{1y} \right\rangle \hat{H} \left\langle T_{1z} \right| &: -1\sqrt{3} \cdot Q_{E_x}^2 \cdot Q_{T_{1x}} + \sqrt{3} \cdot Q_{E_y}^2 \cdot Q_{T_{1x}} - Q_{E_x} \cdot Q_{E_y} \cdot Q_{T_{1x}}
\end{aligned} \tag{3.49}$$

$$\begin{aligned}
\left| T_{1x} \right\rangle \hat{H} \left\langle T_{1y} \right| &: \sqrt{3} \cdot Q_{A_1} \cdot Q_{E_x} \cdot Q_{T_{1z}} + Q_{A_1} \cdot Q_{E_y} \cdot Q_{T_{1z}} \\
\left| T_{1x} \right\rangle \hat{H} \left\langle T_{1z} \right| &: -Q_{A_1} \cdot Q_{E_y} \cdot Q_{T_{1y}} \\
\left| T_{1y} \right\rangle \hat{H} \left\langle T_{1z} \right| &: -1\sqrt{3} \cdot Q_{A_1} \cdot Q_{E_x} \cdot Q_{T_{1x}} + Q_{A_1} \cdot Q_{E_y} \cdot Q_{T_{1x}}
\end{aligned} \tag{3.50}$$

# Supplementary Information A, B and C

Presented below are the MCTDH operator files for the three main models constructed in this work. The parameter and labels sections have been formatted into two columns per page.

- A- the photo-electron spectrum of cyclo-butadiene
- B- the vibrationally mediated dissociation of acetylene
- C- the Singlet state internal conversion of tolane

#####  
 ## SUPPLEMENTARY INFORMATION A

#####

#####

## PARAMETERS AND LABELS

#####

OP\_DEFINE-SECTION

TITLE

Cyclo-cutadiene neutral and radial cation; photo-electron spectrum

END-TITLE

END-OP\_DEFINE-SECTION

PARAMETER-SECTION

#zeroth order

omega\_1 = 0.17619 , ev  
 omega\_2 = 0.04851 , ev  
 omega\_3 = 0.04851 , ev  
 omega\_7 = 0.12355 , ev  
 omega\_8 = 0.12355 , ev  
 omega\_9 = 0.12627 , ev  
 omega\_10 = 0.14408 , ev  
 omega\_11 = 0.16361 , ev  
 omega\_12 = 0.16452 , ev  
 omega\_18 = 0.42911 , ev

#Neutral

E1 = 0.00001 , ev  
 E2 = 1.51211 , ev  
 E3 = 1.85430 , ev  
 1D\_12 = 25.753174265 , ev  
 1A\_12 = -0.052373178  
 1X\_12 = -0.221097957  
 1E\_12 = -0.003413453 , ev  
 2D\_12 = 25.725101186 , ev  
 2A\_12 = -0.055112240  
 2X\_12 = -0.145069150  
 2E\_12 = -0.001631299 , ev  
 3D\_12 = 25.246940997 , ev  
 3A\_12 = -0.056860370  
 3X\_12 = 0.031319676  
 3E\_12 = -0.000080211 , ev  
 1D\_18 = 23.745371710 , ev  
 1A\_18 = -0.088037946  
 1X\_18 = -0.263056956  
 1E\_18 = -0.012444571 , ev  
 2D\_18 = 22.922364627 , ev  
 2A\_18 = -0.092264372  
 2X\_18 = -0.222185547  
 2E\_18 = -0.009437812 , ev  
 3D\_18 = 24.604118563 , ev  
 3A\_18 = -0.090110844  
 3X\_18 = -0.265342082  
 3E\_18 = -0.013734435 , ev  
 cbd1\_m1o2\_s1\_1 = -0.07273400 , ev  
 cbd2\_m1o4\_s1\_1 = 0.00647390 , ev  
 cbd3\_m1o2\_s2\_2 = 0.01964500 , ev  
 cbd4\_m1o4\_s2\_2 = 0.00365380 , ev  
 cbd5\_m1o2\_s3\_3 = -0.02204400 , ev  
 cbd6\_m1o4\_s3\_3 = 0.00189310 , ev  
 cbd7\_m2o2\_s1\_1 = 0.05163500 , ev  
 cbd8\_m2o4\_s1\_1 = 0.16362000 , ev

cbd9\_m2o2\_s2\_2 = -0.00585170 , ev  
 cbd10\_m2o4\_s2\_2 = 0.11740000 , ev  
 cbd11\_m2o2\_s3\_3 = 0.16944000 , ev  
 cbd12\_m2o4\_s3\_3 = 0.17302000 , ev  
 cbd13\_m3o2\_s1\_1 = 0.05163500 , ev  
 cbd14\_m3o4\_s1\_1 = 0.16362000 , ev  
 cbd15\_m3o2\_s2\_2 = -0.00585170 , ev  
 cbd16\_m3o4\_s2\_2 = 0.11740000 , ev  
 cbd17\_m3o2\_s3\_3 = 0.16944000 , ev  
 cbd18\_m3o4\_s3\_3 = 0.17302000 , ev  
 cbd19\_m7o2\_s1\_1 = -0.00032346 , ev  
 cbd20\_m7o4\_s1\_1 = 0.01611300 , ev  
 cbd21\_m7o2\_s2\_2 = 0.01883900 , ev  
 cbd22\_m7o4\_s2\_2 = -0.01533200 , ev  
 cbd23\_m7o2\_s3\_3 = -0.00381810 , ev  
 cbd24\_m7o4\_s3\_3 = -0.00407250 , ev  
 cbd25\_m8o2\_s1\_1 = -0.00032346 , ev  
 cbd26\_m8o4\_s1\_1 = 0.01611300 , ev  
 cbd27\_m8o2\_s2\_2 = 0.01883900 , ev  
 cbd28\_m8o4\_s2\_2 = -0.01533200 , ev  
 cbd29\_m8o2\_s3\_3 = -0.00381810 , ev  
 cbd30\_m8o4\_s3\_3 = -0.00407250 , ev  
 cbd31\_m9o2\_s1\_1 = -0.01960900 , ev  
 cbd32\_m9o4\_s1\_1 = -0.00085961 , ev  
 cbd33\_m9o2\_s2\_2 = -0.05300300 , ev  
 cbd34\_m9o4\_s2\_2 = -0.00101910 , ev  
 cbd35\_m9o2\_s3\_3 = 0.00555090 , ev  
 cbd36\_m9o4\_s3\_3 = 0.00372730 , ev  
 cbd37\_m1o1\_s1\_2 = 0.5017 , ev  
 cbd38\_m9o1\_s2\_3 = -0.1725 , ev  
 cbd39\_m11o1\_s1\_3 = -0.0073 , ev  
 cbd40\_m10o2\_s1\_1 = -0.0207 , ev  
 cbd41\_m10o2\_s2\_2 = -0.0119 , ev  
 cbd42\_m10o2\_s3\_3 = 0.0054 , ev  
 cbd43\_m11o2\_s1\_1 = -0.0126 , ev  
 cbd44\_m11o2\_s2\_2 = -0.0146 , ev  
 cbd45\_m11o2\_s3\_3 = -0.0150 , ev  
 cbd46\_m1o1\_m10o1\_s1\_1 = 0.0054 , ev  
 cbd47\_m1o1\_m10o1\_s2\_2 = -0.0588 , ev  
 cbd48\_m1o1\_m10o1\_s3\_3 = -0.0263 , ev  
 cbd49\_m1o2\_m12o2\_s1\_1 = 0.00068214 , ev  
 cbd50\_m1o2\_m12o2\_s2\_2 = 0.00147100 , ev  
 cbd51\_m1o2\_m12o2\_s3\_3 = 0.00000361 , ev  
 cbd52\_m1o2\_m12o1\_s1\_1 = 0.00103920 , ev  
 cbd53\_m1o2\_m12o1\_s2\_2 = 0.02485400 , ev  
 cbd54\_m1o2\_m12o1\_s3\_3 = 0.00581450 , ev  
 cbd55\_m1o2\_m18o1\_s1\_1 = 0.00005430 , ev  
 cbd56\_m1o2\_m18o1\_s2\_2 = 0.00002454 , ev  
 cbd57\_m1o2\_m18o1\_s3\_3 = 0.00002042 , ev  
 cbd58\_m1o1\_m7o2\_s2\_2 = 0.00726970 , ev  
 cbd59\_m1o1\_m8o2\_s2\_2 = 0.00726970 , ev  
 cbd60\_m1o1\_m7o2\_s3\_3 = 0.00693910 , ev  
 cbd61\_m1o1\_m8o2\_s3\_3 = 0.00693910 , ev

#cation

EE1 = 7.40002 , ev  
 EE2 = 7.40002 , ev  
 4D\_12 = 24.780444217 , ev  
 4A\_12 = -0.057832937  
 4X\_12 = 0.137859746  
 4E\_12 = -0.001587813 , ev  
 5D\_12 = 24.780444217 , ev

5A\_12 = -0.057832937  
 5X\_12 = 0.137859746  
 5E\_12 = -0.001587813, ev  
 4D\_18 = 25.034504022, ev  
 4A\_18 = -0.085530056  
 4X\_18 = -0.343716459  
 4E\_18 = -0.021010724, ev  
 5D\_18 = 25.034504022, ev  
 5A\_18 = -0.085530056  
 5X\_18 = -0.343716459  
 5E\_18 = -0.021010724, ev  
 cbdp1\_m1o1\_s1\_1 = -0.30625000, ev  
 cbdp2\_m1o2\_s1\_1 = -0.00343840, ev  
 cbdp3\_m1o4\_s1\_1 = 0.00020535, ev  
 cbdp4\_m1o1\_s2\_2 = 0.30625000, ev  
 cbdp5\_m1o2\_s2\_2 = -0.00343840, ev  
 cbdp6\_m1o4\_s2\_2 = 0.00020535, ev  
 cbdp7\_m2o2\_s1\_1 = 0.18963000, ev  
 cbdp8\_m2o4\_s1\_1 = 0.05431000, ev  
 cbdp9\_m2o2\_s2\_2 = 0.29811000, ev  
 cbdp10\_m2o4\_s2\_2 = 0.06053900, ev  
 cbdp11\_m3o2\_s1\_1 = 0.18963000, ev  
 cbdp12\_m3o4\_s1\_1 = 0.05431000, ev  
 cbdp13\_m3o2\_s2\_2 = 0.29811000, ev  
 cbdp14\_m3o4\_s2\_2 = 0.06053900, ev  
 cbdp15\_m7o2\_s1\_1 = 0.00344390, ev  
 cbdp16\_m7o4\_s1\_1 = 0.00387720, ev  
 cbdp17\_m7o2\_s2\_2 = -0.00162260, ev  
 cbdp18\_m7o4\_s2\_2 = 0.00191640, ev  
 cbdp19\_m8o2\_s1\_1 = 0.00344390, ev  
 cbdp20\_m8o4\_s1\_1 = 0.00387720, ev  
 cbdp21\_m8o2\_s2\_2 = -0.00162260, ev  
 cbdp22\_m8o4\_s2\_2 = 0.00191640, ev  
 cbdp23\_m9o2\_s1\_1 = -0.00887180, ev  
 cbdp24\_m9o4\_s1\_1 = -0.00326700, ev  
 cbdp25\_m9o2\_s2\_2 = -0.00887180, ev  
 cbdp26\_m9o4\_s2\_2 = -0.00326700, ev  
 cbdp27\_m10o1\_s1\_1 = 0.02998300, ev  
 cbdp28\_m10o2\_s1\_1 = -0.01361900, ev  
 cbdp29\_m10o4\_s1\_1 = 0.00796420, ev  
 cbdp30\_m10o1\_s2\_2 = -0.02998300, ev  
 cbdp31\_m10o2\_s2\_2 = -0.01361900, ev  
 cbdp32\_m10o4\_s2\_2 = 0.00796420, ev  
 cbdp33\_m11o2\_s1\_1 = -0.03438600, ev  
 cbdp34\_m11o4\_s1\_1 = 0.00999480, ev  
 cbdp35\_m11o2\_s2\_2 = -0.03843000, ev  
 cbdp36\_m11o4\_s2\_2 = 0.01149600, ev  
 cbdp37\_m9o1\_s1\_2 = 0.1111, ev  
 cbdp38\_m1o1\_m10o1\_s1\_1 = -0.0380, ev  
 cbdp39\_m1o1\_m10o1\_s2\_2 = -0.0372, ev  
 cbdp40\_m1o1\_m12o1\_s1\_1 = 0.0043, ev  
 cbdp41\_m1o1\_m12o1\_s2\_2 = 0.0349, ev  
 cbdp42\_m1o1\_m18o1\_s1\_1 = 0.0014, ev  
 cbdp43\_m1o1\_m18o1\_s2\_2 = 0.0176, ev  
 cbdp44\_m1o1\_m9o1\_s1\_2 = 0.0051, ev  
 cbdp45\_m9o1\_m10o1\_s1\_2 = 0.0082, ev  
 cbdp46\_m9o1\_m18o1\_s1\_2 = -0.0046, ev  
 cbdp47\_m1o1\_m2o2\_s1\_1 = 0.00722190, ev  
 cbdp48\_m1o1\_m2o2\_s2\_2 = 0.00722190, ev  
 cbdp49\_m1o1\_m3o2\_s1\_1 = 0.00722190, ev  
 cbdp50\_m1o1\_m3o2\_s2\_2 = 0.00722190, ev

end-parameter-section

LABELS-SECTION

v4m12=morse1[4D\_12,4A\_12,4X\_12,4E\_12]  
 v5m12=morse1[5D\_12,5A\_12,5X\_12,5E\_12]  
 v4m18=morse1[4D\_18,4A\_18,4X\_18,4E\_18]  
 v5m18=morse1[5D\_18,5A\_18,5X\_18,5E\_18]  
 v1m12=morse1[1D\_12,1A\_12,1X\_12,1E\_12]  
 v2m12=morse1[2D\_12,2A\_12,2X\_12,2E\_12]  
 v3m12=morse1[3D\_12,3A\_12,3X\_12,3E\_12]  
 v1m18=morse1[1D\_18,1A\_18,1X\_18,1E\_18]  
 v2m18=morse1[2D\_18,2A\_18,2X\_18,2E\_18]  
 v3m18=morse1[3D\_18,3A\_18,3X\_18,3E\_18]

end-labels-section



#####  
 ## SUPPLEMENTARY INFORMATION A

#####  
 #####

## HAMILTONIAN SECTION

#####

HAMILTONIAN-SECTION

-----  
 modes| v1 | v2 | v3 | v4 | v5 | v6 | v7 | v8 | v9 | v10 |  
 modes| v11 | v12 | v13 | v14 | v15 | v16 | v17 | v18 | el  
 -----

#kinetic energy

1.000000\*omega\_1 |1 KE  
 1.000000\*omega\_2 |2 KE  
 1.000000\*omega\_3 |3 KE  
 1.000000\*omega\_7 |7 KE  
 1.000000\*omega\_8 |8 KE  
 1.000000\*omega\_9 |9 KE  
 1.000000\*omega\_10 |10 KE  
 1.000000\*omega\_11 |11 KE  
 1.000000\*omega\_12 |12 KE  
 1.000000\*omega\_18 |18 KE

#zeroth order model

0.500000\*omega\_1 |1 q^2  
 0.500000\*omega\_2 |2 q^2  
 0.500000\*omega\_3 |3 q^2  
 0.500000\*omega\_7 |7 q^2  
 0.500000\*omega\_8 |8 q^2  
 0.500000\*omega\_9 |9 q^2  
 0.500000\*omega\_10 |10 q^2  
 0.500000\*omega\_11 |11 q^2

#neutral

1.000000*E1		19 S1&1
1.000000*E2		19 S2&2
1.000000*E3		19 S3&3
1.000000	12 v1m12	19 S1&1
1.000000	12 v2m12	19 S2&2
1.000000	12 v3m12	19 S3&3
1.000000	18 v1m18	19 S1&1
1.000000	18 v2m18	19 S2&2
1.000000	18 v3m18	19 S3&3
0.500000*cbd1_m1o2_s1_1	1 q^2	19 S1&1
0.041160*cbd2_m1o4_s1_1	1 q^4	19 S1&1
0.500000*cbd3_m1o2_s2_2	1 q^2	19 S2&2
0.041160*cbd4_m1o4_s2_2	1 q^4	19 S2&2
0.500000*cbd5_m1o2_s3_3	1 q^2	19 S3&3
0.041160*cbd6_m1o4_s3_3	1 q^4	19 S3&3
0.500000*cbd7_m2o2_s1_1	2 q^2	19 S1&1
0.041160*cbd8_m2o4_s1_1	2 q^4	19 S1&1
0.500000*cbd9_m2o2_s2_2	2 q^2	19 S2&2
0.041160*cbd10_m2o4_s2_2	2 q^4	19 S2&2
0.500000*cbd11_m2o2_s3_3	2 q^2	19 S3&3
0.041160*cbd12_m2o4_s3_3	2 q^4	19 S3&3
0.500000*cbd13_m3o2_s1_1	3 q^2	19 S1&1
0.041160*cbd14_m3o4_s1_1	3 q^4	19 S1&1
0.500000*cbd15_m3o2_s2_2	3 q^2	19 S2&2
0.041160*cbd16_m3o4_s2_2	3 q^4	19 S2&2
0.500000*cbd17_m3o2_s3_3	3 q^2	19 S3&3
0.041160*cbd18_m3o4_s3_3	3 q^4	19 S3&3
0.500000*cbd19_m7o2_s1_1	7 q^2	19 S1&1
0.041160*cbd20_m7o4_s1_1	7 q^4	19 S1&1

0.500000*cbd21_m7o2_s2_2	7 q^2	19 S2&2
0.041160*cbd22_m7o4_s2_2	7 q^4	19 S2&2
0.500000*cbd23_m7o2_s3_3	7 q^2	19 S3&3
0.041160*cbd24_m7o4_s3_3	7 q^4	19 S3&3
0.500000*cbd25_m8o2_s1_1	8 q^2	19 S1&1
0.041160*cbd26_m8o4_s1_1	8 q^4	19 S1&1
0.500000*cbd27_m8o2_s2_2	8 q^2	19 S2&2
0.041160*cbd28_m8o4_s2_2	8 q^4	19 S2&2
0.500000*cbd29_m8o2_s3_3	8 q^2	19 S3&3
0.041160*cbd30_m8o4_s3_3	8 q^4	19 S3&3
0.500000*cbd31_m9o2_s1_1	9 q^2	19 S1&1
0.041160*cbd32_m9o4_s1_1	9 q^4	19 S1&1
0.500000*cbd33_m9o2_s2_2	9 q^2	19 S2&2
0.041160*cbd34_m9o4_s2_2	9 q^4	19 S2&2
0.500000*cbd35_m9o2_s3_3	9 q^2	19 S3&3
0.041160*cbd36_m9o4_s3_3	9 q^4	19 S3&3
1.000000*cbd37_m1o1_s1_2	1 q^1	19 S1&2
1.000000*cbd38_m9o1_s2_3	9 q^1	19 S2&3
1.000000*cbd39_m11o1_s1_3	11 q^1	19 S1&3
0.500000*cbd40_m10o2_s1_1	10 q^2	19 S1&1
0.500000*cbd41_m10o2_s2_2	10 q^2	19 S2&2
0.500000*cbd42_m10o2_s3_3	10 q^2	19 S3&3
0.500000*cbd43_m11o2_s1_1	11 q^2	19 S1&1
0.500000*cbd44_m11o2_s2_2	11 q^2	19 S2&2
0.500000*cbd45_m11o2_s3_3	11 q^2	19 S3&3
1.000000*cbd46_m1o1_m10o1_s1_1	1 q^1  10 q^1	19 S1&1
1.000000*cbd47_m1o1_m10o1_s2_2	1 q^1  10 q^1	19 S2&2
1.000000*cbd48_m1o1_m10o1_s3_3	1 q^1  10 q^1	19 S3&3
1.000000*cbd49_m1o2_m12o2_s1_1	1 q^2  12 q^2	19 S1&1
1.000000*cbd50_m1o2_m12o2_s2_2	1 q^2  12 q^2	19 S2&2
1.000000*cbd51_m1o2_m12o2_s3_3	1 q^2  12 q^2	19 S3&3
1.000000*cbd52_m1o2_m12o1_s1_1	1 q^2  12 q^1	19 S1&1
1.000000*cbd53_m1o2_m12o1_s2_2	1 q^2  12 q^1	19 S2&2
1.000000*cbd54_m1o2_m12o1_s3_3	1 q^2  12 q^1	19 S3&3
1.000000*cbd55_m1o2_m18o1_s1_1	1 q^2  18 q^1	19 S1&1
1.000000*cbd56_m1o2_m18o1_s2_2	1 q^2  18 q^1	19 S2&2
1.000000*cbd57_m1o2_m18o1_s3_3	1 q^2  18 q^1	19 S3&3
1.000000*cbd58_m1o1_m7o2_s2_2	1 q^1  7 q^2	19 S2&2
1.000000*cbd59_m1o1_m8o2_s2_2	1 q^1  8 q^2	19 S2&2
1.000000*cbd60_m1o1_m7o2_s3_3	1 q^1  7 q^2	19 S3&3
1.000000*cbd61_m1o1_m8o2_s3_3	1 q^1  8 q^2	19 S3&3

#cation

1.000000*EE1	19 S4&4
1.000000*EE2	19 S5&5
1.000000	12 v4m12  19 S4&4
1.000000	12 v5m12  19 S5&5
1.000000	18 v4m18  19 S4&4
1.000000	18 v5m18  19 S5&5
1.000000*cbdp1_m1o1_s1_1	1 q^1  19 S4&4
0.500000*cbdp2_m1o2_s1_1	1 q^2  19 S4&4
0.041160*cbdp3_m1o4_s1_1	1 q^4  19 S4&4
1.000000*cbdp4_m1o1_s2_2	1 q^1  19 S5&5
0.500000*cbdp5_m1o2_s2_2	1 q^2  19 S5&5
0.041160*cbdp6_m1o4_s2_2	1 q^4  19 S5&5
0.500000*cbdp7_m2o2_s1_1	2 q^2  19 S4&4
0.041160*cbdp8_m2o4_s1_1	2 q^4  19 S4&4
0.500000*cbdp9_m2o2_s2_2	2 q^2  19 S5&5
0.041160*cbdp10_m2o4_s2_2	2 q^4  19 S5&5
0.500000*cbdp11_m3o2_s1_1	3 q^2  19 S4&4
0.041160*cbdp12_m3o4_s1_1	3 q^4  19 S4&4

0.500000*cbdp13_m3o2_s2_2	3 q^2	19 S5&5
0.041160*cbdp14_m3o4_s2_2	3 q^4	19 S5&5
0.500000*cbdp15_m7o2_s1_1	7 q^2	19 S4&4
0.041160*cbdp16_m7o4_s1_1	7 q^4	19 S4&4
0.500000*cbdp17_m7o2_s2_2	7 q^2	19 S5&5
0.041160*cbdp18_m7o4_s2_2	7 q^4	19 S5&5
0.500000*cbdp19_m8o2_s1_1	8 q^2	19 S4&4
0.041160*cbdp20_m8o4_s1_1	8 q^4	19 S4&4
0.500000*cbdp21_m8o2_s2_2	8 q^2	19 S5&5
0.041160*cbdp22_m8o4_s2_2	8 q^4	19 S5&5
0.500000*cbdp23_m9o2_s1_1	9 q^2	19 S4&4
0.041160*cbdp24_m9o4_s1_1	9 q^4	19 S4&4
0.500000*cbdp25_m9o2_s2_2	9 q^2	19 S5&5
0.041160*cbdp26_m9o4_s2_2	9 q^4	19 S5&5
1.000000*cbdp27_m10o1_s1_1	10 q^1	19 S4&4
0.500000*cbdp28_m10o2_s1_1	10 q^2	19 S4&4
0.041160*cbdp29_m10o4_s1_1	10 q^4	19 S4&4
1.000000*cbdp30_m10o1_s2_2	10 q^1	19 S5&5
0.500000*cbdp31_m10o2_s2_2	10 q^2	19 S5&5
0.041160*cbdp32_m10o4_s2_2	10 q^4	19 S5&5
0.500000*cbdp33_m11o2_s1_1	11 q^2	19 S4&4
0.041160*cbdp34_m11o4_s1_1	11 q^4	19 S4&4
0.500000*cbdp35_m11o2_s2_2	11 q^2	19 S5&5
0.041160*cbdp36_m11o4_s2_2	11 q^4	19 S5&5
1.000000*cbdp37_m9o1_s1_2	9 q^1	19 S4&5
1.000000*cbdp38_m1o1_m10o1_s1_1	1 q^1  10 q^1	19 S4&4
1.000000*cbdp39_m1o1_m10o1_s2_2	1 q^1  10 q^1	19 S5&5
1.000000*cbdp40_m1o1_m12o1_s1_1	1 q^1  12 q^1	19 S4&4
1.000000*cbdp41_m1o1_m12o1_s2_2	1 q^1  12 q^1	19 S5&5
1.000000*cbdp42_m1o1_m18o1_s1_1	1 q^1  18 q^1	19 S4&4
1.000000*cbdp43_m1o1_m18o1_s2_2	1 q^1  18 q^1	19 S5&5
1.000000*cbdp44_m1o1_m9o1_s1_2	1 q^1  9 q^1	19 S4&5
1.000000*cbdp45_m9o1_m10o1_s1_2	9 q^1  10 q^1	19 S4&5
1.000000*cbdp46_m9o1_m18o1_s1_2	9 q^1  18 q^1	19 S4&5
1.000000*cbdp47_m1o1_m2o2_s1_1	1 q^1  2 q^2	19 S4&4
1.000000*cbdp48_m1o1_m2o2_s2_2	1 q^1  2 q^2	19 S5&5
1.000000*cbdp49_m1o1_m3o2_s1_1	1 q^1  3 q^2	19 S4&4
1.000000*cbdp50_m1o1_m3o2_s2_2	1 q^1  3 q^2	19 S5&5

END-HAMILTONIAN-SECTION

END-OPERATOR

#\*\*\*\*\*#

```
#####
## SUPPLEMENTARY INFORMATION B
#####
#####
## PARAMETERS AND LABELS
#####
OP_DEFINE-SECTION
TITLE
10-state 7-coordinate acetylene model
END-TITLE
END-OP_DEFINE-SECTION
PARAMETER-SECTION
```

```
#vertical energies
```

```
E1      = 0.00000 , ev
E2      = 6.91857 , ev
E3      = 7.26113 , ev
E4      = 7.26114 , ev
E5      = 8.26326 , ev
E6      = 8.26326 , ev
E7      = 8.57901 , ev
E8      = 8.57901 , ev
E9      = 9.37474 , ev
E10     = 9.37474 , ev
```

```
#Morse potential (radial coordinates (1, 4))
```

```
1D_1 = 6.466600000 , ev
1A_1 = 0.141069884
1X_1 = -0.077787000+16.668
1E_1 = -0.000770189 , ev
2D_1 = 8.705900000 , ev
2A_1 = 0.128314808
2X_1 = -0.478150000+16.668
2E_1 = -0.030830900 , ev
3D_1 = 8.972700000 , ev
3A_1 = 0.125538924
3X_1 = -0.424620000+16.668
3E_1 = -0.024178705 , ev
4D_1 = 8.972700000 , ev
4A_1 = 0.125538924
4X_1 = -0.424620000+16.668
4E_1 = -0.024178705 , ev
5D_1 = 7.846800000 , ev
5A_1 = 0.128590030
5X_1 = -0.068891000+16.668
5E_1 = -0.000610362 , ev
6D_1 = 7.846800000 , ev
6A_1 = 0.128590030
6X_1 = -0.068891000+16.668
6E_1 = -0.000610362 , ev
9D_1 = 7.539600000 , ev
9A_1 = 0.123402812
9X_1 = 0.190820000+16.668
9E_1 = -0.004280484 , ev
10D_1 = 7.539600000 , ev
10A_1 = 0.123402812
10X_1 = 0.190820000+16.668
10E_1 = -0.004280484 , ev
1D_4 = 6.466600000 , ev
1A_4 = 0.141069884
1X_4 = -0.077787000+16.668
1E_4 = -0.000770189 , ev
```

```
2D_4 = 8.705900000 , ev
2A_4 = 0.128314808
2X_4 = -0.478150000+16.668
2E_4 = -0.030830900 , ev
3D_4 = 8.972700000 , ev
3A_4 = 0.125538924
3X_4 = -0.424620000+16.668
3E_4 = -0.024178705 , ev
4D_4 = 8.972700000 , ev
4A_4 = 0.125538924
4X_4 = -0.424620000+16.668
4E_4 = -0.024178705 , ev
5D_4 = 7.846800000 , ev
5A_4 = 0.128590030
5X_4 = -0.068891000+16.668
5E_4 = -0.000610362 , ev
6D_4 = 7.846800000 , ev
6A_4 = 0.128590030
6X_4 = -0.068891000+16.668
6E_4 = -0.000610362 , ev
9D_4 = 7.539600000 , ev
9A_4 = 0.123402812
9X_4 = 0.190820000+16.668
9E_4 = -0.004280484 , ev
10D_4 = 7.539600000 , ev
10A_4 = 0.123402812
10X_4 = 0.190820000+16.668
10E_4 = -0.004280484 , ev
```

```
#morse potential (cc stretch)
```

```
1D_5 = 12.505000000 , ev
1A_5 = 0.052288683
1X_5 = -1.235300000
1E_5 = -0.048926363 , ev
2D_5 = 14.092000000 , ev
2A_5 = 0.039704236
2X_5 = 3.240500000
2E_5 = -0.265672377 , ev
3D_5 = 13.418000000 , ev
3A_5 = 0.040903859
3X_5 = 2.978600000
3E_5 = -0.225263422 , ev
4D_5 = 13.418000000 , ev
4A_5 = 0.040903859
4X_5 = 2.978600000
4E_5 = -0.225263422 , ev
5D_5 = 15.081000000 , ev
5A_5 = 0.043513700
5X_5 = 0.426480000
5E_5 = -0.005291167 , ev
6D_5 = 15.081000000 , ev
6A_5 = 0.043513700
6X_5 = 0.426480000
6E_5 = -0.005291167 , ev
7D_5 = 5.506200000 , ev
7A_5 = 0.059685408
7X_5 = 1.583100000
7E_5 = -0.054070913 , ev
8D_5 = 5.506200000 , ev
8A_5 = 0.059685408
8X_5 = 1.583100000
8E_5 = -0.054070913 , ev
```

```

9D_5 = 17.474000000 , ev
9A_5 = 0.040090461
9X_5 = 0.365540000
9E_5 = -0.003808171 , ev
10D_5 = 17.474000000 , ev
10A_5 = 0.040090461
10X_5 = 0.365540000
10E_5 = -0.003808171 , ev

```

```

#predissociation potential function (folded diabatic coupling between
n a state following a morse potential and a higher
#lying one following a decayling exponential.

```

```

7K1_1 = 2.9738, ev
7K2_1 = 0.15385000
7K3_1 = 0.36221000+16.668
7K4_1 = 0.07123, ev
7K5_1 = 2.56430000
7K6_1 = -0.58519000+16.668
7K7_1 = 3.6603, ev
7K8_1 = 7.0316, ev
7K9_1 = 0.11424000
7K1_4 = 2.9738, ev
7K2_4 = 0.15385000
7K3_4 = 0.36221000+16.668
7K4_4 = 0.07123, ev
7K5_4 = 2.56430000
7K6_4 = -0.58519000+16.668
7K7_4 = 3.6603, ev
7K8_4 = 7.0316, ev
7K9_4 = 0.11424000
8K1_1 = 2.9738, ev
8K2_1 = 0.15385000
8K3_1 = 0.36221000+16.668
8K4_1 = 0.07123, ev
8K5_1 = 2.56430000
8K6_1 = -0.58519000+16.668
8K7_1 = 3.6603, ev
8K8_1 = 7.0316, ev
8K9_1 = 0.11424000
8K1_4 = 2.9738, ev
8K2_4 = 0.15385000
8K3_4 = 0.36221000+16.668
8K4_4 = 0.07123, ev
8K5_4 = 2.56430000
8K6_4 = -0.58519000+16.668
8K7_4 = 3.6603, ev
8K8_4 = 7.0316, ev
8K9_4 = 0.11424000

```

```

#S0 model

```

```

p1_m1o1_m4o1_s0_0 = 0.0041, ev
p2_m2o4_s0_0 = 0.10114, ev
p3_m3o4_s0_0 = 0.10114, ev
p4_m6o4_s0_0 = 0.10114, ev
p5_m7o4_s0_0 = 0.10114, ev
p6_m2o2_s0_0 = 2.1261, ev
p8_m6o2_s0_0 = 2.1261, ev
p9_m7o2_s0_0 = 2.1261, ev
p10_m3o1_m2o3_s0_0 = 0.016238, ev
p11_m3o2_m2o2_s0_0 = 0.025286, ev
p12_m3o3_m2o1_s0_0 = 0.016238, ev
p13_m7o1_m6o3_s0_0 = 0.016238, ev

```

```

p14_m7o2_m6o2_s0_0 = 0.025286, ev
p15_m7o3_m6o1_s0_0 = 0.016238, ev
p17_m7o1_m6o1_s0_0 = 0.0668, ev
p16_m3o1_m2o1_s0_0 = 0.0668, ev

```

```

#parameters coupling radial coordinates (1,4) to Renner-Teller 4D s
ubspace

```

```

p1 = -1.9301000 , ev
p2 = -0.1189100
p3 = 0.55077000
p4 = 0.08799700 , ev
p5 = 2.94650000
p6 = 0.93562000
p7 = 0.33982000 , ev
p8 = -0.1113200
p9 = 3.93640000
p10 = -1.574800 , ev
p11 = 0.9224600
p12 = 0.3073200
p13 = 3.6992000 , ev
p14 = -0.254810
p15 = -0.364960
p16 = 3.8506000 , ev
p17 = 0.0525410
p18 = -1.004200
p19 = 1.6018000 , ev
p20 = 0.1001800
p21 = -1.554700
p22 = 2.4171000 , ev
p23 = -0.065758
p24 = -0.833810
p25 = 2.9423000
p26 = 0.1994400
p27 = 0.1765300
p28 = 3.8840000
p29 = 0.3721200
p30 = 8.9707000
p31 = 3.0463000
p32 = -5.326200
p33 = 1.5309000 , ev
p34 = -0.012014
p35 = -2.539400
p36 = 2.2920000
p37 = -3.235500 , ev
p38 = 0.1935600
p39 = -0.743790
p40 = -2.000000
p41 = 2.5913000 , ev
p42 = -0.050717
p43 = 1.2729000
p44 = 1.7451000
p45 = -2.535900 , ev
p46 = -0.305680
p47 = 0.3774700
p48 = -0.976620
p49 = -0.241630 , ev
p50 = 0.9150700
p51 = 2.9566000
p52 = 0.9001600
p53 = 3.1057000 , ev
p54 = 0.0168290
p55 = 0.4410400

```

p56 = -1.300200  
 p57 = -0.972500 ,ev  
 p58 = 0.0797090  
 p59 = -2.047100  
 p60 = -0.450400

#### #Renner-Teller 4D subspace model

p1\_m1o1\_m4o1\_s1\_1 = 0.0043, ev  
 p2\_m1o1\_m4o1\_s2\_2 = 0.0017, ev  
 p3\_m1o1\_m4o1\_s3\_3 = 0.0017, ev  
 p93\_m2o2\_s1\_1 = 0.73176, ev  
 p33\_m2o4\_s1\_1 = 24.665, ev  
 p94\_m2o2\_s2\_2 = 0.49227, ev  
 p34\_m2o4\_s2\_2 = 10.056, ev  
 p95\_m2o2\_s3\_3 = 0.49227, ev  
 p35\_m2o4\_s3\_3 = 3.4537, ev  
 p96\_m2o2\_s4\_4 = 2.3484, ev  
 p36\_m2o4\_s4\_4 = 4.6506, ev  
 p97\_m2o2\_s5\_5 = 0.42884, ev  
 p37\_m2o4\_s5\_5 = 5.5935, ev  
 p98\_m2o2\_s6\_6 = 0.74085, ev  
 p38\_m2o4\_s6\_6 = 4.7048, ev  
 p99\_m2o2\_s7\_7 = 1.2521, ev  
 p39\_m2o4\_s7\_7 = 3.1806, ev  
 p100\_m2o2\_s8\_8 = 0.29211, ev  
 p40\_m2o4\_s8\_8 = 1.2811, ev  
 p92\_m2o2\_s9\_9 = 0.29211, ev  
 p32\_m2o4\_s9\_9 = 2.2933, ev  
 p102\_m3o2\_s1\_1 = 0.73176, ev  
 p42\_m3o4\_s1\_1 = 24.665, ev  
 p103\_m3o2\_s2\_2 = 0.49227, ev  
 p43\_m3o4\_s2\_2 = 10.056, ev  
 p104\_m3o2\_s3\_3 = 0.49227, ev  
 p44\_m3o4\_s3\_3 = 3.4537, ev  
 p105\_m3o2\_s4\_4 = 2.3484, ev  
 p45\_m3o4\_s4\_4 = 4.6506, ev  
 p106\_m3o2\_s5\_5 = 0.42884, ev  
 p46\_m3o4\_s5\_5 = 5.5935, ev  
 p107\_m3o2\_s6\_6 = 0.74085, ev  
 p47\_m3o4\_s6\_6 = 4.7048, ev  
 p108\_m3o2\_s7\_7 = 1.2521, ev  
 p48\_m3o4\_s7\_7 = 3.1806, ev  
 p109\_m3o2\_s8\_8 = 0.29211, ev  
 p49\_m3o4\_s8\_8 = 1.2811, ev  
 p101\_m3o2\_s9\_9 = 0.29211, ev  
 p41\_m3o4\_s9\_9 = 2.2933, ev  
 p111\_m6o2\_s1\_1 = 0.73176, ev  
 p51\_m6o4\_s1\_1 = 24.665, ev  
 p112\_m6o2\_s2\_2 = 0.49227, ev  
 p52\_m6o4\_s2\_2 = 10.056, ev  
 p113\_m6o2\_s3\_3 = 0.49227, ev  
 p53\_m6o4\_s3\_3 = 3.4537, ev  
 p114\_m6o2\_s4\_4 = 0.42884, ev  
 p54\_m6o4\_s4\_4 = 5.5935, ev  
 p115\_m6o2\_s5\_5 = 2.3484, ev  
 p55\_m6o4\_s5\_5 = 4.6506, ev  
 p116\_m6o2\_s6\_6 = 1.2521, ev  
 p56\_m6o4\_s6\_6 = 3.1806, ev  
 p117\_m6o2\_s7\_7 = 0.74085, ev  
 p57\_m6o4\_s7\_7 = 4.7048, ev  
 p118\_m6o2\_s8\_8 = 0.29211, ev  
 p58\_m6o4\_s8\_8 = 1.2811, ev

p110\_m6o2\_s9\_9 = 0.29211, ev  
 p50\_m6o4\_s9\_9 = 2.2933, ev  
 p120\_m7o2\_s1\_1 = 0.73176, ev  
 p60\_m7o4\_s1\_1 = 24.665, ev  
 p121\_m7o2\_s2\_2 = 0.49227, ev  
 p61\_m7o4\_s2\_2 = 10.056, ev  
 p122\_m7o2\_s3\_3 = 0.49227, ev  
 p62\_m7o4\_s3\_3 = 3.4537, ev  
 p123\_m7o2\_s4\_4 = 0.42884, ev  
 p63\_m7o4\_s4\_4 = 5.5935, ev  
 p124\_m7o2\_s5\_5 = 2.3484, ev  
 p64\_m7o4\_s5\_5 = 4.6506, ev  
 p125\_m7o2\_s6\_6 = 1.2521, ev  
 p65\_m7o4\_s6\_6 = 3.1806, ev  
 p126\_m7o2\_s7\_7 = 0.74085, ev  
 p66\_m7o4\_s7\_7 = 4.7048, ev  
 p127\_m7o2\_s8\_8 = 0.29211, ev  
 p67\_m7o4\_s8\_8 = 1.2811, ev  
 p119\_m7o2\_s9\_9 = 0.29211, ev  
 p59\_m7o4\_s9\_9 = 2.2933, ev  
 p281\_m2o1\_s1\_5 = -1.1168, ev  
 p282\_m2o1\_s1\_6 = 1.2509, ev  
 p283\_m2o1\_s2\_5 = 0.8052, ev  
 p284\_m2o1\_s2\_6 = -0.8082, ev  
 p285\_m2o1\_s3\_4 = 0.8052, ev  
 p286\_m2o1\_s3\_7 = -0.8082, ev  
 p287\_m2o1\_s4\_8 = 0.3317, ev  
 p288\_m2o1\_s5\_9 = -0.3317, ev  
 p289\_m2o1\_s6\_9 = -0.3681, ev  
 p290\_m2o1\_s7\_8 = -0.3681, ev  
 p291\_m3o1\_s1\_5 = -1.1168, ev  
 p292\_m3o1\_s1\_6 = -1.2509, ev  
 p293\_m3o1\_s2\_5 = 0.8052, ev  
 p294\_m3o1\_s2\_6 = 0.8082, ev  
 p295\_m3o1\_s3\_4 = 0.8052, ev  
 p296\_m3o1\_s3\_7 = 0.8082, ev  
 p297\_m3o1\_s4\_8 = -0.3317, ev  
 p298\_m3o1\_s5\_9 = 0.3317, ev  
 p299\_m3o1\_s6\_9 = -0.3681, ev  
 p300\_m3o1\_s7\_8 = -0.3681, ev  
 p301\_m6o1\_s1\_4 = 1.1168, ev  
 p302\_m6o1\_s1\_7 = -1.2509, ev  
 p303\_m6o1\_s2\_4 = 0.8052, ev  
 p304\_m6o1\_s2\_7 = -0.8082, ev  
 p305\_m6o1\_s3\_5 = -0.8052, ev  
 p306\_m6o1\_s3\_6 = 0.8082, ev  
 p307\_m6o1\_s4\_9 = -0.3317, ev  
 p308\_m6o1\_s5\_8 = -0.3317, ev  
 p309\_m6o1\_s6\_8 = 0.3681, ev  
 p310\_m6o1\_s7\_9 = -0.3681, ev  
 p311\_m7o1\_s1\_4 = 1.1168, ev  
 p312\_m7o1\_s1\_7 = 1.2509, ev  
 p313\_m7o1\_s2\_4 = 0.8052, ev  
 p314\_m7o1\_s2\_7 = 0.8082, ev  
 p315\_m7o1\_s3\_5 = -0.8052, ev  
 p316\_m7o1\_s3\_6 = -0.8082, ev  
 p317\_m7o1\_s4\_9 = 0.3317, ev  
 p318\_m7o1\_s5\_8 = 0.3317, ev  
 p319\_m7o1\_s6\_8 = 0.3681, ev  
 p320\_m7o1\_s7\_9 = -0.3681, ev  
 p1\_m1o1\_m4o1\_s1\_1 = 0.0043, ev  
 p2\_m1o1\_m4o1\_s2\_2 = 0.0017, ev

p3\_m1o1\_m4o1\_s3\_3 = 0.0017, ev  
 p264\_m3o1\_m2o1\_s1\_1 = 1.3206, ev  
 p265\_m3o1\_m2o1\_s2\_2 = -0.0752, ev  
 p266\_m3o1\_m2o1\_s3\_3 = -0.0752, ev  
 p267\_m3o1\_m2o1\_s4\_4 = -1.0255, ev  
 p268\_m3o1\_m2o1\_s5\_5 = -1.7517, ev  
 p269\_m3o1\_m2o1\_s6\_6 = 1.5213, ev  
 p270\_m3o1\_m2o1\_s7\_7 = 0.4716, ev  
 p271\_m3o1\_m2o1\_s8\_8 = -0.0292, ev  
 p263\_m3o1\_m2o1\_s9\_9 = -0.0292, ev  
 p273\_m7o1\_m6o1\_s1\_1 = 1.3206, ev  
 p274\_m7o1\_m6o1\_s2\_2 = -0.0752, ev  
 p275\_m7o1\_m6o1\_s3\_3 = -0.0752, ev  
 p276\_m7o1\_m6o1\_s4\_4 = -1.7517, ev  
 p277\_m7o1\_m6o1\_s5\_5 = -1.0255, ev  
 p278\_m7o1\_m6o1\_s6\_6 = 0.4716, ev  
 p279\_m7o1\_m6o1\_s7\_7 = 1.5213, ev  
 p280\_m7o1\_m6o1\_s8\_8 = -0.0292, ev  
 p272\_m7o1\_m6o1\_s9\_9 = -0.0292, ev  
 p69\_m2o2\_s1\_2 = 0.5939, ev  
 p68\_m2o2\_s1\_9 = -0.2654, ev  
 p70\_m2o2\_s2\_9 = 1.1446, ev  
 p71\_m2o2\_s3\_8 = 1.1446, ev  
 p72\_m2o2\_s4\_7 = -0.2441, ev  
 p73\_m2o2\_s5\_6 = 0.7131, ev  
 p75\_m3o2\_s1\_2 = 0.5939, ev  
 p74\_m3o2\_s1\_9 = 0.2654, ev  
 p76\_m3o2\_s2\_9 = -1.1446, ev  
 p77\_m3o2\_s3\_8 = -1.1446, ev  
 p78\_m3o2\_s4\_7 = 0.2441, ev  
 p79\_m3o2\_s5\_6 = -0.7131, ev  
 p81\_m6o2\_s1\_2 = -0.5939, ev  
 p80\_m6o2\_s1\_9 = 0.2654, ev  
 p82\_m6o2\_s2\_9 = 1.1446, ev  
 p83\_m6o2\_s3\_8 = 1.1446, ev  
 p84\_m6o2\_s4\_7 = 0.7131, ev  
 p85\_m6o2\_s5\_6 = -0.2441, ev  
 p87\_m7o2\_s1\_2 = -0.5939, ev  
 p86\_m7o2\_s1\_9 = -0.2654, ev  
 p88\_m7o2\_s2\_9 = -1.1446, ev  
 p89\_m7o2\_s3\_8 = -1.1446, ev  
 p90\_m7o2\_s4\_7 = -0.7131, ev  
 p91\_m7o2\_s5\_6 = 0.2441, ev  
 p4\_m3o1\_m2o1\_s1\_2 = -0.4031, ev  
 p5\_m2o1\_m6o1\_s1\_3 = -1.1879, ev  
 p6\_m2o1\_m6o1\_s1\_8 = -0.2654, ev  
 p7\_m2o1\_m6o1\_s4\_5 = -0.1505, ev  
 p8\_m2o1\_m6o1\_s4\_6 = 0.0052, ev  
 p9\_m2o1\_m6o1\_s5\_7 = 0.0052, ev  
 p10\_m2o1\_m6o1\_s6\_7 = 0.4940, ev  
 p11\_m2o1\_m7o1\_s1\_3 = 0.8062, ev  
 p12\_m2o1\_m7o1\_s2\_8 = -1.3965, ev  
 p13\_m2o1\_m7o1\_s3\_9 = 1.3965, ev  
 p14\_m2o1\_m7o1\_s4\_5 = 1.0427, ev  
 p15\_m2o1\_m7o1\_s4\_6 = -0.3543, ev  
 p16\_m2o1\_m7o1\_s5\_7 = 0.3543, ev  
 p17\_m2o1\_m7o1\_s6\_7 = -1.0669, ev  
 p18\_m3o1\_m6o1\_s1\_3 = 0.8062, ev  
 p19\_m3o1\_m6o1\_s2\_8 = 1.3965, ev  
 p20\_m3o1\_m6o1\_s3\_9 = -1.3965, ev  
 p21\_m3o1\_m6o1\_s4\_5 = 1.0427, ev  
 p22\_m3o1\_m6o1\_s4\_6 = 0.3543, ev  
 p23\_m3o1\_m6o1\_s5\_7 = -0.3543, ev  
 p24\_m3o1\_m6o1\_s6\_7 = -1.0669, ev  
 p25\_m3o1\_m7o1\_s1\_3 = -1.1879, ev  
 p26\_m3o1\_m7o1\_s1\_8 = 0.2654, ev  
 p27\_m3o1\_m7o1\_s4\_5 = -0.1505, ev  
 p28\_m3o1\_m7o1\_s4\_6 = -0.0052, ev  
 p29\_m3o1\_m7o1\_s5\_7 = -0.0052, ev  
 p30\_m3o1\_m7o1\_s6\_7 = 0.4940, ev  
 p31\_m7o1\_m6o1\_s1\_2 = 0.4031, ev  
 p128\_m3o1\_m2o3\_s9\_9 = -0.00020958, ev  
 p177\_m3o2\_m2o2\_s9\_9 = 0.10586, ev  
 p186\_m3o3\_m2o1\_s9\_9 = -0.00020958, ev  
 p197\_m2o2\_m6o2\_s9\_9 = 0.68837, ev  
 p208\_m3o1\_m2o1\_m6o2\_s9\_9 = 0.46064, ev  
 p219\_m3o2\_m6o2\_s9\_9 = 0.68837, ev  
 p230\_m2o2\_m7o1\_m6o1\_s9\_9 = -0.46064, ev  
 p241\_m3o1\_m2o1\_m7o1\_m6o1\_s9\_9 = 2.7456, ev  
 p252\_m3o2\_m7o1\_m6o1\_s9\_9 = -0.46064, ev  
 p129\_m7o1\_m6o3\_s9\_9 = -0.00020958, ev  
 p140\_m2o2\_m7o2\_s9\_9 = 0.68837, ev  
 p151\_m3o1\_m2o1\_m7o2\_s9\_9 = -0.46064, ev  
 p162\_m3o2\_m7o2\_s9\_9 = 0.68837, ev  
 p173\_m7o2\_m6o2\_s9\_9 = -0.10586, ev  
 p176\_m7o3\_m6o1\_s9\_9 = -0.00020958, ev  
 p178\_m3o1\_m2o3\_s1\_1 = -0.54862, ev  
 p179\_m3o2\_m2o2\_s1\_1 = 0.61572, ev  
 p180\_m3o3\_m2o1\_s1\_1 = -0.54862, ev  
 p181\_m2o2\_m6o2\_s1\_1 = 2.5895, ev  
 p182\_m3o1\_m2o1\_m6o2\_s1\_1 = -3.2087, ev  
 p183\_m3o2\_m6o2\_s1\_1 = 1.3162, ev  
 p184\_m2o2\_m7o1\_m6o1\_s1\_1 = -3.2087, ev  
 p185\_m3o1\_m2o1\_m7o1\_m6o1\_s1\_1 = 5.1935, ev  
 p187\_m3o2\_m7o1\_m6o1\_s1\_1 = -3.2087, ev  
 p188\_m7o1\_m6o3\_s1\_1 = -0.54862, ev  
 p189\_m2o2\_m7o2\_s1\_1 = 1.3162, ev  
 p190\_m3o1\_m2o1\_m7o2\_s1\_1 = -3.2087, ev  
 p191\_m3o2\_m7o2\_s1\_1 = 2.5895, ev  
 p192\_m7o2\_m6o2\_s1\_1 = 0.61572, ev  
 p193\_m7o3\_m6o1\_s1\_1 = -0.54862, ev  
 p194\_m3o1\_m2o3\_s2\_2 = -0.49026, ev  
 p195\_m3o2\_m2o2\_s2\_2 = 0.20446, ev  
 p196\_m3o3\_m2o1\_s2\_2 = -0.49026, ev  
 p198\_m2o2\_m6o2\_s2\_2 = 0.048785, ev  
 p199\_m3o1\_m2o1\_m6o2\_s2\_2 = 0.05975, ev  
 p200\_m3o2\_m6o2\_s2\_2 = 0.048785, ev  
 p201\_m2o2\_m7o1\_m6o1\_s2\_2 = 0.05975, ev  
 p202\_m3o1\_m2o1\_m7o1\_m6o1\_s2\_2 = 0.19514, ev  
 p203\_m3o2\_m7o1\_m6o1\_s2\_2 = 0.05975, ev  
 p204\_m7o1\_m6o3\_s2\_2 = -0.49026, ev  
 p205\_m2o2\_m7o2\_s2\_2 = 0.048785, ev  
 p206\_m3o1\_m2o1\_m7o2\_s2\_2 = 0.05975, ev  
 p207\_m3o2\_m7o2\_s2\_2 = 0.048785, ev  
 p209\_m7o2\_m6o2\_s2\_2 = 0.20446, ev  
 p210\_m7o3\_m6o1\_s2\_2 = -0.49026, ev  
 p211\_m3o1\_m2o3\_s3\_3 = -0.37605, ev  
 p212\_m3o2\_m2o2\_s3\_3 = 0.52389, ev  
 p213\_m3o3\_m2o1\_s3\_3 = -0.37605, ev  
 p214\_m2o2\_m6o2\_s3\_3 = 0.16808, ev  
 p215\_m3o1\_m2o1\_m6o2\_s3\_3 = 0.2313, ev  
 p216\_m3o2\_m6o2\_s3\_3 = 0.16808, ev  
 p217\_m2o2\_m7o1\_m6o1\_s3\_3 = 0.2313, ev  
 p218\_m3o1\_m2o1\_m7o1\_m6o1\_s3\_3 = 0.55398, ev

p220\_m3o2\_m7o1\_m6o1\_s3\_3 = 0.2313, ev  
 p221\_m7o1\_m6o3\_s3\_3 = -0.37605, ev  
 p222\_m2o2\_m7o2\_s3\_3 = 0.16808, ev  
 p223\_m3o1\_m2o1\_m7o2\_s3\_3 = 0.2313, ev  
 p224\_m3o2\_m7o2\_s3\_3 = 0.16808, ev  
 p225\_m7o2\_m6o2\_s3\_3 = 0.52389, ev  
 p226\_m7o3\_m6o1\_s3\_3 = -0.37605, ev  
 p227\_m3o1\_m2o3\_s4\_4 = 0.20941, ev  
 p228\_m3o2\_m2o2\_s4\_4 = 1.101, ev  
 p229\_m3o3\_m2o1\_s4\_4 = 0.20941, ev  
 p231\_m2o2\_m6o2\_s4\_4 = 0.1863, ev  
 p232\_m3o1\_m2o1\_m6o2\_s4\_4 = 0.065764, ev  
 p233\_m3o2\_m6o2\_s4\_4 = 0.1863, ev  
 p234\_m2o2\_m7o1\_m6o1\_s4\_4 = 0.063336, ev  
 p235\_m3o1\_m2o1\_m7o1\_m6o1\_s4\_4 = 0.74035, ev  
 p236\_m3o2\_m7o1\_m6o1\_s4\_4 = 0.063336, ev  
 p237\_m7o1\_m6o3\_s4\_4 = -0.057583, ev  
 p238\_m2o2\_m7o2\_s4\_4 = 0.1863, ev  
 p239\_m3o1\_m2o1\_m7o2\_s4\_4 = 0.065764, ev  
 p240\_m3o2\_m7o2\_s4\_4 = 0.1863, ev  
 p242\_m7o2\_m6o2\_s4\_4 = 1.3849, ev  
 p243\_m7o3\_m6o1\_s4\_4 = -0.057583, ev  
 p244\_m3o1\_m2o3\_s5\_5 = -0.057583, ev  
 p245\_m3o2\_m2o2\_s5\_5 = 1.3849, ev  
 p246\_m3o3\_m2o1\_s5\_5 = -0.057583, ev  
 p247\_m2o2\_m6o2\_s5\_5 = 0.033343, ev  
 p248\_m3o1\_m2o1\_m6o2\_s5\_5 = 0.035815, ev  
 p249\_m3o2\_m6o2\_s5\_5 = 0.033343, ev  
 p250\_m2o2\_m7o1\_m6o1\_s5\_5 = 0.038243, ev  
 p251\_m3o1\_m2o1\_m7o1\_m6o1\_s5\_5 = 0.12851, ev  
 p253\_m3o2\_m7o1\_m6o1\_s5\_5 = 0.038243, ev  
 p254\_m7o1\_m6o3\_s5\_5 = 0.20941, ev  
 p255\_m2o2\_m7o2\_s5\_5 = 0.033343, ev  
 p256\_m3o1\_m2o1\_m7o2\_s5\_5 = 0.035815, ev  
 p257\_m3o2\_m7o2\_s5\_5 = 0.033343, ev  
 p258\_m7o2\_m6o2\_s5\_5 = 1.101, ev  
 p259\_m7o3\_m6o1\_s5\_5 = 0.20941, ev  
 p260\_m3o1\_m2o3\_s6\_6 = 0.22487, ev  
 p261\_m3o2\_m2o2\_s6\_6 = 0.89252, ev  
 p262\_m3o3\_m2o1\_s6\_6 = 0.22487, ev  
 p130\_m2o2\_m6o2\_s6\_6 = 0.60318, ev  
 p131\_m3o1\_m2o1\_m6o2\_s6\_6 = 1.2064, ev  
 p132\_m3o2\_m6o2\_s6\_6 = 0.60318, ev  
 p133\_m2o2\_m7o1\_m6o1\_s6\_6 = 0.36563, ev  
 p134\_m3o1\_m2o1\_m7o1\_m6o1\_s6\_6 = 0.73126, ev  
 p135\_m3o2\_m7o1\_m6o1\_s6\_6 = 0.36563, ev  
 p136\_m7o1\_m6o3\_s6\_6 = -0.26556, ev  
 p137\_m2o2\_m7o2\_s6\_6 = 0.60318, ev  
 p138\_m3o1\_m2o1\_m7o2\_s6\_6 = 1.2064, ev  
 p139\_m3o2\_m7o2\_s6\_6 = 0.60318, ev  
 p141\_m7o2\_m6o2\_s6\_6 = 0.37705, ev  
 p142\_m7o3\_m6o1\_s6\_6 = -0.26556, ev  
 p143\_m3o1\_m2o3\_s7\_7 = -0.26556, ev  
 p144\_m3o2\_m2o2\_s7\_7 = 0.37705, ev  
 p145\_m3o3\_m2o1\_s7\_7 = -0.26556, ev  
 p146\_m2o2\_m6o2\_s7\_7 = 0.89819, ev  
 p147\_m3o1\_m2o1\_m6o2\_s7\_7 = -0.95807, ev  
 p148\_m3o2\_m6o2\_s7\_7 = 0.89819, ev  
 p149\_m2o2\_m7o1\_m6o1\_s7\_7 = -0.11733, ev  
 p150\_m3o1\_m2o1\_m7o1\_m6o1\_s7\_7 = 1.9113, ev  
 p152\_m3o2\_m7o1\_m6o1\_s7\_7 = -0.11733, ev  
 p153\_m7o1\_m6o3\_s7\_7 = 0.22487, ev

p154\_m2o2\_m7o2\_s7\_7 = 0.89819, ev  
 p155\_m3o1\_m2o1\_m7o2\_s7\_7 = -0.95807, ev  
 p156\_m3o2\_m7o2\_s7\_7 = 0.89819, ev  
 p157\_m7o2\_m6o2\_s7\_7 = 0.89252, ev  
 p158\_m7o3\_m6o1\_s7\_7 = 0.22487, ev  
 p159\_m3o1\_m2o3\_s8\_8 = -0.015615, ev  
 p160\_m3o2\_m2o2\_s8\_8 = -0.068021, ev  
 p161\_m3o3\_m2o1\_s8\_8 = -0.015615, ev  
 p163\_m2o2\_m6o2\_s8\_8 = 0.1917, ev  
 p164\_m3o1\_m2o1\_m6o2\_s8\_8 = -0.29839, ev  
 p165\_m3o2\_m6o2\_s8\_8 = 0.1917, ev  
 p166\_m2o2\_m7o1\_m6o1\_s8\_8 = -0.29839, ev  
 p167\_m3o1\_m2o1\_m7o1\_m6o1\_s8\_8 = 0.74834, ev  
 p168\_m3o2\_m7o1\_m6o1\_s8\_8 = -0.29839, ev  
 p169\_m7o1\_m6o3\_s8\_8 = -0.015615, ev  
 p170\_m2o2\_m7o2\_s8\_8 = 0.1917, ev  
 p171\_m3o1\_m2o1\_m7o2\_s8\_8 = -0.29839, ev  
 p172\_m3o2\_m7o2\_s8\_8 = 0.1917, ev  
 p174\_m7o2\_m6o2\_s8\_8 = -0.068021, ev  
 p175\_m7o3\_m6o1\_s8\_8 = -0.015615, ev  
 p128\_m3o1\_m2o3\_s9\_9 = 0.09583700, ev  
 p321\_m1o2\_m2o2\_s1\_1 = 0.09583700, ev  
 p322\_m1o2\_m2o2\_s2\_2 = 0.00028878, ev  
 p177\_m3o2\_m2o2\_s9\_9 = 0.00028878, ev  
 p186\_m3o3\_m2o1\_s9\_9 = 0.09583700, ev  
 p323\_m3o2\_m4o2\_s1\_1 = 0.09583700, ev  
 p197\_m2o2\_m6o2\_s9\_9 = 0.00028878, ev  
 p324\_m3o2\_m4o2\_s2\_2 = 0.00028878, ev  
 p208\_m3o1\_m2o1\_m6o2\_s9\_9 = 0.09583700, ev  
 p325\_m1o2\_m6o2\_s1\_1 = 0.09583700, ev  
 p326\_m1o2\_m6o2\_s2\_2 = 0.00028878, ev  
 p219\_m3o2\_m6o2\_s9\_9 = 0.00028878, ev  
 p230\_m2o2\_m7o1\_m6o1\_s9\_9 = 0.09583700, ev  
 p327\_m4o2\_m7o2\_s1\_1 = 0.09583700, ev  
 p241\_m3o1\_m2o1\_m7o1\_m6o1\_s9\_9 = 0.00028878, ev  
 p328\_m4o2\_m7o2\_s2\_2 = 0.00028878, ev  
 p252\_m3o2\_m7o1\_m6o1\_s9\_9 = 0.00037217, ev  
 p329\_m1o2\_m2o2\_s3\_3 = 0.00037217, ev  
 p330\_m3o2\_m4o2\_s3\_3 = 0.00037217, ev  
 p129\_m7o1\_m6o3\_s9\_9 = 0.00037217, ev  
 p331\_m1o2\_m6o2\_s3\_3 = 0.00037217, ev  
 p140\_m2o2\_m7o2\_s9\_9 = 0.00037217, ev  
 p151\_m3o1\_m2o1\_m7o2\_s9\_9 = 0.00037217, ev  
 p332\_m4o2\_m7o2\_s3\_3 = 0.00037217, ev

#ad-hoc functions

7o8T1 = -5.7967, ev  
 7o8T2 = -0.2260  
 7o8T3 = -0.0250  
 7o8T2\_2 = -1.1500  
 gam14\_cd2 = -0.0168, ev  
 gam14\_cdl = 0.0477, ev

#coordinate shifts:

r0 = 16.668  
 pi2 = 1.57079  
 pi = 3.141593

#pulse parameters

dip\_s1 = 1.0  
 A = 2.7726



```

B    = A/pi
C    = B^0.5
s1   = 60.0, ev
width1 = 21.2, fs
zz = 16.0
omega1 = PEN, eV
std   = 6.8, fs
hwidth = 30,fs
t1    = 30,fs
tdip_s2_x = 0.1060
tdip_s2_y = -0.1060
tdip_s34_x = 0.2227
tdip_s34_y = 0.2227
tdip_s34_y = 0.2227
tdip_s56_x = 0.0569
tdip_s56_y = 0.0569
tdip_md5_s56_x = -0.04502
tdip_md5_s56_0 = 0.17

kk = 1.0, ev
end-parameter-section
LABELS-SECTION
pcap = CAP[55,0.0012900,3,1]
rstp = step[40]

# predissiation potential model (coupling folded)
v7m1 = acpot2[7K1_1,7K2_1,7K3_1,7K4_1,7K5_1,7K6_1,7K7_1,
7K8_1,7K9_1]
v8m1 = acpot2[8K1_1,8K2_1,8K3_1,8K4_1,8K5_1,8K6_1,8K7_1,
8K8_1,8K9_1]
v7m4 = acpot2[7K1_4,7K2_4,7K3_4,7K4_4,7K5_4,7K6_4,7K7_4,
7K8_4,7K9_4]
v8m4 = acpot2[8K1_4,8K2_4,8K3_4,8K4_4,8K5_4,8K6_4,8K7_4,
8K8_4,8K9_4]

#morse potential
v1m1 =morse1[1D_1,1A_1,1X_1,1E_1]
v1m4 =morse1[1D_4,1A_4,1X_4,1E_4]
v1m5 =morse1[1D_5,1A_5,1X_5,1E_5]
v2m1 =morse1[2D_1,2A_1,2X_1,2E_1]
v3m1 =morse1[3D_1,3A_1,3X_1,3E_1]
v4m1 =morse1[4D_1,4A_1,4X_1,4E_1]
v5m1 =morse1[5D_1,5A_1,5X_1,5E_1]
v6m1 =morse1[6D_1,6A_1,6X_1,6E_1]
v9m1 =morse1[9D_1,9A_1,9X_1,9E_1]
v10m1=morse1[10D_1,10A_1,10X_1,10E_1]
v2m4 =morse1[2D_4,2A_4,2X_4,2E_4]
v3m4 =morse1[3D_4,3A_4,3X_4,3E_4]
v4m4 =morse1[4D_4,4A_4,4X_4,4E_4]
v5m4 =morse1[5D_4,5A_4,5X_4,5E_4]
v6m4 =morse1[6D_4,6A_4,6X_4,6E_4]
v9m4 =morse1[9D_4,9A_4,9X_4,9E_4]
v10m4=morse1[10D_4,10A_4,10X_4,10E_4]
v2m5 =morse1[2D_5,2A_5,2X_5,2E_5]
v3m5 =morse1[3D_5,3A_5,3X_5,3E_5]
v4m5 =morse1[4D_5,4A_5,4X_5,4E_5]
v5m5 =morse1[5D_5,5A_5,5X_5,5E_5]
v6m5 =morse1[6D_5,6A_5,6X_5,6E_5]
v7m5 =morse1[7D_5,7A_5,7X_5,7E_5]
v8m5 =morse1[8D_5,8A_5,8X_5,8E_5]
v9m5 =morse1[9D_5,9A_5,9X_5,9E_5]
v10m5=morse1[10D_5,10A_5,10X_5,10E_5]

7o8Ttnh14 = tanh[7o8T2, r0]^1.0
7o8Ttnh55 = tanh[7o8T3,0.0]^1.0
7o8Ttnh14_2 = tanh[7o8T2_2,r0]^1.0

qp1 = q[pi]
qp2 = q[pi]^2
qp3 = q[pi]^3
qp4 = q[pi]^4

qq1 = q[pi2]
qq2 = q[pi2]^2
qq3 = q[pi2]^3
qq4 = q[pi2]^4

pstp = step[r0]
nstp = rstp[r0]

rqc2 = q[0.0]^(-2)
rq1 = q[r0]^1
rq2 = q[r0]^2

#cosm are defined in text as G(x)
#cosp = 2.0d0*(1.0d0-cos(aa*(x-x0))), aa= first entry, x0 = second entry

#cosm= 0.25d0*(cos(aa*(x-x0))+3.0d0)*stpf((x-x0),aa,.false.)*stpf
((x-x0),-aa,.true.) + &
# 0.5d0*(stpf((x-x0),aa,.true.) + stpf((x-x0),-aa,.false.))
# where stpf(.,true./false.) and forward/backward step functions. a
a= first entry, x0= second entry

cosm29_1 = cosm[p29,pi]
cosm29_2 = cosm[p29,pi2]
cosm30_1 = cosm[p30,pi]
cosm30_2 = cosm[p30,pi2]
cosm31_1 = cosm[p31,pi]
cosm31_2 = cosm[p31,pi2]
cosm32_1 = cosm[p32,pi]
cosm32_2 = cosm[p32,pi2]
cosm36_1 = cosm[p36,pi]
cosm36_2 = cosm[p36,pi2]
cosm40_1 = cosm[p40,pi]
cosm40_2 = cosm[p40,pi2]
cosm44_1 = cosm[p44,pi]
cosm44_2 = cosm[p44,pi2]
cosm25_1 = cosm[p25,pi]
cosm25_2 = cosm[p25,pi2]
cosm26_1 = cosm[p26,pi]
cosm26_2 = cosm[p26,pi2]
cosm27_2 = cosm[p27,pi2]
cosm27_1 = cosm[p27,pi]
cosm28_2 = cosm[p28,pi2]
cosm28_1 = cosm[p28,pi]
cosm48_1 = cosm[p48,pi]
cosm48_2 = cosm[p48,pi2]
cosm52_1 = cosm[p52,pi]
cosm52_2 = cosm[p52,pi2]
cosm56_1 = cosm[p56,pi]
cosm56_2 = cosm[p56,pi2]
cosm60_2 = cosm[p60,pi2]
cosm60_1 = cosm[p60,pi]

```

```

cosp3_1 = cosp[p3,pi]
cosp3_2 = cosp[p3,pi2]
cosp6_1 = cosp[p6,pi]
cosp6_2 = cosp[p6,pi2]
cosp9_1 = cosp[p9,pi]
cosp9_2 = cosp[p9,pi2]
cosp12_1 = cosp[p12,pi]
cosp12_2 = cosp[p12,pi2]
cosp35_1 = cosp[p35,pi]
cosp35_2 = cosp[p35,pi2]
cosp39_1 = cosp[p39,pi]
cosp39_2 = cosp[p39,pi2]
cosp43_1 = cosp[p43,pi]
cosp43_2 = cosp[p43,pi2]

```

```

sin15_2 = sin[p15,pi2]
sin15_1 = sin[p15,pi]
sin18_2 = sin[p18,pi2]
sin18_1 = sin[p18,pi]
sin21_2 = sin[p21,pi2]
sin21_1 = sin[p21,pi]
sin24_2 = sin[p24,pi2]
sin24_1 = sin[p24,pi]
sin47_2 = sin[p47,pi2]
sin47_1 = sin[p47,pi]
sin51_2 = sin[p51,pi2]
sin51_1 = sin[p51,pi]
sin55_2 = sin[p55,pi2]
sin55_1 = sin[p55,pi]
sin59_2 = sin[p59,pi2]
sin59_1 = sin[p59,pi]

```

```

tanh2 = tanh[p2 ,r0]
tanh5 = tanh[p5 ,r0]
tanh8 = tanh[p8 ,r0]
tanh11 = tanh[p11,r0]
tanh34 = tanh[p34,r0]
tanh14 = tanh[p14,r0]
tanh17 = tanh[p17,r0]
tanh20 = tanh[p20,r0]
tanh23 = tanh[p23,r0]
tanh38 = tanh[p38,r0]
tanh42 = tanh[p42,r0]
tanh46 = tanh[p46,r0]
tanh50 = tanh[p50,r0]
tanh54 = tanh[p54,r0]
tanh58 = tanh[p58,r0]

```

```

#pulse functions
pulse1 = gauss[A/width1^2,t1]
cosom1 = cos[omega1,t1]
step1 = step[-hwidth+t1]
rstep1 = rstep[hwidth+t1]

```

```

end-labels-section
end-parameter-section
LABELS-SECTION

```

```
#####
## SUPPLEMENTARY INFORMATION B
#####
#####
## HAMILTONIAN SECTION
#####
```

# HAMILTONIAN-SECTION

```
-----
modes| v1 | v2 | v3 | v4 | v5 | v6 | v7 | el
-----
```

#pulse exciting the x-plane

```
-tdip_s2_x*s1*C/zz |2 qq1 |8 S1&2 |9 cosom1*pulse1*step1*rstep1
tdip_s2_x*s1*C/zz |3 qq1 |8 S1&2 |9 cosom1*pulse1*step1*rstep1
```

```
-tdip_s34_x*s1*C/zz |2 qq1 |8 S1&4 |9 cosom1*pulse1*step1*rstep1
tdip_s34_x*s1*C/zz |3 qq1 |8 S1&4 |9 cosom1*pulse1*step1*rstep1
-ttdip_s34_x*s1*C/zz |6 qp1 |8 S1&3 |9 cosom1*pulse1*step1*rstep1
tdip_s34_x*s1*C/zz |7 qp1 |8 S1&3 |9 cosom1*pulse1*step1*rstep1
```

#kinetic energy

```
kk |5 KE
-kk*0.5 |1 dq^2
kk*0.5 |1 rqc2 |2 j^2
-kk*0.5 |4 dq^2
kk*0.5 |4 rqc2 |3 j^2
```

#S0:

E1  8 S1&1		
1.0  1 v1m1  8 S1&1		
1.0  4 v1m4  8 S1&1		
1.0  5 v1m5  8 S1&1		
1.000000*p1_m1o1_m4o1_s0_0	1 q^1  4 q^1	8 S1&1
0.041160*p2_m2o4_s0_0	2 q^4	8 S1&1
0.041160*p3_m3o4_s0_0	3 q^4	8 S1&1
0.041160*p4_m6o4_s0_0	6 q^4	8 S1&1
0.041160*p5_m7o4_s0_0	7 q^4	8 S1&1
0.500000*p6_m2o2_s0_0	2 q^2	8 S1&1
0.500000*p7_m3o2_s0_0	3 q^2	8 S1&1
0.500000*p8_m6o2_s0_0	6 q^2	8 S1&1
0.500000*p9_m7o2_s0_0	7 q^2	8 S1&1
1.000000*p10_m3o1_m2o3_s0_0	3 q^1  2 q^3	8 S1&1
1.000000*p11_m3o2_m2o2_s0_0	3 q^2  2 q^2	8 S1&1
1.000000*p12_m3o3_m2o1_s0_0	3 q^3  2 q^1	8 S1&1
1.000000*p13_m7o1_m6o3_s0_0	7 q^1  6 q^3	8 S1&1
1.000000*p14_m7o2_m6o2_s0_0	7 q^2  6 q^2	8 S1&1
1.000000*p15_m7o3_m6o1_s0_0	7 q^3  6 q^1	8 S1&1
1.000000*p16_m3o1_m2o1_s0_0	3 q^1  2 q^1	8 S1&1
1.000000*p17_m7o1_m6o1_s0_0	7 q^1  6 q^1	8 S1&1

#caps for dissociating coordinates

```
1.0 |1 pcap |8 S7&7
1.0 |4 pcap |8 S8&8
1.0 |4 pcap |8 S7&7
1.0 |1 pcap |8 S8&8
1.0 |1 pcap |8 S2&2
1.0 |4 pcap |8 S2&2
1.0 |4 pcap |8 S3&3
1.0 |1 pcap |8 S3&3
1.0 |4 pcap |8 S4&4
1.0 |1 pcap |8 S4&4
```

```

1.0 |4 pcap |8 S5&5
1.0 |1 pcap |8 S5&5
1.0 |4 pcap |8 S6&6
1.0 |1 pcap |8 S6&6
1.0 |4 pcap |8 S10&10
1.0 |1 pcap |8 S10&10
1.0 |4 pcap |8 S9&9
1.0 |1 pcap |8 S9&9

```

## #vertical energies

```

E2 |8 S2&2
E3 |8 S3&3
E4 |8 S4&4
E5 |8 S5&5
E6 |8 S6&6
E7 |8 S7&7
E8 |8 S8&8
E9 |8 S9&9
E10 |8 S10&10

```

## #morse potential for radial coordinates (1,4) and cc stretch

```

1.0 |1 v2m1 |8 S2&2
1.0 |1 v3m1 |8 S3&3
1.0 |1 v4m1 |8 S4&4
1.0 |1 v5m1 |8 S5&5
1.0 |1 v6m1 |8 S6&6
1.0 |1 v9m1 |8 S9&9
1.0 |1 v10m1 |8 S10&10
1.0 |4 v2m4 |8 S2&2
1.0 |4 v3m4 |8 S3&3
1.0 |4 v4m4 |8 S4&4
1.0 |4 v5m4 |8 S5&5
1.0 |4 v6m4 |8 S6&6
1.0 |4 v9m4 |8 S9&9
1.0 |4 v10m4 |8 S10&10
1.0 |5 v2m5 |8 S2&2
1.0 |5 v3m5 |8 S3&3
1.0 |5 v4m5 |8 S4&4
1.0 |5 v5m5 |8 S5&5
1.0 |5 v6m5 |8 S6&6
1.0 |5 v7m5 |8 S7&7
1.0 |5 v8m5 |8 S8&8
1.0 |5 v9m5 |8 S9&9
1.0 |5 v10m5 |8 S10&10
1.0 |1 v7m1 |8 S7&7
1.0 |1 v8m1 |8 S8&8
1.0 |4 v7m4 |8 S7&7
1.0 |4 v8m4 |8 S8&8

```

## # terms coupling radial dissociation coordinates

```

1.000000*p1_m1o1_m4o1_s1_1 |1 rq1 |4 rq1 |8 S2&2
1.000000*p2_m1o1_m4o1_s2_2 |1 rq1 |4 rq1 |8 S3&3
1.000000*p3_m1o1_m4o1_s3_3 |1 rq1 |4 rq1 |8 S4&4

```

## #ad-hoc functions

```

1.000000*gam14_cd1 |1 pstp*rq1 |4 pstp*rq1 |8 S7&7
1.000000*gam14_cd1 |1 pstp*rq1 |4 pstp*rq1 |8 S8&8
1.000000*gam14_cd2 |1 nstp*rq1 |4 pstp*rq1 |8 S7&7
1.000000*gam14_cd2 |1 nstp*rq1 |4 pstp*rq1 |8 S8&8
1.000000*gam14_cd2 |1 pstp*rq1 |4 nstp*rq1 |8 S8&8
1.000000*gam14_cd2 |1 pstp*rq1 |4 nstp*rq1 |8 S7&7
1.000000*7o8T1 |1 7o8Ttnh14 |5 7o8Ttnh55 |4 nstp*7o8Ttnh14_2 |8 S6&6

```

```

1.000000*7o8T1 |4 7o8Ttnh14 |5 7o8Ttnh55 |1 nstp*7o8Ttnh14_2 |8 S6&6
1.000000*7o8T1 |4 7o8Ttnh14 |5 7o8Ttnh55 |1 nstp*7o8Ttnh14_2 |8 S7&7
1.000000*7o8T1 |1 7o8Ttnh14 |5 7o8Ttnh55 |4 nstp*7o8Ttnh14_2 |8 S7&7

```

```

#terms coupling dissociating radial coordinates to Renner–Teller 4D subspace
#cosp = 2.0d0*(1.0d0-cos(aa*(x-x0))), aa= first entry, x0 = second entry

```

```

#cosm= 0.25d0*(cos(aa*(x-x0))+3.0d0)*stpf((x-x0),aa,.false.)*stpf((x-x0),-aa,.true.) + &
# 0.5d0*(stpf((x-x0),aa,.true.) + stpf((x-x0),-aa,.false.))
# where stpf(.,.true./.false.) and forward/backward step functions. aa= first entry, x0= second entry

```

```

+p1 |1 tanh2 |2 cosp3_2 |6 cosm29_1 |8 S7&7
+p1 |1 tanh2 |6 cosp3_1 |2 cosm29_2 |8 S8&8
+p1 |4 tanh2 |7 cosp3_1 |3 cosm29_2 |8 S8&8
+p1 |4 tanh2 |3 cosp3_2 |7 cosm29_1 |8 S7&7
+p4 |1 tanh5 |2 cosp6_2 |6 cosm30_1 |8 S8&8
+p4 |1 tanh5 |6 cosp6_1 |2 cosm30_2 |8 S7&7
+p4 |4 tanh5 |7 cosp6_1 |3 cosm30_2 |8 S7&7
+p4 |4 tanh5 |3 cosp6_2 |7 cosm30_1 |8 S8&8
+p7 |1 tanh8 |2 cosp9_2 |6 cosm31_1 |8 S2&2
+p7 |1 tanh8 |6 cosp9_1 |2 cosm31_2 |8 S2&2
+p7 |4 tanh8 |7 cosp9_1 |3 cosm31_2 |8 S2&2
+p7 |4 tanh8 |3 cosp9_2 |7 cosm31_1 |8 S2&2
+p10 |1 tanh11 |2 cosp12_2 |6 cosm32_1 |8 S4&4
+p10 |1 tanh11 |6 cosp12_1 |2 cosm32_2 |8 S4&4
+p10 |4 tanh11 |7 cosp12_1 |3 cosm32_2 |8 S4&4
+p10 |4 tanh11 |3 cosp12_2 |7 cosm32_1 |8 S4&4
+p33 |1 tanh34 |2 cosp35_2 |6 cosm36_1 |8 S3&3
+p33 |1 tanh34 |6 cosp35_1 |2 cosm36_2 |8 S3&3
+p33 |4 tanh34 |7 cosp35_1 |3 cosm36_2 |8 S3&3
+p33 |4 tanh34 |3 cosp35_2 |7 cosm36_1 |8 S3&3
+p37 |1 tanh38 |2 cosp39_2 |6 cosm40_1 |8 S5&5
+p37 |1 tanh38 |6 cosp39_1 |2 cosm40_2 |8 S6&6
+p37 |4 tanh38 |7 cosp39_1 |3 cosm40_2 |8 S6&6
+p37 |4 tanh38 |3 cosp39_2 |7 cosm40_1 |8 S5&5
+p41 |1 tanh42 |2 cosp43_2 |6 cosm44_1 |8 S6&6
+p41 |1 tanh42 |6 cosp43_1 |2 cosm44_2 |8 S5&5
+p41 |4 tanh42 |7 cosp43_1 |3 cosm44_2 |8 S5&5
+p41 |4 tanh42 |3 cosp43_2 |7 cosm44_1 |8 S6&6
+p13 |1 tanh14 |2 sin15_2 |6 cosm25_1 |8 S2&7
-p13 |4 tanh14 |3 sin15_2 |7 cosm25_1 |8 S2&7
-p13 |1 tanh14 |6 sin15_1 |2 cosm25_2 |8 S2&8
+p13 |4 tanh14 |7 sin15_1 |3 cosm25_2 |8 S2&8
-p16 |4 tanh17 |3 sin18_2 |7 cosm26_1 |8 S3&7
+p16 |1 tanh17 |2 sin18_2 |6 cosm26_1 |8 S3&7
+p16 |1 tanh17 |6 sin18_1 |2 cosm26_2 |8 S3&8
-p16 |4 tanh17 |7 sin18_1 |3 cosm26_2 |8 S3&8
-p16 |4 tanh17 |3 sin18_2 |7 cosm26_1 |8 S4&8
+p16 |1 tanh17 |2 sin18_2 |6 cosm26_1 |8 S4&8
+p16 |4 tanh17 |7 sin18_1 |3 cosm26_2 |8 S4&7
-p16 |1 tanh17 |6 sin18_1 |2 cosm26_2 |8 S4&7
+p19 |4 tanh20 |2 sin21_2 |6 cosm27_1 |8 S2&7
-p19 |1 tanh20 |3 sin21_2 |7 cosm27_1 |8 S2&7
-p19 |4 tanh20 |6 sin21_1 |2 cosm27_2 |8 S2&8
+p19 |1 tanh20 |7 sin21_1 |3 cosm27_2 |8 S2&8
-p22 |1 tanh23 |3 sin24_2 |7 cosm28_1 |8 S3&7
+p22 |4 tanh23 |2 sin24_2 |6 cosm28_1 |8 S3&7
+p22 |4 tanh23 |6 sin24_1 |2 cosm28_2 |8 S3&8
-p22 |1 tanh23 |7 sin24_1 |3 cosm28_2 |8 S3&8
-p22 |1 tanh23 |3 sin24_2 |7 cosm28_1 |8 S4&8
+p22 |4 tanh23 |2 sin24_2 |6 cosm28_1 |8 S4&8
+p22 |1 tanh23 |7 sin24_1 |3 cosm28_2 |8 S4&7

```

```

-p22 |4 tanh23 |6 sin24_1 |2 cosm28_2 |8 S4&7
+p45 |4 tanh46 |3 sin47_2 |7 cosm48_1 |8 S2&6
+p45 |1 tanh46 |2 sin47_2 |6 cosm48_1 |8 S2&6
-p45 |1 tanh46 |6 sin47_1 |2 cosm48_2 |8 S2&5
-p45 |4 tanh46 |7 sin47_1 |3 cosm48_2 |8 S2&5
+p49 |1 tanh50 |3 sin51_2 |7 cosm52_1 |8 S2&6
+p49 |4 tanh50 |2 sin51_2 |6 cosm52_1 |8 S2&6
-p49 |4 tanh50 |6 sin51_1 |2 cosm52_2 |8 S2&5
-p49 |1 tanh50 |7 sin51_1 |3 cosm52_2 |8 S2&5
+p53 |4 tanh54 |3 sin55_2 |7 cosm56_1 |8 S3&6
+p53 |1 tanh54 |2 sin55_2 |6 cosm56_1 |8 S3&6
+p53 |1 tanh54 |6 sin55_1 |2 cosm56_2 |8 S3&5
+p53 |4 tanh54 |7 sin55_1 |3 cosm56_2 |8 S3&5
+p53 |4 tanh54 |3 sin55_2 |7 cosm56_1 |8 S4&5
+p53 |1 tanh54 |2 sin55_2 |6 cosm56_1 |8 S4&5
-p53 |4 tanh54 |7 sin55_1 |3 cosm56_2 |8 S4&6
-p53 |1 tanh54 |6 sin55_1 |2 cosm56_2 |8 S4&6
+p57 |1 tanh58 |3 sin59_2 |7 cosm60_1 |8 S3&6
+p57 |4 tanh58 |2 sin59_2 |6 cosm60_1 |8 S3&6
+p57 |4 tanh58 |6 sin59_1 |2 cosm60_2 |8 S3&5
+p57 |1 tanh58 |7 sin59_1 |3 cosm60_2 |8 S3&5
+p57 |1 tanh58 |3 sin59_2 |7 cosm60_1 |8 S4&5
+p57 |4 tanh58 |2 sin59_2 |6 cosm60_1 |8 S4&5
-p57 |1 tanh58 |7 sin59_1 |3 cosm60_2 |8 S4&6
-p57 |4 tanh58 |6 sin59_1 |2 cosm60_2 |8 S4&6

```

# bounded polynomial terms coupling radial dissociation coordinates (1,4) and 4D Renner–Teller subspace

```

1.000000*p321_m1o2_m2o2_s1_1 |1 rq2 |2 qq2 |8 S2&2
1.000000*p322_m1o2_m2o2_s2_2 |1 rq2 |2 qq2 |8 S3&3
1.000000*p323_m3o2_m4o2_s1_1 |3 qq2 |4 rq2 |8 S2&2
1.000000*p324_m3o2_m4o2_s2_2 |3 qq2 |4 rq2 |8 S3&3
1.000000*p325_m1o2_m6o2_s1_1 |1 rq2 |6 qp2 |8 S2&2
1.000000*p326_m1o2_m6o2_s2_2 |1 rq2 |6 qp2 |8 S3&3
1.000000*p327_m4o2_m7o2_s1_1 |4 rq2 |7 qp2 |8 S2&2
1.000000*p328_m4o2_m7o2_s2_2 |4 rq2 |7 qp2 |8 S3&3
1.000000*p329_m1o2_m2o2_s3_3 |1 rq2 |2 qq2 |8 S4&4
1.000000*p330_m3o2_m4o2_s3_3 |3 qq2 |4 rq2 |8 S4&4
1.000000*p331_m1o2_m6o2_s3_3 |1 rq2 |6 qp2 |8 S4&4
1.000000*p332_m4o2_m7o2_s3_3 |4 rq2 |7 qp2 |8 S4&4
1.000000*p1_m1o1_m4o1_s1_1 |1 rq1 |4 rq1 |8 S2&2
1.000000*p2_m1o1_m4o1_s2_2 |1 rq1 |4 rq1 |8 S3&3
1.000000*p3_m1o1_m4o1_s3_3 |1 rq1 |4 rq1 |8 S4&4

```

# 4D Renner–Teller subspace model

```

1.000000*p4_m3o1_m2o1_s1_2 |3 qq1 |2 qq1 |8 S2&3
1.000000*p5_m2o1_m6o1_s1_3 |2 qq1 |6 qp1 |8 S2&4
1.000000*p6_m2o1_m6o1_s1_8 |2 qq1 |6 qp1 |8 S2&9
1.000000*p7_m2o1_m6o1_s4_5 |2 qq1 |6 qp1 |8 S5&6
1.000000*p8_m2o1_m6o1_s4_6 |2 qq1 |6 qp1 |8 S5&7
1.000000*p9_m2o1_m6o1_s5_7 |2 qq1 |6 qp1 |8 S6&8
1.000000*p10_m2o1_m6o1_s6_7 |2 qq1 |6 qp1 |8 S7&8
1.000000*p11_m2o1_m7o1_s1_3 |2 qq1 |7 qp1 |8 S2&4
1.000000*p12_m2o1_m7o1_s2_8 |2 qq1 |7 qp1 |8 S3&9
1.000000*p13_m2o1_m7o1_s3_9 |2 qq1 |7 qp1 |8 S4&10
1.000000*p14_m2o1_m7o1_s4_5 |2 qq1 |7 qp1 |8 S5&6
1.000000*p15_m2o1_m7o1_s4_6 |2 qq1 |7 qp1 |8 S5&7
1.000000*p16_m2o1_m7o1_s5_7 |2 qq1 |7 qp1 |8 S6&8
1.000000*p17_m2o1_m7o1_s6_7 |2 qq1 |7 qp1 |8 S7&8
1.000000*p18_m3o1_m6o1_s1_3 |3 qq1 |6 qp1 |8 S2&4
1.000000*p19_m3o1_m6o1_s2_8 |3 qq1 |6 qp1 |8 S3&9
1.000000*p20_m3o1_m6o1_s3_9 |3 qq1 |6 qp1 |8 S4&10
1.000000*p21_m3o1_m6o1_s4_5 |3 qq1 |6 qp1 |8 S5&6

```

1.000000*p22_m3o1_m6o1_s4_6	3 qq1  6 qp1	8 S5&7
1.000000*p23_m3o1_m6o1_s5_7	3 qq1  6 qp1	8 S6&8
1.000000*p24_m3o1_m6o1_s6_7	3 qq1  6 qp1	8 S7&8
1.000000*p25_m3o1_m7o1_s1_3	3 qq1  7 qp1	8 S2&4
1.000000*p26_m3o1_m7o1_s1_8	3 qq1  7 qp1	8 S2&9
1.000000*p27_m3o1_m7o1_s4_5	3 qq1  7 qp1	8 S5&6
1.000000*p28_m3o1_m7o1_s4_6	3 qq1  7 qp1	8 S5&7
1.000000*p29_m3o1_m7o1_s5_7	3 qq1  7 qp1	8 S6&8
1.000000*p30_m3o1_m7o1_s6_7	3 qq1  7 qp1	8 S7&8
1.000000*p31_m7o1_m6o1_s1_2	7 qp1  6 qp1	8 S2&3
0.041160*p32_m2o4_s9_9	2 qq4	8 S10&10
0.041160*p33_m2o4_s1_1	2 qq4	8 S2&2
0.041160*p34_m2o4_s2_2	2 qq4	8 S3&3
0.041160*p35_m2o4_s3_3	2 qq4	8 S4&4
0.041160*p36_m2o4_s4_4	2 qq4	8 S5&5
0.041160*p37_m2o4_s5_5	2 qq4	8 S6&6
0.041160*p38_m2o4_s6_6	2 qq4	8 S7&7
0.041160*p39_m2o4_s7_7	2 qq4	8 S8&8
0.041160*p40_m2o4_s8_8	2 qq4	8 S9&9
0.041160*p41_m3o4_s9_9	3 qq4	8 S10&10
0.041160*p42_m3o4_s1_1	3 qq4	8 S2&2
0.041160*p43_m3o4_s2_2	3 qq4	8 S3&3
0.041160*p44_m3o4_s3_3	3 qq4	8 S4&4
0.041160*p45_m3o4_s4_4	3 qq4	8 S5&5
0.041160*p46_m3o4_s5_5	3 qq4	8 S6&6
0.041160*p47_m3o4_s6_6	3 qq4	8 S7&7
0.041160*p48_m3o4_s7_7	3 qq4	8 S8&8
0.041160*p49_m3o4_s8_8	3 qq4	8 S9&9
0.041160*p50_m6o4_s9_9	6 qp4	8 S10&10
0.041160*p51_m6o4_s1_1	6 qp4	8 S2&2
0.041160*p52_m6o4_s2_2	6 qp4	8 S3&3
0.041160*p53_m6o4_s3_3	6 qp4	8 S4&4
0.041160*p54_m6o4_s4_4	6 qp4	8 S5&5
0.041160*p55_m6o4_s5_5	6 qp4	8 S6&6
0.041160*p56_m6o4_s6_6	6 qp4	8 S7&7
0.041160*p57_m6o4_s7_7	6 qp4	8 S8&8
0.041160*p58_m6o4_s8_8	6 qp4	8 S9&9
0.041160*p59_m7o4_s9_9	7 qp4	8 S10&10
0.041160*p60_m7o4_s1_1	7 qp4	8 S2&2
0.041160*p61_m7o4_s2_2	7 qp4	8 S3&3
0.041160*p62_m7o4_s3_3	7 qp4	8 S4&4
0.041160*p63_m7o4_s4_4	7 qp4	8 S5&5
0.041160*p64_m7o4_s5_5	7 qp4	8 S6&6
0.041160*p65_m7o4_s6_6	7 qp4	8 S7&7
0.041160*p66_m7o4_s7_7	7 qp4	8 S8&8
0.041160*p67_m7o4_s8_8	7 qp4	8 S9&9
0.500000*p68_m2o2_s1_9	2 qq2	8 S2&10
0.500000*p69_m2o2_s1_2	2 qq2	8 S2&3
0.500000*p70_m2o2_s2_9	2 qq2	8 S3&10
0.500000*p71_m2o2_s3_8	2 qq2	8 S4&9
0.500000*p72_m2o2_s4_7	2 qq2	8 S5&8
0.500000*p73_m2o2_s5_6	2 qq2	8 S6&7
0.500000*p74_m3o2_s1_9	3 qq2	8 S2&10
0.500000*p75_m3o2_s1_2	3 qq2	8 S2&3
0.500000*p76_m3o2_s2_9	3 qq2	8 S3&10
0.500000*p77_m3o2_s3_8	3 qq2	8 S4&9
0.500000*p78_m3o2_s4_7	3 qq2	8 S5&8
0.500000*p79_m3o2_s5_6	3 qq2	8 S6&7
0.500000*p80_m6o2_s1_9	6 qp2	8 S2&10
0.500000*p81_m6o2_s1_2	6 qp2	8 S2&3
0.500000*p82_m6o2_s2_9	6 qp2	8 S3&10
0.500000*p83_m6o2_s3_8	6 qp2	8 S4&9

0.500000*p84_m6o2_s4_7	6 qp2	8 S5&8
0.500000*p85_m6o2_s5_6	6 qp2	8 S6&7
0.500000*p86_m7o2_s1_9	7 qp2	8 S2&10
0.500000*p87_m7o2_s1_2	7 qp2	8 S2&3
0.500000*p88_m7o2_s2_9	7 qp2	8 S3&10
0.500000*p89_m7o2_s3_8	7 qp2	8 S4&9
0.500000*p90_m7o2_s4_7	7 qp2	8 S5&8
0.500000*p91_m7o2_s5_6	7 qp2	8 S6&7
0.500000*p92_m2o2_s9_9	2 qq2	8 S10&10
0.500000*p93_m2o2_s1_1	2 qq2	8 S2&2
0.500000*p94_m2o2_s2_2	2 qq2	8 S3&3
0.500000*p95_m2o2_s3_3	2 qq2	8 S4&4
0.500000*p96_m2o2_s4_4	2 qq2	8 S5&5
0.500000*p97_m2o2_s5_5	2 qq2	8 S6&6
0.500000*p98_m2o2_s6_6	2 qq2	8 S7&7
0.500000*p99_m2o2_s7_7	2 qq2	8 S8&8
0.500000*p100_m2o2_s8_8	2 qq2	8 S9&9
0.500000*p101_m3o2_s9_9	3 qq2	8 S10&10
0.500000*p102_m3o2_s1_1	3 qq2	8 S2&2
0.500000*p103_m3o2_s2_2	3 qq2	8 S3&3
0.500000*p104_m3o2_s3_3	3 qq2	8 S4&4
0.500000*p105_m3o2_s4_4	3 qq2	8 S5&5
0.500000*p106_m3o2_s5_5	3 qq2	8 S6&6
0.500000*p107_m3o2_s6_6	3 qq2	8 S7&7
0.500000*p108_m3o2_s7_7	3 qq2	8 S8&8
0.500000*p109_m3o2_s8_8	3 qq2	8 S9&9
0.500000*p110_m6o2_s9_9	6 qp2	8 S10&10
0.500000*p111_m6o2_s1_1	6 qp2	8 S2&2
0.500000*p112_m6o2_s2_2	6 qp2	8 S3&3
0.500000*p113_m6o2_s3_3	6 qp2	8 S4&4
0.500000*p114_m6o2_s4_4	6 qp2	8 S5&5
0.500000*p115_m6o2_s5_5	6 qp2	8 S6&6
0.500000*p116_m6o2_s6_6	6 qp2	8 S7&7
0.500000*p117_m6o2_s7_7	6 qp2	8 S8&8
0.500000*p118_m6o2_s8_8	6 qp2	8 S9&9
0.500000*p119_m7o2_s9_9	7 qp2	8 S10&10
0.500000*p120_m7o2_s1_1	7 qp2	8 S2&2
0.500000*p121_m7o2_s2_2	7 qp2	8 S3&3
0.500000*p122_m7o2_s3_3	7 qp2	8 S4&4
0.500000*p123_m7o2_s4_4	7 qp2	8 S5&5
0.500000*p124_m7o2_s5_5	7 qp2	8 S6&6
0.500000*p125_m7o2_s6_6	7 qp2	8 S7&7
0.500000*p126_m7o2_s7_7	7 qp2	8 S8&8
0.500000*p127_m7o2_s8_8	7 qp2	8 S9&9
1.000000*p128_m3o1_m2o3_s9_9	3 qq1  2 qq3	8 S10&10
1.000000*p129_m7o1_m6o3_s9_9	7 qp1  6 qp3	8 S10&10
1.000000*p130_m2o2_m6o2_s6_6	2 qq2  6 qp2	8 S7&7
1.000000*p131_m3o1_m2o1_m6o2_s6_6	3 qq1  2 qq1  6 qp2	8 S7&7
1.000000*p132_m3o2_m6o2_s6_6	3 qq2  6 qp2	8 S7&7
1.000000*p133_m2o2_m7o1_m6o1_s6_6	2 qq2  7 qp1  6 qp1	8 S7&7
1.000000*p134_m3o1_m2o1_m7o1_m6o1_s6_6	3 qq1  2 qq1  7 qp1  6 qp1	8 S7&7
1.000000*p135_m3o2_m7o1_m6o1_s6_6	3 qq2  7 qp1  6 qp1	8 S7&7
1.000000*p136_m7o1_m6o3_s6_6	7 qp1  6 qp3	8 S7&7
1.000000*p137_m2o2_m7o2_s6_6	2 qq2  7 qp2	8 S7&7
1.000000*p138_m3o1_m2o1_m7o2_s6_6	3 qq1  2 qq1  7 qp2	8 S7&7
1.000000*p139_m3o2_m7o2_s6_6	3 qq2  7 qp2	8 S7&7
1.000000*p140_m2o2_m7o2_s9_9	2 qq2  7 qp2	8 S10&10
1.000000*p141_m7o2_m6o2_s6_6	7 qp2  6 qp2	8 S7&7
1.000000*p142_m7o3_m6o1_s6_6	7 qp3  6 qp1	8 S7&7
1.000000*p143_m3o1_m2o3_s7_7	3 qq1  2 qq3	8 S8&8
1.000000*p144_m3o2_m2o2_s7_7	3 qq2  2 qq2	8 S8&8
1.000000*p145_m3o3_m2o1_s7_7	3 qq3  2 qq1	8 S8&8



1.000000*p146_m2o2_m6o2_s7_7	2 qq2  6 qp2	8 S8&8
1.000000*p147_m3o1_m2o1_m6o2_s7_7	3 qq1  2 qq1  6 qp2	8 S8&8
1.000000*p148_m3o2_m6o2_s7_7	3 qq2  6 qp2	8 S8&8
1.000000*p149_m2o2_m7o1_m6o1_s7_7	2 qq2  7 qp1  6 qp1	8 S8&8
1.000000*p150_m3o1_m2o1_m7o1_m6o1_s7_7	3 qq1  2 qq1  7 qp1  6 qp1	8 S8&8
1.000000*p151_m3o1_m2o1_m7o2_s9_9	3 qq1  2 qq1  7 qp2	8 S10&10
1.000000*p152_m3o2_m7o1_m6o1_s7_7	3 qq2  7 qp1  6 qp1	8 S8&8
1.000000*p153_m7o1_m6o3_s7_7	7 qp1  6 qp3	8 S8&8
1.000000*p154_m2o2_m7o2_s7_7	2 qq2  7 qp2	8 S8&8
1.000000*p155_m3o1_m2o1_m7o2_s7_7	3 qq1  2 qq1  7 qp2	8 S8&8
1.000000*p156_m3o2_m7o2_s7_7	3 qq2  7 qp2	8 S8&8
1.000000*p157_m7o2_m6o2_s7_7	7 qp2  6 qp2	8 S8&8
1.000000*p158_m7o3_m6o1_s7_7	7 qp3  6 qp1	8 S8&8
1.000000*p159_m3o1_m2o3_s8_8	3 qq1  2 qq3	8 S9&9
1.000000*p160_m3o2_m2o2_s8_8	3 qq2  2 qq2	8 S9&9
1.000000*p161_m3o3_m2o1_s8_8	3 qq3  2 qq1	8 S9&9
1.000000*p162_m3o2_m7o2_s9_9	3 qq2  7 qp2	8 S10&10
1.000000*p163_m2o2_m6o2_s8_8	2 qq2  6 qp2	8 S9&9
1.000000*p164_m3o1_m2o1_m6o2_s8_8	3 qq1  2 qq1  6 qp2	8 S9&9
1.000000*p165_m3o2_m6o2_s8_8	3 qq2  6 qp2	8 S9&9
1.000000*p166_m2o2_m7o1_m6o1_s8_8	2 qq2  7 qp1  6 qp1	8 S9&9
1.000000*p167_m3o1_m2o1_m7o1_m6o1_s8_8	3 qq1  2 qq1  7 qp1  6 qp1	8 S9&9
1.000000*p168_m3o2_m7o1_m6o1_s8_8	3 qq2  7 qp1  6 qp1	8 S9&9
1.000000*p169_m7o1_m6o3_s8_8	7 qp1  6 qp3	8 S9&9
1.000000*p170_m2o2_m7o2_s8_8	2 qq2  7 qp2	8 S9&9
1.000000*p171_m3o1_m2o1_m7o2_s8_8	3 qq1  2 qq1  7 qp2	8 S9&9
1.000000*p172_m3o2_m7o2_s8_8	3 qq2  7 qp2	8 S9&9
1.000000*p173_m7o2_m6o2_s9_9	7 qp2  6 qp2	8 S10&10
1.000000*p174_m7o2_m6o2_s8_8	7 qp2  6 qp2	8 S9&9
1.000000*p175_m7o3_m6o1_s8_8	7 qp3  6 qp1	8 S9&9
1.000000*p176_m7o3_m6o1_s9_9	7 qp3  6 qp1	8 S10&10
1.000000*p177_m3o2_m2o2_s9_9	3 qq2  2 qq2	8 S10&10
1.000000*p178_m3o1_m2o3_s1_1	3 qq1  2 qq3	8 S2&2
1.000000*p179_m3o2_m2o2_s1_1	3 qq2  2 qq2	8 S2&2
1.000000*p180_m3o3_m2o1_s1_1	3 qq3  2 qq1	8 S2&2
1.000000*p181_m2o2_m6o2_s1_1	2 qq2  6 qp2	8 S2&2
1.000000*p182_m3o1_m2o1_m6o2_s1_1	3 qq1  2 qq1  6 qp2	8 S2&2
1.000000*p183_m3o2_m6o2_s1_1	3 qq2  6 qp2	8 S2&2
1.000000*p184_m2o2_m7o1_m6o1_s1_1	2 qq2  7 qp1  6 qp1	8 S2&2
1.000000*p185_m3o1_m2o1_m7o1_m6o1_s1_1	3 qq1  2 qq1  7 qp1  6 qp1	8 S2&2
1.000000*p186_m3o3_m2o1_s9_9	3 qq3  2 qq1	8 S10&10
1.000000*p187_m3o2_m7o1_m6o1_s1_1	3 qq2  7 qp1  6 qp1	8 S2&2
1.000000*p188_m7o1_m6o3_s1_1	7 qp1  6 qp3	8 S2&2
1.000000*p189_m2o2_m7o2_s1_1	2 qq2  7 qp2	8 S2&2
1.000000*p190_m3o1_m2o1_m7o2_s1_1	3 qq1  2 qq1  7 qp2	8 S2&2
1.000000*p191_m3o2_m7o2_s1_1	3 qq2  7 qp2	8 S2&2
1.000000*p192_m7o2_m6o2_s1_1	7 qp2  6 qp2	8 S2&2
1.000000*p193_m7o3_m6o1_s1_1	7 qp3  6 qp1	8 S2&2
1.000000*p194_m3o1_m2o3_s2_2	3 qq1  2 qq3	8 S3&3
1.000000*p195_m3o2_m2o2_s2_2	3 qq2  2 qq2	8 S3&3
1.000000*p196_m3o3_m2o1_s2_2	3 qq3  2 qq1	8 S3&3
1.000000*p197_m2o2_m6o2_s9_9	2 qq2  6 qp2	8 S10&10
1.000000*p198_m2o2_m6o2_s2_2	2 qq2  6 qp2	8 S3&3
1.000000*p199_m3o1_m2o1_m6o2_s2_2	3 qq1  2 qq1  6 qp2	8 S3&3
1.000000*p200_m3o2_m6o2_s2_2	3 qq2  6 qp2	8 S3&3
1.000000*p201_m2o2_m7o1_m6o1_s2_2	2 qq2  7 qp1  6 qp1	8 S3&3
1.000000*p202_m3o1_m2o1_m7o1_m6o1_s2_2	3 qq1  2 qq1  7 qp1  6 qp1	8 S3&3
1.000000*p203_m3o2_m7o1_m6o1_s2_2	3 qq2  7 qp1  6 qp1	8 S3&3
1.000000*p204_m7o1_m6o3_s2_2	7 qp1  6 qp3	8 S3&3
1.000000*p205_m2o2_m7o2_s2_2	2 qq2  7 qp2	8 S3&3
1.000000*p206_m3o1_m2o1_m7o2_s2_2	3 qq1  2 qq1  7 qp2	8 S3&3
1.000000*p207_m3o2_m7o2_s2_2	3 qq2  7 qp2	8 S3&3

1.000000*p208_m3o1_m2o1_m6o2_s9_9	3 qq1  2 qq1  6 qp2	8 S10&10
1.000000*p209_m7o2_m6o2_s2_2	7 qp2  6 qp2	8 S3&3
1.000000*p210_m7o3_m6o1_s2_2	7 qp3  6 qp1	8 S3&3
1.000000*p211_m3o1_m2o3_s3_3	3 qq1  2 qq3	8 S4&4
1.000000*p212_m3o2_m2o2_s3_3	3 qq2  2 qq2	8 S4&4
1.000000*p213_m3o3_m2o1_s3_3	3 qq3  2 qq1	8 S4&4
1.000000*p214_m2o2_m6o2_s3_3	2 qq2  6 qp2	8 S4&4
1.000000*p215_m3o1_m2o1_m6o2_s3_3	3 qq1  2 qq1  6 qp2	8 S4&4
1.000000*p216_m3o2_m6o2_s3_3	3 qq2  6 qp2	8 S4&4
1.000000*p217_m2o2_m7o1_m6o1_s3_3	2 qq2  7 qp1  6 qp1	8 S4&4
1.000000*p218_m3o1_m2o1_m7o1_m6o1_s3_3	3 qq1  2 qq1  7 qp1  6 qp1	8 S4&4
1.000000*p219_m3o2_m6o2_s9_9	3 qq2  6 qp2	8 S10&10
1.000000*p220_m3o2_m7o1_m6o1_s3_3	3 qq2  7 qp1  6 qp1	8 S4&4
1.000000*p221_m7o1_m6o3_s3_3	7 qp1  6 qp3	8 S4&4
1.000000*p222_m2o2_m7o2_s3_3	2 qq2  7 qp2	8 S4&4
1.000000*p223_m3o1_m2o1_m7o2_s3_3	3 qq1  2 qq1  7 qp2	8 S4&4
1.000000*p224_m3o2_m7o2_s3_3	3 qq2  7 qp2	8 S4&4
1.000000*p225_m7o2_m6o2_s3_3	7 qp2  6 qp2	8 S4&4
1.000000*p226_m7o3_m6o1_s3_3	7 qp3  6 qp1	8 S4&4
1.000000*p227_m3o1_m2o3_s4_4	3 qq1  2 qq3	8 S5&5
1.000000*p228_m3o2_m2o2_s4_4	3 qq2  2 qq2	8 S5&5
1.000000*p229_m3o3_m2o1_s4_4	3 qq3  2 qq1	8 S5&5
1.000000*p230_m2o2_m7o1_m6o1_s9_9	2 qq2  7 qp1  6 qp1	8 S10&10
1.000000*p231_m2o2_m6o2_s4_4	2 qq2  6 qp2	8 S5&5
1.000000*p232_m3o1_m2o1_m6o2_s4_4	3 qq1  2 qq1  6 qp2	8 S5&5
1.000000*p233_m3o2_m6o2_s4_4	3 qq2  6 qp2	8 S5&5
1.000000*p234_m2o2_m7o1_m6o1_s4_4	2 qq2  7 qp1  6 qp1	8 S5&5
1.000000*p235_m3o1_m2o1_m7o1_m6o1_s4_4	3 qq1  2 qq1  7 qp1  6 qp1	8 S5&5
1.000000*p236_m3o2_m7o1_m6o1_s4_4	3 qq2  7 qp1  6 qp1	8 S5&5
1.000000*p237_m7o1_m6o3_s4_4	7 qp1  6 qp3	8 S5&5
1.000000*p238_m2o2_m7o2_s4_4	2 qq2  7 qp2	8 S5&5
1.000000*p239_m3o1_m2o1_m7o2_s4_4	3 qq1  2 qq1  7 qp2	8 S5&5
1.000000*p240_m3o2_m7o2_s4_4	3 qq2  7 qp2	8 S5&5
1.000000*p241_m3o1_m2o1_m7o1_m6o1_s9_9	3 qq1  2 qq1  7 qp1  6 qp1	8 S10&10
1.000000*p242_m7o2_m6o2_s4_4	7 qp2  6 qp2	8 S5&5
1.000000*p243_m7o3_m6o1_s4_4	7 qp3  6 qp1	8 S5&5
1.000000*p244_m3o1_m2o3_s5_5	3 qq1  2 qq3	8 S6&6
1.000000*p245_m3o2_m2o2_s5_5	3 qq2  2 qq2	8 S6&6
1.000000*p246_m3o3_m2o1_s5_5	3 qq3  2 qq1	8 S6&6
1.000000*p247_m2o2_m6o2_s5_5	2 qq2  6 qp2	8 S6&6
1.000000*p248_m3o1_m2o1_m6o2_s5_5	3 qq1  2 qq1  6 qp2	8 S6&6
1.000000*p249_m3o2_m6o2_s5_5	3 qq2  6 qp2	8 S6&6
1.000000*p250_m2o2_m7o1_m6o1_s5_5	2 qq2  7 qp1  6 qp1	8 S6&6
1.000000*p251_m3o1_m2o1_m7o1_m6o1_s5_5	3 qq1  2 qq1  7 qp1  6 qp1	8 S6&6
1.000000*p252_m3o2_m7o1_m6o1_s9_9	3 qq2  7 qp1  6 qp1	8 S10&10
1.000000*p253_m3o2_m7o1_m6o1_s5_5	3 qq2  7 qp1  6 qp1	8 S6&6
1.000000*p254_m7o1_m6o3_s5_5	7 qp1  6 qp3	8 S6&6
1.000000*p255_m2o2_m7o2_s5_5	2 qq2  7 qp2	8 S6&6
1.000000*p256_m3o1_m2o1_m7o2_s5_5	3 qq1  2 qq1  7 qp2	8 S6&6
1.000000*p257_m3o2_m7o2_s5_5	3 qq2  7 qp2	8 S6&6
1.000000*p258_m7o2_m6o2_s5_5	7 qp2  6 qp2	8 S6&6
1.000000*p259_m7o3_m6o1_s5_5	7 qp3  6 qp1	8 S6&6
1.000000*p260_m3o1_m2o3_s6_6	3 qq1  2 qq3	8 S7&7
1.000000*p261_m3o2_m2o2_s6_6	3 qq2  2 qq2	8 S7&7
1.000000*p262_m3o3_m2o1_s6_6	3 qq3  2 qq1	8 S7&7
1.000000*p263_m3o1_m2o1_s9_9	3 qq1  2 qq1	8 S10&10
1.000000*p264_m3o1_m2o1_s1_1	3 qq1  2 qq1	8 S2&2
1.000000*p265_m3o1_m2o1_s2_2	3 qq1  2 qq1	8 S3&3
1.000000*p266_m3o1_m2o1_s3_3	3 qq1  2 qq1	8 S4&4
1.000000*p267_m3o1_m2o1_s4_4	3 qq1  2 qq1	8 S5&5
1.000000*p268_m3o1_m2o1_s5_5	3 qq1  2 qq1	8 S6&6
1.000000*p269_m3o1_m2o1_s6_6	3 qq1  2 qq1	8 S7&7

1.000000*p270_m3o1_m2o1_s7_7	3 qq1	2 qq1	8 S8&8
1.000000*p271_m3o1_m2o1_s8_8	3 qq1	2 qq1	8 S9&9
1.000000*p272_m7o1_m6o1_s9_9	7 qp1	6 qp1	8 S10&10
1.000000*p273_m7o1_m6o1_s1_1	7 qp1	6 qp1	8 S2&2
1.000000*p274_m7o1_m6o1_s2_2	7 qp1	6 qp1	8 S3&3
1.000000*p275_m7o1_m6o1_s3_3	7 qp1	6 qp1	8 S4&4
1.000000*p276_m7o1_m6o1_s4_4	7 qp1	6 qp1	8 S5&5
1.000000*p277_m7o1_m6o1_s5_5	7 qp1	6 qp1	8 S6&6
1.000000*p278_m7o1_m6o1_s6_6	7 qp1	6 qp1	8 S7&7
1.000000*p279_m7o1_m6o1_s7_7	7 qp1	6 qp1	8 S8&8
1.000000*p280_m7o1_m6o1_s8_8	7 qp1	6 qp1	8 S9&9
1.000000*p281_m2o1_s1_5	2 qq1		8 S2&6
1.000000*p282_m2o1_s1_6	2 qq1		8 S2&7
1.000000*p283_m2o1_s2_5	2 qq1		8 S3&6
1.000000*p284_m2o1_s2_6	2 qq1		8 S3&7
1.000000*p285_m2o1_s3_4	2 qq1		8 S4&5
1.000000*p286_m2o1_s3_7	2 qq1		8 S4&8
1.000000*p287_m2o1_s4_8	2 qq1		8 S5&9
1.000000*p288_m2o1_s5_9	2 qq1		8 S6&10
1.000000*p289_m2o1_s6_9	2 qq1		8 S7&10
1.000000*p290_m2o1_s7_8	2 qq1		8 S8&9
1.000000*p291_m3o1_s1_5	3 qq1		8 S2&6
1.000000*p292_m3o1_s1_6	3 qq1		8 S2&7
1.000000*p293_m3o1_s2_5	3 qq1		8 S3&6
1.000000*p294_m3o1_s2_6	3 qq1		8 S3&7
1.000000*p295_m3o1_s3_4	3 qq1		8 S4&5
1.000000*p296_m3o1_s3_7	3 qq1		8 S4&8
1.000000*p297_m3o1_s4_8	3 qq1		8 S5&9
1.000000*p298_m3o1_s5_9	3 qq1		8 S6&10
1.000000*p299_m3o1_s6_9	3 qq1		8 S7&10
1.000000*p300_m3o1_s7_8	3 qq1		8 S8&9
1.000000*p301_m6o1_s1_4	6 qp1		8 S2&5
1.000000*p302_m6o1_s1_7	6 qp1		8 S2&8
1.000000*p303_m6o1_s2_4	6 qp1		8 S3&5
1.000000*p304_m6o1_s2_7	6 qp1		8 S3&8
1.000000*p305_m6o1_s3_5	6 qp1		8 S4&6
1.000000*p306_m6o1_s3_6	6 qp1		8 S4&7
1.000000*p307_m6o1_s4_9	6 qp1		8 S5&10
1.000000*p308_m6o1_s5_8	6 qp1		8 S6&9
1.000000*p309_m6o1_s6_8	6 qp1		8 S7&9
1.000000*p310_m6o1_s7_9	6 qp1		8 S8&10
1.000000*p311_m7o1_s1_4	7 qp1		8 S2&5
1.000000*p312_m7o1_s1_7	7 qp1		8 S2&8
1.000000*p313_m7o1_s2_4	7 qp1		8 S3&5
1.000000*p314_m7o1_s2_7	7 qp1		8 S3&8
1.000000*p315_m7o1_s3_5	7 qp1		8 S4&6
1.000000*p316_m7o1_s3_6	7 qp1		8 S4&7
1.000000*p317_m7o1_s4_9	7 qp1		8 S5&10
1.000000*p318_m7o1_s5_8	7 qp1		8 S6&9
1.000000*p319_m7o1_s6_8	7 qp1		8 S7&9
1.000000*p320_m7o1_s7_9	7 qp1		8 S8&10

END-HAMILTONIAN-SECTION

END-OPERATOR

#####

```
#####
## SUPPLEMENTARY INFORMATION C
#####
#####
## PARAMETERS AND LABELS
#####
```

# OP\_DEFINE-SECTION

## TITLE

Tolane 9-state model (energy transfer)

## END-TITLE

## END-OP\_DEFINE-SECTION

## PARAMETER-SECTION

### #vertical energies

```
E1      = 0.00011 , ev
E2      = 4.13352 , ev
E3      = 4.18876 , ev
E4      = 4.19937 , ev
E5      = 4.84265 , ev
E6      = 5.10388 , ev
E7      = 5.54524 , ev
E8      = 5.57082 , ev
E9      = 6.44960 , ev
```

### #ag mode 56 morse potential function parameters

```
1D_56 = 21.365000000 , ev
1A_56 = 0.083009605
1X_56 = -0.345830000
1E_56 = -0.017109896 , ev
2D_56 = 912.540000000 , ev
2A_56 = 0.010966387
2X_56 = 0.923650000
2E_56 = -0.094579412 , ev
3D_56 = 11.726000000 , ev
3A_56 = 0.096143465
3X_56 = 0.032257000
3E_56 = -0.000113132 , ev
4D_56 = 16.484000000 , ev
4A_56 = 0.081359644
4X_56 = 0.051395000
4E_56 = -0.000289427 , ev
5D_56 = 22.246000000 , ev
5A_56 = 0.068843581
5X_56 = 1.363500000
5E_56 = -0.215463863 , ev
6D_56 = 22.348000000 , ev
6A_56 = 0.064710136
6X_56 = 0.935840000
6E_56 = -0.087100243 , ev
7D_56 = 17.515000000 , ev
7A_56 = 0.067316345
7X_56 = 0.116760000
7E_56 = -0.001090574 , ev
```

### #zeroth order model parameters

```
omega_2      = 0.00541 , ev
omega_4      = 0.01520 , ev
omega_5      = 0.01680 , ev
omega_6      = 0.03189 , ev
omega_7      = 0.03210 , ev
omega_10     = 0.04933 , ev
omega_12     = 0.05745 , ev
omega_14     = 0.06379 , ev
omega_20     = 0.08718 , ev
```

```
omega_24     = 0.10491 , ev
omega_29     = 0.11781 , ev
omega_33     = 0.12503 , ev
omega_38     = 0.14382 , ev
omega_54     = 0.20415 , ev
omega_56     = 0.27477 , ev
```

### #S0 model

```
p1_m4o1_s1_1 = -0.0459 , ev
p2_m9o1_s1_1 = -0.0778 , ev
p3_m12o1_s1_1 = -0.1005 , ev
p4_m13o1_s1_1 = 0.0114 , ev
p5_m14o1_s1_1 = -0.0103 , ev
p6_m1o2_s1_1 = 0.0647 , ev
p7_m2o2_s1_1 = 0.0736 , ev
p8_m3o2_s1_1 = 0.0533 , ev
p9_m4o2_s1_1 = 0.0021 , ev
p10_m5o2_s1_1 = 0.1085 , ev
p11_m6o2_s1_1 = 0.0224 , ev
p12_m8o2_s1_1 = 0.0315 , ev
p13_m9o2_s1_1 = 0.0061 , ev
p14_m10o2_s1_1 = 0.0480 , ev
p15_m11o2_s1_1 = 0.0433 , ev
p16_m12o2_s1_1 = 0.0035 , ev
p17_m13o2_s1_1 = 0.0013 , ev
p18_m14o2_s1_1 = -0.0045 , ev
p19_m8o1_m3o1_s1_1 = -0.0262 , ev
p20_m13o1_m4o1_s1_1 = -0.0002 , ev
p21_m15o1_m4o1_s1_1 = 0.0161 , ev
p22_m13o1_m15o1_s1_1 = 0.0179 , ev
```

### #excited states

```
p1_m2o2_s8_8 = -0.02930000 , ev
p2_m2o4_s8_8 = 0.03219400 , ev
p3_m4o2_s5_5 = -0.06119100 , ev
p4_m4o4_s5_5 = 0.05162700 , ev
p5_m4o2_s8_8 = -0.13984000 , ev
p6_m4o4_s8_8 = 0.08389300 , ev
p7_m5o2_s2_2 = 0.01277500 , ev
p8_m5o4_s2_2 = 0.00383380 , ev
p9_m5o2_s3_3 = 0.03594600 , ev
p10_m5o4_s3_3 = 0.00135830 , ev
p11_m5o2_s4_4 = 0.03594600 , ev
p12_m5o4_s4_4 = 0.00135830 , ev
p13_m5o2_s5_5 = 0.00851120 , ev
p14_m5o4_s5_5 = 0.00489220 , ev
p15_m5o2_s8_8 = 0.08868300 , ev
p16_m5o4_s8_8 = 0.01692900 , ev
p17_m7o2_s5_5 = -0.09558600 , ev
p18_m7o4_s5_5 = 0.03152400 , ev
p19_m7o2_s8_8 = -0.04215300 , ev
p20_m7o4_s8_8 = 0.06601000 , ev
p21_m14o2_s8_8 = 0.04829700 , ev
p22_m14o4_s8_8 = 0.00250890 , ev
p23_m56o1_s8_8 = -0.30078000 , ev
p24_m56o2_s8_8 = -0.09413400 , ev
p25_m56o4_s8_8 = -0.01392900 , ev
p26_m56o1_s9_9 = -0.18176000 , ev
p27_m56o2_s9_9 = 0.01419400 , ev
p28_m56o4_s9_9 = 0.01352200 , ev
p29_m6o1_s1_1 = -0.0459 , ev
p30_m6o1_s2_2 = -0.0748 , ev
p31_m6o1_s3_3 = -0.0447 , ev
p32_m6o1_s4_4 = -0.0447 , ev
```

p33\_m6o1\_s5\_5 = -0.0366, ev  
 p34\_m6o1\_s6\_6 = -0.0448, ev  
 p35\_m6o1\_s7\_7 = -0.0415, ev  
 p36\_m6o1\_s8\_8 = -0.0415, ev  
 p37\_m20o1\_s1\_1 = -0.0778, ev  
 p38\_m20o1\_s2\_2 = -0.0604, ev  
 p39\_m20o1\_s3\_3 = -0.0580, ev  
 p40\_m20o1\_s4\_4 = -0.0624, ev  
 p41\_m20o1\_s5\_5 = -0.0638, ev  
 p42\_m20o1\_s6\_6 = -0.0427, ev  
 p43\_m20o1\_s7\_7 = -0.0461, ev  
 p44\_m20o1\_s8\_8 = -0.0547, ev  
 p45\_m33o1\_s1\_1 = -0.1005, ev  
 p46\_m33o1\_s2\_2 = -0.0310, ev  
 p47\_m33o1\_s3\_3 = -0.0168, ev  
 p48\_m33o1\_s4\_4 = -0.0108, ev  
 p49\_m33o1\_s5\_5 = -0.0271, ev  
 p50\_m33o1\_s6\_6 = 0.0103, ev  
 p51\_m33o1\_s7\_7 = -0.0288, ev  
 p52\_m33o1\_s8\_8 = -0.0579, ev  
 p53\_m38o1\_s1\_1 = 0.0114, ev  
 p54\_m38o1\_s2\_2 = -0.0802, ev  
 p55\_m38o1\_s3\_3 = -0.0920, ev  
 p56\_m38o1\_s4\_4 = -0.0920, ev  
 p57\_m38o1\_s5\_5 = -0.0102, ev  
 p58\_m38o1\_s6\_6 = -0.1378, ev  
 p59\_m38o1\_s7\_7 = -0.0623, ev  
 p60\_m38o1\_s8\_8 = -0.0008, ev  
 p61\_m54o1\_s1\_1 = -0.0103, ev  
 p62\_m54o1\_s2\_2 = -0.1627, ev  
 p63\_m54o1\_s3\_3 = -0.0017, ev  
 p64\_m54o1\_s4\_4 = -0.0013, ev  
 p65\_m54o1\_s5\_5 = -0.0931, ev  
 p66\_m54o1\_s6\_6 = -0.2431, ev  
 p67\_m54o1\_s7\_7 = -0.0444, ev  
 p68\_m54o1\_s8\_8 = -0.0415, ev  
 p69\_m5o1\_s8\_9 = -0.3981, ev  
 p70\_m6o1\_s5\_8 = 0.0144, ev  
 p71\_m6o1\_s6\_7 = -0.0144, ev  
 p72\_m10o1\_s2\_5 = 0.0610, ev  
 p73\_m10o1\_s2\_8 = -0.0033, ev  
 p74\_m14o1\_s8\_9 = 0.5135, ev  
 p75\_m20o1\_s5\_8 = 0.0914, ev  
 p76\_m20o1\_s6\_7 = 0.0587, ev  
 p77\_m24o1\_s2\_5 = 0.0639, ev  
 p78\_m24o1\_s2\_8 = -0.0201, ev  
 p79\_m29o1\_s2\_5 = 0.0397, ev  
 p80\_m29o1\_s2\_8 = 0.0068, ev  
 p81\_m33o1\_s5\_8 = 0.0303, ev  
 p82\_m33o1\_s6\_7 = 0.0239, ev  
 p83\_m38o1\_s5\_8 = 0.0328, ev  
 p84\_m38o1\_s6\_7 = 0.0205, ev  
 p85\_m54o1\_s5\_8 = 0.0543, ev  
 p86\_m54o1\_s6\_7 = 0.0043, ev  
 p87\_m56o1\_s5\_8 = 0.0225, ev  
 p88\_m56o1\_s6\_7 = 0.0050, ev  
 p89\_m2o2\_s1\_1 = 0.0647, ev  
 p90\_m2o2\_s2\_2 = 0.0481, ev  
 p91\_m2o2\_s3\_3 = 0.0481, ev  
 p92\_m2o2\_s4\_4 = 0.0481, ev  
 p93\_m2o2\_s5\_5 = 0.0581, ev  
 p94\_m2o2\_s6\_6 = 0.0422, ev

p95\_m2o2\_s7\_7 = 0.0491, ev  
 p96\_m2o2\_s8\_8 = -0.0019, ev  
 p97\_m4o2\_s1\_1 = 0.0736, ev  
 p98\_m4o2\_s2\_2 = 0.0429, ev  
 p99\_m4o2\_s3\_3 = 0.0498, ev  
 p100\_m4o2\_s4\_4 = 0.0498, ev  
 p101\_m4o2\_s6\_6 = 0.0294, ev  
 p102\_m4o2\_s7\_7 = 0.0215, ev  
 p103\_m4o2\_s9\_9 = 0.2481, ev  
 p104\_m5o2\_s1\_1 = -1.1533, ev  
 p105\_m5o2\_s3\_3 = 0.0375, ev  
 p106\_m5o2\_s4\_4 = 0.0403, ev  
 p107\_m5o2\_s5\_5 = 0.0022, ev  
 p108\_m5o2\_s6\_6 = 0.0216, ev  
 p109\_m5o2\_s7\_7 = 0.0283, ev  
 p110\_m5o2\_s9\_9 = 0.0074, ev  
 p111\_m6o2\_s1\_1 = 0.0021, ev  
 p112\_m6o2\_s2\_2 = -0.0022, ev  
 p113\_m6o2\_s3\_3 = -0.0005, ev  
 p114\_m6o2\_s4\_4 = -0.0005, ev  
 p115\_m6o2\_s5\_5 = -0.0002, ev  
 p116\_m6o2\_s6\_6 = -0.0011, ev  
 p117\_m6o2\_s7\_7 = -0.0022, ev  
 p118\_m6o2\_s8\_8 = -0.0022, ev  
 p119\_m6o2\_s9\_9 = -0.0021, ev  
 p120\_m7o2\_s1\_1 = 0.1141, ev  
 p121\_m7o2\_s2\_2 = 0.0630, ev  
 p122\_m7o2\_s3\_3 = 0.0834, ev  
 p123\_m7o2\_s4\_4 = 0.0834, ev  
 p124\_m7o2\_s6\_6 = 0.0285, ev  
 p125\_m7o2\_s7\_7 = 0.0588, ev  
 p126\_m7o2\_s9\_9 = 0.2141, ev  
 p127\_m10o2\_s1\_1 = 0.0224, ev  
 p128\_m10o2\_s2\_2 = 0.0199, ev  
 p129\_m10o2\_s3\_3 = 0.0029, ev  
 p130\_m10o2\_s4\_4 = 0.0029, ev  
 p131\_m10o2\_s5\_5 = 0.0108, ev  
 p132\_m10o2\_s6\_6 = 0.0106, ev  
 p133\_m10o2\_s7\_7 = -0.0021, ev  
 p134\_m10o2\_s8\_8 = 0.0285, ev  
 p135\_m14o2\_s1\_1 = 0.0315, ev  
 p136\_m14o2\_s2\_2 = -0.0095, ev  
 p137\_m14o2\_s3\_3 = 0.0300, ev  
 p138\_m14o2\_s4\_4 = 0.0300, ev  
 p139\_m14o2\_s5\_5 = 0.0817, ev  
 p140\_m14o2\_s6\_6 = 0.0234, ev  
 p141\_m14o2\_s7\_7 = 0.0201, ev  
 p142\_m14o2\_s9\_9 = 0.0143, ev  
 p143\_m20o2\_s1\_1 = 0.0061, ev  
 p144\_m20o2\_s2\_2 = 0.0006, ev  
 p145\_m20o2\_s3\_3 = -0.0023, ev  
 p146\_m20o2\_s4\_4 = -0.0071, ev  
 p147\_m20o2\_s5\_5 = 0.0251, ev  
 p148\_m20o2\_s6\_6 = 0.0130, ev  
 p149\_m20o2\_s7\_7 = -0.0209, ev  
 p150\_m20o2\_s8\_8 = -0.0376, ev  
 p151\_m24o2\_s1\_1 = 0.0480, ev  
 p152\_m24o2\_s2\_2 = 0.0473, ev  
 p153\_m24o2\_s3\_3 = 0.0298, ev  
 p154\_m24o2\_s4\_4 = 0.0298, ev  
 p155\_m24o2\_s5\_5 = 0.0374, ev  
 p156\_m24o2\_s6\_6 = 0.0190, ev

p157\_m24o2\_s7\_7 = 0.0269, ev  
 p158\_m24o2\_s8\_8 = 0.0476, ev  
 p159\_m29o2\_s1\_1 = 0.0433, ev  
 p160\_m29o2\_s2\_2 = 0.0354, ev  
 p161\_m29o2\_s3\_3 = 0.0263, ev  
 p162\_m29o2\_s4\_4 = 0.0263, ev  
 p163\_m29o2\_s5\_5 = 0.0358, ev  
 p164\_m29o2\_s6\_6 = 0.0272, ev  
 p165\_m29o2\_s7\_7 = 0.0235, ev  
 p166\_m29o2\_s8\_8 = 0.0343, ev  
 p167\_m33o2\_s1\_1 = 0.0035, ev  
 p168\_m33o2\_s2\_2 = 0.0003, ev  
 p169\_m33o2\_s3\_3 = 0.0045, ev  
 p170\_m33o2\_s4\_4 = 0.0013, ev  
 p171\_m33o2\_s5\_5 = 0.0042, ev  
 p172\_m33o2\_s6\_6 = 0.0048, ev  
 p173\_m33o2\_s7\_7 = -0.0021, ev  
 p174\_m33o2\_s8\_8 = -0.0184, ev  
 p175\_m38o2\_s1\_1 = 0.0013, ev  
 p176\_m38o2\_s2\_2 = -0.0050, ev  
 p177\_m38o2\_s5\_5 = -0.0028, ev  
 p178\_m38o2\_s6\_6 = -0.0018, ev  
 p179\_m38o2\_s7\_7 = -0.0158, ev  
 p180\_m38o2\_s8\_8 = -0.0203, ev  
 p181\_m54o2\_s1\_1 = -0.0045, ev  
 p182\_m54o2\_s2\_2 = -0.0049, ev  
 p183\_m54o2\_s3\_3 = 0.0001, ev  
 p184\_m54o2\_s4\_4 = 0.0014, ev  
 p185\_m54o2\_s5\_5 = -0.0014, ev  
 p186\_m54o2\_s6\_6 = -0.0576, ev  
 p187\_m54o2\_s7\_7 = -0.0469, ev  
 p188\_m54o2\_s8\_8 = -0.0572, ev  
 p189\_m5o1\_m14o1\_s1\_1 = -0.0262, ev  
 p190\_m5o1\_m14o1\_s2\_2 = -0.0050, ev  
 p191\_m5o1\_m14o1\_s3\_3 = -0.0159, ev  
 p192\_m5o1\_m14o1\_s4\_4 = -0.0159, ev  
 p193\_m5o1\_m14o1\_s5\_5 = -0.0186, ev  
 p194\_m5o1\_m14o1\_s6\_6 = -0.0033, ev  
 p195\_m5o1\_m14o1\_s7\_7 = -0.0135, ev  
 p196\_m5o1\_m14o1\_s8\_8 = -0.0475, ev  
 p197\_m5o1\_m14o1\_s9\_9 = -0.0329, ev  
 p198\_m20o1\_m6o1\_s2\_2 = 0.0043, ev  
 p199\_m20o1\_m6o1\_s3\_3 = 0.0019, ev  
 p200\_m20o1\_m6o1\_s4\_4 = 0.0051, ev  
 p201\_m20o1\_m6o1\_s5\_5 = 0.0023, ev  
 p202\_m20o1\_m6o1\_s6\_6 = -0.0021, ev  
 p203\_m20o1\_m6o1\_s7\_7 = -0.0041, ev  
 p204\_m20o1\_m6o1\_s8\_8 = -0.0045, ev  
 p205\_m38o1\_m6o1\_s1\_1 = -0.0002, ev  
 p206\_m38o1\_m6o1\_s2\_2 = 0.0025, ev  
 p207\_m38o1\_m6o1\_s3\_3 = -0.0008, ev  
 p208\_m38o1\_m6o1\_s4\_4 = -0.0008, ev  
 p209\_m38o1\_m6o1\_s5\_5 = -0.0033, ev  
 p210\_m38o1\_m6o1\_s6\_6 = -0.0104, ev  
 p211\_m38o1\_m6o1\_s7\_7 = -0.0021, ev  
 p212\_m38o1\_m6o1\_s8\_8 = -0.0280, ev  
 p213\_m56o1\_m6o1\_s1\_1 = 0.0161, ev  
 p214\_m56o1\_m6o1\_s2\_2 = 0.0140, ev  
 p215\_m56o1\_m6o1\_s3\_3 = 0.0190, ev  
 p216\_m56o1\_m6o1\_s4\_4 = 0.0061, ev  
 p217\_m56o1\_m6o1\_s5\_5 = -0.0027, ev  
 p218\_m56o1\_m6o1\_s6\_6 = 0.0133, ev

p219\_m56o1\_m6o1\_s7\_7 = -0.0090, ev  
 p220\_m56o1\_m6o1\_s8\_8 = 0.0270, ev  
 p221\_m38o1\_m20o1\_s2\_2 = 0.0030, ev  
 p222\_m38o1\_m20o1\_s3\_3 = 0.0024, ev  
 p223\_m38o1\_m20o1\_s4\_4 = 0.0041, ev  
 p224\_m38o1\_m20o1\_s5\_5 = 0.0079, ev  
 p225\_m38o1\_m20o1\_s6\_6 = -0.0014, ev  
 p226\_m38o1\_m20o1\_s7\_7 = -0.0051, ev  
 p227\_m56o1\_m20o1\_s2\_2 = 0.0149, ev  
 p228\_m56o1\_m20o1\_s3\_3 = 0.0132, ev  
 p229\_m56o1\_m20o1\_s4\_4 = 0.0054, ev  
 p230\_m56o1\_m20o1\_s5\_5 = 0.0169, ev  
 p231\_m56o1\_m20o1\_s6\_6 = 0.0330, ev  
 p232\_m56o1\_m20o1\_s7\_7 = 0.0055, ev  
 p233\_m56o1\_m38o1\_s1\_1 = 0.0179, ev  
 p234\_m56o1\_m38o1\_s2\_2 = 0.0225, ev  
 p235\_m56o1\_m38o1\_s3\_3 = 0.0040, ev  
 p236\_m56o1\_m38o1\_s4\_4 = 0.0040, ev  
 p237\_m56o1\_m38o1\_s5\_5 = 0.0216, ev  
 p238\_m56o1\_m38o1\_s6\_6 = 0.0137, ev  
 p239\_m56o1\_m38o1\_s7\_7 = 0.0046, ev  
 p240\_m56o1\_m38o1\_s8\_8 = 0.0149, ev  
 p241\_m2o2\_s4\_8 = 0.0118, ev  
 p242\_m2o2\_s5\_8 = 0.0169, ev  
 p243\_m2o2\_s6\_7 = 0.0012, ev  
 p244\_m4o2\_s5\_8 = 0.0059, ev  
 p245\_m4o2\_s6\_7 = 0.0026, ev  
 p246\_m5o2\_s5\_8 = 0.0137, ev  
 p247\_m5o2\_s6\_7 = 0.0060, ev  
 p248\_m6o2\_s5\_8 = 0.0032, ev  
 p249\_m6o2\_s6\_7 = 0.0032, ev  
 p250\_m7o2\_s5\_8 = -0.0176, ev  
 p251\_m10o2\_s5\_8 = 0.0145, ev  
 p252\_m10o2\_s6\_7 = 0.0138, ev  
 p253\_m14o2\_s5\_8 = 0.0200, ev  
 p254\_m14o2\_s6\_7 = -0.0073, ev  
 p255\_m20o2\_s5\_8 = 0.0062, ev  
 p256\_m20o2\_s6\_7 = -0.0017, ev  
 p257\_m24o2\_s5\_8 = 0.0131, ev  
 p258\_m24o2\_s6\_7 = -0.0068, ev  
 p259\_m29o2\_s5\_8 = 0.0103, ev  
 p260\_m29o2\_s6\_7 = 0.0008, ev  
 p261\_m33o2\_s5\_8 = -0.0016, ev  
 p262\_m33o2\_s6\_7 = -0.0027, ev  
 p263\_m38o2\_s5\_8 = 0.0063, ev  
 p264\_m38o2\_s6\_7 = 0.0111, ev  
 p265\_m54o2\_s5\_8 = 0.0103, ev  
 p266\_m54o2\_s6\_7 = 0.0055, ev  
 p267\_m5o1\_m4o1\_s2\_5 = 0.0092, ev  
 p268\_m5o1\_m4o1\_s2\_8 = 0.0309, ev  
 p269\_m4o1\_m14o1\_s2\_5 = 0.0216, ev  
 p270\_m4o1\_m14o1\_s2\_8 = -0.0382, ev  
 p271\_m5o1\_m6o1\_s8\_9 = -0.0058, ev  
 p272\_m5o1\_m7o1\_s2\_5 = 0.0331, ev  
 p273\_m5o1\_m7o1\_s2\_8 = 0.0139, ev  
 p274\_m5o1\_m14o1\_s5\_8 = -0.0324, ev  
 p275\_m5o1\_m14o1\_s6\_7 = 0.0061, ev  
 p276\_m14o1\_m6o1\_s8\_9 = 0.0061, ev  
 p277\_m20o1\_m6o1\_s5\_8 = -0.0074, ev  
 p278\_m20o1\_m6o1\_s6\_7 = 0.0015, ev  
 p279\_m38o1\_m6o1\_s5\_8 = -0.0049, ev  
 p280\_m38o1\_m6o1\_s6\_7 = -0.0026, ev

p281\_m14o1\_m7o1\_s2\_5 = 0.0305, ev  
 p282\_m14o1\_m7o1\_s2\_8 = -0.0540, ev  
 p283\_m38o1\_m20o1\_s5\_8 = -0.0162, ev  
 p284\_m38o1\_m20o1\_s6\_7 = 0.0035, ev  
 p285\_m56o1\_m38o1\_s5\_8 = 0.0176, ev  
 p286\_m56o1\_m38o1\_s6\_7 = -0.0092, ev  
 p287\_m24o1\_m5o1\_m14o1\_s2\_8 = -0.00228340, ev  
 p288\_m24o1\_m5o1\_m14o1\_s2\_5 = 0.00515890, ev  
 p289\_m5o1\_m14o1\_m29o1\_s2\_8 = -0.00283230, ev  
 p290\_m5o1\_m14o1\_m29o1\_s2\_5 = 0.00114330, ev  
 p291\_m10o1\_m5o1\_m14o1\_s2\_8 = -0.00334740, ev  
 p292\_m10o1\_m5o1\_m14o1\_s2\_5 = 0.00196120, ev  
 p293\_m56o1\_m5o1\_s8\_9 = 0.09500000, ev  
 p294\_m56o1\_m14o1\_s8\_9 = -0.08011100, ev  
 p295\_m56o1\_m5o1\_m14o1\_s8\_8 = -0.00501230, ev  
 p296\_m56o1\_m5o2\_m14o2\_s8\_8 = -0.00040690, ev  
 p297\_m5o1\_m6o1\_s8\_9 = -0.00822000, ev  
 p298\_m14o1\_m6o1\_s8\_9 = 0.00789990, ev  
 p299\_m56o1\_m5o2\_s2\_2 = 0.00560220, ev  
 p300\_m56o1\_m14o2\_s2\_2 = -0.00386880, ev  
 p301\_m38o1\_m5o2\_s2\_2 = -0.00118600, ev  
 p302\_m38o1\_m14o2\_s2\_2 = -0.00275280, ev  
 p303\_m20o1\_m5o2\_s2\_2 = -0.00191530, ev  
 p304\_m20o1\_m14o2\_s2\_2 = -0.00262070, ev  
 p305\_m5o2\_m6o1\_s2\_2 = -0.00039297, ev  
 p306\_m14o2\_m6o1\_s2\_2 = -0.00014303, ev  
 p307\_m20o1\_m5o1\_s8\_9 = -0.00810500, ev  
 p308\_m20o1\_m14o1\_s8\_9 = 0.00790300, ev

end-parameter-section

LABELS-SECTION

v1m56=morse1[1D\_56,1A\_56,1X\_56,1E\_56]  
 v2m56=morse1[2D\_56,2A\_56,2X\_56,2E\_56]  
 v3m56=morse1[3D\_56,3A\_56,3X\_56,3E\_56]  
 v4m56=morse1[4D\_56,4A\_56,4X\_56,4E\_56]  
 v5m56=morse1[5D\_56,5A\_56,5X\_56,5E\_56]  
 v6m56=morse1[6D\_56,6A\_56,6X\_56,6E\_56]  
 v7m56=morse1[7D\_56,7A\_56,7X\_56,7E\_56]

end-labels-section

```
#####
## SUPPLEMENTARY INFORMATION C
#####
#####
## HAMILTONIAN SECTION
#####
```

# HAMILTONIAN-SECTION

```
-----
modes |v2 |v4 |v5 |v6 |
modes |v7 |v10 |v12 |v14 |
modes |v20 |v24 |v29 |v33 |
modes |v38 |v54 |v56 |el
-----
```

## #kinetic energy

```
omega_2 |1 KE
omega_4 |2 KE
omega_5 |3 KE
omega_6 |4 KE
omega_7 |5 KE
omega_10 |6 KE
omega_12 |7 KE
omega_14 |8 KE
omega_20 |9 KE
omega_24 |10 KE
omega_29 |11 KE
omega_33 |12 KE
omega_38 |13 KE
omega_54 |14 KE
omega_56 |15 KE
```

## #\erOTH order

```
omega_2 |1 q^2
omega_4 |2 q^2
omega_5 |3 q^2
omega_6 |4 q^2
omega_7 |5 q^2
omega_10 |6 q^2
omega_12 |7 q^2
omega_14 |8 q^2
omega_20 |9 q^2
omega_24 |10 q^2
omega_29 |11 q^2
omega_33 |12 q^2
omega_38 |13 q^2
omega_54 |14 q^2
omega_56 |15 q^2
```

## #vertical energies

```
E1 |16 S1&1
E2 |16 S2&2
E3 |16 S3&3
E4 |16 S4&4
E5 |16 S5&5
E6 |16 S6&6
E7 |16 S7&7
E8 |16 S8&8
E9 |16 S9&9
```

## #ag mode 56 morse potential functions

```
1.0 |13 v2m56 |16 S2&2
1.0 |13 v3m56 |16 S3&3
1.0 |13 v4m56 |16 S4&4
1.0 |13 v5m56 |16 S5&5
1.0 |13 v6m56 |16 S6&6
```



1.0 |13 v7m56 |16 S7&7  
 1.0 |13 v1m56 |16 S1&1

#S0 model

1.000000*p1_m4o1_s1_1	4 q^1	16 S1&1
1.000000*p2_m9o1_s1_1	9 q^1	16 S1&1
1.000000*p3_m12o1_s1_1	12 q^1	16 S1&1
1.000000*p4_m13o1_s1_1	13 q^1	16 S1&1
1.000000*p5_m14o1_s1_1	14 q^1	16 S1&1
0.500000*p6_m1o2_s1_1	1 q^2	16 S1&1
0.500000*p7_m2o2_s1_1	2 q^2	16 S1&1
0.500000*p8_m3o2_s1_1	3 q^2	16 S1&1
0.500000*p9_m4o2_s1_1	4 q^2	16 S1&1
0.500000*p10_m5o2_s1_1	5 q^2	16 S1&1
0.500000*p11_m6o2_s1_1	6 q^2	16 S1&1
0.500000*p12_m8o2_s1_1	8 q^2	16 S1&1
0.500000*p13_m9o2_s1_1	9 q^2	16 S1&1
0.500000*p14_m10o2_s1_1	10 q^2	16 S1&1
0.500000*p15_m11o2_s1_1	11 q^2	16 S1&1
0.500000*p16_m12o2_s1_1	12 q^2	16 S1&1
0.500000*p17_m13o2_s1_1	13 q^2	16 S1&1
0.500000*p18_m14o2_s1_1	14 q^2	16 S1&1
1.000000*p19_m8o1_m3o1_s1_1	8 q^1  3 q^1	16 S1&1
1.000000*p20_m13o1_m4o1_s1_1	13 q^1  4 q^1	16 S1&1
1.000000*p21_m15o1_m4o1_s1_1	15 q^1  4 q^1	16 S1&1
1.000000*p22_m13o1_m15o1_s1_1	13 q^1  15 q^1	16 S1&1

# excited states

0.500000*p1_m2o2_s8_8	1 q^2	16 S8&8
0.041160*p2_m2o4_s8_8	1 q^4	16 S8&8
0.500000*p3_m4o2_s5_5	2 q^2	16 S5&5
0.041160*p4_m4o4_s5_5	2 q^4	16 S5&5
0.500000*p5_m4o2_s8_8	2 q^2	16 S8&8
0.041160*p6_m4o4_s8_8	2 q^4	16 S8&8
0.500000*p7_m5o2_s2_2	3 q^2	16 S2&2
0.041160*p8_m5o4_s2_2	3 q^4	16 S2&2
0.500000*p9_m5o2_s3_3	3 q^2	16 S3&3
0.041160*p10_m5o4_s3_3	3 q^4	16 S3&3
0.500000*p11_m5o2_s4_4	3 q^2	16 S4&4
0.041160*p12_m5o4_s4_4	3 q^4	16 S4&4
0.500000*p13_m5o2_s5_5	3 q^2	16 S5&5
0.041160*p14_m5o4_s5_5	3 q^4	16 S5&5
0.500000*p15_m5o2_s8_8	3 q^2	16 S8&8
0.041160*p16_m5o4_s8_8	3 q^4	16 S8&8
0.500000*p17_m7o2_s5_5	5 q^2	16 S5&5
0.041160*p18_m7o4_s5_5	5 q^4	16 S5&5
0.500000*p19_m7o2_s8_8	5 q^2	16 S8&8
0.041160*p20_m7o4_s8_8	5 q^4	16 S8&8
0.500000*p21_m14o2_s8_8	8 q^2	16 S8&8
0.041160*p22_m14o4_s8_8	8 q^4	16 S8&8
1.000000*p23_m56o1_s8_8	15 q^1	16 S8&8
0.500000*p24_m56o2_s8_8	15 q^2	16 S8&8
0.041160*p25_m56o4_s8_8	15 q^4	16 S8&8
1.000000*p26_m56o1_s9_9	15 q^1	16 S9&9
0.500000*p27_m56o2_s9_9	15 q^2	16 S9&9
0.041160*p28_m56o4_s9_9	15 q^4	16 S9&9
0.500000*p90_m2o2_s2_2	1 q^2	16 S2&2
0.500000*p91_m2o2_s3_3	1 q^2	16 S3&3
0.500000*p92_m2o2_s4_4	1 q^2	16 S4&4
0.500000*p93_m2o2_s5_5	1 q^2	16 S5&5
0.500000*p94_m2o2_s6_6	1 q^2	16 S6&6
0.500000*p95_m2o2_s7_7	1 q^2	16 S7&7
0.500000*p96_m2o2_s8_8	1 q^2	16 S8&8

0.500000*p98_m4o2_s2_2	2 q^2	16 S2&2
0.500000*p99_m4o2_s3_3	2 q^2	16 S3&3
0.500000*p100_m4o2_s4_4	2 q^2	16 S4&4
0.500000*p101_m4o2_s6_6	2 q^2	16 S6&6
0.500000*p102_m4o2_s7_7	2 q^2	16 S7&7
0.500000*p103_m4o2_s9_9	2 q^2	16 S9&9
0.500000*p105_m5o2_s3_3	3 q^2	16 S3&3
0.500000*p106_m5o2_s4_4	3 q^2	16 S4&4
0.500000*p107_m5o2_s5_5	3 q^2	16 S5&5
0.500000*p108_m5o2_s6_6	3 q^2	16 S6&6
0.500000*p109_m5o2_s7_7	3 q^2	16 S7&7
0.500000*p110_m5o2_s9_9	3 q^2	16 S9&9
0.500000*p112_m6o2_s2_2	4 q^2	16 S2&2
0.500000*p113_m6o2_s3_3	4 q^2	16 S3&3
0.500000*p114_m6o2_s4_4	4 q^2	16 S4&4
0.500000*p115_m6o2_s5_5	4 q^2	16 S5&5
0.500000*p116_m6o2_s6_6	4 q^2	16 S6&6
0.500000*p117_m6o2_s7_7	4 q^2	16 S7&7
0.500000*p118_m6o2_s8_8	4 q^2	16 S8&8
0.500000*p119_m6o2_s9_9	4 q^2	16 S9&9
0.500000*p121_m7o2_s2_2	5 q^2	16 S2&2
0.500000*p122_m7o2_s3_3	5 q^2	16 S3&3
0.500000*p123_m7o2_s4_4	5 q^2	16 S4&4
0.500000*p124_m7o2_s6_6	5 q^2	16 S6&6
0.500000*p125_m7o2_s7_7	5 q^2	16 S7&7
0.500000*p126_m7o2_s9_9	5 q^2	16 S9&9
0.500000*p128_m10o2_s2_2	6 q^2	16 S2&2
0.500000*p129_m10o2_s3_3	6 q^2	16 S3&3
0.500000*p130_m10o2_s4_4	6 q^2	16 S4&4
0.500000*p131_m10o2_s5_5	6 q^2	16 S5&5
0.500000*p132_m10o2_s6_6	6 q^2	16 S6&6
0.500000*p133_m10o2_s7_7	6 q^2	16 S7&7
0.500000*p134_m10o2_s8_8	6 q^2	16 S8&8
0.500000*p136_m14o2_s2_2	8 q^2	16 S2&2
0.500000*p137_m14o2_s3_3	8 q^2	16 S3&3
0.500000*p138_m14o2_s4_4	8 q^2	16 S4&4
0.500000*p139_m14o2_s5_5	8 q^2	16 S5&5
0.500000*p140_m14o2_s6_6	8 q^2	16 S6&6
0.500000*p141_m14o2_s7_7	8 q^2	16 S7&7
0.500000*p142_m14o2_s9_9	8 q^2	16 S9&9
0.500000*p144_m20o2_s2_2	9 q^2	16 S2&2
0.500000*p145_m20o2_s3_3	9 q^2	16 S3&3
0.500000*p146_m20o2_s4_4	9 q^2	16 S4&4
0.500000*p147_m20o2_s5_5	9 q^2	16 S5&5
0.500000*p148_m20o2_s6_6	9 q^2	16 S6&6
0.500000*p149_m20o2_s7_7	9 q^2	16 S7&7
0.500000*p150_m20o2_s8_8	9 q^2	16 S8&8
0.500000*p152_m24o2_s2_2	10 q^2	16 S2&2
0.500000*p153_m24o2_s3_3	10 q^2	16 S3&3
0.500000*p154_m24o2_s4_4	10 q^2	16 S4&4
0.500000*p155_m24o2_s5_5	10 q^2	16 S5&5
0.500000*p156_m24o2_s6_6	10 q^2	16 S6&6
0.500000*p157_m24o2_s7_7	10 q^2	16 S7&7
0.500000*p158_m24o2_s8_8	10 q^2	16 S8&8
0.500000*p160_m29o2_s2_2	11 q^2	16 S2&2
0.500000*p161_m29o2_s3_3	11 q^2	16 S3&3
0.500000*p162_m29o2_s4_4	11 q^2	16 S4&4
0.500000*p163_m29o2_s5_5	11 q^2	16 S5&5
0.500000*p164_m29o2_s6_6	11 q^2	16 S6&6
0.500000*p165_m29o2_s7_7	11 q^2	16 S7&7
0.500000*p166_m29o2_s8_8	11 q^2	16 S8&8
0.500000*p168_m33o2_s2_2	12 q^2	16 S2&2

0.500000*p169_m33o2_s3_3	12 q^2	16 S3&3
0.500000*p170_m33o2_s4_4	12 q^2	16 S4&4
0.500000*p171_m33o2_s5_5	12 q^2	16 S5&5
0.500000*p172_m33o2_s6_6	12 q^2	16 S6&6
0.500000*p173_m33o2_s7_7	12 q^2	16 S7&7
0.500000*p174_m33o2_s8_8	12 q^2	16 S8&8
0.500000*p176_m38o2_s2_2	13 q^2	16 S2&2
0.500000*p177_m38o2_s5_5	13 q^2	16 S5&5
0.500000*p178_m38o2_s6_6	13 q^2	16 S6&6
0.500000*p179_m38o2_s7_7	13 q^2	16 S7&7
0.500000*p180_m38o2_s8_8	13 q^2	16 S8&8
0.500000*p182_m54o2_s2_2	14 q^2	16 S2&2
0.500000*p183_m54o2_s3_3	14 q^2	16 S3&3
0.500000*p184_m54o2_s4_4	14 q^2	16 S4&4
0.500000*p185_m54o2_s5_5	14 q^2	16 S5&5
0.500000*p186_m54o2_s6_6	14 q^2	16 S6&6
0.500000*p187_m54o2_s7_7	14 q^2	16 S7&7
0.500000*p188_m54o2_s8_8	14 q^2	16 S8&8
#gradients (ag modes)		
1.000000*p30_m6o1_s2_2	4 q^1	16 S2&2
1.000000*p31_m6o1_s3_3	4 q^1	16 S3&3
1.000000*p32_m6o1_s4_4	4 q^1	16 S4&4
1.000000*p33_m6o1_s5_5	4 q^1	16 S5&5
1.000000*p34_m6o1_s6_6	4 q^1	16 S6&6
1.000000*p35_m6o1_s7_7	4 q^1	16 S7&7
1.000000*p36_m6o1_s8_8	4 q^1	16 S8&8
1.000000*p38_m20o1_s2_2	9 q^1	16 S2&2
1.000000*p39_m20o1_s3_3	9 q^1	16 S3&3
1.000000*p40_m20o1_s4_4	9 q^1	16 S4&4
1.000000*p41_m20o1_s5_5	9 q^1	16 S5&5
1.000000*p42_m20o1_s6_6	9 q^1	16 S6&6
1.000000*p43_m20o1_s7_7	9 q^1	16 S7&7
1.000000*p44_m20o1_s8_8	9 q^1	16 S8&8
1.000000*p46_m33o1_s2_2	12 q^1	16 S2&2
1.000000*p47_m33o1_s3_3	12 q^1	16 S3&3
1.000000*p48_m33o1_s4_4	12 q^1	16 S4&4
1.000000*p49_m33o1_s5_5	12 q^1	16 S5&5
1.000000*p50_m33o1_s6_6	12 q^1	16 S6&6
1.000000*p51_m33o1_s7_7	12 q^1	16 S7&7
1.000000*p52_m33o1_s8_8	12 q^1	16 S8&8
1.000000*p54_m38o1_s2_2	13 q^1	16 S2&2
1.000000*p55_m38o1_s3_3	13 q^1	16 S3&3
1.000000*p56_m38o1_s4_4	13 q^1	16 S4&4
1.000000*p57_m38o1_s5_5	13 q^1	16 S5&5
1.000000*p58_m38o1_s6_6	13 q^1	16 S6&6
1.000000*p59_m38o1_s7_7	13 q^1	16 S7&7
1.000000*p60_m38o1_s8_8	13 q^1	16 S8&8
1.000000*p62_m54o1_s2_2	14 q^1	16 S2&2
1.000000*p63_m54o1_s3_3	14 q^1	16 S3&3
1.000000*p64_m54o1_s4_4	14 q^1	16 S4&4
1.000000*p65_m54o1_s5_5	14 q^1	16 S5&5
1.000000*p66_m54o1_s6_6	14 q^1	16 S6&6
1.000000*p67_m54o1_s7_7	14 q^1	16 S7&7
1.000000*p68_m54o1_s8_8	14 q^1	16 S8&8
#first order coupling		
1.000000*p69_m5o1_s8_9	3 q^1	16 S8&9
1.000000*p70_m6o1_s5_8	4 q^1	16 S5&8
1.000000*p71_m6o1_s6_7	4 q^1	16 S6&7
1.000000*p72_m10o1_s2_5	6 q^1	16 S2&5
1.000000*p73_m10o1_s2_8	6 q^1	16 S2&8
1.000000*p74_m14o1_s8_9	8 q^1	16 S8&9
1.000000*p75_m20o1_s5_8	9 q^1	16 S5&8

1.000000*p76_m20o1_s6_7	9 q^1	16 S6&7
1.000000*p77_m24o1_s2_5	10 q^1	16 S2&5
1.000000*p78_m24o1_s2_8	10 q^1	16 S2&8
1.000000*p79_m29o1_s2_5	11 q^1	16 S2&5
1.000000*p80_m29o1_s2_8	11 q^1	16 S2&8
1.000000*p81_m33o1_s5_8	12 q^1	16 S5&8
1.000000*p82_m33o1_s6_7	12 q^1	16 S6&7
1.000000*p83_m38o1_s5_8	13 q^1	16 S5&8
1.000000*p84_m38o1_s6_7	13 q^1	16 S6&7
1.000000*p85_m54o1_s5_8	14 q^1	16 S5&8
1.000000*p86_m54o1_s6_7	14 q^1	16 S6&7
1.000000*p87_m56o1_s5_8	15 q^1	16 S5&8
1.000000*p88_m56o1_s6_7	15 q^1	16 S6&7
# second order coupling		
0.500000*p241_m2o2_s4_8	1 q^2	16 S4&8
0.500000*p242_m2o2_s5_8	1 q^2	16 S5&8
0.500000*p243_m2o2_s6_7	1 q^2	16 S6&7
0.500000*p244_m4o2_s5_8	2 q^2	16 S5&8
0.500000*p245_m4o2_s6_7	2 q^2	16 S6&7
0.500000*p246_m5o2_s5_8	3 q^2	16 S5&8
0.500000*p247_m5o2_s6_7	3 q^2	16 S6&7
0.500000*p248_m6o2_s5_8	4 q^2	16 S5&8
0.500000*p249_m6o2_s6_7	4 q^2	16 S6&7
0.500000*p250_m7o2_s5_8	5 q^2	16 S5&8
0.500000*p251_m10o2_s5_8	6 q^2	16 S5&8
0.500000*p252_m10o2_s6_7	6 q^2	16 S6&7
0.500000*p253_m14o2_s5_8	8 q^2	16 S5&8
0.500000*p254_m14o2_s6_7	8 q^2	16 S6&7
0.500000*p255_m20o2_s5_8	9 q^2	16 S5&8
0.500000*p256_m20o2_s6_7	9 q^2	16 S6&7
0.500000*p257_m24o2_s5_8	10 q^2	16 S5&8
0.500000*p258_m24o2_s6_7	10 q^2	16 S6&7
0.500000*p259_m29o2_s5_8	11 q^2	16 S5&8
0.500000*p260_m29o2_s6_7	11 q^2	16 S6&7
0.500000*p261_m33o2_s5_8	12 q^2	16 S5&8
0.500000*p262_m33o2_s6_7	12 q^2	16 S6&7
0.500000*p263_m38o2_s5_8	13 q^2	16 S5&8
0.500000*p264_m38o2_s6_7	13 q^2	16 S6&7
0.500000*p265_m54o2_s5_8	14 q^2	16 S5&8
0.500000*p266_m54o2_s6_7	14 q^2	16 S6&7
# modes 5 and 14		
1.000000*p190_m5o1_m14o1_s2_2	3 q^1  8 q^1	16 S2&2
1.000000*p191_m5o1_m14o1_s3_3	3 q^1  8 q^1	16 S3&3
1.000000*p192_m5o1_m14o1_s4_4	3 q^1  8 q^1	16 S4&4
1.000000*p193_m5o1_m14o1_s5_5	3 q^1  8 q^1	16 S5&5
1.000000*p194_m5o1_m14o1_s6_6	3 q^1  8 q^1	16 S6&6
1.000000*p195_m5o1_m14o1_s7_7	3 q^1  8 q^1	16 S7&7
1.000000*p196_m5o1_m14o1_s8_8	3 q^1  8 q^1	16 S8&8
1.000000*p197_m5o1_m14o1_s9_9	3 q^1  8 q^1	16 S9&9
# ag modes correlation		
1.000000*p198_m20o1_m6o1_s2_2	9 q^1  4 q^1	16 S2&2
1.000000*p199_m20o1_m6o1_s3_3	9 q^1  4 q^1	16 S3&3
1.000000*p200_m20o1_m6o1_s4_4	9 q^1  4 q^1	16 S4&4
1.000000*p201_m20o1_m6o1_s5_5	9 q^1  4 q^1	16 S5&5
1.000000*p202_m20o1_m6o1_s6_6	9 q^1  4 q^1	16 S6&6
1.000000*p203_m20o1_m6o1_s7_7	9 q^1  4 q^1	16 S7&7
1.000000*p204_m20o1_m6o1_s8_8	9 q^1  4 q^1	16 S8&8
1.000000*p206_m38o1_m6o1_s2_2	13 q^1  4 q^1	16 S2&2
1.000000*p207_m38o1_m6o1_s3_3	13 q^1  4 q^1	16 S3&3
1.000000*p208_m38o1_m6o1_s4_4	13 q^1  4 q^1	16 S4&4
1.000000*p209_m38o1_m6o1_s5_5	13 q^1  4 q^1	16 S5&5
1.000000*p210_m38o1_m6o1_s6_6	13 q^1  4 q^1	16 S6&6

1.000000*p211_m38o1_m6o1_s7_7	13 q^1	4 q^1	16 S7&7
1.000000*p212_m38o1_m6o1_s8_8	13 q^1	4 q^1	16 S8&8
1.000000*p214_m56o1_m6o1_s2_2	15 q^1	4 q^1	16 S2&2
1.000000*p215_m56o1_m6o1_s3_3	15 q^1	4 q^1	16 S3&3
1.000000*p216_m56o1_m6o1_s4_4	15 q^1	4 q^1	16 S4&4
1.000000*p217_m56o1_m6o1_s5_5	15 q^1	4 q^1	16 S5&5
1.000000*p218_m56o1_m6o1_s6_6	15 q^1	4 q^1	16 S6&6
1.000000*p219_m56o1_m6o1_s7_7	15 q^1	4 q^1	16 S7&7
1.000000*p220_m56o1_m6o1_s8_8	15 q^1	4 q^1	16 S8&8
1.000000*p221_m38o1_m20o1_s2_2	13 q^1	9 q^1	16 S2&2
1.000000*p222_m38o1_m20o1_s3_3	13 q^1	9 q^1	16 S3&3
1.000000*p223_m38o1_m20o1_s4_4	13 q^1	9 q^1	16 S4&4
1.000000*p224_m38o1_m20o1_s5_5	13 q^1	9 q^1	16 S5&5
1.000000*p225_m38o1_m20o1_s6_6	13 q^1	9 q^1	16 S6&6
1.000000*p226_m38o1_m20o1_s7_7	13 q^1	9 q^1	16 S7&7
1.000000*p227_m56o1_m20o1_s2_2	15 q^1	9 q^1	16 S2&2
1.000000*p228_m56o1_m20o1_s3_3	15 q^1	9 q^1	16 S3&3
1.000000*p229_m56o1_m20o1_s4_4	15 q^1	9 q^1	16 S4&4
1.000000*p230_m56o1_m20o1_s5_5	15 q^1	9 q^1	16 S5&5
1.000000*p231_m56o1_m20o1_s6_6	15 q^1	9 q^1	16 S6&6
1.000000*p232_m56o1_m20o1_s7_7	15 q^1	9 q^1	16 S7&7
1.000000*p234_m56o1_m38o1_s2_2	15 q^1	13 q^1	16 S2&2
1.000000*p235_m56o1_m38o1_s3_3	15 q^1	13 q^1	16 S3&3
1.000000*p236_m56o1_m38o1_s4_4	15 q^1	13 q^1	16 S4&4
1.000000*p237_m56o1_m38o1_s5_5	15 q^1	13 q^1	16 S5&5
1.000000*p238_m56o1_m38o1_s6_6	15 q^1	13 q^1	16 S6&6
1.000000*p239_m56o1_m38o1_s7_7	15 q^1	13 q^1	16 S7&7
1.000000*p240_m56o1_m38o1_s8_8	15 q^1	13 q^1	16 S8&8
1.000000*p277_m20o1_m6o1_s5_8	9 q^1	4 q^1	16 S5&8
1.000000*p278_m20o1_m6o1_s6_7	9 q^1	4 q^1	16 S6&7
1.000000*p279_m38o1_m6o1_s5_8	13 q^1	4 q^1	16 S5&8
1.000000*p280_m38o1_m6o1_s6_7	13 q^1	4 q^1	16 S6&7
1.000000*p276_m14o1_m6o1_s8_9	8 q^1	4 q^1	16 S8&9
1.000000*p283_m38o1_m20o1_s5_8	13 q^1	9 q^1	16 S5&8
1.000000*p284_m38o1_m20o1_s6_7	13 q^1	9 q^1	16 S6&7
1.000000*p285_m56o1_m38o1_s5_8	15 q^1	13 q^1	16 S5&8
1.000000*p286_m56o1_m38o1_s6_7	15 q^1	13 q^1	16 S6&7

# coupling states along modes 4 and 7 (b2g) with 5 and 14i (b3g)

1.000000*p267_m5o1_m4o1_s2_5	3 q^1	2 q^1	16 S2&5
1.000000*p268_m5o1_m4o1_s2_8	3 q^1	2 q^1	16 S2&8
1.000000*p269_m4o1_m14o1_s2_5	2 q^1	8 q^1	16 S2&5
1.000000*p270_m4o1_m14o1_s2_8	2 q^1	8 q^1	16 S2&8
1.000000*p271_m5o1_m6o1_s8_9	3 q^1	4 q^1	16 S8&9
1.000000*p272_m5o1_m7o1_s2_5	3 q^1	5 q^1	16 S2&5
1.000000*p273_m5o1_m7o1_s2_8	3 q^1	5 q^1	16 S2&8
1.000000*p274_m5o1_m14o1_s5_8	3 q^1	8 q^1	16 S5&8
1.000000*p275_m5o1_m14o1_s6_7	3 q^1	8 q^1	16 S6&7
1.000000*p281_m14o1_m7o1_s2_5	8 q^1	5 q^1	16 S2&5
1.000000*p282_m14o1_m7o1_s2_8	8 q^1	5 q^1	16 S2&8
# modes 5 and 14 (b3g) with ag			
1.000000*p293_m56o1_m5o1_s8_9	15 q^1	3 q^1	16 S8&9
1.000000*p294_m56o1_m14o1_s8_9	15 q^1	8 q^1	16 S8&9
1.000000*p297_m5o1_m6o1_s8_9	3 q^1	4 q^1	16 S8&9
1.000000*p298_m14o1_m6o1_s8_9	8 q^1	4 q^1	16 S8&9
1.000000*p299_m56o1_m5o2_s2_2	15 q^1	3 q^2	16 S2&2
1.000000*p300_m56o1_m14o2_s2_2	15 q^1	8 q^2	16 S2&2
1.000000*p301_m38o1_m5o2_s2_2	13 q^1	3 q^2	16 S2&2
1.000000*p302_m38o1_m14o2_s2_2	13 q^1	8 q^2	16 S2&2
1.000000*p303_m20o1_m5o2_s2_2	9 q^1	3 q^2	16 S2&2
1.000000*p304_m20o1_m14o2_s2_2	9 q^1	8 q^2	16 S2&2
1.000000*p305_m5o2_m6o1_s2_2	3 q^2	4 q^1	16 S2&2

1.000000*p306_m14o2_m6o1_s2_2	8 q <sup>2</sup>	4 q <sup>1</sup>		16 S2&2
1.000000*p307_m20o1_m5o1_s8_9	9 q <sup>1</sup>	3 q <sup>1</sup>		16 S8&9
1.000000*p308_m20o1_m14o1_s8_9	9 q <sup>1</sup>	8 q <sup>1</sup>		16 S8&9
# coupling states along b1g modes (10,24,29) with b3g (5,14)				
1.000000*p287_m24o1_m5o1_m14o1_s2_8	10 q <sup>1</sup>	3 q <sup>1</sup>	8 q <sup>1</sup>	16 S2&8
1.000000*p288_m24o1_m5o1_m14o1_s2_5	10 q <sup>1</sup>	3 q <sup>1</sup>	8 q <sup>1</sup>	16 S2&5
1.000000*p289_m5o1_m14o1_m29o1_s2_8	3 q <sup>1</sup>	8 q <sup>1</sup>	11 q <sup>1</sup>	16 S2&8
1.000000*p290_m5o1_m14o1_m29o1_s2_5	3 q <sup>1</sup>	8 q <sup>1</sup>	11 q <sup>1</sup>	16 S2&5
1.000000*p291_m10o1_m5o1_m14o1_s2_8	6 q <sup>1</sup>	3 q <sup>1</sup>	8 q <sup>1</sup>	16 S2&8
1.000000*p292_m10o1_m5o1_m14o1_s2_5	6 q <sup>1</sup>	3 q <sup>1</sup>	8 q <sup>1</sup>	16 S2&5
1.000000*p295_m56o1_m5o1_m14o1_s8_8	15 q <sup>1</sup>	3 q <sup>1</sup>	8 q <sup>1</sup>	16 S8&8
1.000000*p296_m56o1_m5o2_m14o2_s8_8	15 q <sup>1</sup>	3 q <sup>2</sup>	8 q <sup>2</sup>	16 S8&8

END-HAMILTONIAN-SECTION

END-OPERATOR

#####

# Bibliography

- [1] J. M. L. Pecourt, J. Peon, and B. Kohler, “Ultrafast internal conversion of electronically excited rna and dna nucleosides in water,” *Journal of the American Chemical Society*, vol. 122, no. 38, pp. 9348–9349, 2000.
- [2] A. Stolow, “The three pillars of photo-initiated quantum molecular dynamics,” *Faraday Discussions*, vol. 163, pp. 9–32, 2013.
- [3] H. Niikura, F. Legare, R. Hasbani, A. D. Bandrauk, M. Y. Ivanov, D. M. Villeneuve, and P. B. Corkum, “Sub-laser-cycle electron pulses for probing molecular dynamics,” *Nature*, vol. 417, no. 6892, pp. 917–922, 2002.
- [4] Y. L. Yung, M. Allen, and J. P. Pinto, “Photochemistry of the atmosphere of titan - comparison between model and observations,” *Astrophysical Journal Supplement Series*, vol. 55, no. 3, pp. 465–506, 1984.
- [5] M. J. Bearpark, F. Bernardi, S. Clifford, M. Olivucci, M. A. Robb, B. R. Smith, and T. Vreven, “The azulene s-1 state decays via a conical intersection: A casscf study with mmvb dynamics,” *Journal of the American Chemical Society*, vol. 118, no. 1, pp. 169–175, 1996.
- [6] D. S. N. Parker, R. S. Minns, T. J. Penfold, G. A. Worth, and H. H. Fielding, “Ultrafast dynamics of the s-1 excited state of benzene,” *Chemical Physics Letters*, vol. 469, no. 1-3, pp. 43–47, 2009.

- 
- [7] J. von Neumann and E. Wigner, "Concerning the behaviour of eigenvalues in adiabatic processes," *Physikalische Zeitschrift*, vol. 30, pp. 467–470, 1929.
- [8] B. O. Roos, K. Andersson, M. P. Fulscher, P. A. Malmqvist, L. SerranoAndres, K. Pierloot, and M. Merchán, "Multiconfigurational perturbation theory: Applications in electronic spectroscopy," *Advances in Chemical Physics, Vol Xciii*, vol. 93, pp. 219–331, 1996.
- [9] A. H. Zewail, "Femtochemistry. past, present, and future," *Pure and Applied Chemistry*, vol. 72, no. 12, pp. 2219–2231, 2000.
- [10] M. A. Robb, F. Bernardi, and M. Olivucci, "Conical intersections as a mechanistic feature of organic-photochemistry," *Pure and Applied Chemistry*, vol. 67, no. 5, pp. 783–789, 1995.
- [11] W. Fuss, S. Lochbrunner, A. M. Müller, T. Schikarski, W. E. Schmid, and S. A. Trushin, "Pathway approach to ultrafast photochemistry: potential surfaces, conical intersections and isomerizations of small polyenes," *Chemical Physics*, vol. 232, no. 1-2, pp. 161–174, 1998.
- [12] M. Chatteraj, B. A. King, G. U. Bublitz, and S. G. Boxer, "Ultra-fast excited state dynamics in green fluorescent protein: Multiple states and proton transfer," *Proceedings of the National Academy of Sciences of the United States of America*, vol. 93, no. 16, pp. 8362–8367, 1996.
- [13] S. F. Swallen, R. Kopelman, J. S. Moore, and C. Devadoss, "Dendrimer photoantenna supermolecules: energetic funnels, exciton hopping and correlated excimer formation," *Journal of Molecular Structure*, vol. 485, pp. 585–597, 1999.



- 
- [14] M. A. Fox, "Polymeric and supramolecular arrays for directional energy and electron-transport over macroscopic distances," *Accounts of Chemical Research*, vol. 25, no. 12, pp. 569–574, 1992.
- [15] D. Nozaki and K. Yoshizawa, "Molecular orbital engineering of single-molecular light emission," *Chemical Physics Letters*, vol. 394, no. 1-3, pp. 194–197, 2004.
- [16] M. Baer, "Adiabatic and diabatic representations for atom-molecule collisions - treatment of collinear arrangement," *Chemical Physics Letters*, vol. 35, no. 1, pp. 112–118, 1975.
- [17] H. A. Jahn and E. Teller, "Stability of polyatomic molecules in degenerate electronic states. i. orbital degeneracy," *Proceedings of the Royal Society of London Series a-Mathematical and Physical Sciences*, vol. 161, no. A905, pp. 220–235, 1937.
- [18] D. J. Tannor, "Jahn-teller effects in the photodissociation of ozone," *Journal of the American Chemical Society*, vol. 111, no. 8, pp. 2772–2776, 1989.
- [19] V. Kokoouline and C. H. Greene, "Photofragmentation of the h-3 molecule, including jahn-teller coupling effects," *Physical Review A*, vol. 69, no. 3, 2004.
- [20] G. A. Worth, M. A. Robb, and B. Lasorne, "Solving the time-dependent schrodinger equation for nuclear motion in one step: direct dynamics of non-adiabatic systems," *Molecular Physics*, vol. 106, no. 16-18, pp. 2077–2091, 2008.
- [21] M. H. Beck, A. Jackle, G. A. Worth, and H. D. Meyer, "The multiconfiguration time-dependent hartree (mctdh) method: a highly efficient

- algorithm for propagating wavepackets,” *Physics Reports-Review Section of Physics Letters*, vol. 324, no. 1, pp. 1–105, 2000.
- [22] L. S. Cederbaum, H. Koppel, and W. Domcke, “Multimode vibronic coupling effects in molecules,” *International Journal of Quantum Chemistry*, vol. 20, pp. 251–267, 1981.
- [23] T. M. Ticich, M. D. Likar, H. R. Dubal, L. J. Butler, and F. F. Crim, “Vibrationally mediated photodissociation of hydrogen-peroxide,” *Journal of Chemical Physics*, vol. 87, no. 10, pp. 5820–5829, 1987.
- [24] D. M. Bishop, *Group Theory and Chemistry*. Oxford University Press, 1973.
- [25] P. R. Bunker and P. Jensen, *Fundamentals of molecular symmetry*. Institute of Physics, 2005.
- [26] M. Baer, “Beyond born-oppenheimer, electronic nonadiabatic coupling terms and conical intersections,” 2006.
- [27] C. A. Mead and D. G. Truhlar, “Conditions for the definition of a strictly diabatic electronic basis for molecular-systems,” *Journal of Chemical Physics*, vol. 77, no. 12, pp. 6090–6098, 1982.
- [28] G. A. Worth and L. S. Cederbaum, “Beyond born-oppenheimer: Molecular dynamics through a conical intersection,” *Annual Review of Physical Chemistry*, vol. 55, pp. 127–158, 2004.
- [29] P. Garcia-Fernandez and I. B. Bersuker, “Pseudo jahn-teller origin of bending distortions in renner-teller molecules and its spectroscopic implications,” *International Journal of Quantum Chemistry*, vol. 112, no. 18, pp. 3025–3032, 2012.

- 
- [30] A. Szabo and N. S. Ostlund, *Modern quantum chemistry : introduction to advanced electronic structure theory*. Free Press ; Collier Macmillan, 1982.
- [31] T. Helgaker, P. Jørgensen, and J. Olsen, *Molecular electronic-structure theory*. John Wiley and Sons, 2000.
- [32] P. Hohenberg and W. Kohn, “Inhomogeneous electron gas,” *Physical Review B*, vol. 136, no. 3B, pp. B864–+, 1964.
- [33] A. D. Becke, “Density-functional thermochemistry .3. the role of exact exchange,” *Journal of Chemical Physics*, vol. 98, no. 7, pp. 5648–5652, 1993.
- [34] C. T. Lee, W. T. Yang, and R. G. Parr, “Development of the collesalvetti correlation-energy formula into a functional of the electron-density,” *Physical Review B*, vol. 37, no. 2, pp. 785–789, 1988.
- [35] S. Grimme and M. Waletzke, “A combination of kohn-sham density functional theory and multi-reference configuration interaction methods,” *Journal of Chemical Physics*, vol. 111, no. 13, pp. 5645–5655, 1999.
- [36] F. R. W. Byron, Frederick W., *Mathematics of classical and quantum physics*. Dover, 1969.
- [37] H. Meyer, “Theoretische chemie ss 2010. introduction to mctdh. lecture notes,” 2011.
- [38] A. Raab, G. A. Worth, H. D. Meyer, and L. S. Cederbaum, “Molecular dynamics of pyrazine after excitation to the s(2) electronic state using a realistic 24-mode model hamiltonian,” *Journal of Chemical Physics*, vol. 110, no. 2, pp. 936–946, 1999.

- 
- [39] D. B. Fogel, “An introduction to simulated evolutionary optimization,” *Ieee Transactions on Neural Networks*, vol. 5, no. 1, pp. 3–14, 1994.
- [40] L. B. Booker, D. E. Goldberg, and J. H. Holland, “Classifier systems and genetic algorithms,” *Artificial Intelligence*, vol. 40, no. 1-3, pp. 235–282, 1989.
- [41] T. A. El-Mihoub, A. A. Hopgood, L. Nolle, and A. Battersby, “Self-adaptive baldwinian search in hybrid genetic algorithms,” *Computational Intelligence, Theory and Application*, pp. 597–602, 2006.
- [42] M. Hansen, A. Ostermeier, and Ieee, “Adapting arbitrary normal mutation distributions in evolution strategies: The covariance matrix adaptation,” *1996 Ieee International Conference on Evolutionary Computation (Icec '96), Proceedings Of*, pp. 312–317, 1996.
- [43] N. Hansen and A. Ostermeier, “Completely derandomized self-adaptation in evolution strategies,” *Evolutionary Computation*, vol. 9, no. 2, pp. 159–195, 2001.
- [44] N. Hansen, “The cma evolution strategy: A tutorial,” 2011.
- [45] H.-J. Werner, P. J. Knowles, G. Knizia, F. R. Manby, M. Schütz, P. Celani, T. Korona, R. Lindh, A. Mitrushenkov, G. Rauhut, K. R. Shamasundar, T. B. Adler, R. D. Amos, A. Bernhardsson, A. Berning, D. L. Cooper, M. J. O. Deegan, A. J. Dobbyn, F. Eckert, E. Goll, C. Hampel, A. Hesselmann, G. Hetzer, T. Hrenar, G. Jansen, C. Köppl, Y. Liu, A. W. Lloyd, R. A. Mata, A. J. May, S. J. McNicholas, W. Meyer, M. E. Mura, A. Nicklass, D. P. O'Neill, P. Palmieri, D. Peng, K. Pflüger, R. Pitzer, M. Reiher, T. Shiozaki, H. Stoll, A. J. Stone,

- R. Tarroni, T. Thorsteinsson, and M. Wang, “Molpro, version 2012.1, a package of ab initio programs,” 2012.
- [46] T. Bally and S. Masamune, “Cyclobutadiene,” *Tetrahedron*, vol. 36, no. 3, pp. 343–370, 1980.
- [47] S. Koseki and A. Toyota, “Energy component analysis of the pseudo-jahn-teller effect in the ground and electronically excited states of the cyclic conjugated hydrocarbons: Cyclobutadiene, benzene, and cyclooctatetraene,” *Journal of Physical Chemistry A*, vol. 101, no. 31, pp. 5712–5718, 1997.
- [48] T. Saito, S. Nishihara, Y. Kitagawa, T. Kawakami, S. Yamanaka, M. Okumura, and K. Yamaguchi, “A broken-symmetry study on the automerization of cyclobutadiene. comparison with uno- and dno-mrcc methods,” *Chemical Physics Letters*, vol. 498, no. 4-6, pp. 253–258, 2010.
- [49] P. B. Karadakov, “Ground- and excited-state aromaticity and antiaromaticity in benzene and cyclobutadiene,” *Journal of Physical Chemistry A*, vol. 112, no. 31, pp. 7303–7309, 2008.
- [50] F. Dijkstra, J. H. Van Lenthe, R. W. A. Havenith, and L. W. Jenneskens, “Valence bond descriptions of benzene and cyclobutadiene and their counterparts with localized bonds,” *International Journal of Quantum Chemistry*, vol. 91, no. 4, pp. 566–574, 2003.
- [51] D. W. Whitman and B. K. Carpenter, “Limits on the activation parameters for automerization of cyclobutadiene-1,2-d<sub>2</sub>,” *Journal of the American Chemical Society*, vol. 104, no. 23, pp. 6473–6474, 1982.

- 
- [52] K. Nakamura, Y. Osamura, and S. Iwata, "2nd-order jahn-teller effect of cyclobutadiene in low-lying states - an mcsf study," *Chemical Physics*, vol. 136, no. 1, pp. 67–77, 1989.
- [53] S. Saddique and G. A. Worth, "Applying the vibronic coupling model hamiltonian to the photoelectron spectrum of cyclobutadiene," *Chemical Physics*, vol. 329, no. 1-3, pp. 99–108, 2006.
- [54] T. Wang, S. V. Levchenko, and A. I. Krylov, "Analytic gradients for the eom-sf-ccsd and eom-ee-ccsd methods: Theory and applications," *Abstracts of Papers of the American Chemical Society*, vol. 228, pp. U252–U252, 2004.
- [55] M. Sumita and K. Saito, "Tetra-radical and ionic s-1/s-0 conical intersections of cyclobutadiene," *Chemical Physics*, vol. 371, no. 1-3, pp. 30–35, 2010.
- [56] B. R. Arnold and J. Michl, "Ultraviolet and polarized infrared-spectroscopy of matrix-isolated cyclobutadiene and its isotopomers," *Journal of Physical Chemistry*, vol. 97, no. 50, pp. 13348–13354, 1993.
- [57] M. Eckert-Maksic, M. Vazdar, M. Barbatti, H. Lischka, and Z. B. Maksic, "Automerization reaction of cyclobutadiene and its barrier height: An ab initio benchmark multireference average-quadratic coupled cluster study," *Journal of Chemical Physics*, vol. 125, no. 6, pp. 064310–064320, 2006.
- [58] D. W. Kohn and P. Chen, "Vibrational structure in the photoelectron-spectrum of cyclobutadiene as a probe of structure," *Journal of the American Chemical Society*, vol. 115, no. 7, pp. 2844–2848, 1993.

- 
- [59] W. T. Borden, E. R. Davidson, and D. Feller, "The potential surface for the cyclobutadiene radical cation," *Journal of the American Chemical Society*, vol. 103, no. 19, pp. 5725–5729, 1981.
- [60] J. Kreile, N. Munzel, A. Schweig, and H. Specht, "Uv photoelectron-spectrum of cyclobutadiene - free cyclobutadiene stable up to high-temperatures," *Chemical Physics Letters*, vol. 124, no. 2, pp. 140–146, 1986.
- [61] P. Carsky, R. J. Bartlett, G. Fitzgerald, J. Noga, and V. Spirko, "Ab-initio calculations on the energy of activation and tunneling in the automerization of cyclobutadiene," *Journal of Chemical Physics*, vol. 89, no. 5, pp. 3008–3015, 1988.
- [62] M. Roeselova, T. Bally, P. Jungwirth, and P. Carsky, "Cyclobutadiene radical-cation - an ab-initio study of the jahn-teller surface," *Chemical Physics Letters*, vol. 234, no. 4-6, pp. 395–404, 1995.
- [63] D. I. Lyakh, V. F. Lotrich, and R. J. Bartlett, "The 'tailored' ccscd(t) description of the automerization of cyclobutadiene," *Chemical Physics Letters*, vol. 501, no. 4-6, pp. 166–171, 2011.
- [64] X. Li and J. Paldus, "Accounting for the exact degeneracy and quasidegeneracy in the automerization of cyclobutadiene via multireference coupled-cluster methods," *Journal of Chemical Physics*, vol. 131, no. 11, pp. 114103–11413, 2009.
- [65] K. Bhaskaran-Nair, O. Demel, and J. Pittner, "Multireference state-specific mukherjee's coupled cluster method with noniterative triexcitations," *Journal of Chemical Physics*, vol. 129, no. 18, pp. 3125–3128, 2008.

- [66] J. Shen, T. Fang, S. Li, and Y. Jiang, “Performance of block correlated coupled cluster method with the casscf reference function for the prediction of activation barriers, spectroscopic constants in diatomic molecules, and singlet-triplet gaps in diradicals,” *Journal of Physical Chemistry A*, vol. 112, no. 48, pp. 12518–12525, 2008.
- [67] U. S. Mahapatra, S. Chattopadhyay, and R. K. Chaudhuri, “Second-order state-specific multireference moller plesset perturbation theory: Application to energy surfaces of diimide, ethylene, butadiene, and cyclobutadiene,” *Journal of Computational Chemistry*, vol. 32, no. 2, pp. 325–337, 2011.
- [68] M. J. Frisch, G. W. Trucks, H. B. Schlegel, G. E. Scuseria, M. A. Robb, J. R. Cheeseman, J. A. Montgomery, Jr., T. Vreven, K. N. Kudin, J. C. Burant, J. M. Millam, S. S. Iyengar, J. Tomasi, V. Barone, B. Mennucci, M. Cossi, G. Scalmani, N. Rega, G. A. Petersson, H. Nakatsuji, M. Hada, M. Ehara, K. Toyota, R. Fukuda, J. Hasegawa, M. Ishida, T. Nakajima, Y. Honda, O. Kitao, H. Nakai, M. Klene, X. Li, J. E. Knox, H. P. Hratchian, J. B. Cross, V. Bakken, C. Adamo, J. Jaramillo, R. Gomperts, R. E. Stratmann, O. Yazyev, A. J. Austin, R. Cammi, C. Pomelli, J. W. Ochterski, P. Y. Ayala, K. Morokuma, G. A. Voth, P. Salvador, J. J. Dannenberg, V. G. Zakrzewski, S. Dapprich, A. D. Daniels, M. C. Strain, O. Farkas, D. K. Malick, A. D. Rabuck, K. Raghavachari, J. B. Foresman, J. V. Ortiz, Q. Cui, A. G. Baboul, S. Clifford, J. Cioslowski, B. B. Stefanov, G. Liu, A. Liashenko, P. Piskorz, I. Komaromi, R. L. Martin, D. J. Fox, T. Keith, M. A. Al-Laham, C. Y. Peng, A. Nanayakkara, M. Challacombe, P. M. W. Gill, B. Johnson, W. Chen, M. W. Wong, C. Gonzalez, and J. A. Pople, “Gaussian 03, Revision C.02.”



- 
- [69] A. Viel and W. Einfeld, “Effects of higher order jahn-teller coupling on the nuclear dynamics,” *Journal of Chemical Physics*, vol. 120, no. 10, pp. 4603–4613, 2004.
- [70] W. Einfeld and A. Viel, “Higher order (a+e)circle times e pseudo-jahn-teller coupling,” *Journal of Chemical Physics*, vol. 122, no. 20, pp. 204317–204326, 2005.
- [71] F. Gieres, *Symmetries in Physics*:. Editions Frontières, 1997.
- [72] W. Stein *et al.*, *Sage Mathematics Software (Version x.y.z)*. The Sage Development Team, 2014.
- [73] S. L. Altmann and P. Herzog, *Point-Group Theory Tables*. 2011.
- [74] D. Opalka and W. Domcke, “High-order expansion of t(2)xt(2) jahn-teller potential-energy surfaces in tetrahedral molecules,” *Journal of Chemical Physics*, vol. 132, no. 15, pp. 134–138, 2010.
- [75] R. P. Schmid, T. ArusiParpar, R. J. Li, I. Bar, and S. Rosenwaks, “Photodissociation of rovibrationally excited c2h2: Observation of two pathways,” *Journal of Chemical Physics*, vol. 107, no. 2, pp. 385–391, 1997.
- [76] C. K. Ingold and G. W. King, “Excited states of acetylene .1. possibilities of interaction between sigma-bond hybridisation and pi-electron excitation with resulting changes of shape during transitions,” *Journal of the Chemical Society*, vol. 0, no. 549, pp. 2702–2704, 1953.
- [77] J. K. Lundberg, Y. Q. Chen, J. P. Pique, and R. W. Field, “Ultraviolet optical double-resonance study of the predissociated (c)over-tilde-’lag state of acetylene,” *Journal of Molecular Spectroscopy*, vol. 156, no. 1, pp. 104–122, 1992.

- 
- [78] T. R. Fletcher and S. R. Leone, "Photodissociation dynamics of  $\text{C}_2\text{H}_2$  at 193-nm - vibrational distributions of the  $\text{CCH}$  radical and the rotational state distribution of the  $\text{a}$ -approximately(010) state by time-resolved fourier-transform infrared-emission," *Journal of Chemical Physics*, vol. 90, no. 2, pp. 871–879, 1989.
- [79] T. Nakayama and K. Watanabe, "Absorption + photoionization coefficients of acetylene propyne + 1-butyne," *Journal of Chemical Physics*, vol. 40, no. 2, pp. 558–, 1964.
- [80] K. Malsch, G. Hohlneicher, R. Schork, and H. Koppel, "A quantum dynamical examination of the vibronic structure of singlet and triplet spectra of acetylene," *Physical Chemistry Chemical Physics*, vol. 3, no. 24, pp. 5393–5407, 2001.
- [81] F. Laruelle, S. Boye-Peronne, D. Gauyacq, and J. Lievin, "Revisiting mulliken's concepts about rydberg states and rydberg-valence interactions from large-scale ab initio calculations on the acetylene molecule," *Journal of Physical Chemistry A*, vol. 113, no. 47, pp. 13210–13220, 2009.
- [82] B. Schubert, H. Koppel, and H. Lischka, "A wave-packet simulation of the low-lying singlet electronic transitions of acetylene," *Journal of Chemical Physics*, vol. 122, no. 18, pp. 184312–184321, 2005.
- [83] Q. Cui and K. Morokuma, "Ab initio mo studies on the photodissociation of  $\text{C}_2\text{H}_2$  from the  $\text{s-1}((1)\text{a(u)})$  state .2. mechanism involving triplet states," *Chemical Physics Letters*, vol. 272, no. 5-6, pp. 319–327, 1997.
- [84] H. Koepfel, B. Schubert, and H. Lischka, "Conical intersections and strong nonadiabatic coupling effects in singlet-excited acetylene: An ab

- initio quantum dynamical study,” *Chemical Physics*, vol. 343, no. 2-3, pp. 319–328, 2008.
- [85] L. Liu and J. T. Muckerman, “Vibrational eigenvalues and eigenfunctions for planar acetylene by wave-packet propagation, and its mode-selective infrared excitation,” *Journal of Chemical Physics*, vol. 107, no. 9, pp. 3402–3416, 1997.
- [86] Y. Liu, I. B. Bersuker, W. Zou, and J. E. Boggs, “Pseudo jahn-teller versus renner-teller effects in the instability of linear molecules,” *Chemical Physics*, vol. 376, no. 1-3, pp. 30–35, 2010.
- [87] Q. Cui, K. Morokuma, and J. F. Stanton, “Ab initio mo studies on the photodissociation of c2h2 from the s-1((1)a(u)) state. non-adiabatic effects and s-t interaction,” *Chemical Physics Letters*, vol. 263, no. 1-2, pp. 46–53, 1996.
- [88] S. J. Humphrey, C. G. Morgan, A. M. Wodtke, K. L. Cunningham, S. Drucker, and R. W. Field, “Laser excited metastable states of acetylene in the 5.5-5.7 ev region,” *Journal of Chemical Physics*, vol. 107, no. 1, pp. 49–53, 1997.
- [89] A. Haijima, M. Fujii, and M. Ito, “Predissociation of the acetylene a1au state and its mechanism,” *Journal of Chemical Physics*, vol. 92, no. 2, pp. 959–968, 1990.
- [90] D. H. Mordaunt, M. N. R. Ashfold, R. N. Dixon, P. Loffler, L. Schnieder, and K. H. Welge, “Near threshold photodissociation of acetylene,” *Journal of Chemical Physics*, vol. 108, no. 2, pp. 519–526, 1998.

- 
- [91] P. Dupre, R. Jost, M. Lombardi, P. G. Green, E. Abramson, and R. W. Field, "Anomalous behavior of the anticrossing density as a function of excitation-energy in the c2h2 molecule," *Chemical Physics*, vol. 152, no. 3, pp. 293–318, 1991.
- [92] K. L. Bittinger, W. L. Virgo, and R. W. Field, "Spectral signatures of inter-system crossing mediated by energetically distant doorway levels: Examples from the acetylene s-1 state," *Journal of Physical Chemistry A*, vol. 115, no. 43, pp. 11921–11943, 2011.
- [93] M. Fujii, S. Tanabe, Y. Okuzawa, and M. Ito, "Ir-uv double-resonance spectrum of acetylene below and above the predissociation threshold," *Laser Chemistry*, vol. 14, no. 1-3, pp. 161–182, 1994.
- [94] Y. Ganot, A. Golan, X. Z. Sheng, S. Rosenwaks, and I. Bar, "Non-adiabatic dissociation of rovibrationally excited acetylene," *Physical Chemistry Chemical Physics*, vol. 5, no. 24, pp. 5399–5404, 2003.
- [95] E. Ventura, M. Dallos, and H. Lischka, "The valence-excited states t-1-t-4 and s-1-s-2 of acetylene: A high-level mr-cisd and mr-aqcc investigation of stationary points, potential energy surfaces, and surface crossings," *Journal of Chemical Physics*, vol. 118, no. 4, pp. 1702–1713, 2003.
- [96] S. H. S. Wilson, C. L. Reed, D. H. Mordaunt, M. N. R. Ashfold, and M. Kawasaki, "Near-threshold photodissociation of c2h2, c2hd, and c2d2 studied by h(d) atom photofragment translational spectroscopy," *Bulletin of the Chemical Society of Japan*, vol. 69, no. 1, pp. 71–76, 1996.

- 
- [97] A. M. Wodtke and Y. T. Lee, "Photodissociation of acetylene at 193.3 nm," *Journal of Physical Chemistry*, vol. 89, no. 22, pp. 4744–4751, 1985.
- [98] J. Zhang, C. W. Riehn, M. Dulligan, and C. Wittig, "Propensities toward  $c2h((a)\text{over-tilde}(2)\pi)$  in acetylene photodissociation," *Journal of Chemical Physics*, vol. 103, no. 15, pp. 6815–6818, 1995.
- [99] R. P. Schmid, Y. Ganot, T. Arusi-Parpar, R. J. Li, I. Bar, and S. Rosenwaks, *State-selective dissociation of acetylene isotopomers*, vol. 3271, pp. 28–35. 1998.
- [100] Y. Ganot, X. Z. Sheng, I. Bar, and S. Rosenwaks, "Differing reactivities in the predissociation of acetylene isotopomers pre-excited with three c-h stretching quanta," *Chemical Physics Letters*, vol. 361, no. 1-2, pp. 175–181, 2002.
- [101] M. N. R. Ashfold, G. A. King, D. Murdock, M. G. D. Nix, T. A. A. Oliver, and A. G. Sage, " $\pi$  sigma\* excited states in molecular photochemistry," *Physical Chemistry Chemical Physics*, vol. 12, no. 6, pp. 1218–1238, 2010.
- [102] K. Malsch, R. Rebentisch, P. Swiderek, and G. Hohlneicher, "Excited states of acetylene: a caspt2 study," *Theoretical Chemistry Accounts*, vol. 100, no. 1-4, pp. 171–182, 1998.
- [103] N. C. Handy, "The derivation of vibration-rotation kinetic-energy operators, in internal coordinates," *Molecular Physics*, vol. 61, no. 1, pp. 207–223, 1987.

- 
- [104] F. S. Crawford, "Radial kinetic energy term in schrodinger equation for central force," *American Journal of Physics*, vol. 32, no. 8, pp. 611–, 1964.
- [105] Z. Chernia, T. Livneh, I. Pri-Bar, and J. E. Koresh, "Mode assignment for linear phenyl acetylene sequence: phenylacetylene, diphenylacetylene and 1,4-di(phenylethynyl)benzene," *Vibrational Spectroscopy*, vol. 25, no. 2, pp. 119–131, 2001.
- [106] Y. Tanizaki, H. Inoue, T. Hoshi, and Shiraish.J, "Localized and delocalized electronic transitions in diphenylacetylene, stilbene and diphenylbutadiene," *Zeitschrift Fur Physikalische Chemie-Frankfurt*, vol. 74, no. 1-2, pp. 45–, 1971.
- [107] Y. Hirata, T. Okada, N. Mataga, and T. Nomoto, "Picosecond time-resolved absorption-spectrum measurements of the higher excited singlet-state of diphenylacetylene in the solution phase," *Journal of Physical Chemistry*, vol. 96, no. 16, pp. 6559–6563, 1992.
- [108] K. Okuyama, T. Hasegawa, M. Ito, and N. Mikami, "Electronic-spectra of tolane in a supersonic free jet - large-amplitude torsional motion," *Journal of Physical Chemistry*, vol. 88, no. 9, pp. 1711–1716, 1984.
- [109] M. Gutmann, M. Gudipati, P. F. Schonhart, and G. Hohlneicher, "Electronic-spectra of matrix-isolated tolan - site selective one-photon and 2-photon spectra," *Journal of Physical Chemistry*, vol. 96, no. 6, pp. 2433–2442, 1992.
- [110] J. Saltiel and V. K. R. Kumar, "Photophysics of diphenylacetylene: Light from the dark state," *Journal of Physical Chemistry A*, vol. 116, no. 43, pp. 10548–10558, 2012.

- 
- [111] D. R. Borst, S. G. Chou, and D. W. Pratt, "Identification of the light-absorbing states in tolane with potential relevance to self-similar phenylacetylene dendrimers," *Chemical Physics Letters*, vol. 343, no. 3-4, pp. 289–295, 2001.
- [112] M. Z. Zgierski and E. C. Lim, "Nature of the 'dark' state in diphenylacetylene and related molecules: state switch from the linear  $\pi\pi^*$  state to the bent  $\pi\sigma^*$  state," *Chemical Physics Letters*, vol. 387, no. 4-6, pp. 352–355, 2004.
- [113] V. D. Kleiman, J. S. Melinger, and D. McMorro, "Ultrafast dynamics of electronic excitations in a light-harvesting phenylacetylene dendrimer," *Journal of Physical Chemistry B*, vol. 105, no. 24, pp. 5595–5598, 2001.
- [114] C. Ferrante, U. Kensy, and B. Dick, "Does diphenylacetylene (tolan) fluoresce from its 2nd excited singlet-state - semiempirical molecular calculations and fluorescence quantum yield measurements," *Journal of Physical Chemistry*, vol. 97, no. 51, pp. 13457–13463, 1993.
- [115] Y. Amatatsu and M. Hosokawa, "Theoretical study on the photochemical behavior of diphenylacetylene in the low-lying excited states," *Journal of Physical Chemistry A*, vol. 108, no. 46, pp. 10238–10244, 2004.
- [116] T. Ishibashi and H. Hamaguchi, "Structure and dynamics of s-2 and s-1 diphenylacetylene in solution studied by picosecond time-resolved laser spectroscopy," *Journal of Physical Chemistry A*, vol. 102, no. 13, pp. 2263–2269, 1998.
- [117] J. L. Palma, E. Atas, L. Hardison, T. B. Marder, J. C. Collings, A. Beeby, J. S. Melinger, J. L. Krause, V. D. Kleiman, and A. E. Roit-

- berg, “Electronic spectra of the nanostar dendrimer: Theory and experiment,” *Journal of Physical Chemistry C*, vol. 114, no. 48, pp. 20702–20712, 2010.
- [118] B. Schmidt, C. Sobotta, S. Malkmus, S. Laimgruber, M. Braun, W. Zinth, and P. Gilch, “Femtosecond fluorescence and absorption dynamics of an azobenzene with a strong push-pull substitution,” *Journal of Physical Chemistry A*, vol. 108, no. 20, pp. 4399–4404, 2004.
- [119] I. Hartl, P. Gilch, and W. Zinth, “Ultrafast redistribution of vibrational excitation of ch-stretching modes probed via anti-stokes raman scattering,” *Applied Physics B-Lasers and Optics*, vol. 71, no. 3, pp. 397–403, 2000.
- [120] H. Koppel, W. Domcke, and L. S. Cederbaum, “Theory of vibronic coupling in linear-molecules,” *Journal of Chemical Physics*, vol. 74, no. 5, pp. 2945–2968, 1981.
- [121] J. C. Tully, “Molecular-dynamics with electronic-transitions,” *Journal of Chemical Physics*, vol. 93, no. 2, pp. 1061–1071, 1990.
- [122] T. Mondal and A. J. C. Varandas, “Quadratic coupling treatment of the jahn-teller effect in triply-degenerate electronic state of  $\text{CH}_4^+$ : Can one account for floppiness?,” *Journal of Chemical Physics*, vol. 137, no. 21, pp. 214320–214329, 2012.
- [123] U. Opik and M. H. L. Pryce, “Studies of the jahn teller effect .1 a survey of the static problem,” *Journal of Chemical Physics*, vol. 238, no. 1215, pp. 425–447, 1957.